1-1-2021

Identification Of New Per- And Polyfluoroalkyl Substances (PFAS) In Aqueous Film-Forming Foam (AFFF)

Venus Rivera Larson

IDENTIFICATION OF NEW PER- AND POLYFLUOROALKYL SUBSTANCES (PFAS) IN AQUEOUS FILM-FORMING FOAM (AFFF)

by

Venus Rivera Larson, PE, LEED AP
Bachelor of Science, United States Air Force Academy, 2001
Master of Science, University of North Dakota, 2004

A Dissertation

Submitted to the Graduate Faculty

of the

University of North Dakota

in partial fulfillment of the requirements

for the degree of

Doctor of Philosophy in Environmental Engineering

Grand Forks, North Dakota

May
2021

Name: Venus Rivera Larson

Degree: Doctor of Philosophy

This document, submitted in partial fulfillment of the requirements for the degree from the University of North Dakota, has been read by the Faculty Advisory Committee under whom the work has been done and is hereby approved.

DocuSigned by:
Dr. Feng Xiao
BD73D5A4B860469...
Dr. Feng Xiao

DocuSigned by:
Dr. Michael Mann
40E32E674D9D44F...
Dr. Michael Mann

DocuSigned by:
7BBE8E3786EC4DA...
Dr. Aaron Dotson

DocuSigned by:
Mikhail Golovko
450E25915F2D41E...
Dr. Mikhail Golovko

DocuSigned by:
Dr. Alena Kubatova
A63A7CCAD7D74DD...
Dr. Alena Kubatova

This document is being submitted by the appointed advisory committee as having met all the requirements of the School of Graduate Studies at the University of North Dakota and is hereby approved.

DocuSigned by:
Chris Nelson
2E0AF088C7334O3...
Chris Nelson
Dean of the School of Graduate Studies

5/3/2021
Date

PERMISSION

Title Identification of New Per- And Polyfluoroalkyl Substances (PFAS) in Aqueous Film-Forming Foam (AFFF)

Department Environmental Engineering
Degree Doctor of Philosophy

In presenting this dissertation in partial fulfillment of the requirements for a graduate degree from the University of North Dakota, I agree that the library of this University shall make it freely available for inspection. I further agree that permission for extensive copying for scholarly purposes may be granted by the professor who supervised my dissertation work or, in her (or his) absence, by the Chairperson of the department or the dean of the School of Graduate Studies. It is understood that any copying or publication or other use of this thesis (or dissertation) or part thereof for financial gain shall not be allowed without my written permission. It is also understood that due recognition shall be given to me and to the University of North Dakota in any scholarly use which may be made of any material in my dissertation.

Venus Rivera Larson, PE, LEED

3 May 2021
Date

TABLE OF CONTENTS

LIST OF FIGURES

LIST OF TABLES

LIST OF EQUATIONS

ACKNOWLEDGMENTS

I wish to express my sincere appreciation to my Advisory Committee members, especially to Dr. Feng Xiao, for their guidance and support during my online PhD program at the University of North Dakota amid the pandemic. The instruction and assistance of Dr. Xiao in analyzing the data were indispensable.

I also wish to acknowledge Swetha Mallula and Augustus Postiglione for helping me obtain the data required for this research.

Special appreciation is extended to the Alaska Department of Transportation, Division of Statewide Aviation, particularly the members at Fairbanks Airport and Gustavus Airport, and the fine service men and women at Eielson AFB for their support in this research.

Thank you to Veteran Affairs for funding my education!

To my husband, Kass, and my sons, Magnus and Xavier, for all your love and support.

Aurora and Mom, gone but not forgotten. Thank you, God, for blessing my life!

ABSTRACT

The extraordinary number of unknown per- and polyfluoroalkyl substances (PFAS) necessitates identifying the substances as a first step to understanding them and their risks. From an environmental engineering perspective (preventing, controlling, and remediating), PFAS remediation and control measures are only as effective as the tools used to detect them. Focusing on aqueous film-forming foam (AFFF), several researchers have elucidated the structures of unknown PFAS, with each study accomplishing PFAS identification differently. A range of software and practices were used to improve mass spectrometry (MS) results or elucidate chemical structures. Different identification approaches were compared in the current research, including suspected identification and a Kendrick mass defect (KMD) method. Focusing on the interpretation of MS results methods, several commonalities appeared, including suspect identification (exact/accurate mass), fragmentation identification, and KMD. These three identification methods were employed in this study for analyzing several legacy AFFF samples manufactured by the 3M Company from 1979 to 2002 and soil samples collected from past AFFF release sites.

The results obtained indicated how AFFF composition has changed over time. Other PFAS were found, i.e., beyond those targeted by the United States Environmental Protection Agency (USEPA) and the new 40 classes of PFAS identified by Brazen-Hanson et al. (2017). The suspect identification method identified most, if not all, PFAS in the 40 classes detected by Brazen-Hanson et al. (2017). However, the KMD approach detected a much smaller number of PFAS compounds in the AFFF samples. Continuous MS scanning enables identifying new PFAS from other PFAS elucidation studies, i.e., non-targeted analysis (NTA). The NTA approach of complete scan data could facilitate future standards without having to resample and thereby

having to expand on past efforts. The current study shows the strengths and limitations of three PFAS identification methods of soils and legacy AFFF products at known AFFF release sites. Overall, this study shows that multiple methods are required to identify PFAS because of the inherent disadvantages associated with each particular method.

I - Background

Per- and polyfluoroalkyl substances (PFAS) are organic compounds with strong carbon and fluoride bonds (3M, 1999; Ahrens et al., 2011). The commonly known PFAS are perfluorooctanesulfonic acid (PFOS), perfluorooctanoic acid (PFOA), and perfluorohexane sulfonic acid (PFHxS) (Dauchy et al., 2017). PFAS have a tendency to be charged and to persist in soil once released (Barzen-Hanson et al., 2017b). The main difference between PFAS and other organic contaminants is that many perfluoroalkyl substances, such as PFOS and PFOA, are resistant to biological and chemical degradation (Xiao, 2017). Therefore, it is difficult to remove and treat PFAS once released to the soil. PFAS has been used in several applications, but the production of PFAS has been identified as a health concern only within the last number of years (Houtz et al., 2018, Yeung et al., 2017). The urgency to control and treat PFAS released to the environment has increased after the detrimental effects of the substances have become known. In numerous studies, the parameters that control PFAS have reviewed and evaluated, but considerably more information is required (Ateia et al., 2019; Ruan & Jiang, 2017). Even with the increased understanding of PFAS movement in soil, the many PFAS unknowns are further complicated by an increasing number of newly discovered PFAS, which current methods have not been able to identify yet (Barzen-Hanson et al., 2017b; Place et al., 2012).

As regards the newly discovered PFAS in aqueous film-forming foam (AFFF) and their release to soil and water, PFAS identification is limited to a small number of targeted substances, although the number of PFAS listed in the United States Environmental Protection Agency (USEPA/EPA) COMPTOX database (USEPA, 2020a) exceeds 8,000. Recently, numerous cationic or zwitterionic PFAS structures have been identified (Backe et al., 2013; Barzen-Hanson et al., 2017b; D'Agostino & Mabury, 2014, 2017; Munoz et al., 2016; Place & Field, 2012; Xiao

et al., 2017. These cationic or zwitterionic PFAS have been shown to sorb strongly to natural soils (Xiao et al., 2019) and, therefore, be decomposed to form currently regulated perfluoroalkyl substances (Jin et al., 2020; Xiao et al., 2018).

The goal of this dissertation is to understand the movement of AFFF PFAS in soil and to characterize the type of PFAS in commercial AFFF samples and AFFF-impacted soils. In this study, six samples of historical AFFF compositions were analyzed and the soil of three past AFFF release sites to identify new PFAS classes. Identifying the new PFAS and PFAS compositions in the historical AFFF compositions and AFFF-impacted sites demonstrates how AFFF has changed over the years. The following three methods were used, namely suspect identification, fragmentation identification, and KMD. This research helps to improve PFAS identification at AFFF contamination sites for treatment, track transformed or degraded PFAS, adapt to the changing AFFF commercial products, identify the specific characteristics of PFAS and, subsequently, use such enhanced understanding in helping predict PFAS movement. The ability to predict PFAS movement in soil helps in controlling PFAS contamination and its associated health risks.

Predominately, PFOS, PFOA, and others listed in Table 1 are identified typically in environmental samples, posing potential risks to human health and the environment. In some countries, industrial manufacturers have ceased the production of some PFAS, such as PFOS and PFOA. However, the characteristics of PFAS are still required to support consumer needs, such as water/oil waterproofing in cooking, clothing, chemical production (cleaning products), and fire protection (Backe et al., 2013; D'Agostino & Mabury, 2014). PFAS were created to utilize their ability to control oil and water, i.e., their hydrophobic and lipophobic characteristics (Fetter et al., 2018; Yan et al., 2012). Several US federal agencies still use and require the public use of

PFAS-containing products as a firefighting measure because no suitable replacement is available (FAA, 2004). Consequently, utilizing PFAS is set to continue in the US and the rest of the world.

Table 1

Major PFAS Compounds Typically Present in Environmental and Biological Samples

PFAS	Name	Carbon Chain Length	Chemical Structure	Linear Formula	Application	Reference
PFOS	Perfluorooctanesulfonic acid	C-8 Long Carbon Chain		CF3 (CF2)7SO3Na	Perfluorooctanesulfonic acid is a long carbon chain compound used as fabric protector, stain repellent, aqueous film forming foam (AFFF), metal plating and a number of industrial applications	Xiao et al, 2017; Wang et al, 2013; Higgins et al, 2005
PFOA	Perfluorooctanoic acid	C-8 Long Carbon Chain		CF3 (CF2)6COOH	Perfluorooctanoic acid is a long chain perfluorocarboxylic acid (PFCA) used for several industrial applications, including carpeting, upholstery, apparel, floor wax, textiles, sealants,	Xiao et al, 2017; Wang et al, 2013; Higgins et al, 2005
PFPeA	Perfluoropentanoic acid	C-5 Short Carbon Chain	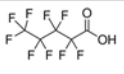	CF3(CF2)3COOH	Perfluoropentanoic acid is a short-chain perfluorocarboxylic acid (PFCA) generally used as an industrial surfactant and surface protector	Arvaniti et al, 2015; Wang et al, 2013
PFBS	Perfluorobutanesulfonic acid	C-4 Short Carbon Chain		CF3(CF2)3SO3K	Perfluorobutanesulfonic acid (PFBS) is a chemical compound with a four carbon fluorocarbon chain and a sulfonic acid functional group and used as stain repellents and commercial	Arvaniti et al, 2015; Wang et al, 2013
PFHxA	Perfluorohexanoic acid	C-6 Short Carbon Chain	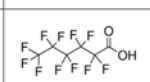	CF(CF2)5COOH	Short-chain perfluorocarboxylic acid (PFCA) used to breakdown product of stain- and grease-proof coatings on food packaging and household products	Arvaniti et al, 2015; Wang et al, 2013
PFHxS	Perfluorohexane sulfonic acid	C-6 Short Carbon Chain		CF(CF2)6SO3	PFOS/PFOA alternative	Arvaniti et al, 2015; Wang et al, 2013; Higgins et al, 2005
PFDA	Perfluorodecanoic acid	C-10 Long Carbon Chain	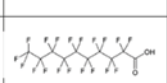	CF(CF2)9COOH	PFOS/PFOA alternative	Xiao et al, 2017; Wang et al, 2019; Higgins et al, 2005
PFNA	Perfluorononanoic acid	C-9 Long Carbon Chain		CF(CF2)8COOH	PFOS/PFOA alternative	Arvaniti et al, 2015; Wang et al, 2013; Higgins et al, 2005
PFUnDA	Perfluorotetradecanoic acid	C-11 Long Carbon Chain		CF(CF2)10COOH	PFOS/PFOA alternative	Arvaniti et al, 2015; Higgins et al, 2005
8:2 FTCA	8:2 fluorotelomer carboxylic acid	at least C-10 Long Carbon Chain		CF(CF2CF2)nCHCOOH	Compound found in AFFF	Wang et al, 2013
8:2 FTUCA	8:2 fluorotelomer unsaturated carboxylic acids	at least C-10 Long Carbon Chain		CF(CF2CF2)nCH=COOH	Compound found in AFFF	Mittal et al, 2016; Wang et al, 2013

II - Movement of PFAS in Soil

As mentioned, PFAS were created to utilize their ability to control oil and water, i.e., their hydrophobic and lipophobic characteristics (Fetter et al., 2018; Yan et al., 2012). These traits have made PFAS a primary component in many applications, such as for non-stick cookware and waterproofing (Zhao et al., 2012). As PFAS are useful in countless industries, they

are used abundantly and can be detected everywhere, even in the blood of polar bears in Antarctica (Zhao et al., 2012). PFAS are crucial in combating fuel fires at fuel distribution/production sites and aircraft fires to save lives during such events. However, although PFAS are a benefit and convenience to society, they also pose significant threats to human health and the environment. PFAS have been shown to interrupt the endocrinological system (thyroid, reproductive system), slow down child development, and they have been linked to high cholesterol, high blood pressure, and cancer (Salgado-Freiria et al., 2018; USEPA, 2016, 2017a). For effective PFAS control and removal, it is crucial to understand PFAS movement behaviors and characteristics. The list of other undetected PFAS is not only extensive but is also ever-growing.

Moreover, these substances are being emitted into the environment without being regulated. These other PFAS could pose similar health risks, e.g., perfluorohexanesulfonate (PFHxS) shows behaviors similar to those of perfluorooctanoic acid (PFOA), whereas F-35B, a commercial fluorotelomer-based compound, mimics the harmful behaviors of perfluorooctanesulfonic acid (PFOS) (Wang et al., 2013; Yin et al., 2018). It would be many years before these other chemicals are studied or even considered for study. Accordingly, for the sake of human health, it is vital to expand the PFAS research focus to include all other PFAS, as they could all be potential precursors to PFOS/PFOA and could have similar adverse health effects.

This current critical review shows how influencing factors are not the only aspect affecting PFAS transport, as other PFAS could also affect sampling readings.

Review of Influencing Factors to PFAS Movement

To understand the movement of PFAS in soil, we compared several studies that focused on factors influencing the transport of PFAS. A summary of the studies is shown in Table 2. These studies show that PFAS movement in soil is influenced by several factors, as well as the interactions between these factors. As shown in Table 2, some of the common factors in PFAS retention are soil organic content, positively charged soil surface, increasing length of PFAS carbon chains (different chemical structures of PFAS), and the unsaturated soil zone. The following sections present detail on the common factors that relate to PFAS movement in the soil.

Table 2

Transport Studies and Movement Influencing Factors

		PFAS Sorption Influencing Factor													
References	Year	Increasing Organic Content	Increase Salinity	Increasing pH	Soil Surface positive charge	PFAS Sulfuric Moiety	Increasing Iron Oxides	Increasing Length of PFAS carbon chain	Increasing Soil Particle Surface area	Unsaturated zone	Clay	Other	PFAS Compound	Soil Type	Summary Result
Higgins et al., 2006	2006	↑*	↑	↓	↑	↑	↑	↑	-	-	-	-	PFOS, PFOA, PFNA, PFDA, PFUnA, PFDS, N-MeFOSAA, N-EtFOSAA	5 different freshwater sediments with varying amounts of organic carbon, sand, silt and clay	Sorption of PFAS on 5 different freshwater sediments was influenced by greater soil organic content, greater salinity, lower pH, more positive soil surface charge, PFAS containing a sulfur moiety and increasing length of the PFAS chain
Johnson et al., 2007	2007	↑*		↓	↑		↑	↑	↑	-	-	-	PFOS	goethite, kaolinite, high iron sand, Ottawa sand	Key to PFOS adsorption were organic carbon and electrostatic effects with surface area of the soil particle an influencing by not dominant factor
You et al., 2010	2010	↑*	↑	↑	↑	-	-	-	-	-	-	-	PFOS	Natural Sediment from two water sources in China	The sorption of PFOS on the sediment was affected significantly by increasing salinity, pH and soil organic carbon content. Sorption became more irreversible incring $CaCl_2$ concentration
Jeon et al., 2011	2011	↑*	↑	-	-	-	-	-	-	-	-	-	PFOS, PFOA	Sediment from three estuarine locations in South Korea; varying montmorillonite clay and Kaolinite clay mixed with humic acid, tannic acid and natural Suwannee river organic matter	Greater sorption of PFAS in soil with increasing amount of salinity and the presence of dissolved organic matter could make PFAS more mobile
Ferrey et al., 2012	2012	↑	↑	↓	-	-	↑*	-	-	-	-	-	PFOS, PFOA	Aquifer sediment downgradient from land in Minneapolis-t Paul . MN, USA	PFOS and PFOA sorption was controlled by electrostatic sorption on ferric oxide in the soil and not organic clay content
Gueflo & Higgins, 2013	2013	↑	-	-	-	↑	-	↑	-	-	-	↑ Presences of other contaminants	PFOS, PFOA, PFNA, PFDA, PFUnA, PFDS, PFPeA, PFHxA, PFHpA, PFBS, PFHxS, 6:2 FTSA, 8:2 FTSA	loamy sand, loam and sandy clay (high iron oxide content)	Sorption of PFAS on 3 different soil were affected by the presence of contaminants (TCE, SDS, AO) depending on Carbon chain length of the PFAS. Short chain PFAS increase soil sorption and decreased with long chain PFAS with SDS presence in loam and sandy loam soils. Low concentration of PFOS decrease in soil sorption with presence of contaminants. Detailed site-specific information is needed to predict PFAS transport
Milinovic et al., 2015	2015	↑	-	-	-	-	-	↑*	-	-	-	-	PFOS, PFOA, PFBS	5 natural and agricultural soils Iberian Peninsula; peat soil from Belarus - all soils from top soil layer	Sorption of PFAS is controlled physicochemical characteristics of PFASs (carbon chain length/hydrophobicity) in soil with PFOS sorption the most irreversible
Lv et al., 2018	2018		↑		↑	-	-	-	-	-	-	↑ Increasing ionic strength of the solution*	PFOA	quartz sand and finely crushed limestone with little or no clay content	Sorption of PFOA in soil increased with the ionic strength of the solution in saturated soil. Ionic strength was increase by increasing the salinity or adding NaCl and $CaCl_2$. CaCl2 had higher PFOA retention than NaCl since Ca is more effective in neutralizing soil surface negative charges
Lyu et al., 2018	2018	-	-	-	-	-	-	-	-	↑*	-	-	PFOA	two size of fine mesh quartz sand	Air-water interface adsorption is a significant source of retention (50%-75%) of PFAS in unsaturated soil
Brusseau, 2018; Brusseau et al., 2019	2019	↑	↑	-	↑	-	-	-	-	↑*	-	↑ Presences of other contaminants*	PFOS, PFOA	natural quartz sand and surface soil with a moderate amount of organic carbon content	PFAS retardation due to sorption/retention in soil model based on solid- phase adsorption, air-water interface, partitioning to soil atmosphere as gas, NAPL-water interface, partitioning to NAPL. Air-water interface and NAPL-water interface will the dominant form of PFAS retention.
Anderson et al, 2019	2019	↑*	-	-	↑	-	-	↑	-	↑*	↓	↓ increased flushing (precipitation)	PFOS, PFOA, PFNA, PFDA, PFPA, PFUnA, PFDS, PFTeDA, PFDoDA PFTrDA PFHxA, PFHpA, PFBS, PFHxS, 6:2 FTSA, 8:2 FTSA	Varied - at least 50 different soil samples with varying characteristics	The effect of soil clay content, TOC, pH, soil flushing (precipitation effect) and PFAS carbon chain length on soil adsorption to create a model for PFAS subsurface transport using a samples from actual contamination sites. Clay content and TOC was thought to be key variable for the model but Clay content had a negative on adsorption. Result show that AEC, TOC, Flushing and length of PFAS chain are key factors in PFAS transport
Dauchy et al., 2019	2019	-	-	-	-	-	-	↑	-	↑*	-	-	24 types of PFAS	Varied - 44 soil core samples: 30 from 2-4m deep and 14 4-15m deep around 5 location at an active Fire Training site	Shorter chain PFAS are more mobile than longer chain PFAS such as PFOS. At greater depth, the prominent PFAS were the short chain and, at shallow depth, long chain PFAS. It may be inferred that the longer chained fluorotelomer could have degraded to the shorter form PFAS at deeper soil depths

Note. ↑: Increase PFAS sorption; ↓: Decrease PFAS sorption;: Key factor to PFAS sorption; -:Not determined in the study.*

Influence of Organic Content

The organic content of soil influences the retardation of PFAS movement, similar to that of other contaminants. Adsorption occurs when sediment or soil is porous, i.e., the contaminant (PFAS) can diffuse into the particle and be sorbed onto interior surfaces (Fetter et al., 2018). Regarding clay with high organic carbon content, the soil organic carbon enables the sorption of PFOS (Wei et al., 2017). In all soil types, the higher the organic carbon content of the surrounding soil, the greater the likelihood of PFAS being adsorbed (Ahrens et al., 2009; Kwadijk et al., 2013). The observed hydrophobic interactions of the PFAS are fundamental to PFAS sorption (Brazen-Hanson et al., 2017; Fetter et al., 2018). The longer the carbon chain of a PFAS, the more hydrophobic would be the PFAS (Arvaniti & Stasinakis, 2012). This factor explains why long-chain PFAS, with ≥ 8 perfluorinated carbons, is adsorbed more readily into the organic carbon in soils than is short-chain carbon PFAS (Arvaniti & Stasinakis, 2015; Gallen et al., 2018; Xiao et al., 2011). Although soils all differ, there are PFAS-contaminated sites where the soil has little or no organic content. With little or no organic carbon content, the electrostatic attraction of the minerals in soil could play an essential role in the sorption of PFAS (Johnson et al., 2007).

Effects of Charges on Soil Surfaces

To identify the charge on soil surfaces, the soil can be tested for anionic exchange capacity (AEC) or cationic exchange capacity (CEC) (Anderson et al., 2019; Milinovic et al., 2015). AEC measures the ability of positively charged soil surfaces to adsorb and exchange anions (Anderson et al., 2019; Milinovic et al., 2015), whereas CEC measures the ability of the negatively charged soil surfaces to adsorb and exchange cations (Anderson et al., 2019; Milinovic et al., 2015). Similarly, assessing the soil zeta potential, measuring the electric

potential at the soil surface indicates where the soil surface is positive or negative (Ferrey et al., 2012; Lv et al., 2018; You et al., 2010). Studies have shown that larger and more positive CEC equates to a more positive surface and higher PFAS sorption (Anderson et al., 2019; Milinovic et al., 2015). The same is true for zeta potential, i.e., the larger and more positive the measurement, the more positive would be the surface, enabling PFAS to sorb more readily (Ferrey et al., 2012; Lv et al., 2018; You et al., 2010). Measuring ionic strength or charge density is another method to measure the soil surface charge, with the same principles as those of AEC/CEC and zeta potential (Johnson et al., 2007). The soil surface charge is dependent on the soil surface composition, i.e., metals or other minerals, such as iron or silica, and the surrounding environment. A study by Lv et al. (2018) showed nearly no PFOA sorption on silica surfaces, as these surfaces have an overall negative charge. The existence of ferric oxides at the soil surface accounts for PFAS adsorption in the absence of organic content (Ferrey et al., 2012). The charge of a soil surface could change depending on the groundwater properties or solution with which the soil comes into contact. Influenced by groundwater salinity and pH, a positively charged soil surface equates to more significant adsorption, which supports the presence of electrostatic forces (Johnson et al., 2007). Focusing on the negative nature of PFAS, any positive ions influence the movement of the PFAS. The negatively charged PFAS use divalent cations (e.g., Ca(II) and Mg(II)) as a bridge to the positive organic carbon and are adsorbed (Arvaniti & Stasinakis, 2015). The effect of monovalent cations (e.g., Na(I)) is mainly compression of the electrical double layer of soil/sediment particles, which enhances the adsorption of anionic PFAS (Xiao et al., 2011).

Unlike the two previously mentioned common factors, an increase in PFAS carbon chain length (chemical structure of PFAS) and soil unsaturated zone factors pose additional

considerations and information gaps. Overall, the mentioned factor studies showed an increase in PFAS retention or adsorption for their targeted factor(s). Predicting PFAS movement on one factor only is not reliable. Therefore, for accurate PFAS prediction, detailed information is required on the site, soil, PFAS types, and other contaminants (Guelfo & Higgins, 2013). The gaps in the list of PFAS movements influence factor studies, i.e., such studies limit their focus to a minimal number of PFAS structures (< 1%) and do not consider other possible factors, such as the effects of the different ionic forms of PFAS. Aspects such as whether the sample was collected from the saturated or unsaturated zones, or the existence of other contaminants/chemicals in the samples, are, therefore, not considered. The following case study demonstrates the impact of such factor gaps.

Case Study

Several models have been created to understand PFAS movement to protect vital water sources. However, the correlations are not precise or accurate when applied in locations different from those for which the models were developed. A greater number of factors is not considered.

PFAS comprises over 8,000 different chemicals (USEPA, 2020a). Even with well-studied chemicals, the isotopes of a chemical could react and behave differently because of a difference in the chemical structure. Also, each PFAS reacts differently; therefore, unique treatment approaches are required.

In Washington County, Minnesota, a landfill is the source of the PFAS in the local area (Minnesota Pollution Control Agency [MPCA], 2007, 2008b). This landfill is one of four disposal sites for the 3M Company, a manufacturer of commercial PFAS such as AFFF. The site was initially mined for sand and gravel and, in 1968, the area was designated a sanitary landfill. It was permitted as a solid waste facility and received both municipal and industrial waste from

1969 to 1975 when it was capped and closed (MPCA, 2008a). The landfill contains an estimated 73% resident and 26% commercial/industrial waste.

When it was converted to a landfill, it was not lined and, in 1983, nearby wells were found to have high levels of volatile organic compounds (VOCs) (MPCA, 2008a). VOC treatment of extraction wells and spray irrigation was employed to control VOC movement and effectively treat the compounds. The on-site spray irrigation employed allowed the extracted groundwater to come into contact with the ambient air, leading to the VOCs being volatilized and removed from the groundwater before it was returned to the environment. This treatment effectively raised the groundwater level in the area. In 2004, PFAS were detected in the wells surrounding the landfill (MPCA, 2008c). Well testing and monitoring were expanded significantly and indicated the widespread presence of PFAS. Subsequently, additional treatment was implemented to remove PFAS from the drinking water, and the site was remediated. In 2009, the landfill was reconstructed on-site with a liner system, and the VOC treatment was disabled (MPCA, 2009). Monitoring of the wells and monitoring stations continue to the present day.

With the source of PFAS effectively controlled, the PFAS concentration at the monitoring wells was expected to decrease. However, the analysis of monitoring results showed the opposite effect.

Data obtained from the Minnesota Pollution Control Agency (MPCA) website contained water sampling results from 1996 to 2020 (2013). Twenty monitoring wells/stations were monitored and sampled for PFAS, but only for a small number of targeted PFAS, starting in 2004. Before 2004, only a few wells were assessed as part of the landfill closure monitoring

program, which did not include testing for PFAS. MPCA had started testing for PFAS only in 2004.

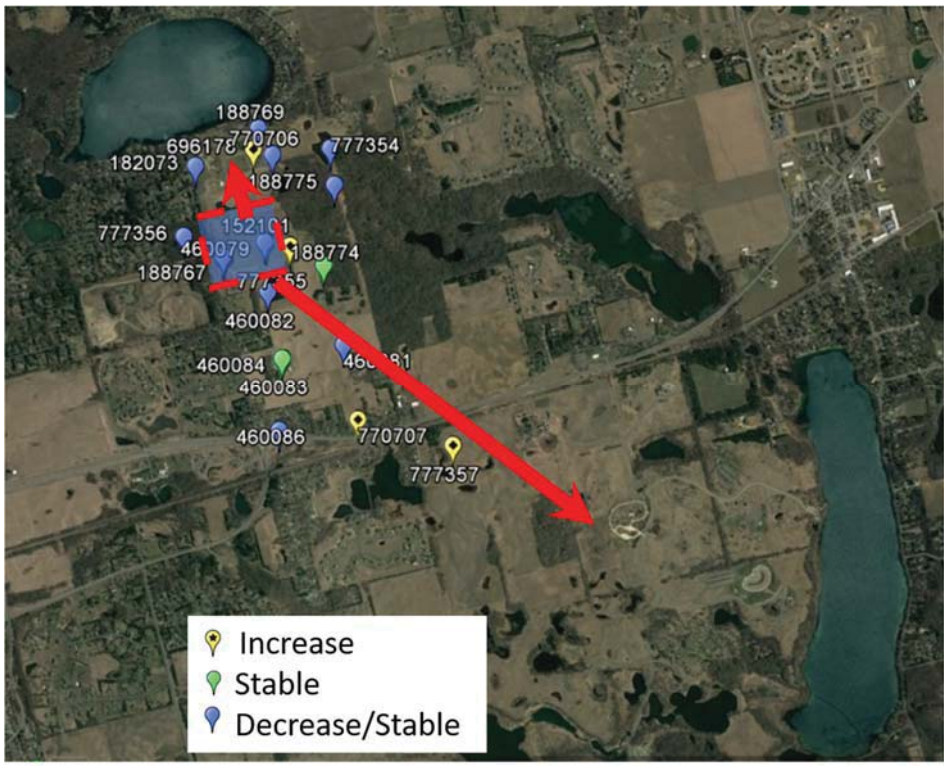

Figure 1: *Map of Closed Landfill and Monitoring Wells/Stations*

This map (Figure 1) shows the landfill in the red dashed line box and the testing wells or stations around the landfill, with the markers representing the stations. Although the bedrock is shallow and highly fractured, groundwater flow is generally south to southeastward, but the flow is northward at one station. At most stations, the concentrations show a stable or slight decrease in some targeted PFAS (shown in Figure 2), but an increase was detected in some stations over time (shown in Figure 3). Station 152101, with the appearance of a decreasing or stable trend, has an $R^{2,}$ of 0.088513 but it is not a statistically significant correlation with a P-value of 0.2734 (> 0.05). Whereas station 188744 has the appearance of a slightly positive trend, but with an R^2 of 0.034125, there is no correlation. However, looking at perflurobutanoic acid (PFBA) results, the R^2 is 0.7933 with a P-value of <0.001, a statistically significant positive correlation. At

Station 152101, Perfluorobutane sulfonate (PFBS) results have an R^2 of 0.5587 with a P-value of <0.001, a statistically significant positive correlation. In Figure 2, there appears to be a decline from 2012 to 2014, but, statistically, the R^2 is 0.0003 with a P-value of 0.7940, a statistically

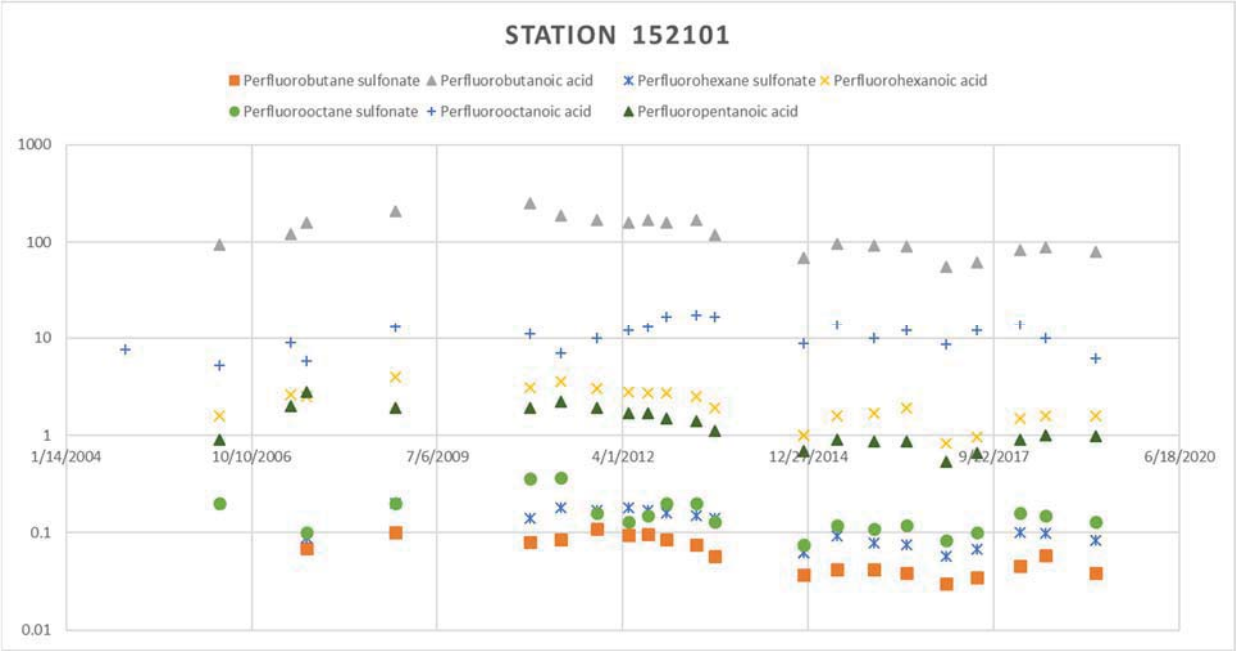

Figure 2: *Graph of Station 152101, with Decreasing/Stable PFAS Concentrations*

insignificant correlation. All results that were lower than the detection limit were not included in the statistical analysis to prevent an artificial skewing of the statistics. The individually observed targeted PFAS statistically have a rise in concentrations, but overall, all the data on targeted PFAS generally reflect stable concentrations. The cause for a few PFAS to increase in the well concentration over time remains unclear. All the samples were sent to the same analytical laboratory and no change in testing procedures was noted.

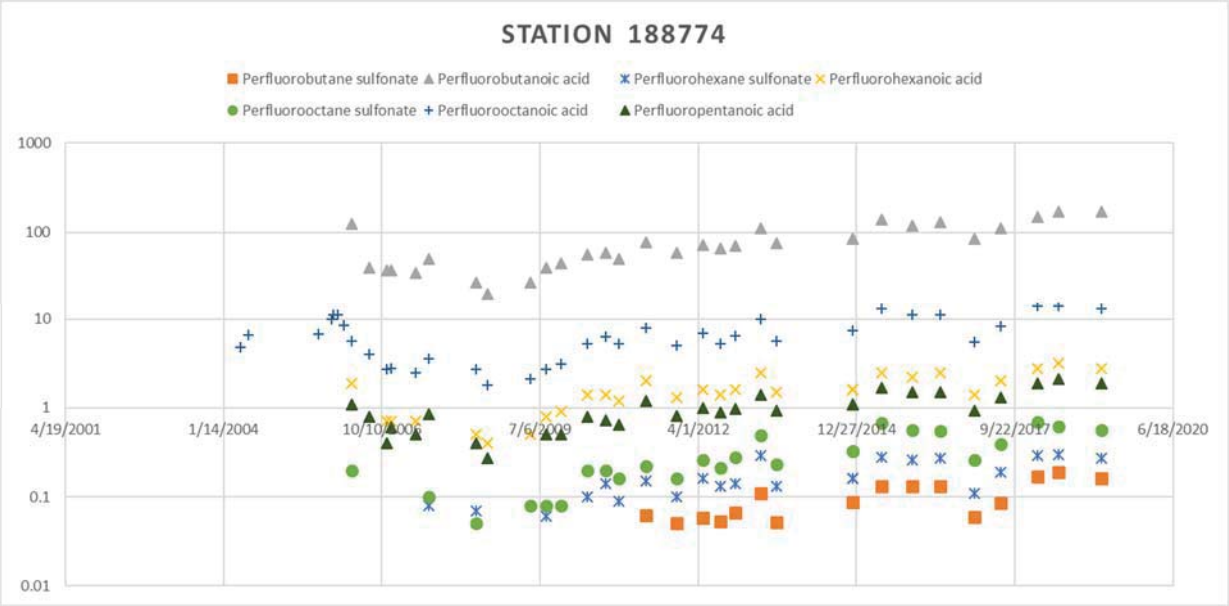

Figure 3: *Graph of Station 188774, with Increasing PFAS Concentrations*

The following list indicates other site parameters that were considered or noted as part of the sampling of wells/stations:

- depth of sampling
- pH
- specific conductance
- temperature
- alkalinity
- Total dissolved solids (TDS)/Total suspended solids (TSS)
- nitrogen
- chloride
- ammonia
- sulfates
- anion/cation ratio
- dissolved oxygen (DO)
- iron

Not all the sampling stations were examined for all the listed parameters. However, the few well locations assessed for all these parameters during the same period had varying results. There is no apparent correlation between the PFAS concentrations and these parameters. Stations monitoring results vary upon location and the distance from the source or landfill and the

direction of ground flow. Five stations' results were analyzed that were equidistant from the source and in the general direction of the observed groundwater flow to determine if there were any statistically significant correlations between the other parameters and the PFAS concentrations. Lower than detection limits (or LOD) results were excluded. The most consistently reported parameters for these 5 stations were pH, temperature, DO, oxidation-reduction potential (ORP), Turbidity, and Specific conductance. The following R2/p-values resulted respectively for more than1300 sample results: 0.0063/0.0032, 0.0035/0.0295 0.0020/0.0020, 0.0046/0.0158, 0.0030/0.053, 0.0250/<0.001. All parameters had very weak correlations that were significant. Other less reported parameters like depth and iron content showed correlations or R^2 with no significance or p values greater than 0.05. Past studies have shown these parameters to influence the PFAS concentration, but not in this case study. There could be other contributing factors affecting PFAS concentrations.

These sample results can be ascribed probably to physical barriers in the soil that delay PFAS movement, another PFAS source in the area, or the breakdown of PFAS already in the environment but not previously detected.

Physical barriers, such as the shallow and highly fractured bedrock, in this case, could prevent the movement of PFAS to a certain extent and, subsequently, could release the PFAS at a later stage. The soil in this area can readily adsorb rain or other precipitation to cause groundwater flow (MPCA, 2007, 2008a, 2009). Therefore, increases in the water table, similar to the mentioned treatment for VOCs, could lead to PFAS movement. A study by the US Air Force (USAF) on AFFF has shown how flushing or increased precipitation could cause increased PFAS movement (Anderson et al., 2019).

Alternatively, there could be another PFAS source in the area. Other nearby landfills and the 3M manufacturing plant (~5 miles [8.05 km] away) could have produced another plume, causing an increase in the PFAS. The land surrounding this closed landfill is rural farmland, with no industrial development or other potential sources of PFAS.

Lastly, the results indicating increased PFAS could reflect the natural breakdown of the previously released but undetected PFAS, which could be precursors of the targeted or tested PFAS. Some of the PFAS eventually degrade to PFOS/PFOA or similar persistent PFAS that bioaccumulate and pose similar health risks (Ahrens et al., 2009; Becker et al., 2010; Gebbink et al., 2015; Houtz et al., 2013; Murakami et al. 2009; Sinclair et al., 2009; Xiao et al., 2012, 2013). Fluorotelomers (FT) are polyfluorinated alkyl substances in which some carbon atoms do not have a strong fluorine bond and which are more easily broken down into smaller compounds (Dauchy et al., 2019). Other long-chained PFAS can break down to create shorter and more resistant PFAS (Dauchy et al., 2019). The undetected PFAS could affect the concentrations of PFAS commonly detected or those included in the current standards of USEPA (2009, 2019) and the American Society for Testing and Materials (ASTM) (2019).

Concern is growing about these precursors that are the replacement PFAS for PFOS and PFOA, as their presence is increasing in the environment and, once degraded, they are a significant source of regulated PFOS/PFOA (Ruan et al., 2015; Schultz et al., 2006; Xiao, 2017). For example, N-ethyl perfluorooctane sulfonamidoacetic acid (EtFOSAA), n-methyl perfluorooctane sulfonamidoacetic acid (MeFOSAA), and perfluorooctanesulfonamide (FOSA) degrade to PFOS (Boulanger et al., 2005; Gebbink et al., 2015). Fluorotelomer-based compounds primarily degrade to PFOA, and the remainder are transformed to PFDA (perfluorodecanoic acid) and PFHxA (Gebbink et al., 2015). Further, some of these PFAS could degrade to different

PFAS depending on the mode of degradation or the surrounding medium (Bolan et al., 2021; Zhao & Zhu, 2017). For instance, 10:2 fluorotelomer alcohol (10:2 FTOH) has been shown to be degraded to perfluorodecanoic acid (PFDA), perfluorononanoic acid (PFNA), and PFOA by soil microorganisms; PFDA, perfluorohexanoic acid (PFHxA), and perfluoropentanoic acid (PFPeA) by wheat roots, and PFDA and PFNA by earthworms (Bolan et al., 2021; Zhao & Zhu, 2017). Substances such as 10:2 FTOH and other long-chain PFAS that have been shown to degrade to other common PFAS are currently not included in the USEPA standard for soil or water testing (Dauchy et al., 2019). Shorter-chained PFAS are transported and detected sooner, whereas longer-chained PFAS, such as 10:2 FTOH, takes longer to be transported (Anderson et al., 2019; Lyu et al., 2018). The additional time could provide time for degradation and could produce short-chained, more common PFAS. Therefore, any meaningful reduction of harmful PFAS needs to consider the precursors of these substances. PFAS precursors have been shown to increase the concentration of the currently detected and regulated PFAS over time (Weber et al., 2017).

Reflecting on the Minnesota case study, the varying levels in the targeted PFAS over almost two decades of testing and monitoring could not be explained by the differing site conditions at each of the 20 wells. There is no known release of other PFAS in the area, and the original PFAS source (landfill) is lined and capped, with appropriate leak detection and prevention measures in place. The original PFAS was released from the landfill; consequently, the increase in targeted PFAS could be ascribed logically to the breakdown or degradation of previously undetected PFAS. The presence of PFOA and PFOS has increased in both wastewater and water treatment processes through chemical (Xiao et al., 2018) and biological processes

(Xiao et al., 2012). Therefore, identifying the other PFAS (other than the targeted PFAS) could help shed light on this aspect.

Different Chemical Structure of PFAS

Expanding PFAS identification entails more than simply expanding the targeted PFAS analyte list, as adjusted approaches to analytical methods are required. Current USEPA (2009, 2019) and ASTM (2019) PFAS standards consider a few targeted PFAS through MS, operating in negative mode or detecting only the resulting negative ions. However, recent research has shown the presence of cationic (positive), zwitterionic (both positive and negative), neutral, and amphoteric (reacts to acids and bases) PFAS (Barzen-Hanson et al., 2017b; Xiao et al., 2019). These non-anionic PFAS might not be detected in negative mode and, therefore, will proceed undetected. Further, several studies have indicated that more than 90% of PFAS are not detected when current methods are employed (Houtz et al., 2018; Miyake et al., 2007; Wiener et al., 2013).

In the table listing the studies on influencing factors (Table 2), the focus is on one or a small fraction of the negative existing PFAS structures. The results of these factor studies do not demonstrate the behaviors of PFAS that are cationic, zwitterionic, neutral, and amphoteric because they are not being detected. These other PFAS also show different behaviors, particularly with factors dependent on the chemical charge interactions between the soil surface and groundwater, such as pH, salinity, and the composition of soil and water. Under the current USEPA (2009, 2019) and ASTM (2019) standards, MS is conducted in the negative mode on a limited number of PFAS. Specific analytical equipment or extraction methods can only be run in one ionic form, such as anionic PFAS, and different forms require additional runs, more samples, and different sample preparations. The additional effort required would probably limit research

efforts to the already established PFAS identification methods. However, various new studies have demonstrated how both negative and positive PFAS can be detected in the same MS scan using inductively coupled plasma mass spectrometry or the fast polarity switching ionization mode, resulting in the identification of a greater number of PFAS (Jamari et al., 2019; Mejia-Avendano et al., 2017).

Effects of the Presence of Different Ions (pH and Salinity)

Regarding pH, H+ or OH- ions affect the surface of soil particles and influence the electrostatic interactions between PFAS and soil. In previous studies observing anionic PFAS, the PFAS sorption on soil/clay increased as pH decreased (You et al., 2010; Xiao et al., 2011). Depending on the solids, Ferrey et al. (2010) and Johnson et al. (2007) showed that, as pH decreased, becoming more acidic with more hydrogen ions, the sorption of PFAS increased. As the pH increased, goethite and kaolinite soil showed less adsorbed PFAS because the increased pH made the soil surface less positive, leading to a repelling force on the PFAS (Johnson et al., 2007). In contrast, You et al. (2010) showed that PFOS sorption was six times greater when the pH was changed from 7 to 8 (from neutral to basic solution); however, in the You et al. (2010) study, soil was used that differed from that used by Johnson et al. (2007). The soil surface strongly influences soil sorption capabilities (Guelfo & Higgins, 2013; Johnson et al., 2007), explaining the varying results obtained by different studies. If these studies considered all the ionic forms of PFAS, the adsorption results would also vary. Where anionic PFAS increases adsorption, cationic PFAS would be repelled and would continue to move. In Xiao et al. (2019), adsorption of cationic PFAS to soil was observed with increasing ions in the solution. In a neutral state (e.g., zwitterionic PFAS), the PFAS would be less likely affected by electrostatic interactions or no sorption (Anderson et al., 2019; Xiao et al., 2019). Similar effects could be

expected under different levels of salinity. PFAS studies report differing accounts on the effects of salinity and PFAS adsorption. Salinity could aid in anionic PFAS sorption to neutralize the negatively charged component of the soil surface (Lv et al., 2018). An increase in salinity reduces the electrostatic repulsion between PFAA molecules and the negatively charged soil particles, leading to adsorption (Jeon et al., 2011; Lv et al., 2018; You et al., 2010; Xiao et al., 2011). A high level of saltwater or salinity creates a "salting out" effect (Xiao et al., 2011). Salting out refers to a high level of ions present in saltwater that prevents the disassociation of other solutes, such as PFAS, and prevents adsorption to the environment (Jeon et al., 2011; You et al., 2010). Therefore, both concepts are correct, in that increasing salinity in the solution creates a more positive soil surface for PFAS to sorb (Jeon et al., 2011; You et al., 2010), but high salinity solutions, such as saltwater, retain PFAS in their neutral form (Ololadea et al., 2018).

Unsaturated and Saturated Soil Zones

Some of the previous factor studies listed (Table 2) do not indicate whether sampling was conducted at the saturated zone (at or below the water table) or at the unsaturated zone (above the water table). Studies on PFAS adsorption have been focused primarily on solid-phase adsorption in the saturated soil zones. However, recent studies have shown more significant adsorption and, therefore, greater PFAS retardation occurring in the unsaturated soil zone than in the saturated zone (Brusseau et al., 2019; Lyu & Brusseau, 2020). Lyu et al. (2018) have indicated that the unsaturated zone accounts for most (50–70%) of PFAS adsorption and takes place at the air–water interface, or PFAS adsorbing to the air or voids in the soil. Considering both the type of PFAS and the soil sample location, a longer-chained PFAS (C8 or higher) would be located closer to the topsoil layer, and a shorter-chained (C6 or lower) would be found in the

deeper layers (Dauchy et al., 2019). These authors have indicated shorter-chained PFAS, FHxSA (perfluorohexane sulfonamide), PFPeS (perfluoropentane sulfonate), and 6:2 FTSAS-SO (6:2 fluorotelomer[FT] thioether amido sulfonate) at the deepest level of soil boring (13 to 15 m below the surface), whereas longer-chained PFAS, such as PFOS, remain closer to the surface (Dauchy et al., 2019).

The primary transport mode for contaminants is through advection (groundwater flow), influenced by dispersion (the flow paths in the soil) (Das, 1998; Fetter et al., 2018; Fitts, 2002). Physical barriers (rocks, impermeable barriers, or physical items in soil) could affect groundwater flow (Das, 1998; Fetter et al., 2018; Fitts, 2002). Physical barriers are the soil components that could prevent or change the movement of any given contaminant and the groundwater flow (advection)(see SI). Bedrock or impermeable soils, such as compacted clay, could stop or change the flow of groundwater and contaminants (Das, 1998; Fetter et al., 2018, Fitts, 2002). Nearby water bodies, such as lakes and rivers, could also function as barriers. Lakes and rivers recharged by groundwater could be a point of deposition of the PFAS contaminant. Dispersion includes diffusion (movement from higher concentrations to lower concentrations) (Fetter et al., 2018). The groundwater concentrations move toward stabilization, and other chemicals or substances in the groundwater could affect the contaminant concentration equilibrium process (Fitts, 2002).

Sorption

Other than physical barriers, sorption to soils is the main reason contaminants retard or slow their flow (Higgins & Luthy, 2006; Miller & Weber, 1984). As regards PFAS, the hydrophobic effect explains adsorption to the soil, as shown in studies on anionic PFAS, particularly that of Xiao et al. (2019). The hydrophobic effect refers to an electrically neutral

compound with polarity being attracted to surfaces that are less polar than water or the inability of the chemical structure of the organic contaminant to form bonds with polar ions such as water (Fetter et al., 2018). Many dissolved organic compounds in water can be adsorbed onto soil particles by the hydrophobic effect (Roy & Griffin., 1985). Organic compounds have a compulsion to complete the outer valence shell. In hydrocarbons, the external hydrogen atoms have an incomplete electron shell. As regards to PFAS, the external fluorine atoms have incomplete electron shells (Bird et al., 1999; Schwarzenbach et al., 2003; Williams, 2019). The incomplete electron shell could cause organic contaminants to be sorbed to minerals in the soil or adsorbed into micropores in carbonaceous sorbent particles, such as carbon or coal (Fetter et al., 2018; Xiao & Pignatello, 2015, 2016). Physisorption, or physical adsorption, occurs when the electronic structure of the atom or molecule is barely adsorbed to the sorbent but does not bond or change the chemical structure of the interacting molecules, such as in π–π electron donor–acceptor interactions and hydrogen bonding (Xiao & Pignatello, 2015; Xiao et al., 2011). The fundamental interacting force of physisorption is caused by Van der Waals forces, which have weak interaction energies (~10 to 100 meV or 1x10 to 15 kJ) (Fetter et al., 2018; Schwarzenbach et al., 2003). Van der Waals forces include the electronic donor–acceptor effect and electrostatic interactions (Fetter et al., 2018; Margenau, 1939; Schwarzenbach et al., 2003). Weak sorption, or Van der Waals forces, refers to the attraction or repulsion of two close atoms (Schwarzenbach et al., 2003; Williams, 2019). Hydrophobic contaminants in water are repelled by water molecules and are readily attached to soil surfaces (Schwarzenbach et al., 2003; Williams, 2019). The charge or partial charge source results from the size of the atoms in a molecule and the electrons are attracted more to larger atoms (Schwarzenbach et al., 2003; Williams, 2019). Such attraction increases the electron density, making the larger atom side more negative (Schwarzenbach et al.,

2003; Williams, 2019). In theory, the most likely PFAS to adsorb into the soil are the PFAS with larger carbon chains, particularly anionic PFAS that includes a sulfur atom, followed by the PFAS with a larger chain with carboxylic acid moiety, followed by the PFAS with a shorter chain with sulfur and, lastly, the shorter-chain PFAS with carboxylic acid moiety (Guelfo & Higgins, 2013; Johnson et al., 2007). The different ionic forms of PFAS have different interactions, but this aspect has not been studied well and, therefore, is not understood well.

The retardation factor can represent the adsorption of PFAS. The following equation represents the retardation of a contaminant:

$$R = \frac{v_x}{v_c} \tag{1}$$

where R is the retardation factor and v_c is contaminant velocity (distance/time) (Fetter et al., 2018; Fitts, 2002). When R is equal to 1, no contaminant is adsorbed, whereas less than 1 represents the amount of contaminant adsorbed. In terms of linear sorption, Equation 2 can be expanded to:

$$R = 1 + \frac{K_d \rho_b}{\theta_w} \tag{2}$$

where K_d is the coefficient representing the contaminant concentration in two mediums or the contaminant concentration in soil compared with the contaminant concentration in the water (Fetter et al., 2018). In nonlinear sorption, a constant also represents this ratio. This constant can be calculated through isotherms or the contaminant concentration with a changing factor or condition, such as water content, depth, or distance from the contaminant source. Certain factors propagate or retard contaminant movement in soil (Xiao et al., 2015). The factors that retard or prevent a contaminant from moving increase the challenge for control and remediation. One such factor is the presence of other contaminants or chemicals in the sampling environment. Guelfo &

Higgins (2013) investigated how PFAS sorption is affected by co-contaminants present in AFFF, specifically non-aqueous phase liquids (NAPLs), such as fuels or AFFF components other than PFAS (chlorinated solvents).

Sorption Because of Other Contaminants

Other contaminants could influence the sorption of PFAS by competing for sorption sites, becoming a sorbent of PFAS, or by preventing or enhancing the sorption of AFFF (Guelfo & Higgins, 2013). Other contaminants generally increase the sorption of short-chained PFAS and decrease long-chained PFAS presence in the soil (Guelfo & Higgins, 2013). Studies by Brusseau (2018) and Brusseau and co-workers (2019) elaborated on the effects of NAPLs on the sorption of PFAS at multiple interfaces, namely soil–atmosphere (as gas in soil voids), air–water, NAPL–water, NAPL, and the solid phase (such as soil) (Brusseau, 2018; Brusseau et al., 2019; Guo et al., 2020). These studies have shown that co-contaminants are critical to adsorption, with the two most critical interfaces for adsorption being the air–water interface and the NAPL–water interface (Brusseau, 2018; Brusseau et al., 2019). These authors used two porous media, namely quartz sand and soil, and PFOS as the model PFAS (Brusseau, 2018; Brusseau et al., 2019; Guo et al., 2020). Air–water interfacial adsorption is a significant retention source for PFOS in these two mediums, contributing more than 80% of total retention for the sand and 32% for the soil (Brusseau, 2018; Brusseau et al., 2019; Guo et al., 2020). In experiments conducted with decane residual emplaced within the sand, adsorption at the decane–water interface contributed more than 70% of the total retention of PFOS transport (Brusseau, 2018; Brusseau et al., 2019). To understand PFAS movement, Brusseau (2018) and Brusseau and co-workers (2019) developed and evaluated a PFAS transport model that considers various adsorption interfaces and partitioning in the soil. The Brusseau model defines the effects of the different interfaces and co-

contaminants on PFAS movement that accurately predicts sorption on their tested soils in saturated and unsaturated zones. To illustrate the effects of PFAS adsorption, Brusseau et al. (2019) modified the retardation equation:

$$R = 1 + \frac{K_d \rho_b}{\theta_w} + \frac{K_a \theta_a}{\theta_w} + \frac{K_{aw} \theta_{aw}}{\theta_w} + \frac{K_n \theta_n}{\theta_w} + \frac{K_{nw} \theta_{nw}}{\theta_w} + \frac{K_{an} \theta_{an}}{\theta_w} \quad (3)$$

where K_d is the solid-phase adsorption coefficient (volume/mass), K_n is the NAPL–water partition coefficient, K_a is the air–water partition coefficient (Henry's coefficient), K_{aw} is the air–water interfacial adsorption coefficient (volume–area), K_{nw} is the NAPL–water interfacial adsorption coefficient (volume–area), K_{an} is the air–NAPL interfacial adsorption coefficient (cm^3–cm^2), A_{aw} is the specific air–water interfacial area (area–volume), A_{nw} is the specific NAPL–water interfacial area (area–volume), A_{an} is the specific air–NAPL interfacial area (area–volume), θ_a is volumetric air content, θ_n is volumetric NAPL content, and θ_w is volumetric water content.

When contaminants are adsorbed onto the soil, there is a possibility of the soil releasing the contaminants later, re-contamination, or spreading of the contamination, which all put public safety at risk. Adsorbed contaminants desorb, based on certain changing conditions, and re-contaminate groundwater (Fetter et al., 2018). Desorption takes place when a sorbate (contaminant) is released from the sorbent (soil) (Fetter et al., 2018). Desorption is driven by balancing the contaminant concentration or the flow of contaminants from a high to a low concentration (Fetter et al., 2018). When a PFAS is adsorbed into the pores of organic carbon, the adsorbed PFAS stops and remains in the soil unless induced to desorb (Wei et al., 2017). PFAS represents many chemicals with different behaviors, particularly in respect of their ionic forms. In Xiao et al. (2019), desorption has been demonstrated to differ between anionic, cationic, and zwitterionic PFAS. Zwitterionic and cationic PFAS sorption depends mainly on the

surrounding environment, such as soil organic content and soil minerals, making sorption nonlinear (Xiao et al., 2019). Similar to anionic PFAS, the amount of soil organic content strongly influences desorption of cationic PFAS; however, in regards to zwitterionic PFAS, the combination of its concentration and low soil organic content shows the most significant influence on its sorption behavior (Xiao et al., 2019). Desorption can occur over time (hysteretic desorption) by flushing as precipitation passes through the contaminated soil or induced by the pumping of fluids in and out of a contaminated site.

Flushing

After a contaminant is released into the soil, its movement can be affected by the volume of precipitation at the site, which causes desorption by precipitation (Fetter et al., 2018). According to Anderson et al. (2019), studying USAF AFFF sites, metadata showed a significant difference between groundwater PFAS concentrations at low flushed sites (low precipitation) and high flushed sites (high precipitation). The PFAS concentration at high flushed sites was 12 times that of the low flushed areas (Anderson et al., 2019). The results of this study also showed under-prediction of the PFAS amounts flushed, whereas, in high flushed areas, the concentration was over-predicted, but the hysteretic desorption of PFAS could not be validated (Anderson et al., 2019). In another study, the flushing concept is described as the level of water infiltration to the soil either by snowmelt or additional water from firefighting training (Høisæter et al., 2019). As in the study by Anderson et al. (2019), it was found that high infiltration increases the movement of PFAS, particularly in unsaturated soils (Høisæter et al., 2019). The distinction between the two studies is that Høisæter et al. (2019) show that short-chain PFAS are more likely to move than are long-chain PFAS. The results of Weber et al. (2017) support the finding that short-chain PFAS transport is faster than long-chain PFAS transport.

Flushing can also be induced mechanically and some contaminants are treated by the flushing of soil. Flushing is done by pumping water into areas located before the contaminated areas and extracted again beyond the contaminated site in the direction of groundwater flow (Fetter et al., 2018). The concept is to flush out the soil contaminants by artificially creating groundwater with a low contaminant concentration, which promotes the contaminants to desorb from the soil and, in that way, they are removed from the site. However, no amount of flushing can move contaminants sequestered deep within the soil particle micropores and outside the reach of flowing water. This finding indicates that permanent PFAS sorption exists, with the implication being that such adsorbed contaminants are resistant to treatment by chemicals and bacteria simply because they are out of the reach of such treatments.

Aging/Sequestration—Removing Toxicity

Several studies on organic contaminants have shown the effects of aging on contaminated soil (Liang et al., 2010; Leppänen & Kukkonen, 2000; Ma et al., 2012; White et al., 1997). These studies found that the longer the organic contaminant is sorbed into the soil, the less likely or more challenging it would be for such contaminant to be desorbed (Liang et al., 2010; Leppänen & Kukkonen, 2000; Ma et al., 2012; White et al., 1997). In a study by White et al. (1997) on soil spiked with a contaminant, the contaminant remained sorbed in the soil for varying amounts of time. This study showed that the longer the contaminant was left sorbed in the soil, the significantly smaller was the amount recovered through vigorous and extensive extraction (White et al., 1997). Even in a simulation of human digestion with simulated gastric fluid, the same result was obtained, i.e., the longer the contaminant was sorbed, the smaller was the amount extracted (Jin et al., 1999). In another study with earthworms consuming contaminated soil, lower contaminant concentrations were found in the worms on soil that had been allowed to

age (Liang et al., 2010; Leppänen & Kukkonen, 2000; Ma et al., 2012; White et al., 1997). No specific type of sorption was identified as causing extra retention by the contaminant aging in the soil. Any sorption could remove the contaminant out of reach of groundwater, treatment chemicals, or biodegradation. Aging could also account for contaminant persistence in soils or the environment because no treatment can reach the contaminant (White et al., 1997). An increase in contact time with the contaminant leads to the contaminant diffusing further into the internal micropores of soil particles, effectively sequestering the contaminant and preventing permanent desorption from the soil (Hatzinger & Alexander, 1995; Liang et al., 2010; Ma et al., 2012; Steinberg et al., 1987; White et al., 1997). However, permanent sorption renders the contaminant less toxic than predicted (Ma et al., 2012). These studies were conducted on non-PFAS contaminants; however, PFAS would probably show similar behaviors. In a recent study, the irreversibility of PFAS sorption has suggested that certain types of PFAS were entrapped because of the size of the pores in the soils, causing a size-exclusion effect (Xiao et al., 2019). This study has indicated that aged cationic/zwitterionic PFAS in past release sites would be less accessible to forms of degradation or remediation (Xiao et al., 2019).

The information gained from previous studies obviously enhances the knowledge on the movement of PFAS; however, it is essential to realize that such information is only a part of the puzzle. PFAS remain essential to basic human life, from the mundane fast-food wrap and non-stick pan convenience to life-saving firefighting; therefore, broadening the identification of PFAS is required to understand the health risks posed by these PFAS and to establish the necessary protection controls. There are gaps in the research, such as the behaviors of more than 8,000 PFAS, including precursor PFAS, different ionic forms of PFAS, sampling locations at saturated or unsaturated zones, and the presence of other contaminants that could affect PFAS

concentrations in the soil. The ability to control and mitigate PFAS health risks and effects remains limited or incomplete with such knowledge gaps. More relevant research could improve the predictability of all PFAS movements and enhance insight into the controls or the necessary remediation actions. Broadening the identification of PFAS would allow future research to fill such knowledge gaps.

III - MS Identification: The Need for Non-Targeted Analysis

Currently, PFAS identification is limited to a few known substances, as indicated in Table 3. The yellow highlighted cells show the additional PFAS compared with the previous version of the identification method or all previous methods. In 2009, USEPA released PFAS identification Method 537 and, in 2018, an updated Method 537.1. Both methods detect a few additional PFAS, mostly long-chained PFAS (≥ 8 perfluorinated carbons). In 2019, Method 533 was released, covering short-chained PFAS to complement Method 537.1 (long-chain PFAS). Combined, both current USEPA methods could identify 29 PFAS (USEPA, 2019a). All these methods are targeted PFAS identification (USEPA, 2020b).

Table 3

List of PFAS Targeted by USEPA and ASTM MethodsWith current identification

Analyte	Abbreviation	CASRN	UCMR3	Method 533	Method 537.1	Method 537	ASTM D7968 (PFAS in Soil)
11-Chloroeicosafluoro-3-oxaundecane-1-sulfonic acid	11Cl-PF3OUdS	763051-92-9		x	x		
9-Chlorohexadecafluoro-3-oxanonane-1-sulfonic acd	9Cl-PF3ONS	756426-58-1		x	x		
4,8-Dioxa-3H-perfluorononanoic acid	ADONA	919005-14-4		x	x		
Hexafluoropropylene oxide dimer acid	HFPO-DA	13252-13-6		x	x		
Perfluorobutanesulfonic acid	PFBS	375-73-5	x	x	x	x	x
Perfluorodecanoic acid	PFDA	335-76-2		x	x	x	x
Perfluorododecanoic acid	PFDoA	307-55-1		x	x	x	x
Perfluoroheptanoic acid	PFHpA	375-85-9	x	x	x	x	x
Perfluorohexanoic acid	PFHxA	307-24-4		x	x	x	x
Perfluorohexanesulfonic acid	PFHxS	355-46-4	x	x	x	x	x
Perfluorononanoic acid	PFNA	375-95-1	x	x	x	x	x
Perfluorooctanoic acid	PFOA	335-67-1		x	x	x	x
Perfluorooctanesulfonic acid	PFOS	1763-23-1	x	x	x	x	x
Perfluoroundecanoic acid	PFUnA	2058-94-8	x	x	x	x	x
1H,1H, 2H, 2H-Perfluorohexane sulfonic acid	4:2FTS	757124-72-4		x			
1H,1H, 2H, 2H-Perfluorooctane sulfonic acid	6:2FTS	27619-97-2		x			
1H,1H, 2H, 2H-Perfluorodecane sulfonic acid	8:2FTS	39108-34-4		x			
Nonafluoro-3,6-dioxaheptanoic acid	NFDHA	151772-58-6		x			
Perfluorobutanoic acid	PFBA	375-22-4		x			x
Perfluoro(2-ethoxyethane)sulfonic acid	PFEESA	113507-82-7		x			
Perfluoroheptanesulfonic acid	PFHpS	375-92-8		x			
Perfluoro-4-methoxybutanoic acid	PFMBA	863090-89-5		x			
Perfluoro-3-methoxypropanoic acid	PFMPA	377-73-1		x			
Perfluoropentanoic acid	PFPeA	2706-90-3		x			x
Perfluoropentanesulfonic acid	PFPeS	2706-91-4		x			
N-ethyl perfluorooctanesulfonamidoacetic acid	NEtFOSAA	2991-50-6			x	x	
N-methyl perfluorooctanesulfonamidoacetic acid	NMeFOSAA	2355-31-9			x	x	
Perfluorotetradecanoic acid	PFTA	376-06-7			x	x	
Perfluorotridecanoic acid	PFTrDA	72629-94-8			x	x	
Decaluoro-4-(pentafluoroethyl)cyclohexanesulfonate	PFecHS						x
Perfluorotridecanoate	PFTriA						x
Perfluorotetradecanoate	PFTreA						x
3-perfluoropheptyl propanoic acid	FHpPA						x
2H-perfluoro-2-decenoic acid	FOUEA						x
2-perfluorodecyl ethanoic acid	FDEA						x
2-perfluorooctyl ethanoic acid	FOEA						x
2H-perfluoro-2-octenoic acid	FHUEA						x
2-perfluorohexyl ethanoic acid	FHEA						x
Total PFAS			**6.00**	**25.00**	**18.00**	**14.00**	**21.00**

References –UMCR3:USEPA, 2017b;Method 533:USEPA, 2019a, 2019b;Method 537:USEPA, 2019b;Method 537.1: USEPA, 2009, 2019b; D7968: ASTM, 2019

methods focused on a limited number of targeted PFAS, recent studies have shown that other PFAS, such as poly-PFAS, remain unidentified (Xiao et al., 2017). Although the current USEPA and ASTM standards focus only on up to 29 PFAS, the USEPA COMPTOX database (2020) (a collection of research from academia, USEPA, and other nations) lists over 8,000 PFAS structures. Several studies have shown that more than 90% of PFAS are not detected (Houtz et al., 2018; Miyake et al., 2017; Wiener et al., 2013). With such a large gap in identification, broadening the identification of PFAS is the logical next step to controlling PFAS, particularly in AFFF, about which there are many litigations and much public concern. Focusing on AFFF, the

current research analyzed the results from multiple PFAS identification methods, particularly AFFF PFAS elucidation studies, and used the information to broaden PFAS identification.

Review of Current PFAS Identification Methods

In PFAS identification studies relating to AFFF, the apparent difference in both target analysis and NTA is the number of different PFAS structures identified (Table 4). The current USEPA (2009, 2019) and ASTM (2019) standards are the targeted methods. For targeted identification, the methods are prescriptive. Target identification scans the pure form of the targeted PFAS and compares it to the sample results from water samples, soil samples, or other sample media. In NTA, combinations of different steps are employed. A comparison of targeted and NTA studies indicated quite apparent differences. The NTA listed or the elucidation studies have a more complex approach, with several steps, and incorporate different software systems to identify the new PFAS structures. In an USEPA trial considering the NTA methods of at least 25 commercial laboratories, it was found that the laboratories all employed different procedures and equipment (Sobus, 2020; USEPA, 2018). However, Table 4 shows that a few similar practices are used in all analytical methods.

Targeted approaches are the established standards for identification, resulting in a high level of confidence in PFAS identification (Hollender et al., 2019; Schymanski et al., 2014). However, currently, there is no established standard for NTA and, therefore, the identification confidence level is lower. With the discovery and identification of novel PFAS, identification quality assurance is crucial because no reference standard exists. There are five levels of identification in HRMS, namely "certain identification" with a standard (level 1); "probable identification" with an unambiguous match of MS library spectrum (level 2A); "probable identification" based on diagnostic evidence, but not confirmed by standard or literature

information (level 2B); "tentative identification of a structure," where multiple structures are possible (level 3); "unequivocal molecular formula," particular molecular formula but no structure (level 4) and, finally, a "measured exact mass of interest" (level 5) (Hollender et al., 2019; Schymanski et al., 2014). Presently, level 1 identification is not possible. Levels 2A or B could be sufficient to identify the new PFAS until a standard is established. With recent elucidation studies expanding MS databases to identify novel PFAS, levels 2A or 2B are possible.

Table 4

Comparison of PFAS Identification Studies—Targeted/Non-Targeted Analysis

Reference	Martix/ Media - Form of Sample (liquid, soil, gas)	Targeted/ Non-Targeted	# of PFAS	Year	Instrument	Chromatographic Separation	Type of MS identification/interpretation/ Structure Elucidation	Software	Suspect Identification (Exact/Accurate Mass)	Fragment Identification	KMD	Other Mass Defect	Peak Search	Retention Time	Other	Extraction Method/Sample Preparation	Extracting Chemical	Filtered during extraction	Type of Ionization
EPA 537.1 (USEPA, 2009)	PFAS Analyte (Drinking Water)	Targeted	Known (18)	2009	LC/MS-MS	-	Reference Standards	-	-	-	-	-	✓	✓	Reference Standard	SPE (MeOH)	MeOH	-	ESI-
EPA 533 (USEPA, 2019)	PFAS Analyte (Drinking Water)	Targeted	Known (25)	2019	LC/MS-MS	C18 liquid chromatography column (2 x 50 mm) packed with 3 µm C18 solid phase particles	Reference Standards	-	-	-	-	-	✓	✓	Reference Standard	SPE (MeOH)	MeOH	-	ESI-
ASTM D7968 (ASTM, 2019)	Soil	Targeted	Known (21)	2017	LC/MS-MS	UPLC	Reference Standards	-	-	✓	-	-	✓	-	Reference Standard	SPE (MeOH)	MeOH	✓	-
Plumlee et al., 2015	Water, Sediment, Fish, Meat and Human Milk	Targeted	Known PFAS (+27)	2015	Turbo V source in electrospray (ESI) negative ion (NI) mode at an ionspray voltage of –4,500 V on an QqTOF AB SCIEX TripleTOF™ 5600 system	Agilent 1200 Infinity (Agilent, Waldbronn, Germany) using a Poroshell 12 EC-C18 column of 50×30 mm internal diameter, 2.7 µm (Agilent)	Reference Standards	Analyst, Peak View 1.0 with the application XIC Manager and Formula Finder and MultiQuant 2.0; Peak View	✓	✓ Isotopic Patterns		✓ software calculated mass error		✓	MS/MS Library	Various dependent on Media	Various dependent on Media	N/A	ESI-
D' Agostino and Mabury , 2017	Surface Waters	Targeted	Known PFAS (+27)	2017	Acuity UPLC-Xevo TQ-S system Waters, Milford, MA; Xevo TQ-S in -ESI	Acquity UPLC–Xevo TQ-S system (Waters, Milford, MA). An Acquity UPLC BEH C18 column (1.7 µm, 2.1 mm × 75 mm)	Mann-Whitney test for detection	OriginPro 2017	-	-	-	-	-	✓	Reference Standard	Oasis SPE WAX	MeOH	N/A	ESI -/+ mode
Yeung et al, 2017	River and Rain Water Samples	Targeted	Known PFAS (+27)	2017	Xevo TQ-Standem mass spectrometer (MS/MS – Waters Corporation, MA,USA) operated in negative ionization mode with an atmospheric electrospray interface	Eight different types of Acquity UPC2columnswere evaluated including Viridis BEH (3.0 mm x 100 mm, 1.7 m), Viridis BEH 2-EP (3.0 mm x 100 mm, 1.7 m), Viridis HSS C18 SB(3.0 mm x 150 mm, 1.8 m), Viridis CSH Fluoro-Phenyl (3.0 mm x100 mm, 1.7 m), Torus 2-PIC (3.0 mm x 100 mm, 1.7 m), TorusDEA (3.0 mm x 100 mm, 1.7 m), Torus DIOL (3.0 mm x 100 mm,1.7 m), and Torus 1-AA (3.0 mm x 100 mm, 1.7 m) columns(Waters, MA, USA) and Acquity UPLC System for standard targeted PFAS identification	Reference Standards	Convergence chromatography manager with an active back pres-sure regulator (ABPR), a sample manager, a binary solvent manager,a column manager, and a post column pre-convergence managerspliti	-	-	-	-	✓	✓	Comparison MS using two MS systems	Oasis SPE WAX	MeOH (0.5% NH4OH)	N/A	ESI-
Place and Field, 2012	AFFF/Commerical Surfactants	Non-Targeted	New PFAS (27)	2012	Waters Xevo G2 QTOF	Waters Acquity H-Class UPLC (Waters, Milfor, MA)	Suspect ion list-> Exact mass filtering -> Matching spectrum -> ID	MassLynx	✓	✓	-	✓ Actual / theoretical ion mass - nominal ion mass	-	-	Patent Information	Dilution (MeOH)	MeOH	N/A	Fast atom bombardment
Backe et al., 2013	AFFF formulas and water samples from known AFFF release sites	Targeted & Non-targeted	26 New PFAS (Cationic perfluorosalkylsulfonamidoamines [C4–C8 PFSAmN] and zwitterionic perfluorosulfonamide amino carboxylate [C4–C8 PFSaAmA]	2013	TQ Detector (Waters Corporation, Milford, MA) triple quadrupole mass spectrometer that was operated in multiple-reaction monitoring (MRM) mode and controlled by MassLynx (Version 4.1). The HPLC/MS/MS system was interfaced with an electrospray ionization source.	Agilent 1100 series HPLC (Santa Clara, CA) that was modified to perform 900 µL injections (Agilent part # G1816A) 4.6 × 12.5 mm × 5 µm Zorbax Silica (Sil) guard column that was connected in series to an Agilent 4.6 × 12.5 mm × 5 µm Zorbax propylamine (NH2) guard column that as connected in series to a Zorbax Eclipse Plus C18 4.6 × 50 mm × 1.8 µm analytical column.	Analytes with authentic analytical standards commercially available; Semiquantitative (Sq) data Oregon State University	MassLynx (Version 4.1).	-	-	-	-	✓	Reference Standards/ Patent Information /MSDS	Dilution (MeOH)	MeOH	N/A	ESI -/+ mode
Beduel et al., 2017	AFFF in soil and concrete samples form a fire training ground	Non-Targeted	4 New Classes and 8 Previous Classes	2017	Shimadzu Nexera X2 ultra high-pressure liquid chroma tography (UHPLC) system equipped with a binary pump and a reverse-phase Luna C18 column (3 µm × 2 mm x 150 mm, Phenomenex) combined with Triple-TOF 5600 system (AB Sciex)	Shimadzu Nexera X2 ultrahigh-pressure liquid chroma tography (UHPLC) system equipped with a binary pump and a reverse-phase Luna C18 column (3 µm × 2 mm × 150 mm, Phenomenex)	mass filtering then a manual PFAS homologue search can be performed KMD or by searching for m/z spacing by ±50 (i.e. -CF2-) or ±100 (i.e. -CF2-CF2-) as PFASs	PeakView software (AB Sciex) to verify unknown PFAS not listed	✓	-	✓	-	-	-	-	MeOH/NH3aq	MeOH/NH3aq	Yes	ESI-
Barzen-Hanson et al., 2017	Historic AFFFs and AFFF-Impacted Groundwater	Non-Targeted	40 New Classes of PFAS (~31 New PFAS)	2017	SCIEX TripleTOF 5600+ (Framingham, MA) QTOF-MS with electrospray ionization (ESI)	Shimadzu LC-30AD (Columbia, MO)	Subtract Background, Suspect Screens using targeted and non-targeted approachs using peak finding, Mass Defects/KMD, Fragmentation ID and Patent Search with proposed structures using ChemBioDraf Ultra 14.0 software	ChemBioDraf Ultra 14.0; Mass Frontier	✓	✓	✓	✓	✓	✓	-	Micro Liquid-Liquid Extraction	HCl and 2,2,2-trifluoroethanol in ethyl acetate	N/A	ESI -/+ mode
Houtz et al., 2013	Wastewater from Treatment Plant	Targeted & Non-Target	Ten Previous PFAS classes and 5 new PFAS Classes	2013	Shimadzu Nexera UPLC and a SciEx 5500 QTrap (Targeted); Agilent 1290 UPLC interfaced with an Agilent 6550 QTOF (Agilent Technologies, Santa Clara, CA) operating in electrospray ionization (ESI) negative mode (untargeted)	Shimadzu Nexera UPLC (Targeted); Agilent Zorbax Extend-C18 column (2.1 × 50 mm, 1.8 µm) (Untargeted)	After Targeted analysis used TOP Assay for total PFAS amount and general identify unknown PFAS	Agilent MassHunter Qual/Agilent Mass Professional Profiler (MPP) software	✓	✓	-	✓	✓	✓	-	Oasis SPE WAX	MeOH (0.5% NH4OH)	N/A	ESI-
D' Agostino and Mabury, 2014	AFFF/Commerical Surfactants	Non-Targeted	12 New; 81 Previous PFAS/fluorinated surfactants	2014	AB/Sciex QStar XL, MDS aiex, Concord, ON Canada	Waters Acquity H-Class UPLC system (Waters Corporation, Milford, MA, USA)	Compare Total Organic Fluorine to FTICR-MS, QTOF-MS and LC MS/MS	Analyst 1.5.1	✓	✓	-	✓ software calculated mass error	✓	✓	Pre-screen with TOF-DIC	2 way of SPE faction method Oasis weak anion (WAX) and Oasis weak cation ex (WCX)	MeOH	N/A	ESI -/+ mode
Liu et al., 2015	Wastewater released from a fluorochemical manufacturing park	Non-Targeted	New (36)	2015	Orbitrap Elite, Thermo Fisher Scientific, CA,USA)	In-line Reversed-phase C18 HPLC column (Hypersil Gold, 5 cm length, 2.1 mm i.d., 1.9 µm particles)	Two injections. The first injection simultaneously accomplished untargted HPLC retention time flagging, and empirical formula assignment. The second injection was used for targeted MS/MS in HRMS mode for empirical formula confirmation and structural characterization.	Xcalibur	-	✓	✓	-	-	✓	Double Injection (repeated MS/MS)	In-line C18 SPE column (Hypersil Gold, 2cm length, 2.1 mm i.d., 12 µm particle)	N/A	N/A	ESI-
Mejia-Avendaño et al., 2017	AFFF Impacted Soil	Targeted/Non-Targeted	55 New; 7 New Classes	2017	Quantitative analysis - Shimadzu UHPLC on a AB Sciex 5500 Qtrap mass spectrometer Qualitative Analysis - Agilent Zorbax SB-C8 column (3.5 µm, 100 × 2.1 mm) on a Dionex UHPLC system(Q Exactive Orbitrap mass spectrometer (both from Thermo Fischer Scientific)	Thermo C18 Hypersil Gold column (1.9 µm, 100 × 2.1 mm).	Obtain full scan MS with both positive and negative mode and find exact mass match with 5ppm window	-	✓	-	-	-	-	-	Standards for known PFAS	MeOH plus 0.1% NH4OH	MeOH plus 0.1% NH4OH	N/A	-/+ heated electrospray ionization (fast polarity switching mode)
Munoz et al., 2016	River Sediment	Targeted/Non-Targeted	New PFAS from other AFFF PFAS studies (60 PFAS total)	2016	Ultra-high performance liquid chromatography coupled to Orbitrap mass spectrometry through polarity-switching electrospray ionization	Dionex Ultimate 3000 LC chain was controlled via the Chromeleon 7.2 Software (ThermoFisherScientific, Waltham,MA,USA,and Dionex Sofiron GMbH part of Thermo Fisher Scientific, Germany) with A Thermo Hypersil Gold eQ column(100x2 1mm;dp=1.9 µm) was used for analyte separation.	Used known standards for common PFAS, data match with recreated PFAS and exact match/fragment identification for other PFAS from other AFFF PFAS studies	For Chromatography - Chromeleon 7.2 Software For MS - Xcalibur 2.3 software	✓	✓	-	-	-	✓	-	Standards for known PFAS; Recreation of some PFAS	MeOH plus 0.1% NH4OH	MeOH plus 0.1% NH4OH	N/A	-/+ heated electrospray ionization (fast polarity switching mode)
Xiao et al., 2017	AFFF formulas	Non-Targeted	New (47); Infrequent Known (43); Known (24)	2017	Waters hybrid QTOF-MS (Synapt G2-S, Waters Corporation, Milford, MA, USA)	Waters Acquity UPLC system: Waters Acquity UPLC BEH Shield RP18 column (100 × 2.1 mm; 130 Å; 1.7 mm) with a Waters Acquity UPLC BEH Shield RP18 VanGuard pre-column (5 × 2.1 mm; 130 Å; 1.7 mm)	High-resolution parent ion search (HRPS) function to Parent Ion fragments of PFAS and associated the product ion scan spectra data were analysed by researchers and MassLynx 4.1 software to propose chemical structures within 20 ppm of candidate m/z	MassLynx V4.1	✓	✓ Parent Ion Search	-	✓	✓	-	Dilution (MeOH)	MeOH	N/A	ESI -/+ mode

Logically, the approach to identifying PFAS differs between different media, and the current study focuses on AFFF-related identification. Concentrating on the interpretation of the MS results from Table 4, some commonalities are apparent. Employing chromatography and HRMS provides chemical attributes, such as retention time, peaks, abundance, charge, and mass to charge values (*m/z*) from the mass spectrum for targeted ions or associated fragments (Barzen-Hanson et al., 2017b). This information can be used to broaden PFAS identification to include currently unknown chemicals. Several aspects should be considered in PFAS chemical elucidation, with the most common being suspect identification (exact/accurate mass), fragmentation, and mass defect.

In the current study, six samples of historical AFFF compositions were analyzed and the soil of three past AFFF release sites to identify new PFAS classes. Identifying the new PFAS and PFAS compositions in the historical AFFF site and the AFFF-impacted site demonstrated how AFFF has changed over time. The following methods were employed, namely suspect identification, fragmentation identification, and KMD. This research could help improve PFAS identification at AFFF contamination sites for treatment, track transformed or degraded PFAS, adapt to changing AFFF commercial products, identify the specific characteristics of PFAS and, subsequently, use this knowledge to help predict PFAS movement.

IV - Methods/Testing

Sample Collections

Historical Commercial AFFF Samples

Six samples of historical AFFF commercial products were obtained from the 3M company from the years 1979, 1989, 1990 (two different manufacturing events), 1997, and 1998.

AFFF Release Sites Soil Samples

The AFFF soil samples were obtained from three airports. The samples of two sites (sites F and G) are from firefighting training areas and one sample is from an aircraft fire/explosion site (Site E). The amount of AFFF used is unknown. For the fire training sites, the use of AFFF was discontinued recently, and the aircraft fire/explosion site dates from 1989 (ADEC, 2019).

The soil of Site G is sandy, with no clay or other fines, and the sand particle size gradually decreases with depth. During sampling at Site G, the groundwater table was penetrated at approximately two feet (60.96 cm). The soils of sites E and F are similar, with a loamy first layer transitioning to silt and deepest layers of clay. The samples at sites E and F do not reach the water table or the saturated zone.

Soil sample collection was based on the procedure by Xiao et al. (2015). After carefully removing stones and vegetation from the sampling surface, each soil sample was obtained using a stainless steel auger. The approximate mass of each sample was 50 g. The samples were placed in pre-cleaned polyethylene bags and taken to the laboratory for further treatment and analyses. To avoid cross-contamination, the auger was cleaned after each sample was processed by 1) cleaning with a tissue to remove the soil/particles attached to it, 2) rinsing with a mixture of methanol and reverse osmosis (RO) water, 3) cleaning again with a clean tissue, 4) rinsing with RO water, 5) wiping with a clean tissue, 6) rinsing with RO water, and 6) wiping with a clean tissue. To assess the adequacy of the cleaning process employed during the sampling procedure, three rinse blanks were prepared using RO water to rinse to decontaminate the auger. Three field blanks were prepared using a mixture of domestic soil obtained from a site with no known PFAS contamination or release or any known use or production of PFAS chemicals. The uncontaminated domestic soil samples were carried in three pre-cleaned polyethylene bags to

each sampling site. The bags were opened, and the mixtures were exposed to the sampling environment of the three sites, sites E, F, G. The blanks were processed and treated as field samples. The blanks were placed in sample containers for handling, shipment, and analysis, identical to the field samples.

Each field sample bag was cut open to allow a thin layer of soil to be exposed to the air. The soil air-dried overnight. Each sample was subsequently sieved through a 2-mm stainless steel mesh to remove stones/other coarse materials mixed thoroughly. Subsequently, the sample was ground and homogenized with a methanol-rinsed mortar and pestle and separated into polyethylene containers. After processing a sample, the mortar and pestle were cleaned with methanol and RO water. An additional soil blank (not exposed to the sample sites) was processed to observe the possible ambient PFAS condition of the laboratory environment or the drying processes.

Other quality assurance and quality control (QA/QC) considerations included using nitrile gloves, wearing old clothing (laundered several times), avoiding pre-wrapped food and snacks, and not wearing water-resistant clothing and insect repellant/sunscreen (Erickson, 2008; Xiao et al., 2015).

Sample Preparation

Soil Extraction Method

Soil extraction was modified slightly from the same method used in Barzen-Hanson et al. (2017a), Houtz et al. (2013), and Xiao et al. (2015). Briefly, 10 mL of 0.5 M HCl in methanol (pH < 0.5) was added to a 50-mL centrifuge tube containing 10 g of dried soil. The mixture was shaken by hand (wrist action) to ensure contact with the solution and soil, followed by sonication for 30 min in a heated bath (45 °C; VWR, Symphony™, Avantor®, USA).

The vials were centrifuged at 3,000 rpm for 15 min, and the supernatant was decanted into a separate tube. The extraction process was repeated three times. Barzen-Hanson et al. (2017a) have indicated that three extraction rounds are sufficient to recover > 97% of all analytes. The resulting analytes were allowed to evaporate under a laboratory hood until 5 ml remained. The analytes were injected into analyte bottles passing through a 2-μm filter before liquid chromatography and mass spectrum analyses.

Analysis

PFAS chemical analysis followed the same procedure as that of Xiao et al. (2017). Certified standards of 24 PFAS in methanol were purchased from Wellington Laboratories (Guelph, Canada). Chemicals in group #1 (per-PFAS group) included 1) five linear perfluoroalkyl sulfonates (per-PFSAs): perfluorobutanesulfonate (PFBS), perfluorohexanesulfonate (PFHxS), perfluoroheptanesulfonate (PFHpS), PFOS, perfluorodecanesulfonate (PFDS); and 2) ten linear perfluoroalkyl carboxylates (per-PFCAs): perfluoropentanoate (PFPeA), perfluorohexanoate (PFHxA), perfluoroheptanoate (PFHpA), PFOA, perfluorononanoate (PFNA), perfluorodecanoate (PFDA), perfluoroundecanoate (PFUnDA), perfluorododecanoate (PFDoDA), perfluorotridecanoate (PFTrDA), and perfluorotetradecanoate (PFTeDA). The chemicals in group #2 (poly-PFAS group) included 1) four alternative compounds to PFOS/PFOA: 2,3,3,3-tetrafluoro-2-(1,1,2,2,3,3,3-heptafluoropropoxy) propanoic acid (HFPO-DA or GenX [42-45]), dodecafluoro-3H-4,8-dioxanonanoate (ADONA), 6:2 and 8:2 chlorinated polyfluorinated ether sulfonates (6:2 and 8:2 Cl-PFAESs or F-53B); and 2) five poly-PFAS: 6:2 and 8:2 fluorotelomer sulfonates (6:2 and 8:2 FTS), 8:2 fluorotelomer unsaturated acid (8:2 FTUCA), N-methyl and N-ethyl perfluorooctane sulfonamide acetates (N-Me- and N-Et-FOSAAs).

Small aliquots of the standards were added to a solution of 20% (v/v) methanol (Optima™; LC/MS grade) in deionized water (18MU cm, Millipore Synergy 185) to a concentration of 10, 20, 40, or 200 ng/mL for ultra-performance liquid chromatography (UPLC) Time-of-Flight(TOF)-Mass Spectrometry $(MS)^E$ analysis. Twenty microliters of the surfactant liquid were dissolved in 50 mL of methanol (Optima™; LC/MS grade) and equilibrated for 48 h. Subsequently, a 200-mL aliquot of the methanol solution was added to 800 mL deionized water for UPLC-ToF-MS^E analysis.

The analysis was conducted on a Waters Acquity UPLC system, coupled with a Waters hybrid (QToF)-MS (Synapt G2-S, Waters Corporation, Milford, MA, USA), available in the Department of Biomedical Sciences of the University of North Dakota (see Figure 4).

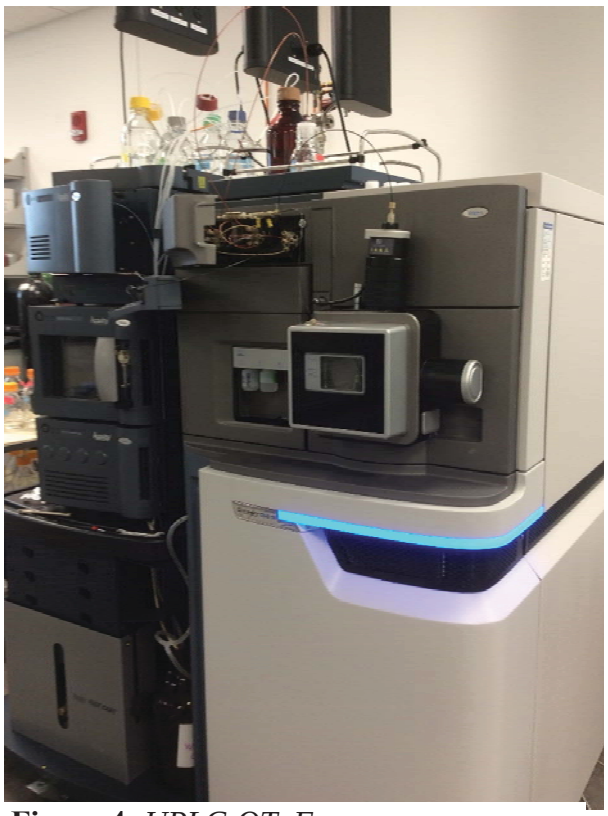

Figure 4: *UPLC-QToF*

Chromatographic Method

Chromatography was performed using a Waters Acquity UPLC BEH Shield RP18 column (100 x 2.1 mm; 130 Å; 1.7 µm) with a Waters Acquity UPLC BEH Shield RP18 VanGuard pre-column (5 x 2.1 mm; 130 Å; 1.7 µm). The mobile phase consisted of eluent A (2 mM ammonium formate in Optima™ water; LC/MS grade) and eluent B (2 mM ammonium formate in Optima™ methanol; LC/MS grade). The elution started at 20% B for 0.5 min and was linearly increased to 85% B in 5 min, further increased to 98% B in 0.1 min and kept isocratic for 1.5 min. At 7.1 min, the A/B ratio returned

to the initial value of 80/20 over 0.1 min to re-equilibrate the column for another 1.3 min. Analytes were eluted using a Waters Acquity UPLC pump with a well-plate autosampler at 8 °degrees C. The flow rate was maintained at 0.45 mL/min, and the column temperature was 55 °degrees C.

Mass Spectrometry Method

The MS analysis was performed using the Synapt G2-S QToF-MS, Waters Corporation, USA, with an electrospray ionization (ESI) source operated in either the negative or positive ion modes (ESI^- or ESI^+). The MS operating conditions were as follows: cone voltage, 20 V; capillary voltage, 1.8 kV; source temperature, 110 °C; desolvation temperature, 350 °C; cone gas flow rate, 10 L/h; and desolvation gas flow, 1,000 L/h. The analyzer was operated with an extended dynamic range at 10,000 resolution (fwhm at *m/z* 554), with an acquisition time of 0.1 s. The Synapt G2-S ToF MS^E mode was used to collect data, with the T-wave element alternated between a low energy of 2 V (MS) and high energy ($MS^{E)}$ states in which the transfer T-wave element voltage ranged from 10 to 25 V [51]). Leucine enkephalin (400 pg/µL) was infused at a rate of 10 mL/min for mass correction. MassLynx V4.1 software (Waters Corporation, USA) was used for instrument control, acquisition, and mass analysis.

MS Identification

The identification methods examined in this study are suspect identification, fragmentation identification, and KMD.

Suspect Identification

Suspect identification refers to identification through accurate masses (Hollender et al., 2019). In other PFAS structural elucidation research, the term suspect identification is related to the screening methods or narrowing to mass/charge (m/z) values with the most potential to be

identified as PFAS (Barzen-Hanson et al., 2017b). In the current study, suspect identification is referred to as PFAS identification using the available database/library exact/accurate masses.

Suspect identification or finding the exact mass could be as simple as inputting the desired m/z value to the MS analysis software or could refer to a more in-depth data-mining approach. Accurate masses can be found in full-scan mass chromatograms from ultra-performance liquid chromatography and tandem mass spectrometry (UPLC/MS-MS) equivalent or more advanced chromatography and mass spectrometry methods (Place et al., 2012; Xiao et al., 2017). Other attributes of the detected masses can also be captured by MS. These attributes can be used to enhance suspect identification, such as peaks in the mass spectrum (Barzen-Hanson et al., 2017b) and retention time (Liu et al., 2019).

Suspect identification could be limited by excess background data or noise in the mass spectrum. To deal with any background data, using laboratory blanks or focusing on results with adequate resolving power (>103) could improve the identification results (Harris & Charles, 2016, p. 97, 563; Watson & Sparkman, 2007, p. 200).

Building on other PFAS structural elucidation studies, the m/z values can be used in suspect identification. Armed with such knowledge, future PFAS studies and testing could also identify the new PFAS. Without a reference standard for the new PFAS, the previous studies provide a reference point for potential chemical identification. However, basing identification solely on accurate mass has a low confidence level with respect to true chemical identification (Hollender et al., 2019; Schymanski et al., 2014). Additional data need to be analyzed to validate such chemical identification (Harris & Charles, p. 570). Suspect identification can be used as a screening tool to focus on the scan portion with the most potential, leading to identification at a higher confidence level (Ruan & Jiang, 2017).

A full-scan mass spectrum was obtained for each sample in both positive and negative ionization modes. For each of the new AFFF PFAS (40 classes) and the known PFAS with reference standards, exact mass or mass/charge (*m/z*) values were searched, and peaks were found in the resulting chromatography utilizing the software MassLynx, Waters Corporation, USA. Using the peaks, a mass spectrum graph was obtained, and the exact *m/z* value, if found, was identified using the suspect identification method, as shown in Figure 5.

The error between the exact mass and measured mass was limited to +/- 20 ppm, using the following calculation (Xiao et al., 2017):

$$\text{error (in mDa)} = \left[\text{measured mass (Da)} - \text{exact mass (Da)}\right] \times 100 \; ; \qquad (4)$$

$$\text{error (in ppm)} = \left[\text{error (in mDa)} / \text{exact mass}\right] \times 10^6$$

The PFAS within +/- 20 ppm error were identified as candidate PFAS.

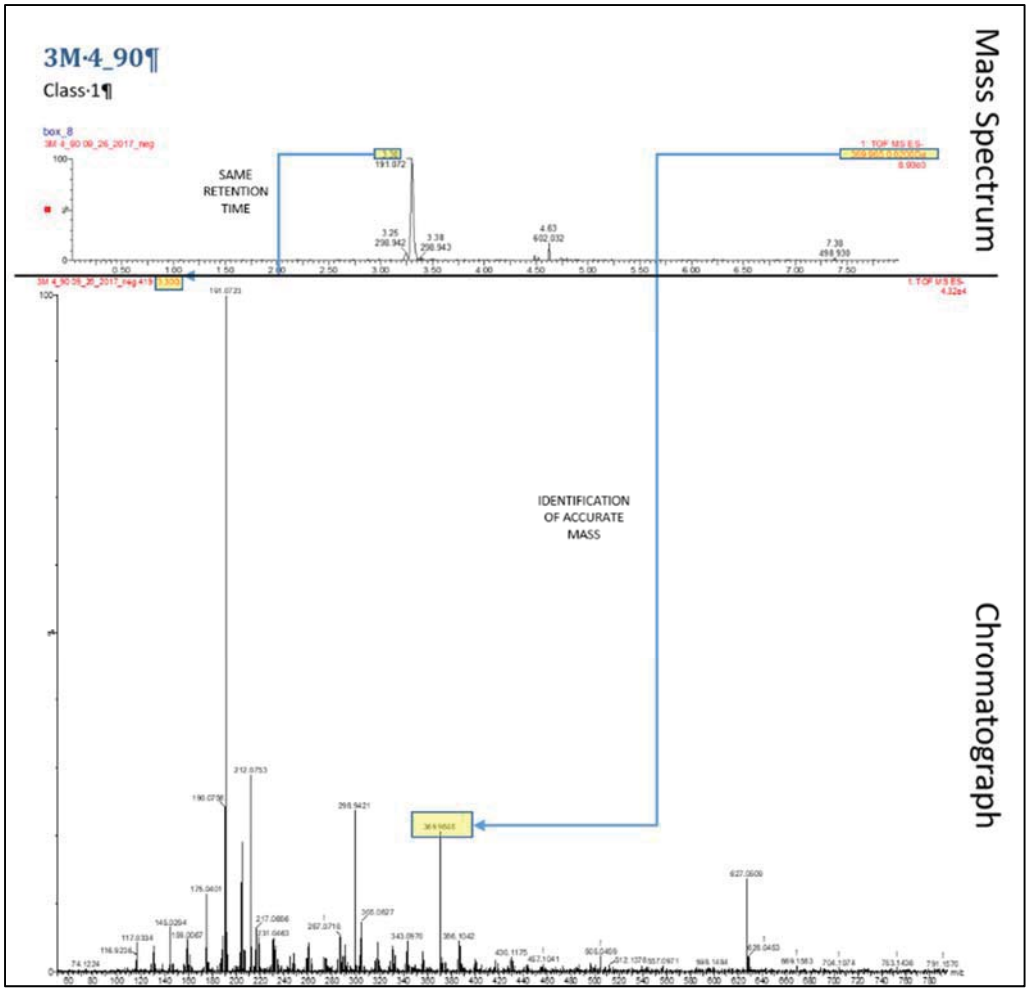

Figure 5: *Suspect Identification Example*

Fragmentation Identification

Full-scan MS spectrum results can identify PFAS by identifying fragments that are typically detected for a specific PFAS chemical structure (Barzen-Hanson et al., 2017b; Harris & Charles, 2016, p. 570; Hollender et al., 2019; Watson & Sparkman, 2007, pp. 433–443). Fragmentation can be accomplished by finding peaks and matching the isotopes of the specific chemical structures (Barzen-Hanson et al., 2017b; Harris & Charles, 2016, p. 570; Watson & Sparkman, 2007, pp. 433–443). Another study used a high-resolution parent ion search (HRPIS) to identify fragments of a specific PFAS (Xiao et al., 2017). One aspect of fragment

identification that must be considered is that each atom within a PFAS structure can vary in molecular mass, such as carbon, hydrogen, sulfur, and oxygen, which typically compose PFAS (Harris & Charles, 565). Carbon atoms naturally exist in at least 15 different isotopes (ScienceStruck, 2020). PFAS comprises mainly carbon atoms, which implies that the mass of any specific PFAS could vary depending on which carbon isotopes are present in that particular PFAS. The same is assumed for the other PFAS chemical structure components. This aspect explains why comparing MS scans to a known database (Watson & Sparkman, 2007, pp. 433–443) or repeat MS scans could help verify the fragments of specific PFAS and their isotopes (Liu et al., 2015).

Fragmentation identification has been used to identify or predict the structures of unknown chemicals. However, trace amounts of a specific chemical could result in ineffective analysis. Although employing advanced MS systems lead to high mass accuracy and resolution, the problems of high background noise and insignificant data remain (Ateia, 2019; Cerveny et al., 2016; Lin et al., 2016; Lorenzo et al., 2018; Zacs & Bartkevics, 2015), which could make fragment analysis ineffective. Combined with trace amounts of a specific PFAS, such noise and superfluous data could lead to non-identification. The low abundance of one particular PFAS structure could lead to fragmentation identification being insufficient to identify the structure, which implies that additional analysis, such as KMD plots, is required (Barzen-Hanson et al., 2017b).

For the current study, fragmentation identification was conducted only on the ionization results of the suspect identification negative mode. For fragmentation identification methods, the results of negative ionization mode suspect identification were focused on those *m/z* values most likely to be identified as PFAS. Two types of fragmentation identification were used, namely

identifying results with expected fragment ion from a database (CFM-ID) and HRPIS. The first method compares MS scan data for a specified PFAS *m/z* value with the database MS scan (Figure 6). If multiple fragment ions match between the MS results and the MS database, the fragmentation identification results are likely identified PFAS.

According to Xiao et al. (2017), a first step is to perform HRPIS (Function of MS^e) on PFAS characteristic fragments to identify candidate PFAS parent ions from UPLC-ESI-ToF-MS^E chromatograms. Next, the production scan spectrums of these candidate PFAS ions are studied (see supplemental information for more information). Possible formulas are matched with the reference standard PFAS and the new 40 classes of PFAS using MassLynx V4.1 software, with a mass error tolerance of 20 ppm. PFAS compounds are identified as candidate PFAS with a +/- 20 ppm, following the same error formula as suspect identification.

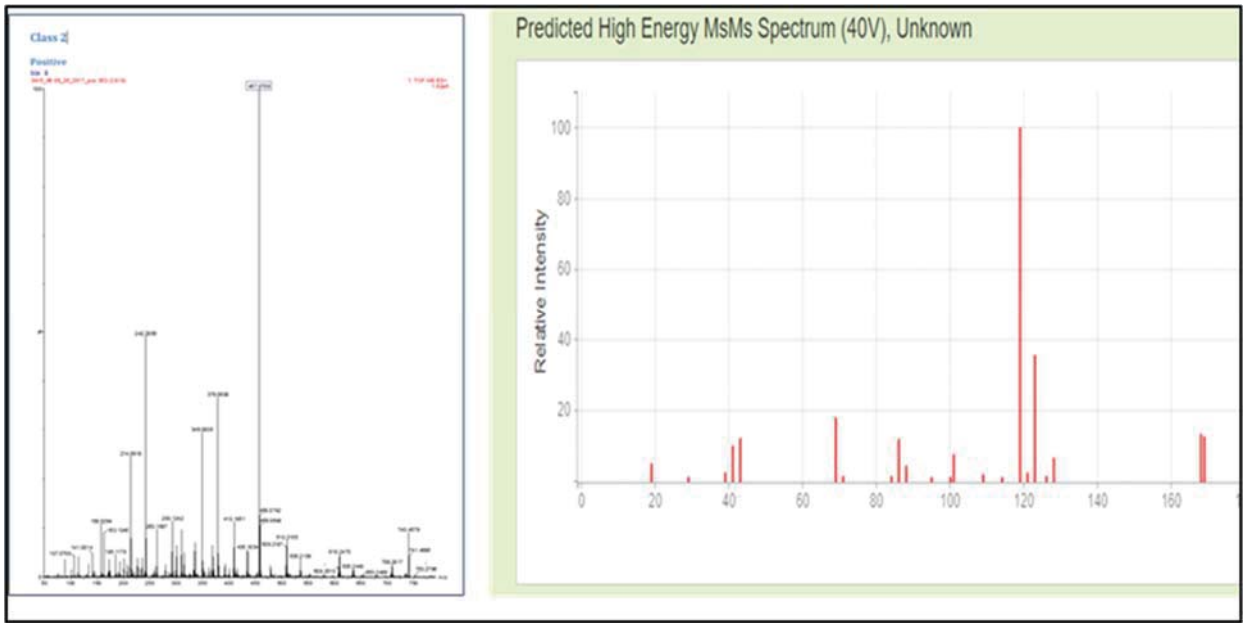

Figure 6: *Example of fragmentation identification by database comparison*

Kendrick Mass Defect

KMD plotting has been used to identify unknown hydrocarbon compounds but could also be used for other chemical structures with a common repeating structure (Hughey et al., 2001; Kendrick, 1963). This method uses a repeating structure in a chemical, such as CH_2 in hydrocarbons, to focus on the unique portion of the chemical (Hughey et al., 2001; Kendrick, 1963). For PFAS, the repeating structure is CF_2. The repeating CF_2 chain is common to all PFAS (Barzen-Hanson et al., 2017b; EUROFINS, E. A., 2020; Xiao et al., 2017). Using this trait, KMD plots, using the equation below, can identify the unique PFAS in MS data (Barzen-Hanson et al., 2017b; EUROFINS, E. A., 2020). KMD is calculated using Equation 5:

Kendrick mass defect = nominal Kendrick mass – exact Kendrick mass. (5)

Other types of mass defects are calculated utilizing the CF_2 chain, but the difference in the KMD approach is that it considers the nominal mass of the PFAS and the exact mass of the CF_2 chains to focus more on the unique portion of the PFAS (Place & Field, 2012). Other mass defect calculations use only the nominal mass of CF_2 (Place & Field, 2012). The calculated KMD is used to detect PFAS with the same unique chemical structure but differs by the number of CF_2 chains. M/Z values that differ by multiples of CF_2 mass are considered PFAS (see Figure 7). KMD takes advantage of the greater precision of HRMS. KMD has been used successfully to identify many new PFAS structures (Barzen-Hanson et al., 2017b).

Using the full-scan mass spectrum obtained for each sample, only in negative mode, all the resulting data are grouped by *m/z* values that had a difference of +/- 50 Da. 50 is the nominal mass of CF^2. Therefore, if the m/z values with the same first two whole integers and first decimal point are grouped, this represents the m/z values separated by 100 Da or two CF^2 chains. Then add m/z values +/- 50 Da, one CF^2 chain, from the previous step would be one grouping. This

grouping brings together the *m/z* value of the ions with the most similar chemical structure that varies in the number of CF_2 chains. KMD is calculated using Equation 5.

The grouped *m/z* values are plotted with the calculated KMDs over each *m/z* value. When three or more *m/z* values have the same KMD, they are identified PFAS or PFAS fragments created by the MS (see Figure 7). Similar to fragmentation identification, KMD builds on a proceeding suspect screening to produce a focused PFAS candidate list. The same KMD value is defined as having a difference between the two KMD values equal to or less than 0.001+/-. The limit is set to reduce false identifications, and this boundary fits the parameters of known PFAS KMD plots.

Once the ions with the same KMD are determined, the *m/z* values are matched to one of the 40 PFAS classes and validated again through the suspect identification method, MS exact mass match, and peak finding.

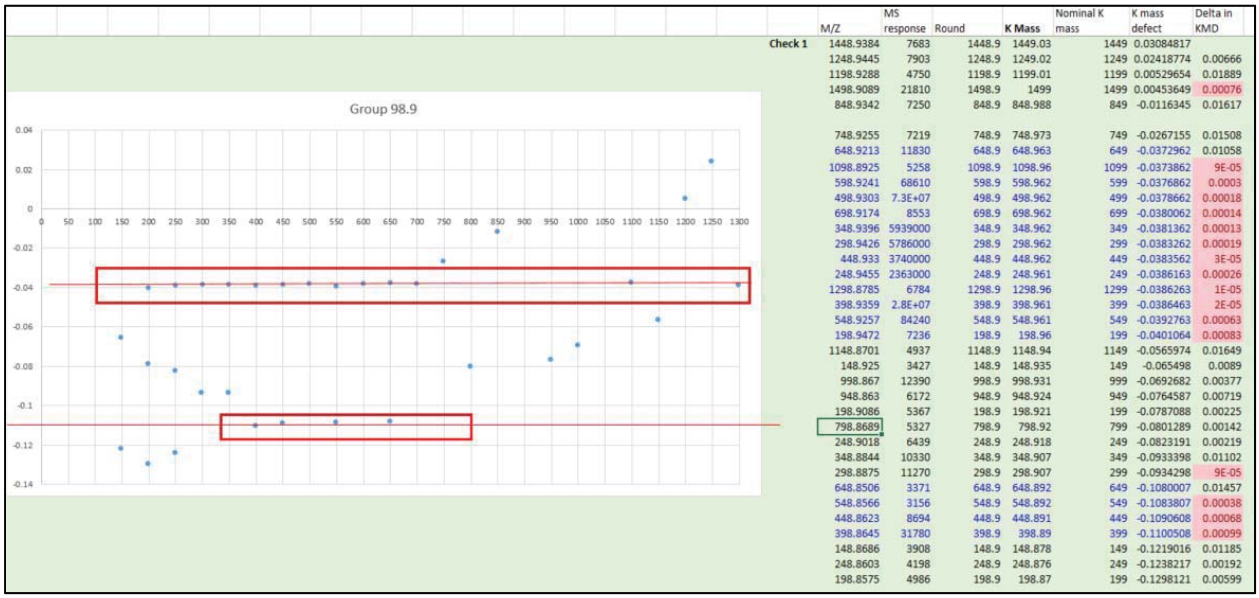

	M/Z	MS response	Round	K Mass	Nominal K mass	K mass defect	Delta in KMD
Check 1	1448.9384	7683	1448.9	1449.03	1449	0.03084817	
	1248.9445	7903	1248.9	1249.02	1249	0.02418774	0.00666
	1198.9288	4750	1198.9	1199.01	1199	0.00529654	0.01889
	1498.9089	21810	1498.9	1499	1499	0.00453649	0.00076
	848.9342	7250	848.9	848.988	849	-0.0116345	0.01617
	748.9255	7219	748.9	748.973	749	-0.0267155	0.01508
	648.9213	11830	648.9	648.963	649	-0.0372962	0.01058
	1098.8925	5258	1098.9	1098.96	1099	-0.0373862	9E-05
	598.9241	68610	598.9	598.962	599	-0.0376862	0.0003
	498.9303	7.3E+07	498.9	498.962	499	-0.0378662	0.00018
	698.9174	8553	698.9	698.962	699	-0.0380062	0.00014
	348.9396	5939000	348.9	348.962	349	-0.0381362	0.00013
	298.9426	5786000	298.9	298.962	299	-0.0383262	0.00019
	448.933	3740000	448.9	448.962	449	-0.0383562	3E-05
	248.9455	2363000	248.9	248.961	249	-0.0386163	0.00026
	1298.8785	6784	1298.9	1298.96	1299	-0.0386263	1E-05
	398.9359	2.8E+07	398.9	398.961	399	-0.0386463	2E-05
	548.9257	84240	548.9	548.961	549	-0.0392763	0.00063
	198.9472	7236	198.9	198.96	199	-0.0401064	0.00083
	1148.8701	4937	1148.9	1148.94	1149	-0.0565974	0.01649
	148.925	3427	148.9	148.935	149	-0.065498	0.0089
	998.867	12390	998.9	998.931	999	-0.0692682	0.00377
	948.863	6172	948.9	948.924	949	-0.0764587	0.00719
	198.9086	5367	198.9	198.921	199	-0.0787088	0.00225
	798.8689	5327	798.9	798.92	799	-0.0801289	0.00142
	248.9018	6439	248.9	248.918	249	-0.0823191	0.00219
	348.8844	10330	348.9	348.907	349	-0.0933398	0.01102
	298.8875	11270	298.9	298.907	299	-0.0934298	9E-05
	648.8506	3371	648.9	648.892	649	-0.1080007	0.01457
	548.8566	3156	548.9	548.892	549	-0.1083807	0.00038
	448.8623	8694	448.9	448.891	449	-0.1090608	0.00068
	398.8645	31780	398.9	398.89	399	-0.1100508	0.00099
	148.8686	3908	148.9	148.878	149	-0.1219016	0.01185
	248.8603	4198	248.9	248.876	249	-0.1238217	0.00192
	198.8575	4986	198.9	198.87	199	-0.1298121	0.00599

Figure 7: *KMD Plot of PFAS in AFFF Product Example*

V - Results

Suspect Identification

AFFF compositions have evolved over time. The results of suspect identification show the change in legacy AFFF commercial products. The history of AFFF is based initially on long-chained PFAS, such as PFOS/PFOA (≥ 8 perfluorinated carbons) (Ateia et al., 2019; Duachy et al., 2017; Houtz et al., 2013). With additional regulations (in the US local or state regulations, but not federal), companies switched to shorter-chained PFAS, such as GenX, ADONA, and F53B (Ateia et al., 2019; Duachy et al., 2017; Houtz et al., 2013). The shorter-chain replacement PFAS could explain the change of prominent PFAS found in the environment to PFBS, a short-chain PFAS (Ateia et al., 2019; Duachy et al., 2017; Houtz et al., 2013). The previously dominant PFOS is being replaced by PFBS (Earnshaw et al., 2014). PFBS exposure has been shown to interfere with the female reproductive system, pregnancy, and kidney functions, which are similar to the adverse health effects of PFOS (USDHHS, 2017).

Table 2

Suspect Identification Results of Forty New PFAS Classes in Six AFFF Products

	PFAS classes (*n* = 30) present in six AFFF samples (A–F) available in PI Xiao's laboratory																													
AFFF	1	2	3	4	5	8	9	10	11	12	13	14	15	16	17	19	21	23	24	25	26	28	29	31	32	33	34	35	37	40
A		X	X	X	X		X	X	X		X				X	X		X				X	X	X			X			
B		X		X	X		X		X		X													X	X		X			
C	X	X	X	X	X	X	X	X	X	X	X		X	X			X	X		X		X		X	X	X	X	X	X	
D		X	X	X	X	X	X	X	X		X	X	X		X	X	X	X	X	X				X	X	X	X	X	X	
E		X	X				X		X													X	X							
F		X	X								X	X	X	X	X					X	X	X					X			X

Anionic, zwitterionic, and cationic PFAS classes (Barzen-Hanson et al. , ***Environmental Science & Technology***, 51, 2047-2057, 2017) are marked in blue, red, and green, respectively.

The results summarized in Table 5 (see APPENDIX A for complete data) show how AFFF commercial products have generally remained the same except for three years with

noticeable differences, namely B (1989), E (1997), and F (1998). Only 30 of the 40 classes were discovered in Barzen-Hanson et al. (2017b).

Combining the results with the previous study by Barzen-Hanson et al. (2017b), the composition of AFFF through the year is shown in Table 6.

Table 3

Forty New Classes Identified in AFFF Products from 1979 to 2001

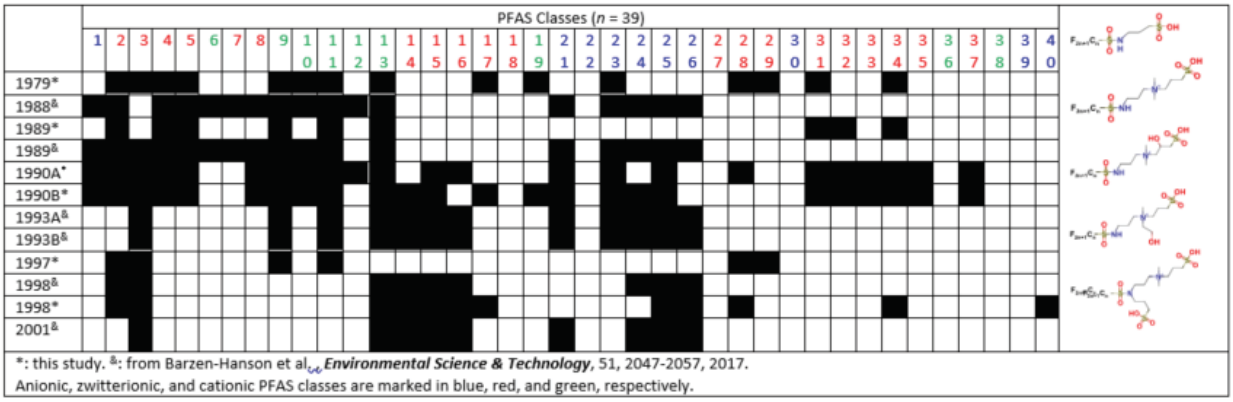

As noted in Place and Field (2012), at least seven different companies have produced AFFF commercially from 1976 to the present. In these different companies, a few different PFAS were unique to the particular manufacturing company (Place & Field, 2012). Accordingly, AFFF compositions could change between various manufacturers, and changes in chemical compositions could lead to even more new and unidentified PFAS in AFFF. Therefore, continuing with the current USEPA targeted methods is inadequate to adapt to the changing AFFF commercial industry, as the newer PFAS cannot be detected. Therefore, the need for NTA is clear.

However, basing identification solely on accurate mass has a low confidence level with respect to true chemical identification (Hollender et al., 2019; Schymanski et al., 2014). Additional data need to be analyzed to validate such chemical identification. Suspect

identification can be used as a screening tool, leading to identification at a higher confidence level (Ruan & Jiang, 2017).

Fragmentation Identification

Fragment identification, notably parent ion search, could further validate the identified new PFAS in AFFF (Xiao et al., 2017). However, in the current research, achieving this has proven challenging, as the fragment ions that were expected to be found were not found. Further, other studies have found new PFAS by different fragment identification methods; however, again, in the current study, the parent ion search did not identify the same PFAS (Barzen-Hanson et al., 2017; Place & Field, 2012). Comparing results with the CFM-ID database produced similar non-identification. Non-identification of some of the 40 classes of PFAS occurred in many of the AFFF samples that could be ascribed probably to a low concentration of new PFAS (Barzen-Hanson et al., 2017b; Ruan & Jiang, 2017). Because of the lack of PFAS identification in the negative mode, fragmentation identification was not included.

In other studies analyzing other commercial AFFF or PFAS products, the AFFF in these studies were probably produced or manufactured by a slightly different process, although still considered the same product by the manufacturer. Further, these are legacy formulas manufactured several years ago and subjected to degradation over time.

Kendrick Mass Defect

As KMD analysis was accomplished only in the negative mode scan, only the negative mode PFAS ions were identified. Supporting data can be found in APPENDIX B. Only 21 PFAS classes could be detected in the negative mode.

Table 4

KMD Analysis of New forty Classes of PFAS in Six AFFF Products in Negative Mode

AFFF	PFAS classes (n =21) present in six AFFF samples (A-F) in Negative Mode																							
	1	2	3	5	6	7	16	20	21	22	23	24	25	26	27	29	30	32	36	39	40	PR-3[a]	Class S[b]	Class R[b]	Class 3B[c]
A (5_79)											X											X			
B (1_89)																									
C (4_90)									X		X											X			
D (6_90)											X											X			
E (4_97)																									
F (3_98)											X	X										X	X	X	X

[a] - listed at previously identified in Barzen-Hanson et al, 2017; [b] - D'Agostino and Mabury, 2014; [c] - Place and Field, 2012

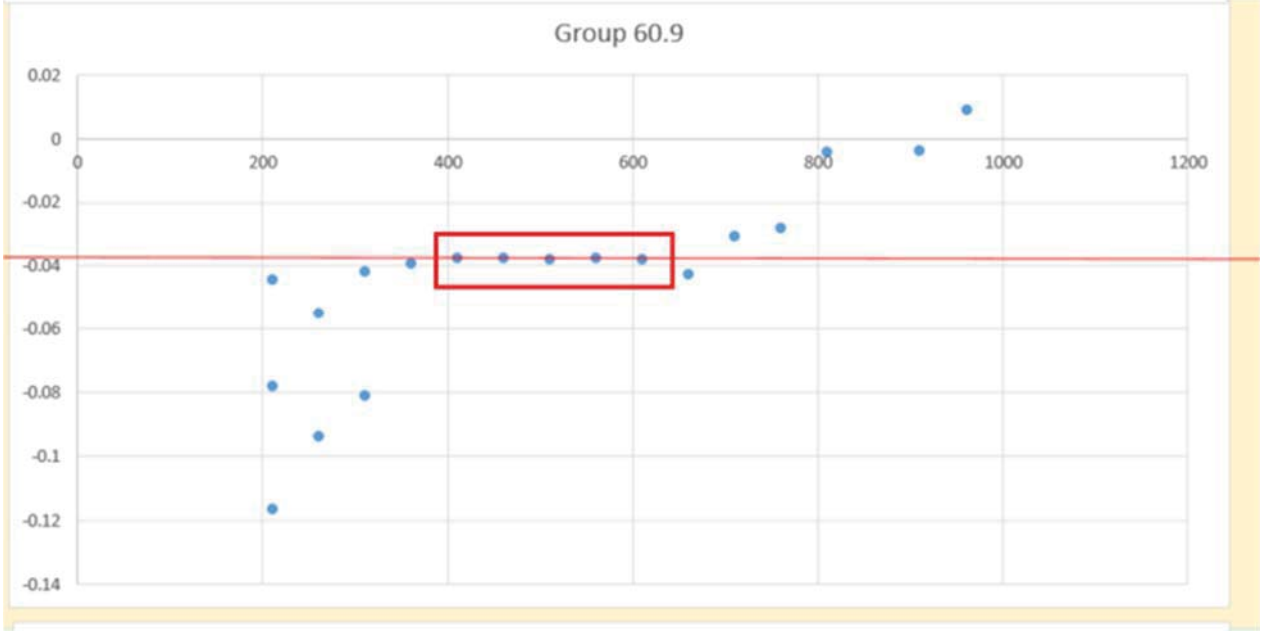

Figure 8: *KMD Identification of Class 23 in a Legacy AFFF*

***Figure 9**: KMD Identification of Class 21 in a Legacy AFFF*

Employing the KMD method, far fewer PFAS classes were identified than the suspect identification method (see Table 7). The suspect identification results detected 30 of 40 classes in the combined results of all six AFFF commercial products but, in the KMD, only three of the 21 negative mode classes were identified. The Barzen-Hanson et al. (2017b) PFAS classes identified in the samples by the KMD method are 21, 23, and 24. In class 21, one graph had two KMD identification lines (shown in Figure 9). As the KMDs are so close, roughly 0.01 *m/z* difference in KMD, the second line is probably simply an isotope of PFAS in class 21. None of the Barzen-Hanson et al. (2017b) PFAS classes were identified in the 1989 or 1997 AFFF samples.

Such non-identification demonstrates the effect of the zwitterionic and cationic nature of PFAS ions that do not show up on a negative mode scan. Of the 40 classes, 9 classes could be

identified only in the positive mode, and 20 could be identified in either positive or negative mode (Barzen-Hanson et al., 2017b). Additional classes could have been identified if the positive mode were analyzed. The current PFAS identification standards only run in the negative ionization mode (ASTM, 2017; USAEPA, 2019). Another possibility for non-identification is the difference between each KMD value of less than 0.001 *m/z* used in the current study, which could be more limiting than those used in the study by Barzen-Hanson et al. (2017b). Such a limit could lead to a lesser amount of PFAS being identified. Barzen-Hanson et al. (2017b) used software to accomplish the KMD analysis. In the current study, a manual review was conducted of each KMD plot; however, the software algorithms could have additional parameters that are not feasible in a manual review.

Some KMD *m/z* values noted the repeating CF_2, such as seen in Figure 10, but these were not *m/z* values identified by Barzen-Hanson et al. (2017b). Using Equation 4, the errors calculated between these results and the theoretical *m/z* values of the Barzen-Hanson et al. (2017b) PFAS classes were too great for identification. In some instances, the difference was several thousand parts per million. Beyond the 40 classes of Barzen-Hanson et al. (2017b), the KMD results were compared with other PFAS elucidation studies, and additional PFAS were identified**.**

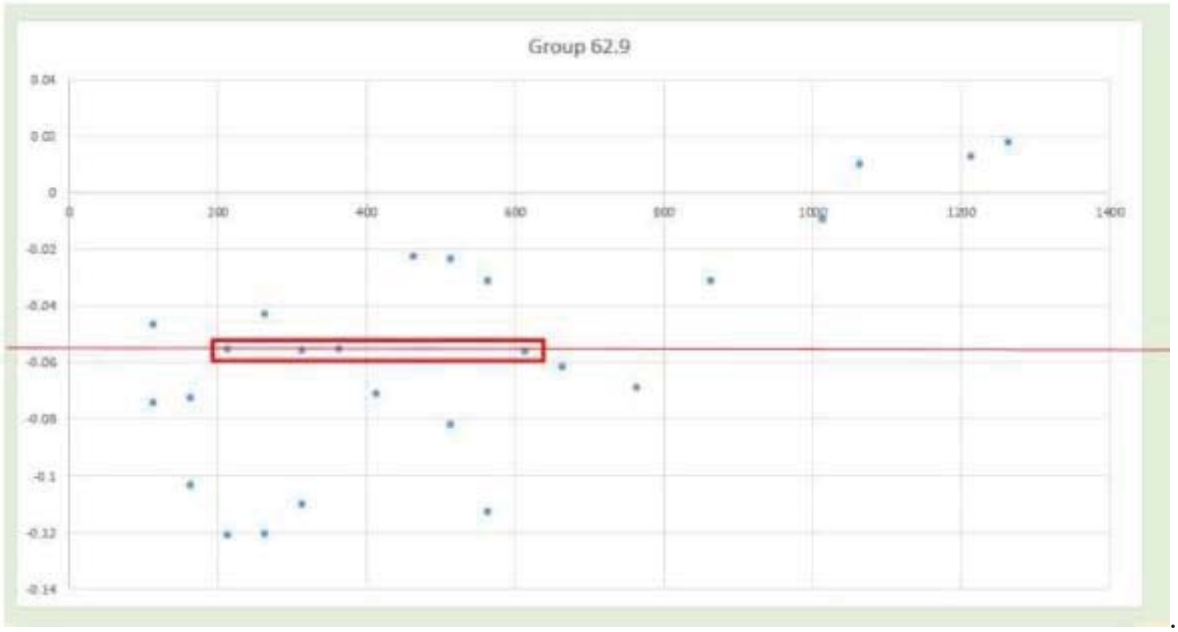

Figure 10: *KMD Identification of Other PFAS in a Legacy AFFF*

Many of the commonly identified PFAS were identified in all the samples. The PR-3 structure was identified for the 1979, 1990, and 1998 AFFF samples. PR-3 is one of 17 previously discovered PFAS classes found in AFFF commercial products and AFFF-impacted groundwater before the 40 classes discovered by Barzen-Hanson et al. (2017b). For the 1998 sample, Class S and Class R were identified from D'Agostino and Mabury (2014) and Class 3B from Place and Field (2012). These three classes have the same *m/z* value but have different retention times and are, therefore, assumed separate, distinct structures. A PFAS commonly found in aircraft hydraulic fluid, a non-AFFF function, was also identified. The cyclohexane sulfonate class from De Silva et al. (2011) was identified in all the samples, except the 1979 and 1989 samples. This current study only identified a few PFAS already identified by other PFAS AFFF elucidation studies. Similar to KMD identification of the forty classes of Barzen-Hanson et al. (2017b), the differences in KMD application/parameters and chemical degradation could explain the inability to identify PFAS in the six AFFF samples.

Although only a few of the 40 classes previously identified by Barzen-Hanson et al. (2017b) were found in the current research using the KMD method (Figure 11), employing the non-targeted approach of the full mass spectrum scan and KMD identification allowed additional identification of other PFAS from other PFAS elucidation studies. The suspect identification results were also compared with the *m/z* values of other studies and additional PFAS were identified, similar to the KMD results. As there is no standard for identifying the majority of the new PFAS, employing full-scan data or a non-targeted approach allows broader identification of PFAS, taking advantage of the knowledge obtained from several previous research efforts and studies. That NTA could utilize current and future studies or standards is particularly significant, as some of these other PFAS are precursors to currently regulated PFAS, such as PFOS and PFOA.

In summary, all three methods employed in the current study were labor-intensive, as listed in the comparison table (Table 8), but only some of the new PFAS were identified, as shown in Figure 11. Based on the HRMS confidence levels for identification and reviewing the procedures of some of the elucidation studies, suspect identification is considered only a screening step and not sufficient to positively identify the new PFAS (Hollender et al., 2019; Schymanski et al., 2014). Fragment identification is also considered a screening tool but, if used along with other methods, could lead to identification; however, for these new PFAS, the resulting fragments from an MS scan are unknown (Barzen-Hanson et al., 2017b; Ruan & Jiang, 2017). Without historical and validated MS scans of the new PFAS, accomplishing fragmentation identification (Hollender et al., 2019; Sobus, 2020; Sobus et al., 2018; USAEPA, 2020) may not be possible, particularly considering the low quantities of new PFAS present in the samples (Barzen-Hanson et al., 2017b; Ruan & Jiang, 2017). The KMD method appears to be the standard for identification; however,

only a small number of new PFAS were identified in the current study. Owing to the labor-intensive demands of the KMD method, computer software was employed in some studies instead of manual or technician review of each data point. During a review of three identification software applications employed to identify the extensive list of PFAS, the different applications identified a few different PFAS but, overall, shared identification of the same PFAS (Nason et al., 2020).

Table 5

Comparison of Identification Methods

Identification Method	Positives (+)	Negatives (-)	Labor/Time Needed
Suspect Identification	Use a screening tool for further analysis	Low confidence	** 2–3 months per six samples
Fragment Identification	Use a screening tool for further analysis	-Limited to available established MS databases -Lead to non-identification owing to low levels	**** 3–6 months per three samples in negative mode
KMD	Higher confidence	-Computer programs have varied results -Lead to false identification	***** 6+ months (years) per three samples in negative mode Most labor-intensive

Figure 11: *KMD and Suspect Identification Results*

The results could probably vary because of the different coding and parameters or system sensitives. During an educational discussion on Mar 15, 2021, Dr. Feng Xiao indicated that, in another research effort using one chemical software application, PFAS identification analysis of an AFFF sample, known to contain PFOS or PFOA, could not detect PFOS or PFOA. In another study, manual identification was the preferred mode of analysis (Baduel et al., 2017). More research into standardizing the identification of other PFAS is still required.

AFFF Soil Results

At all three investigated sites, PFAS were detected, but only in extremely low amounts owing to these low amounts; the other/new PFAS could not be identified. Despite the high resolution and accuracy of UPLC and QToF-MS analysis of PFAS, environmental samples have high background noise and significant interference on the chromatograms, leading to ineffective analysis (Ateia et al., 2019; Cerveny et al., 2016; Lin et al., 2016; Lorenzo et al., 2018; Zacs & Bartkevics, 2015). At the sample sites, one year or more had passed since the last AFFF event. Precipitation (snow and rain) could probably have flushed the soil and moved the PFAS to the groundwater (Anderson et al., 2019). The three locations receive several inches of precipitation

annually, leading to a lower level of PFAS in the soil samples. These locations are in areas with a cold climate and the transport of PFAS would vary depending on the degree of infiltration. This situation is similar to that in a study in Norway, where high infiltration showed more PFAS movement and low infiltration showed no PFAS movement (Høisæter et al., 2019). One of the locations, Site G, has a high water table, which could contribute to lower soil PFAS levels. PFAS movement in the soil is affected by the saturation level of the soil (Brusseau et al., 2019; Lyu & Brusseau, 2020; Silva et al., 2019).

In the current study, some samples could not be processed because of the potential presence of other chemicals that could damage the analytical equipment. To obtain accurate results and adjust to the different chemical properties, LC and MS equipment must be calibrated explicitly for the analyte of interest (Watson & Sparkman, 2007, pp. 537–538; Harris & Charles, 2016, p. 586). Other contaminants could be more acidic or more viscous than PFAS, such as hydrocarbons, which could damage the testing equipment. The field and laboratory observations in the current study indicated that the samples varied significantly in color, consistency/texture, and form (see Figure 12).

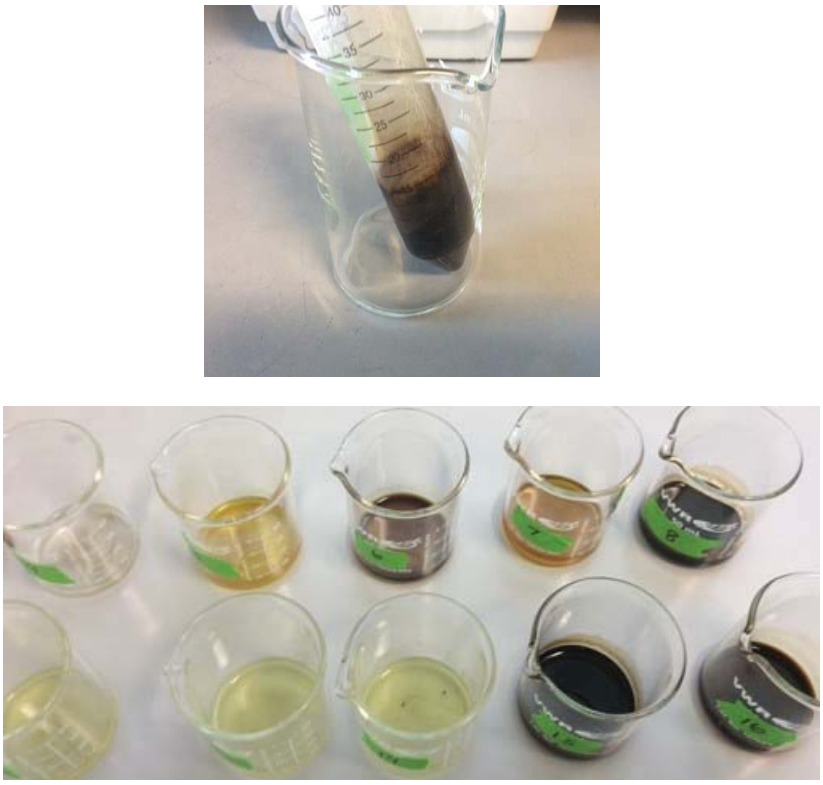

Figure 12: *Extractions from Soil Samples for PFAS Identification*

From 37 soil sample extractions, only 16 were analyzed. A few samples from each of the three investigated sites were processed, showing the presence of PFAS in the soil at extremely low levels (see Table 9). The specific samples that were processed are highlighted in yellow in Table 9.

AFFF is used to control fuel fires and, because the deployment of AFFF at a site includes other contaminants, these other contaminants were present in each soil sample. Testing other contaminants is outside the scope of the current study; however, this finding reveals the need for pre-processing of soil samples before identifying PFAS. Brusseau (2018) developed a model to account for the effects of air, soil, water, and other contaminants (fuel) on PFAS concentration. Brusseau et al. (2019) experimented with another contaminant (non-PFAS) concerning PFAS movement and retardation in soil. The effect of the other contaminant was applied theoretically

to PFAS movement, but the other contaminant was not mixed with or did not interact with the PFAS. The ASTM D7968 -17a standard (2019) focuses only on the extraction of targeted PFAS from the soil samples and does not address other possible contaminants. Therefore, not considering any other contaminants could affect the accuracy of the results. Other contaminants could retain PFAS on the site (Brusseau, 2018; Brusseau et al., 2019). A study by Bugsel and Zwiener (2020) on PFAS-contaminated soil identified more than 61 PFAS, using a non-targeted approach with methods similar to those employed in the current study. However, the PFAS contamination source identified in Bugsel and Zwiener (2020) is compost mixed with paper sludge that contains PFAS and is not AFFF from firefighting events. The study by Bugsel and Zwiener (2020) was not hampered by the same concerns as those of the current study. No special processing is described in Bugsel and Zwiener (2020) to account for other possible interfering chemicals. The potential presence of other contaminants was probably not a concern in previous soil sample testing and, therefore, it was not dealt with. Without an official or standardized approach to deal with the other contaminants, it is unclear how such other contaminants should be considered in PFAS testing.

All the current study samples were processed at site G and were taken from both unsaturated and saturated soil zones. Even at low levels, the results appeared to show a greater concentration of PFOS (a long-chained PFAS) in the soils above the water table compared with the samples in the saturated zone. This finding supports the concept that longer-chained PFAS are less mobile than are shorter-chained PFAS, as demonstrated in Høisæter et al. (2019) and Weber et al. (2017).

Table 6

PFAS Results at Three AFFF Release Sites

Sample ID	Sample Name	Media	Sample Amount	Depth Extracted (in)	Comments	Summary Results (ug/l)
1	F1	Soil/Extraction	2 ml	0-5		Could not be analyzed
2	F2	Soil/Extraction	2 ml	10-15	Sediment at bottom of centrifuge tube; require addition methanol and evaporation	Could not be analyzed
2a	F2	Soil/Extraction	0.5 ml	10-15	2nd part - Sediment at bottom of centrifuge tube; require addition methanol and evaporation	Could not be analyzed
3	F3	Soil/Extraction	2 ml	15-20	Sediment at bottom of centrifuge tube; require addition methanol and evaporation	1.263 (PFBA); 0.325 (PFHpA); 69.7444 (PFOS)
3a	F3	Soil/Extraction	2 ml	15-20	2nd part - Sediment at bottom of centrifuge tube; require addition methanol and evaporation	5.66 (PFBA); 1.471 (PFHpA); 0.219 (PFOA) 6.241 (PFOS)
4	F4	Soil/Extraction	2 ml	20-25		Could not be analyzed
5	F5	Soil/Extraction	2 ml	25-30	Sediment at bottom of centrifuge tube; require addition methanol and evaporation	Could not be analyzed
5a	F5	Soil/Extraction	2 ml	25-30	2nd part - Sediment at bottom of centrifuge tube; require addition methanol and evaporation	Could not be analyzed
6	F6	Soil/Extraction	2 ml	30-35		Could not be analyzed
7	F7	Soil/Extraction	2 ml	35-40	Sediment at bottom of centrifuge tube; require addition methanol and evaporation	7.688 (PFBA); 0.407 (PFOA); 0.0157 (PFDA); 0.603 (PFUnDA); 1.823 (PFOS)
7a	F7	Soil/Extraction	0.5 ml	35-40	2nd part - Sediment at bottom of centrifuge tube; require addition methanol and evaporation	6.882 (PFBA); 0.745 (PFHpA); 0.445 (PFUnDA); 0.291 (PFOS)
9	G1	Soil/Extraction	2 ml	0-5		5.29 (PFBA); 1.994 (PFPeA); 1.132 (PFUnDA); 3.366 (PFBS)
10	G2	Soil/Extraction	2 ml	10-15	Congealed liquid at bottom of centrifuge; require addition methanol and evaporation	6.357 (PFBA); 0.266 (PFHpA); 0.075 (PFNA)
10a	G2	Soil/Extraction	0.5 ml	10-15	2nd part - Congealed liquid at bottom of centrifuge; require addition methanol and evaporation	0.166 (PFHpA); 0.329 (PFHpA); 0.695 (PFDA); 0.683 (PFUnDA); 35.326 (PFOS)
11	G3	Soil/Extraction	2 ml	15-20	Soil at water table; Congealed liquid at bottom of centrifuge; require addition methanol and evaporation	3.10 (PFBA); 0.162 (PFOA); 0.297 (PFNA); 0.269 (PFUnDA); 1.063 (PFHxS); 0.546 (PFOS)
11a	G3	Soil/Extraction	0.5 ml	15-20	2nd part - Soil at water table; Congealed liquid at bottom of centrifuge require addition methanol and evaporation	0.206 (PFUnDA); 2.101 (PFHxS)
12	G4	Soil/Extraction	2 ml	20-25	Below water table; Congealed liquid at bottom of centrifuge; require addition methanol and evaporation	2.956 (PFBA); 0.419 (PFHpA); 0.93 (PFBS); 2.591 (PFOS)
12a	G4	Soil/Extraction	0.5 ml	20-25	2nd part - Below water table; Congealed liquid at bottom of centrifuge require addition methanol and evaporation	3.429 (PFBA); 0.267 (PFNA); 0.14 (PFDA); 0.166 (PFUnDA)
13	G5	Soil/Extraction	2 ml	25-30	Below water table; Congealed liquid at bottom of centrifuge; require addition methanol and evaporation	2.779 (PFBA); 0.841 (PFPeA); 0.487 (PFHpA); 0.469 (PFNA); 0.082 (PFNA)
13a	G5	Soil/Extraction	0.5 ml	25-30	2nd part - Below water table; Congealed liquid at bottom of centrifuge; require addition methanol and evaporation	0.533 (PFHpA); 1.544 (PFOS)
14	G6	Soil/Extraction	2 ml	30-35	Below water table	3.006 (PFBA); 0.348 (PFOA); 1.022 (PFOS)
16	E1	Soil/Extraction	2 ml	0-5		Could not be analyzed
17	E2	Soil/Extraction	2 ml	10-15		Could not be analyzed
18	E3	Soil/Extraction	2 ml	15-20		Could not be analyzed
19	E4	Soil/Extraction	2 ml	20-25		Could not be analyzed
20	E5	Soil/Extraction	2 ml	25-30	Sediment at bottom of centrifuge tube; require addition methanol and evaporation	Could not be analyzed
20a	E5	Soil/Extraction	0.5 ml	25-30	2nd part - Sediment at bottom of centrifuge tube; require addition methanol and evaporation	Could not be analyzed
21	E6	Soil/Extraction	2 ml	30-35		3.579 (PFBA); 1.158 (PFPeA); 2.078 (PFOS
22	E7	Soil/Extraction	2 ml	35-40		2.915 (PFBA); 0.216 (PFOA); 0.152 (PFNA); 0.423 (PFBS); 0.851 (PFOS)

VI - Discussion

Although the study results were limited, areas requiring improvements were identified, and some of these improvements are already being developed. NTA is considered to produce identification at a lower confidence level than targeted analysis but, with further study, the knowledge gaps could be filled. Therefore, NTA could benefit environmental regulation and reduce PFAS risks.

Benefits of Non-Targeted Analysis

The benefits of NTA have been recognized nationally and worldwide, and non-targeted identification is required to adapt to the ever-evolving chemical industry. According to the USEPA and other international organizations, such an approach is necessary to regulate, understand, and track the risk and behaviors of the new and unknown chemicals being released into the environment (American Chemistry Society [ACS], 2020; Hollender et al., 2019; Sobus et al., 2018; Sobus, 2020; USEPA, 2018).

Access to past MS scans during this study and having other University of North Dakota associates review, process, and validate the results showed the benefit of access to full scans to future efforts in PFAS management. For instance, past data could be reanalyzed in different ways without the need to conduct resampling. Retaining the full MS scan could facilitate identifying those PFAS for which no standard of identification currently exists once such standards have been developed and established. Without the full scan, reanalysis for previously undetected PFAS would not be possible. Even if standards were not established, access to complete scan data could help future standards research and development.

Numerous Approaches to Non-Target Identification/Identification Level of Confidence

Without established standards/reference standards for non-targeted identification of each different PFAS, it is difficult to achieve the highest confidence level of identification. However, building on the PFAS structure elucidation research from academia could enhance the confidence level, thereby bringing the identification of new PFAS closer to reality. Although this type of identification is currently considered to have a lower confidence rating, the new PFAS could be traced and tracked, mainly when a full-scan mass spectrum is obtained. The ability to trace and track could help in discovering the pathway of risks and in establishing and implementing precautions (ACS, 2020; Hollender et al., 2019).

As shown in Table 4, there are many approaches to non-target identification. The proprietary nature of the AFFF commercial industry keeps the evolution of AFFF formulations confidential and, to keep pace with the changes, untargeted identification is required. However, not all untargeted identification is the same. The USEPA Non-Targeted Analysis Collaboration Trial (ENTACT), a multi-year study, has three phases, which are (1) reviewing the accuracy of using a blind analysis—known chemicals are sent to each laboratory and the accuracy of the results are recorded; (2) unblinded analysis to help improve each laboratory NTA approach; and (3) analysis of individual chemical substances to create a database that would enable other laboratories, or future chemical analyses, to compare results with this database, thereby improving identification (USAEPA, 2020; Sobus, 2020; Sobus et al., 2018). Each laboratory has different equipment and processes for NTA; however, the process is the most crucial aspect of NTA results' accuracy. During the 2020 American Chemistry Society (ACS) Fall Meeting, TOXI Broadcast, on August 19, 2020, USEPA Scientist Jon Sobus, co-leader of ENTACT, stated that the effectiveness of NTA did not depend that much on the brand or type of mass spectrometer

employed but rather the procedure involved in the identification processes. During this same broadcast, a panel of experts disputed QToF-MS results' accuracy due to the amount of background noise in the data, which could lead to misidentification.

Further, according to these experts, an ion trap mass analyzer (Orbitrap) showed greater precision and produced reliable data because of its much higher resolving power than QToF. However, the ENTACT study continues, and the results are not available at this time. The ENTACT efforts help improve the accuracy and reliability of NTA, considering that a consolidated database is vital to the effectiveness of NTA (Hollender et al., 2019).

Ultra-Short/Short PFAS Identification

PFAS containing only two to three CF_2 chains (C_2 or C_3) are considered ultra-short/short PFAS. Because of the short-chain, these PFAS elute early and are not clearly visible in MS scans (Ateia et al., 2019). Ultra-performance convergence chromatography has been evaluated to resolve the detection issue in HRMS. For instance, Yeung et al. (2017) have identified short-chained PFAS, but with limited ability to quantify the quantity of short-chain PFAS in the sample compared with typical HPLC/QToF results. In another study focused on ultra-short PFAS, no concerns were detected in QToF-MS identifying and quantifying the C_2–C_3 PFAS. However, as total organic fluoride analysis was not included, possibly, not all short-chain PFAS were identified (Barzen-Hanson & Field, 2015). For future NTA, ultra-short/short-chain PFAS need to be considered because of the increasing presence of C_2–C_3 PFAS in the environment, with probably similar health risks (Ateia et al., 2019; Barzen-Hanson & Field, 2015; Yeung et al., 2017).

PFAS Fingerprinting

Once the PFAS chemical structures were identified using NTA, the new PFAS sources and behaviors could be explored and defined (Plumb, 2004). USEPA has researched and developed "chemical fingerprinting" for PFAS to show PFAS characteristics and origins (Lougee, 2020). The challenges in chemical fingerprinting are that the selected sample preparation techniques and analytical platforms, such as NTA, when combined, could lead to deciphering the complete chemical composition of a sample (Lougee, 2020). The code style used in the USEPA study is the publicly available Chemical Subgraph and Reactions Markup Language (CSRML) (Lougee, 2020; Yang et al., 2015). USEPA has already identified more than 160 PFAS fingerprints using CSRML (Lougee, 2020).

Fingerprinting is a chemical code to the unique structure in a specific PFAS that could facilitate PFAS to be analyzed in ways differing from those used previously (Plumb, 2004). Chemical fingerprinting can show how the chemical, PFAS, was likely manufactured and can note the chemical traits based on the assigned code expected for a specific structure (Benotti et al., 2020).

For example, PFAS are purposely human-made and created through electrochemical fluorination (ECF) or telemorization. The branched PFAS are formed in ECF, whereas linear PFAS result from telemorization (Benotti, 2020; Benotti et al., 2020). ECF is used in the metal plating process and the production process of AFFF by the 3M Company, whereas other AFFF manufacturing companies use telemorization. Knowing how PFAS are made could give insight into the source of the PFAS (Benotti, 2020; Benotti et al., 2020). When a source is known, it could be analyzed and remediated, and further releases could be prevented.

VII - Conclusion/Areas for Potential Research

The expansion of PFAS identification beyond the current USEPA methods has proven to be challenging. The goal of the current study was to demonstrate the identification of 40 new classes discovered by Barzen-Hanson et al. (2017b) in legacy AFFF commercial products and known AFFF release sites. However, unforeseen complications arose. The efforts in the current study indicated that a standardized NTA approach and additional guidance to multiple chemical releases at AFFF release sites are indispensable. Further advancements in NTA could help track currently unknown precursor PFAS that transform or degrade, contributing to the greater prevalence of targeted (regulated) PFAS, thereby providing insight into the unexplainable increase in PFAS concentrations. Besides, NTA could facilitate tracking and studying of other unknown PFAS. With the additional knowledge obtained through ENTACT and USEPA COMPTOX, establishing an NTA standard is possible. Below are some potential areas for future research.

- Using PFAS elucidation research to broaden the identification of PFAS could provide a greater understanding of PFAS behaviors, such as degradation and the associated health risks and remediation controls
- Potential aspects for further research include identifying PFAS concentrations in the presence of other contaminants/chemicals and software development to conduct suspect identification (exact mass), fragmentation, KMD, and other PFAS identification methods, with the aim being to expedite the processing of samples. All three methods used in this study were labor intensive but, with improved software, NTA could be completed in days rather than months. Timely results are preferred in the investigation of chemical releases.

- The impact of other contaminants on the concentration of PFAS in the environmental samples and the appropriate pre-processing needed to prevent damage to analytical equipment and reflect the actual PFAS concentrations in environmental samples.
- The impact of precursor PFAS on the concentration of common PFAS or currently regulated PFAS to show the requirement for further remediation.
- Use NTA to identify new PFAS created through thermal processes such as fire, incineration, and thermal destruction/disposal methods
- Study the desorption of PFAS on paved surfaces like asphalt and concrete pavements and the potential of recontaminating environment
- Aging soil, i.e., the sequestering of contaminants deep within the micropores of soil particles, could remove the adverse effects of such contaminants from public water sources. Focusing research on PFAS to demonstrate naturally-aging PFAS impacted soil and whether or not desorption of the different PFAS is reduced.
- Formulating a model that accounts for the different PFAS and soil characteristics increases the versatility of the model and possibly the accuracy of detecting PFAS movement in the soil.

APPENDIX A - SUSPECT IDENTIFICATION RESULTS

Table A-1: Suspect Identification Results Listing

Class	+/-	Theoretical m/z	Spectrum Observed m/z	Retention Time (min)	MS Response of the highest peak	Spectrum Error (mDa)	Spectrum Error (ppm)	Yr	Chemical	Comments
PFBS	-	298.9424	298.9424	3.28	3.44E+05	0.00	0.00	1979	3M 5_79	Detected
PFHxS	-	398.9361	398.9368	4.29	1.33E+06	0.70	1.75	1979	3M 5_79	Detected
PFHpS	-	448.9329	448.9331	4.63	3.16E+05	0.20	0.45	1979	3M 5_79	Detected
PFOS	-	498.9297	498.9300	4.93	2.91E+06	0.30	0.60	1979	3M 5_79	Detected
PFDS	-	598.9233	598.9210	5.33	1.16E+04	-2.30	-3.84	1979	3M 5_79	Detected
PFHxA	-	312.9723	312.9713	3.76	1.11E+04	-1.00	-3.20	1979	3M 5_79	Detected
PFHpA	-	362.9691	362.9682	4.24	3.02E+03	-0.90	-2.48	1979	3M 5_79	Detected
PFOA	-	412.9659	412.9657	4.59	2.23E+04	-0.20	-0.48	1979	3M 5_79	Detected
2	+	507.0665	507.0755	3.86	6.87E+03	9.00	17.75	1979	3M 5_79	Detected; Clear Peak
2	+	557.0633	557.0623	4.09	1.35E+03	-1.00	-1.80	1979	3M 5_79	Detected; Clear Peak
2	+	607.0601	607.0604	4.50	3.69E+04	0.30	0.49	1979	3M 5_79	Detected; Clear Peak
3	+	473.0646	473.0642	2.86	9.19E+03	-0.40	-0.85	1979	3M 5_79	Detected; Clear Peak
3	+	523.0614	523.0613	3.61	7.94E+04	-0.10	-0.19	1979	3M 5_79	Detected; Clear Peak
3	+	573.0582	573.0592	4.14	5.77E+04	1.00	1.75	1979	3M 5_79	Detected; Clear Peak
3	+	623.0550	623.0551	4.53	4.51E+05	0.10	0.16	1979	3M 5_79	Detected; Clear Peak
4	+	537.0770	537.0771	3.45	2.53E+04	0.10	0.19	1979	3M 5_79	Detected; Clear Peak
4	+	587.0738	587.0741	3.98	2.12E+04	0.30	0.51	1979	3M 5_79	Detected; Clear Peak
4	+	637.0706	637.0707	4.40	2.14E+05	0.10	0.16	1979	3M 5_79	Detected; Clear Peak
5	+	579.0734	579.0811	4.84	2.22E+04	7.70	13.30	1979	3M 5_79	Detected; Clear Peak
5	+	629.0702	629.0758	5.10	7.93E+04	5.60	8.90	1979	3M 5_79	Detected; Clear Peak
5	+	679.0670	679.0677	3.85	5.62E+02	0.70	1.03	1979	3M 5_79	Potential Detection with clear peak but still too much noise
5	+	729.0638	729.0597	4.24	6.98E+03	-4.10	-5.62	1979	3M 5_79	Detected; Clear Peak
9	+	423.1183	423.1186	3.12	2.84E+04	0.30	0.71	1979	3M 5_79	Potential Detection with clear peak but other close peaks
9	+	473.1151	473.1161	3.75	7.76E+04	1.00	2.11	1979	3M 5_79	Detected; Clear Peak
9	+	523.1190	523.1126	4.22	9.20E+04	-6.40	-12.23	1979	3M 5_79	Detected; Clear Peak
9	+	573.1087	573.1091	4.59	6.57E+05	0.40	0.70	1979	3M 5_79	Detected; Clear Peak
9	+	623.1055	623.1027	4.90	3.09E+03	-2.80	-4.49	1979	3M 5_79	Potential Detection with clear peak but other close peaks
9	+	673.1023	673.0974	5.14	6.93E+03	-4.90	-7.28	1979	3M 5_79	Detected; Clear Peak
10	+	445.0838	445.0847	4.03	6.84E+04	0.90	2.02	1979	3M 5_79	Detected; Clear Peak
10	+	495.0806	495.0811	4.47	5.05E+04	0.50	1.01	1979	3M 5_79	Detected; Clear Peak
10	+	545.0774	545.0778	4.82	4.79E+05	0.40	0.73	1979	3M 5_79	Detected; Clear Peak
11	+	329.0953	329.0951	2.43	9.85E+02	-0.20	-0.61	1979	3M 5_79	Potential Detection with clear peak but other close peaks
11	+	379.0921	379.0928	2.81	3.45E+04	0.70	1.85	1979	3M 5_79	Detected; Clear Peak
11	+	429.0889	429.0896	3.58	2.27E+05	0.70	1.63	1979	3M 5_79	Detected; Clear Peak
11	+	479.0857	479.0865	4.12	2.47E+05	0.80	1.67	1979	3M 5_79	Detected; Clear Peak
11	+	529.0825	529.0840	4.53	1.71E+06	1.50	2.84	1979	3M 5_79	Detected; Clear Peak
11	+	579.0793	579.0789	4.84	2.22E+04	-0.40	-0.69	1979	3M 5_79	Detected; Clear Peak
11	+	629.0761	629.0756	5.10	7.93E+04	-0.50	-0.79	1979	3M 5_79	Detected; Clear Peak
13	+	349.0815	349.0811	2.80	7.14E+03	-0.40	-1.15	1979	3M 5_79	Detected; Clear Peak
13	+	399.0783	399.0786	3.58	3.74E+04	0.30	0.75	1979	3M 5_79	Detected; Clear Peak
13	+	449.0751	449.0753	4.14	4.43E+04	0.20	0.45	1979	3M 5_79	Detected; Clear Peak
13	+	499.0719	499.0728	4.53	4.48E+05	0.90	1.80	1979	3M 5_79	Detected; Clear Peak
13	+	549.0688	549.0688	4.85	3.26E+03	0.00	0.00	1979	3M 5_79	Detected; Clear Peak
13	+	599.0656	599.0660	5.12	1.57E+04	0.40	0.67	1979	3M 5_79	Detected; Clear Peak
19	+	523.0719	523.0616	3.68	9.81E+03	-10.30	-19.69	1979	3M 5_79	Detected; Clear Peak
19	+	623.0660	623.0573	4.54	3.76E+05	-8.70	-13.96	1979	3M 5_79	Detected; Clear Peak
19	+	723.0592	723.0461	5.13	1.35E+04	-13.10	-18.12	1979	3M 5_79	Detected; Clear Peak

Yellow Highlight: Spectrometry and Chromatography graphs provided

Class	+/-	Theoretical m/z	Spectrum Observed m/z	Retention Time (min)	MS Response of the highest peak	Spectrum Error (mDa)	Spectrum Error (ppm)	Yr	Chemical	Comments
28	+	567.0876	567.0876	3.44	9.09E+04	0.00	0.00	1979	3M 5_79	Detected; Clear Peak
28	+	617.0844	617.0858	3.98	8.76E+04	1.40	2.27	1979	3M 5_79	Detected; Clear Peak
28	+	667.0812	667.0814	4.39	6.65E+05	0.20	0.30	1979	3M 5_79	Detected; Clear Peak
29	+	661.0600	661.0610	3.10	6.51E+04	1.00	1.51	1979	3M 5_79	Detected; Clear Peak
29	+	711.0569	711.0573	3.66	4.95E+04	0.40	0.56	1979	3M 5_79	Detected; Clear Peak
29	+	761.0537	761.0546	4.09	4.29E+05	0.90	1.18	1979	3M 5_79	Detected; Clear Peak
31	+	471.0826	471.0919	3.11	2.76E+02	9.30	19.74	1979	3M 5_79	Potential Detection with clear peak but other close peaks
31	+	521.0796	521.0880	3.72	9.21E+02	8.40	16.12	1979	3M 5_79	Detected; Clear Peak
31	+	571.0789	571.0684	4.20	8.72E+02	-10.50	-18.39	1979	3M 5_79	Potential Detection with clear peak but other close peaks
31	+	621.0757	621.0743	4.57	1.37E+04	-1.40	-2.25	1979	3M 5_79	Detected; Clear Peak
32	+	515.0751	515.0688	4.66	2.19E+04	-6.30	-12.23	1979	3M 5_79	Potential Detection with clear peak but other close peaks
32	+	565.0719	565.0611	6.00	1.71E+03	-10.80	-19.11	1979	3M 5_79	Potential Detection with clear peak but other close peaks
32	+	615.0687	615.0698	5.51	5.83E+04	1.10	1.79	1979	3M 5_79	Detected; Clear Peak
32	+	665.0655	665.0641	3.10	5.60E+02	-1.40	-2.11	1979	3M 5_79	Potential Detection with clear peak but still too much noise
33	+	531.0700	531.0731	4.78	5.32E+04	3.10	5.84	1979	3M 5_79	Detected; Clear Peak
33	+	631.0637	631.0748	5.11	2.38E+03	11.10	17.59	1979	3M 5_79	Potential Detection with clear peak but still too much noise
34	+	451.0768	451.0750	4.14	9.63E+02	-1.80	-3.99	1979	3M 5_79	Potential Detection with clear peak but still too much noise
34	+	501.0736	501.0697	4.53	1.70E+04	-3.90	-7.78	1979	3M 5_79	Detected; Clear Peak
34	+	551.0736	551.0712	3.79	9.19E+02	-2.40	-4.36	1979	3M 5_79	Potential Detection with clear peak but still too much noise
34	+	601.0730	601.0635	5.51	3.90E+04	-9.50	-15.81	1979	3M 5_79	Detected; Clear Peak
37	+	479.0493	479.0533	3.54	1.12E+03	4.00	8.35	1979	3M 5_79	Detected; Clear Peak
3M	+	385.0632	385.0630	4.30	6.26E+04	-0.20	-0.52	1979	3M 5_79	Detected; Clear Peak
3M	+	457.0844	457.0817	3.77	8.93E+02	-2.70	-5.91	1979	3M 5_79	Potential Detection with clear peak but still too much noise
3M	+	485.0568	485.0570	4.68	4.72E+05	0.20	0.41	1979	3M 5_79	Detected; Clear Peak
3M	+	507.0812	507.0768	3.85	9.47E+03	-4.40	-8.68	1979	3M 5_79	Detected; Clear Peak
3M	+	557.0780	557.0739	NC	5.40E+02	-4.10	-7.36	1979	3M 5_79	Potential Detection with clear peak but still too much noise
Buckeye	+	532.0769	532.0856	4.53	6.90E+03	8.70	16.35	1979	3M 5_79	Potential Detection with clear peak but still too much noise
Chemguard	+	581.1144	581.1205	NC	3.02E+02	6.10	10.50	1979	3M 5_79	Potential Detection with clear peak but still too much noise
Fireade	+	613.0818	613.0784	5.99	3.61E+02	-3.40	-5.55	1979	3M 5_79	Potential Detection with clear peak but still too much noise
Fireade	+	671.0872	671.0901	3.85	2.03E+03	2.90	4.32	1979	3M 5_79	Potential Detection with clear peak but other close peaks
Fireade	+	871.0745	871.0657	5.51	1.90E+04	-8.80	-10.10	1979	3M 5_79	Potential Detection with clear peak but other close peaks
National Foam	+	613.0818	613.0890	5.99	3.61E+02	7.20	11.74	1979	3M 5_79	Potential Detection with clear peak but still too much noise
National Foam	+	671.0872	671.0901	3.85	2.03E+03	2.90	4.32	1979	3M 5_79	Potential Detection with clear peak but other close peaks
National Foam	+	871.0745	871.0657	5.51	1.90E+04	-8.80	-10.10	1979	3M 5_79	Detected; Clear Peak

Class	+/-	Theoretical m/z	Spectrum Observed m/z	Retention Time (min)	MS Response of the highest peak	Spectrum Error (mDa)	Spectrum Error (ppm)	Yr	Chemical	Comments
1	-	369.9648	369.9712	4.55	8.04E+02	6.40	17.30	1979	3M 5_79	Detected; Clear Peak
21	-	356.9119	356.9161	3.29	1.90E+02	4.20	11.77	1979	3M 5_79	Potential Detection with clear peak but still too much noise
21	-	406.9087	406.9009	4.24	4.03E+02	-7.80	-19.17	1979	3M 5_79	Potential Detection with clear peak but still too much noise
21	-	456.9055	456.9062	4.58	2.07E+02	0.70	1.53	1979	3M 5_79	Potential Detection with clear peak but still too much noise
21	-	506.9023	506.8951	4.87	2.81E+02	-7.20	-14.20	1979	3M 5_79	Potential Detection with clear peak but still too much noise
21	-	556.8991	556.8995	5.12	8.60E+02	0.40	0.72	1979	3M 5_79	Potential Detection with clear peak but still too much noise
21	-	656.8927	656.8801	5.50	1.84E+03	-12.60	-19.18	1979	3M 5_79	Potential Detection with clear peak but still too much noise
23	-	360.9398	360.9371	3.91	1.23E+03	-2.70	-7.48	1979	3M 5_79	Potential Detection with clear peak but other dose peaks
23	-	410.9366	410.9366	4.27	1.72E+03	0.00	0.00	1979	3M 5_79	Detected; Clear Peak
23	-	460.9334	460.9334	4.58	6.10E+04	0.00	0.00	1979	3M 5_79	Potential Detection with clear peak but other dose peaks
23	-	510.9302	510.9232	4.87	9.73E+02	-7.00	-13.70	1979	3M 5_79	Detected; Clear Peak
23	-	560.9270	560.9173	5.10	1.09E+03	-9.70	-17.29	1979	3M 5_79	Potential Detection with clear peak but other dose peaks
23	-	610.9238	610.9161	5.26	1.17E+03	-7.70	-12.60	1979	3M 5_79	Potential Detection with clear peak but other dose peaks
23	-	710.9175	710.9255	5.53	2.70E+02	8.00	11.25	1979	3M 5_79	Potential Detection with clear peak but other dose peaks
24	-	442.9428	442.9409	4.61	4.24E+03	-1.90	-4.29	1979	3M 5_79	Potential Detection with clear peak but other dose peaks
25	-	230.9556	230.9513	1.70	6.00E+02	-4.30	-18.62	1979	3M 5_79	Potential Detection with clear peak but other dose peaks
25	-	330.9492	330.9500	3.14	5.18E+02	0.80	2.42	1979	3M 5_79	Potential Detection with clear peak but other dose peaks
25	-	380.9460	380.9448	3.66	6.29E+02	-1.20	-3.15	1979	3M 5_79	Potential Detection with clear peak but still too much noise
25	-	430.9396	430.9425	4.58	1.69E+02	2.90	6.73	1979	3M 5_79	Potential Detection with clear peak but still too much noise
25	-	480.9396	480.9393	4.68	4.28E+03	-0.30	-0.62	1979	3M 5_79	Potential Detection with clear peak but other dose peaks
26	-	362.9555	362.9619	4.28	3.46E+02	6.40	17.63	1979	3M 5_79	Potential Detection with clear peak but still too much noise
26	-	462.9491	462.9443	4.69	1.36E+03	-4.80	-10.37	1979	3M 5_79	Detected; Clear Peak
29	-	609.0487	609.0443	2.32	6.05E+03	-4.40	-7.22	1979	3M 5_79	Detected; Clear Peak
29	-	659.0455	659.0400	3.10	2.58E+04	-5.50	-8.35	1979	3M 5_79	Detected; Clear Peak
29	-	709.0423	709.0394	3.67	2.23E+04	-2.90	-4.09	1979	3M 5_79	Detected; Clear Peak
29	-	759.0391	759.0378	4.09	2.22E+05	-1.30	-1.71	1979	3M 5_79	Detected; Clear Peak
Angus	-	586.0391	586.0353	4.86	2.40E+02	-3.80	-6.48	1979	3M 5_79	Potential Detection with clear peak but still too much noise
Angus	-	602.0341	602.0334	4.27	1.42E+02	-0.70	-1.16	1979	3M 5_79	Potential Detection with clear peak but still too much noise
PFBS	-	298.9424	298.9428	3.28	2.32E+04	0.40	1.34	1989	3M1_89	Detected
PFHxS	-	398.9361	398.9361	4.28	1.35E+05	0.00	0.00	1989	3M1_89	Detected
PFHpS	-	448.9329	448.9312	4.63	9.56E+03	-1.70	-3.79	1989	3M1_89	Detected
PFOS	-	498.9297	498.9287	4.90	3.63E+05	-1.00	-2.00	1989	3M1_89	Detected
PFOA	-	412.9659	412.9627	4.60	1.71E+03	-3.20	-7.75	1989	3M1_89	Detected
2	+	457.0696	457.0775	2.77	4.13E+02	7.90	17.28	1989	3M1_89	Potential Detection with clear peak but still too much noise
2	+	507.0665	507.0667	3.55	5.15E+03	0.20	0.39	1989	3M1_89	Detected; Clear Peak
2	+	557.0633	557.0612	4.09	3.50E+03	-2.10	-3.77	1989	3M1_89	Detected; Clear Peak
2	+	607.0601	607.0599	4.50	4.03E+04	-0.20	-0.33	1989	3M1_89	Detected; Clear Peak
2	+	657.0569	657.0529	4.85	1.47E+02	-4.00	-6.09	1989	3M1_89	Potential Detection with clear peak but still too much noise
2	+	707.0537	707.0525	5.08	7.57E+02	-1.20	-1.70	1989	3M1_89	Potential Detection with clear peak but still too much noise
4	+	587.0738	587.0646	5.50	1.10E+03	-9.20	-15.67	1989	3M1_89	Detected; Clear Peak
4	+	637.0706	637.0676	4.48	8.21E+02	-3.00	-4.71	1989	3M1_89	Potential Detection with clear peak but other dose peaks
5	+	629.0702	629.0768	5.11	1.68E+03	6.60	10.49	1989	3M1_89	Potential Detection with clear peak but other dose peaks
5	+	679.0670	679.0660	3.86	8.64E+02	-1.00	-1.47	1989	3M1_89	Detected; Clear Peak
5	+	729.0638	729.0613	4.24	1.23E+04	-2.50	-3.43	1989	3M1_89	Detected; Clear Peak
5	+	829.0574	829.0656	4.89	2.68E+02	8.20	9.89	1989	3M1_89	Potential Detection with clear peak but still too much noise
8	+	451.0991	451.0964	2.18	1.54E+02	-2.70	-5.99	1989	3M1_89	Potential Detection with clear peak but still too much noise
8	+	551.0927	551.0927	3.74	4.14E+03	0.00	0.00	1989	3M1_89	Potential Detection with clear peak but other dose peaks
8	+	601.0895	601.0886	4.18	3.07E+03	-0.90	-1.50	1989	3M1_89	Potential Detection with clear peak but other dose peaks

Class	+/-	Theoretical m/z	Spectrum Observed m/z	Retention Time (min)	MS Response of the highest peak	Spectrum Error (mDa)	Spectrum Error (ppm)	Yr	Chemical	Comments
8	+	651.0863	651.0864	4.60	3.91E+04	0.10	0.15	1989	3M1_89	Potential Detection with clear peak but other close peaks
8	+	701.0831	701.0844	4.77	1.81E+02	1.30	1.85	1989	3M1_89	Potential Detection with clear peak but still too much noise
8	+	751.0799	751.0844	5.16	8.44E+02	4.50	5.99	1989	3M1_89	Potential Detection with clear peak but other close peaks
9	+	373.1215	373.1181	6.13	2.42E+03	-3.40	-9.11	1989	3M1_89	Detected; Clear Peak
9	+	423.1183	423.1142	3.11	8.58E+02	-4.10	-9.69	1989	3M1_89	Detected; Clear Peak
9	+	473.1151	473.1186	3.74	3.34E+03	3.50	7.40	1989	3M1_89	Detected; Clear Peak
9	+	623.1055	623.1008	5.99	7.41E+02	-4.70	-7.54	1989	3M1_89	Detected; Clear Peak
11	+	379.0921	379.0939	2.86	1.77E+03	1.80	4.75	1989	3M1_89	Potential Detection with clear peak but other close peaks
11	+	429.0889	429.0888	3.59	5.37E+03	-0.10	-0.23	1989	3M1_89	Detected; Clear Peak
11	+	479.0857	479.0855	4.12	9.88E+03	-0.20	-0.42	1989	3M1_89	Detected; Clear Peak
11	+	529.0825	529.0832	4.52	1.33E+05	0.70	1.32	1989	3M1_89	Detected; Clear Peak
11	+	629.0761	629.0768	5.11	1.68E+03	0.70	1.11	1989	3M1_89	Detected; Clear Peak
13	+	349.0815	349.0813	2.86	5.45E+02	-0.20	-0.57	1989	3M1_89	Potential Detection with clear peak but other close peaks
13	+	399.0783	399.0788	3.59	1.90E+03	0.50	1.25	1989	3M1_89	Detected; Clear Peak
13	+	449.0751	449.0738	4.12	1.76E+03	-1.30	-2.89	1989	3M1_89	Detected; Clear Peak
13	+	499.0719	499.0724	4.53	6.57E+04	0.50	1.00	1989	3M1_89	Detected; Clear Peak
13	+	549.0688	549.0685	4.85	3.49E+02	-0.30	-0.55	1989	3M1_89	Potential Detection with clear peak but still too much noise
13	+	599.0656	599.0656	5.11	8.14E+02	0.00	0.00	1989	3M1_89	Potential Detection with clear peak but still too much noise
14	+	571.0931	571.0831	4.26	4.78E+02	-10.00	-17.51	1989	3M1_89	Potential Detection with clear peak but still too much noise
19	+	623.0660	623.0688	4.57	1.52E+03	2.80	4.49	1989	3M1_89	Detected; Clear Peak
19	+	723.0592	723.0562	5.15	1.32E+02	-3.00	-4.15	1989	3M1_89	Potential Detection with clear peak but still too much noise
31	+	471.0826	471.0785	3.07	6.20E+02	-4.10	-8.70	1989	3M1_89	Detected; Clear Peak
31	+	521.0796	521.0861	3.74	1.21E+03	6.50	12.47	1989	3M1_89	Detected; Clear Peak
31	+	571.0789	571.0812	4.20	1.11E+03	2.30	4.03	1989	3M1_89	Detected; Clear Peak
31	+	621.0757	621.0754	4.57	2.59E+04	-0.30	-0.48	1989	3M1_89	Detected; Clear Peak
32	+	515.0751	515.0674	4.67	8.85E+03	-7.70	-14.95	1989	3M1_89	Detected; Clear Peak
32	+	565.0719	565.0613	6.00	2.51E+02	-10.60	-18.76	1989	3M1_89	Potential Detection with clear peak but still too much noise
32	+	615.0687	615.0715	5.51	2.47E+04	2.80	4.55	1989	3M1_89	Detected; Clear Peak
33	+	531.0700	531.0805	4.51	3.25E+03	10.50	19.77	1989	3M1_89	Detected; Clear Peak
34	+	451.0768	451.0825	4.11	2.01E+02	5.70	12.64	1989	3M1_89	Potential Detection with clear peak but still too much noise
34	+	601.0730	601.0630	5.51	1.46E+04	-10.00	-16.64	1989	3M1_89	Detected; Clear Peak
3M	+	385.0632	385.0624	3.77	6.42E+03	-0.80	-2.08	1989	3M1_89	Potential Detection with clear peak but other close peaks
3M	+	435.0600	435.0600	4.29	5.72E+03	0.02	0.05	1989	3M1_89	Potential Detection with clear peak but still too much noise
3M	+	485.0568	485.0579	4.68	5.90E+04	1.10	2.27	1989	3M1_89	Detected; Clear Peak
3M	+	507.0812	507.0778	3.84	9.16E+02	-3.40	-6.71	1989	3M1_89	Potential Detection with clear peak but other close peaks
Buckeye	+	514.0863	514.0857	3.86	1.28E+02	-0.60	-1.17	1989	3M1_89	Potential Detection with clear peak but still too much noise
Buckeye	+	532.0769	532.0854	4.51	4.15E+02	8.50	15.98	1989	3M1_89	Potential Detection with clear peak but still too much noise
Chemguard	+	681.1080	681.1012	4.61	3.35E+02	-6.80	-9.98	1989	3M1_89	Potential Detection with clear peak but other close peaks
Fireade	+	871.0745	871.0660	5.51	4.69E+03	-8.50	-9.76	1989	3M1_89	Potential Detection with clear peak but other close peaks
30	-	635.0561	635.0485	4.60	7.00E+02	-7.60	-11.97	1989	3M1_89	Potential Detection with clear peak but other close peaks
3M	-	398.9361	398.9360	4.28	1.29E+05	-0.10	-0.25	1989	3M1_89	Detected; Clear Peak
3M	-	448.9329	448.9312	4.63	8.97E+03	-1.70	-3.79	1989	3M1_89	Potential Detection with clear peak but other close peaks
3M	-	498.9297	498.9292	4.90	3.47E+05	-0.50	-1.00	1989	3M1_89	Detected; Clear Peak
2	+	457.0696	457.0722	2.81	1.36E+05	2.60	5.69	1990	3M 4_90	Detected; Clear Peak
2	+	507.0665	507.0681	3.60	9.35E+05	1.60	3.16	1990	3M 4_90	Detected; Clear Peak
2	+	557.0633	557.0647	4.15	7.95E+05	1.40	2.51	1990	3M 4_90	Detected; Clear Peak

Class	+/-	Theoretical m/z	Spectrum Observed m/z	Retention Time (min)	MS Response of the highest peak	Spectrum Error (mDa)	Spectrum Error (ppm)	Yr	Chemical	Comments
2	+	607.0601	607.0608	4.56	3.16E+06	0.70	1.15	1990	3M 4_90	Detected; Clear Peak
2	+	657.0569	657.0560	4.88	5.26E+04	-0.90	-1.37	1990	3M 4_90	Detected; Clear Peak
2	+	707.0537	707.0527	5.14	2.04E+05	-1.00	-1.41	1990	3M 4_90	Detected; Clear Peak
3	+	473.0646	473.0664	3.01	7.44E+03	1.80	3.80	1990	3M 4_90	Detected; Clear Peak
3	+	523.0614	523.0583	3.64	2.42E+04	-3.10	-5.93	1990	3M 4_90	Detected; Clear Peak
3	+	573.0582	573.0561	4.12	2.03E+04	-2.10	-3.66	1990	3M 4_90	Detected; Clear Peak
3	+	623.0550	623.0571	4.49	9.23E+04	2.10	3.37	1990	3M 4_90	Detected; Clear Peak
4	+	587.0738	587.0832	4.73	1.16E+04	9.40	16.01	1990	3M 4_90	Potential Detection with clear peak but other close peaks
4	+	637.0706	637.0682	4.54	6.80E+04	-2.40	-3.77	1990	3M 4_90	Potential Detection with clear peak but other close peaks
5	+	579.0734	579.0741	2.70	8.90E+04	0.70	1.21	1990	3M 4_90	Detected; Clear Peak
5	+	629.0702	629.0687	3.40	3.31E+05	-1.50	-2.38	1990	3M 4_90	Detected; Clear Peak
5	+	679.0670	679.0670	3.92	2.78E+05	0.00	0.00	1990	3M 4_90	Detected; Clear Peak
5	+	729.0638	729.0641	4.32	1.22E+06	0.30	0.41	1990	3M 4_90	Detected; Clear Peak
5	+	779.0606	779.0549	4.64	2.23E+04	-5.70	-7.32	1990	3M 4_90	Detected; Clear Peak
5	+	829.0574	829.0566	4.91	7.26E+04	-0.80	-0.96	1990	3M 4_90	Detected; Clear Peak
8	+	501.0959	501.0982	3.10	1.23E+05	2.30	4.59	1990	3M 4_90	Detected; Clear Peak
8	+	551.0927	551.0937	3.74	2.19E+05	1.00	1.81	1990	3M 4_90	Potential Detection with clear peak but other close peaks
8	+	601.0895	601.0901	4.22	1.67E+05	0.60	1.00	1990	3M 4_90	Potential Detection with clear peak but other close peaks
8	+	651.0863	651.0862	4.64	1.53E+06	-0.10	-0.15	1990	3M 4_90	Potential Detection with clear peak but other close peaks
8	+	701.0831	701.0782	4.91	9.56E+03	-4.90	-6.99	1990	3M 4_90	Potential Detection with clear peak but other close peaks
8	+	751.0799	751.0772	5.16	3.73E+04	-2.70	-3.59	1990	3M 4_90	Potential Detection with clear peak but other close peaks
9	+	423.1183	423.1179	3.08	3.43E+04	-0.40	-0.95	1990	3M 4_90	Detected; Clear Peak
9	+	473.1151	473.1162	3.75	1.20E+05	1.10	2.33	1990	3M 4_90	Detected; Clear Peak
9	+	523.1190	523.1130	4.21	6.57E+04	-6.00	-11.47	1990	3M 4_90	Detected; Clear Peak
9	+	573.1087	573.1093	4.59	1.09E+06	0.60	1.05	1990	3M 4_90	Detected; Clear Peak
9	+	673.1023	673.1001	5.16	2.17E+04	-2.20	-3.27	1990	3M 4_90	Detected; Clear Peak
10	+	445.0838	445.0855	4.06	2.45E+04	1.70	3.82	1990	3M 4_90	Detected; Clear Peak
10	+	495.0806	495.0809	4.50	1.96E+04	0.30	0.61	1990	3M 4_90	Detected; Clear Peak
10	+	545.0774	545.0804	4.85	3.42E+05	3.00	5.50	1990	3M 4_90	Detected; Clear Peak
11	+	379.0921	379.0942	2.82	5.78E+04	2.10	5.54	1990	3M 4_90	Detected; Clear Peak
11	+	429.0889	429.0910	3.60	4.16E+05	2.10	4.89	1990	3M 4_90	Detected; Clear Peak
11	+	479.0857	479.0876	4.13	3.35E+05	1.90	3.97	1990	3M 4_90	Detected; Clear Peak
11	+	529.0825	529.0834	4.54	3.39E+06	0.90	1.70	1990	3M 4_90	Detected; Clear Peak
11	+	579.0793	579.0741	2.70	8.90E+04	-5.20	-8.98	1990	3M 4_90	Potential Detection with clear peak but other close peaks
11	+	629.0761	629.0692	3.40	3.31E+05	-6.90	-10.97	1990	3M 4_90	Potential Detection with clear peak but other close peaks
12	+	513.0876	513.0964	4.45	1.48E+05	8.80	17.15	1990	3M 4_90	Detected; Clear Peak
13	+	349.0815	349.0846	2.81	3.91E+04	3.10	8.88	1990	3M 4_90	Detected; Clear Peak
13	+	399.0783	399.0804	3.60	2.17E+05	2.10	5.26	1990	3M 4_90	Detected; Clear Peak
13	+	449.0751	449.0773	4.15	1.58E+05	2.20	4.90	1990	3M 4_90	Detected; Clear Peak
13	+	499.0719	499.0769	4.55	2.08E+06	5.00	10.02	1990	3M 4_90	Detected; Clear Peak
13	+	549.0688	549.0674	4.88	1.36E+04	-1.40	-2.55	1990	3M 4_90	Detected; Clear Peak
13	+	599.0656	599.0665	5.14	6.68E+04	0.90	1.50	1990	3M 4_90	Detected; Clear Peak
15	+	615.0829	615.0736	5.55	3.73E+05	-9.30	-15.12	1990	3M 4_90	Detected; Clear Peak
16	+	543.0618	543.0655	4.69	6.55E+04	3.70	6.81	1990	3M 4_90	Detected; Clear Peak
28	+	567.0876	567.0853	3.48	1.92E+03	-2.30	-4.06	1990	3M 4_90	Detected; Clear Peak
28	+	667.0812	667.0839	4.42	1.01E+04	2.70	4.05	1990	3M 4_90	Detected; Clear Peak

Class	+/-	Theoretical m/z	Spectrum Observed m/z	Retention Time (min)	MS Response of the highest peak	Spectrum Error (mDa)	Spectrum Error (ppm)	Yr	Chemical	Comments
29	+	761.0537	761.0502	4.16	5.51E+03	-3.50	-4.60	1990	3M 4_90	Potential Detection with clear peak but other close peaks
31	+	471.0826	471.0830	3.10	5.12E+04	0.40	0.85	1990	3M 4_90	Detected; Clear Peak
31	+	521.0796	521.0829	3.75	1.59E+05	3.30	6.33	1990	3M 4_90	Detected; Clear Peak
31	+	571.0789	571.0802	4.23	1.21E+05	1.30	2.28	1990	3M 4_90	Detected; Clear Peak
31	+	621.0757	621.0775	4.61	1.29E+06	1.80	2.90	1990	3M 4_90	Detected; Clear Peak
32	+	515.0751	515.0680	4.69	4.61E+05	-7.10	-13.78	1990	3M 4_90	Detected; Clear Peak
32	+	565.0719	565.0623	5.00	2.65E+03	-9.60	-16.99	1990	3M 4_90	Detected; Clear Peak
32	+	665.0655	665.0659	4.38	5.13E+03	0.40	0.60	1990	3M 4_90	Detected; Clear Peak
33	+	531.0700	531.0784	4.54	1.56E+05	8.40	15.82	1990	3M 4_90	Detected; Clear Peak
33	+	631.0637	631.0665	3.40	4.88E+04	2.80	4.44	1990	3M 4_90	Detected; Clear Peak
33	+	681.0605	681.0629	3.91	4.54E+04	2.40	3.52	1990	3M 4_90	Detected; Clear Peak
34	+	601.0730	601.0676	5.56	1.90E+05	-5.40	-8.98	1990	3M 4_90	Detected; Clear Peak
37	+	479.0493	479.0525	2.82	5.11E+03	3.20	6.68	1990	3M 4_90	Detected; Clear Peak
37	+	529.0461	529.0530	3.60	1.11E+04	6.90	13.04	1990	3M 4_90	Detected; Clear Peak
3M	+	385.0632	385.0657	3.79	1.38E+06	2.50	6.49	1990	3M 4_90	Detected; Clear Peak
3M	+	435.0600	435.0620	4.30	1.11E+06	2.00	4.60	1990	3M 4_90	Detected; Clear Peak
3M	+	457.0844	457.0882	3.81	5.88E+04	3.80	8.31	1990	3M 4_90	Potential Detection with clear peak but other close peaks
3M	+	485.0568	485.0582	4.70	5.69E+06	1.40	2.89	1990	3M 4_90	Detected; Clear Peak
3M	+	507.0812	507.0804	4.29	4.84E+04	-0.80	-1.58	1990	3M 4_90	Potential Detection with clear peak but other close peaks
3M	+	557.0780	557.0768	4.68	2.24E+05	-1.20	-2.15	1990	3M 4_90	Potential Detection with clear peak but other close peaks
Buckeye	+	632.0705	632.0755	5.42	8.99E+03	5.00	7.91	1990	3M 4_90	Potential Detection with clear peak but other close peaks
Chemguard	+	681.1080	681.0988	4.50	7.44E+03	-9.20	-13.51	1990	3M 4_90	Potential Detection with clear peak but still too much noise
Fireade	+	871.0745	871.0661	5.56	1.21E+05	-8.40	-9.64	1990	3M 4_90	Detected; Clear Peak
National Foam	+	871.0745	871.0658	5.56	1.21E+05	-8.70	-9.99	1990	3M 4_90	Detected; Clear Peak
1	-	369.9648	369.9648	3.30	8.93E+05	0.00	0.00	1990	3M 4_90	Detected; Clear Peak
1	-	419.9628	419.9603	3.91	5.66E+03	-2.50	-5.95	1990	3M 4_90	Detected; Clear Peak
1	-	519.9564	519.9553	4.68	4.49E+04	-1.10	-2.12	1990	3M 4_90	Detected; Clear Peak
2	-	455.0547	455.0541	2.81	6.04E+04	-0.60	-1.32	1990	3M 4_90	Detected; Clear Peak
2	-	505.0523	505.0525	3.60	2.02E+05	0.20	0.40	1990	3M 4_90	Detected; Clear Peak
2	-	555.0491	555.0468	4.15	1.79E+05	-2.30	-4.14	1990	3M 4_90	Detected; Clear Peak
2	-	605.0461	605.0438	4.55	7.94E+05	-2.30	-3.80	1990	3M 4_90	Detected; Clear Peak
3	-	521.0468	521.0443	3.64	1.64E+03	-2.50	-4.80	1990	3M 4_90	Potential Detection with clear peak but still too much noise
3	-	621.0404	621.0410	4.49	8.49E+03	0.60	0.97	1990	3M 4_90	Detected; Clear Peak
5	-	577.0585	577.0578	2.70	5.45E+04	-0.70	-1.21	1990	3M 4_90	Detected; Clear Peak
5	-	627.0558	627.0546	3.40	1.54E+05	-1.20	-1.91	1990	3M 4_90	Detected; Clear Peak
5	-	677.0529	677.0517	3.91	9.45E+04	-1.20	-1.77	1990	3M 4_90	Detected; Clear Peak
5	-	727.0513	727.0462	4.31	4.61E+05	-5.10	-7.01	1990	3M 4_90	Detected; Clear Peak
16	-	441.0536	441.0484	3.79	1.89E+03	-5.20	-11.79	1990	3M 4_90	Potential Detection with clear peak but still too much noise
16	-	491.0504	491.0529	4.30	1.47E+03	2.50	5.09	1990	3M 4_90	Potential Detection with clear peak but still too much noise
16	-	541.0472	541.0439	4.69	6.89E+03	-3.30	-6.10	1990	3M 4_90	Detected; Clear Peak
21	-	356.9119	356.9091	3.83	1.49E+03	-2.80	-7.85	1990	3M 4_90	Detected; Clear Peak
21	-	406.9087	406.9066	4.30	1.02E+04	-2.10	-5.16	1990	3M 4_90	Detected; Clear Peak
21	-	456.9055	456.9008	4.65	1.14E+04	-4.70	-10.29	1990	3M 4_90	Detected; Clear Peak
21	-	506.9023	506.9019	4.94	1.20E+04	-0.40	-0.79	1990	3M 4_90	Detected; Clear Peak
21	-	556.8991	556.8990	5.18	2.31E+04	-0.10	-0.18	1990	3M 4_90	Detected; Clear Peak
21	-	656.8927	656.8906	5.54	2.68E+05	-2.10	-3.20	1990	3M 4_90	Detected; Clear Peak
23	-	410.9366	410.9351	4.33	3.17E+04	-1.50	-3.65	1990	3M 4_90	Detected; Clear Peak
23	-	460.9334	460.9319	4.66	6.27E+05	-1.50	-3.25	1990	3M 4_90	Detected; Clear Peak

Class	+/-	Theoretical m/z	Spectrum Observed m/z	Retention Time (min)	MS Response of the highest peak	Spectrum Error (mDa)	Spectrum Error (ppm)	Yr	Chemical	Comments
23	-	510.9302	510.9300	4.93	5.59E+04	-0.20	-0.39	1990	3M 4_90	Detected; Clear Peak
23	-	560.9270	560.9249	5.16	1.96E+04	-2.10	-3.74	1990	3M 4_90	Potential Detection with clear peak but other close peaks
23	-	610.9238	610.9193	5.36	2.03E+04	-4.50	-7.37	1990	3M 4_90	Detected; Clear Peak
23	-	660.9206	660.9199	5.44	1.40E+04	-0.70	-1.06	1990	3M 4_90	Detected; Clear Peak
23	-	710.9175	710.9173	5.59	1.07E+04	-0.20	-0.28	1990	3M 4_90	Detected; Clear Peak
24	-	342.9492	342.9510	3.38	5.88E+03	1.80	5.25	1990	3M 4_90	Potential Detection with clear peak but other close peaks
24	-	392.9460	392.9456	4.29	5.53E+03	-0.40	-1.02	1990	3M 4_90	Detected; Clear Peak
25	-	180.9588	180.9573	0.78	2.49E+03	-1.50	-8.29	1990	3M 4_90	Detected; Clear Peak
25	-	230.9556	230.9533	1.75	9.10E+03	-2.30	-9.96	1990	3M 4_90	Detected; Clear Peak
25	-	280.9524	280.9518	2.45	1.13E+04	-0.60	-2.14	1990	3M 4_90	Detected; Clear Peak
25	-	330.9492	330.9485	3.20	1.05E+04	-0.70	-2.12	1990	3M 4_90	Detected; Clear Peak
25	-	380.9460	380.9448	3.72	8.08E+03	-1.20	-3.15	1990	3M 4_90	Potential Detection with clear peak but other close peaks
25	-	430.9396	430.9404	4.21	5.43E+03	0.80	1.86	1990	3M 4_90	Potential Detection with clear peak but other close peaks
26	-	462.9491	462.9470	4.76	6.98E+04	-2.10	-4.54	1990	3M 4_90	Potential Detection with clear peak but other close peaks
29	-	659.0455	659.0458	3.17	8.04E+02	0.30	0.46	1990	3M 4_90	Potential Detection with clear peak but other close peaks
29	-	759.0391	759.0317	4.17	3.63E+03	-7.40	-9.75	1990	3M 4_90	Detected; Clear Peak
30	-	635.0561	635.0539	4.63	3.17E+04	-2.20	-3.46	1990	3M 4_90	Potential Detection with clear peak but other close peaks
32	-	513.0606	513.0513	4.69	2.96E+04	-9.30	-18.13	1990	3M 4_90	Detected; Clear Peak
32	-	563.0574	563.0563	3.49	5.23E+02	-1.10	-1.95	1990	3M 4_90	Potential Detection with clear peak but still too much noise
32	-	663.0510	663.0535	4.38	2.01E+03	2.50	3.77	1990	3M 4_90	Detected; Clear Peak
3M	-	398.9361	398.9353	4.36	7.05E+06	-0.80	-2.01	1990	3M 4_90	Detected; Clear Peak
3M	-	448.9329	448.9332	4.69	2.08E+06	0.30	0.67	1990	3M 4_90	Detected; Clear Peak
3M	-	498.9297	498.9290	4.97	2.13E+07	-0.70	-1.40	1990	3M 4_90	Detected; Clear Peak
Angus	-	602.0341	602.0342	4.62	5.82E+05	0.10	0.17	1990	3M 4_90	Detected; Clear Peak
Chemguard	-	586.0391	586.0479	5.14	8.77E+02	8.80	15.02	1990	3M 4_90	Potential Detection with clear peak but still too much noise
PFBS	-	298.9424	298.9425	3.35	1.85E+06	0.10	0.33	1990	3M 4_90	Detected
PFHpS	-	448.9329	448.9315	4.69	2.11E+06	-1.40	-3.12	1990	3M 4_90	Detected
PFOS	-	498.9297	498.9288	4.97	2.22E+07	-0.90	-1.80	1990	3M 4_90	Detected
PFDS	-	598.9233	598.9224	5.31	5.92E+04	-0.90	-1.50	1990	3M 4_90	Detected
PFHxA	-	312.9723	312.9731	3.83	7.51E+04	0.80	2.56	1990	3M 4_90	Detected
PFHpA	-	362.9691	362.9679	4.30	5.12E+04	-1.20	-3.31	1990	3M 4_90	Detected
PFOA	-	412.9659	412.9653	4.66	1.40E+05	-0.60	-1.45	1990	3M 4_90	Detected
PFBS	-	298.9424	298.9420	3.35	2.34E+06	-0.40	-1.34	1990	3M 6_90	Detected
PFHxS	-	398.9361	398.9355	4.36	8.31E+06	-0.60	-1.50	1990	3M 6_90	Detected
PFHpS	-	448.9329	448.9325	4.69	2.47E+06	-0.40	-0.89	1990	3M 6_90	Detected
PFOS	-	498.9297	498.9292	4.97	2.28E+07	-0.50	-1.00	1990	3M 6_90	Detected
PFDS	-	598.9233	598.9233	5.31	7.38E+04	0.00	0.00	1990	3M 6_90	Detected
PFHpA	-	362.9691	362.9697	4.30	5.60E+04	0.60	1.65	1990	3M 6_90	Detected
PFOA	-	412.9659	412.9663	4.66	1.59E+05	0.40	0.97	1990	3M 6_90	Detected
2	+	457.0696	457.0709	2.81	1.62E+05	1.30	2.84	1990	3M 6_90	Detected; Clear Peak

Class	+/-	Theoretical m/z	Spectrum Observed m/z	Retention Time (min)	MS Response of the highest peak	Spectrum Error (mDa)	Spectrum Error (ppm)	Yr	Chemical	Comments
2	+	507.0665	507.0684	3.60	1.09E+06	1.90	3.75	1990	3M 6_90	Detected; Clear Peak
2	+	557.0633	557.0644	4.15	9.80E+05	1.10	1.97	1990	3M 6_90	Detected; Clear Peak
2	+	607.0601	607.0594	4.56	3.68E+06	-0.70	-1.15	1990	3M 6_90	Detected; Clear Peak
2	+	657.0569	657.0555	4.88	5.13E+04	-1.40	-2.13	1990	3M 6_90	Detected; Clear Peak
2	+	707.0537	707.0525	5.14	2.49E+05	-1.20	-1.70	1990	3M 6_90	Detected; Clear Peak
3	+	473.0646	473.0648	3.01	1.83E+04	0.20	0.42	1990	3M 6_90	Detected; Clear Peak
3	+	523.0614	523.0617	3.64	5.09E+04	0.30	0.57	1990	3M 6_90	Detected; Clear Peak
3	+	573.0582	573.0599	4.11	4.13E+04	1.70	2.97	1990	3M 6_90	Detected; Clear Peak
3	+	623.0550	623.0565	4.49	2.00E+05	1.50	2.41	1990	3M 6_90	Detected; Clear Peak
4	+	537.0770	537.0786	3.59	5.81E+03	1.60	2.98	1990	3M 6_90	Potential Detection with clear peak but other close peaks
4	+	637.0706	637.0690	4.53	7.65E+04	-1.60	-2.51	1990	3M 6_90	Detected; Clear Peak
5	+	579.0734	579.0746	2.70	1.04E+05	1.20	2.07	1990	3M 6_90	Detected; Clear Peak
5	+	629.0702	629.0701	3.40	3.79E+05	-0.10	-0.16	1990	3M 6_90	Detected; Clear Peak
5	+	679.0670	679.0665	3.91	3.25E+05	-0.50	-0.74	1990	3M 6_90	Detected; Clear Peak
5	+	729.0638	729.0634	4.32	1.35E+06	-0.40	-0.55	1990	3M 6_90	Detected; Clear Peak
5	+	779.0606	779.0588	4.64	2.64E+04	-1.80	-2.31	1990	3M 6_90	Detected; Clear Peak
5	+	829.0574	829.0558	4.91	7.77E+04	-1.60	-1.93	1990	3M 6_90	Detected; Clear Peak
8	+	451.0991	451.0904	4.13	1.94E+04	-8.70	-19.29	1990	3M 6_90	Detected; Clear Peak
8	+	501.0959	501.0976	3.10	1.30E+05	1.70	3.39	1990	3M 6_90	Detected; Clear Peak
8	+	551.0927	551.0933	3.74	2.34E+05	0.60	1.09	1990	3M 6_90	Potential Detection with clear peak but other close peaks
8	+	601.0895	601.0891	4.22	1.95E+05	-0.40	-0.67	1990	3M 6_90	Potential Detection with clear peak but other close peaks
8	+	651.0863	651.0874	4.64	1.68E+06	1.10	1.69	1990	3M 6_90	Potential Detection with clear peak but other close peaks
8	+	701.0831	701.0775	4.91	1.06E+04	-5.60	-7.99	1990	3M 6_90	Potential Detection with clear peak but other close peaks
8	+	751.0799	751.0781	5.16	4.46E+04	-1.80	-2.40	1990	3M 6_90	Potential Detection with clear peak but other close peaks
9	+	423.1183	423.1209	3.09	2.93E+04	2.60	6.14	1990	3M 6_90	Detected; Clear Peak
9	+	473.1151	473.1165	3.75	1.08E+05	1.40	2.96	1990	3M 6_90	Detected; Clear Peak
9	+	523.1190	523.1119	4.22	6.09E+04	-7.10	-13.57	1990	3M 6_90	Detected; Clear Peak
9	+	573.1087	573.1107	4.59	1.17E+06	2.00	3.49	1990	3M 6_90	Detected; Clear Peak
9	+	623.1055	623.1030	4.90	5.56E+03	-2.50	-4.01	1990	3M 6_90	Detected; Clear Peak
9	+	673.1023	673.1016	5.15	2.44E+04	-0.70	-1.04	1990	3M 6_90	Detected; Clear Peak
10	+	445.0838	445.0851	4.07	5.57E+04	1.30	2.92	1990	3M 6_90	Detected; Clear Peak
10	+	495.0806	495.0811	4.50	4.10E+04	0.50	1.01	1990	3M 6_90	Detected; Clear Peak
10	+	545.0774	545.0792	4.85	8.60E+05	1.80	3.30	1990	3M 6_90	Detected; Clear Peak
11	+	379.0921	379.0941	2.82	6.72E+04	2.00	5.28	1990	3M 6_90	Detected; Clear Peak
11	+	429.0889	429.0906	3.60	5.00E+05	1.70	3.96	1990	3M 6_90	Detected; Clear Peak
11	+	479.0857	479.0875	4.13	4.35E+05	1.80	3.76	1990	3M 6_90	Detected; Clear Peak
11	+	529.0825	529.0838	4.54	4.24E+06	1.30	2.46	1990	3M 6_90	Detected; Clear Peak
11	+	579.0793	579.0746	2.70	1.04E+05	-4.70	-8.12	1990	3M 6_90	Potential Detection with clear peak but other close peaks
11	+	629.0761	629.0701	3.40	3.79E+05	-6.00	-9.54	1990	3M 6_90	Potential Detection with clear peak but other close peaks
12	+	513.0876	513.0882	4.72	5.52E+04	0.60	1.17	1990	3M 6_90	Detected; Clear Peak
13	+	349.0815	349.0840	2.81	4.79E+04	2.50	7.16	1990	3M 6_90	Detected; Clear Peak
13	+	399.0783	399.0808	3.60	2.64E+04	2.50	6.26	1990	3M 6_90	Detected; Clear Peak
13	+	449.0751	449.0771	4.15	2.25E+05	2.00	4.45	1990	3M 6_90	Detected; Clear Peak
13	+	499.0719	499.0733	4.56	2.86E+06	1.40	2.81	1990	3M 6_90	Detected; Clear Peak
13	+	549.0688	549.0688	4.88	2.35E+04	0.00	0.00	1990	3M 6_90	Detected; Clear Peak
13	+	599.0656	599.0668	5.14	1.06E+05	1.20	2.00	1990	3M 6_90	Detected; Clear Peak
14	+	471.0995	471.0905	3.27	3.10E+03	-9.00	-19.10	1990	3M 6_90	Potential Detection with clear peak but other close peaks
14	+	521.0963	521.0977	3.79	5.37E+04	1.40	2.69	1990	3M 6_90	Detected; Clear Peak
14	+	571.0931	571.0924	4.28	6.06E+04	-0.70	-1.23	1990	3M 6_90	Detected; Clear Peak
15	+	515.0904	515.0812	4.92	6.60E+04	-9.20	-17.86	1990	3M 6_90	Detected; Clear Peak
16	+	543.0618	543.0590	5.11	3.58E+03	-2.80	-5.16	1990	3M 6_90	Potential Detection with clear peak but other close peaks

Class	+/-	Theoretical m/z	Spectrum Observed m/z	Retention Time (min)	MS Response of the highest peak	Spectrum Error (mDa)	Spectrum Error (ppm)	Yr	Chemical	Comments
17	+	550.0680	550.0732	4.88	3.56E+03	5.20	9.45	1990	3M 6_90	Detected; Clear Peak
19	+	623.0660	623.0565	4.49	2.00E+05	-9.50	-15.25	1990	3M 6_90	Detected; Clear Peak
19	+	723.0592	723.0642	5.18	4.64E+03	5.00	6.92	1990	3M 6_90	Detected; Clear Peak
31	+	471.0826	471.0887	3.10	5.16E+04	6.10	12.95	1990	3M 6_90	Detected; Clear Peak
31	+	521.0796	521.0827	3.75	1.66E+05	3.10	5.95	1990	3M 6_90	Detected; Clear Peak
31	+	571.0789	571.0804	4.23	1.50E+05	1.50	2.63	1990	3M 6_90	Detected; Clear Peak
31	+	621.0757	621.0767	4.61	1.44E+06	1.00	1.61	1990	3M 6_90	Detected; Clear Peak
32	+	515.0751	515.0682	4.68	3.00E+05	-6.90	-13.40	1990	3M 6_90	Detected; Clear Peak
33	+	531.0700	531.0636	4.82	5.53E+05	-6.40	-12.05	1990	3M 6_90	Detected; Clear Peak
33	+	581.0668	581.0720	2.70	1.62E+04	5.20	8.95	1990	3M 6_90	Detected; Clear Peak
33	+	631.0637	631.0657	3.40	5.92E+04	2.00	3.17	1990	3M 6_90	Detected; Clear Peak
33	+	681.0605	681.0649	3.91	5.08E+04	4.40	6.46	1990	3M 6_90	Detected; Clear Peak
34	+	451.0768	451.0853	4.14	1.79E+04	8.50	18.84	1990	3M 6_90	Detected; Clear Peak
34	+	501.0736	501.0749	4.55	1.89E+05	1.30	2.59	1990	3M 6_90	Detected; Clear Peak
34	+	601.0730	601.0692	5.55	2.43E+05	-3.80	-6.32	1990	3M 6_90	Detected; Clear Peak
37	+	429.0525	429.0548	4.16	2.19E+03	2.30	5.36	1990	3M 6_90	Detected; Clear Peak
37	+	479.0493	479.0550	2.82	4.95E+03	5.70	11.90	1990	3M 6_90	Potential Detection with clear peak but other close peaks
37	+	529.0461	529.0492	3.60	9.78E+03	3.10	5.86	1990	3M 6_90	Detected; Clear Peak
38	+	541.1189	541.1285	4.11	2.14E+03	9.60	17.74	1990	3M 6_90	Potential Detection with clear peak but still too much noise
3M	+	385.0632	385.0653	3.79	1.41E+06	2.10	5.45	1990	3M 6_90	Detected; Clear Peak
3M	+	435.0600	435.0590	4.30	1.46E+06	-1.00	-2.30	1990	3M 6_90	Detected; Clear Peak
3M	+	485.0568	485.0576	4.70	8.55E+06	0.80	1.65	1990	3M 6_90	Detected; Clear Peak
Buckeye	+	432.0833	432.0868	3.99	3.26E+03	3.50	8.10	1990	3M 6_90	Potential Detection with clear peak but other close peaks
Buckeye	+	514.0863	514.0901	4.72	9.80E+03	3.80	7.39	1990	3M 6_90	Detected; Clear Peak
Buckeye	+	532.0769	532.0788	4.54	2.70E+04	1.90	3.57	1990	3M 6_90	Detected; Clear Peak
Buckeye	+	632.0705	632.0643	3.40	1.01E+04	-6.20	-9.81	1990	3M 6_90	Detected; Clear Peak
Chemguard	+	681.1080	681.0956	4.64	6.82E+03	-12.40	-18.21	1990	3M 6_90	Potential Detection with clear peak but other close peaks
Fireade	+	513.0881	513.0888	4.72	5.52E+04	0.70	1.36	1990	3M 6_90	Detected; Clear Peak
Fireade	+	571.0936	571.0911	4.28	6.06E+04	-2.50	-4.38	1990	3M 6_90	Detected; Clear Peak
Fireade	+	871.0745	871.0693	5.56	1.53E+06	-5.20	-5.97	1990	3M 6_90	Detected; Clear Peak
National Foam	+	513.0881	513.0887	4.72	5.52E+04	0.60	1.17	1990	3M 6_90	Detected; Clear Peak
National Foam	+	571.0936	571.0891	4.28	6.06E+04	-4.50	-7.88	1990	3M 6_90	Detected; Clear Peak
National Foam	+	871.0745	871.0667	5.56	1.53E+05	-7.80	-8.95	1990	3M 6_90	Detected; Clear Peak
1	-	369.9648	369.9658	3.30	8.30E+03	1.00	2.70	1990	3M 6_90	Detected; Clear Peak
1	-	519.9564	519.9548	4.68	3.66E+04	-1.60	-3.08	1990	3M 6_90	Detected; Clear Peak
2	-	455.0547	455.0540	2.80	7.83E+04	-0.70	-1.54	1990	3M 6_90	Detected; Clear Peak
2	-	505.0523	505.0511	3.60	2.46E+05	-1.20	-2.38	1990	3M 6_90	Detected; Clear Peak
2	-	555.0491	555.0474	4.15	2.18E+05	-1.70	-3.06	1990	3M 6_90	Detected; Clear Peak
2	-	605.0461	605.0450	4.55	9.86E+05	-1.10	-1.82	1990	3M 6_90	Detected; Clear Peak
3	-	471.0500	471.0471	3.02	1.70E+03	-2.90	-6.16	1990	3M 6_90	Detected; Clear Peak
3	-	521.0468	521.0483	3.64	4.29E+03	1.50	2.88	1990	3M 6_90	Detected; Clear Peak
3	-	571.0436	571.0414	4.12	3.27E+03	-2.20	-3.85	1990	3M 6_90	Detected; Clear Peak
3	-	621.0404	621.0393	4.49	1.72E+04	-1.10	-1.77	1990	3M 6_90	Detected; Clear Peak
5	-	577.0585	577.0566	2.70	6.30E+04	-1.90	-3.29	1990	3M 6_90	Detected; Clear Peak
5	-	627.0558	627.0547	3.40	1.77E+05	-1.10	-1.75	1990	3M 6_90	Detected; Clear Peak
5	-	677.0529	677.0498	3.91	1.13E+05	-3.10	-4.58	1990	3M 6_90	Detected; Clear Peak
5	-	727.0513	727.0490	4.31	5.24E+05	-2.30	-3.16	1990	3M 6_90	Detected; Clear Peak
21	-	356.9119	356.9106	3.83	2.04E+03	-1.30	-3.64	1990	3M 6_90	Detected; Clear Peak

Class	+/-	Theoretical m/z	Spectrum Observed m/z	Retention Time (min)	MS Response of the highest peak	Spectrum Error (mDa)	Spectrum Error (ppm)	Yr	Chemical	Comments
21	-	406.9087	406.9067	4.30	1.09E+04	-2.00	-4.92	1990	3M 6_90	Detected; Clear Peak
21	-	456.9055	456.9023	4.65	1.42E+04	-3.20	-7.00	1990	3M 6_90	Detected; Clear Peak
21	-	506.9023	506.9003	4.93	1.50E+04	-2.00	-3.95	1990	3M 6_90	Detected; Clear Peak
21	-	556.8991	556.8969	5.18	3.26E+04	-2.20	-3.95	1990	3M 6_90	Detected; Clear Peak
21	-	656.8927	656.8903	5.53	3.53E+05	-2.40	-3.65	1990	3M 6_90	Detected; Clear Peak
22	-	520.9321	520.9289	5.17	1.44E+03	-3.20	-6.14	1990	3M 6_90	Detected; Clear Peak
22	-	570.9291	570.9209	5.35	1.01E+03	-8.20	-14.36	1990	3M 6_90	Potential Detection with clear peak but other close peaks
23	-	360.9398	360.9380	3.94	1.32E+04	-1.80	-4.99	1990	3M 6_90	Potential Detection with clear peak but other close peaks
23	-	410.9366	410.9356	4.33	3.98E+04	-1.00	-2.43	1990	3M 6_90	Detected; Clear Peak
23	-	460.9334	460.9324	4.66	7.33E+05	-1.00	-2.17	1990	3M 6_90	Detected; Clear Peak
23	-	510.9302	510.9300	4.93	6.56E+04	-0.20	-0.39	1990	3M 6_90	Detected; Clear Peak
23	-	560.9270	560.9238	5.16	2.55E+04	-3.20	-5.70	1990	3M 6_90	Potential Detection with clear peak but other close peaks
23	-	610.9238	610.9214	5.31	2.38E+04	-2.40	-3.93	1990	3M 6_90	Potential Detection with clear peak but other close peaks
23	-	660.9206	660.9183	5.44	1.72E+04	-2.30	-3.48	1990	3M 6_90	Potential Detection with clear peak but other close peaks
24	-	342.9492	342.9486	3.38	7.24E+03	-0.60	-1.75	1990	3M 6_90	Detected; Clear Peak
24	-	392.9460	392.9452	4.29	6.83E+03	-0.80	-2.04	1990	3M 6_90	Detected; Clear Peak
24	-	442.9428	442.9417	4.54	1.24E+05	-1.10	-2.48	1990	3M 6_90	Potential Detection with clear peak but other close peaks
25	-	180.9588	180.9567	0.75	3.02E+03	-2.10	-11.60	1990	3M 6_90	Potential Detection with clear peak but other close peaks
25	-	230.9556	230.9543	1.75	9.19E+03	-1.30	-5.63	1990	3M 6_90	Detected; Clear Peak
25	-	280.9524	280.9511	2.45	1.06E+04	-1.30	-4.63	1990	3M 6_90	Detected; Clear Peak
25	-	330.9492	330.9489	3.20	1.01E+04	-0.30	-0.91	1990	3M 6_90	Detected; Clear Peak
25	-	380.9460	380.9449	3.71	7.16E+03	-1.10	-2.89	1990	3M 6_90	Potential Detection with clear peak but other close peaks
25	-	480.9396	480.9394	4.74	1.97E+05	-0.20	-0.42	1990	3M 6_90	Potential Detection with clear peak but other close peaks
26	-	462.9491	462.9474	4.76	8.11E+04	-1.70	-3.67	1990	3M 6_90	Potential Detection with clear peak but other close peaks
29	-	609.0487	609.0432	4.55	3.58E+03	-5.50	-9.03	1990	3M 6_90	Detected; Clear Peak
30	-	585.0590	585.0573	4.92	8.80E+03	-1.70	-2.91	1990	3M 6_90	Potential Detection with clear peak but other close peaks
30	-	635.0561	635.0551	4.54	3.87E+04	-1.00	-1.57	1990	3M 6_90	Potential Detection with clear peak but other close peaks
32	-	513.0606	513.0506	4.69	2.21E+04	-10.00	-19.49	1990	3M 6_90	Potential Detection with clear peak but still too much noise
32	-	563.0574	563.0526	4.54	8.39E+02	-4.80	-8.52	1990	3M 6_90	Potential Detection with clear peak but still too much noise
32	-	663.0510	663.0432	4.68	9.60E+02	-7.80	-11.76	1990	3M 6_90	Detected; Clear Peak
40	-	482.9941	482.9872	5.07	8.79E+02	-6.90	-14.29	1990	3M 6_90	Potential Detection with clear peak but still too much noise
3M	-	398.9361	398.9355	4.36	8.06E+06	-0.60	-1.50	1990	3M 6_90	Detected; Clear Peak
3M	-	448.9329	448.9323	4.69	2.43E+06	-0.60	-1.34	1990	3M 6_90	Detected; Clear Peak
3M	-	498.9297	498.9281	4.97	2.21E+07	-1.60	-3.21	1990	3M 6_90	Detected; Clear Peak
2	+	457.0696	457.0777	3.85	2.72E+03	8.10	17.72	1997	3M 4_97	Potential Detection with clear peak but still too much noise
2	+	507.0665	507.0763	4.18	2.16E+03	9.80	19.33	1997	3M 4_97	Potential Detection with clear peak but still too much noise
2	+	607.0601	607.0622	4.55	6.69E+03	2.10	3.46	1997	3M 4_97	Detected; Clear Peak
2	+	657.0569	657.0567	5.25	5.22E+02	-0.20	-0.30	1997	3M 4_97	Potential Detection with clear peak but still too much noise

Class	+/-	Theoretical m/z	Spectrum Observed m/z	Retention Time (min)	MS Response of the highest peak	Spectrum Error (mDa)	Spectrum Error (ppm)	Yr	Chemical	Comments
2	+	707.0537	707.0579	5.14	4.08E+02	4.20	5.94	1997	3M 4_97	Potential Detection with clear peak but still too much noise
3	+	523.0614	523.0612	3.66	3.18E+03	-0.20	-0.38	1997	3M 4_97	Detected; Clear Peak
3	+	573.0582	573.0665	4.19	2.08E+03	8.30	14.48	1997	3M 4_97	Detected; Clear Peak
3	+	623.0550	623.0557	4.59	1.24E+04	0.70	1.12	1997	3M 4_97	Detected; Clear Peak
4	+	587.0738	587.0752	4.01	1.18E+03	1.40	2.38	1997	3M 4_97	Potential Detection with clear peak but still too much noise
4	+	637.0706	637.0690	4.44	7.31E+03	-1.60	-2.51	1997	3M 4_97	Detected; Clear Peak
5	+	629.0702	629.0770	3.40	1.30E+03	6.80	10.81	1997	3M 4_97	Potential Detection with clear peak but still too much noise
5	+	679.0670	679.0599	3.91	8.35E+02	-7.10	-10.46	1997	3M 4_97	Potential Detection with clear peak but still too much noise
5	+	729.0638	729.0589	4.31	6.33E+03	-4.90	-6.72	1997	3M 4_97	Detected; Clear Peak
8	+	501.0959	501.0958	3.10	5.38E+04	-0.10	-0.20	1997	3M 4_97	Detected; Clear Peak
8	+	551.0927	551.0912	3.74	5.63E+03	-1.50	-2.72	1997	3M 4_97	Potential Detection with clear peak but other close peaks
8	+	601.0895	601.0842	4.21	3.07E+03	-5.30	-8.82	1997	3M 4_97	Potential Detection with clear peak but other close peaks
8	+	651.0863	651.0866	4.60	3.14E+04	0.30	0.46	1997	3M 4_97	Potential Detection with clear peak but other close peaks
9	+	473.1151	473.1190	3.73	6.16E+03	3.90	8.24	1997	3M 4_97	Detected; Clear Peak
9	+	523.1190	523.1208	4.21	1.51E+03	1.80	3.44	1997	3M 4_97	Potential Detection with clear peak but still too much noise
9	+	573.1087	573.1109	4.59	4.96E+03	2.20	3.84	1997	3M 4_97	Detected; Clear Peak
11	+	379.0921	379.0914	2.82	5.21E+03	-0.70	-1.85	1997	3M 4_97	Potential Detection with clear peak but still too much noise
11	+	429.0889	429.0910	3.59	1.04E+04	2.10	4.89	1997	3M 4_97	Detected; Clear Peak
11	+	479.0857	479.0873	4.13	5.69E+03	1.60	3.34	1997	3M 4_97	Detected; Clear Peak
11	+	529.0825	529.0829	4.54	1.72E+04	0.40	0.76	1997	3M 4_97	Detected; Clear Peak
11	+	629.0761	629.0686	3.39	1.22E+03	-7.50	-11.92	1997	3M 4_97	Potential Detection with clear peak but still too much noise
13	+	399.0783	399.0785	3.60	3.21E+03	0.20	0.50	1997	3M 4_97	Potential Detection with clear peak but still too much noise
13	+	449.0751	449.0714	4.14	1.52E+03	-3.70	-8.24	1997	3M 4_97	Potential Detection with clear peak but still too much noise
13	+	499.0719	499.0757	4.55	4.27E+03	3.80	7.61	1997	3M 4_97	Potential Detection with clear peak but still too much noise
14	+	421.1027	421.1021	3.01	1.34E+03	-0.60	-1.42	1997	3M 4_97	Potential Detection with clear peak but still too much noise
14	+	571.0931	571.0898	4.71	3.69E+03	-3.30	-5.78	1997	3M 4_97	Potential Detection with clear peak but other close peaks
15	+	615.0829	615.0785	5.55	1.98E+03	-4.40	-7.15	1997	3M 4_97	Potential Detection with clear peak but still too much noise
19	+	623.0660	623.0601	4.60	6.03E+03	-5.90	-9.47	1997	3M 4_97	Detected; Clear Peak
28	+	567.0876	567.0886	3.47	5.53E+03	1.00	1.76	1997	3M 4_97	Detected; Clear Peak
28	+	617.0844	617.0886	4.01	3.40E+03	4.20	6.81	1997	3M 4_97	Detected; Clear Peak
28	+	667.0812	667.0786	4.42	2.09E+04	-2.60	-3.90	1997	3M 4_97	Detected; Clear Peak
29	+	661.0600	661.0621	3.17	3.21E+03	2.10	3.18	1997	3M 4_97	Detected; Clear Peak
29	+	761.0537	761.0495	4.17	1.20E+04	-4.20	-5.52	1997	3M 4_97	Detected; Clear Peak
31	+	471.0826	471.0820	3.09	9.34E+02	-0.60	-1.27	1997	3M 4_97	Potential Detection with clear peak but still too much noise
31	+	521.0796	521.0861	3.75	2.48E+03	6.50	12.47	1997	3M 4_97	Potential Detection with clear peak but still too much noise
31	+	571.0789	571.0834	4.62	2.69E+03	4.50	7.88	1997	3M 4_97	Potential Detection with clear peak but still too much noise
31	+	621.0757	621.0775	4.61	1.26E+04	1.80	2.90	1997	3M 4_97	Detected; Clear Peak
32	+	615.0687	615.0687	5.55	1.98E+03	0.00	0.00	1997	3M 4_97	Potential Detection with clear peak but still too much noise
33	+	531.0700	531.0659	4.83	1.23E+03	-4.10	-7.72	1997	3M 4_97	Potential Detection with clear peak but still too much noise
3M	+	385.0632	385.0643	3.77	2.43E+04	1.10	2.86	1997	3M 4_97	Detected; Clear Peak
3M	+	435.0600	435.0598	4.30	1.23E+04	-0.20	-0.46	1997	3M 4_97	Detected; Clear Peak
3M	+	457.0844	457.0857	3.82	4.49E+04	1.30	2.84	1997	3M 4_97	Detected; Clear Peak
3M	+	485.0568	485.0592	4.69	1.58E+04	2.40	4.95	1997	3M 4_97	Detected; Clear Peak
3M	+	507.0812	507.0806	4.29	2.39E+04	-0.60	-1.18	1997	3M 4_97	Detected; Clear Peak
3M	+	557.0780	557.0788	4.68	7.67E+04	0.80	1.44	1997	3M 4_97	Detected; Clear Peak

Class	+/-	Theoretical m/z	Spectrum Observed m/z	Retention Time (min)	MS Response of the highest peak	Spectrum Error (mDa)	Spectrum Error (ppm)	Yr	Chemical	Comments
Angus	+	596.0916	596.0952	2.89	2.56E+02	3.60	6.04	1997	3M 4_97	Detected; Clear Peak
Buckeye	+	414.0927	414.0944	4.07	3.93E+03	1.70	4.11	1997	3M 4_97	Detected; Clear Peak
Buckeye	+	432.0833	432.0830	4.14	1.24E+04	-0.30	-0.69	1997	3M 4_97	Detected; Clear Peak
Fireade	+	571.0936	571.0911	4.71	3.69E+03	-2.50	-4.38	1997	3M 4_97	Potential Detection with clear peak but other close peaks
National Foam	+	571.0936	571.0891	4.71	3.69E+03	-4.50	-7.88	1997	3M 4_97	Potential Detection with clear peak but other close peaks
1	-	519.9564	519.9546	4.69	6.03E+02	-1.80	-3.46	1997	3M 4_97	Potential Detection with clear peak but still too much noise
2	-	555.0491	555.0569	4.69	1.56E+03	7.80	14.05	1997	3M 4_97	Potential Detection with clear peak but still too much noise
2	-	605.0461	605.0366	4.55	2.26E+03	-9.50	-15.70	1997	3M 4_97	Potential Detection with clear peak but still too much noise
3	-	521.0468	521.0469	3.67	1.39E+03	0.10	0.19	1997	3M 4_97	Potential Detection with clear peak but still too much noise
3	-	621.0404	621.0396	4.59	3.98E+03	-0.80	-1.29	1997	3M 4_97	Detected; Clear Peak
5	-	727.0513	727.0452	4.31	3.29E+03	-6.10	-8.39	1997	3M 4_97	Detected; Clear Peak
29	-	609.0487	609.0518	2.38	8.71E+02	3.10	5.09	1997	3M 4_97	Potential Detection with clear peak but still too much noise
29	-	659.0455	659.0453	3.16	2.34E+03	-0.20	-0.30	1997	3M 4_97	Potential Detection with clear peak but still too much noise
29	-	709.0423	709.0349	3.73	1.70E+03	-7.40	-10.44	1997	3M 4_97	Potential Detection with clear peak but still too much noise
29	-	759.0391	759.0361	4.17	7.57E+03	-3.00	-3.95	1997	3M 4_97	Detected; Clear Peak
3M	-	398.9361	398.9364	4.36	3.30E+05	0.30	0.75	1997	3M 4_97	Detected; Clear Peak
3M	-	448.9329	448.9342	4.69	3.36E+04	1.30	2.90	1997	3M 4_97	Detected; Clear Peak
3M	-	498.9297	498.9287	4.97	1.31E+06	-1.00	-2.00	1997	3M 4_97	Detected; Clear Peak
Angus	-	586.0391	586.0385	5.13	2.57E+05	-0.60	-1.02	1997	3M 4_97	Detected; Clear Peak
Angus	-	602.0341	602.0294	4.62	8.07E+03	-4.70	-7.81	1997	3M 4_97	Detected; Clear Peak
Ansul	-	586.0391	586.0391	5.13	2.57E+05	0.00	0.00	1997	3M 4_97	Detected; Clear Peak
Ansul	-	602.0341	602.0264	4.62	8.07E+03	-7.70	-12.79	1997	3M 4_97	Detected; Clear Peak
Chemguard	-	586.0391	586.0385	5.13	2.57E+05	-0.60	-1.02	1997	3M 4_97	Detected; Clear Peak
PFBS	-	298.9424	298.9424	3.35	6.61E+04	0.00	0.00	1997	3M 4_97	Detected
PFHxS	-	398.9361	398.9364	4.36	3.44E+05	0.30	0.75	1997	3M 4_97	Detected
PFHpS	-	448.9329	448.9326	4.69	3.50E+04	-0.30	-0.67	1997	3M 4_97	Detected
PFOS	-	498.9297	498.9297	4.97	1.39E+06	0.00	0.00	1997	3M 4_97	Detected
PFOA	-	412.9659	412.9662	4.66	4.21E+03	0.30	0.73	1997	3M 4_97	Detected
2	+	507.0665	507.0746	4.50	7.39E+02	8.10	15.97	1998	3M 3_98	Potential Detection with clear peak but still too much noise
2	+	557.0633	557.0729	5.32	1.35E+03	9.60	17.23	1998	3M 3_98	Potential Detection with clear peak but still too much noise
2	+	657.0569	657.0685	5.02	2.62E+03	11.60	17.65	1998	3M 3_98	Detected; Clear Peak
3	+	623.0550	623.0569	4.85	4.44E+02	1.90	3.05	1998	3M 3_98	Detected; Clear Peak
12	+	513.0876	513.0958	4.63	1.57E+03	8.20	15.98	1998	3M 3_98	Potential Detection with clear peak but other close peaks
13	+	349.0815	349.0812	2.81	4.74E+04	-0.30	-0.86	1998	3M 3_98	Detected; Clear Peak
13	+	399.0783	399.0785	3.58	1.35E+05	0.20	0.50	1998	3M 3_98	Detected; Clear Peak
13	+	449.0751	449.0762	4.13	1.48E+05	1.10	2.45	1998	3M 3_98	Detected; Clear Peak
13	+	499.0719	499.0724	4.53	3.93E+05	0.50	1.00	1998	3M 3_98	Detected; Clear Peak
13	+	549.0688	549.0673	4.86	6.33E+03	-1.50	-2.73	1998	3M 3_98	Detected; Clear Peak
13	+	599.0656	599.0662	5.12	1.59E+03	0.60	1.00	1998	3M 3_98	Potential Detection with clear peak but other close peaks
14	+	421.1027	421.1036	2.99	1.50E+05	0.90	2.14	1998	3M 3_98	Detected; Clear Peak
14	+	471.0995	471.1005	3.69	2.06E+05	1.00	2.12	1998	3M 3_98	Detected; Clear Peak
14	+	521.0963	521.0981	4.19	2.39E+05	1.80	3.45	1998	3M 3_98	Detected; Clear Peak
14	+	571.0931	571.0952	4.58	4.24E+05	2.10	3.68	1998	3M 3_98	Detected; Clear Peak
15	+	515.0904	515.0901	3.40	5.90E+04	-0.30	-0.58	1998	3M 3_98	Detected; Clear Peak
15	+	565.0872	565.0866	3.92	3.87E+04	-0.60	-1.06	1998	3M 3_98	Detected; Clear Peak
15	+	615.0829	615.0831	4.32	1.39E+05	0.20	0.33	1998	3M 3_98	Detected; Clear Peak
16	+	393.0714	393.0714	3.01	1.40E+04	0.00	0.00	1998	3M 3_98	Detected; Clear Peak
16	+	443.0682	443.0688	3.74	2.60E+04	0.60	1.35	1998	3M 3_98	Detected; Clear Peak
16	+	493.0650	493.0659	4.24	1.78E+04	0.90	1.83	1998	3M 3_98	Detected; Clear Peak
16	+	543.0618	543.0620	4.63	3.39E+04	0.20	0.37	1998	3M 3_98	Detected; Clear Peak
17	+	450.0733	450.0783	4.13	1.26E+04	5.00	11.11	1998	3M 3_98	Detected; Clear Peak

Class	+/-	Theoretical m/z	Spectrum Observed m/z	Retention Time (min)	MS Response of the highest peak	Spectrum Error (mDa)	Spectrum Error (ppm)	Yr	Chemical	Comments
17	+	550.0680	550.0725	4.87	5.14E+02	4.50	8.18	1998	3M 3_98	Potential Detection with clear peak but other close peaks
19	+	523.0719	523.0769	4.08	2.95E+04	5.00	9.56	1998	3M 3_98	Detected; Clear Peak
19	+	623.0650	623.0686	4.81	7.65E+02	2.60	4.17	1998	3M 3_98	Potential Detection with clear peak but other close peaks
19	+	723.0592	723.0461	5.38	1.99E+02	-13.10	-18.12	1998	3M 3_98	Detected; Clear Peak
28	+	567.0876	567.0852	3.93	1.26E+03	-2.40	-4.23	1998	3M 3_98	Detected; Clear Peak
28	+	617.0844	617.0797	4.32	4.63E+03	-4.70	-7.62	1998	3M 3_98	Detected; Clear Peak
31	+	621.0757	621.0878	4.95	1.92E+03	12.10	19.48	1998	3M 3_98	Potential Detection with clear peak but other close peaks
32	+	515.0751	515.0782	4.87	1.20E+03	3.10	6.02	1998	3M 3_98	Potential Detection with clear peak but other close peaks
32	+	615.0687	615.0777	0.57	1.83E+03	9.00	14.63	1998	3M 3_98	Potential Detection with clear peak but other close peaks
32	+	665.0655	665.0638	0.59	2.09E+02	-1.70	-2.56	1998	3M 3_98	Potential Detection with clear peak but other close peaks
34	+	451.0768	451.0711	4.13	3.89E+03	-5.70	-12.64	1998	3M 3_98	Detected; Clear Peak
34	+	501.0736	501.0702	4.53	1.15E+04	-3.40	-6.79	1998	3M 3_98	Detected; Clear Peak
34	+	551.0736	551.0817	4.87	2.69E+02	8.10	14.70	1998	3M 3_98	Potential Detection with clear peak but still too much noise
34	+	601.0730	601.0684	5.13	1.90E+02	-4.60	-7.65	1998	3M 3_98	Potential Detection with clear peak but still too much noise
37	+	479.0493	479.0582	3.77	5.01E+02	8.90	18.58	1998	3M 3_98	Potential Detection with clear peak but still too much noise
3M	+	385.0632	385.0625	3.78	2.07E+06	-0.70	-1.82	1998	3M 3_98	Detected; Clear Peak
3M	+	435.0600	435.0596	4.30	2.18E+06	-0.40	-0.92	1998	3M 3_98	Detected; Clear Peak
3M	+	457.0844	457.0846	3.78	2.45E+06	0.20	0.44	1998	3M 3_98	Detected; Clear Peak
3M	+	485.0568	485.0569	4.69	8.78E+06	0.10	0.21	1998	3M 3_98	Detected; Clear Peak
3M	+	507.0812	507.0817	4.26	3.05E+06	0.50	0.99	1998	3M 3_98	Detected; Clear Peak
3M	+	557.0780	557.0781	4.64	9.44E+06	0.10	0.18	1998	3M 3_98	Detected; Clear Peak
3M	+	579.1023	579.1024	3.86	2.60E+05	0.10	0.17	1998	3M 3_98	Detected; Clear Peak
3M	+	629.0991	629.0995	4.27	8.54E+05	0.40	0.64	1998	3M 3_98	Detected; Clear Peak
Buckeye	+	614.0799	614.0883	0.63	2.94E+02	8.40	13.68	1998	3M 3_98	Potential Detection with clear peak but other close peaks
Chemguard	+	581.1144	581.1083	3.93	1.78E+03	-6.10	-10.50	1998	3M 3_98	Detected; Clear Peak
Fireade	+	571.0936	571.0939	4.58	4.24E+05	0.30	0.53	1998	3M 3_98	Detected; Clear Peak
Fireade	+	671.0872	671.0850	5.16	5.82E+03	-2.20	-3.28	1998	3M 3_98	Detected; Clear Peak
National Foam	+	571.0936	571.0941	4.58	4.24E+04	0.50	0.88	1998	3M 3_98	Detected; Clear Peak
National Foam	+	671.0872	671.0857	5.16	5.82E+03	-1.50	-2.24	1998	3M 3_98	Detected; Clear Peak
21	-	356.9119	356.9189	3.79	1.41E+02	7.00	19.61	1998	3M 3_98	Potential Detection with clear peak but still too much noise
21	-	456.9055	456.9109	4.58	1.21E+02	5.40	11.82	1998	3M 3_98	Potential Detection with clear peak but still too much noise
21	-	506.9023	506.9012	4.87	5.49E+02	-1.10	-2.17	1998	3M 3_98	Detected; Clear Peak
21	-	556.8991	556.9037	5.10	6.89E+02	4.60	8.26	1998	3M 3_98	Potential Detection with clear peak but other close peaks
21	-	656.8927	656.8849	5.50	2.40E+03	-7.80	-11.87	1998	3M 3_98	Potential Detection with clear peak but other close peaks
23	-	310.9430	310.9404	3.57	3.72E+02	-2.60	-8.36	1998	3M 3_98	Potential Detection with clear peak but other close peaks
23	-	360.9398	360.9380	4.05	3.94E+03	-1.80	-4.99	1998	3M 3_98	Potential Detection with clear peak but other close peaks
23	-	410.9366	410.9407	4.46	1.69E+03	4.10	9.98	1998	3M 3_98	Potential Detection with clear peak but other close peaks
23	-	460.9334	460.9323	4.76	6.92E+04	-1.10	-2.39	1998	3M 3_98	Potential Detection with clear peak but other close peaks

Class	+/-	Theoretical m/z	Spectrum Observed m/z	Retention Time (min)	MS Response of the highest peak	Spectrum Error (mDa)	Spectrum Error (ppm)	Yr	Chemical	Comments
23	-	560.9270	560.9266	5.10	5.75E+02	-0.40	-0.71	1998	3M 3_98	Potential Detection with clear peak but other close peaks
23	-	610.9238	610.9205	5.26	4.87E+02	-3.30	-5.40	1998	3M 3_98	Potential Detection with clear peak but other close peaks
23	-	710.9175	710.9136	5.47	2.06E+02	-3.90	-5.49	1998	3M 3_98	Potential Detection with clear peak but other close peaks
24	-	292.9524	292.9487	3.14	4.76E+02	-3.70	-12.63	1998	3M 3_98	Potential Detection with clear peak but still too much noise
24	-	342.9492	342.9480	3.62	1.58E+03	-1.20	-3.50	1998	3M 3_98	Potential Detection with clear peak but other close peaks
24	-	392.9460	392.9442	4.05	4.17E+03	-1.80	-4.58	1998	3M 3_98	Detected; Clear Peak
24	-	442.9428	442.9421	4.47	7.44E+04	-0.70	-1.58	1998	3M 3_98	Potential Detection with clear peak but other close peaks
25	-	180.9588	180.9610	0.74	1.10E+03	2.20	12.16	1998	3M 3_98	Potential Detection with clear peak but other close peaks
25	-	230.9556	230.9552	1.67	3.77E+03	-0.40	-1.73	1998	3M 3_98	Potential Detection with clear peak but other close peaks
25	-	280.9524	280.9491	2.39	3.26E+03	-3.30	-11.75	1998	3M 3_98	Detected; Clear Peak
25	-	330.9492	330.9485	3.35	7.76E+02	-0.70	-2.12	1998	3M 3_98	Potential Detection with clear peak but other close peaks
25	-	380.9460	380.9435	4.15	1.93E+03	-2.50	-6.56	1998	3M 3_98	Detected; Clear Peak
25	-	480.9396	480.9390	4.67	5.61E+04	-0.60	-1.25	1998	3M 3_98	Potential Detection with clear peak but other close peaks
26	-	462.9491	462.9488	4.69	4.52E+04	-0.30	-0.65	1998	3M 3_98	Detected; Clear Peak
30	-	585.0590	585.0559	5.02	6.82E+02	-3.10	-5.30	1998	3M 3_98	Potential Detection with clear peak but other close peaks
40	-	582.9877	582.9846	4.69	1.94E+02	-3.10	-5.32	1998	3M 3_98	Detected; Clear Peak
3M	-	398.9361	398.9359	4.29	2.09E+06	-0.20	-0.50	1998	3M 3_98	Detected; Clear Peak
3M	-	448.9329	448.9330	4.62	4.34E+05	0.10	0.22	1998	3M 3_98	Detected; Clear Peak
3M	-	498.9297	498.9305	4.90	4.25E+05	0.80	1.60	1998	3M 3_98	Detected; Clear Peak
Angus	-	586.0391	586.0374	5.26	1.54E+02	-1.70	-2.90	1998	3M 3_98	Potential Detection with clear peak but still too much noise
Ansul	-	586.0391	586.0452	5.26	1.54E+02	6.10	10.41	1998	3M 3_98	Potential Detection with clear peak but still too much noise
Ansul	-	602.0341	602.0264	6.18	1.08E+02	-7.70	-12.79	1998	3M 3_98	Potential Detection with clear peak but still too much noise
Chemguard	-	586.0391	586.0469	5.26	1.54E+02	7.80	13.31	1998	3M 3_98	Potential Detection with clear peak but still too much noise
PFBS	-	298.9424	298.9421	3.27	5.98E+05	-0.30	-1.00	1998	3M 3_98	Detected
PFHxS	-	398.9361	398.9358	4.29	2.15E+06	-0.30	-0.75	1998	3M 3_98	Detected
PFHpS	-	448.9329	448.9326	4.62	4.56E+05	-0.30	-0.67	1998	3M 3_98	Detected
PFOS	-	498.9297	498.9301	4.90	4.37E+06	0.40	0.80	1998	3M 3_98	Detected
PFDS	-	598.9233	598.9217	5.35	8.61E+03	-1.60	-2.67	1998	3M 3_98	Detected
PFHpA	-	362.9691	362.9695	4.23	6.42E+03	0.40	1.10	1998	3M 3_98	Detected
3	+	623.0550	623.0565	5.53	2.46E+03	1.50	2.41	2002	Ansol 9_02	Detected; Clear Peak
4	+	587.0738	587.0742	3.73	4.35E+02	0.40	0.68	2002	Ansol 9_02	Potential Detection with clear peak but still too much noise
12	+	513.0876	513.0932	4.46	2.86E+03	5.60	10.91	2002	Ansol 9_02	Potential Detection with clear peak but other close peaks
14	+	571.0931	571.0927	4.70	2.90E+04	-0.40	-0.70	2002	Ansol 9_02	Detected; Clear Peak
15	+	515.0904	515.0879	4.87	2.47E+03	-2.50	-4.85	2002	Ansol 9_02	Detected; Clear Peak
18	+	378.1100	378.1089	3.85	5.55E+02	-1.10	-2.91	2002	Ansol 9_02	Potential Detection with clear peak but still too much noise
18	+	478.1046	478.1012	4.75	1.75E+03	-3.40	-7.11	2002	Ansol 9_02	Detected; Clear Peak
19	+	523.0719	523.0723	5.09	2.12E+03	0.40	0.76	2002	Ansol 9_02	Detected; Clear Peak
19	+	623.0660	623.0730	5.53	2.46E+03	7.00	11.23	2002	Ansol 9_02	Detected; Clear Peak
Buckeye	+	414.0927	414.0929	4.07	2.66E+04	0.20	0.48	2002	Ansol 9_02	Detected; Clear Peak
Buckeye	+	432.0833	432.0841	4.14	1.00E+05	0.80	1.85	2002	Ansol 9_02	Detected; Clear Peak
Buckeye	+	514.0863	514.0871	4.87	1.18E+04	0.80	1.56	2002	Ansol 9_02	Detected; Clear Peak
Buckeye	+	532.0769	532.0773	4.91	3.88E+04	0.40	0.75	2002	Ansol 9_02	Detected; Clear Peak

Class	+/-	Theoretical m/z	Spectrum Observed m/z	Retention Time (min)	MS Response of the highest peak	Spectrum Error (mDa)	Spectrum Error (ppm)	Yr	Chemical	Comments
Fireade	+	571.0936	571.0919	4.70	2.90E+04	-1.70	-2.98	2002	Ansol 9_02	Detected; Clear Peak
Fireade	+	671.0872	671.0989	5.27	8.46E+02	11.70	17.43	2002	Ansol 9_02	Potential Detection with clear peak but still too much noise
National Foam	+	513.0881	513.0953	4.46	2.86E+03	7.20	14.03	2002	Ansol 9_02	Potential Detection with clear peak but other close peaks
National Foam	+	571.0936	571.0919	4.70	2.90E+04	-1.70	-2.98	2002	Ansol 9_02	Detected; Clear Peak
National Foam	+	671.0872	671.0851	5.27	8.46E+02	-2.10	-3.13	2002	Ansol 9_02	Potential Detection with clear peak but still too much noise
Angus	-	586.0391	586.0397	5.13	1.60E+06	0.60	1.02	2002	Ansol 9_02	Detected; Clear Peak
Angus	-	602.0341	602.0342	4.61	7.34E+04	0.10	0.17	2002	Ansol 9_02	Detected; Clear Peak
Ansul	-	586.0391	586.0392	5.13	1.60E+06	0.10	0.17	2002	Ansol 9_02	Detected; Clear Peak
Ansul	-	602.0341	602.0342	4.61	7.34E+04	0.10	0.17	2002	Ansol 9_02	Detected; Clear Peak
Ansul	-	686.0328	686.0231	5.51	7.25E+03	-9.70	-14.14	2002	Ansol 9_02	Detected; Clear Peak
Chemguard	-	586.0391	586.0401	5.13	1.60E+06	1.00	1.71	2002	Ansol 9_02	Detected; Clear Peak

3M 5_79 – Mass Spectrums and Chromatographs

Figure A1: Class 2 of 3M 5_79 - Positive

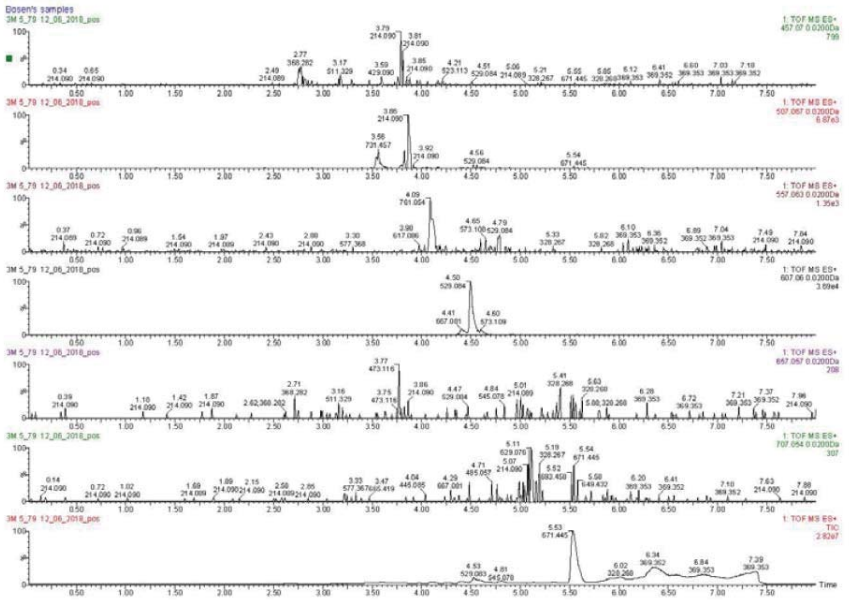

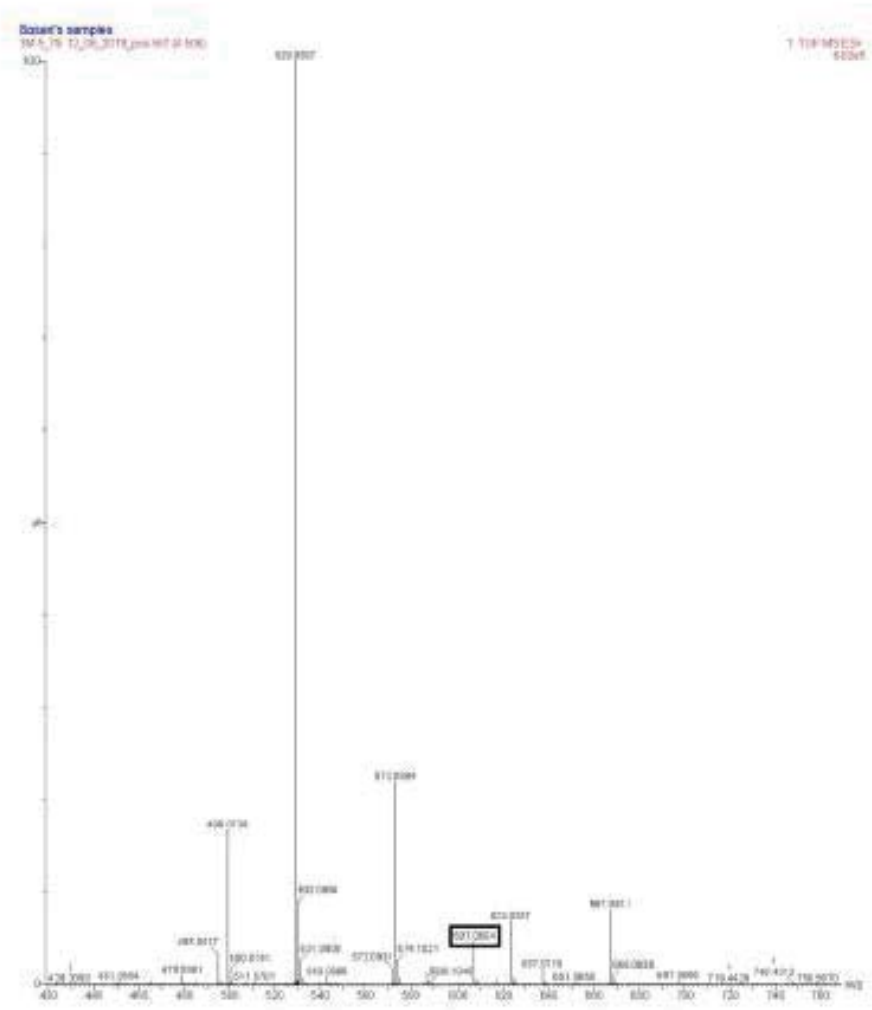

Mass value is found 607.0604 m/z

Figure A2: Class 3 of 3M 5_79 - Positive

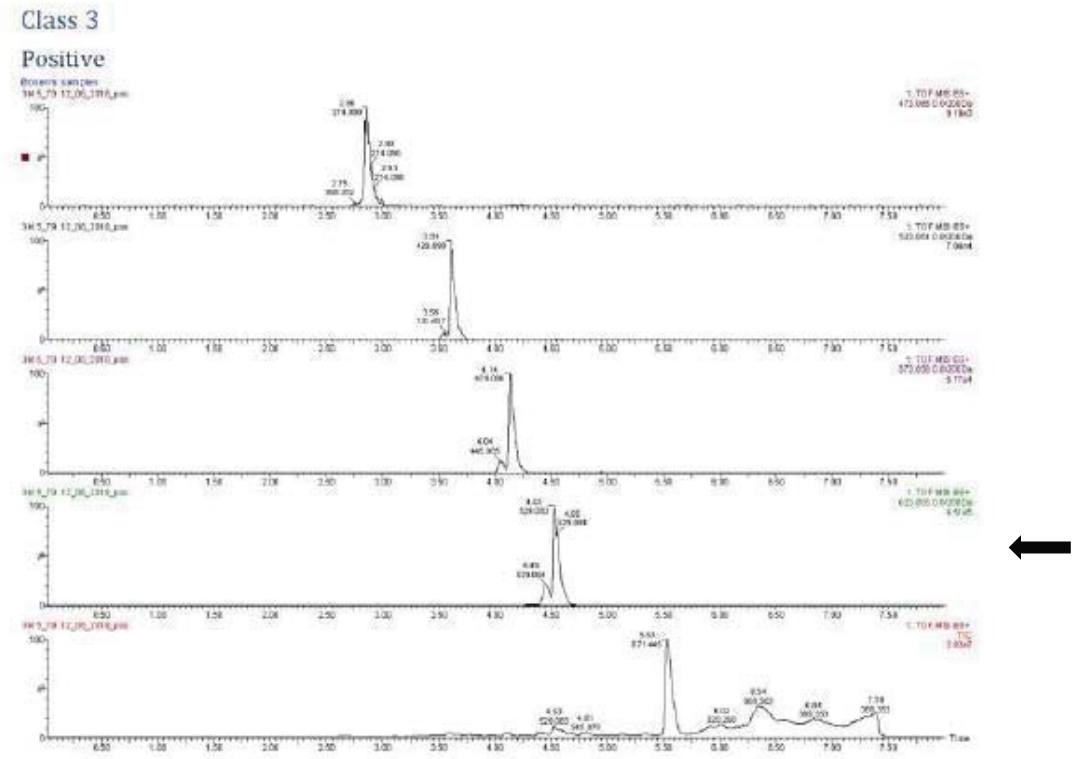

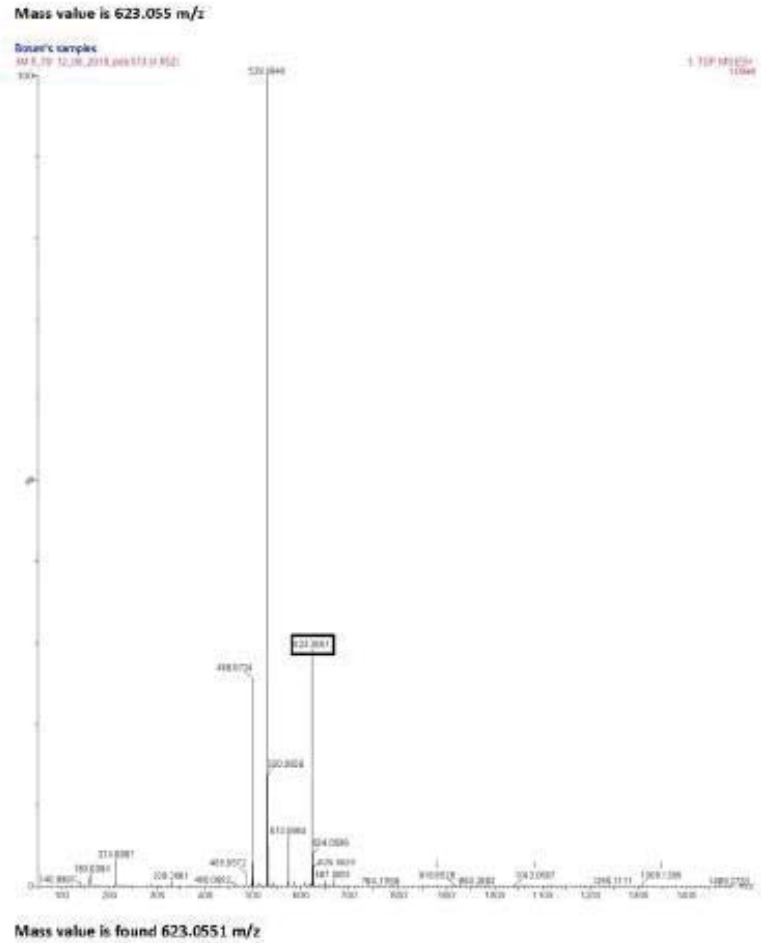

Figure A3: Class 4 of 3M 5_79 - Positive

Class 4

Positive

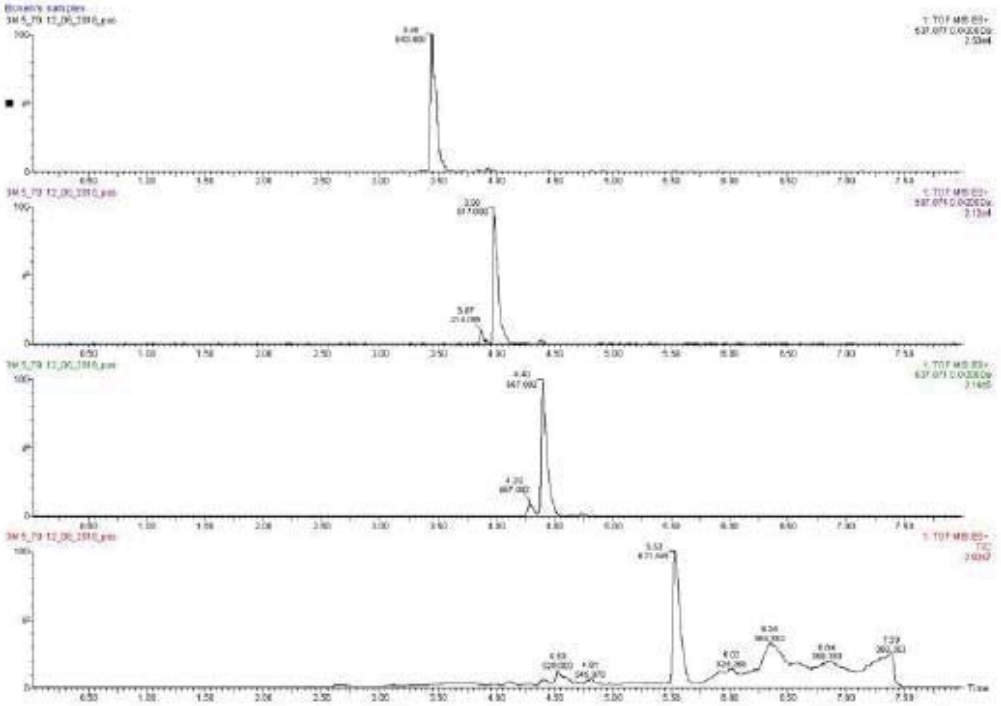

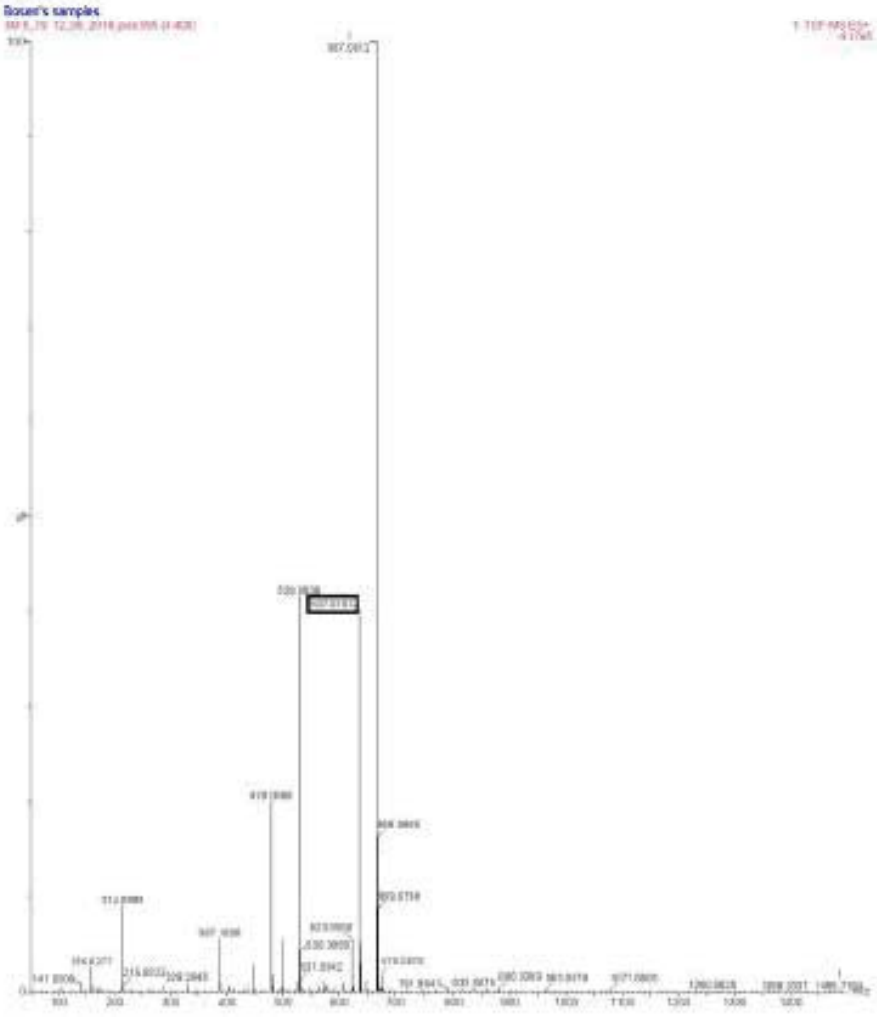

Mass value is found 637.070 m/z

Figure A4: Class 5 of 3M 5_79 - Positive

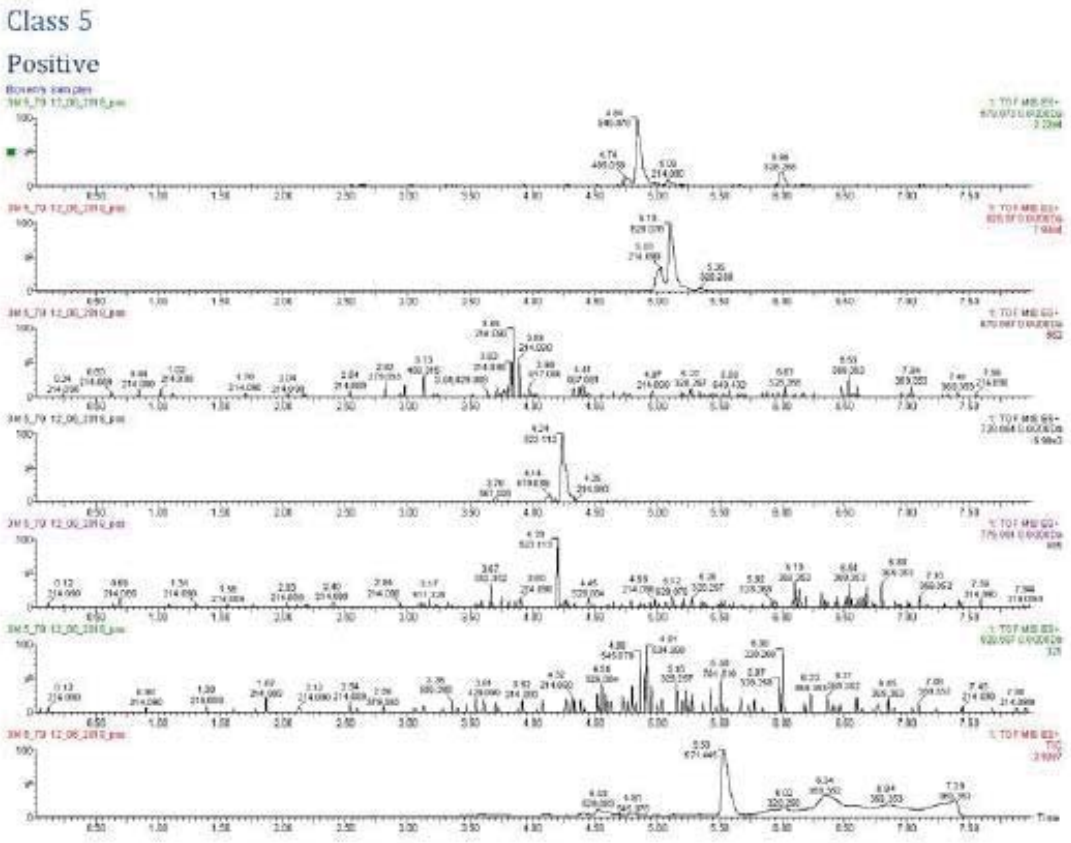

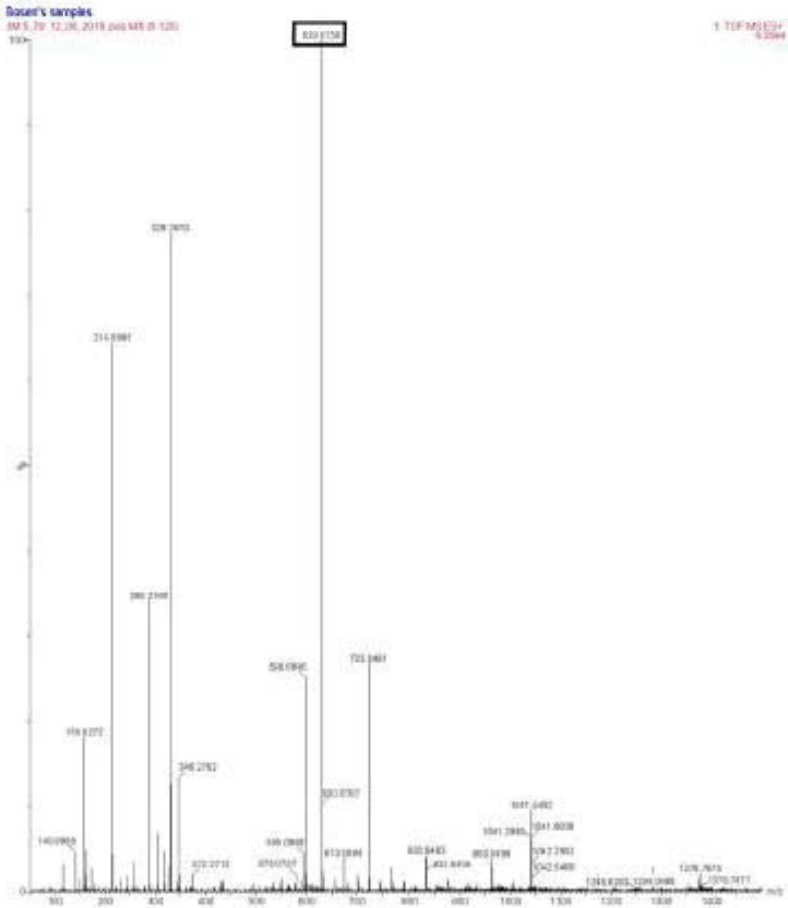

Mass value is found 629.0758 m/z

Figure A5: Class 9 of 3M 5_79 - Positive

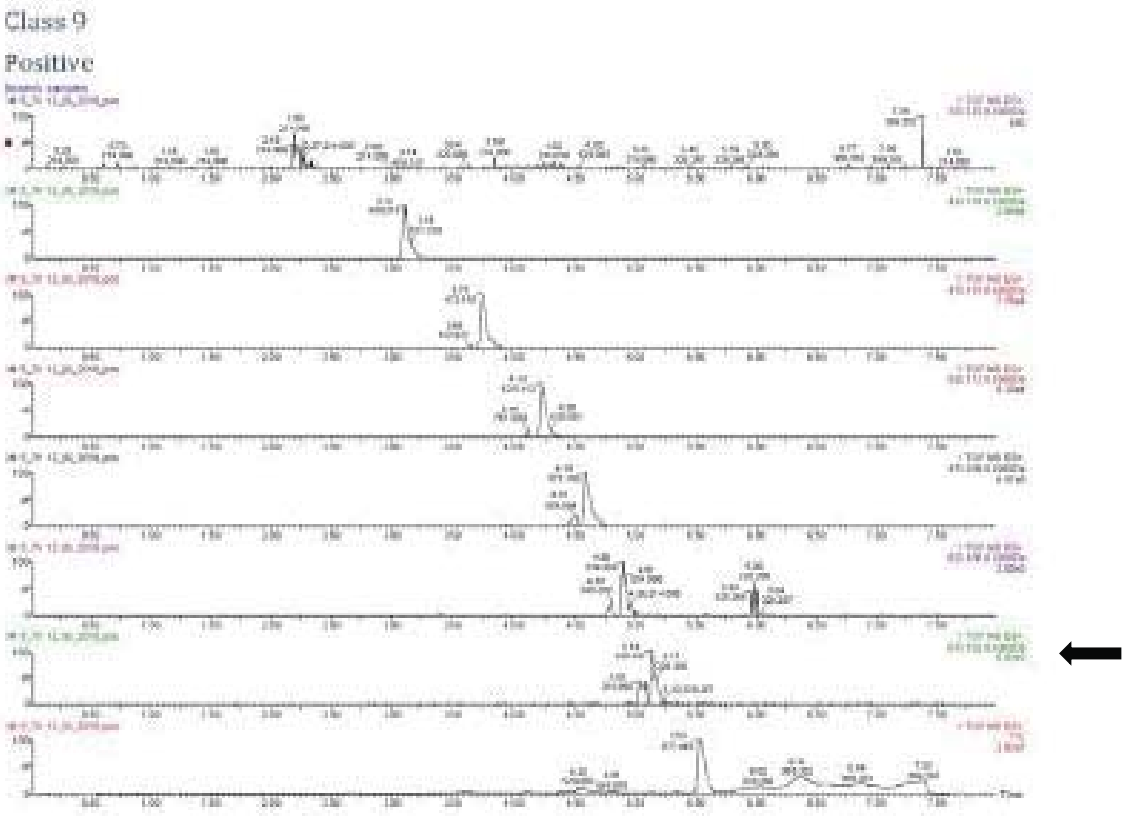

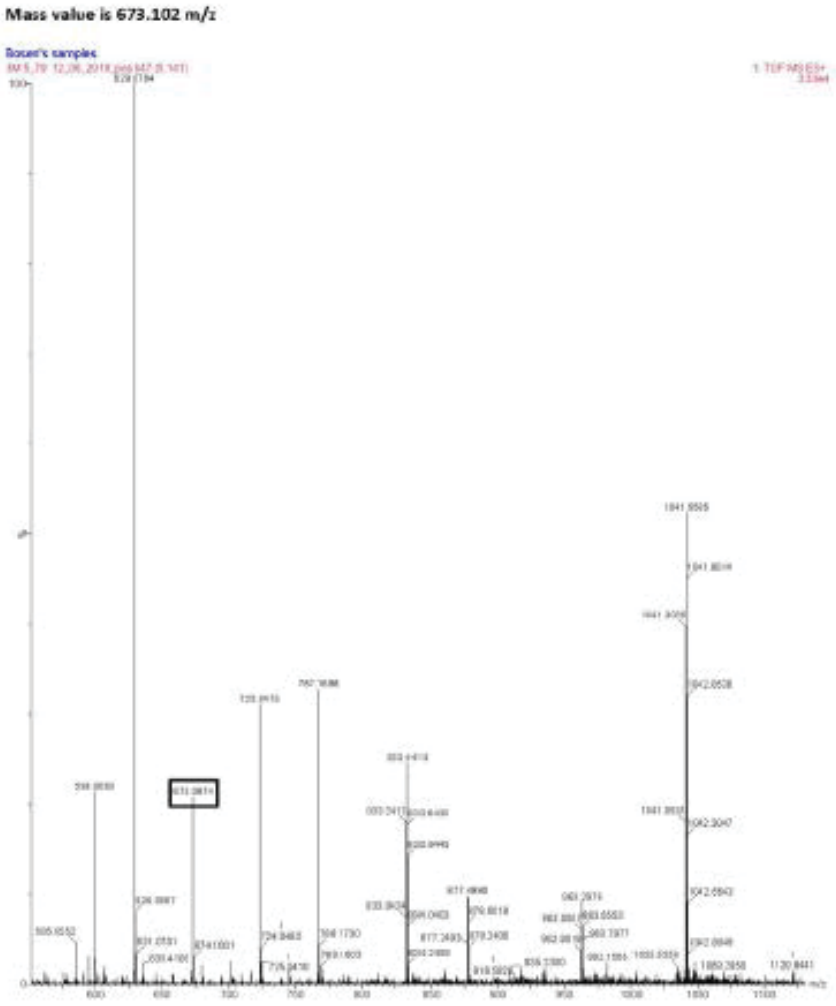

Figure A6: Class 10 of 3M 5_79 - Positive

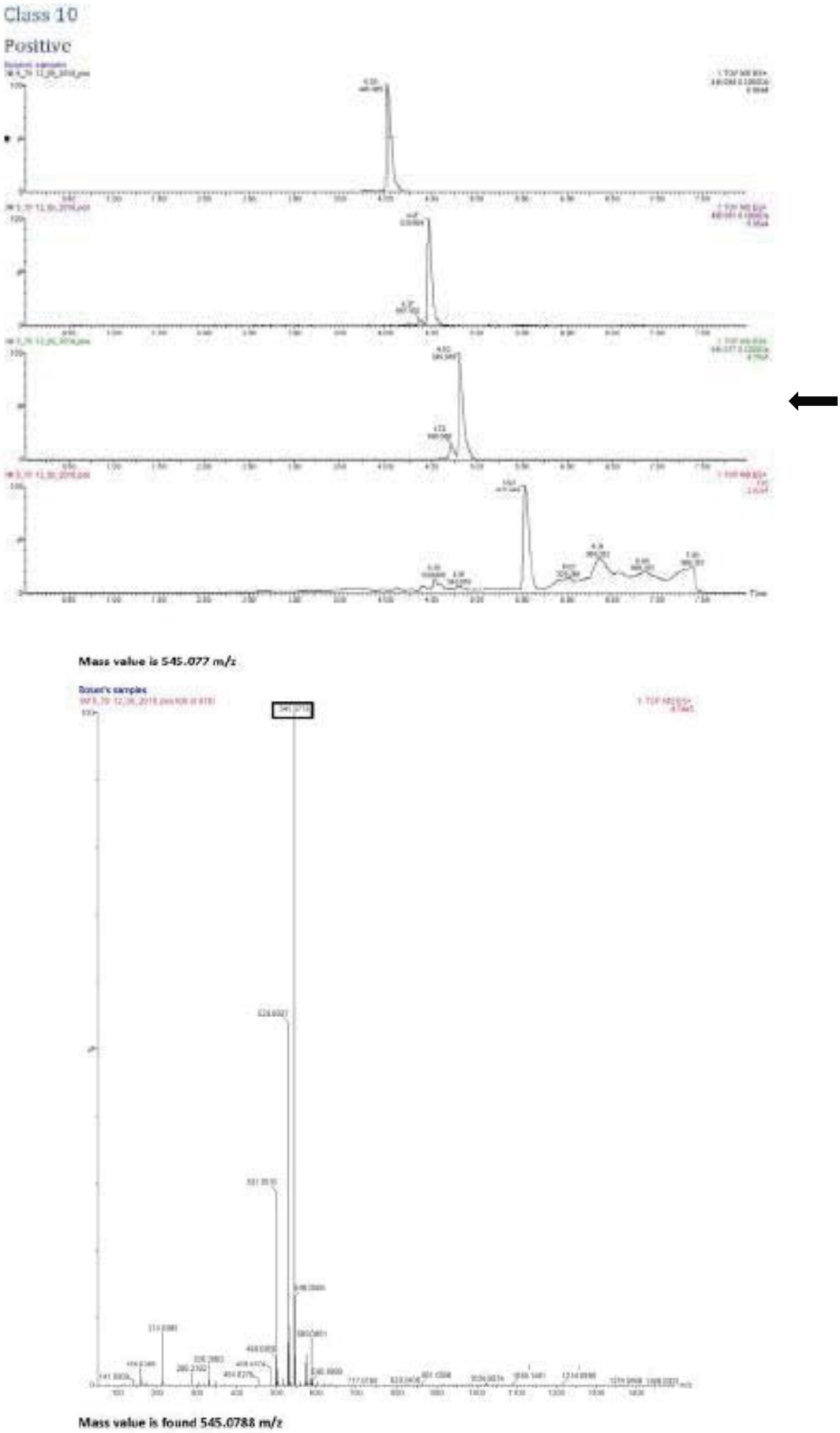

Figure A7: Class 11 of 3M 5_79 - Positive

Class 11

Positive

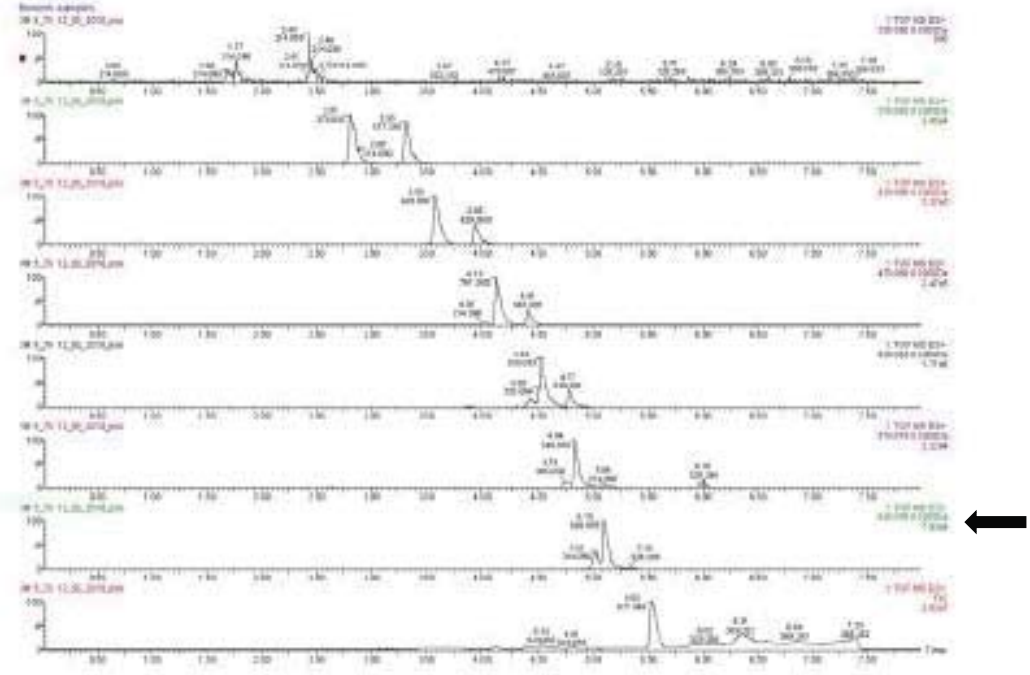

Mass value is 629.076 m/z

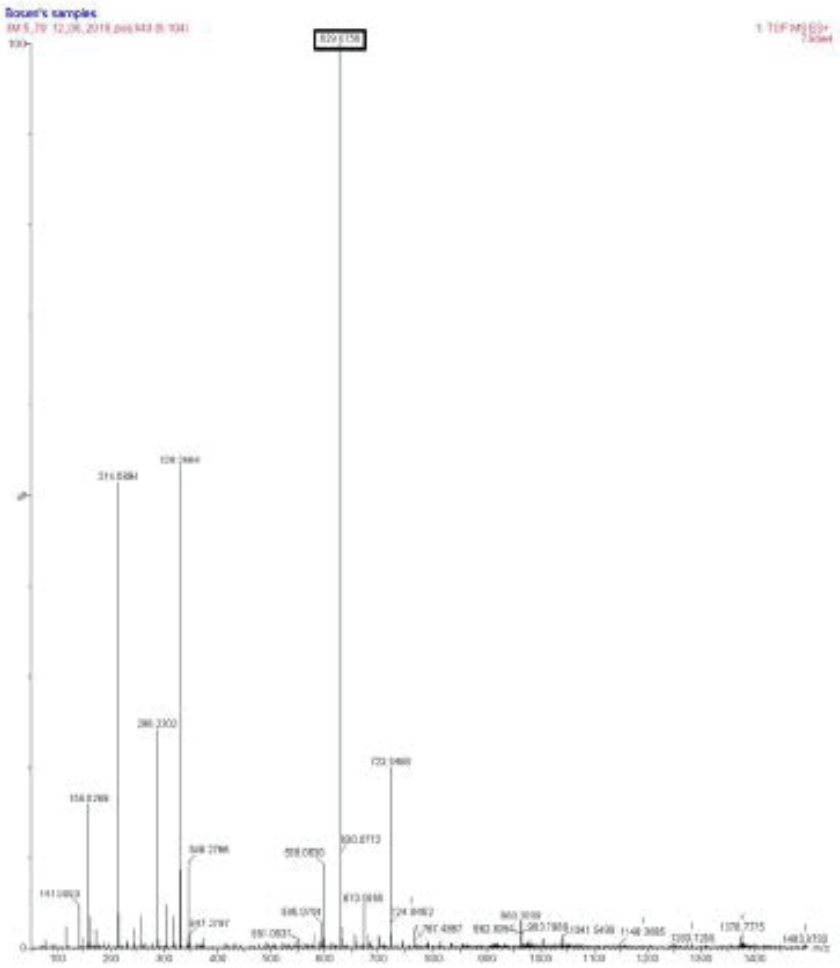

Mass value is found 629.0756 m/z

Figure A8: Class 13 of 3M 5_79 - Positive

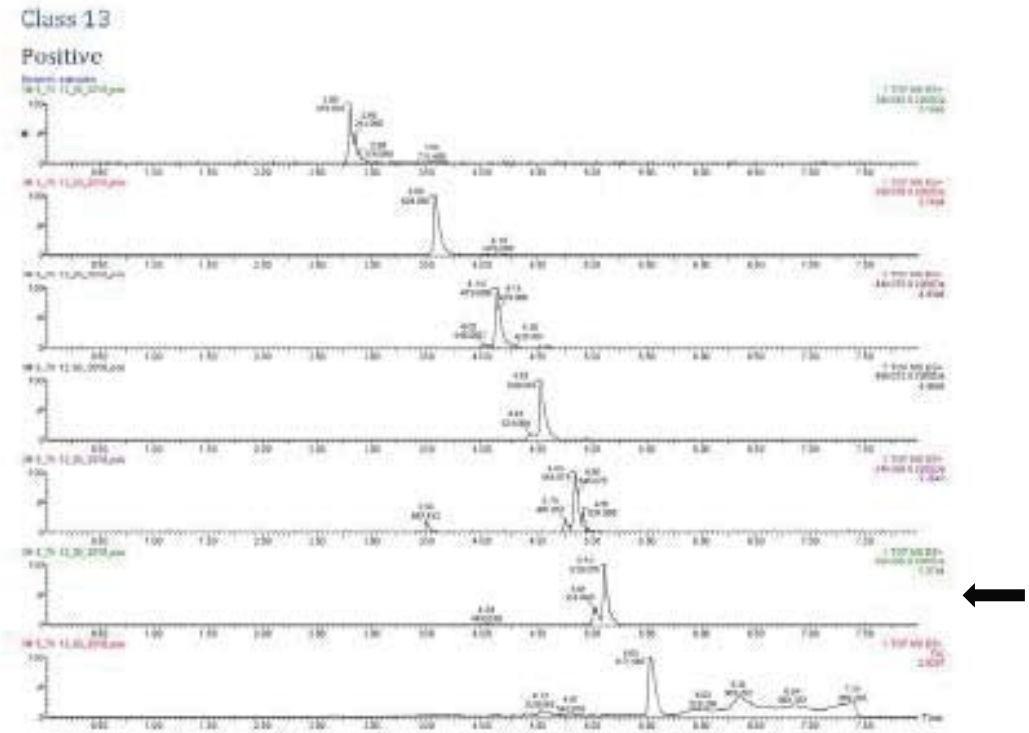

Mass value is 599.066 m/z

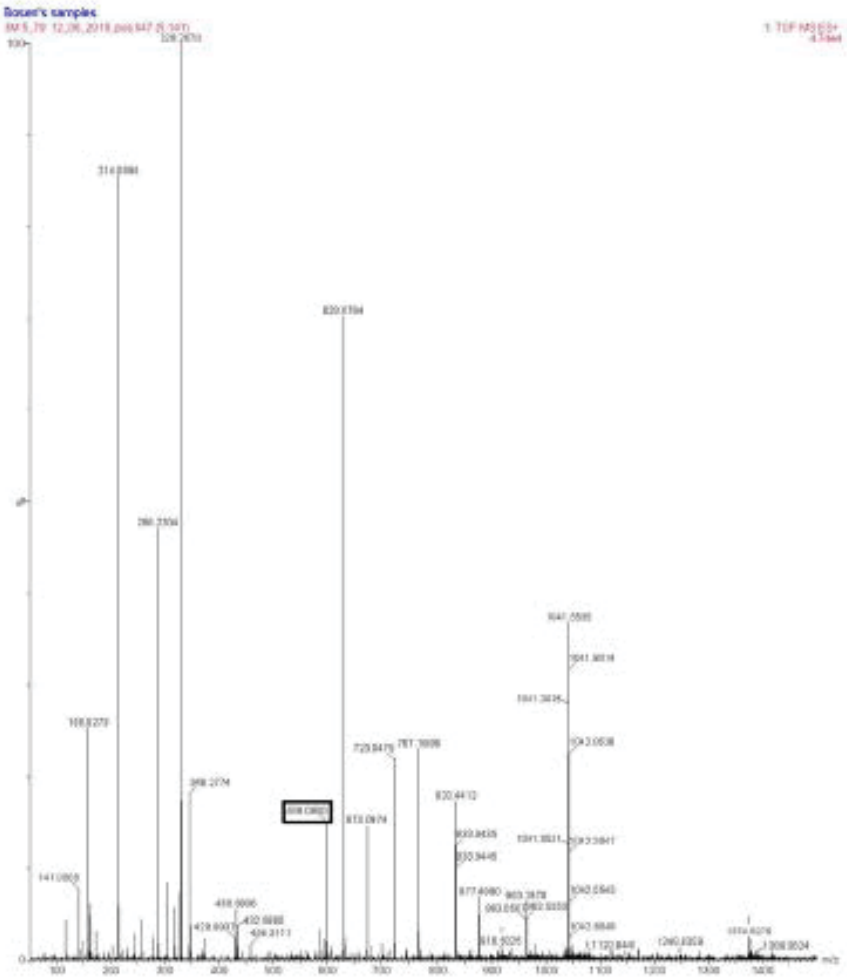

Mass value is found 599.0660 m/z

Figure A9: Class 19 of 3M 5_79 - Positive

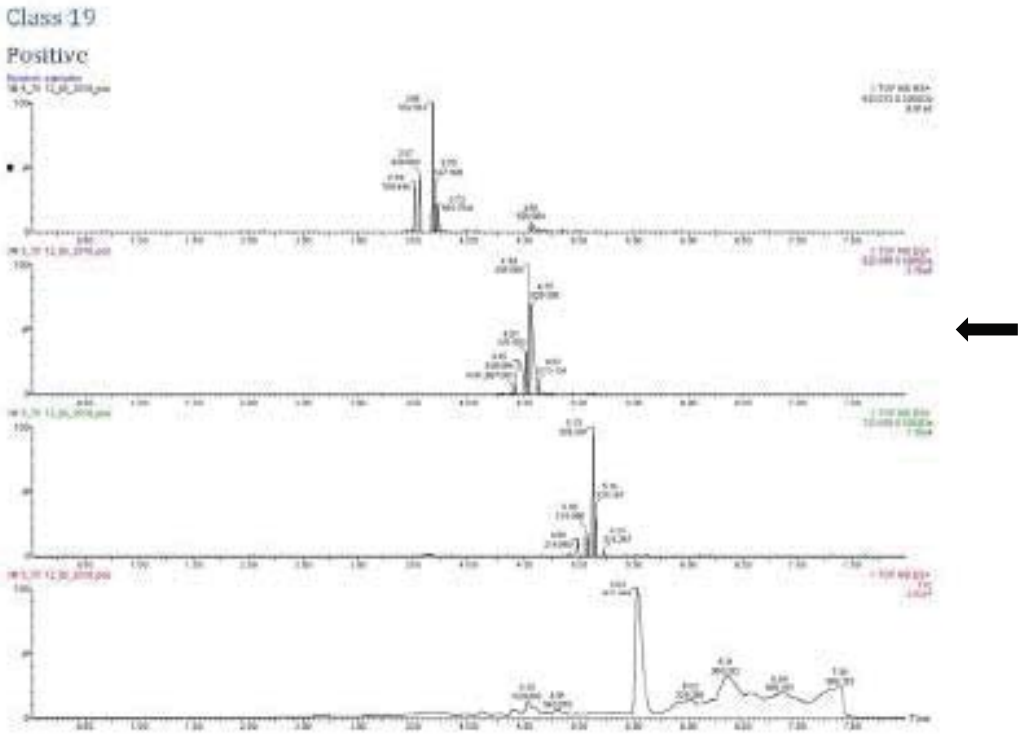

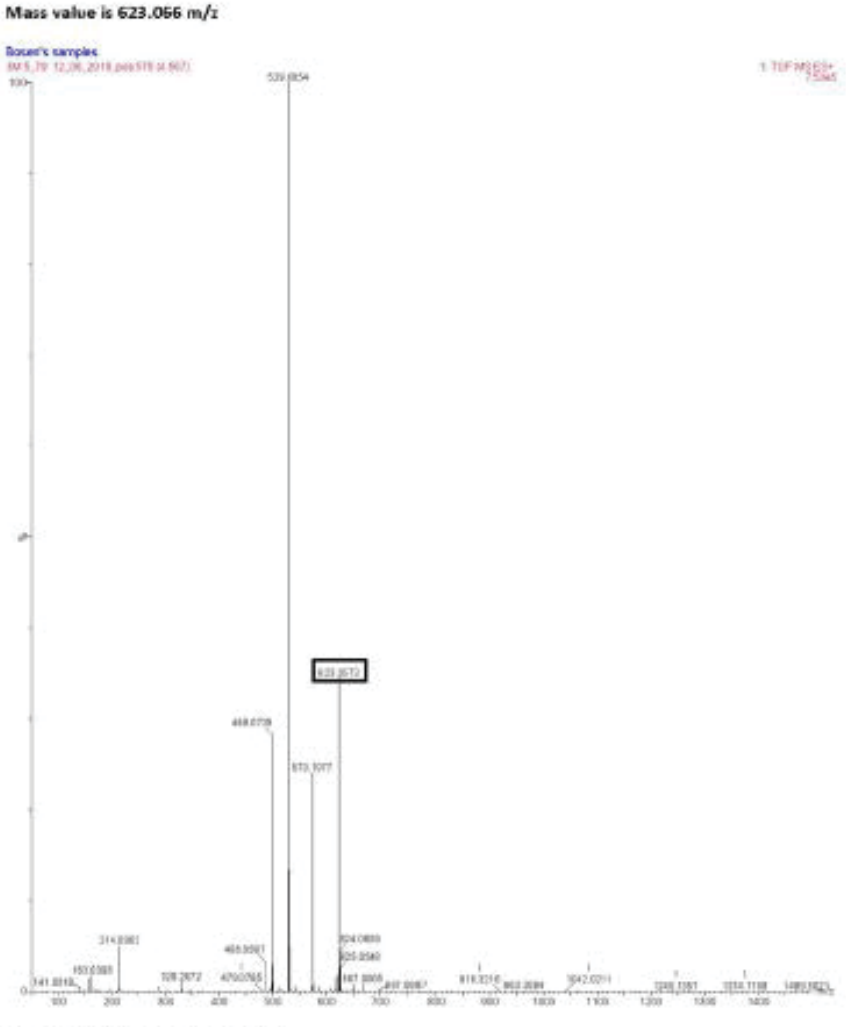

Figure A10: Class 28 of 3M 5_79 - Positive

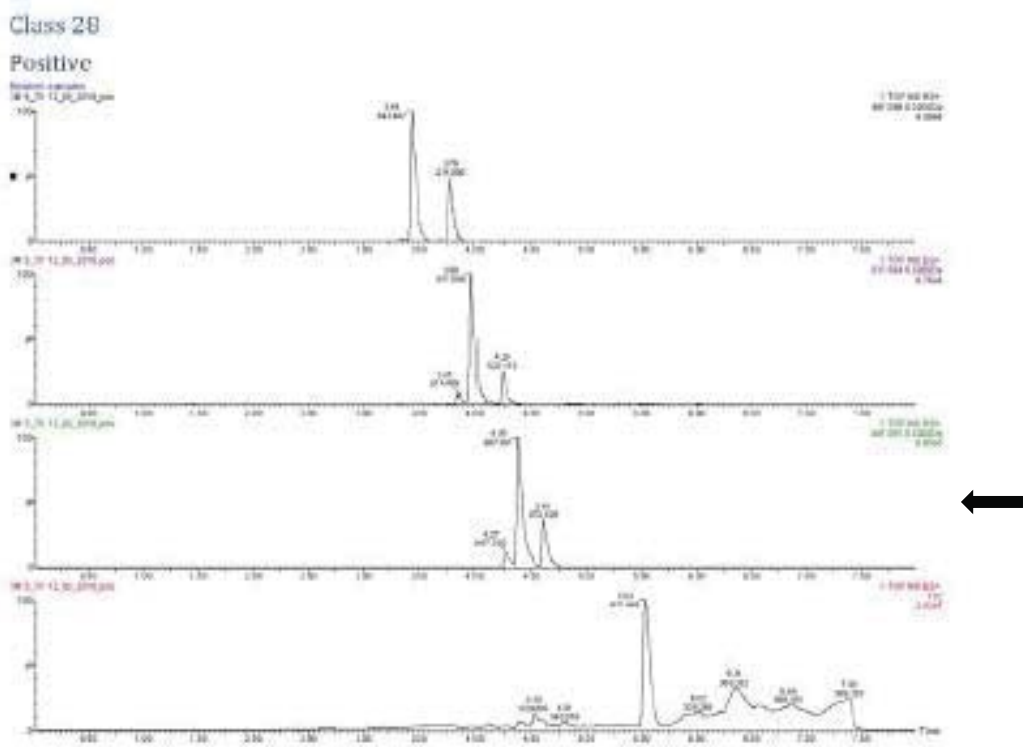

Mass value is 667.081 m/z

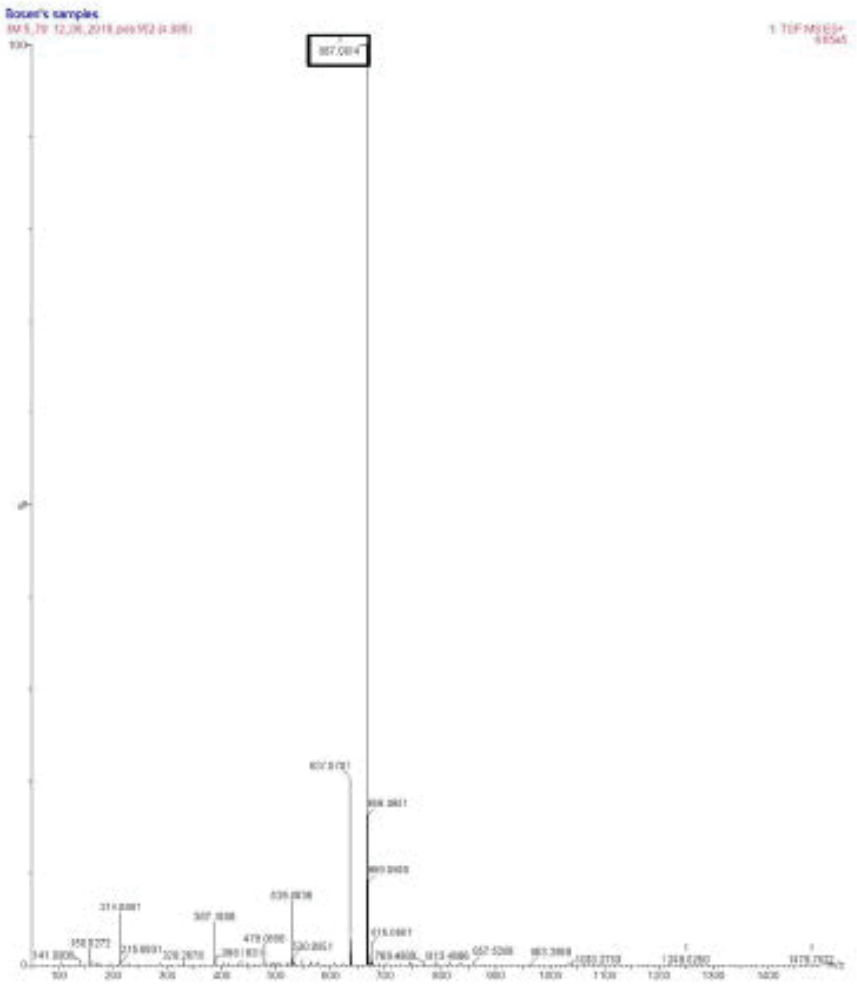

Mass value is 667.0814 m/z

Figure A11: Class 29 of 3M 5_79 - Positive

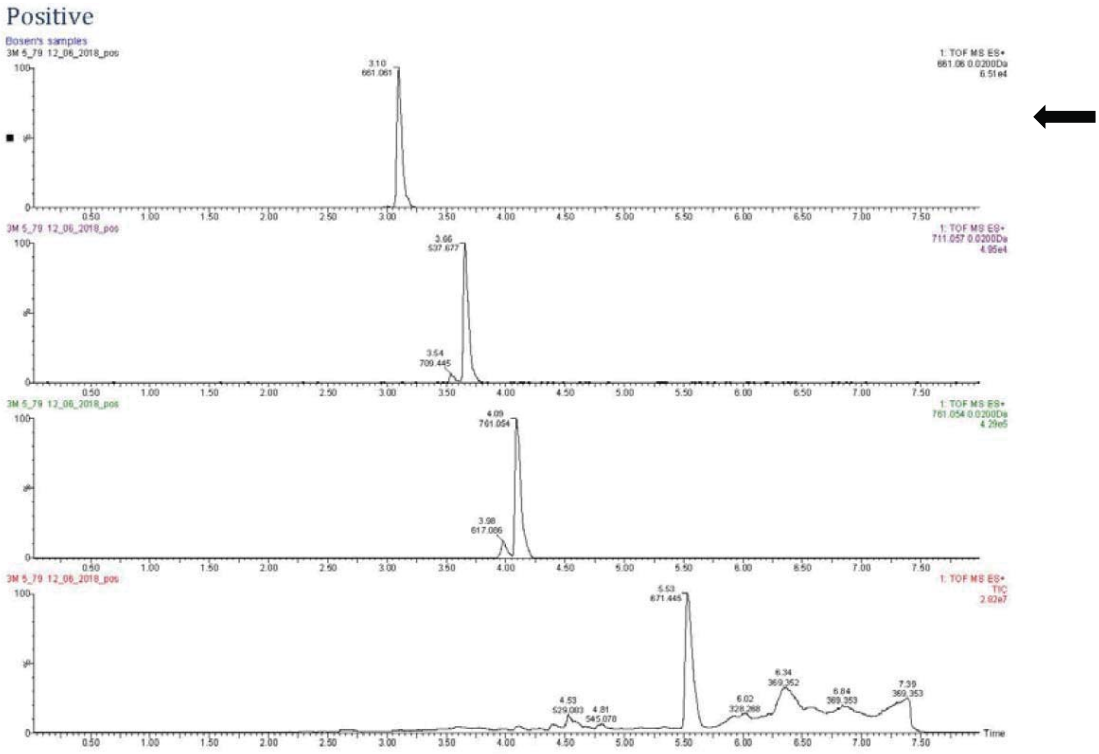

Mass value is 661.06 m/z

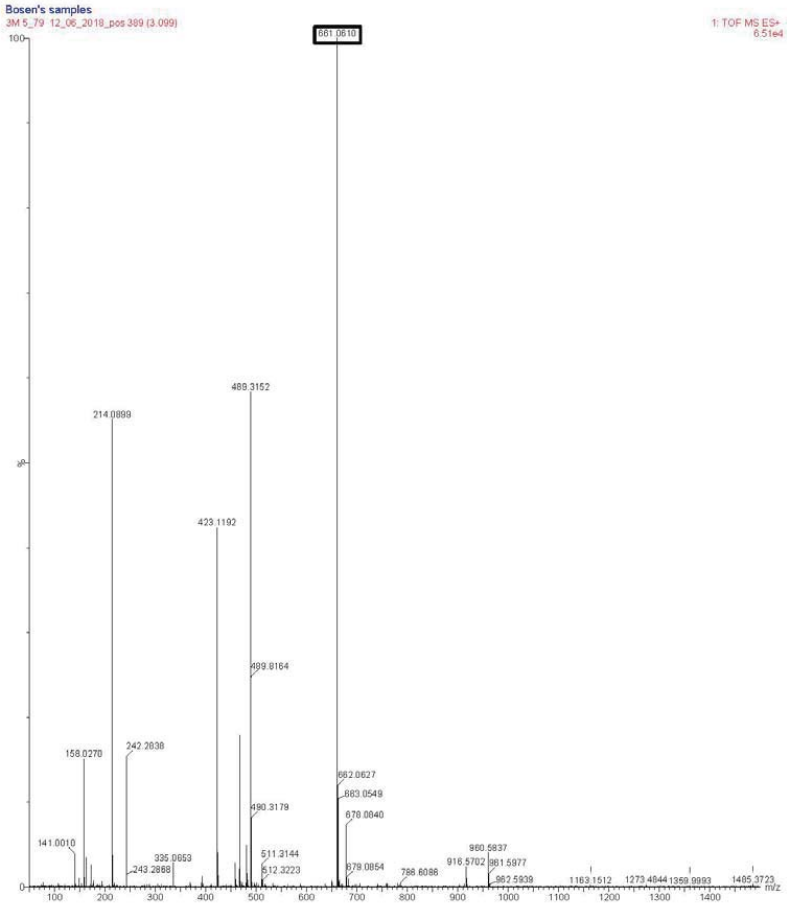

Mass value is found 661.0610 m/z

Figure A12: Class 31 of 3M 5_79 - Positive

Class 31

Positive

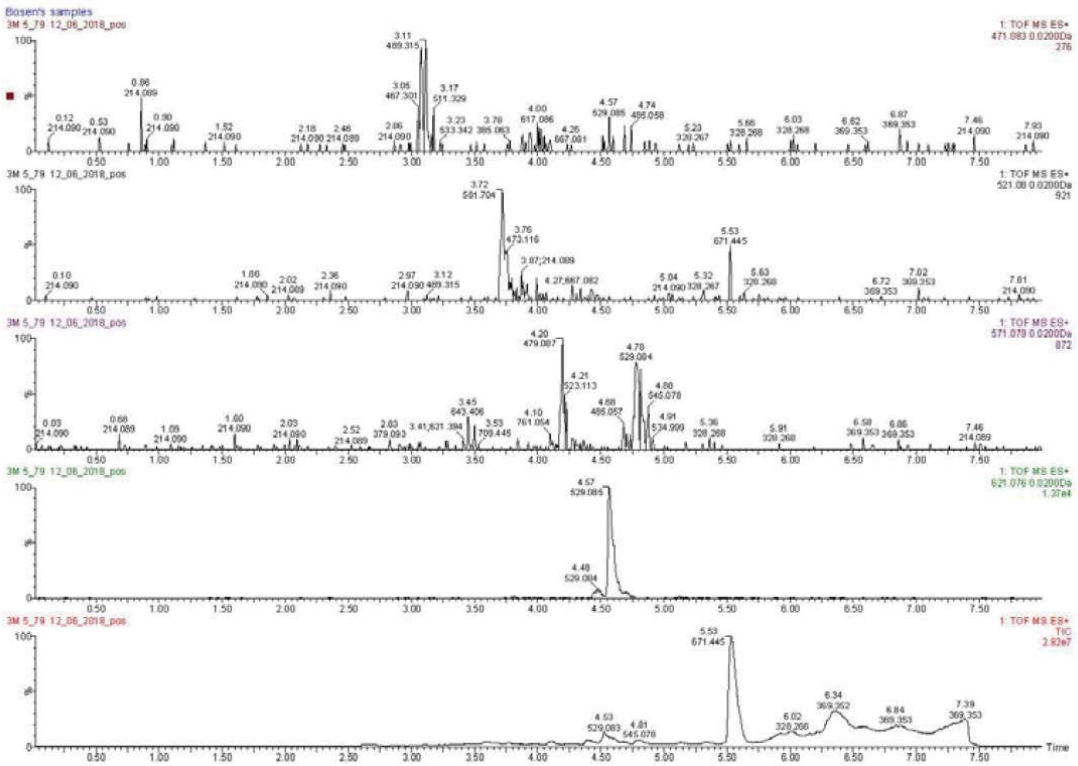

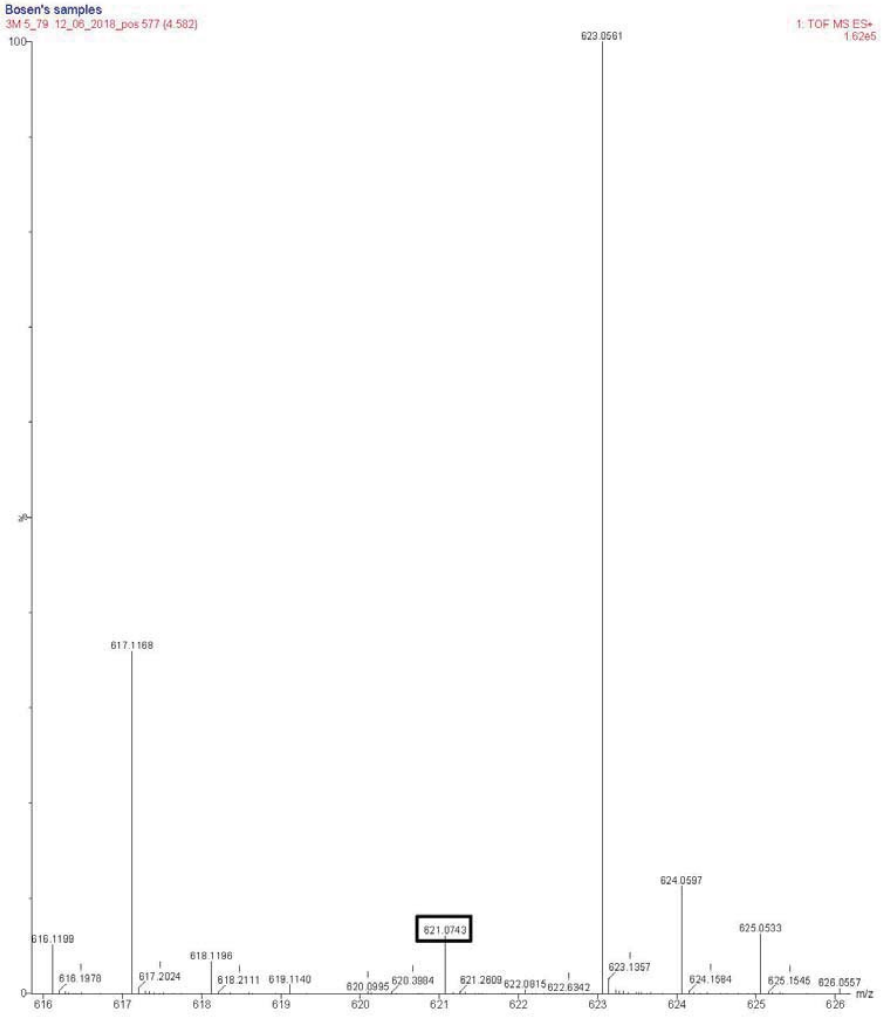

Mass value is 621.0743 m/z

Figure A13: Class 32 of 3M 5_79 - Positive

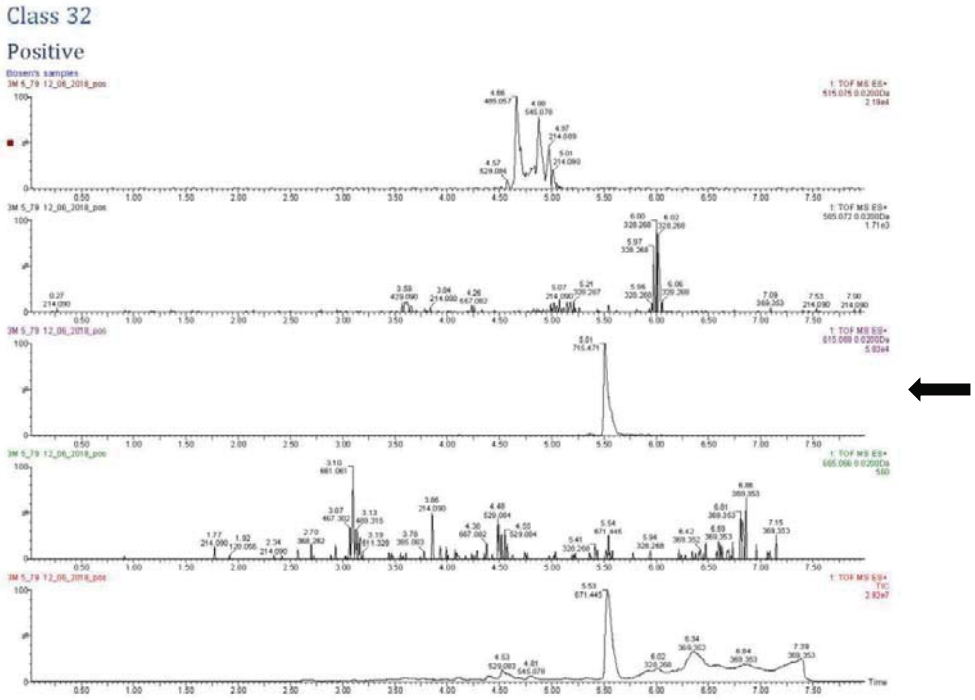

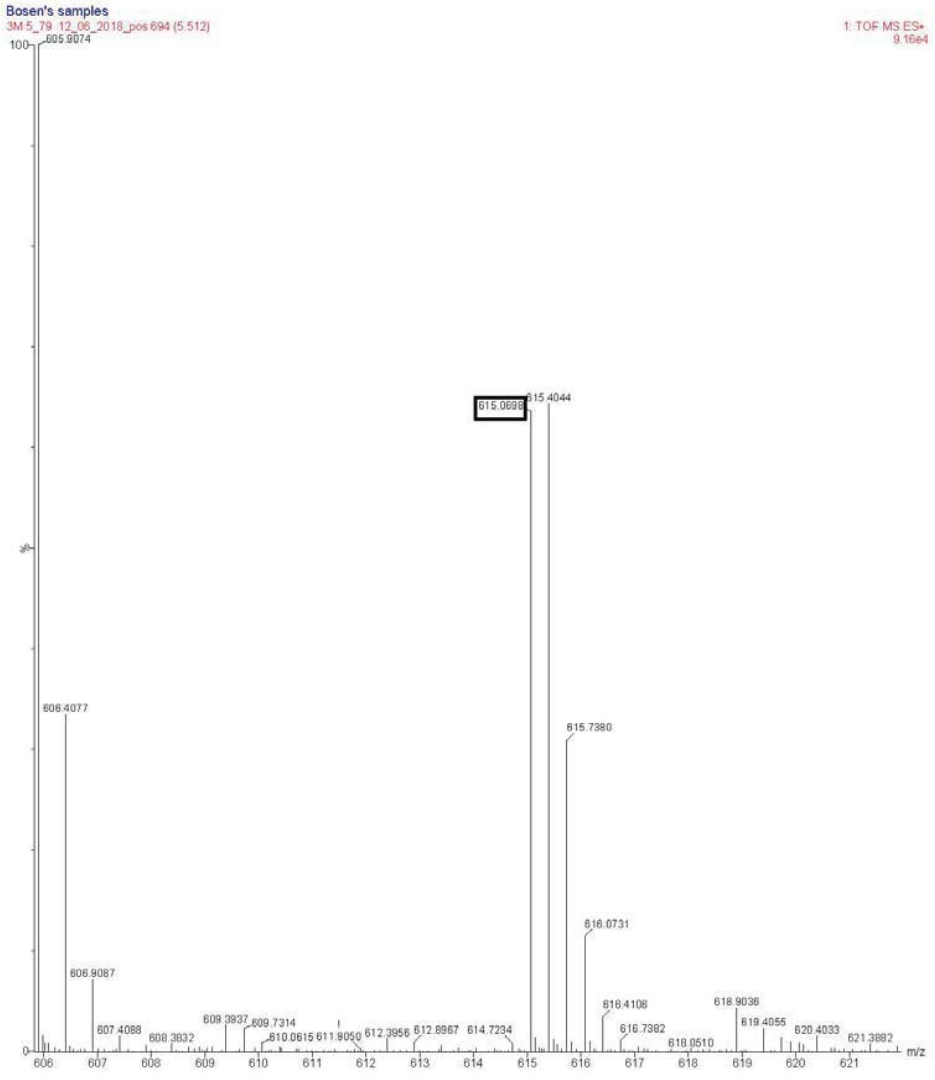

Mass value is found 615.0698 m/z

Figure A14: Class 33 of 3M 5_79 - Positive

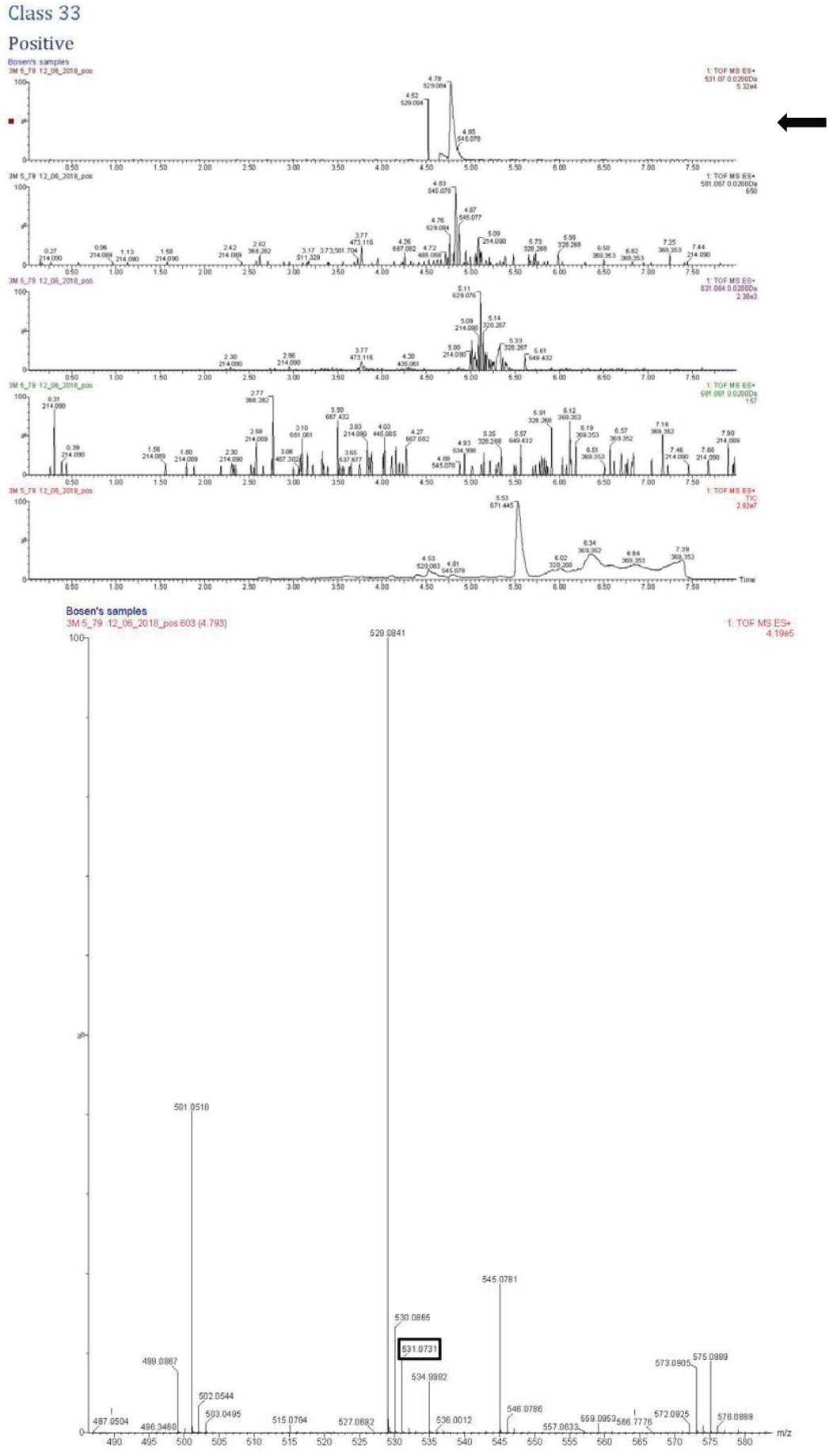

Mass value is 531.0731 m/z

Figure A15: Class 34 of 3M 5_79 - Positive

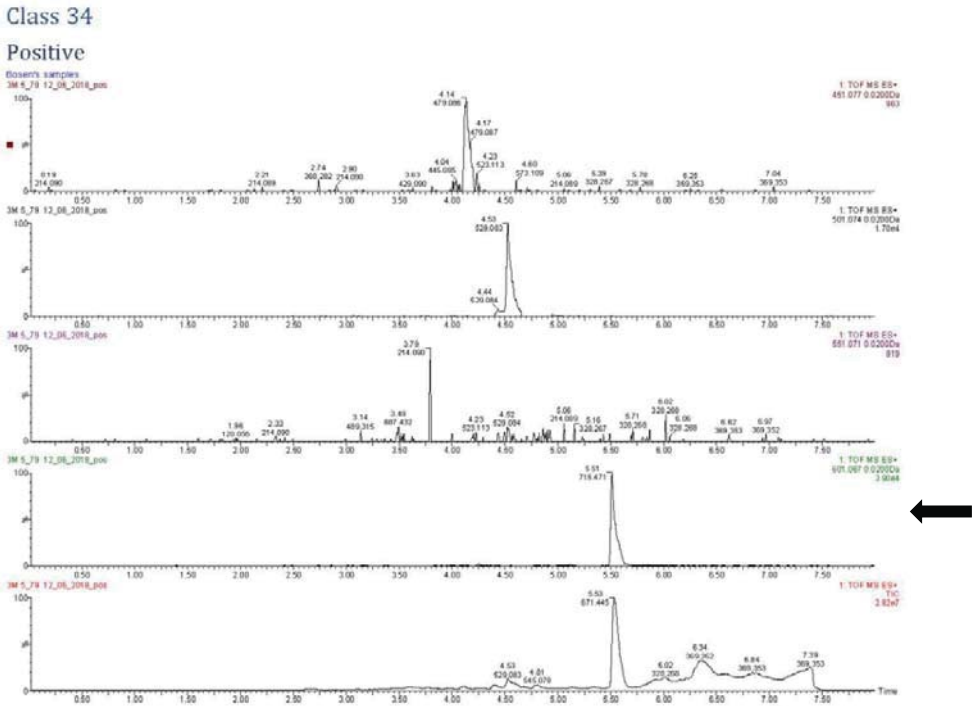

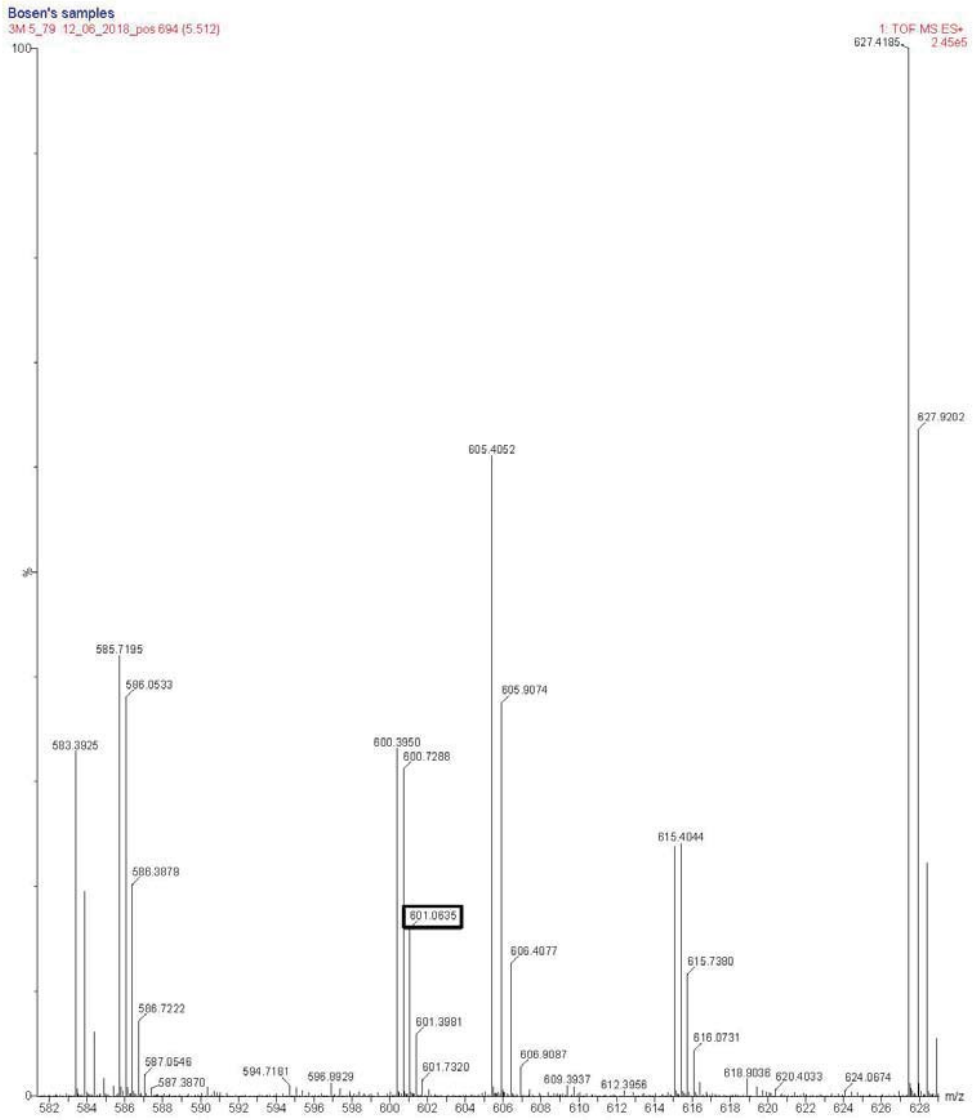

Mass value is found 601.0635 m/z

Figure A16: Class 1 of 3M 5_79 - Negative

3M 5_79

Class 1

Negative

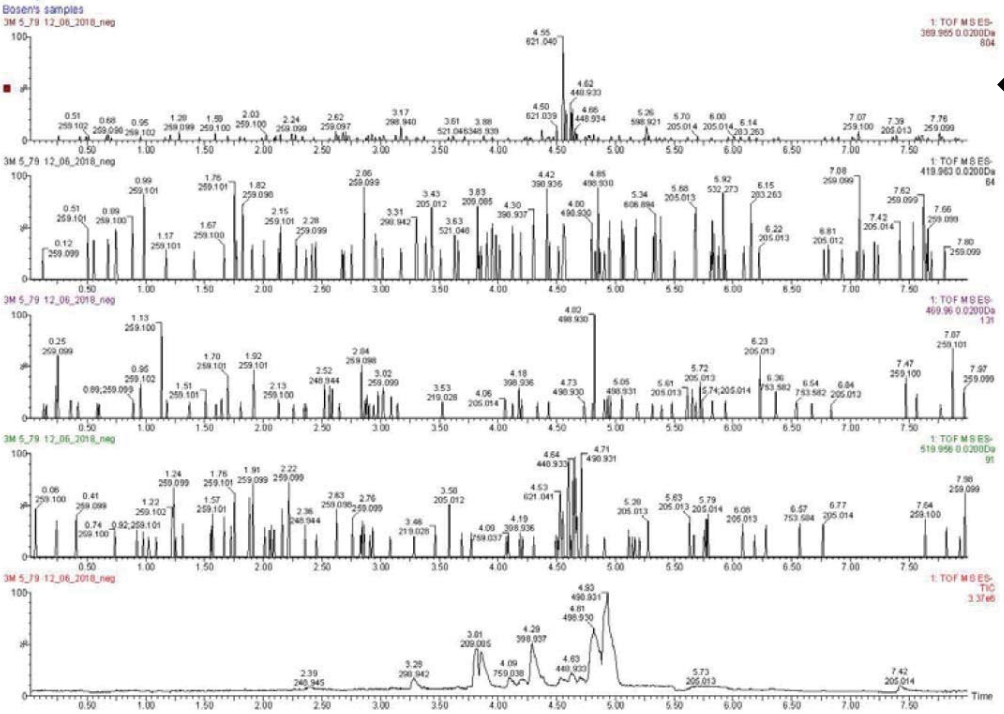

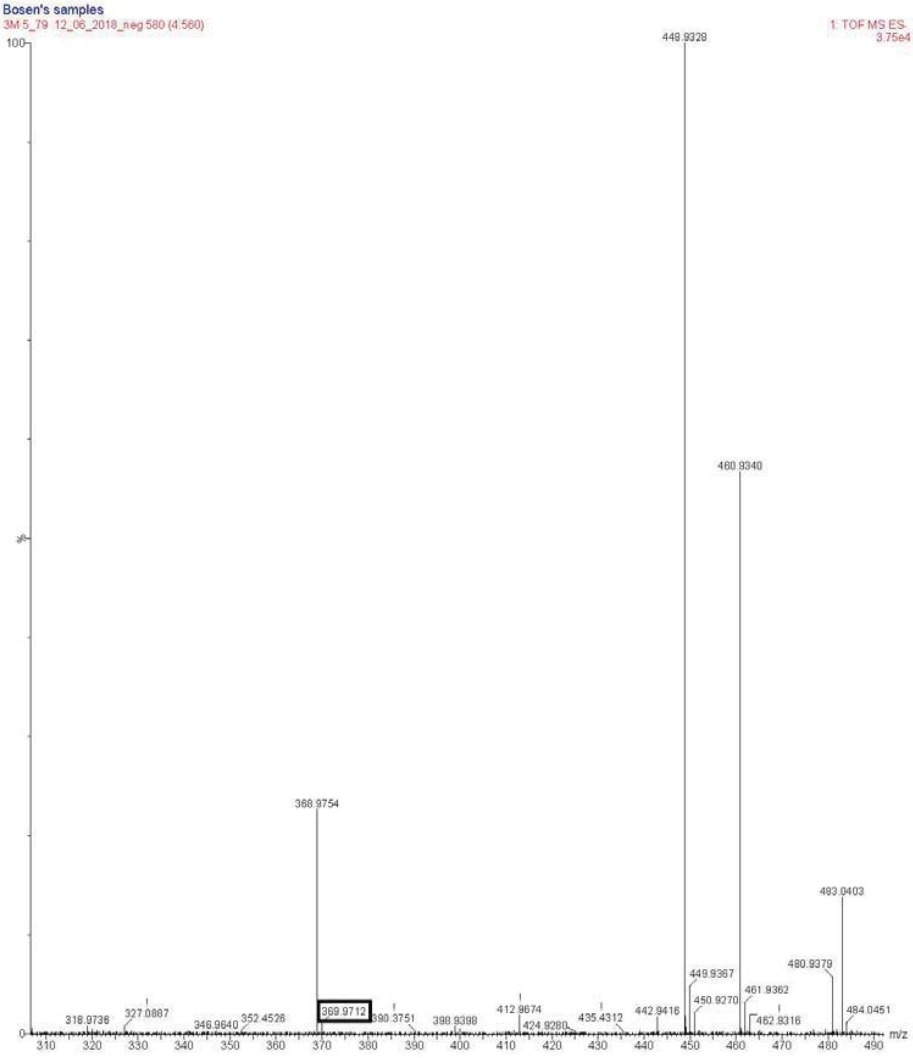

Mass value is found 369.9712 m/z

Figure A17: Class 21 of 3M 5_79 - Negative

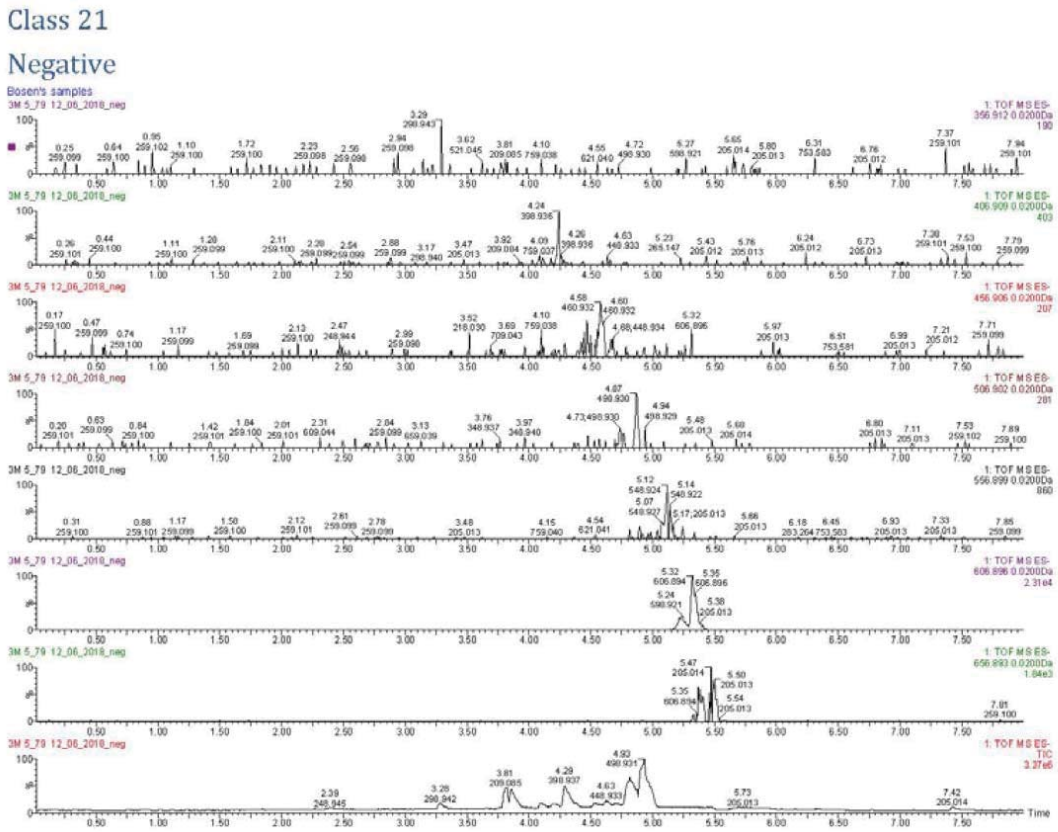

Mass value is found 656.896 m/z

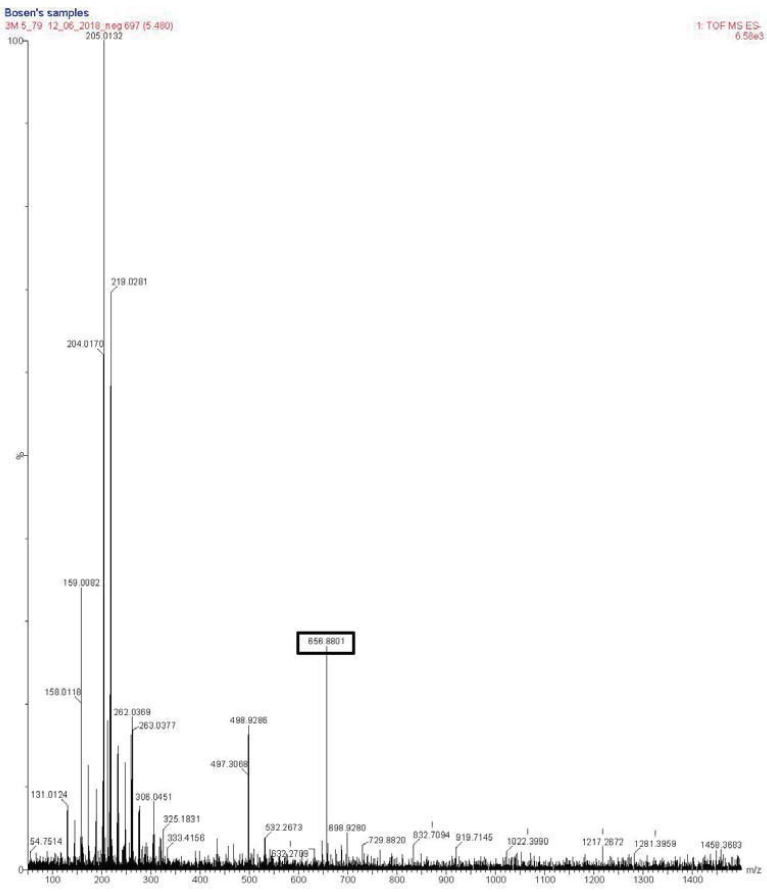

Mass value is found 656.8801 m/z

Figure A18: Class 23 of 3M 5_79 - Negative

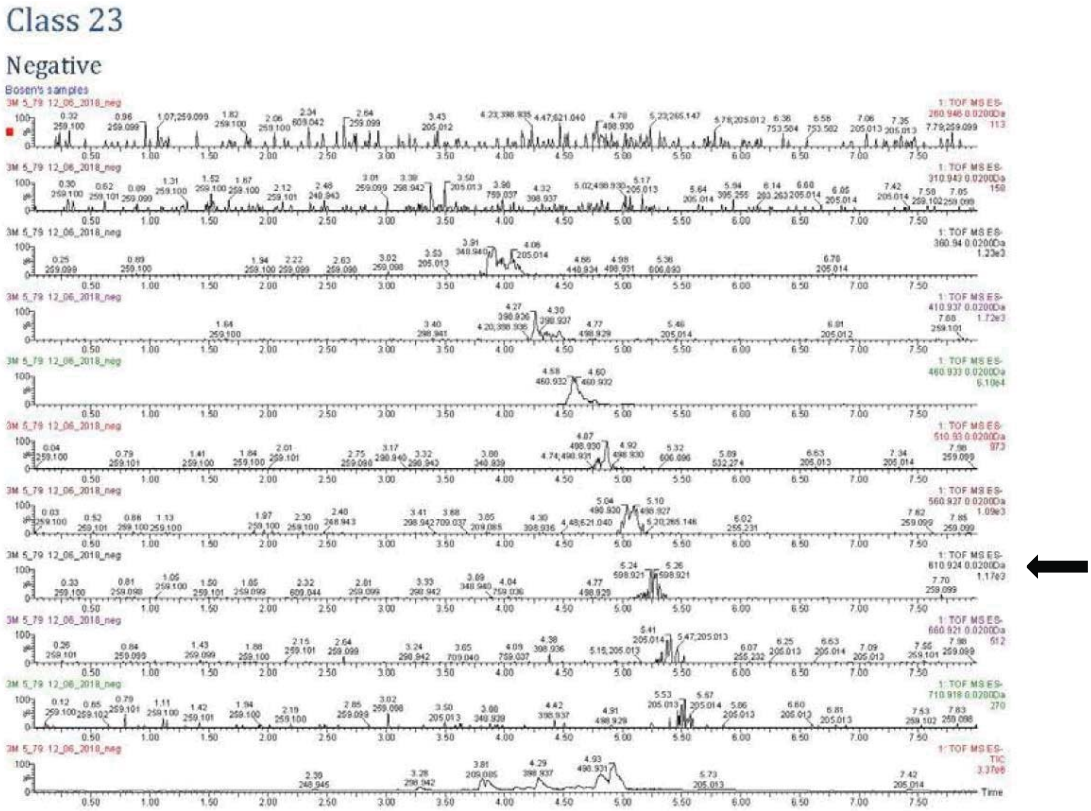

Mass value is 610.921 m/z

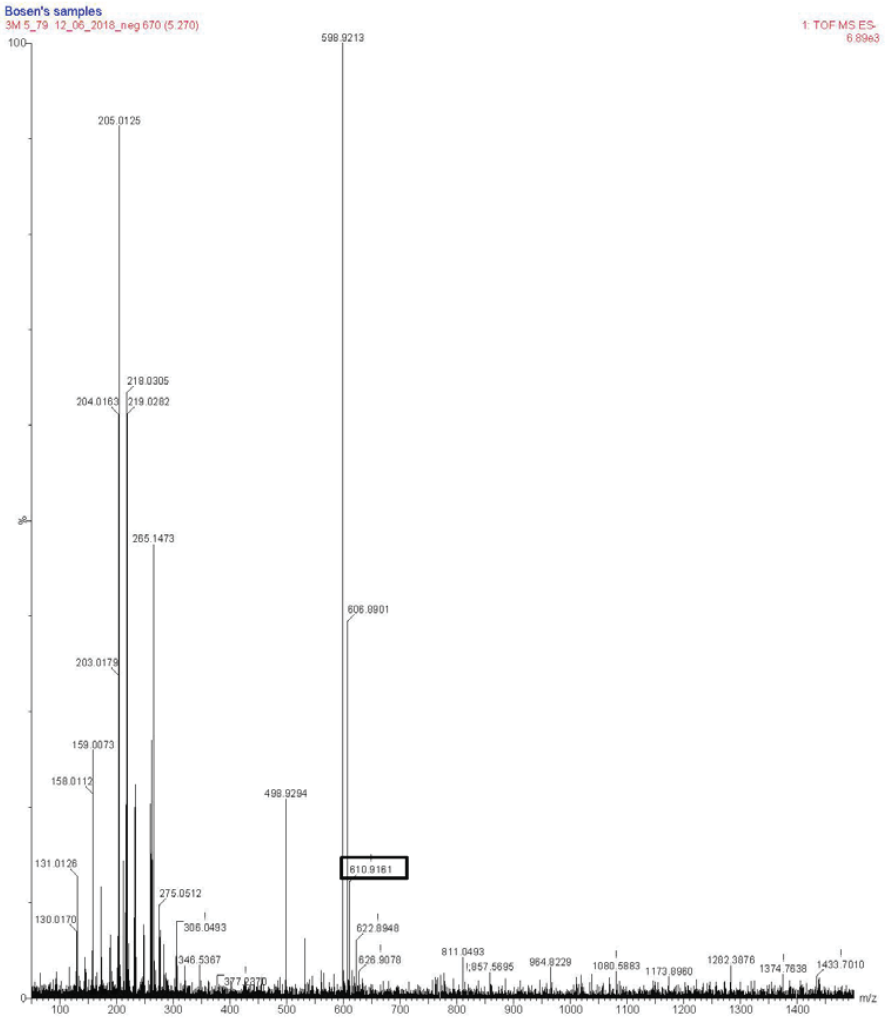

Mass value is found 610.9161 m/z

Figure A19: Class 24 of 3M 5_79 - Negative

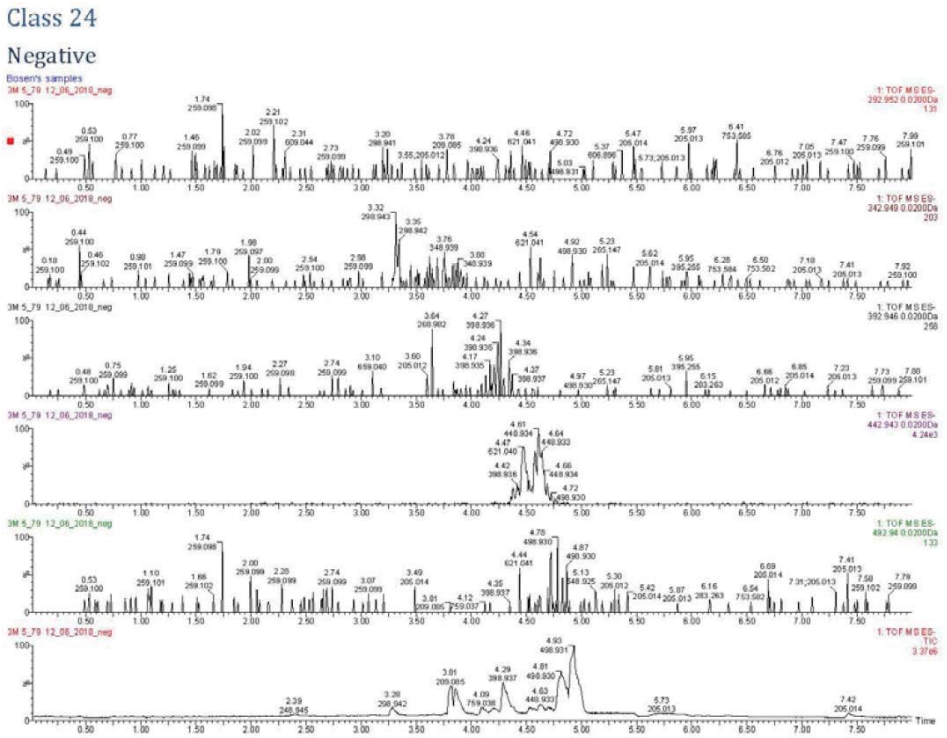

Mass value is 442.943 m/z

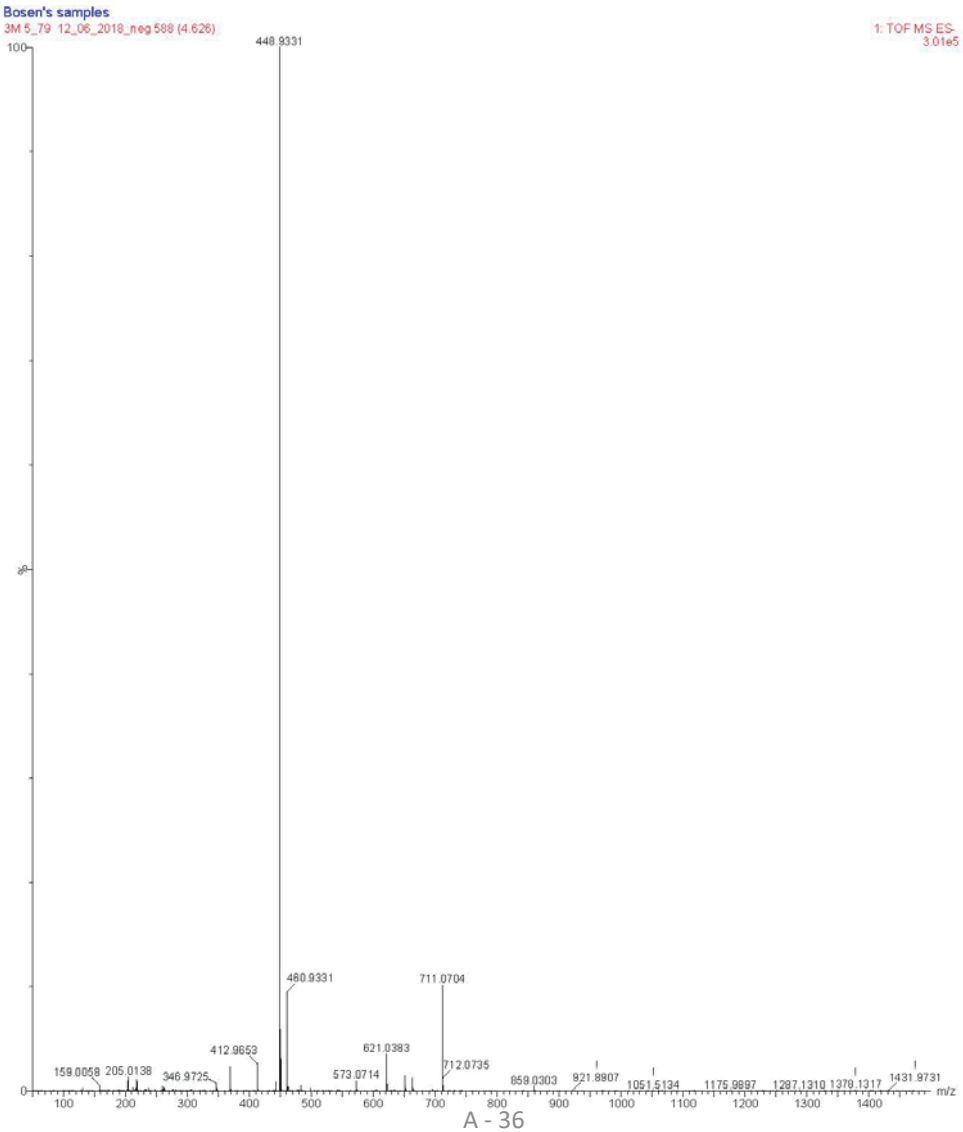

Figure A20: Class 25 of 3M 5_79 - Negative

Class 25

Negative

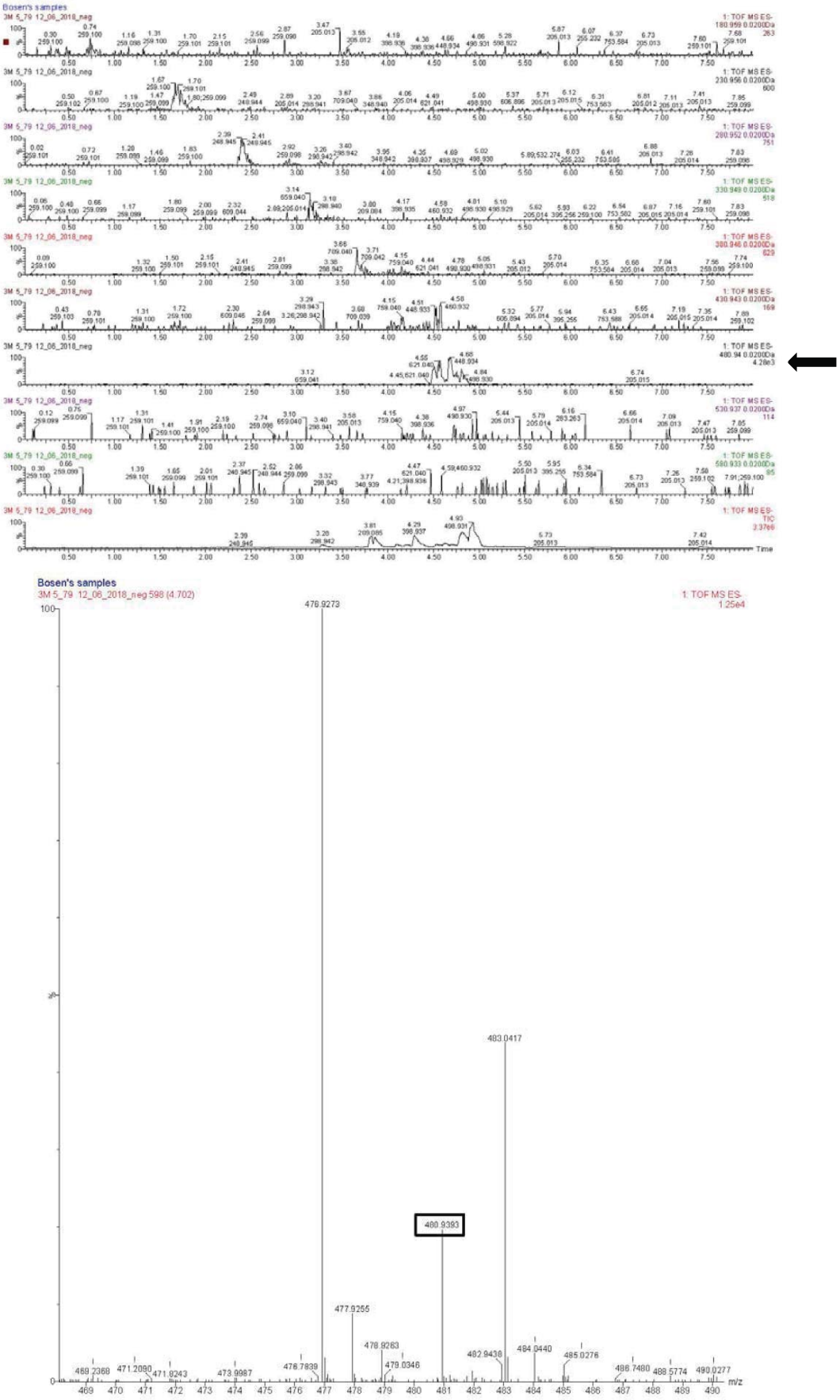

Mass value is 480.9393 m/z

Figure A21: Class 26 of 3M 5_79 - Negative

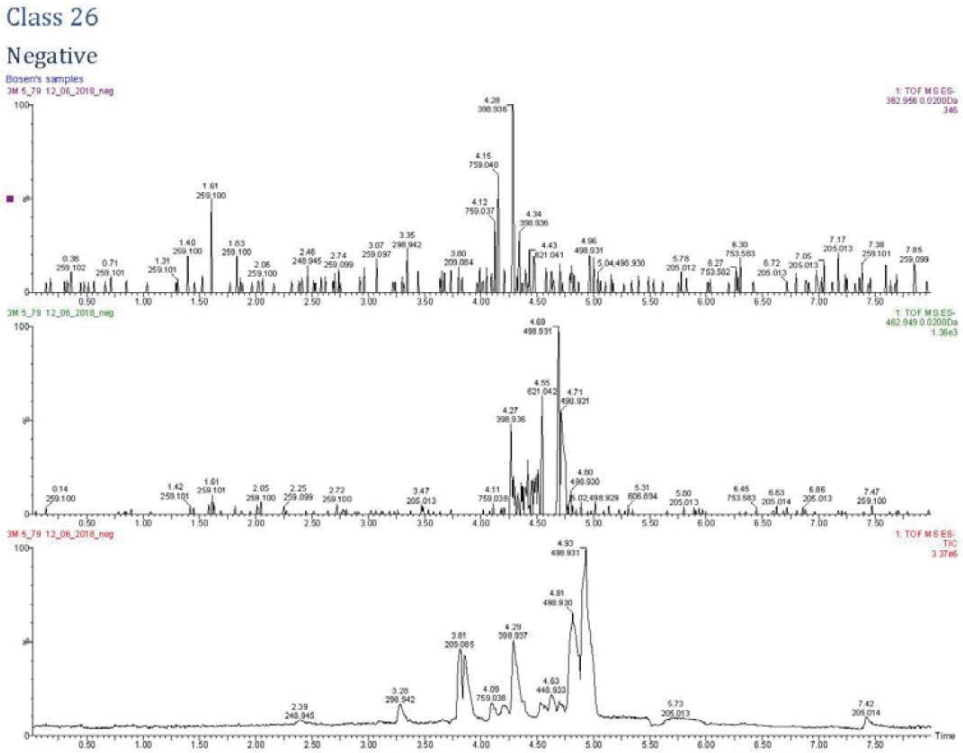

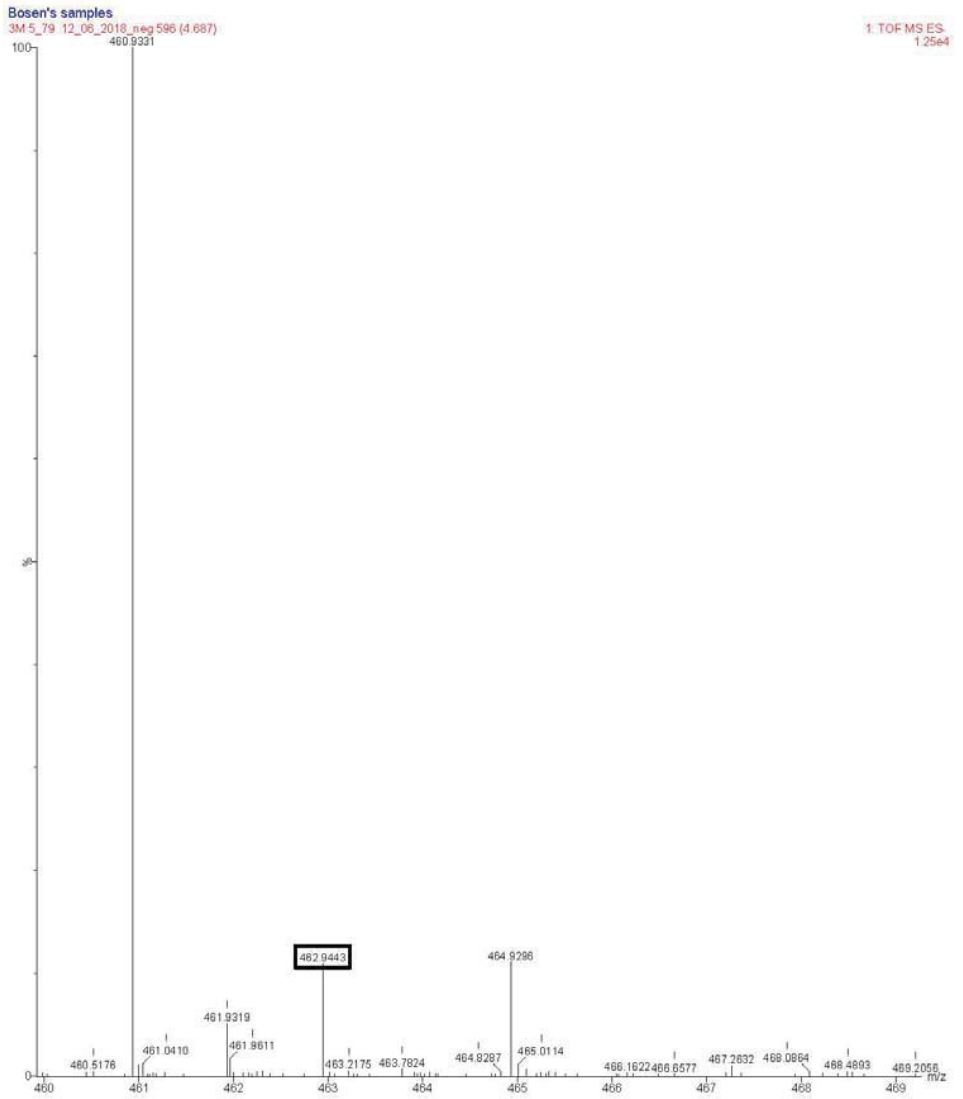

Mass value is found 462.9443 m/z

Figure A22: Class 29 of 3M 5_79 - Negative

Class 29

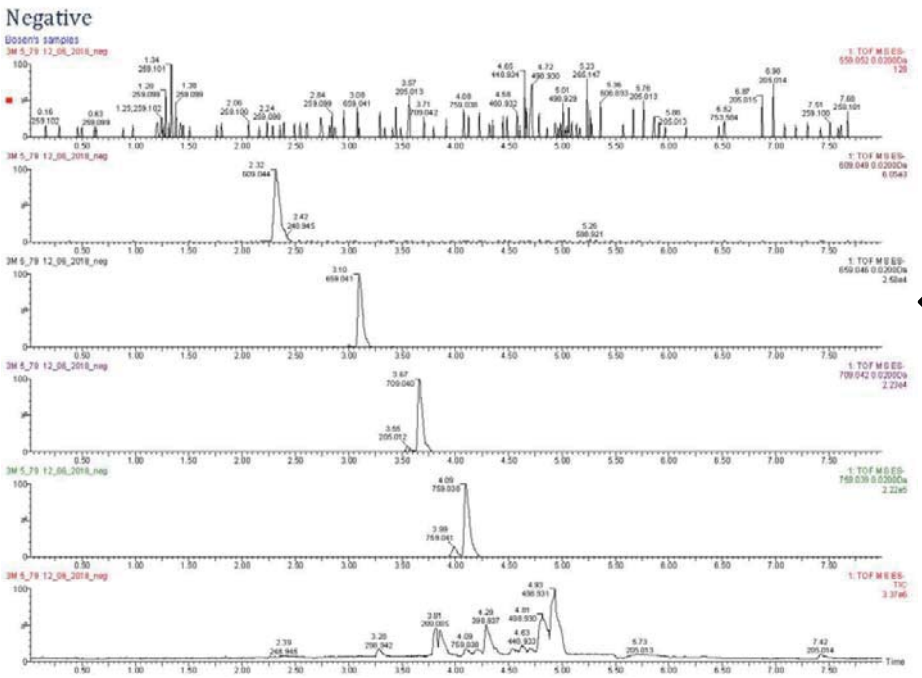

Mass value is 659.046 m/z

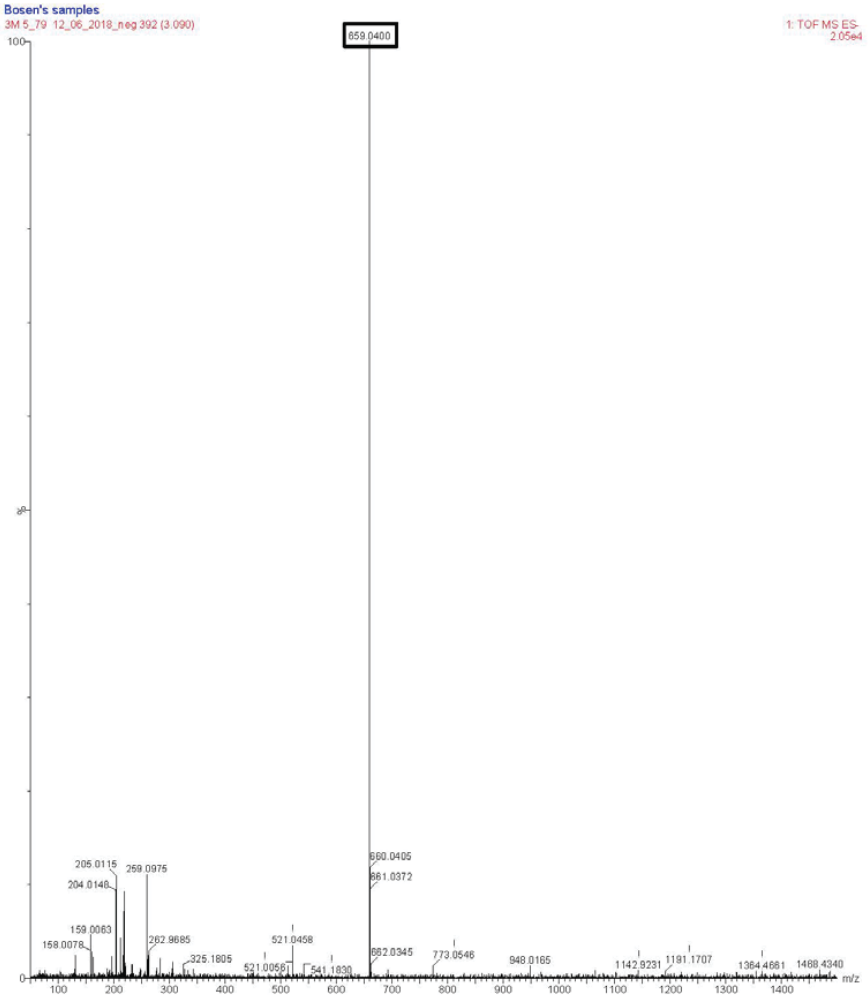

Mass value is found 659.0400 m/z

Figure A2-1: Class 2 of 3M 1_89 - Positive

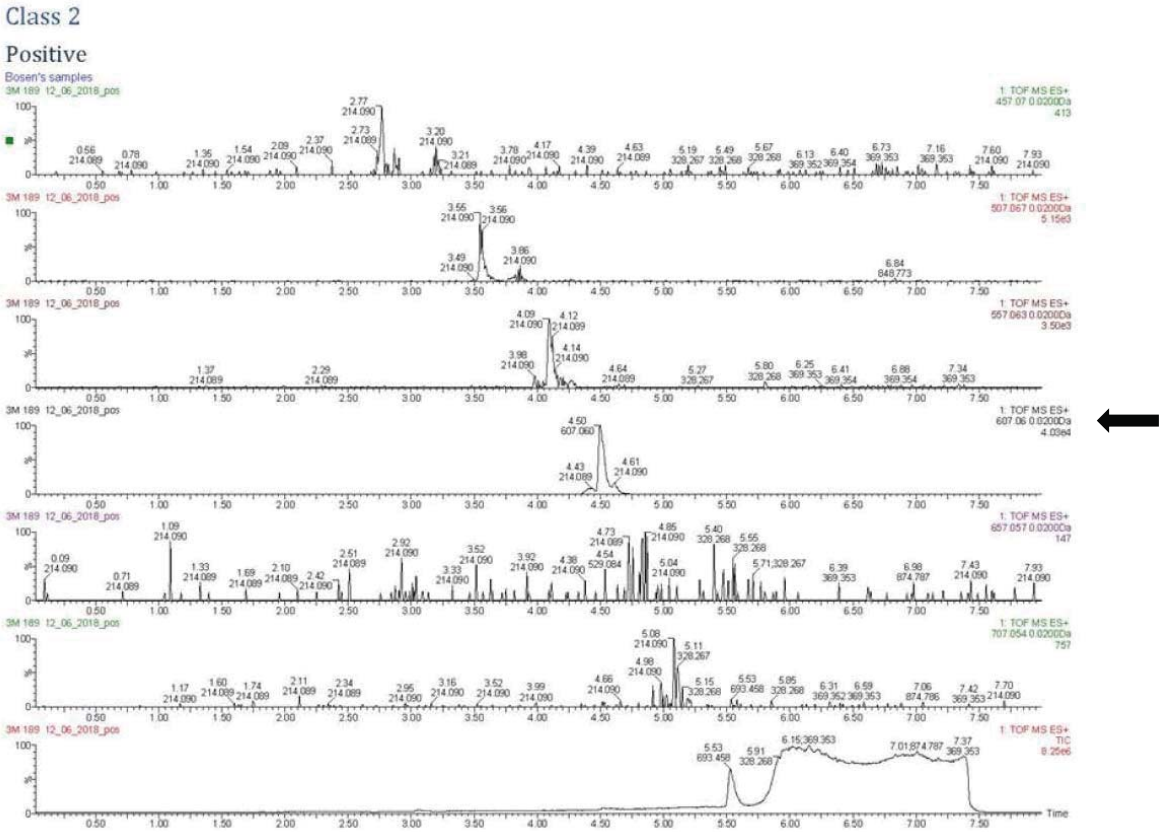

Mass value is 607.06 m/z

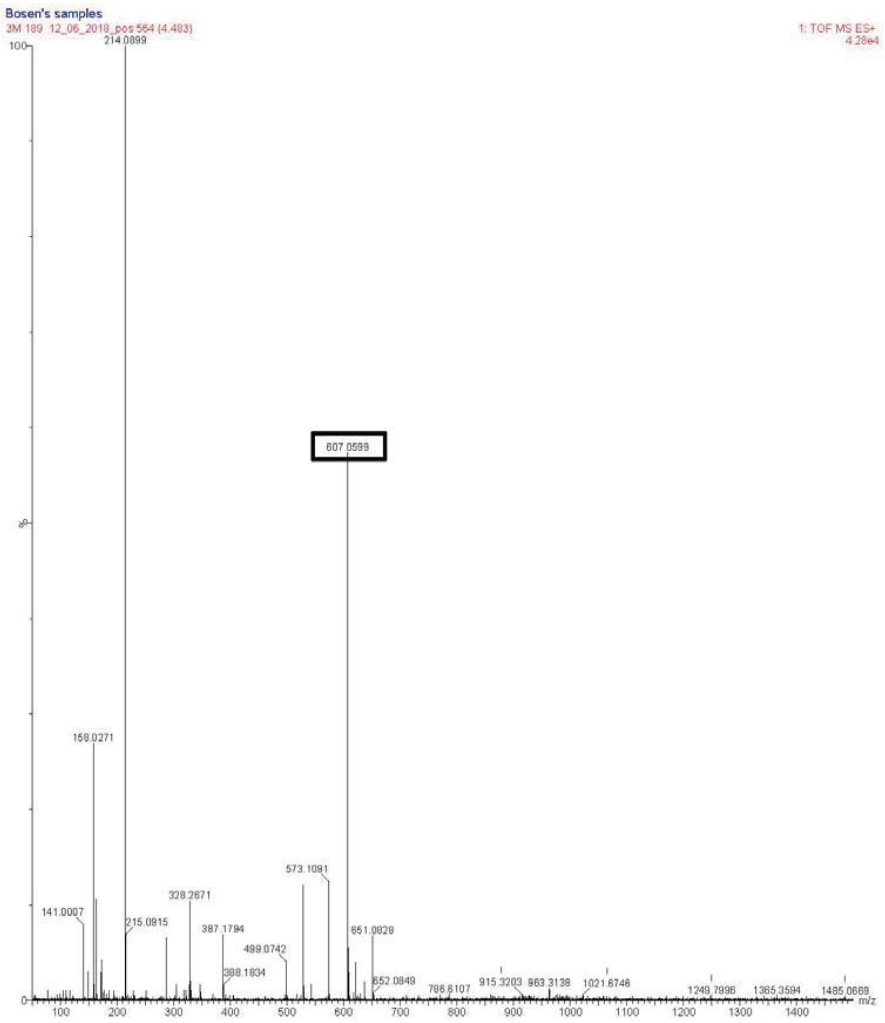

Mass value is found 607.0599 m/z

Figure A2-2: Class 4 of 3M 1_89 - Positive

Class 4

Positive

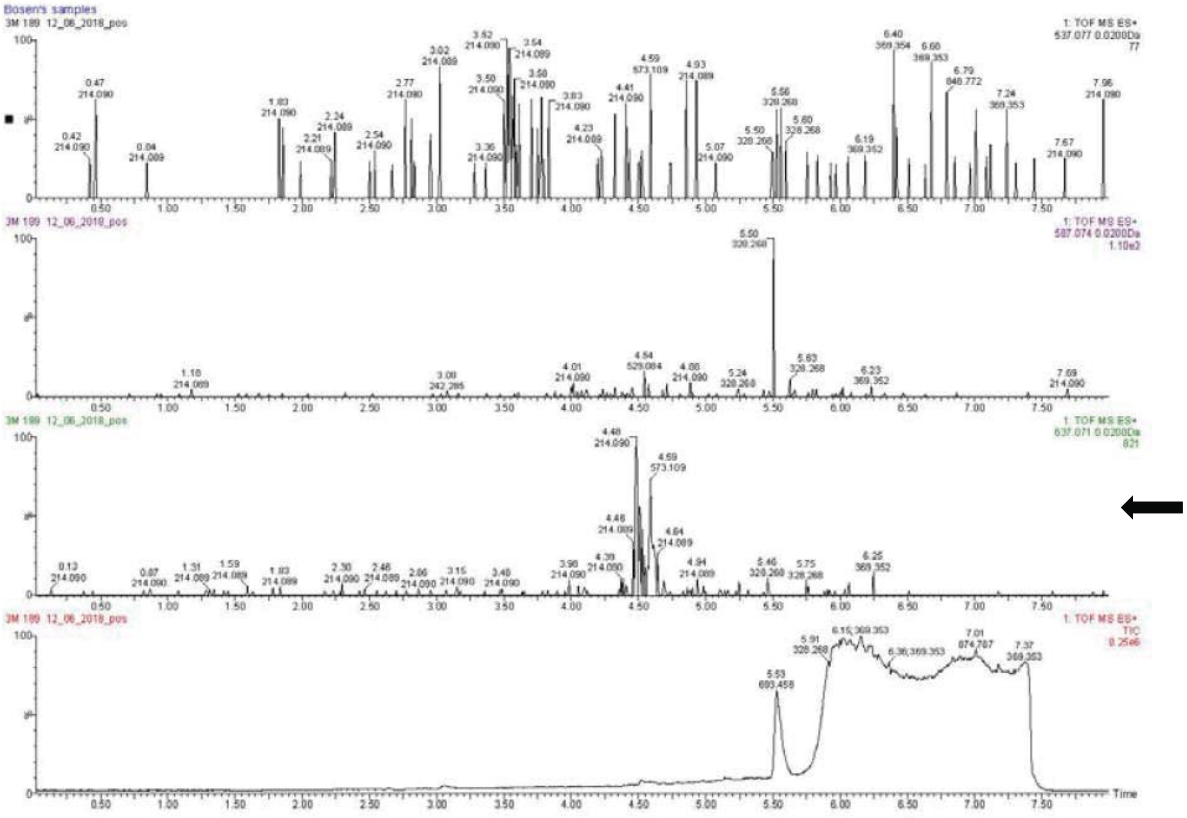

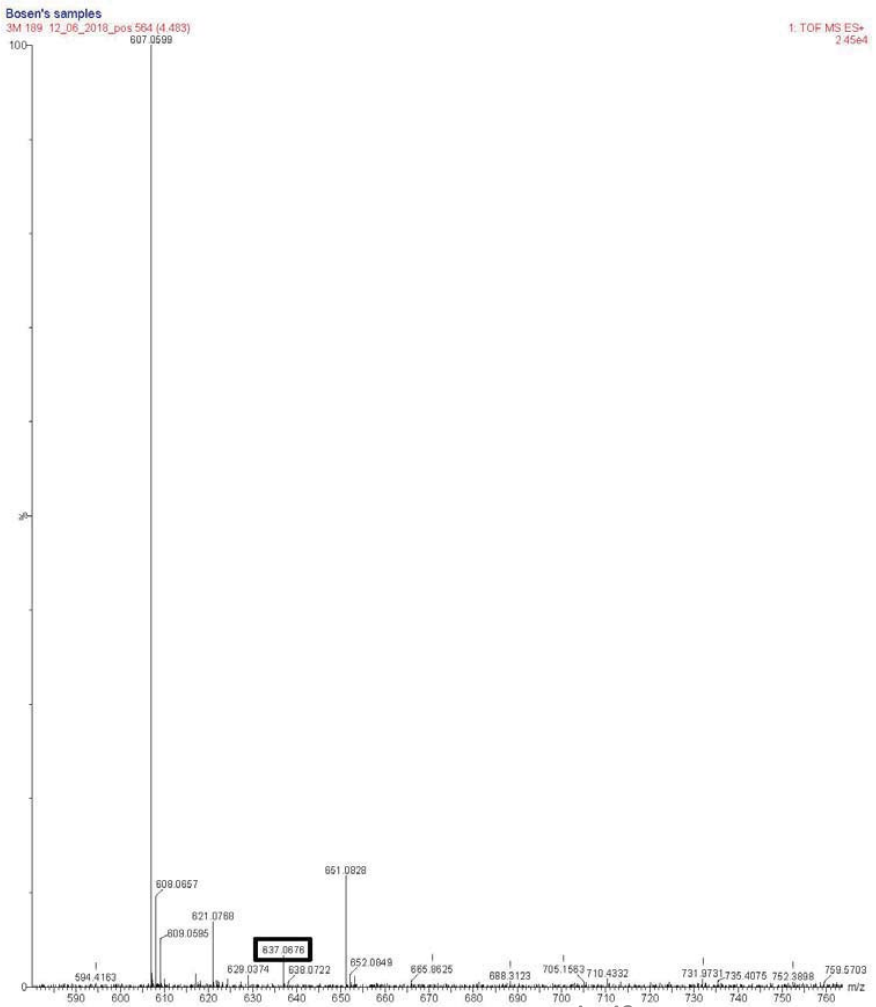

Mass value is found 637.0676 m/z

Figure A2-3: Class 5 of 3M 1_89 - Positive

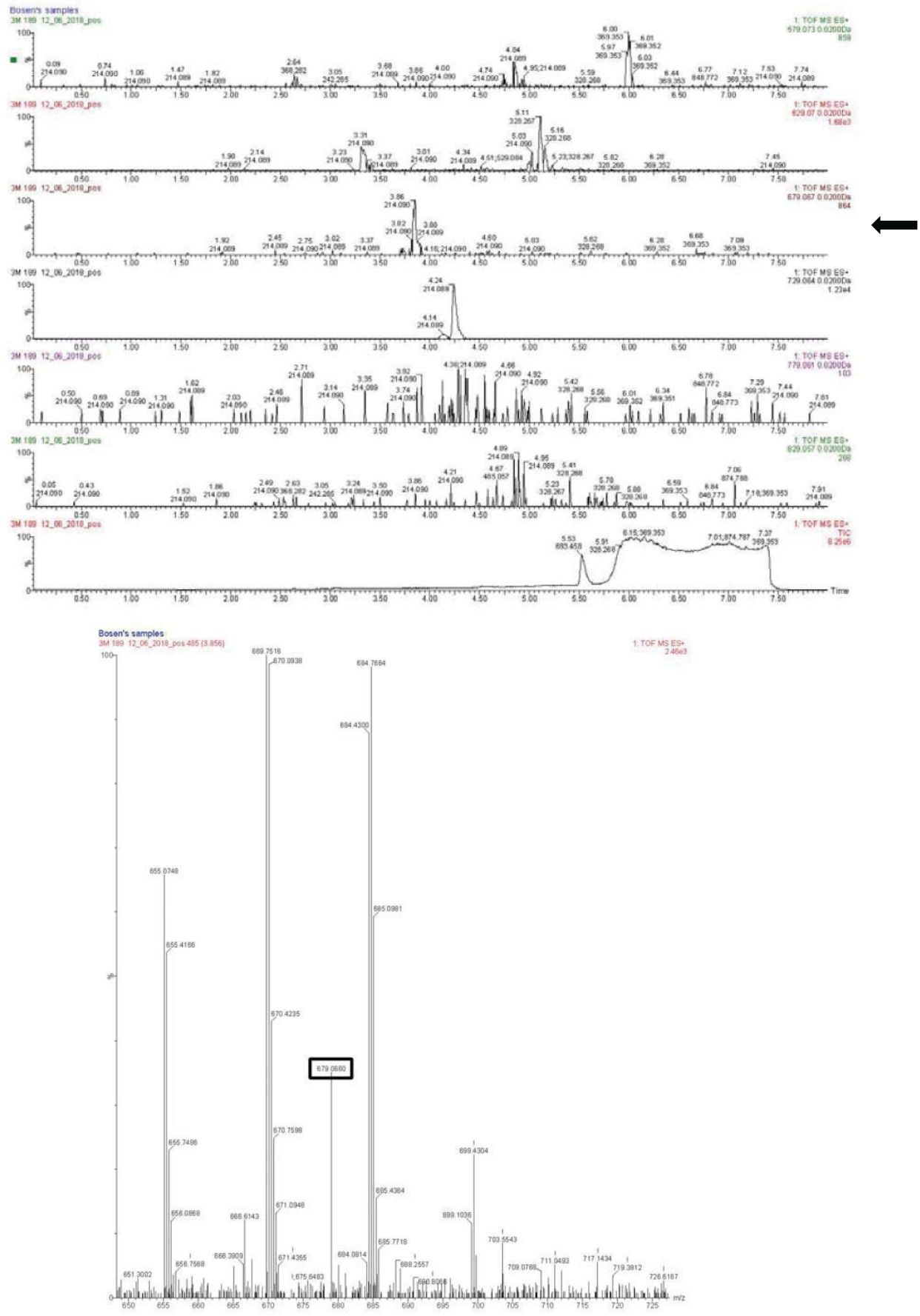

Mass value is 679.0660 m/z

Figure A2-4: Class 8 of 3M 1_89 - Positive

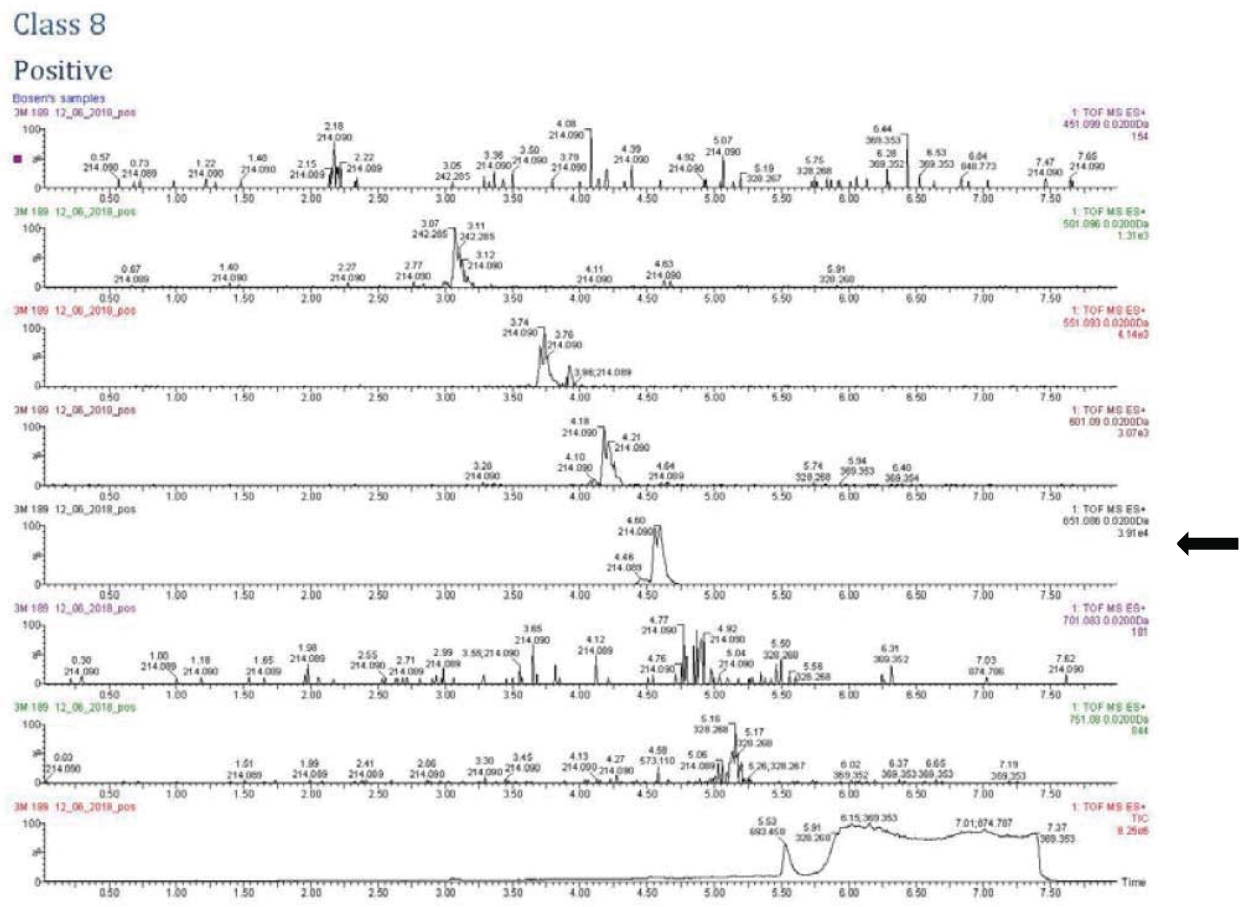

Mass value is found 651.086 m/z

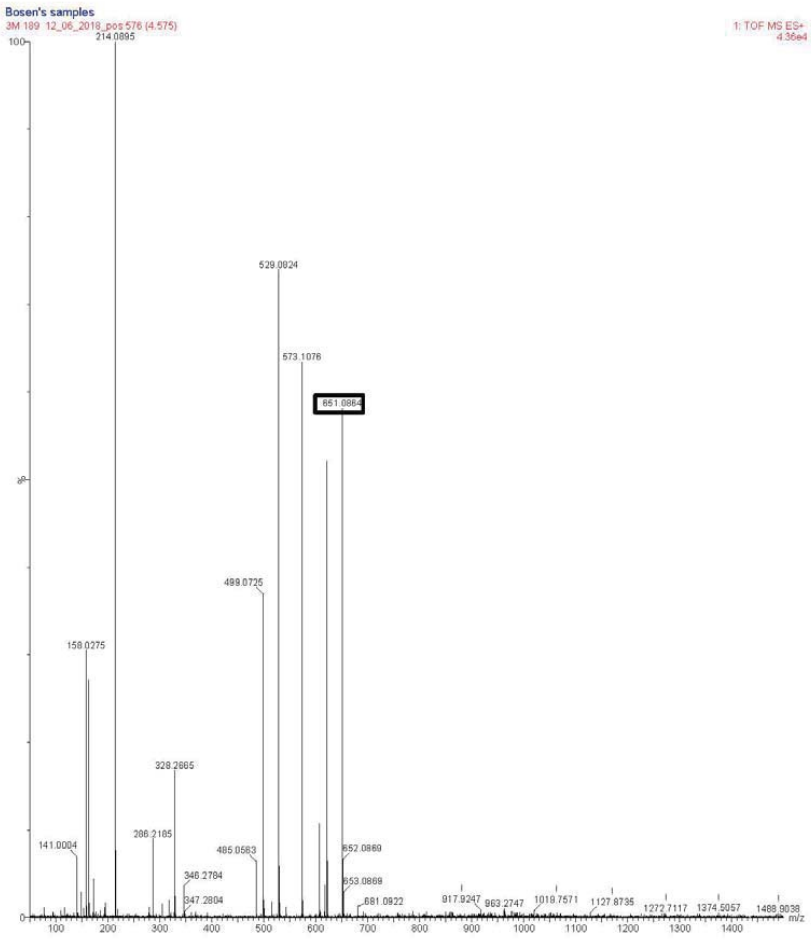

Mass value is found 651.0964 m/z

Figure A2-5: Class 9 of 3M 1_89 - Positive

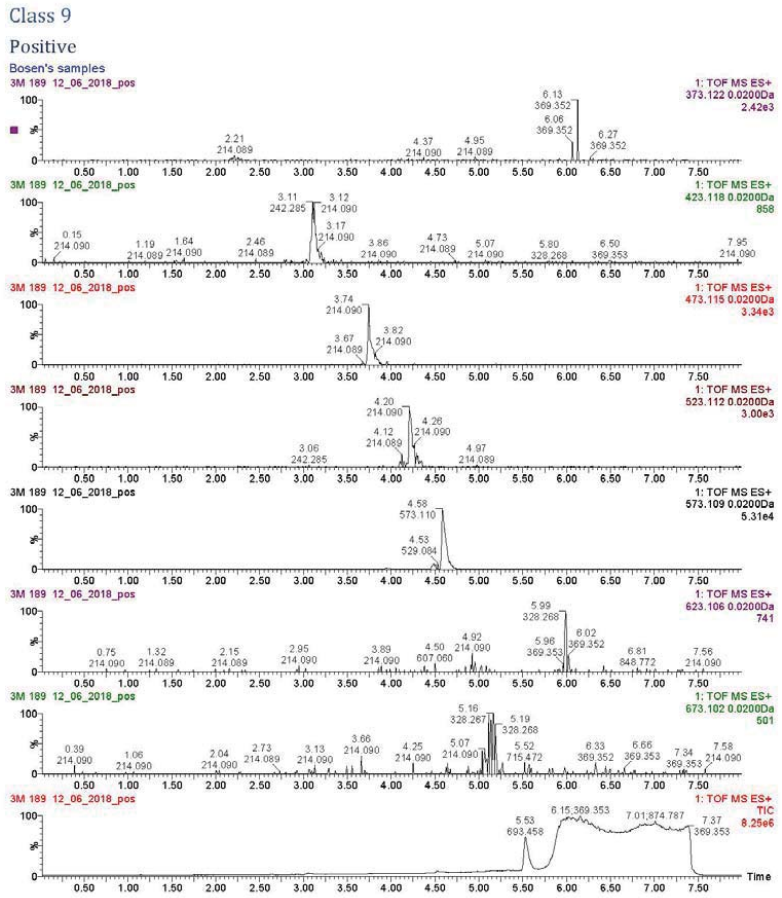

Mass value is 473.115 m/z

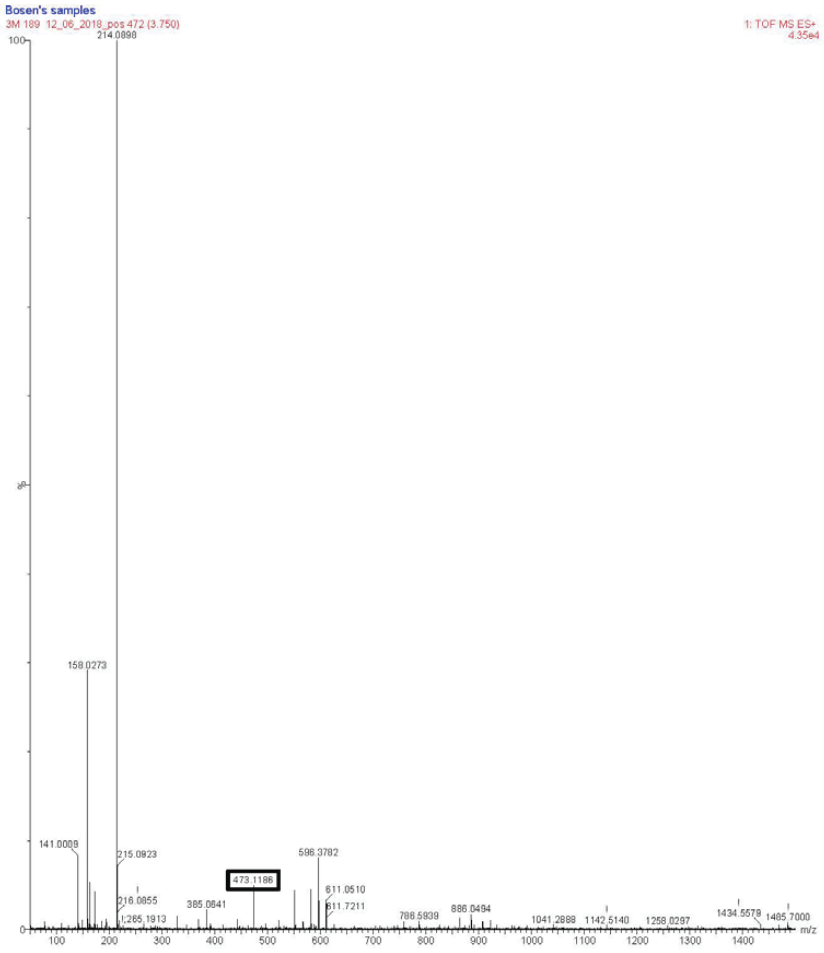

Mass value is found 473.1186 m/z

Figure A2-6: Class 11 of 3M 1_89 - Positive

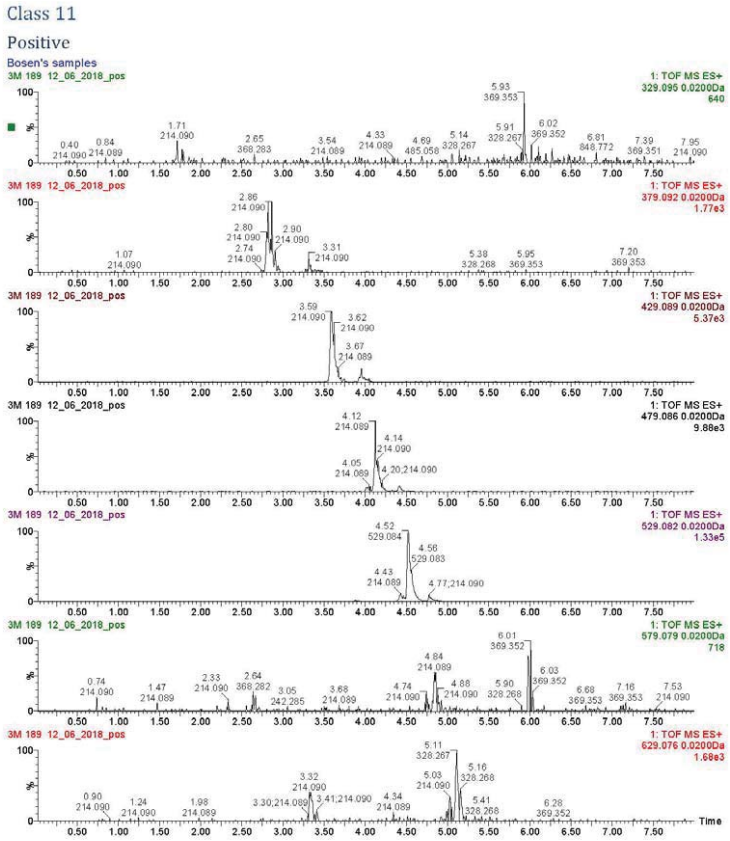

Mass value is 629.076 m/z

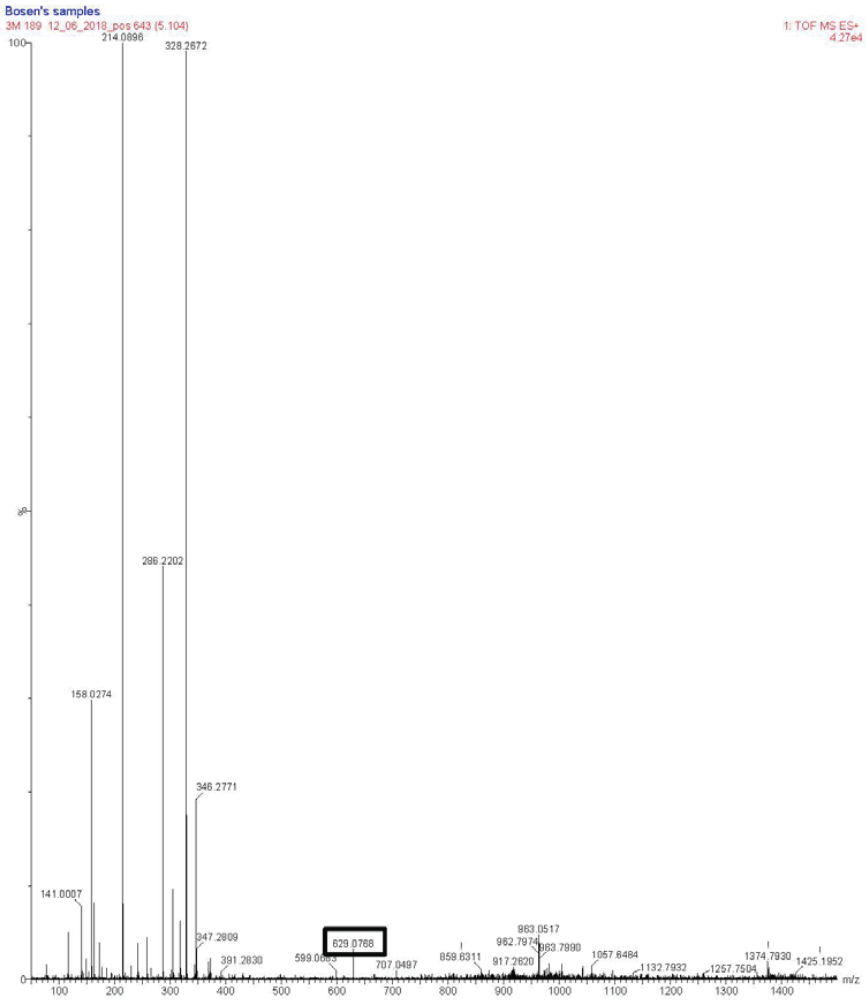

Mass value is found 629.0768 m/z

Figure A2-7: Class 13 of 3M 1_89 - Positive

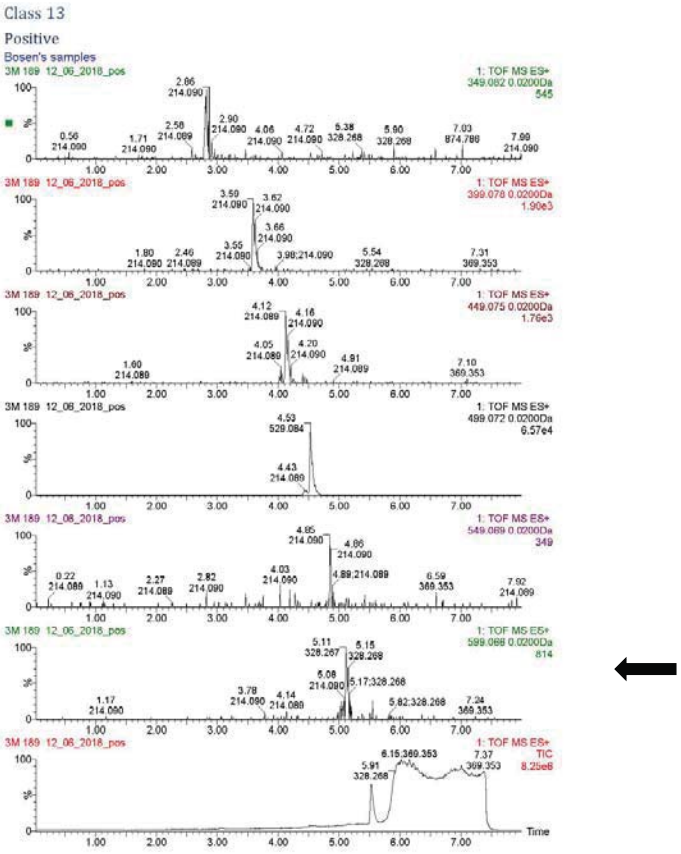

Mass value is 599.066 m/z

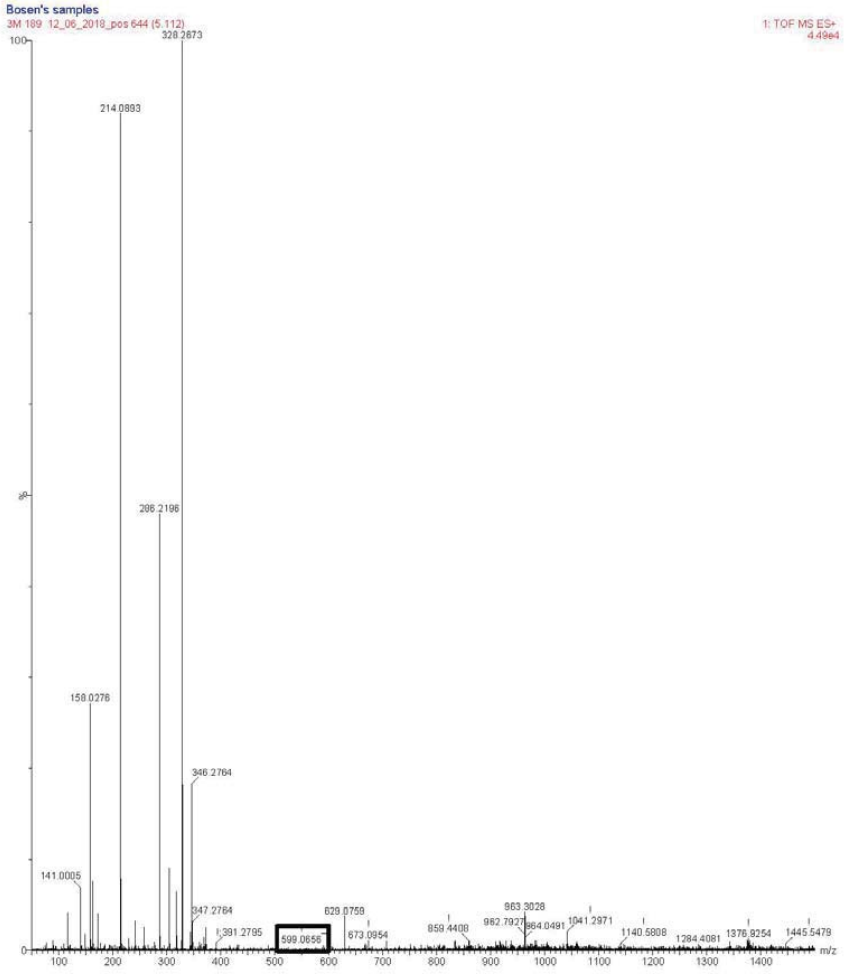

Mass value is found 599.0656 m/z

Figure A2-8: Class 14 of 3M 1_89 - Positive

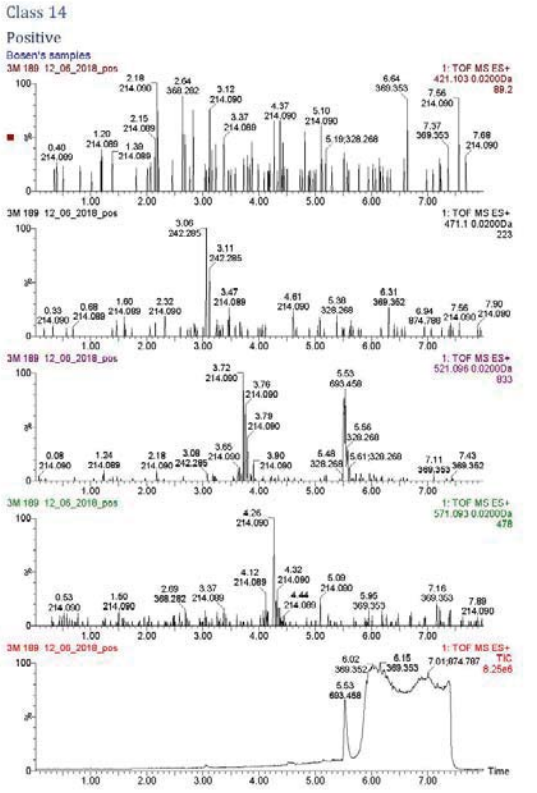

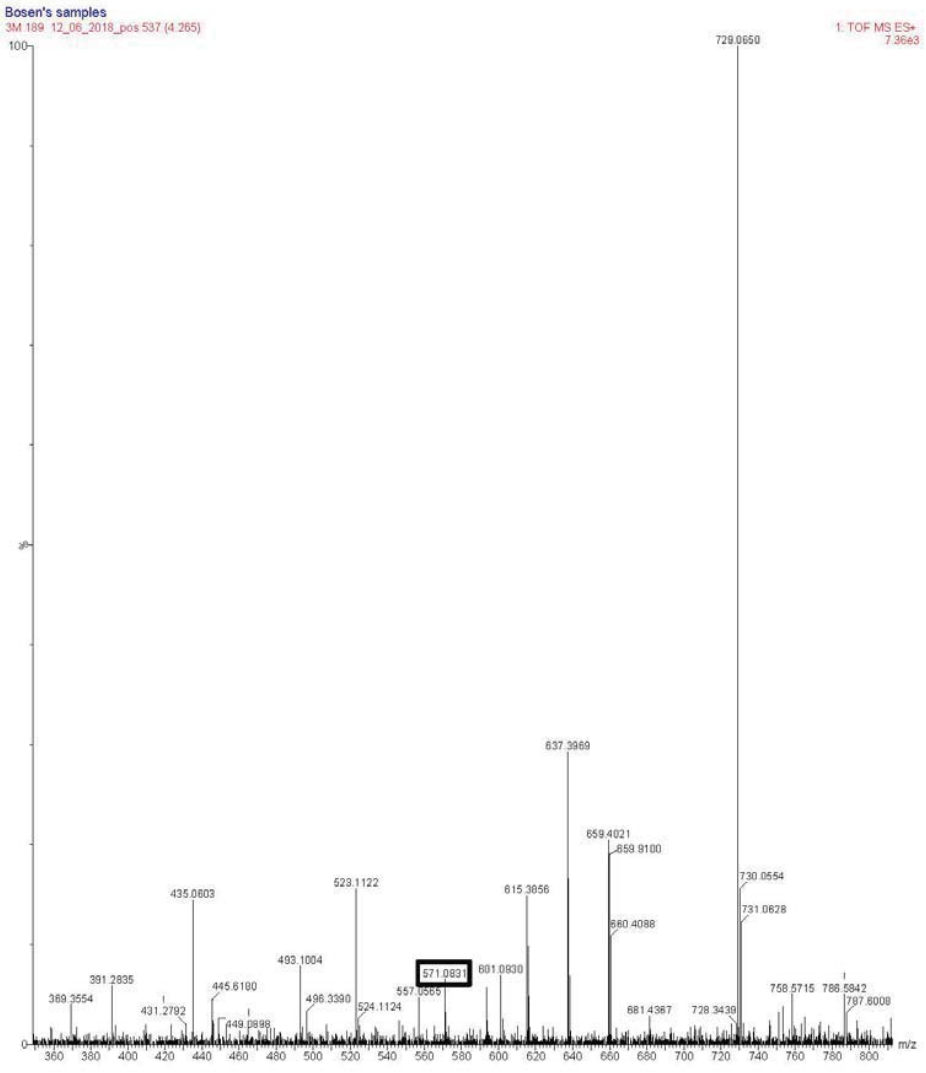

Mass value is found 571.0831 m/z

Figure A2-9: Class 19 of 3M 1_89 - Positive

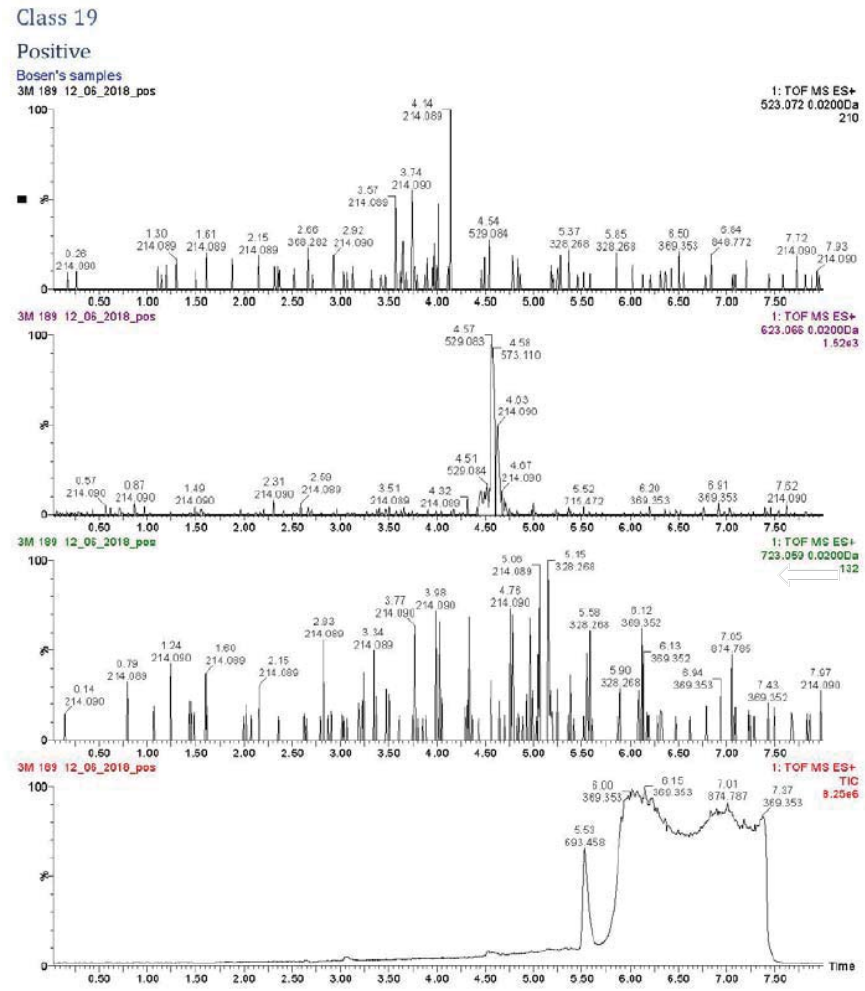

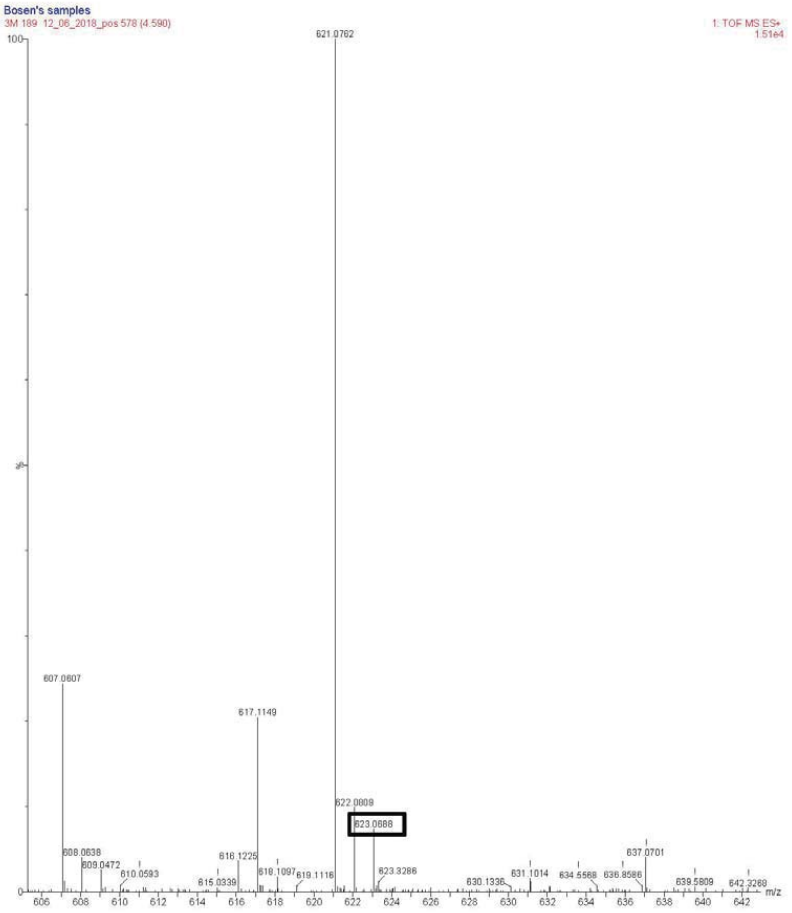

Mass value is found 623.0688 m/z

Figure A2-10: Class 31 of 3M 1_89 - Positive

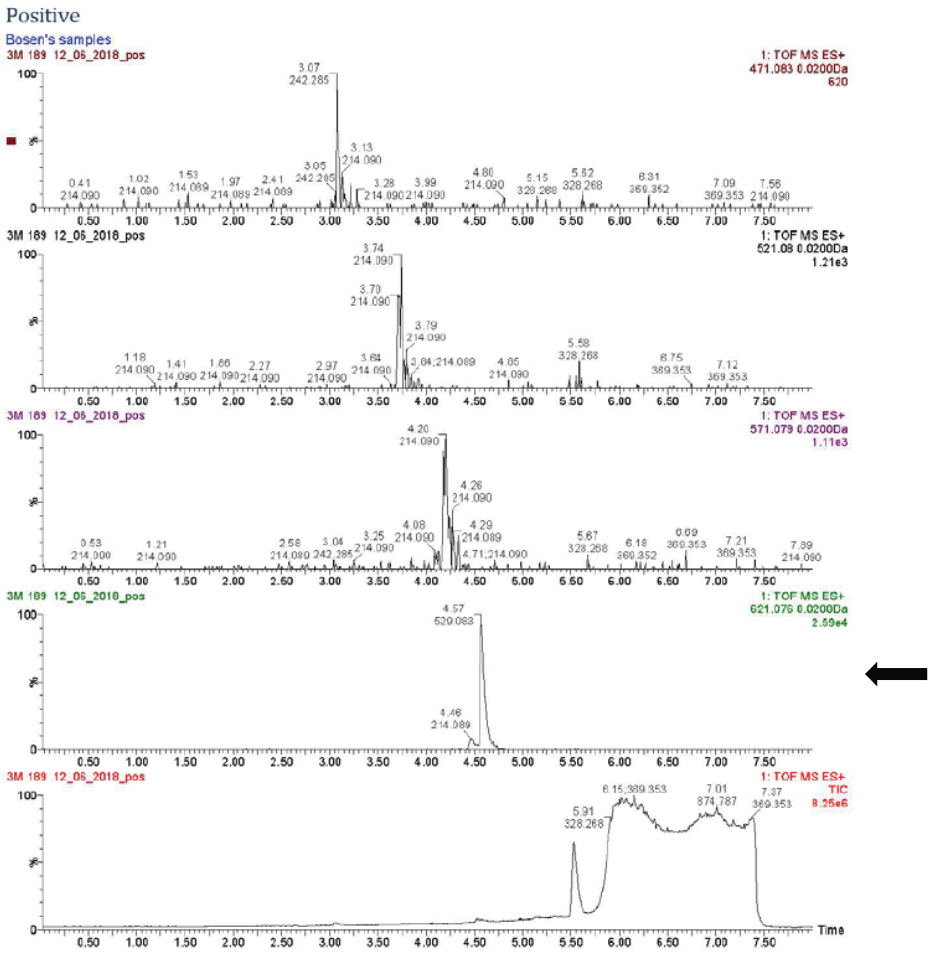

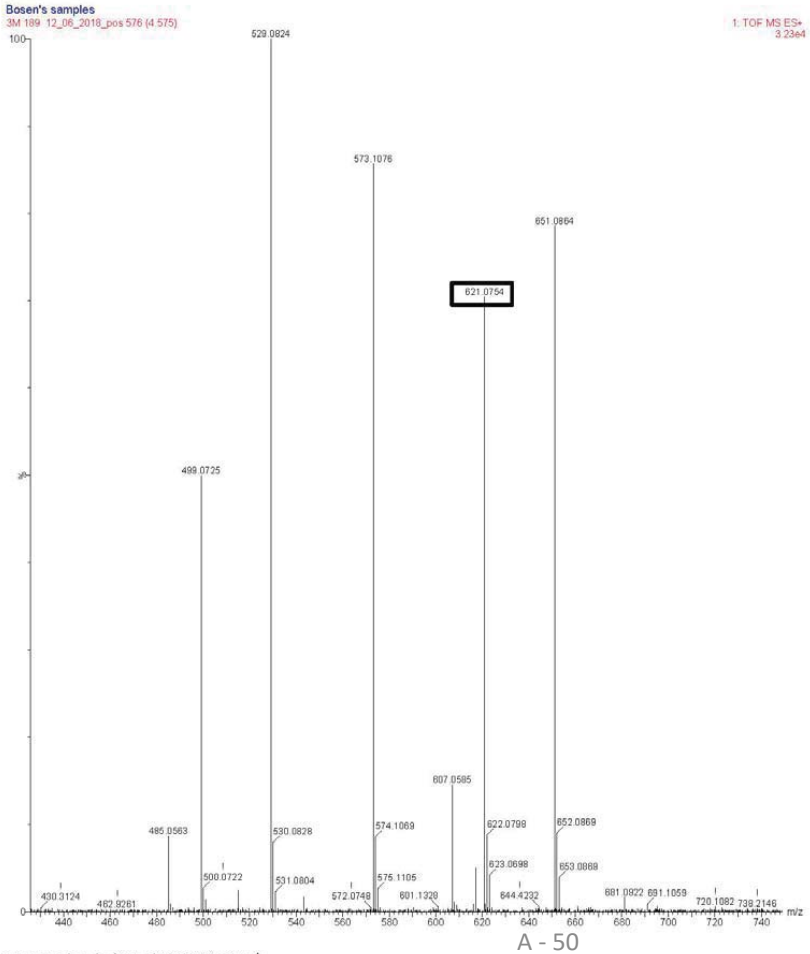

Mass value is found 621.0754 m/z

Figure A2-11: Class 32 of 3M 1_89 - Positive

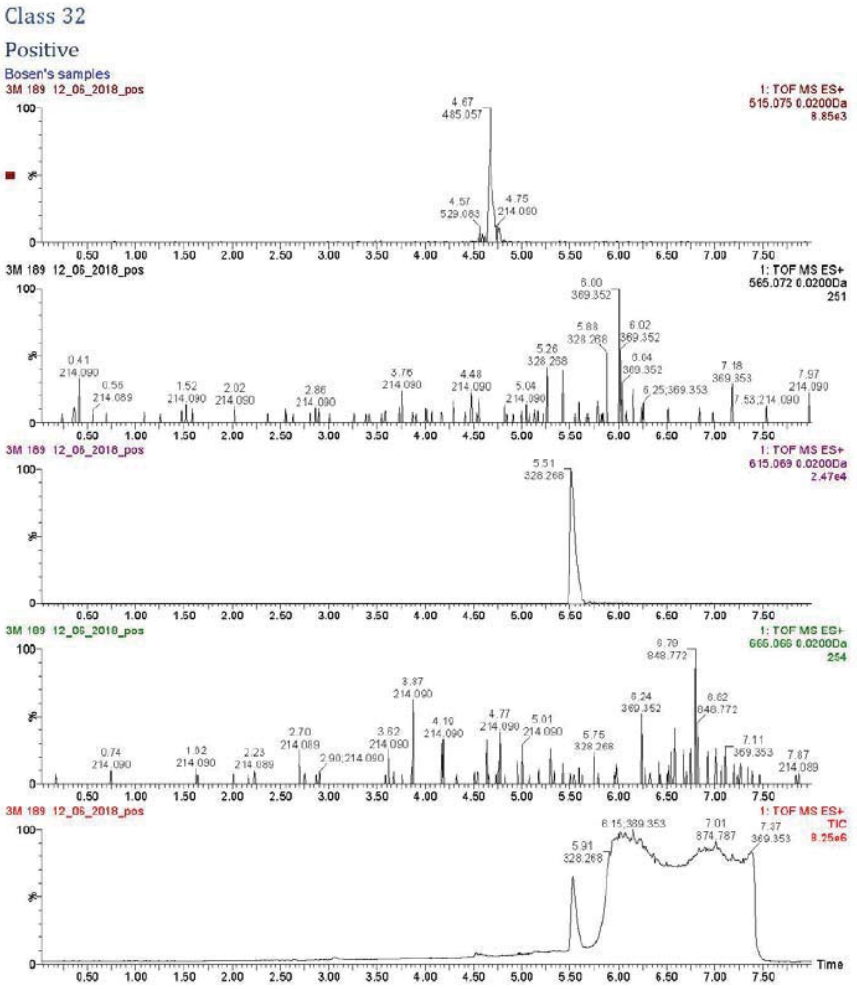

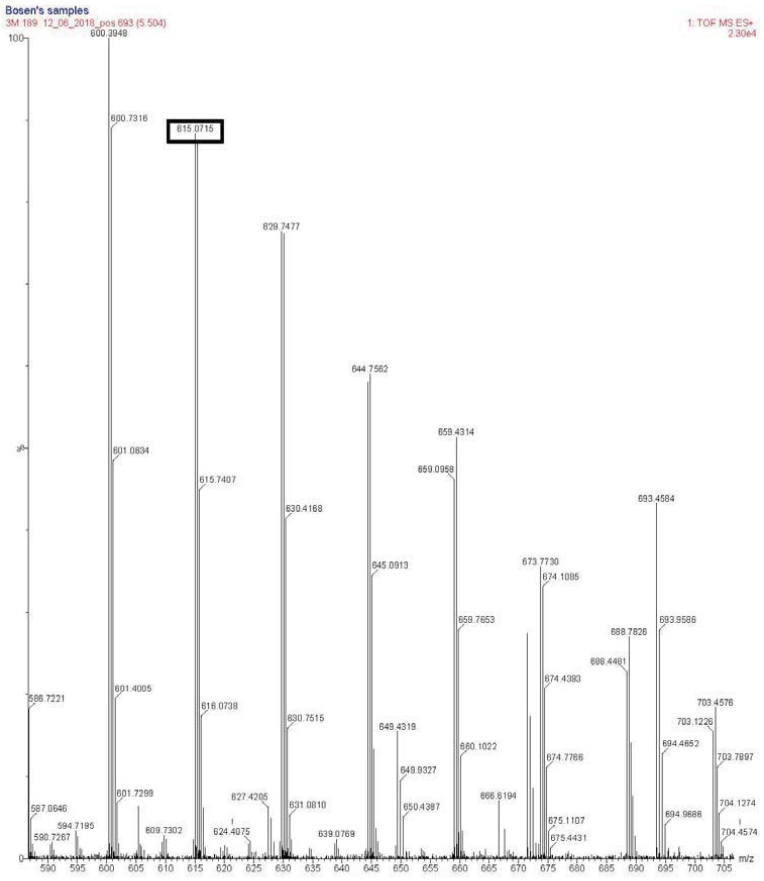

Mass value is found 615.0715 m/z

Figure A2-12: Class 33 of 3M 1_89 - Positive

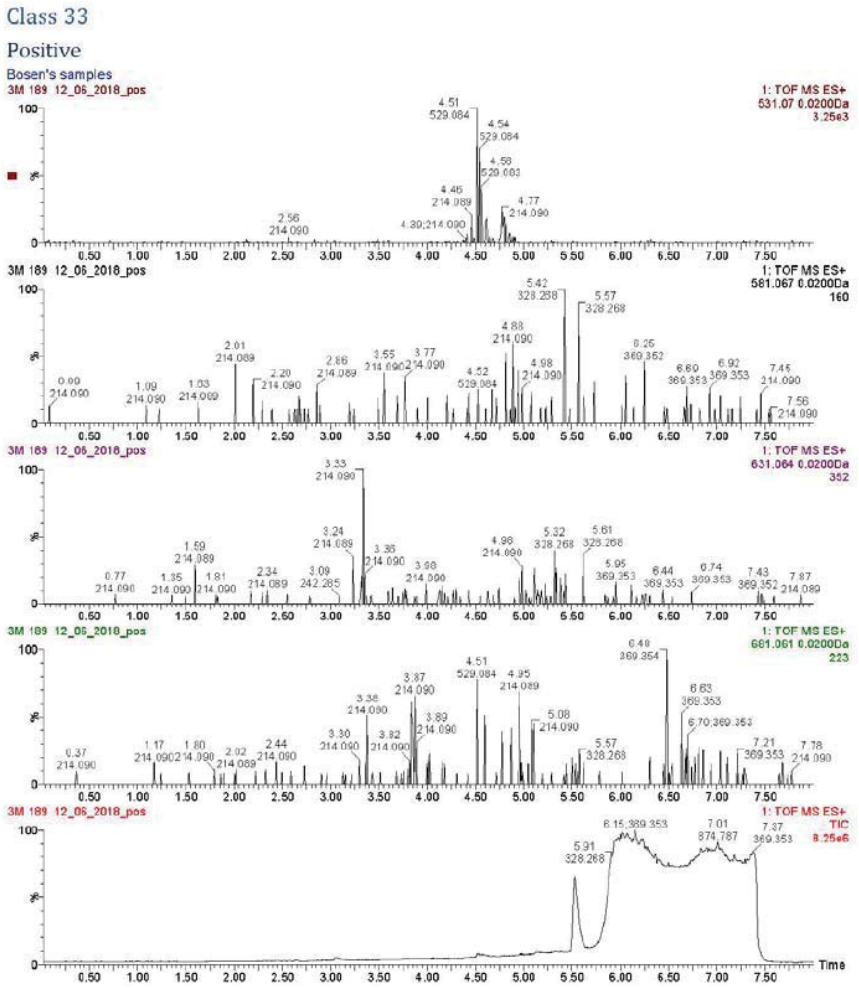

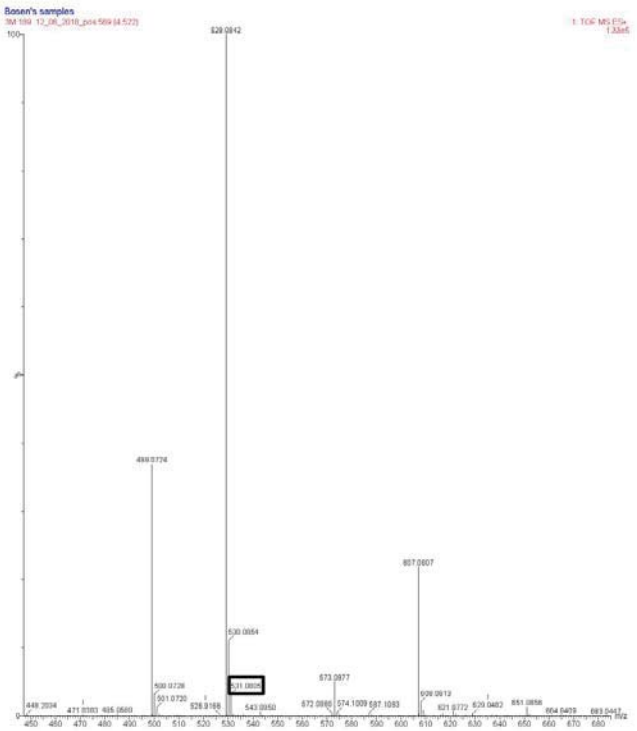

Mass value is found 531.0805 m/z

Figure A2-13: Class 34 of 3M 1_89 - Positive

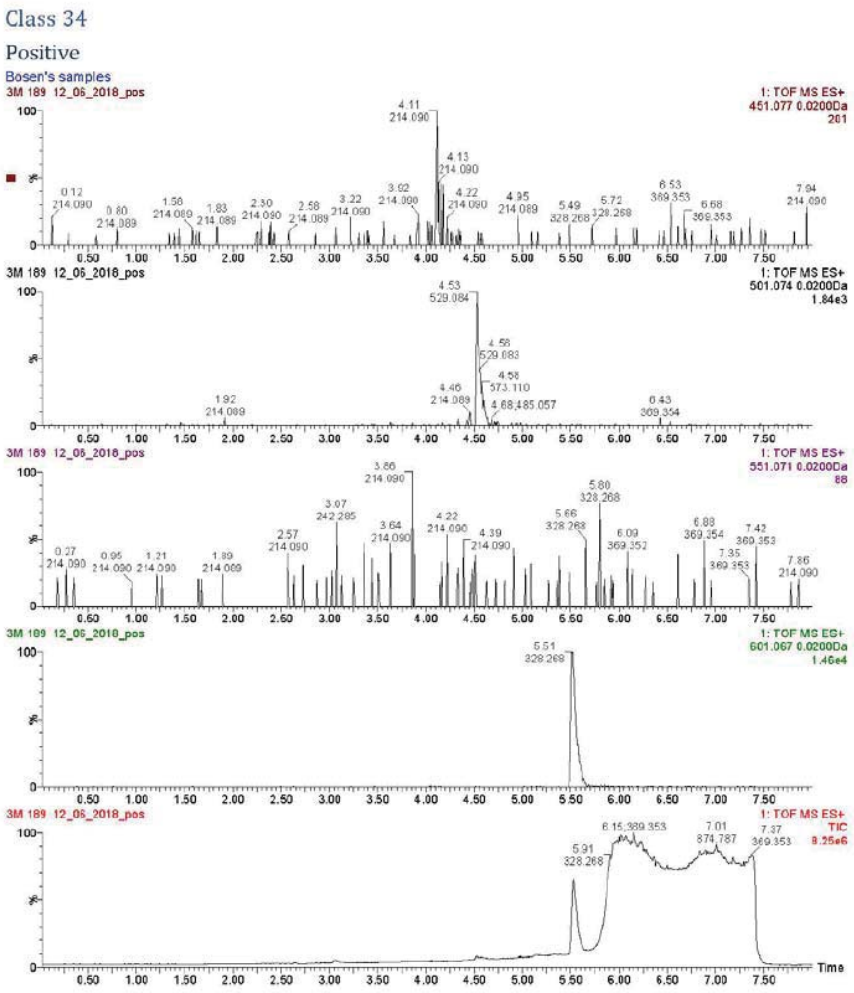

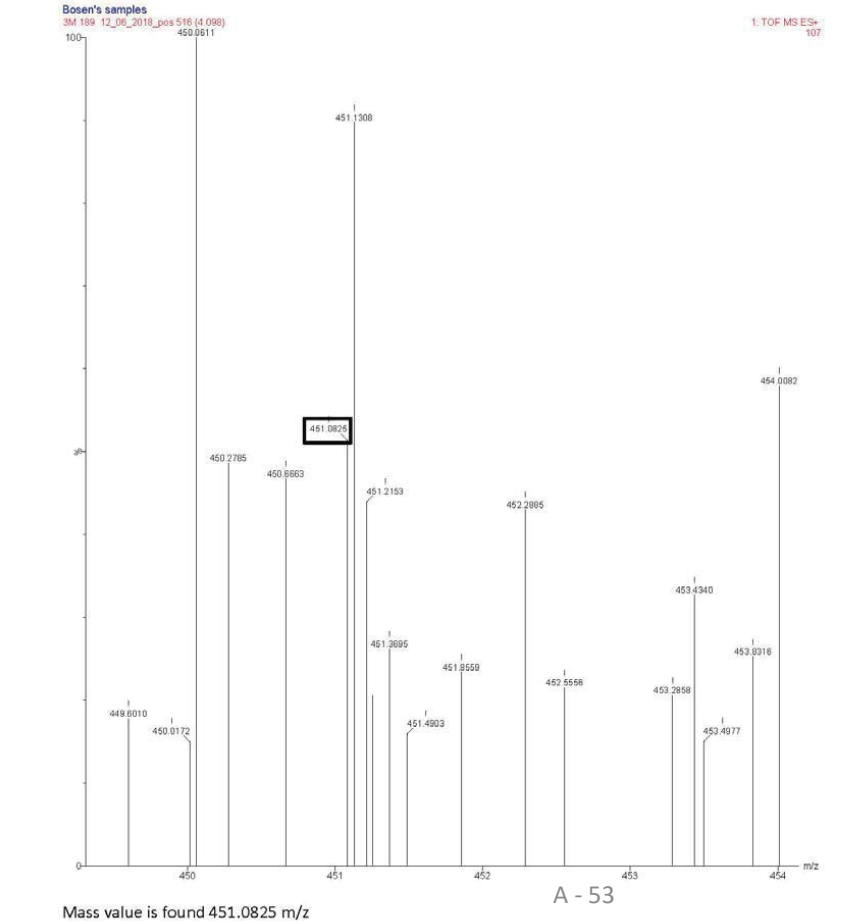

Mass value is found 451.0825 m/z

3M 4_90 – Mass Spectrums and Chromatographs

Figure A3-1: Class 2 of 3M 4_90 - Positive

Class 2

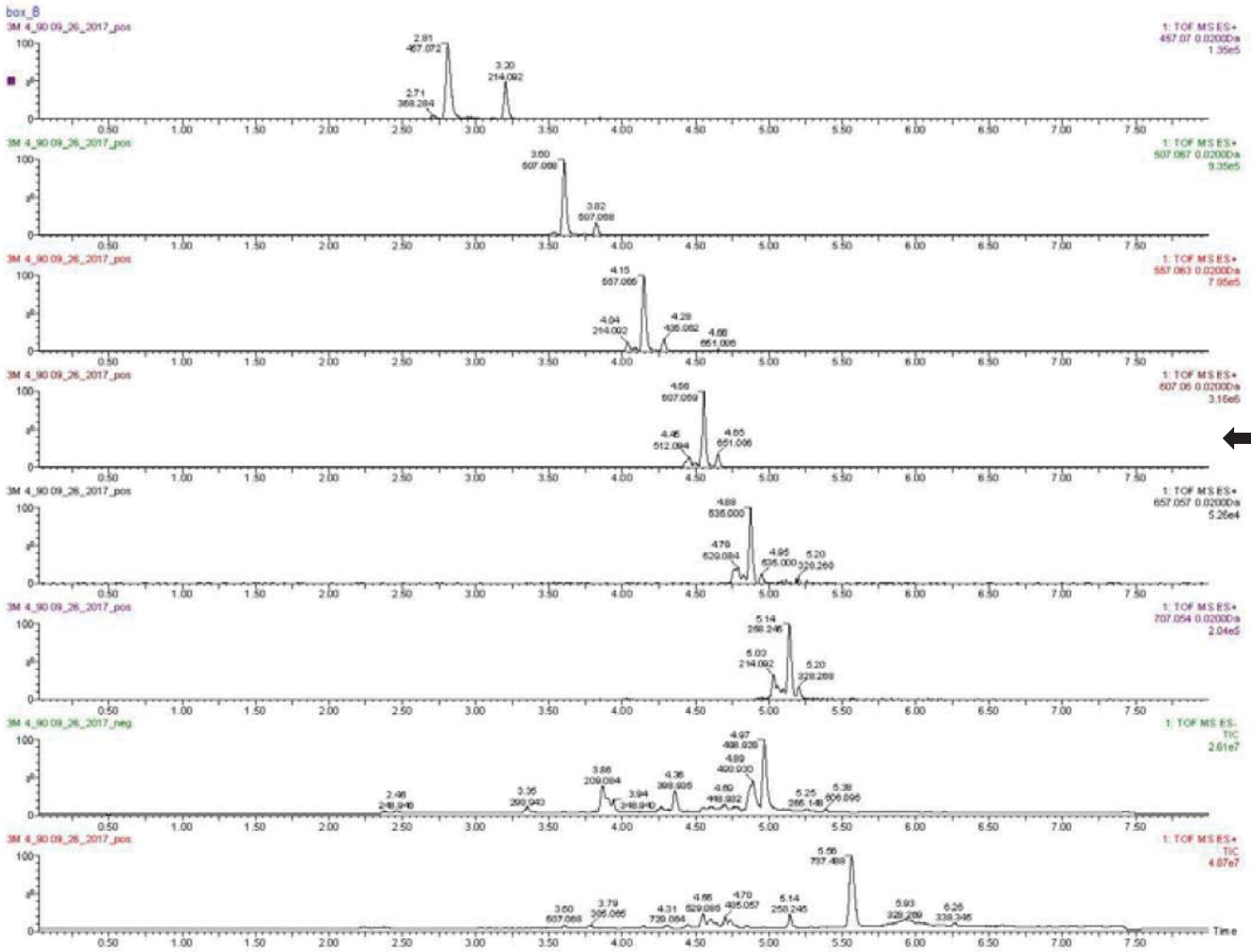

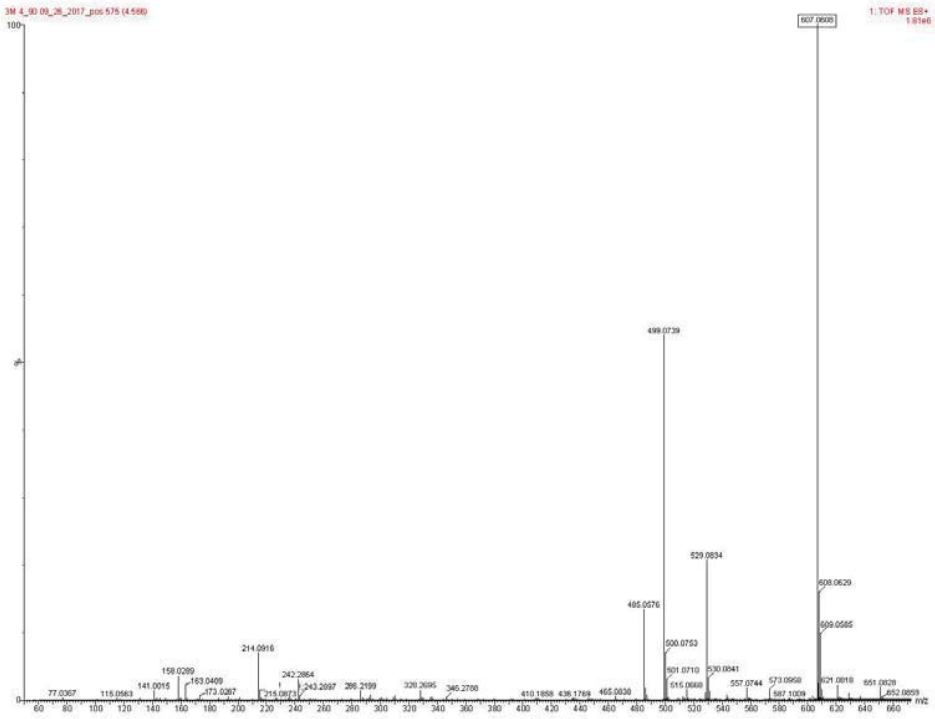

607.0608 m/z

Figure A3-2: Class 3 of 3M 4_90 - Positive

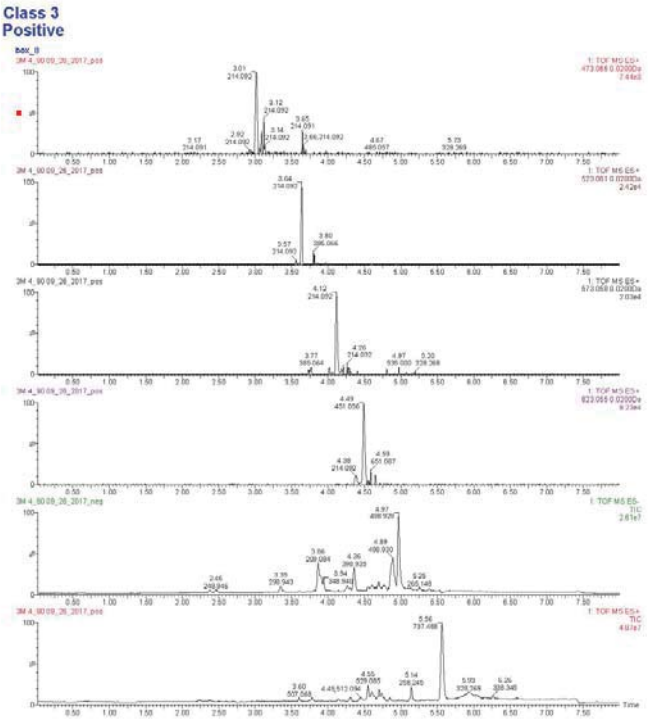

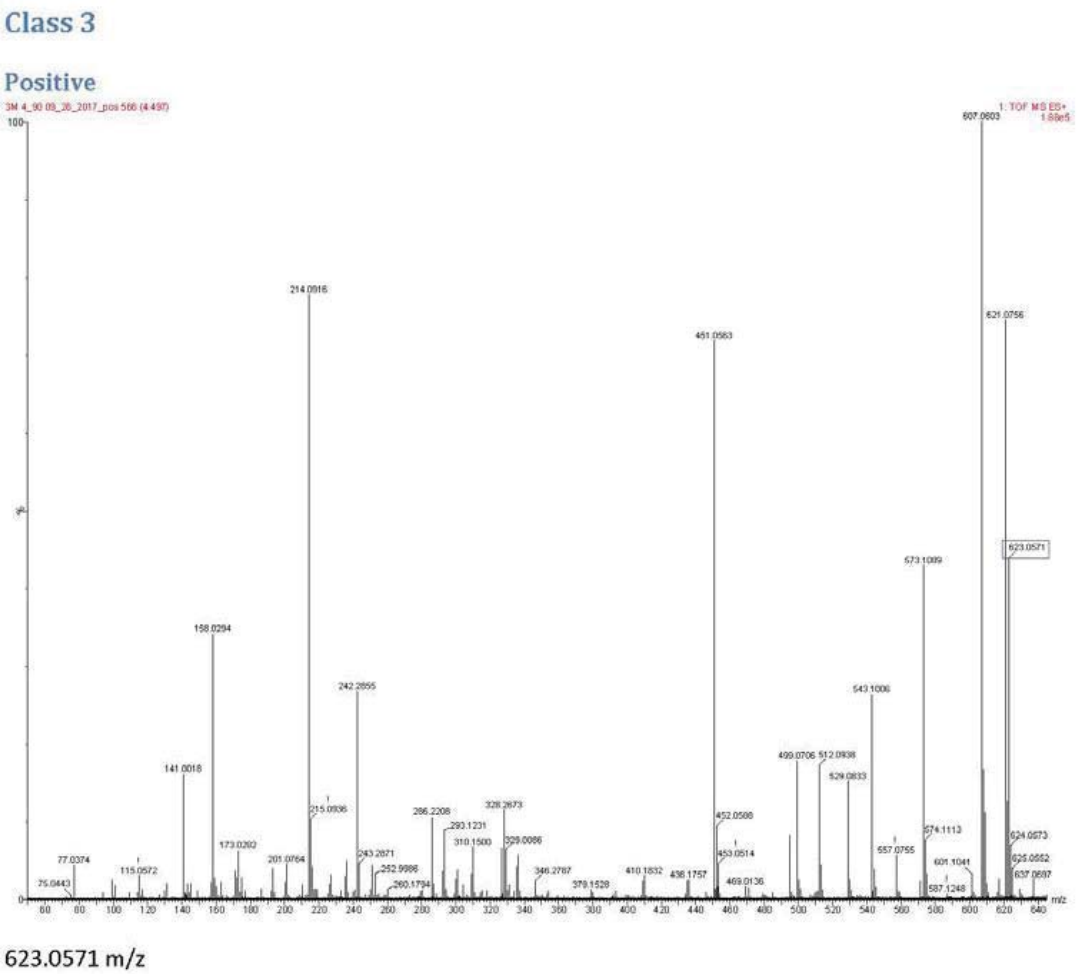

623.0571 m/z

Figure A3-3: Class 4 of 3M 4_90 - Positive

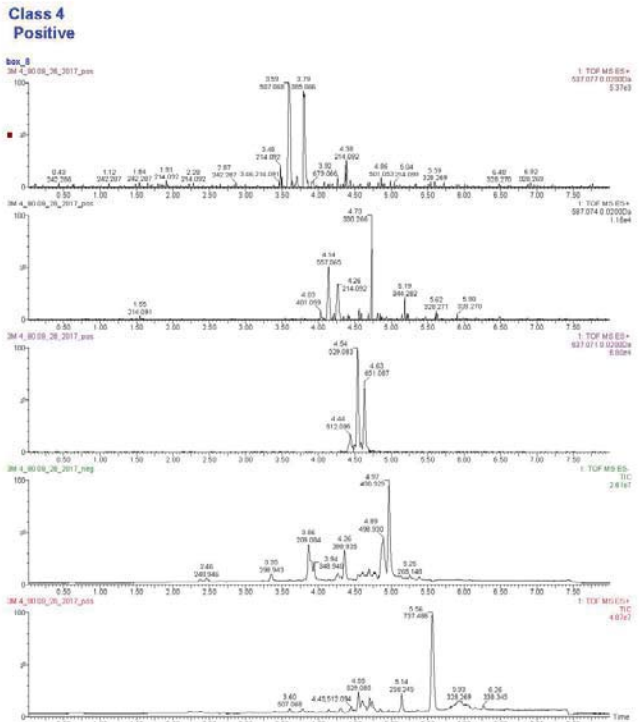

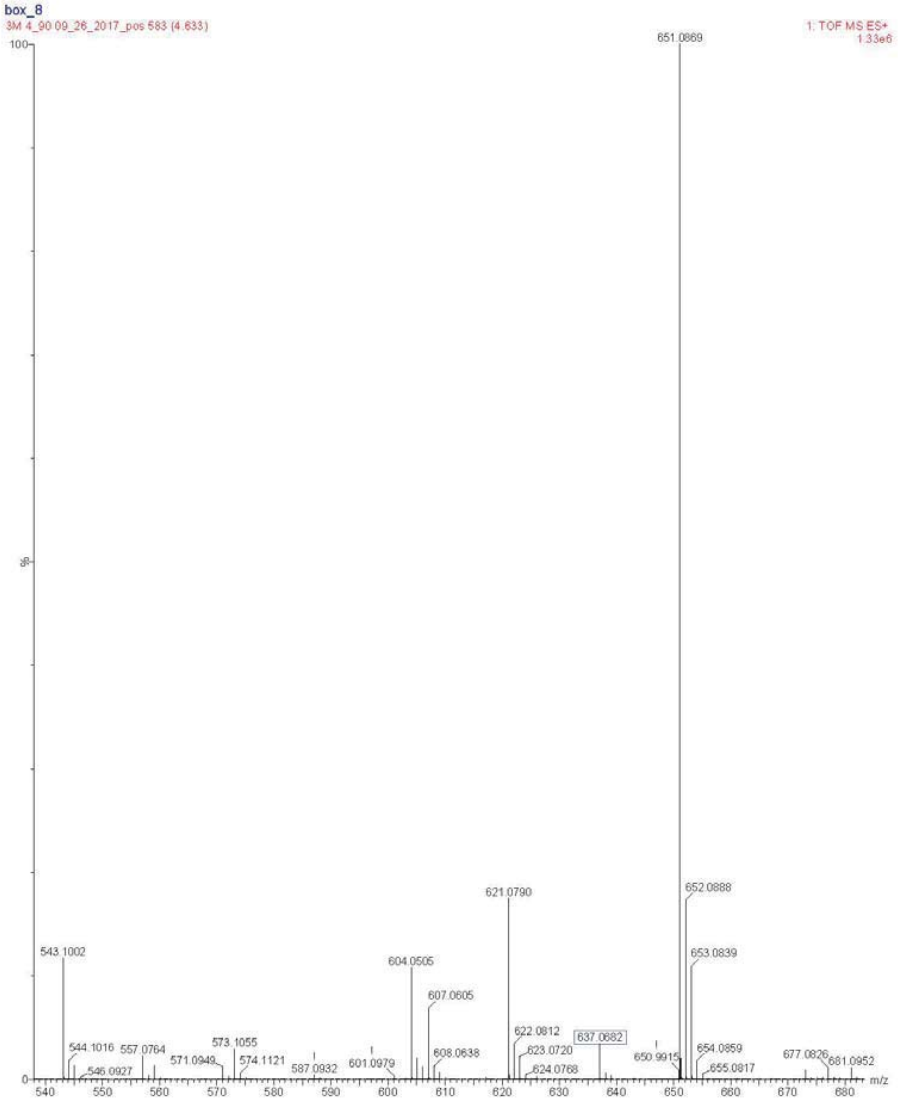

637.0682 m/z

Figure A3-4: Class 5 of 3M 4_90 - Positive

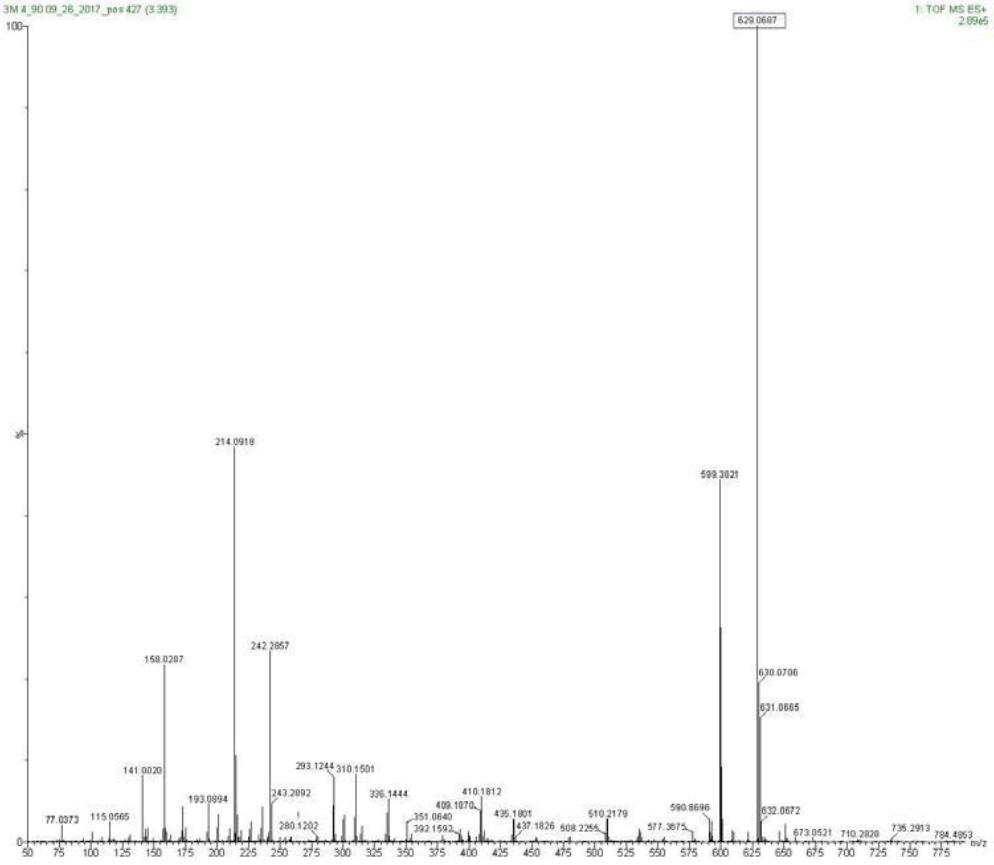

629.0687 m/z

Figure A3-5: Class 8 of 3M 4_90 - Positive

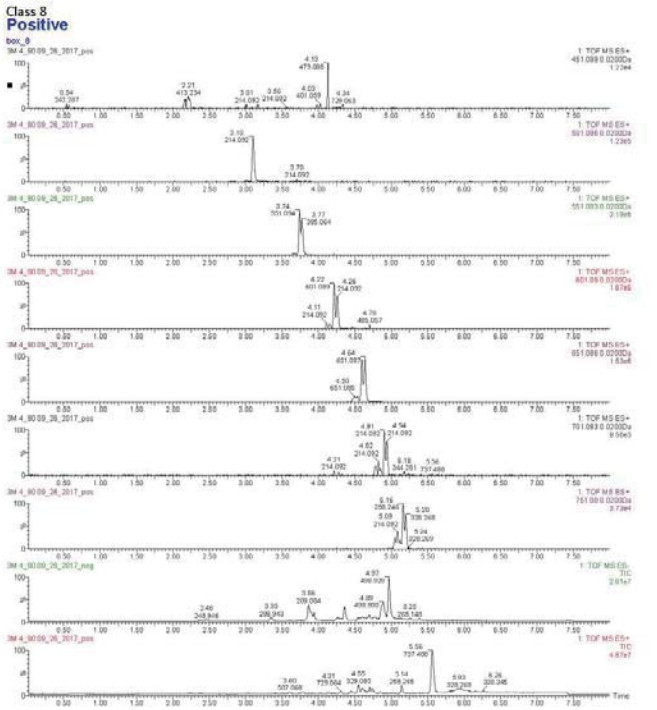

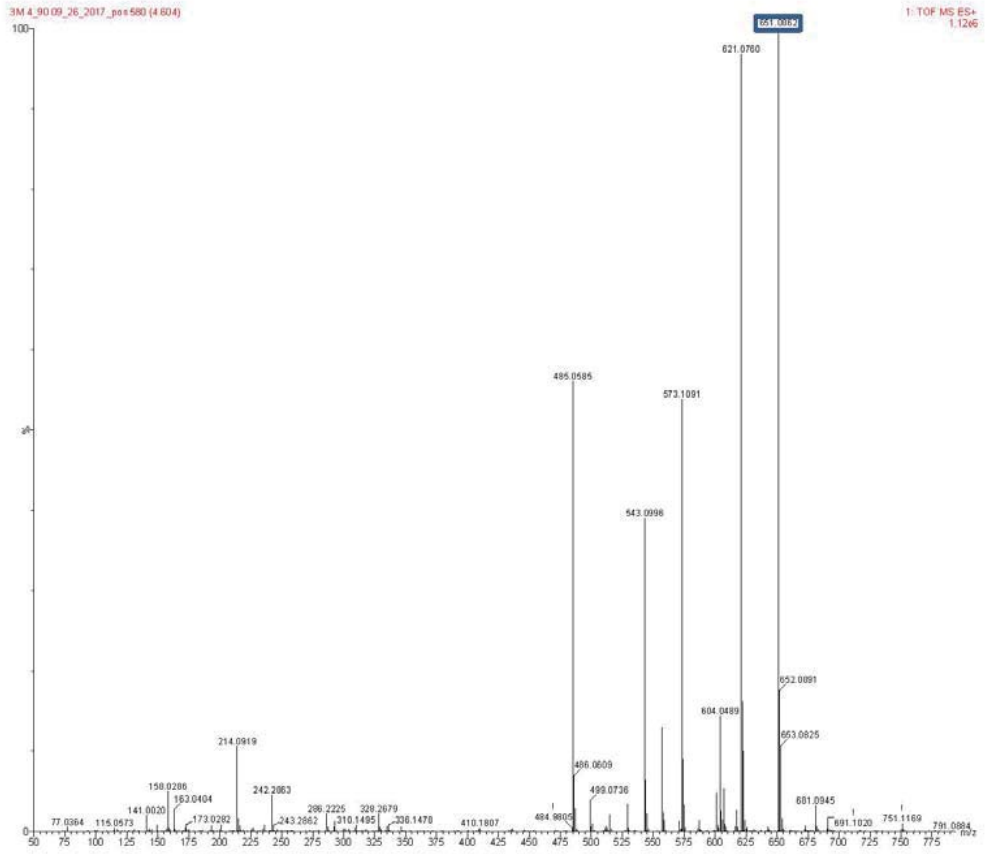

651.0862m/z

Figure A3-6: Class 9 of 3M 4_90 - Positive

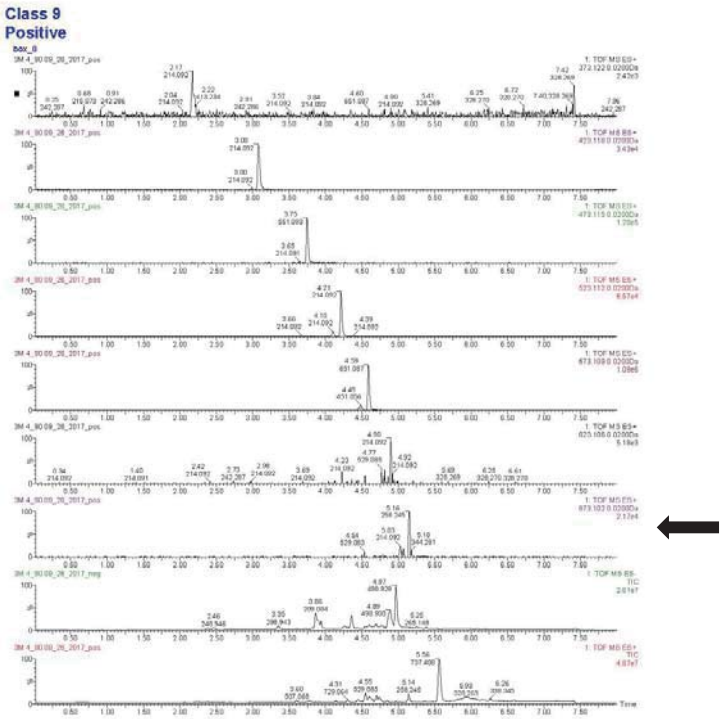

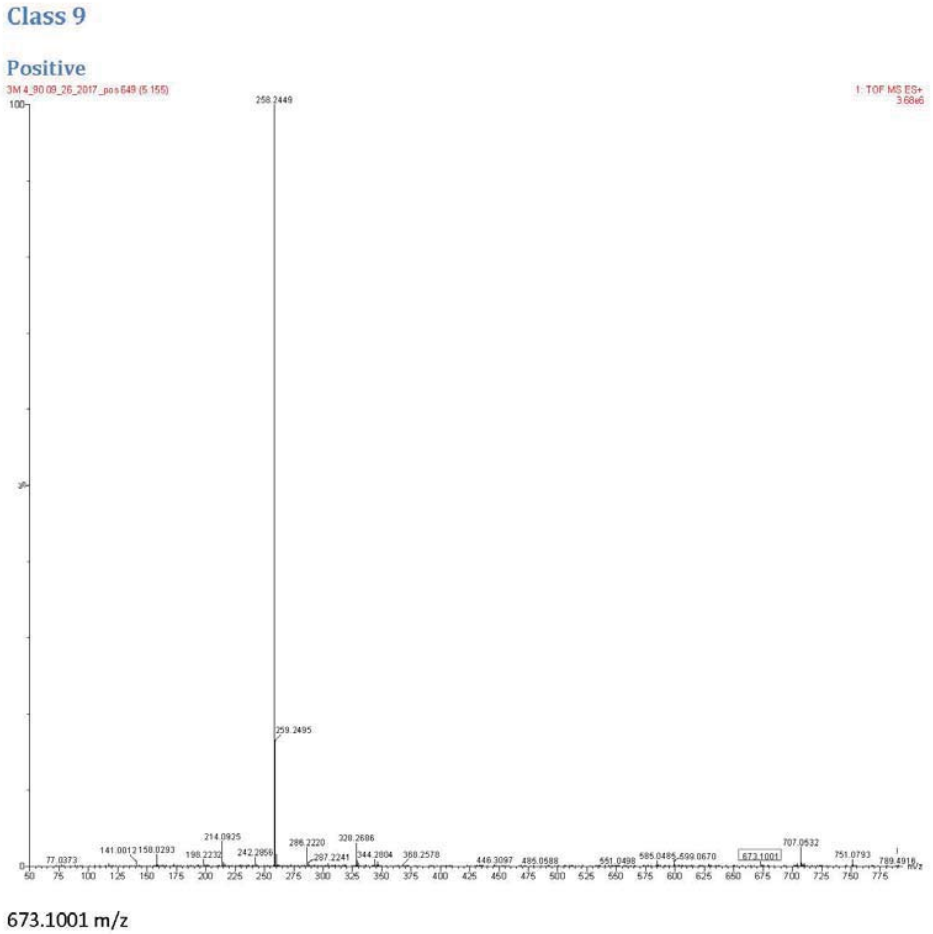

673.1001 m/z

Figure A3-7: Class 10 of 3M 4_90 - Positive

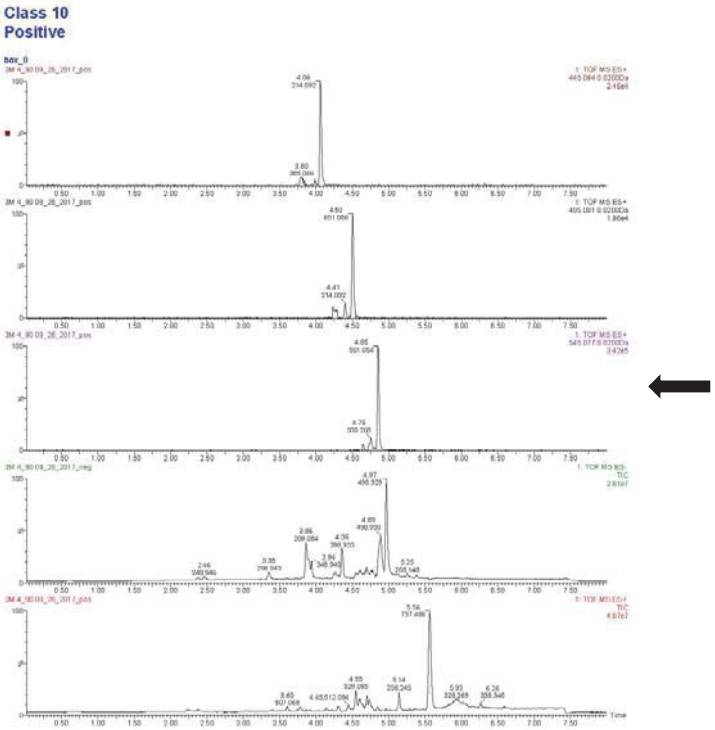

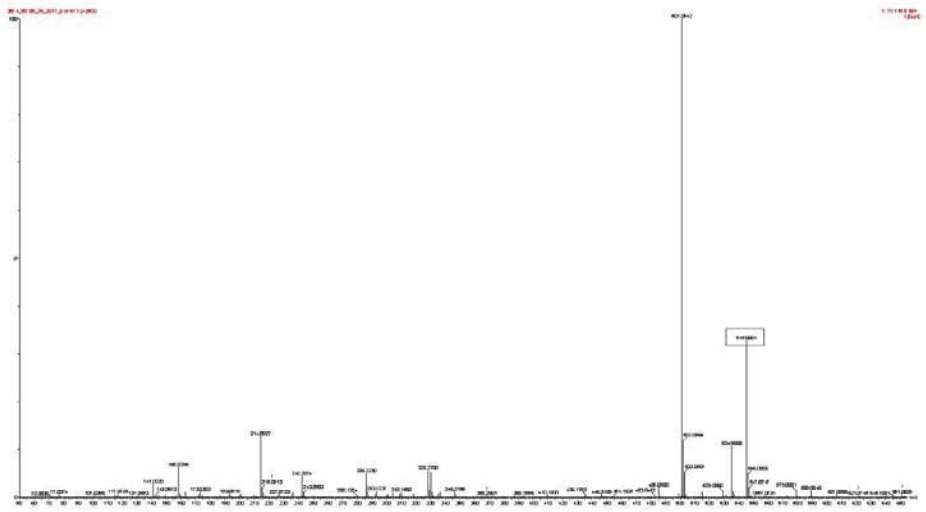

545.0804 m/z

Figure A3-8: Class 11 of 3M 4_90 - Positive

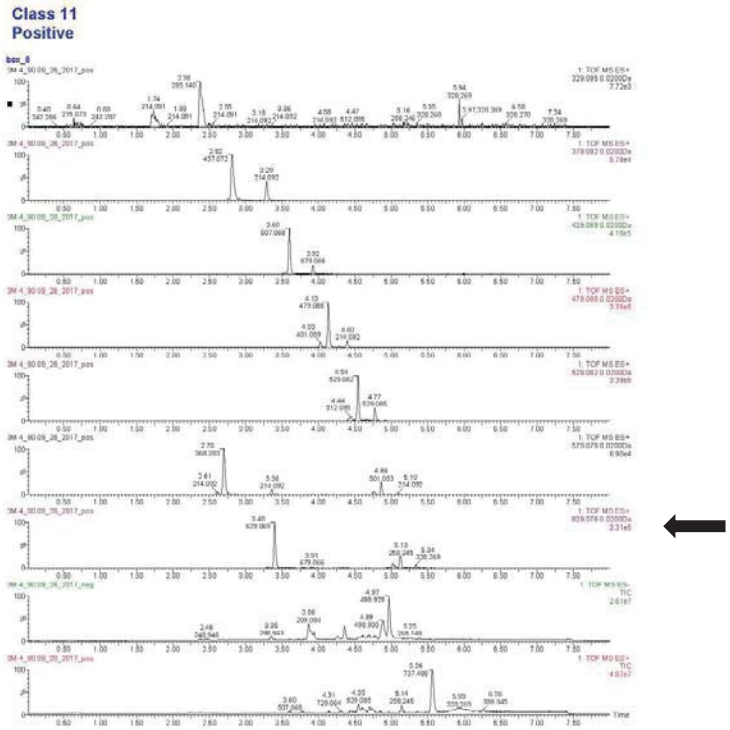

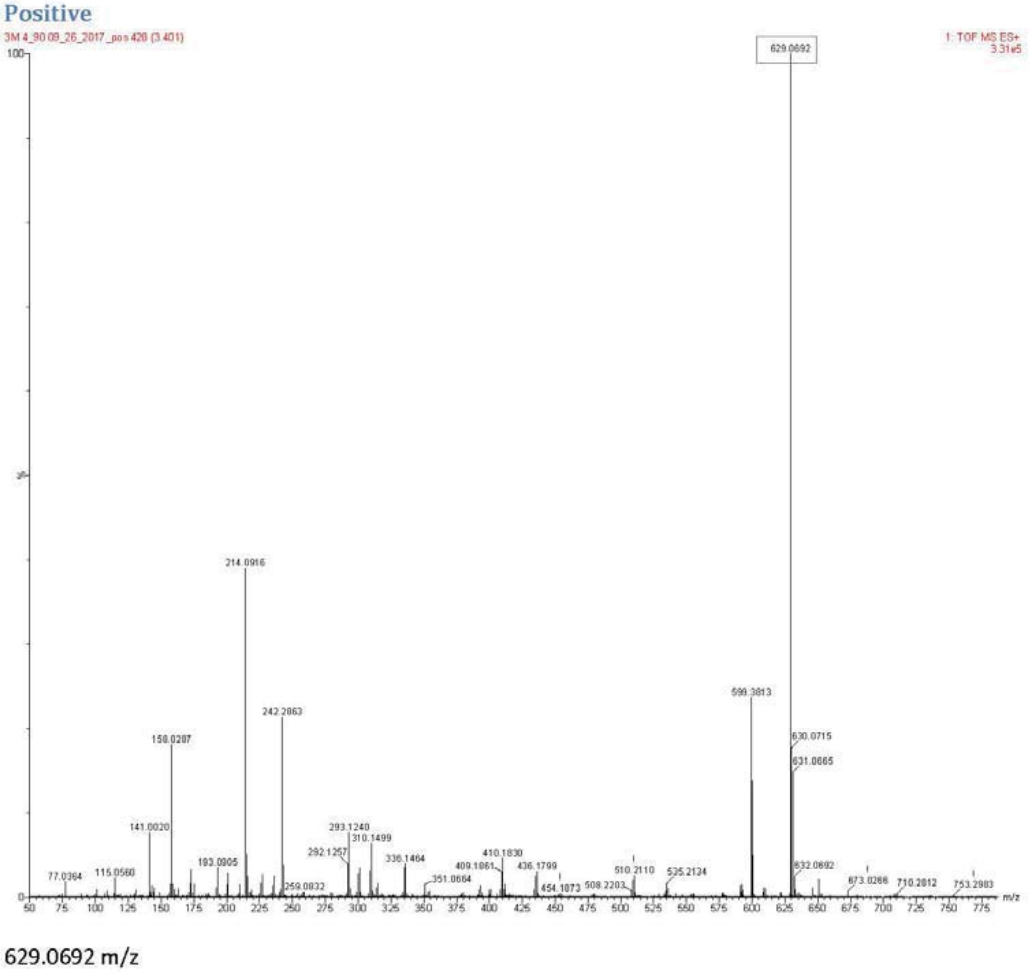

Figure A3-9: Class 12 of 3M 4_90 - Positive

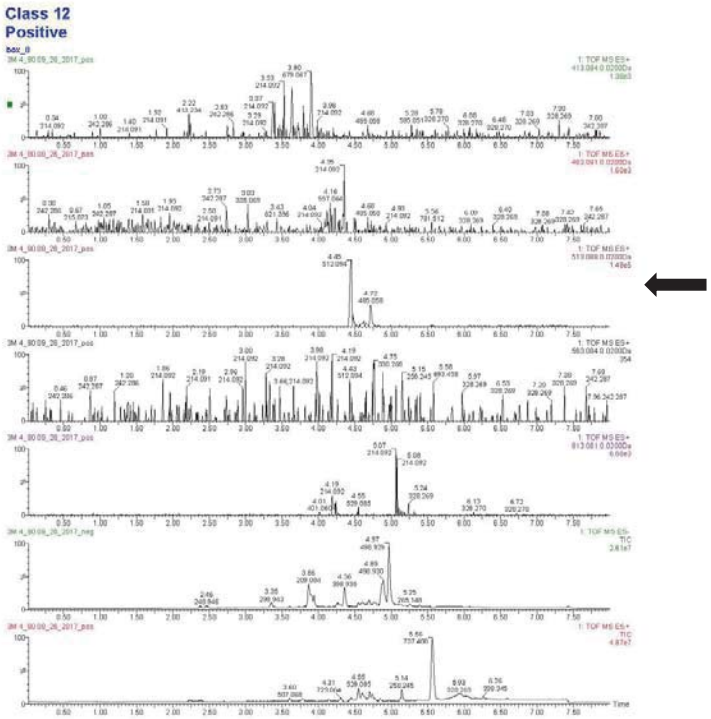

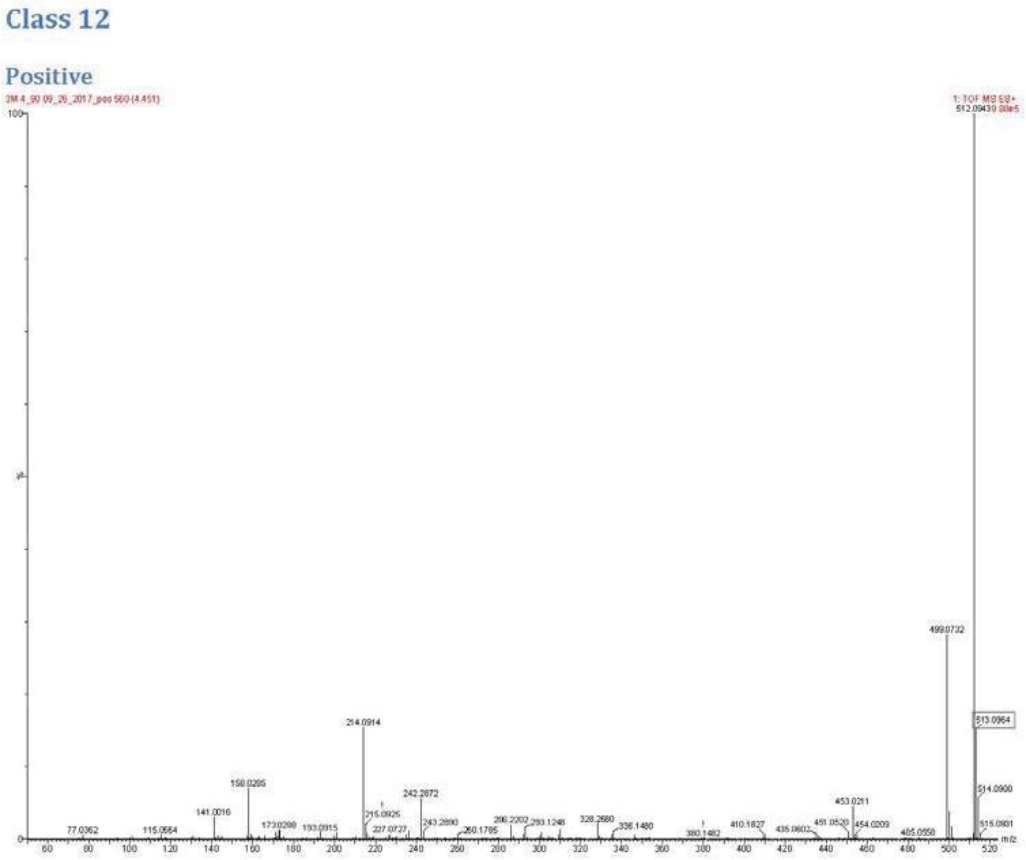

513.0964 m/z (only one of 5 was clear)

Figure A3-10: Class 13 of 3M 4_90 - Positive

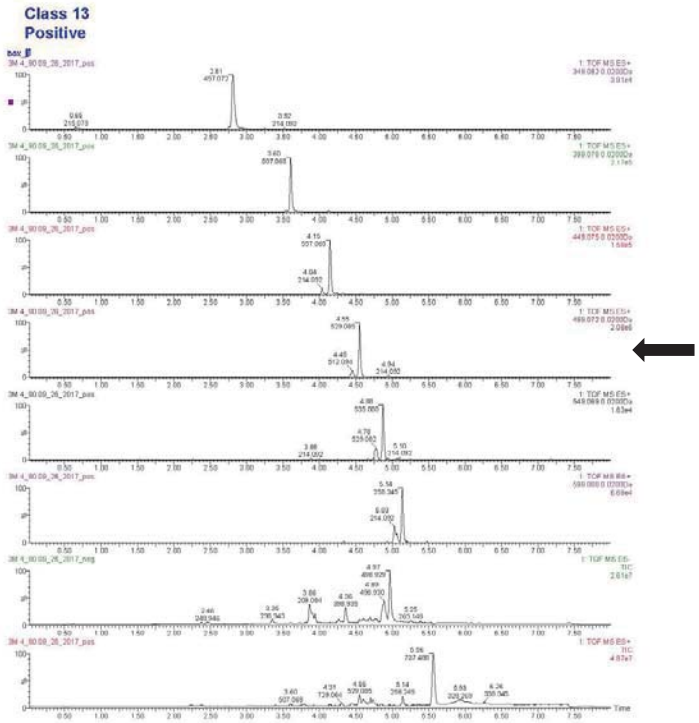

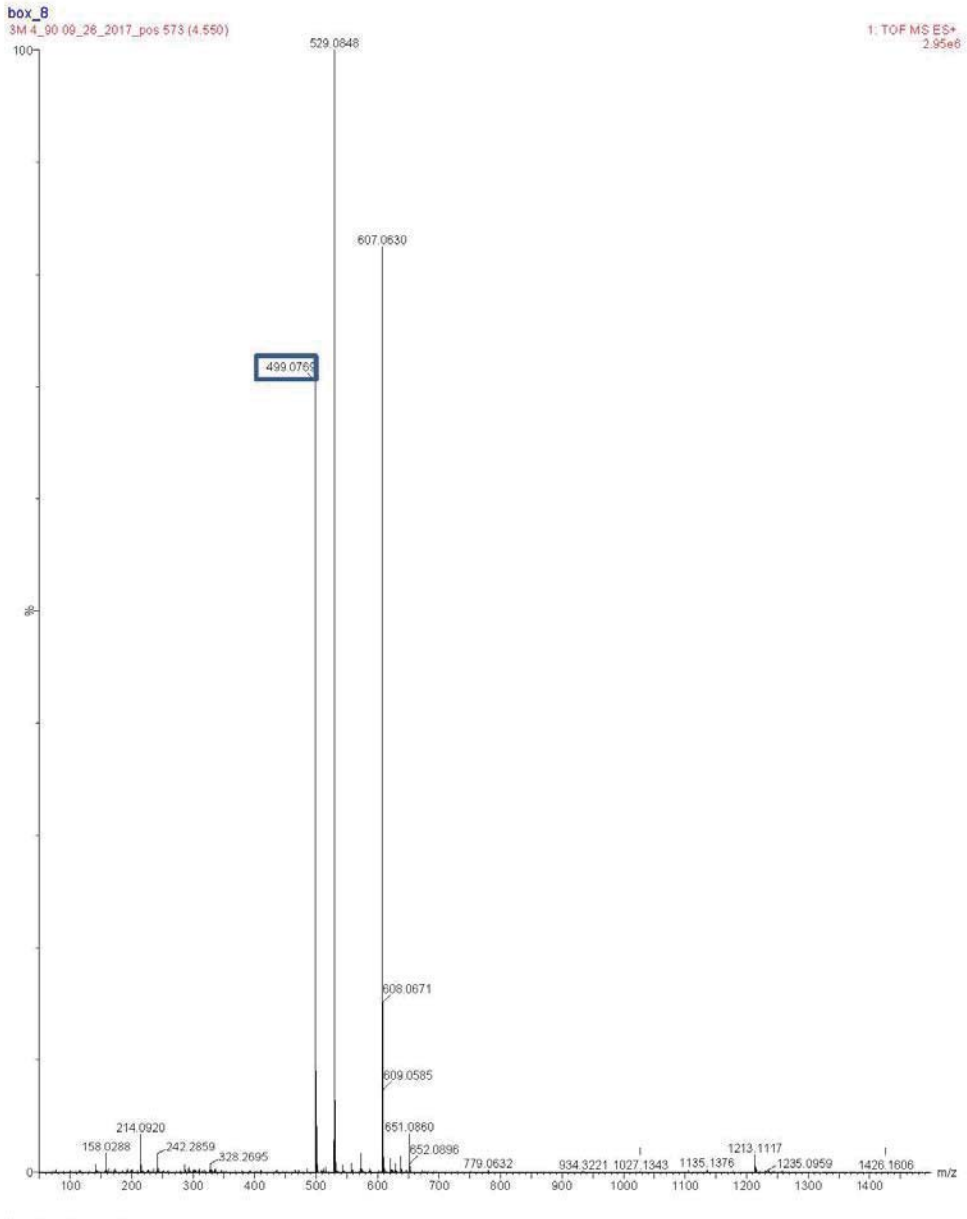

499.0769 m/z

Figure A3-11: Class 15 of 3M 4_90 - Positive

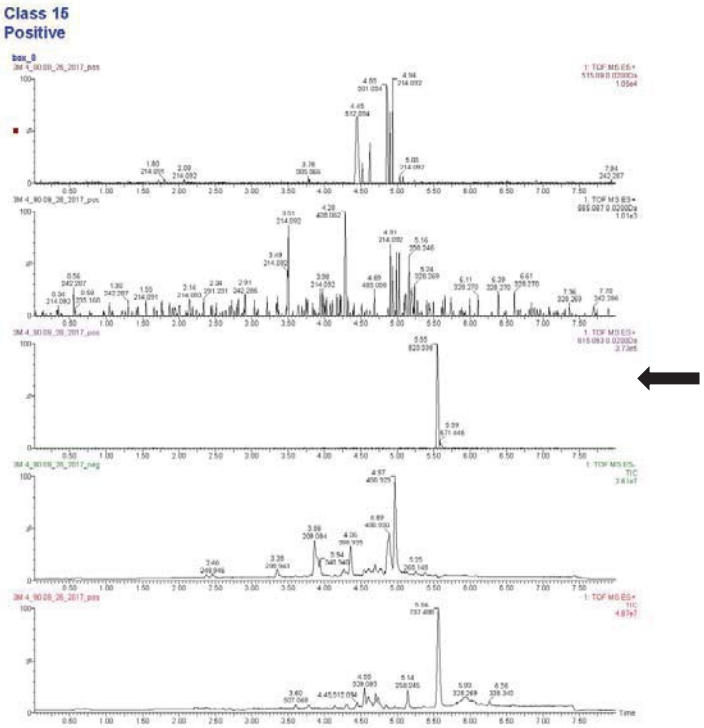

Class 15

Positive

box_8

3M 4_90 09_26_2017_pos 700 (5.557)

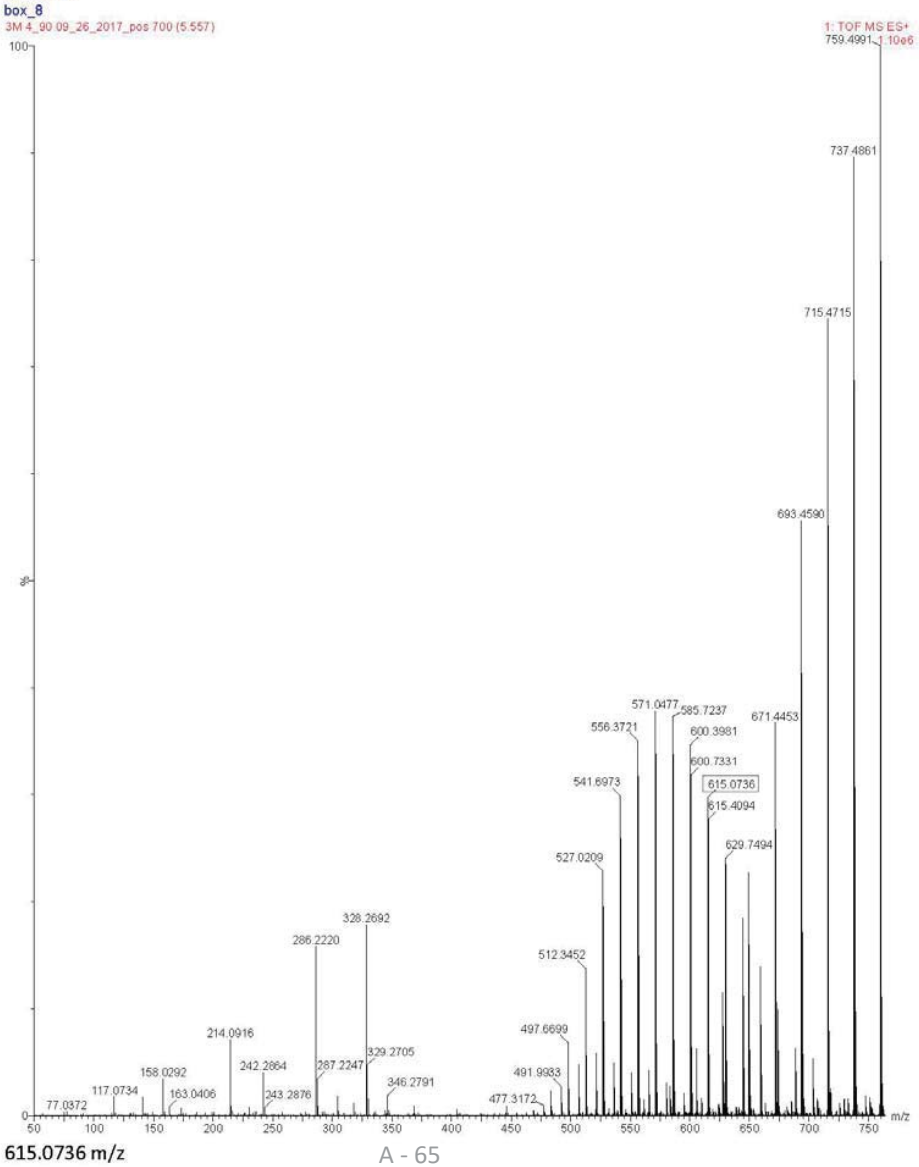

Figure A3-12: Class 16 of 3M 4_90 - Positive

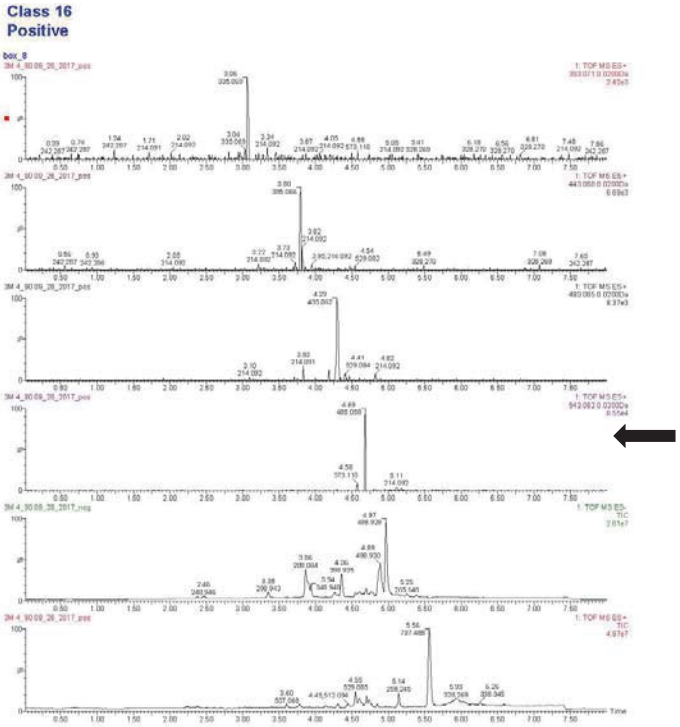

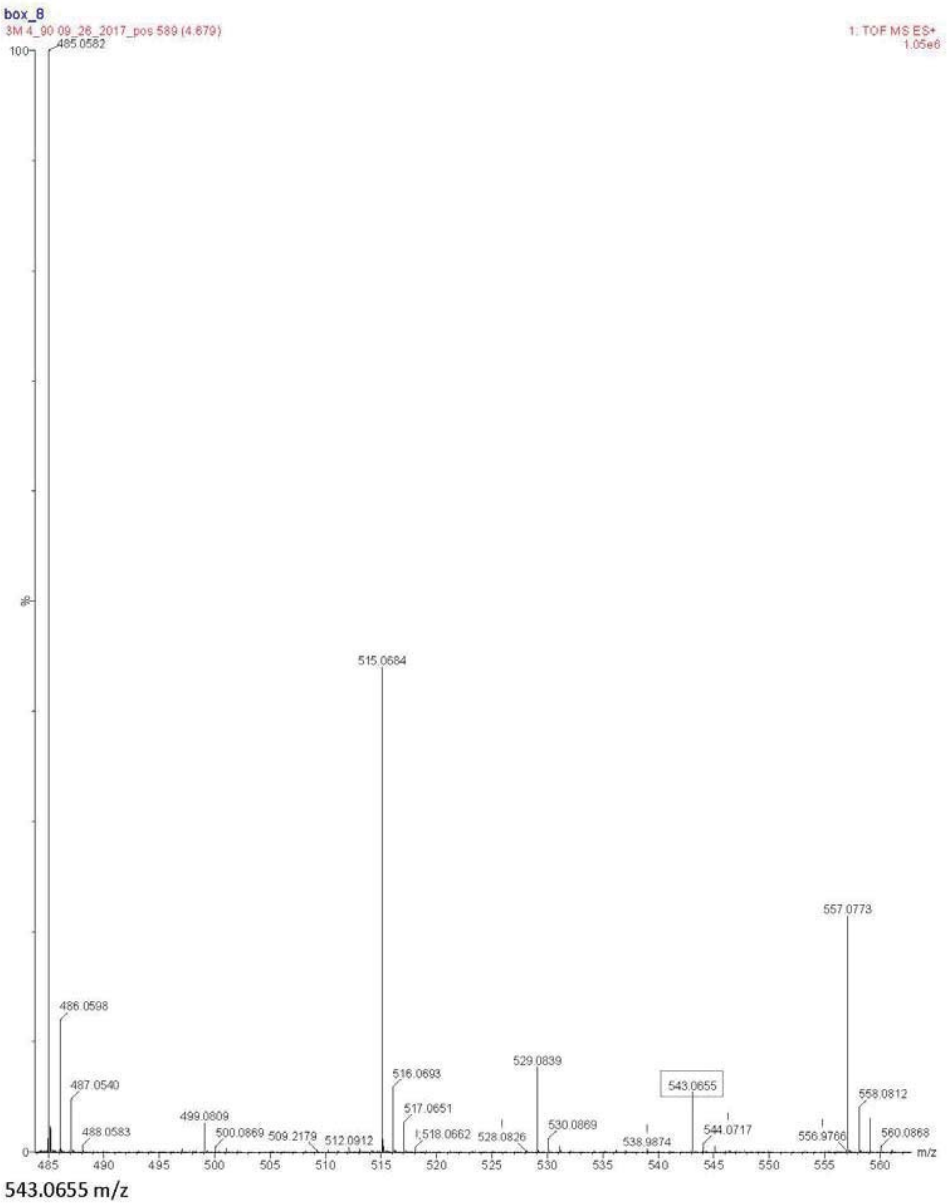

Figure A3-13: Class 28 of 3M 4_90 - Positive

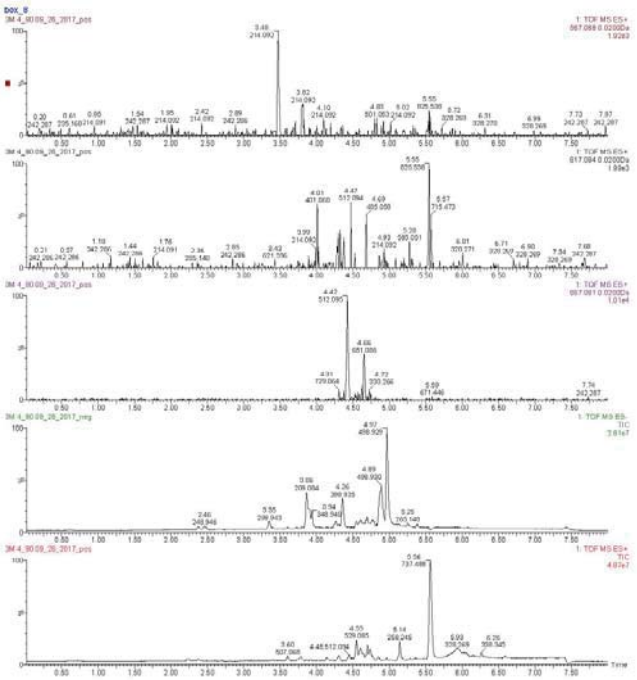

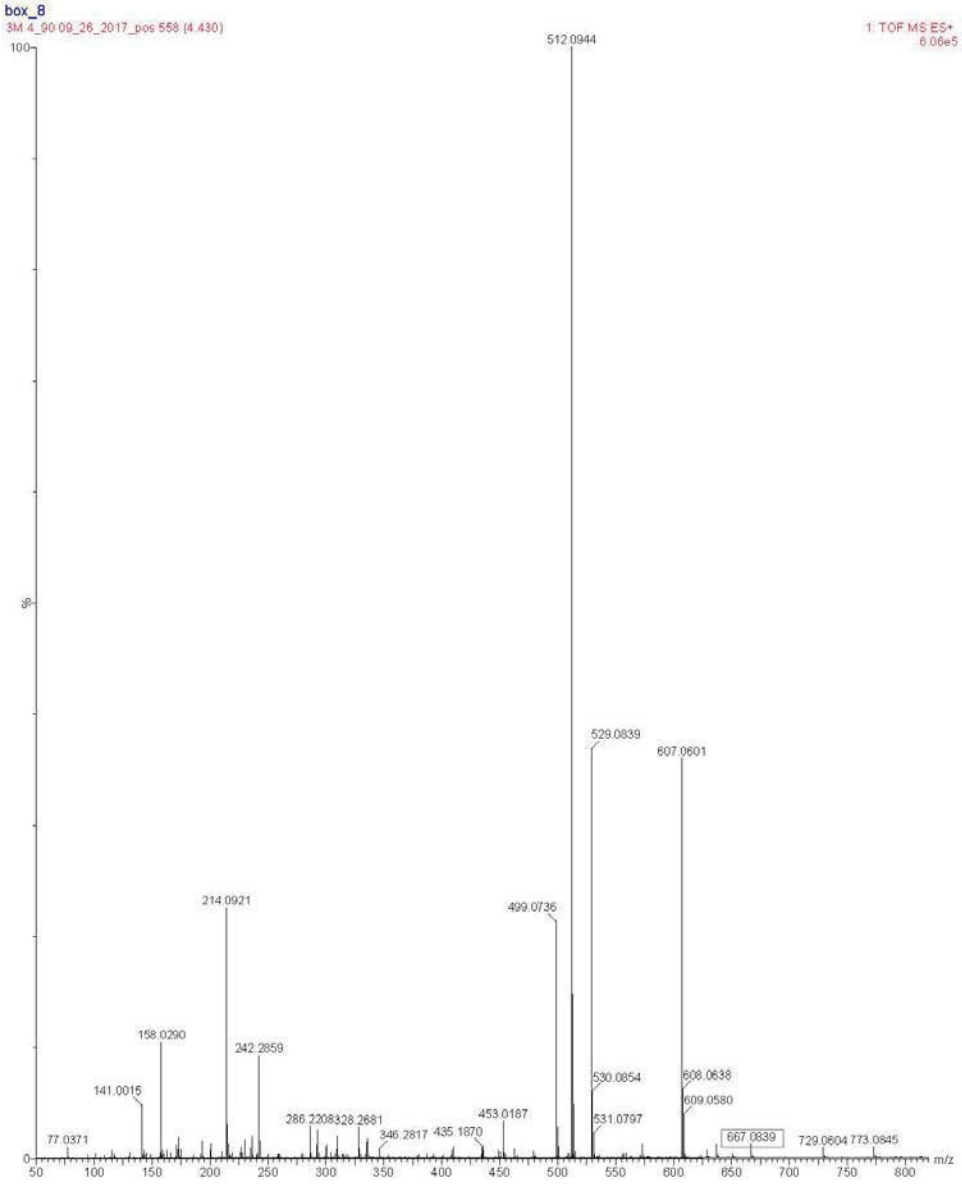

667.0839 m/z

Figure A3-14: Class 29 of 3M 4_90 - Positive

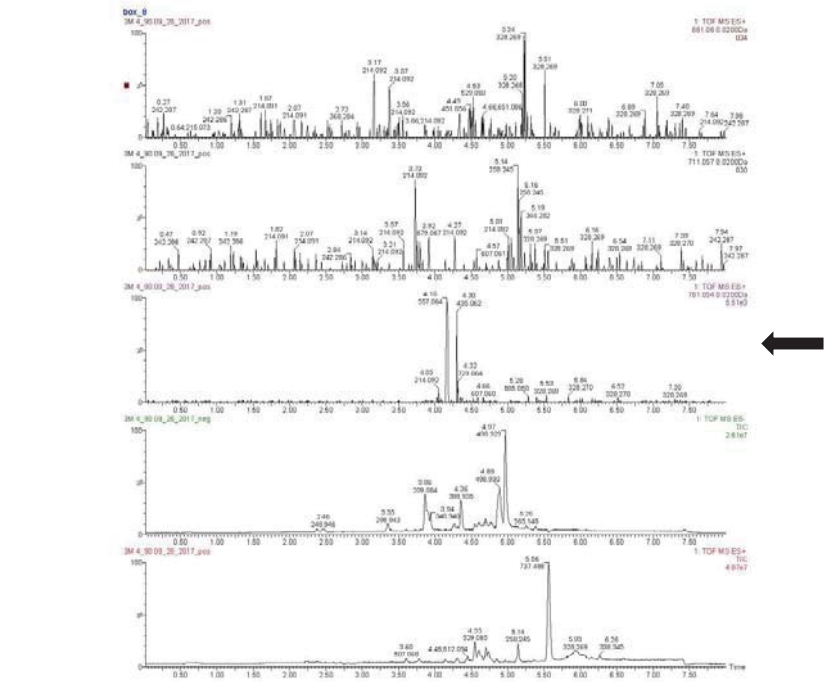

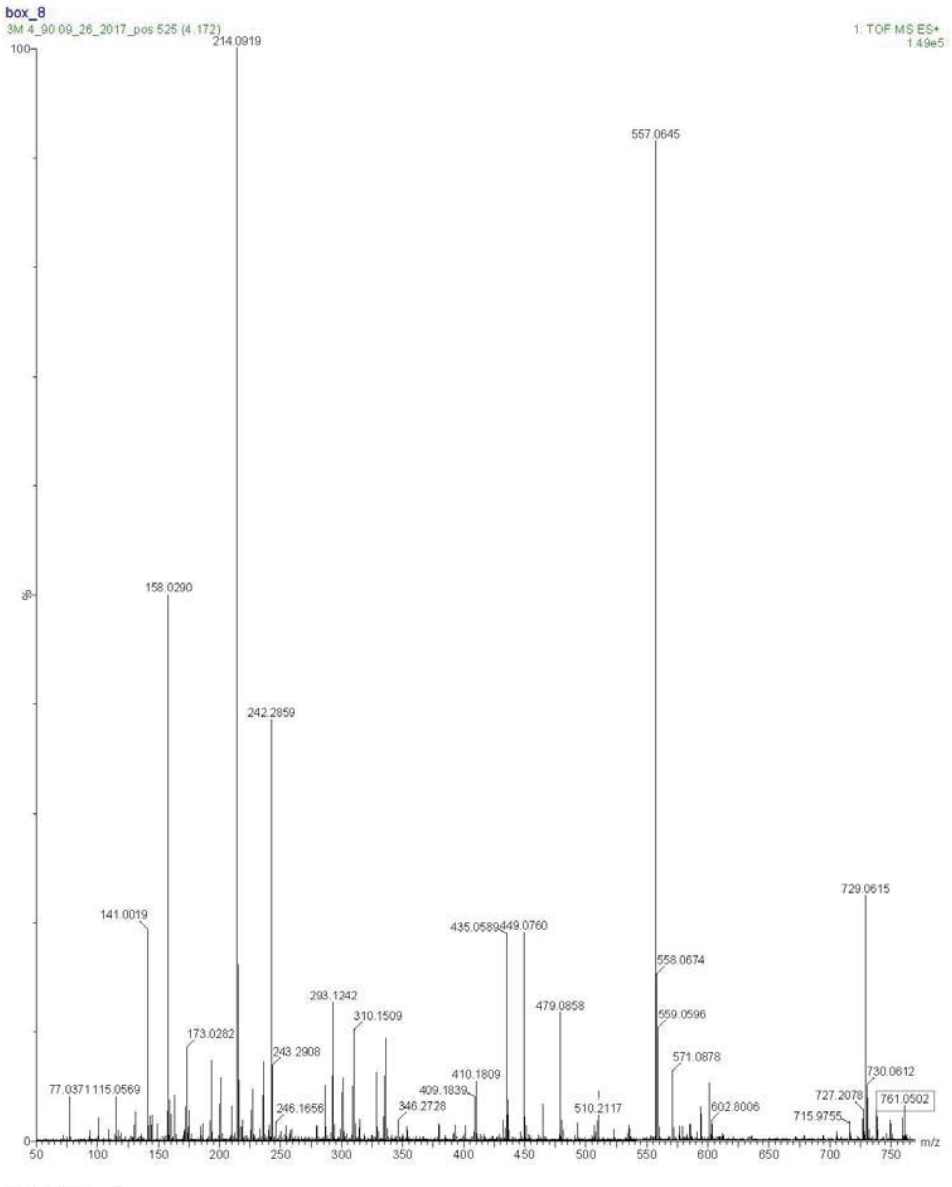

761.0502 m/z

Figure A3-15: Class 31 of 3M 4_90 - Positive

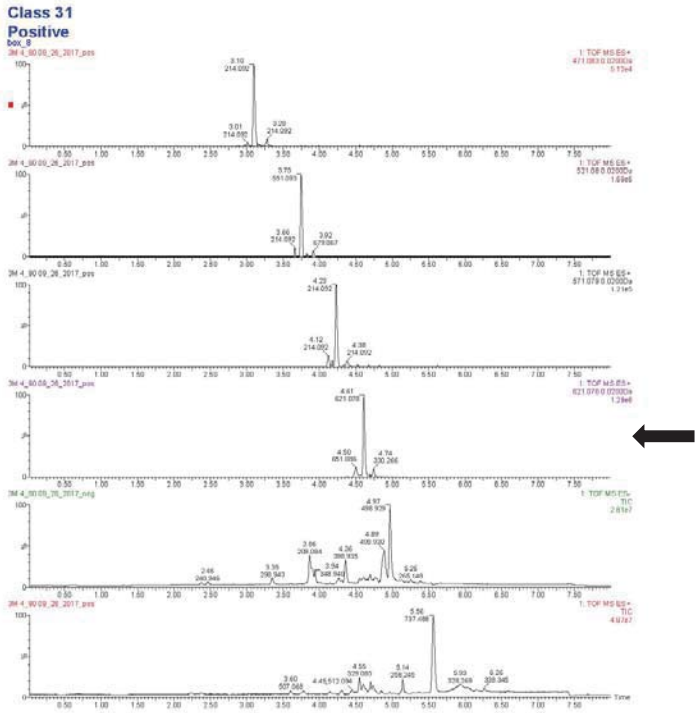

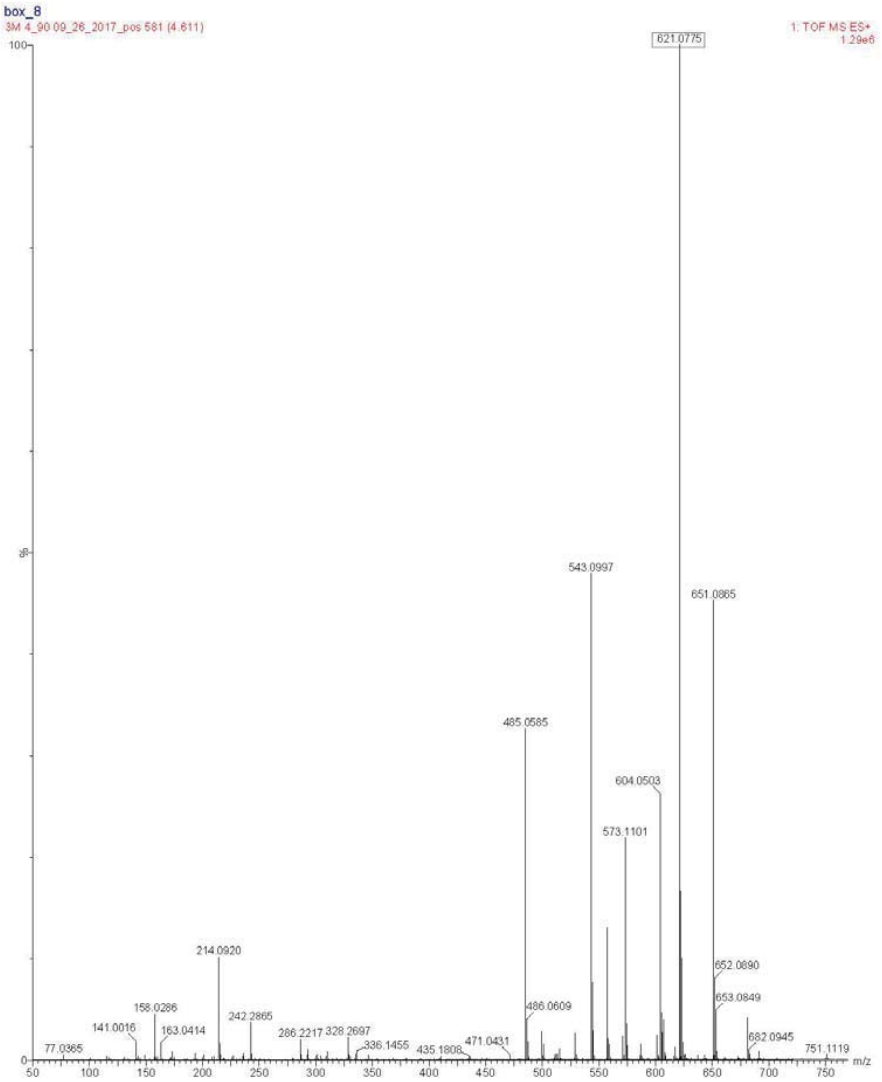

621.0775m/z

Figure A3-16: Class 32 of 3M 4_90 - Positive

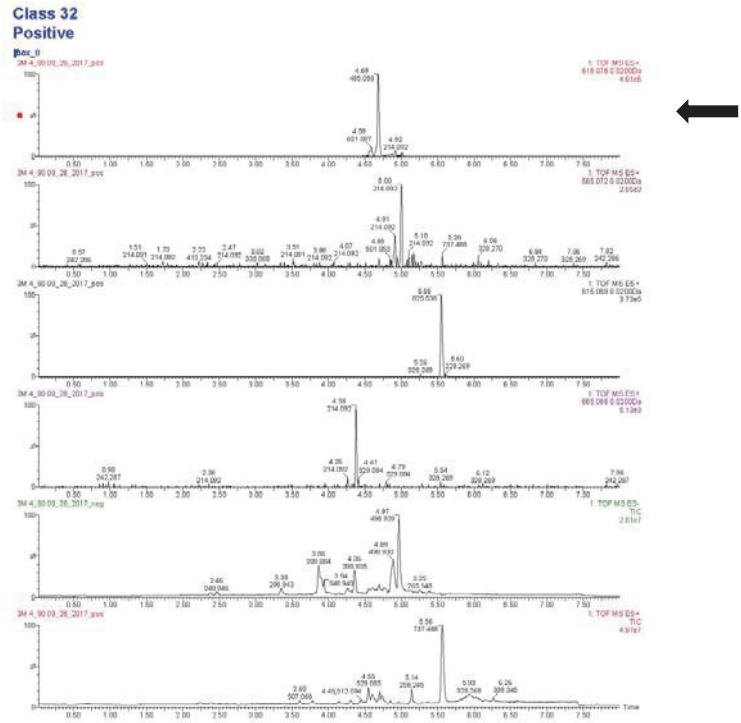

Class 32

Positive

box_8

3M 4_90 09_26_2017_pos 590 (4.686)

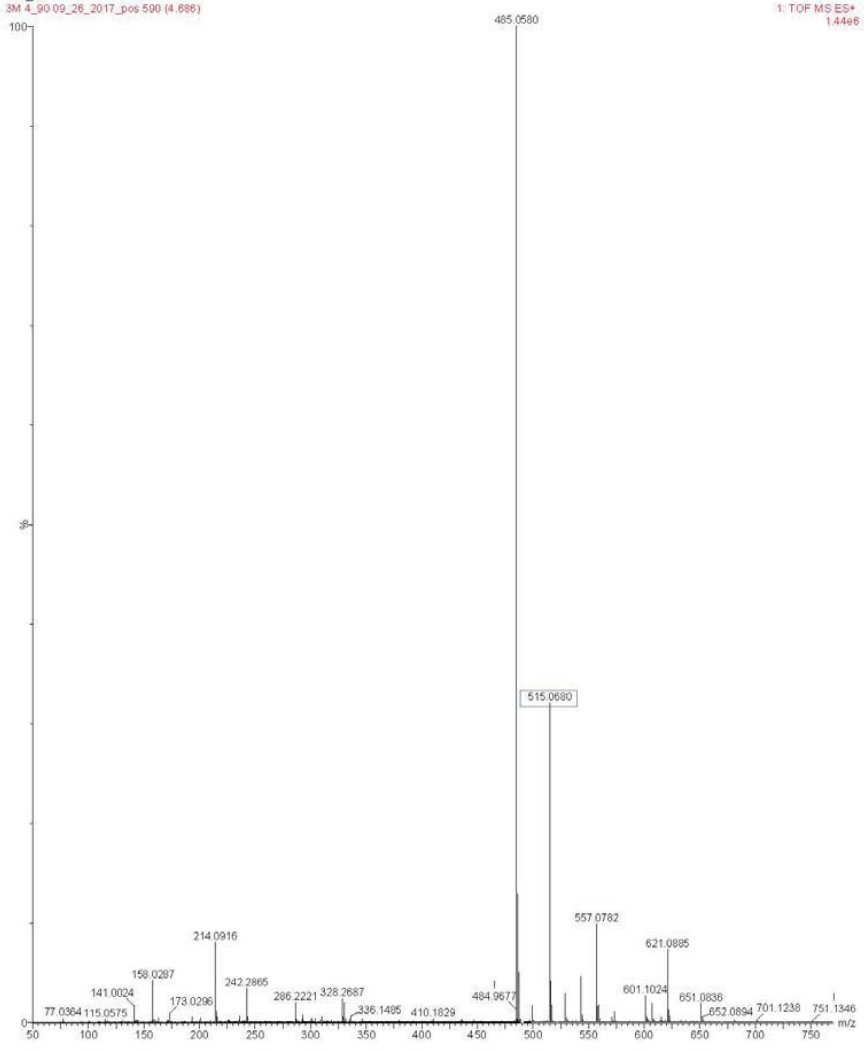

515.0680 m/z

Figure A3-17: Class 33 of 3M 4_90 - Positive

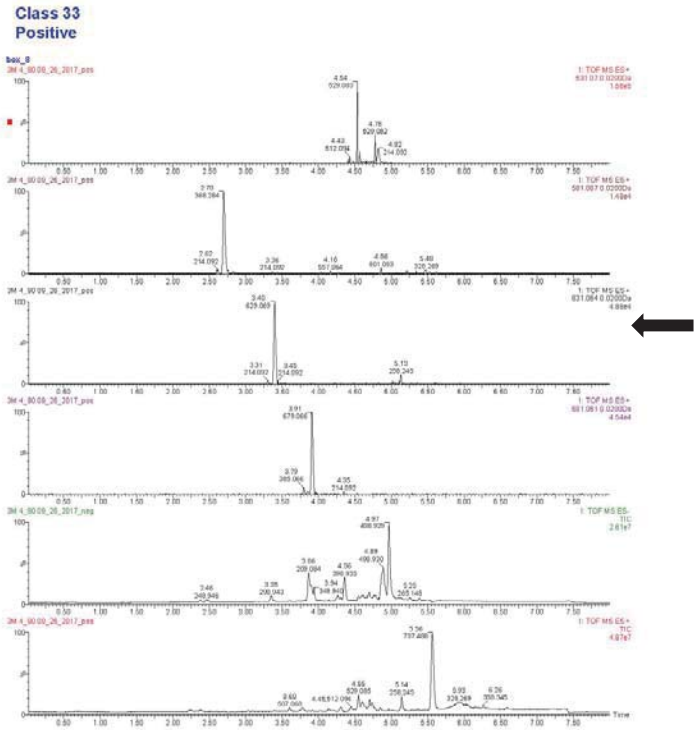

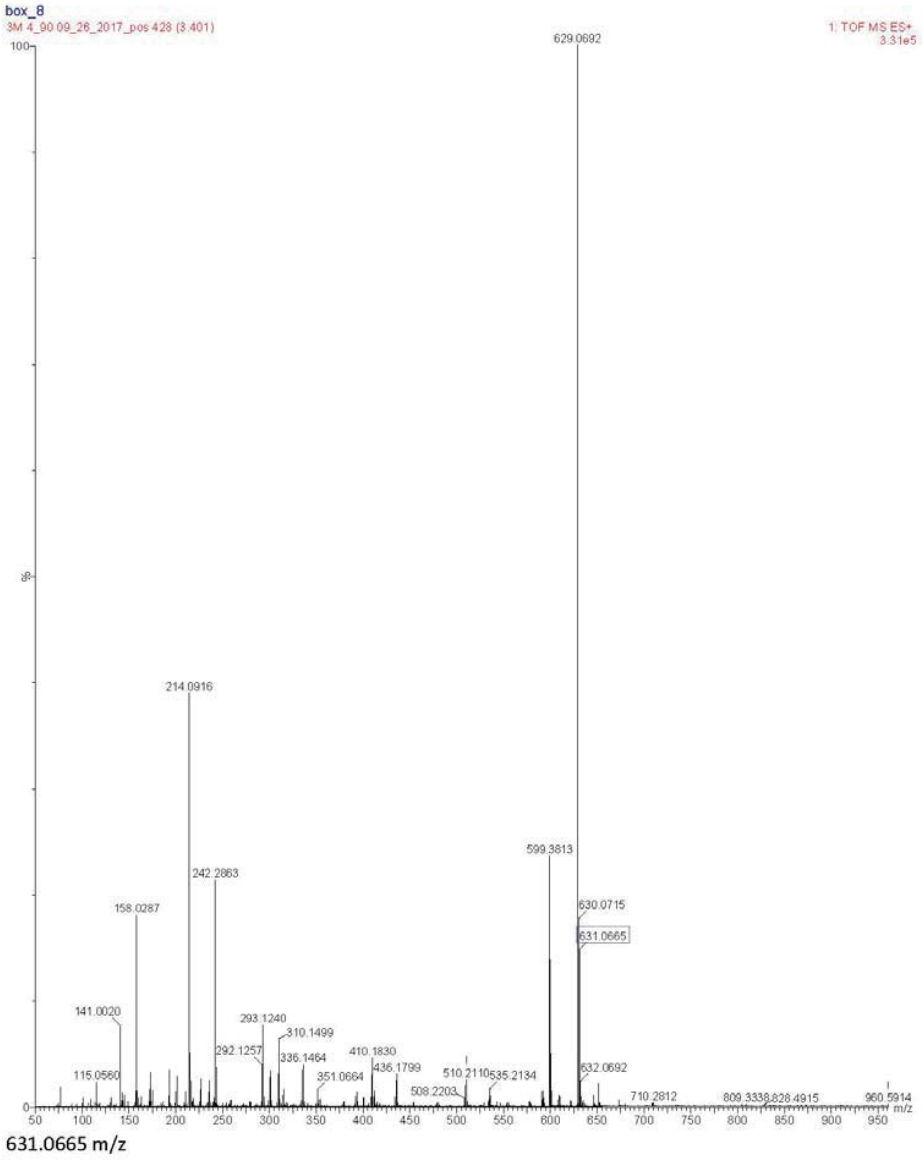

Figure A3-18: Class 34 of 3M 4_90 - Positive

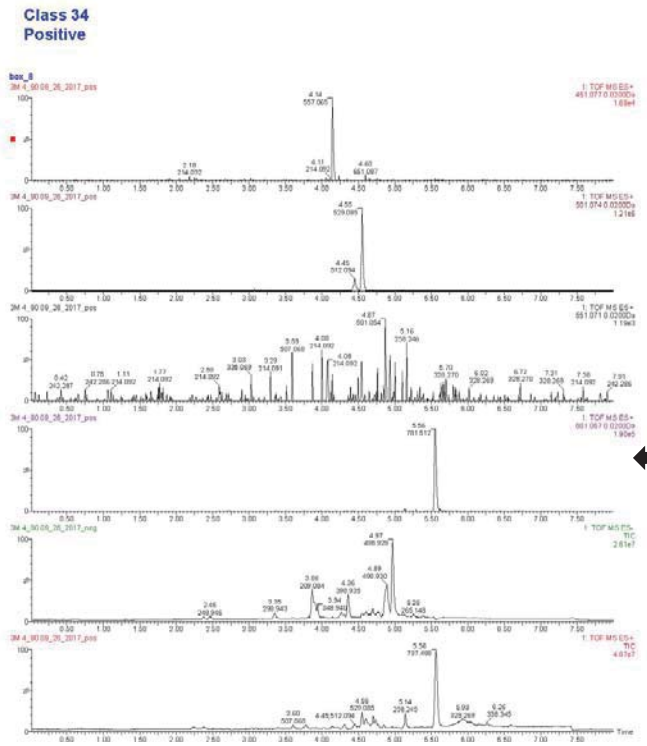

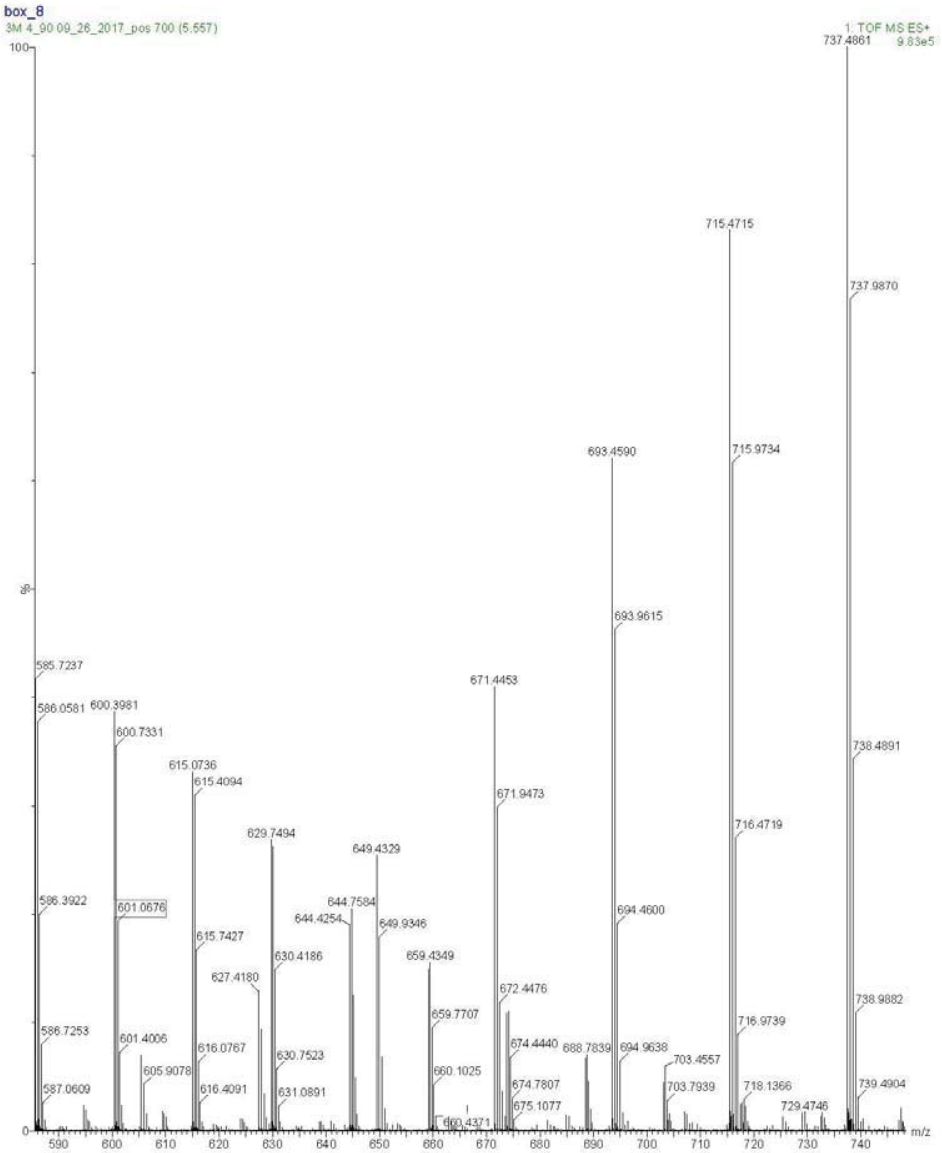

601.0676 m/z

Figure A3-19: Class 37 of 3M 4_90 - Positive

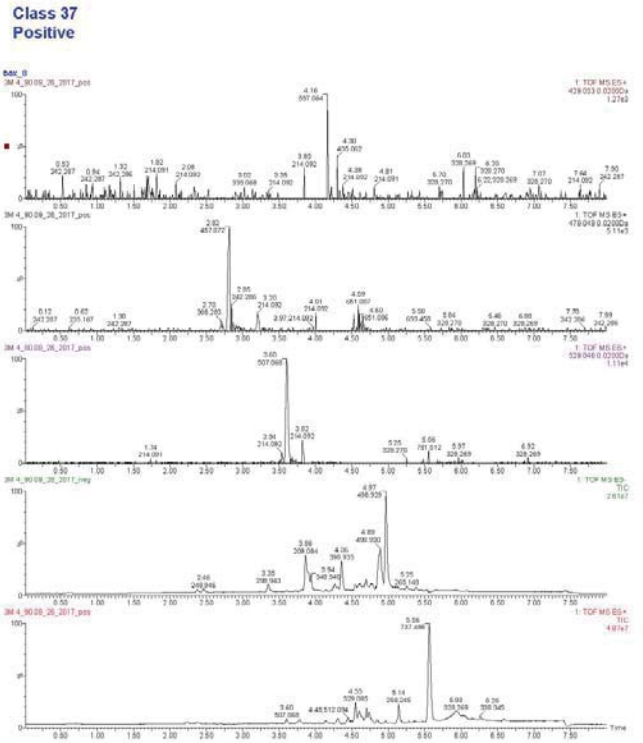

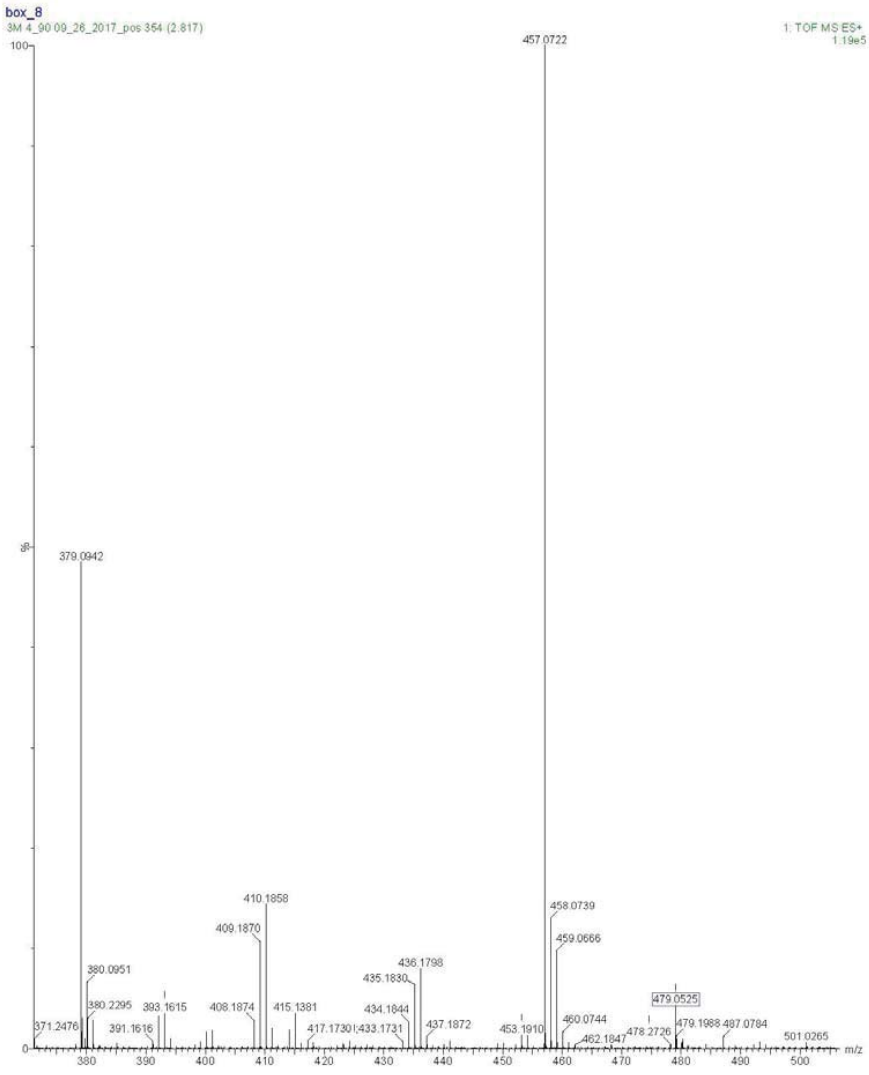

479.0525 m/z

Figure A3-19: Class 1 of 3M 4_90 - Negative

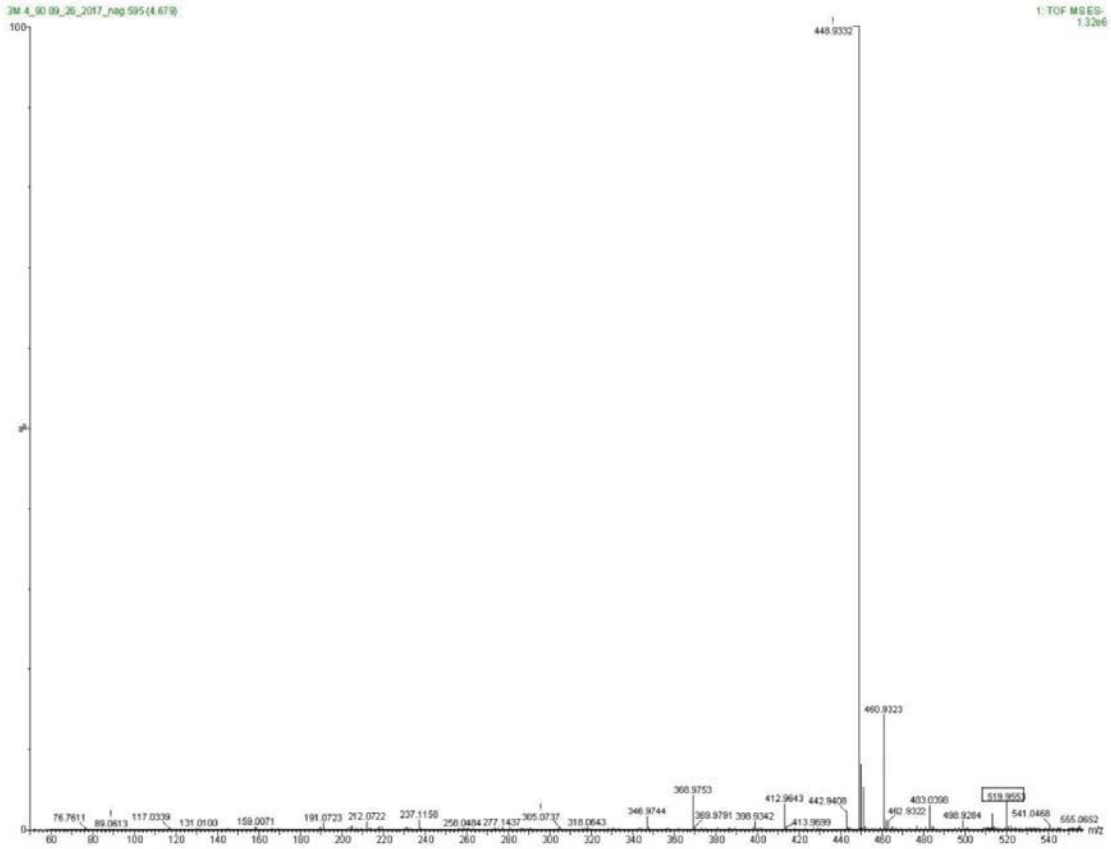

519.9553 m/z

Figure A3-20: Class 2 of 3M 4_90 - Negative

Class 2

Negative

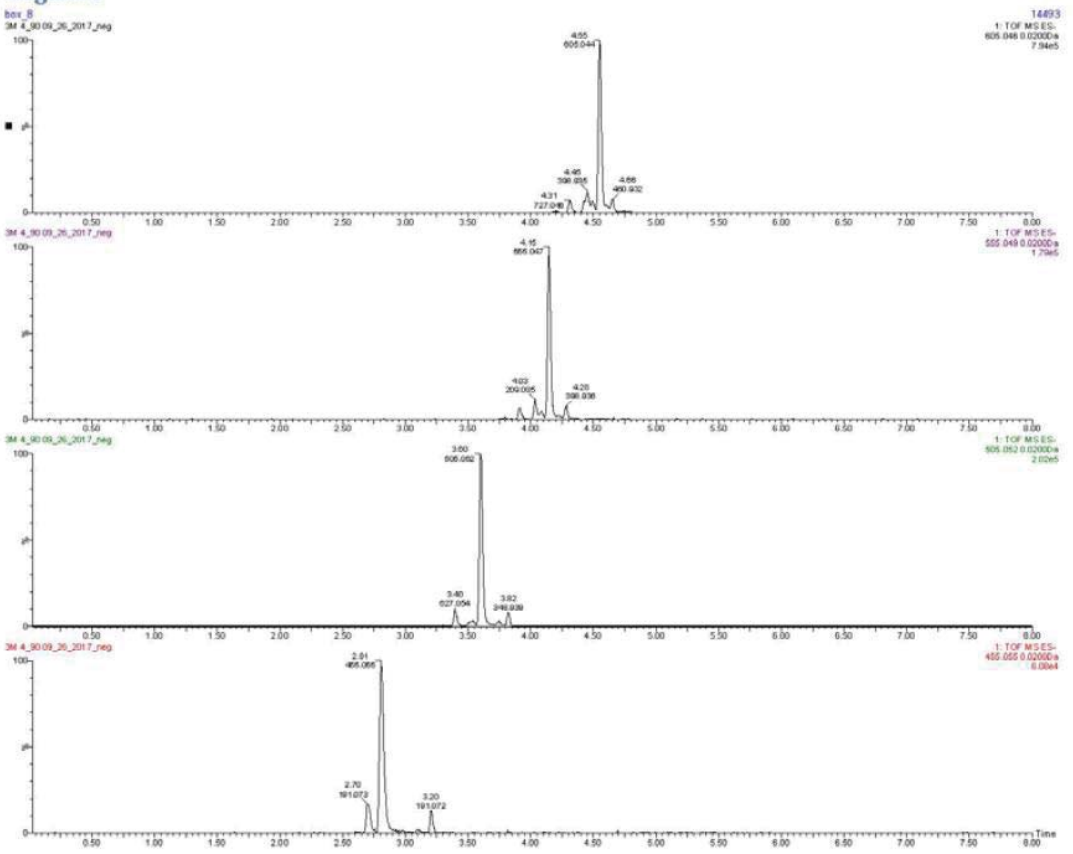

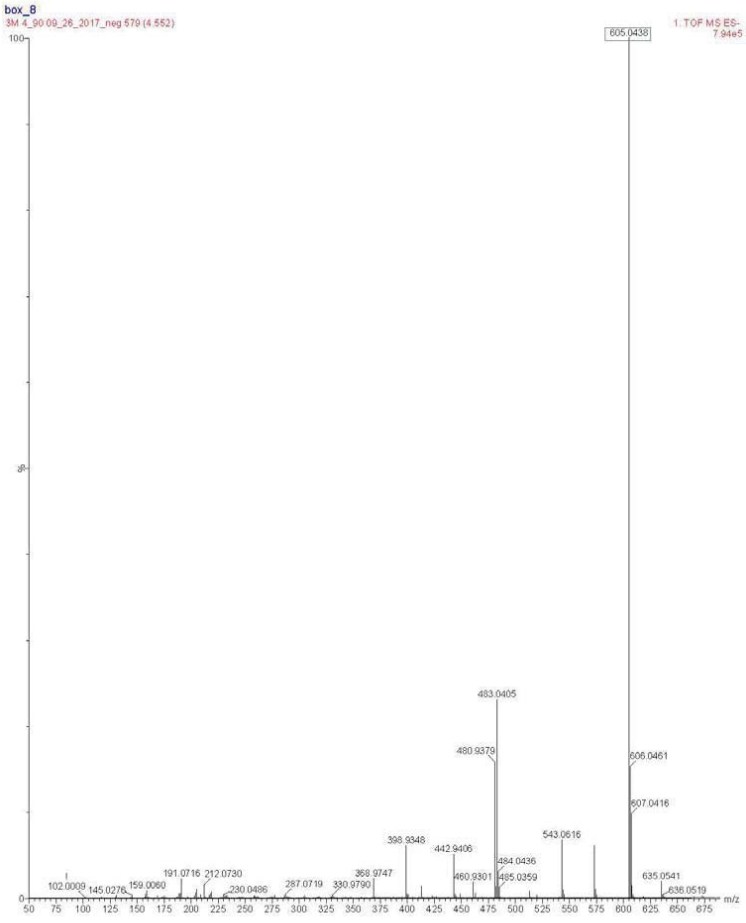

605.0438 m/z

Figure A3-21: Class 3 of 3M 4_90 - Negative

Class 3

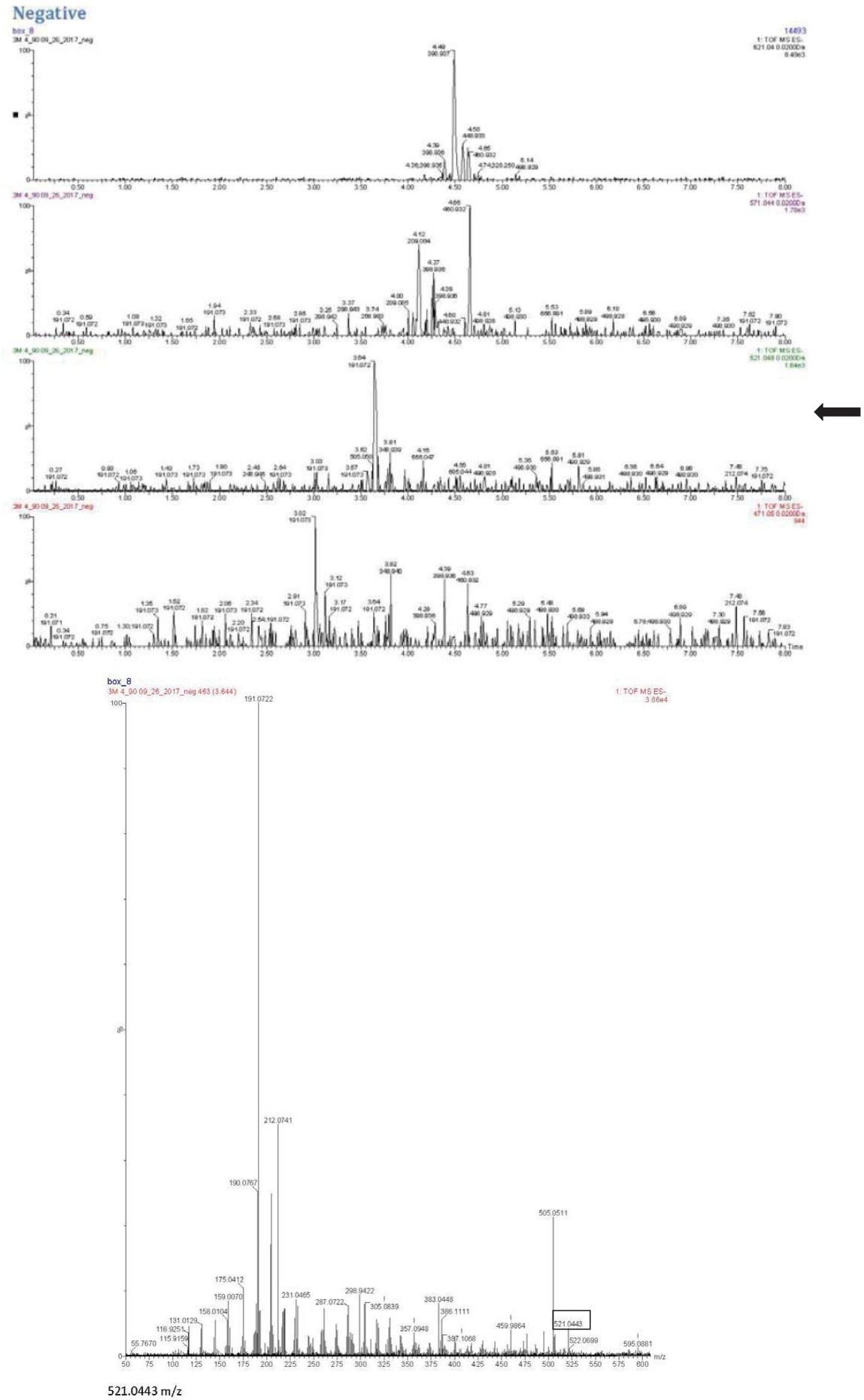

521.0443 m/z

Figure A3-22: Class 5 of 3M 4_90 - Negative

Class 5

Negative

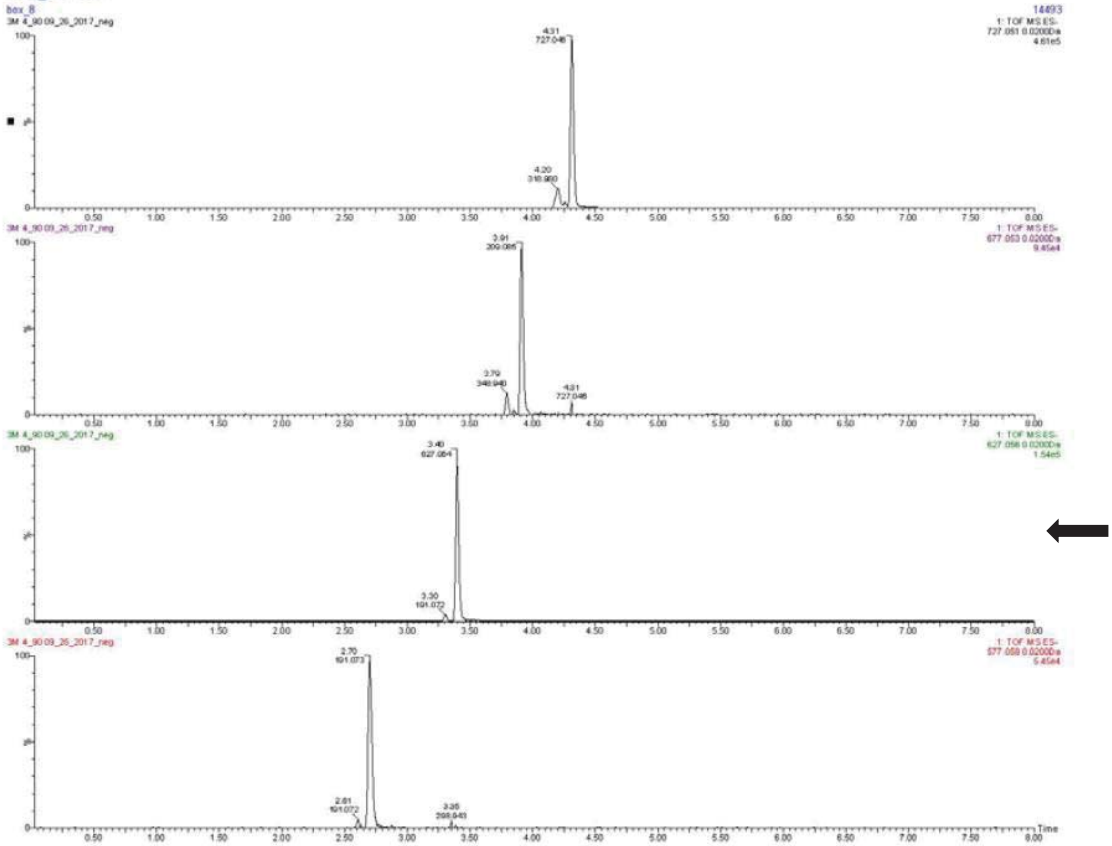

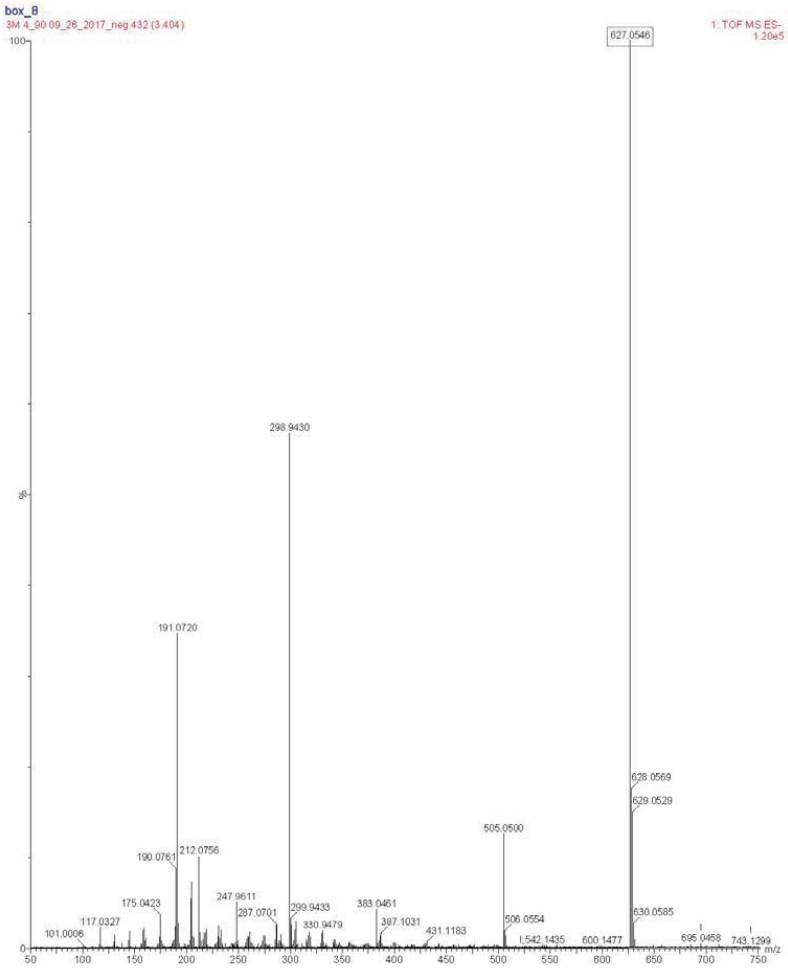

627.0546 m/z

Figure A3-23: Class 16 of 3M 4_90 - Negative

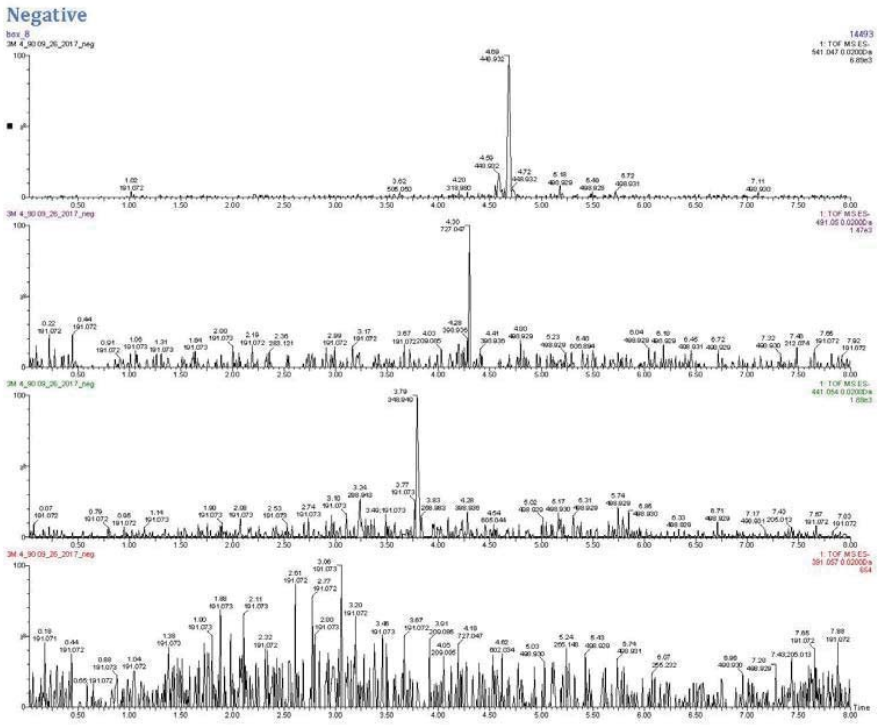

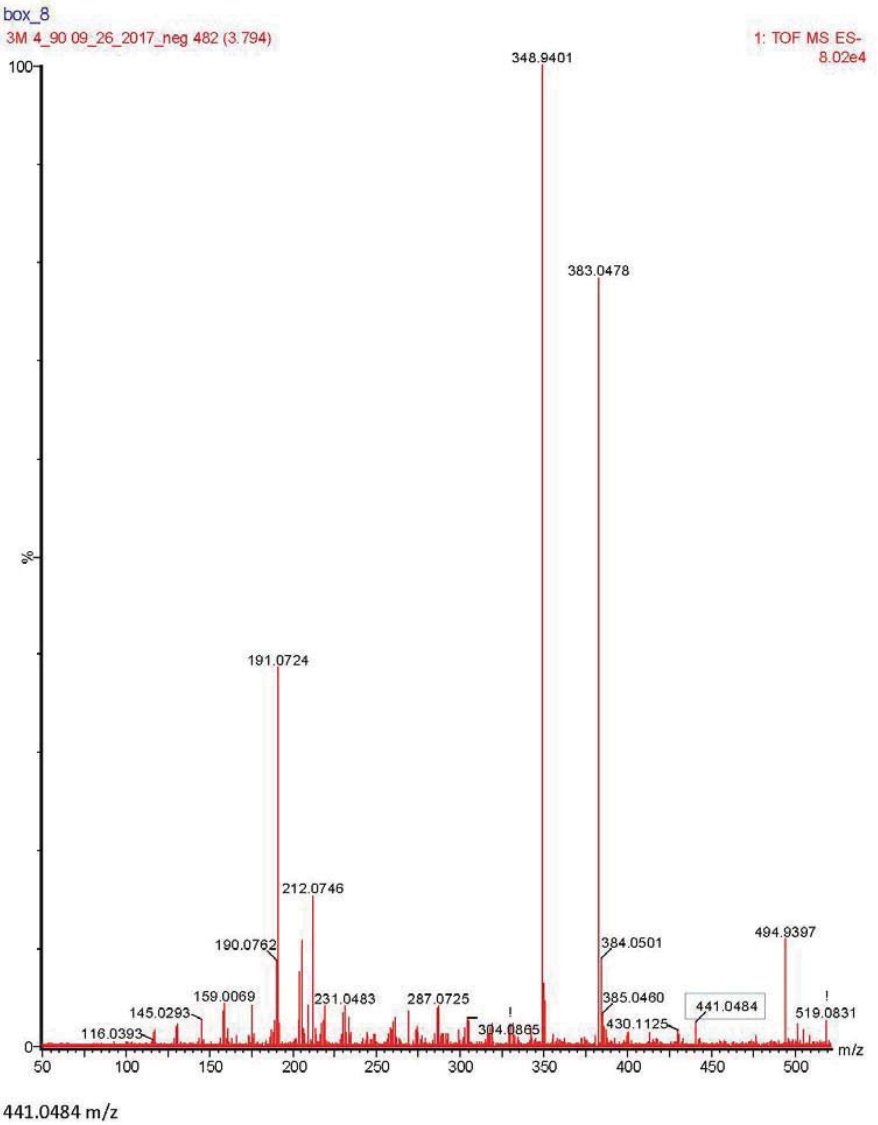

441.0484 m/z

Figure A3-24: Class 21 of 3M 4_90 - Negative

Class 21 - Negative

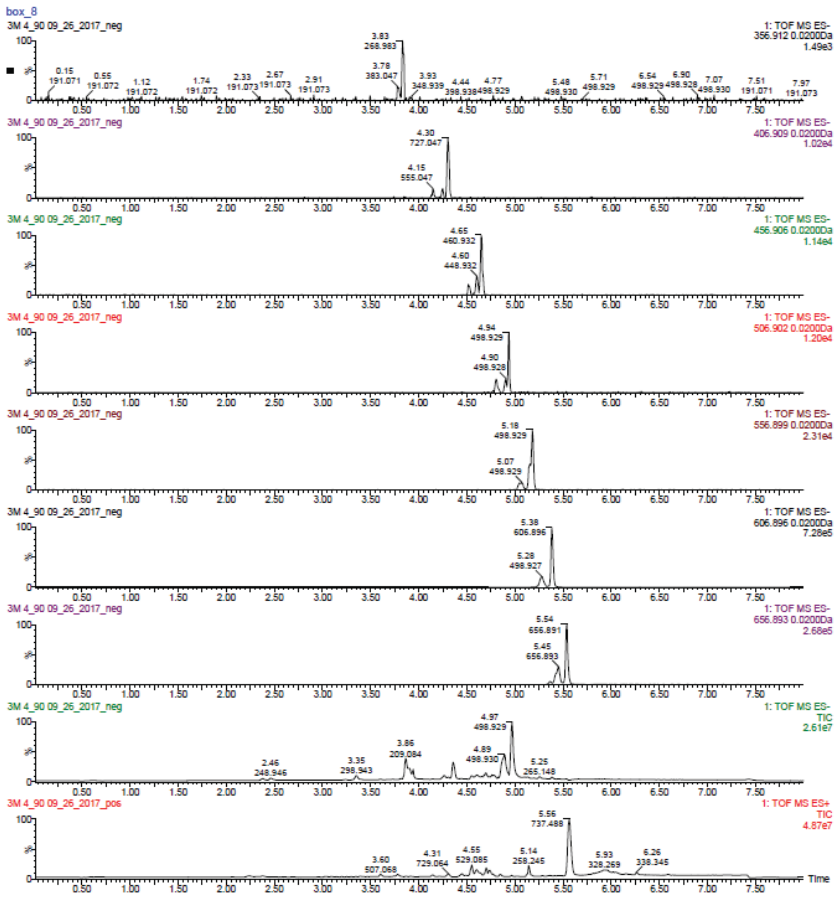

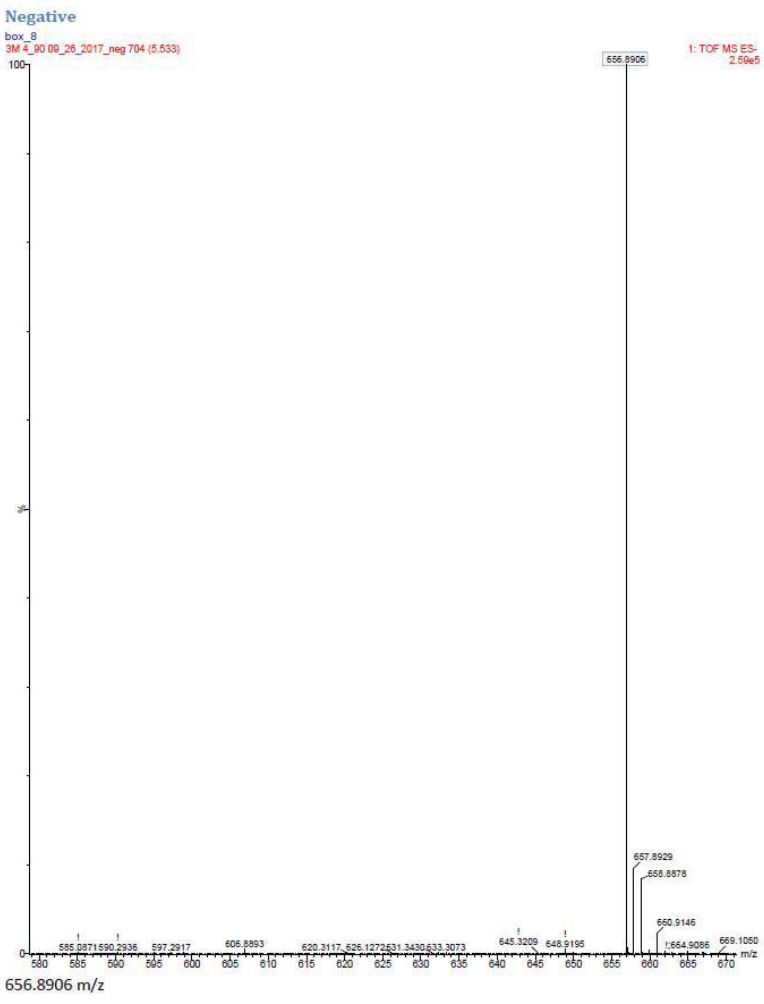

656.8906 m/z

Figure A3-25: Class 23 of 3M 4_90 - Negative

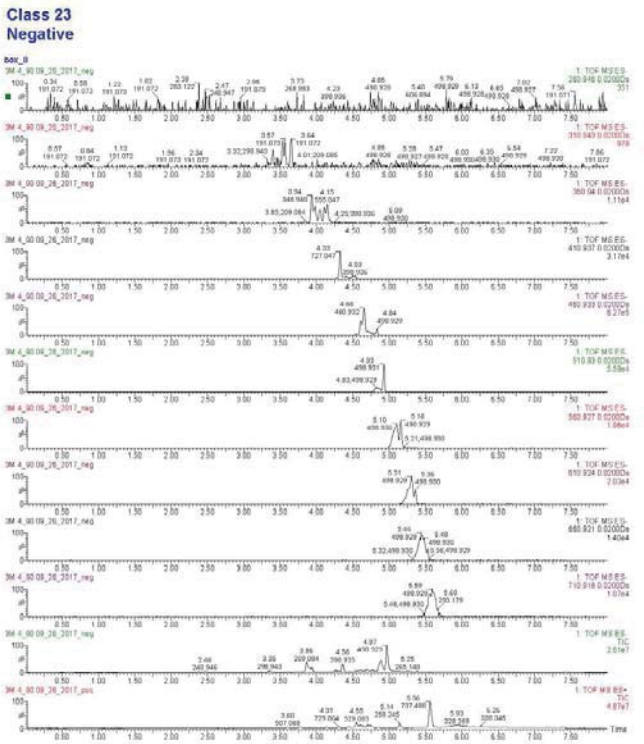

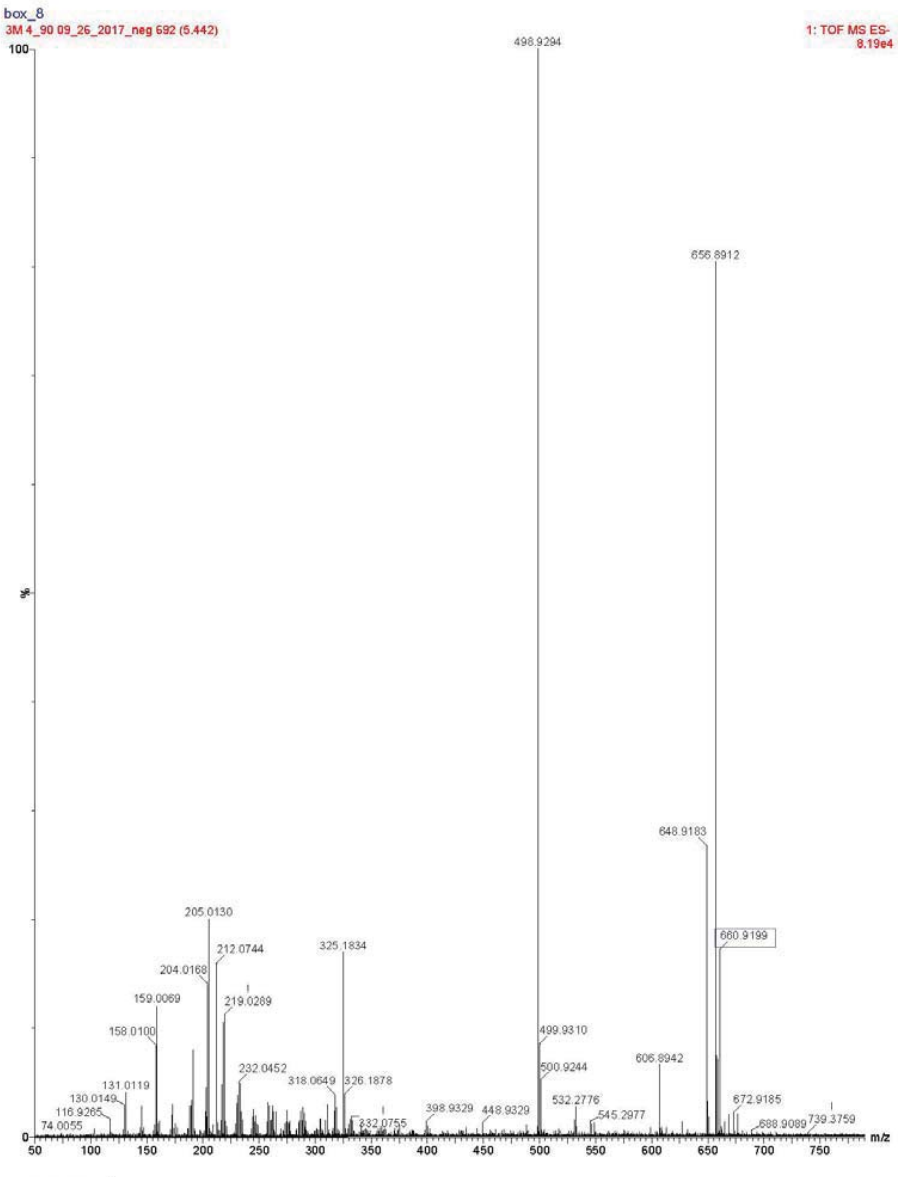

660.9199 m/z

Figure A3-26: Class 24 of 3M 4_90 - Negative

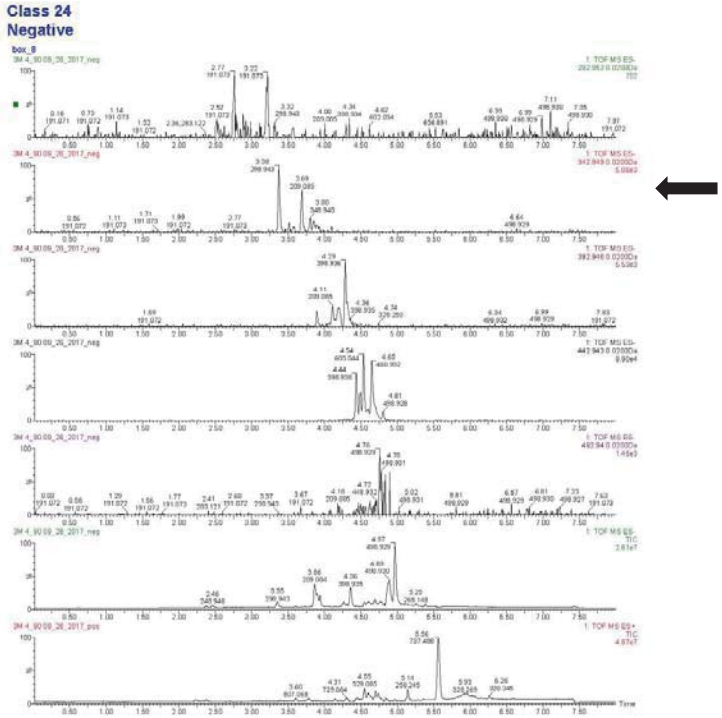

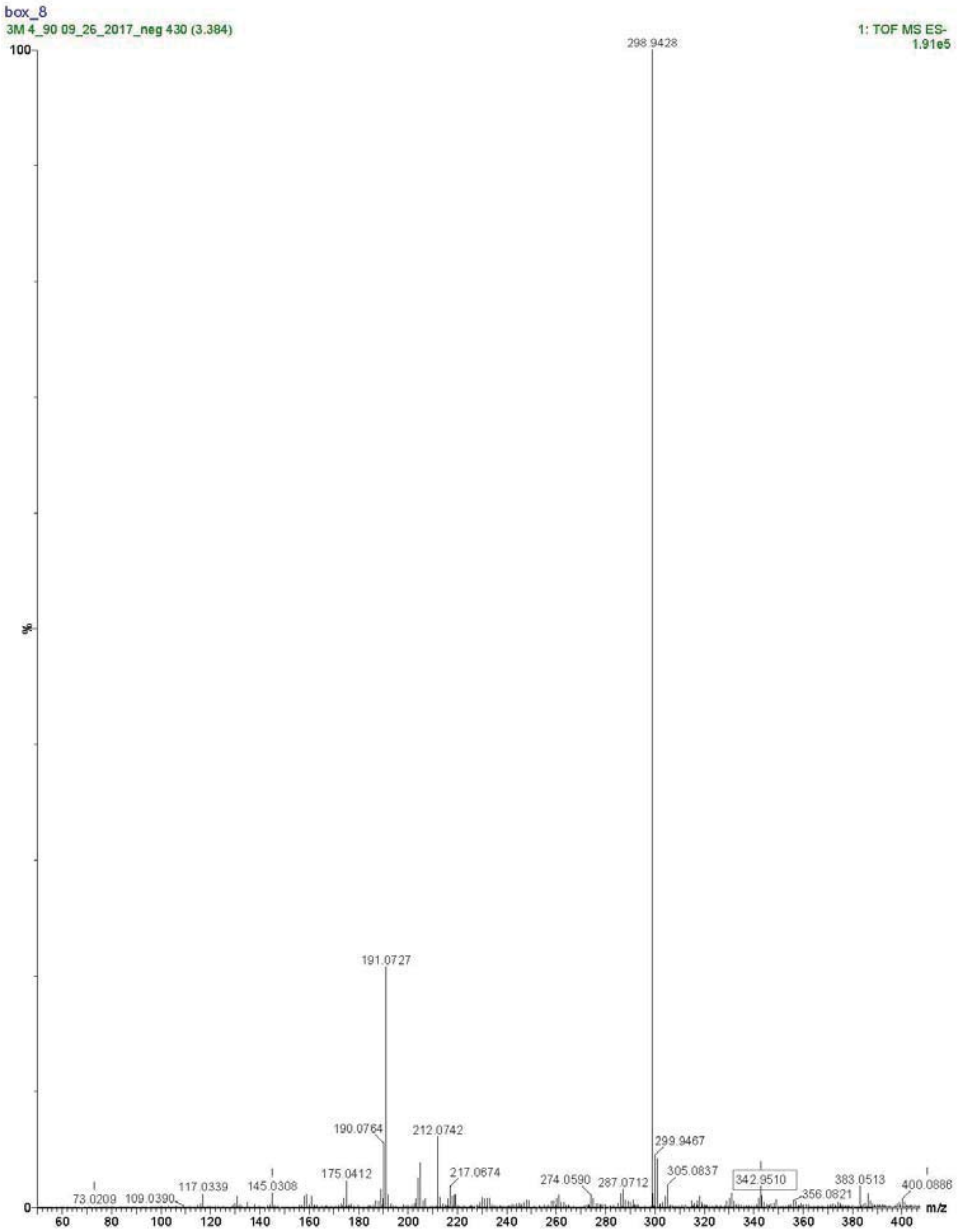

342.9510 m/z

Figure A3-27: Class 25 of 3M 4_90 - Negative

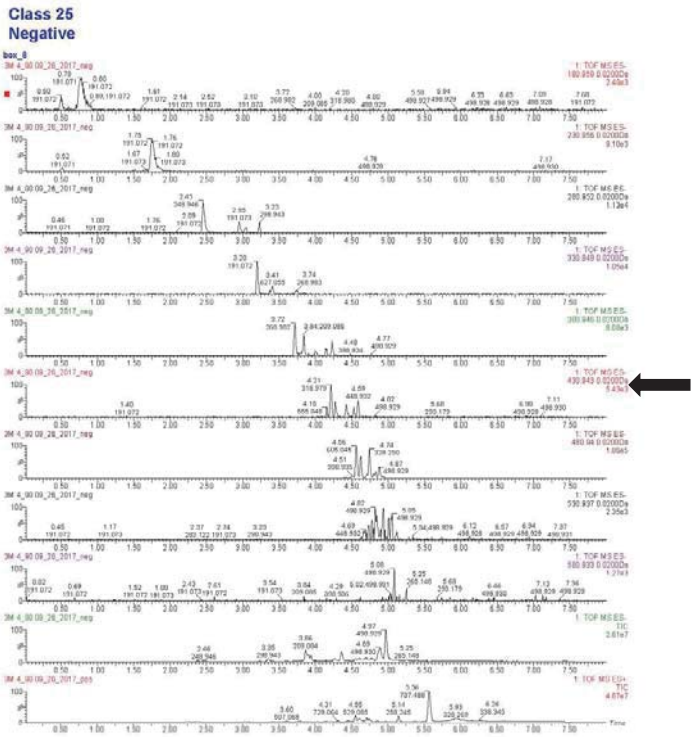

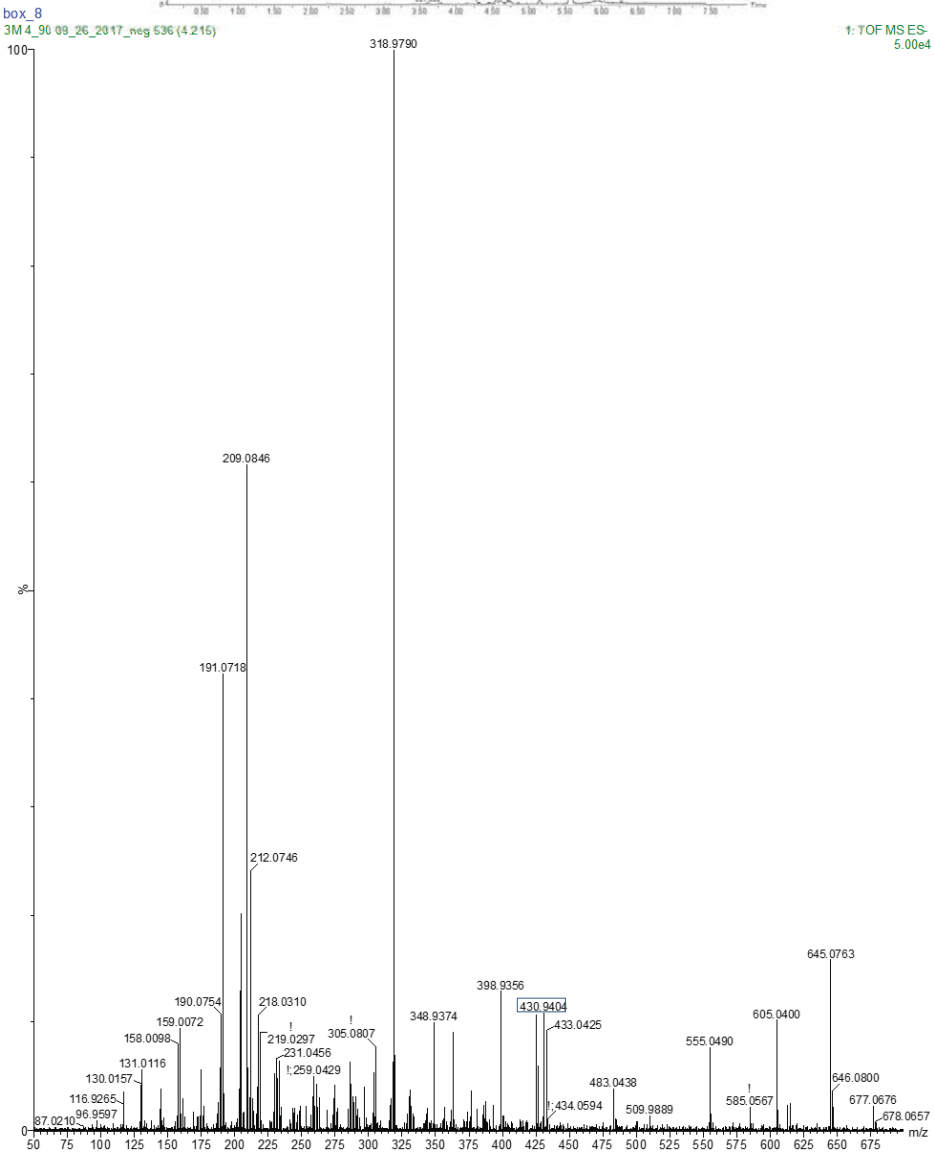

430.9494 m/z

Figure A3-28: Class 26 of 3M 4_90 - Negative

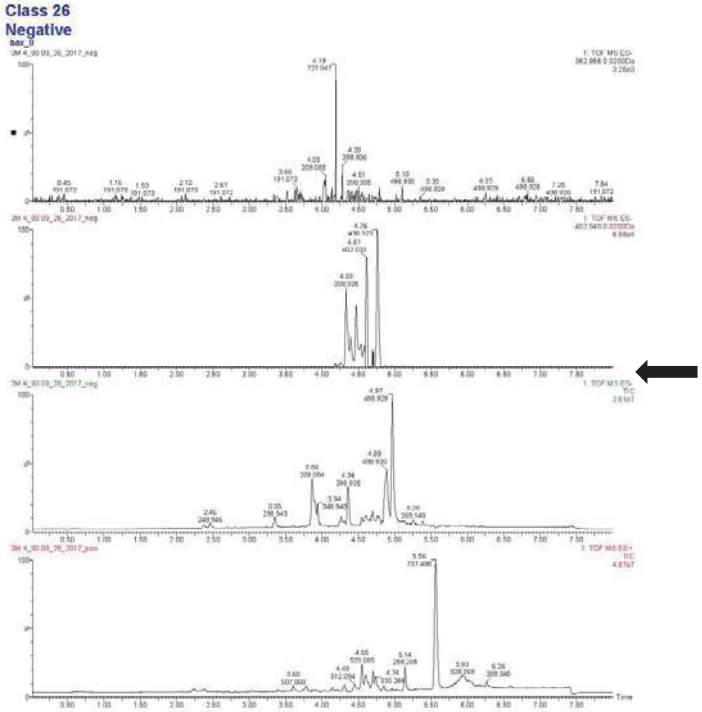

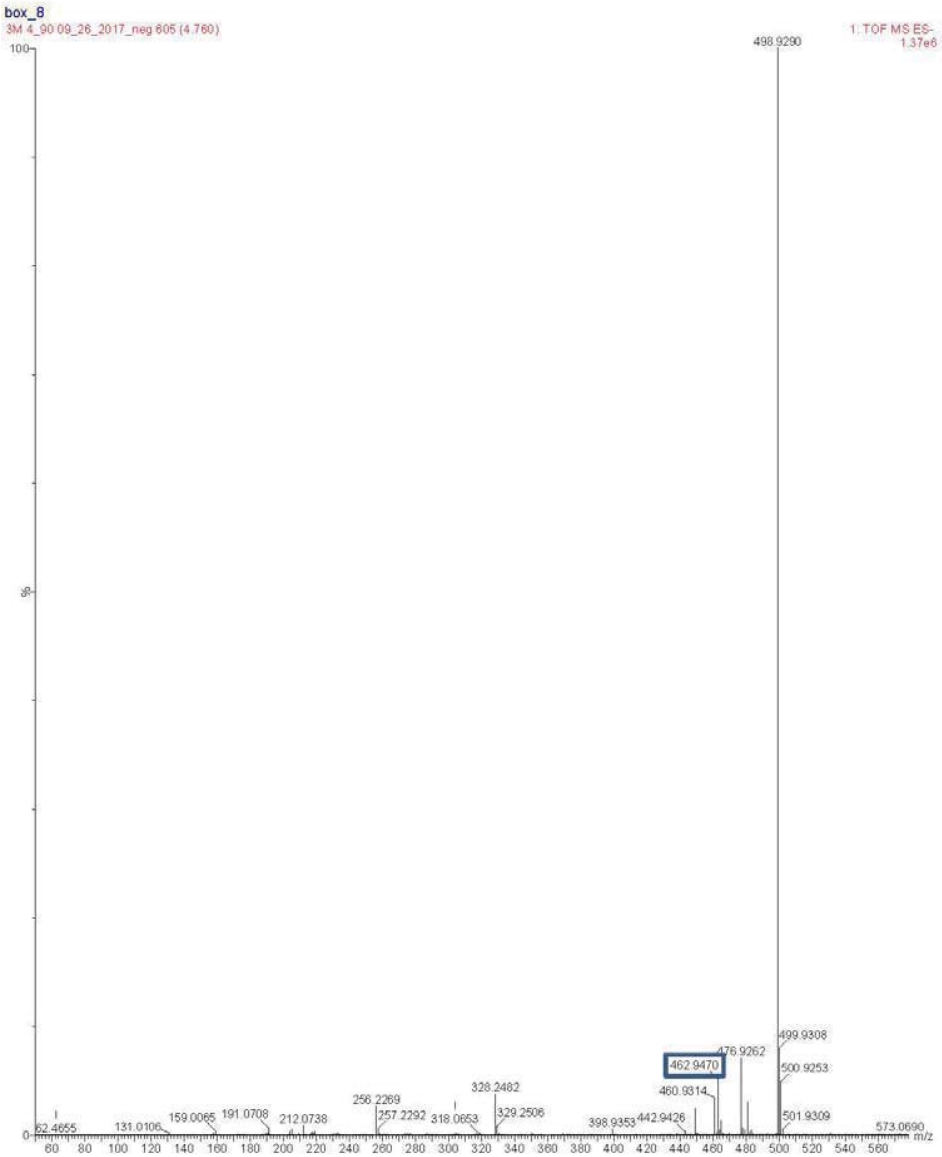

462.9470 m/z

Figure A3-29: Class 29 of 3M 4_90 - Negative

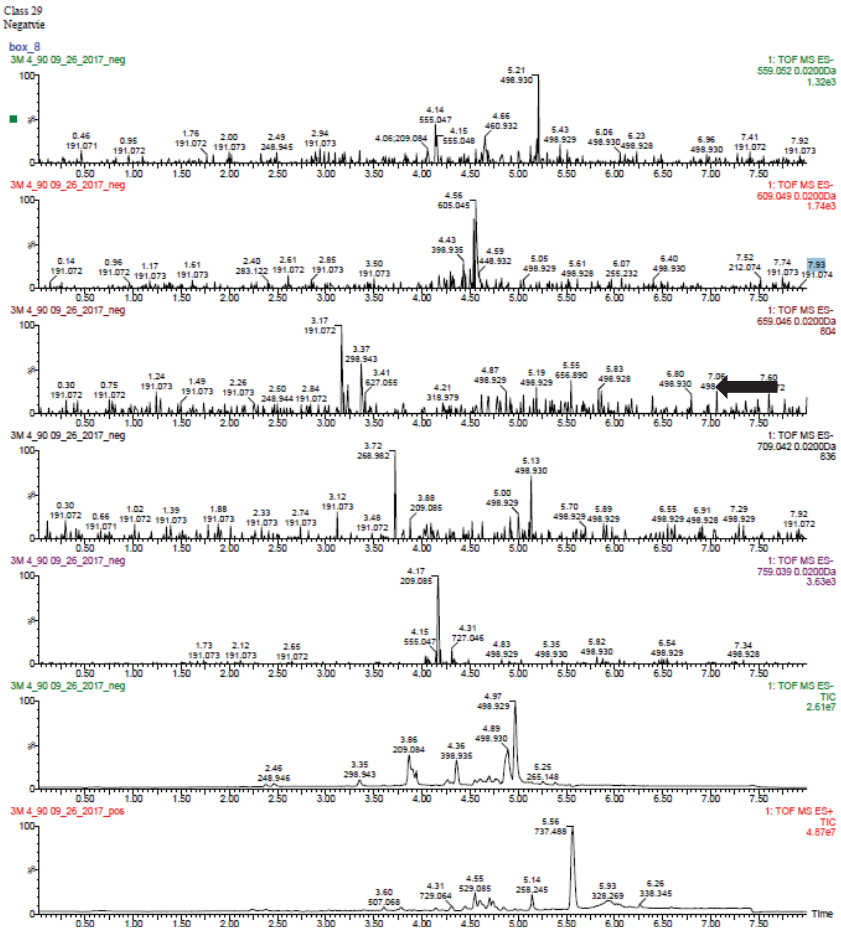

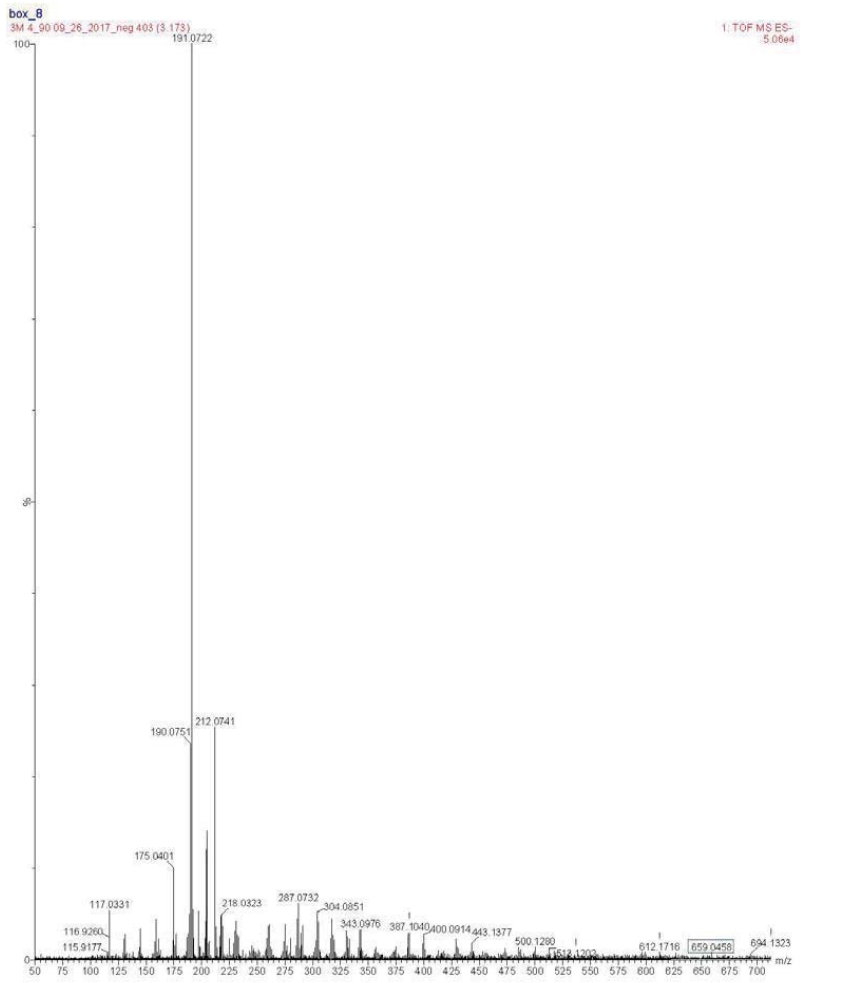

659.0458 m/z

Figure A3-30: Class 30 of 3M 4_90 - Negative

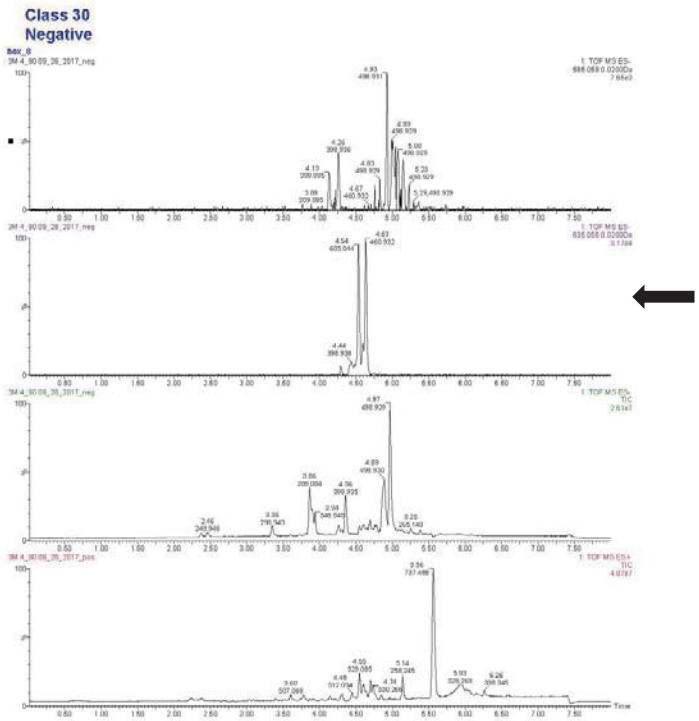

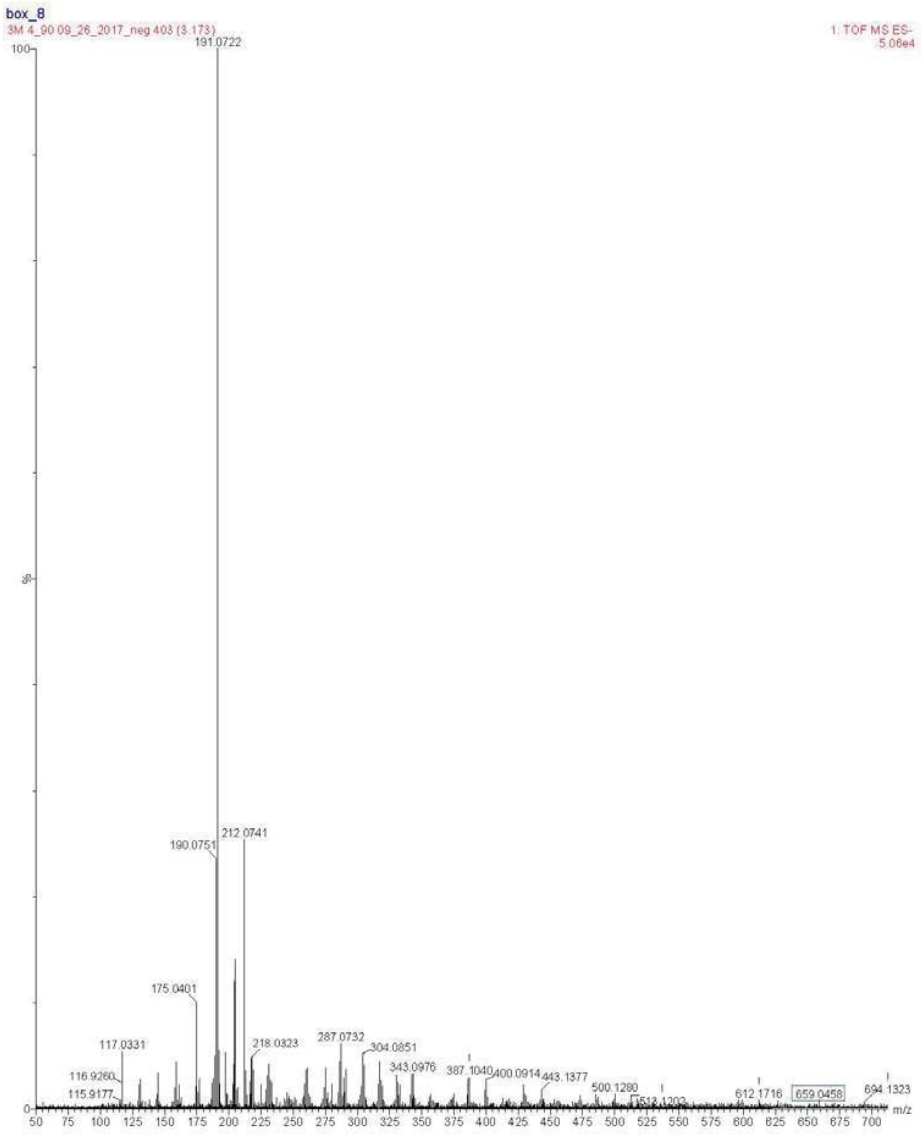

659.0458 m/z

Figure A3-31: Class 32 of 3M 4_90 - Negative

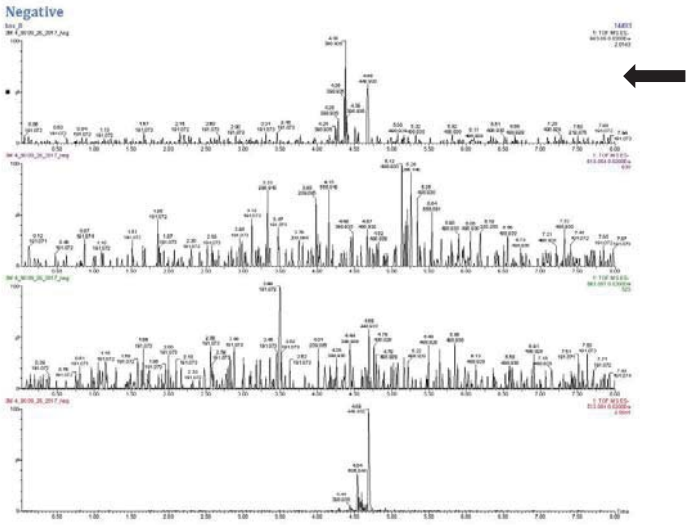

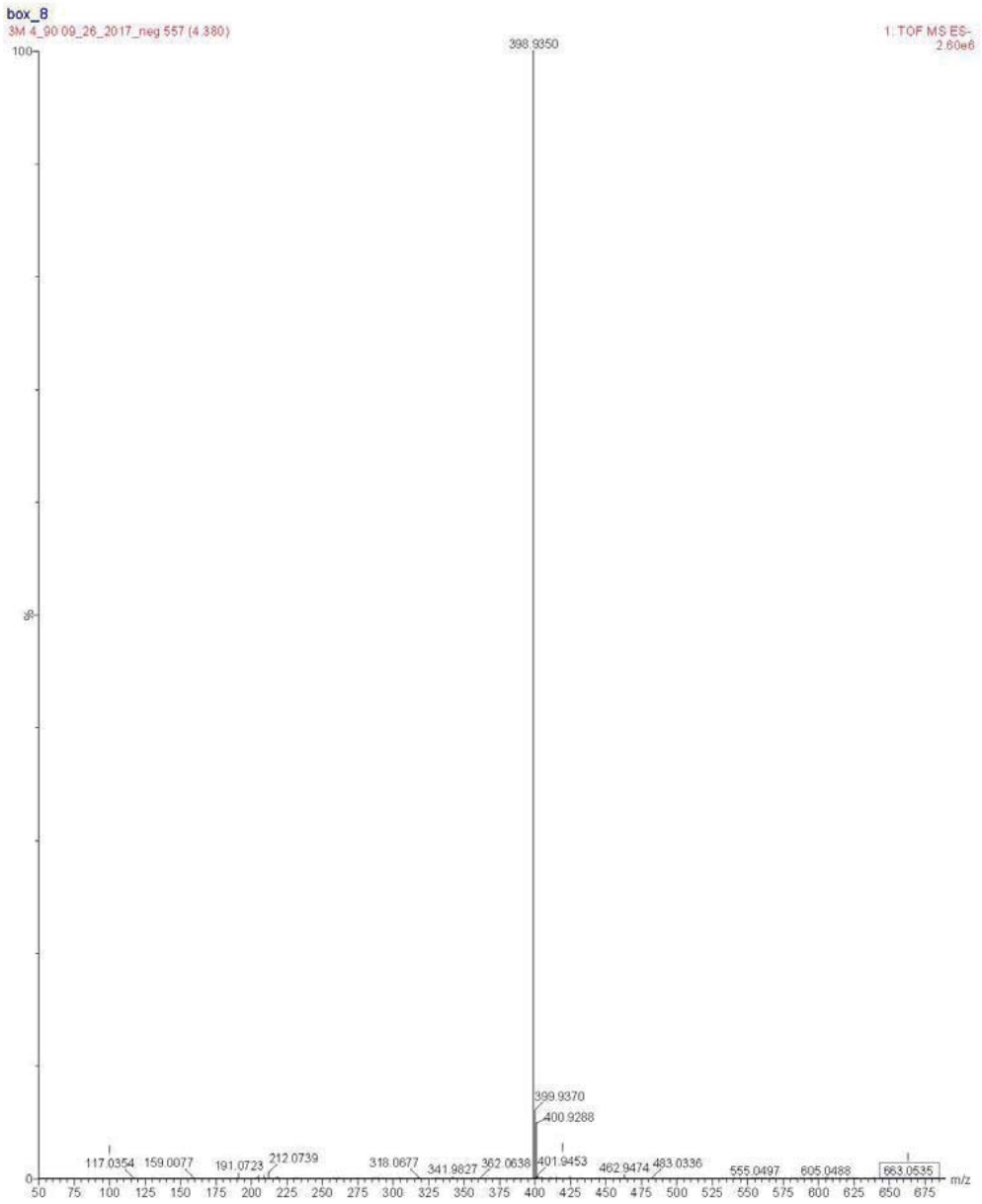

663.050 m/z

3M 6_90 – Mass Spectrums and Chromatographs

Figure A4-1: Class 2 of 3M 6_90 - Positive

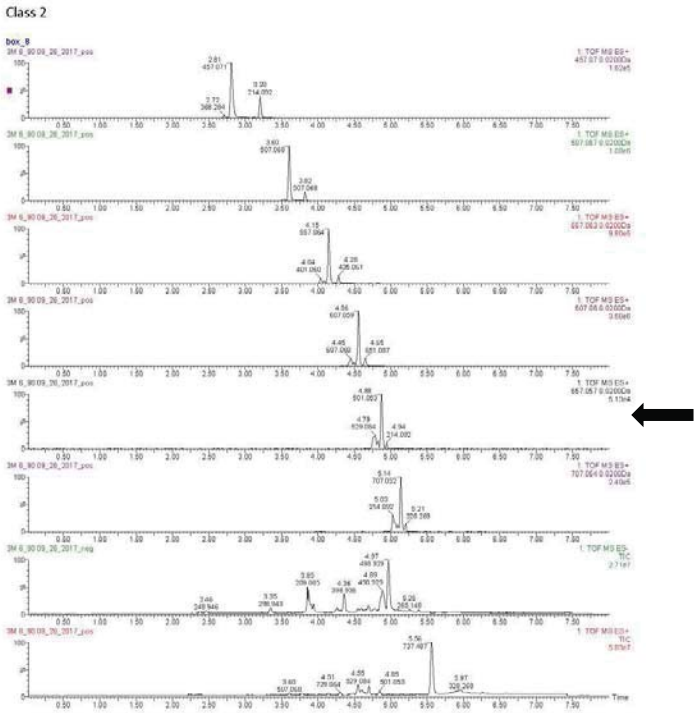

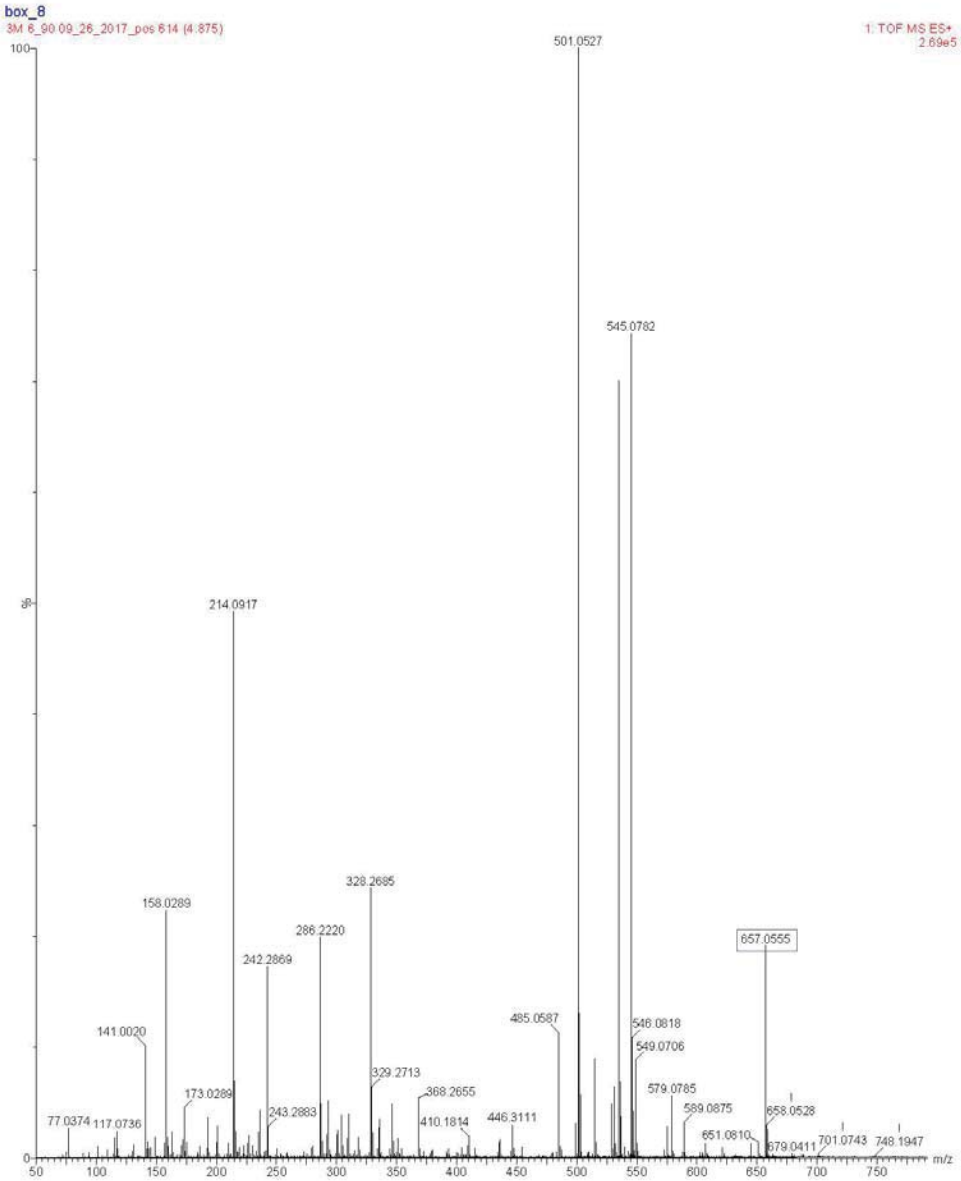

657.0555 m/z

Figure A4-2: Class 3 of 3M 6_90 - Positive

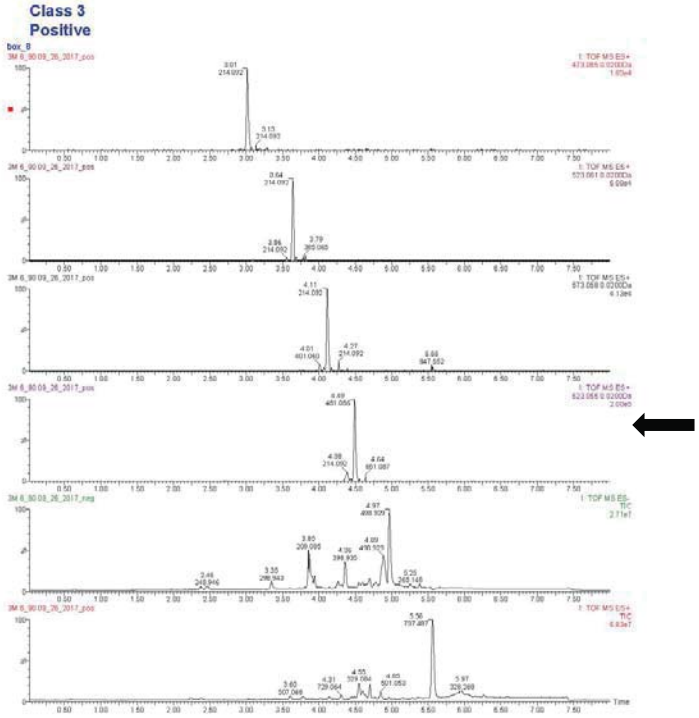

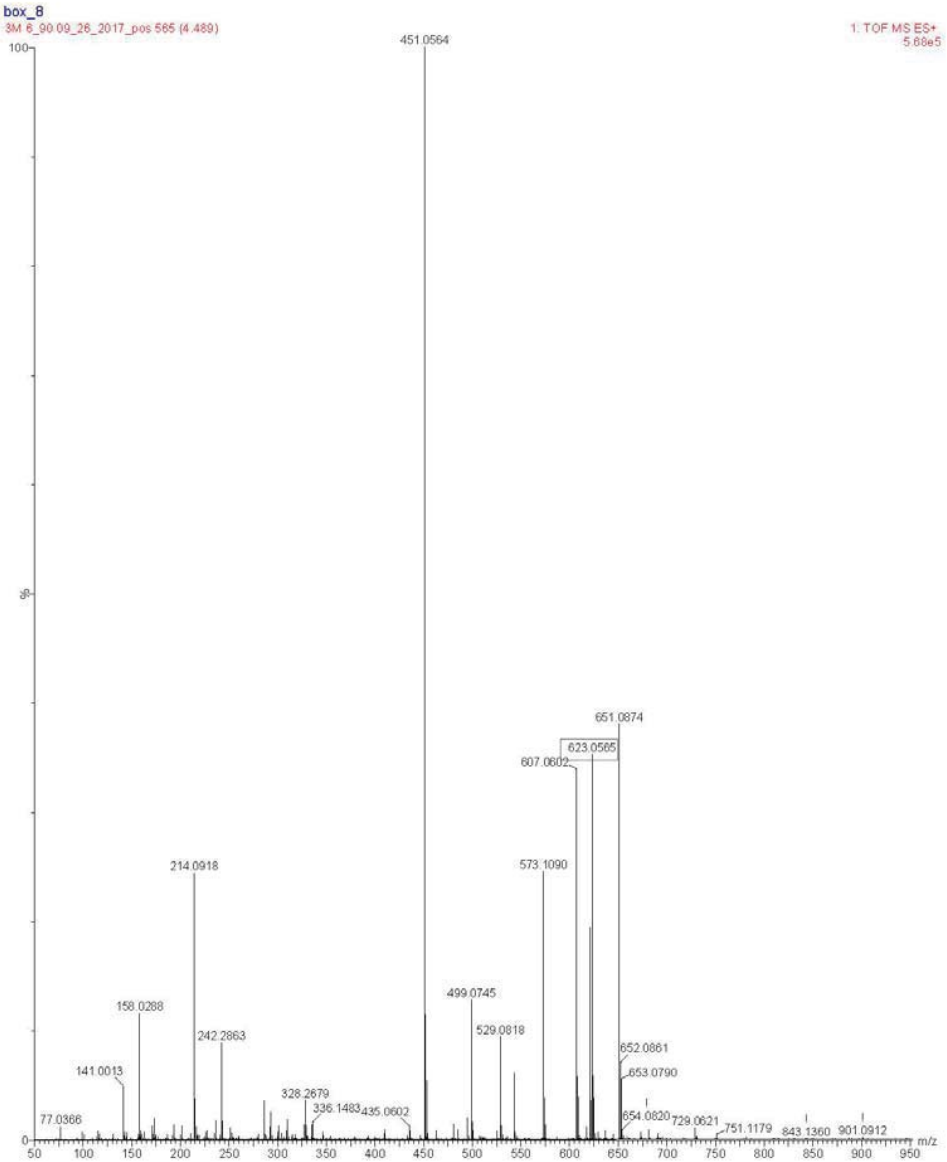

623.0565 m/z

Figure A4-3: Class 4 of 3M 6_90 - Positive

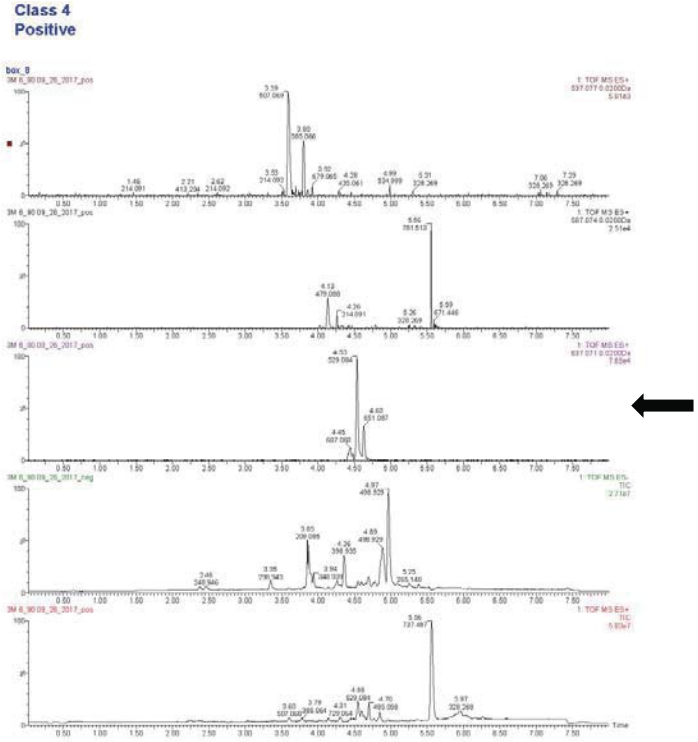

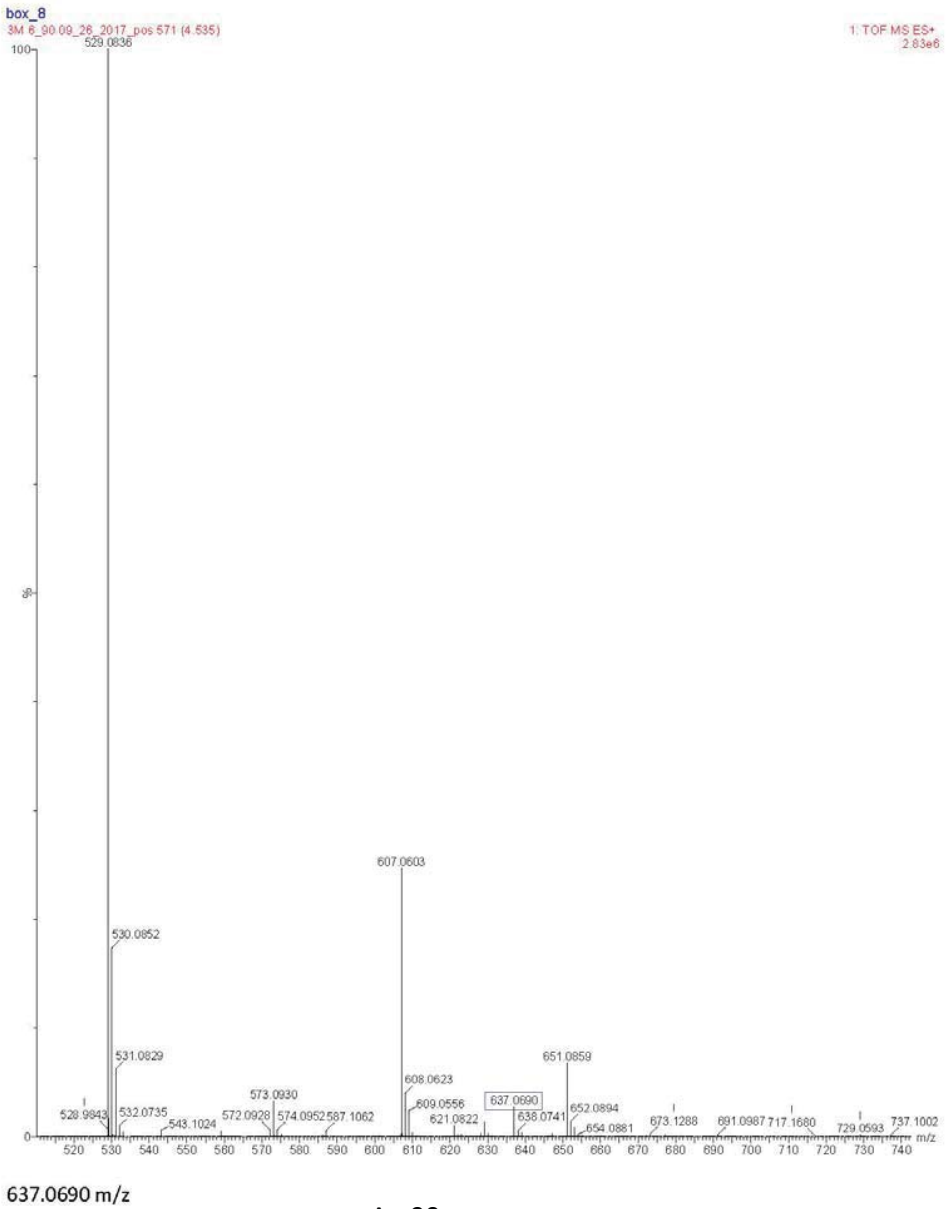

637.0690 m/z

Figure A4-4: Class 5 of 3M 6_90 - Positive

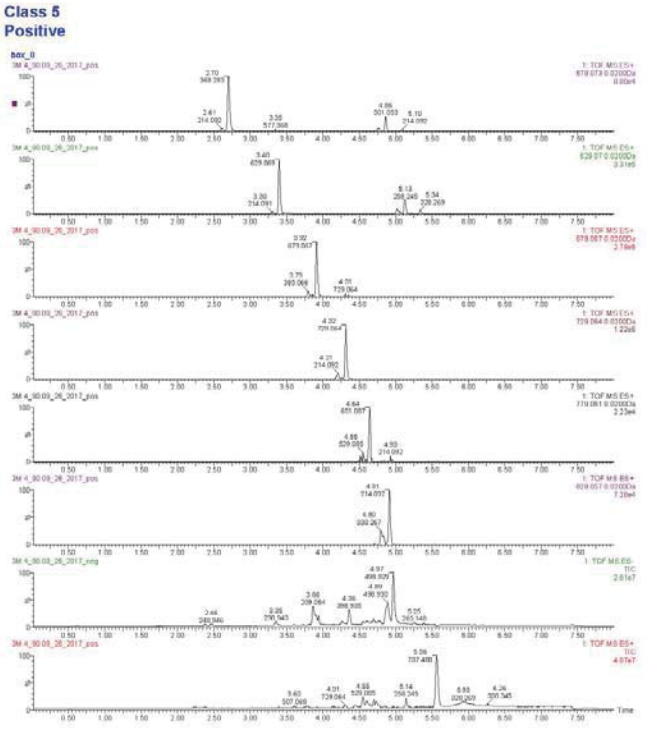

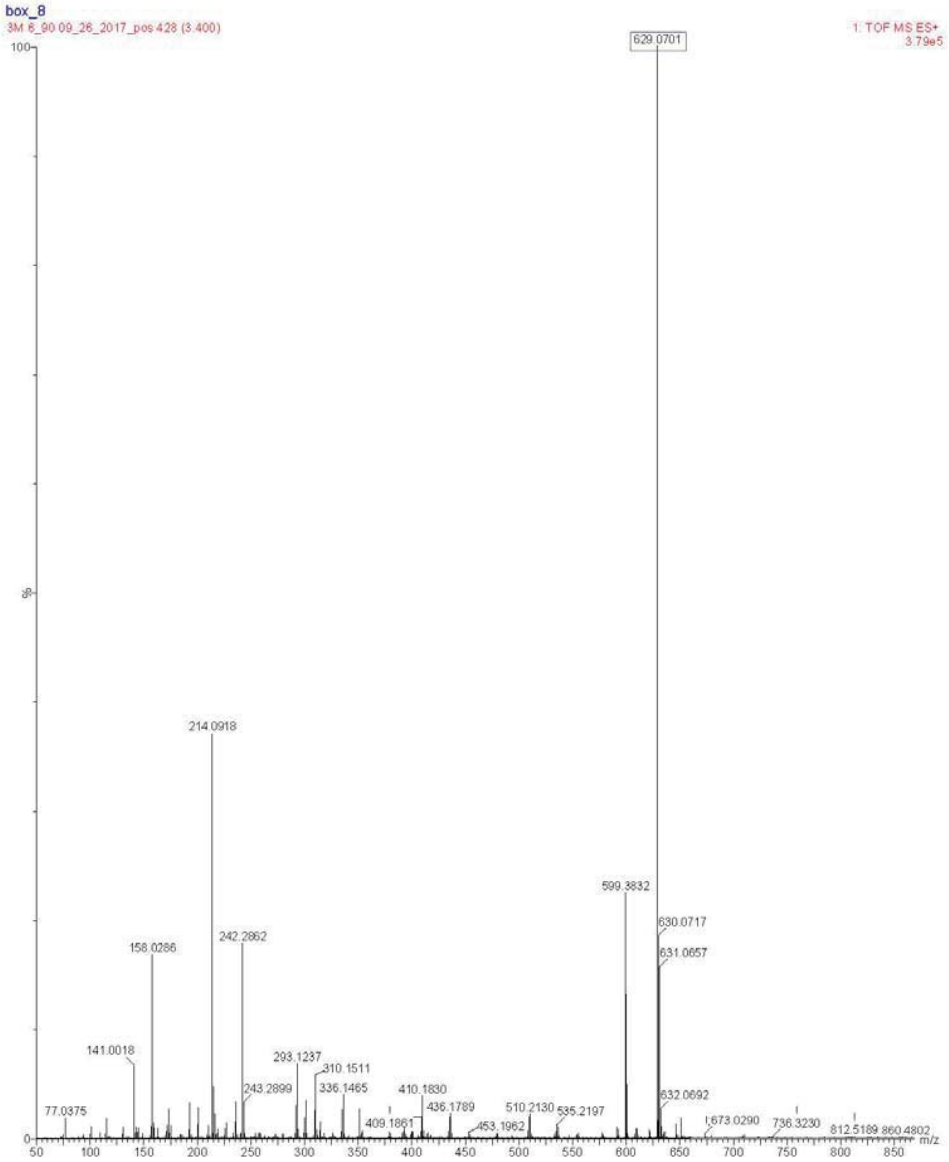

629.0701 m/z

Figure A4-5: Class 8 of 3M 6_90 - Positive

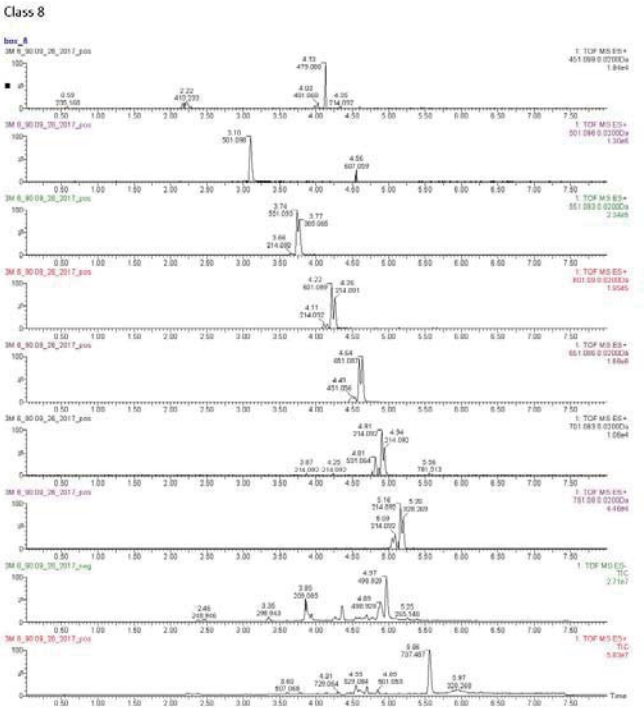

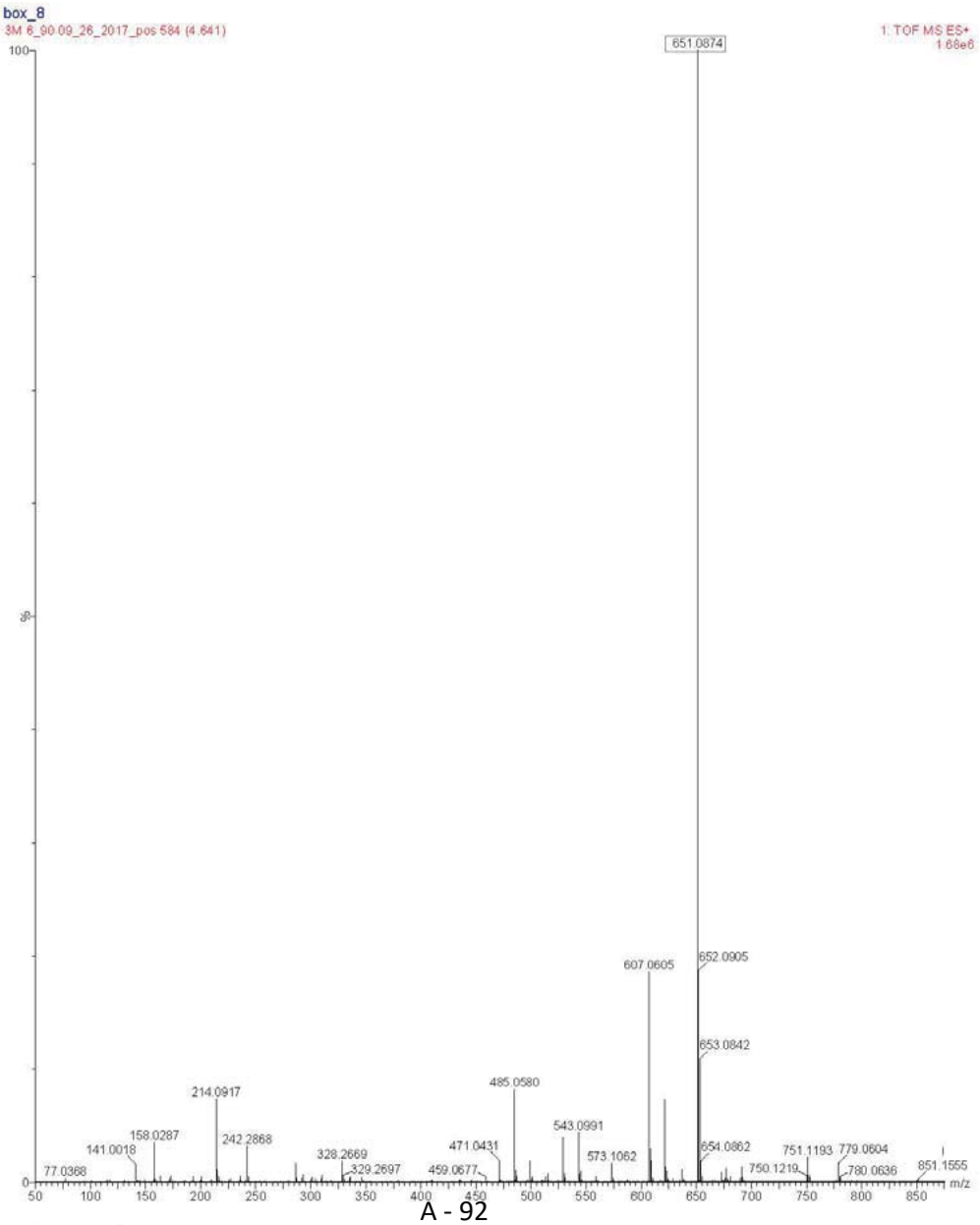

651.0874 m/z

Figure A4-6: Class 9 of 3M 6_90 - Positive

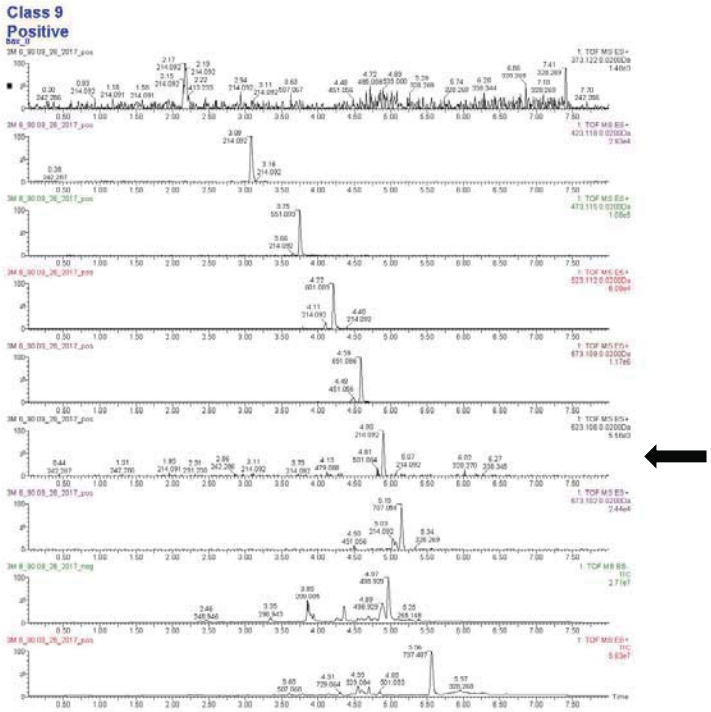

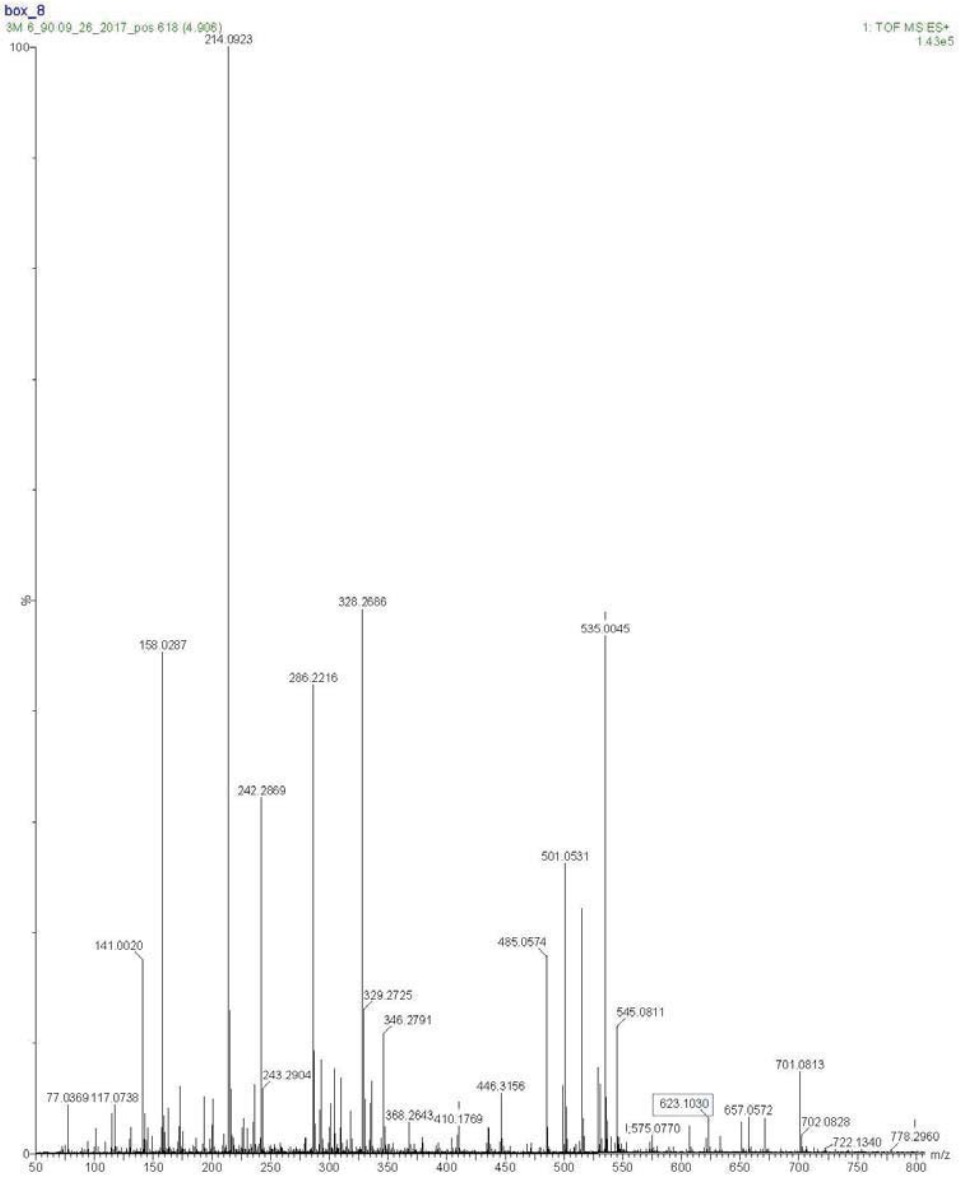

623.1030 m/z

Figure A4-7: Class 10 of 3M 6_90 - Positive

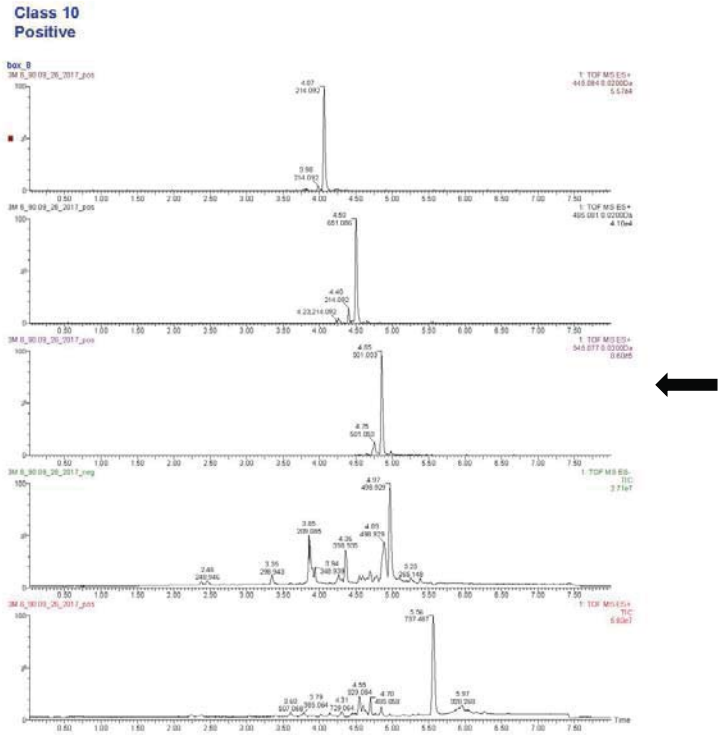

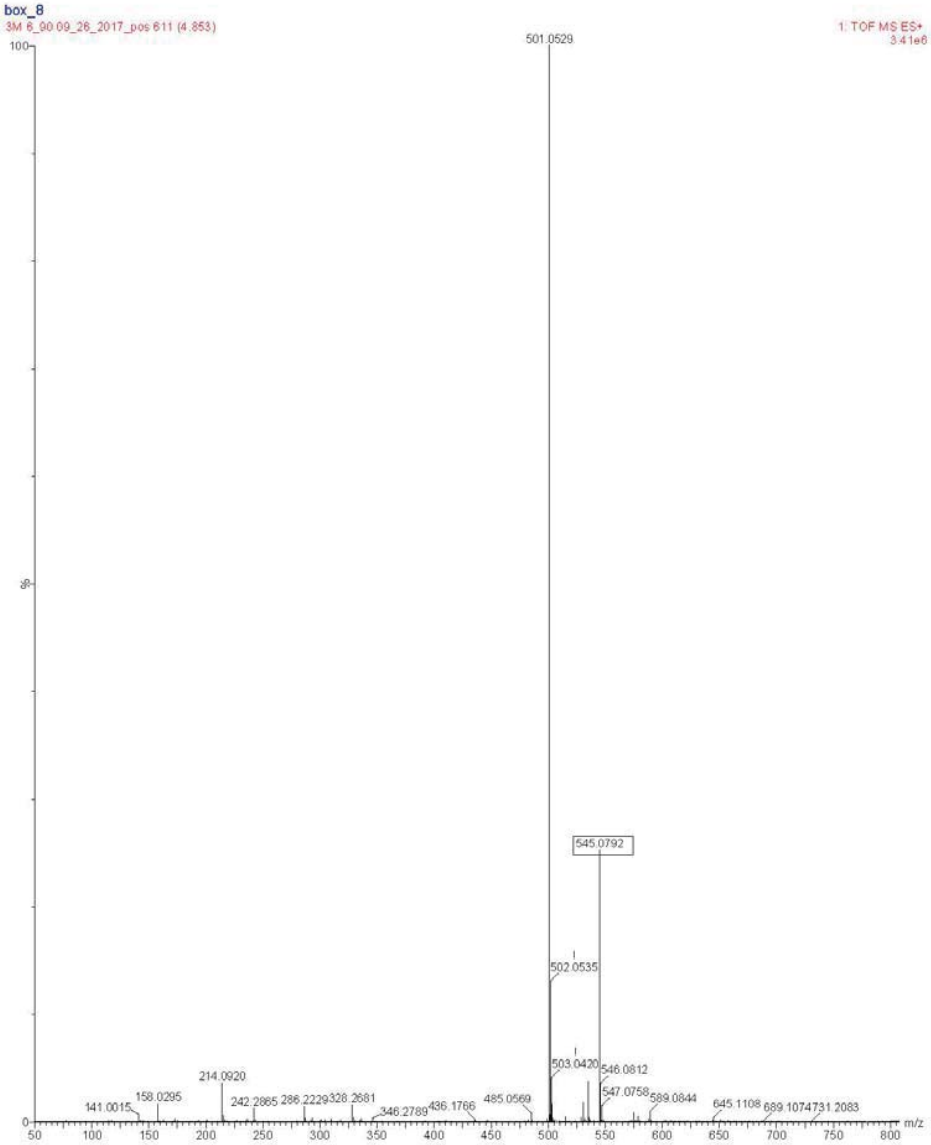

545.0792 m/z

Figure A4-8: Class 11 of 3M 6_90 - Positive

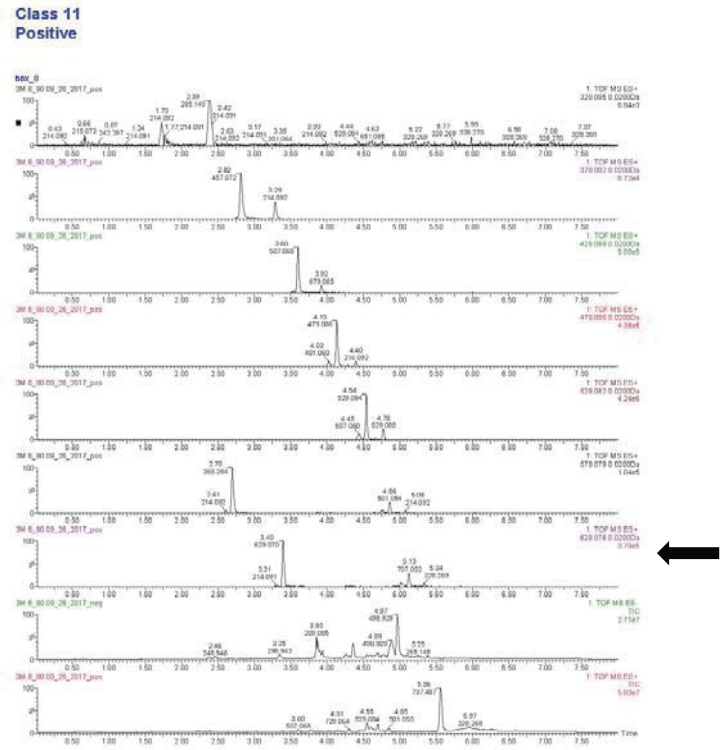

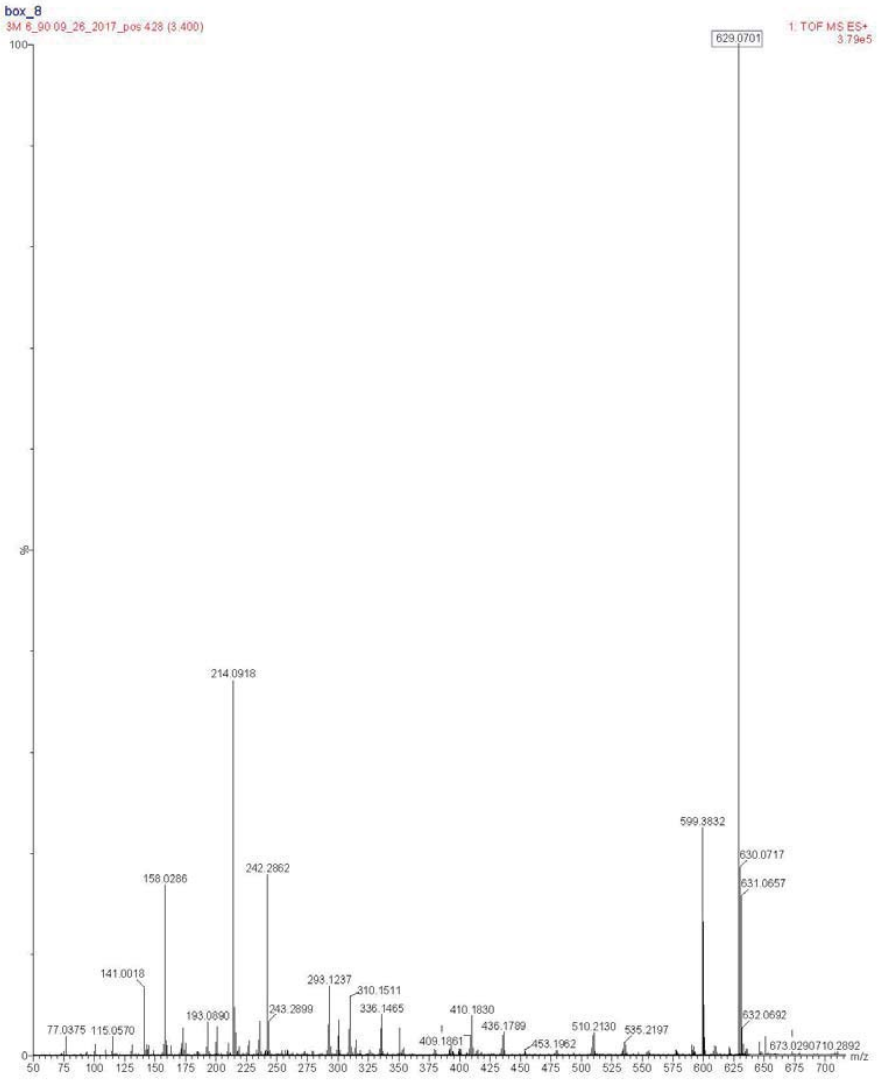

629.0701 m/z

Figure A4-9: Class 12 of 3M 6_90 - Positive

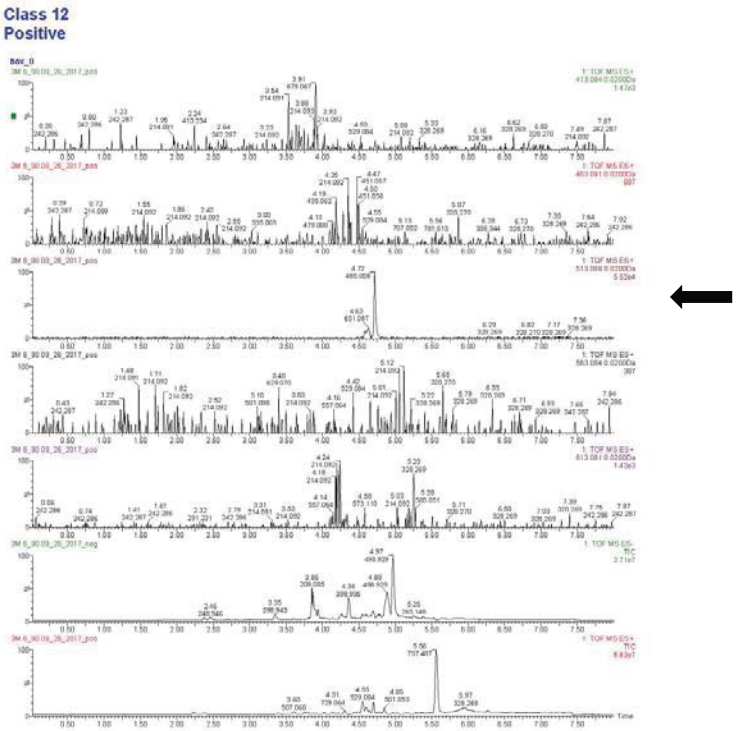

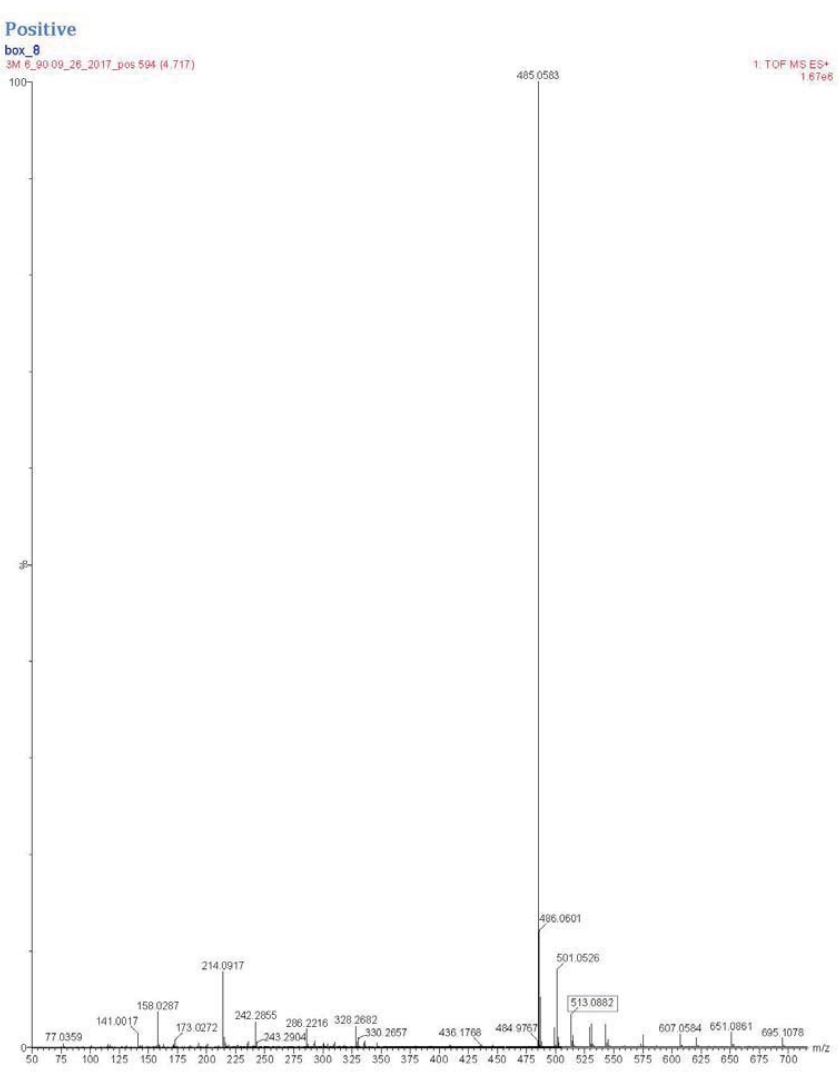

513.0882 m/z (one of 5 clear)

Figure A4-10: Class 13 of 3M 6_90 - Positive

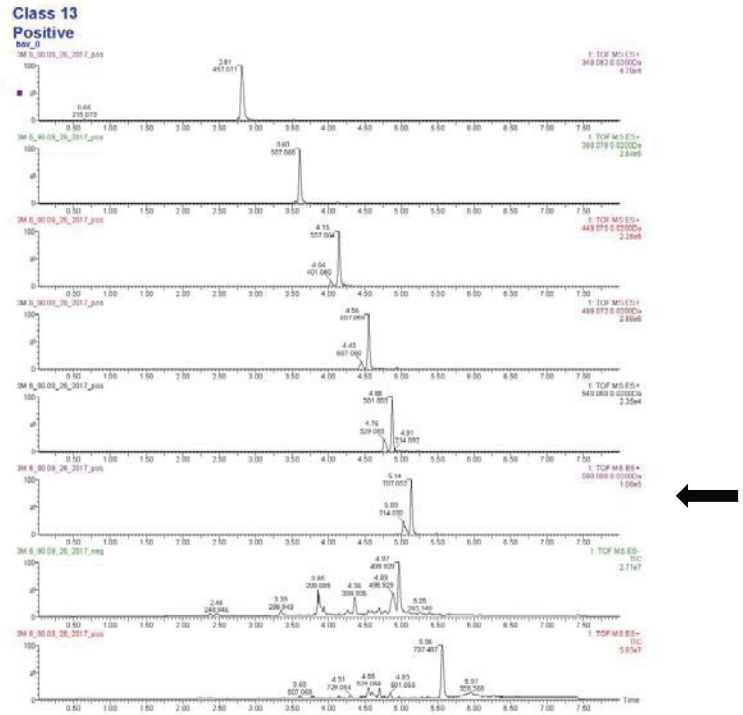

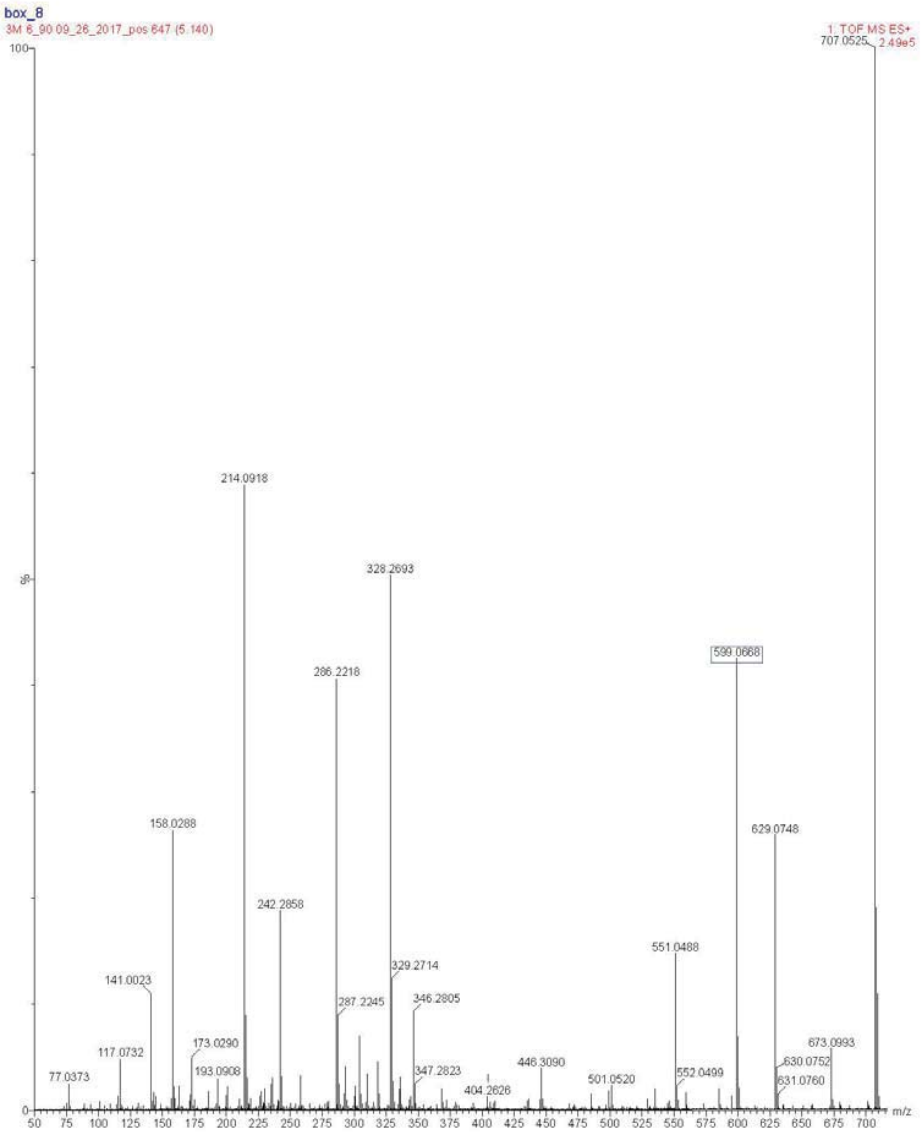

599.0668 m/z

Figure A4-11: Class 14 of 3M 6_90 - Positive

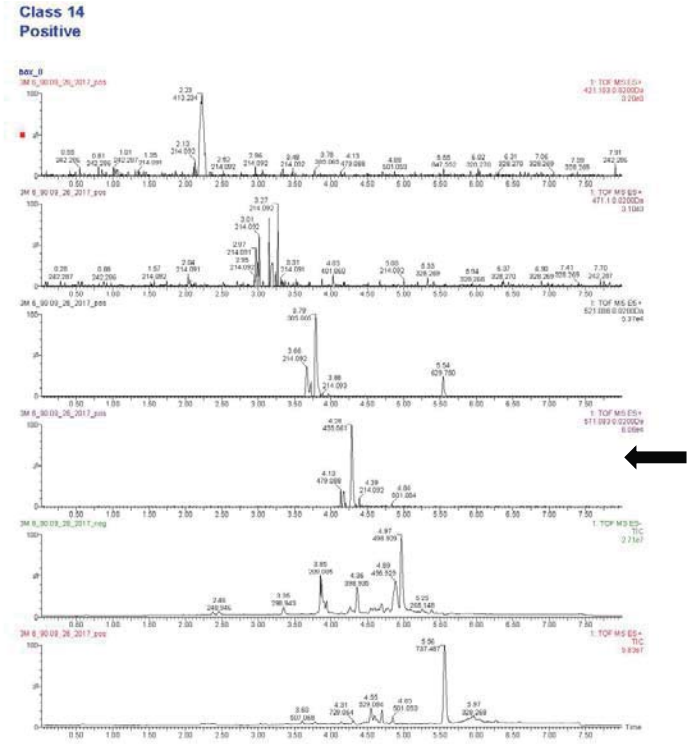

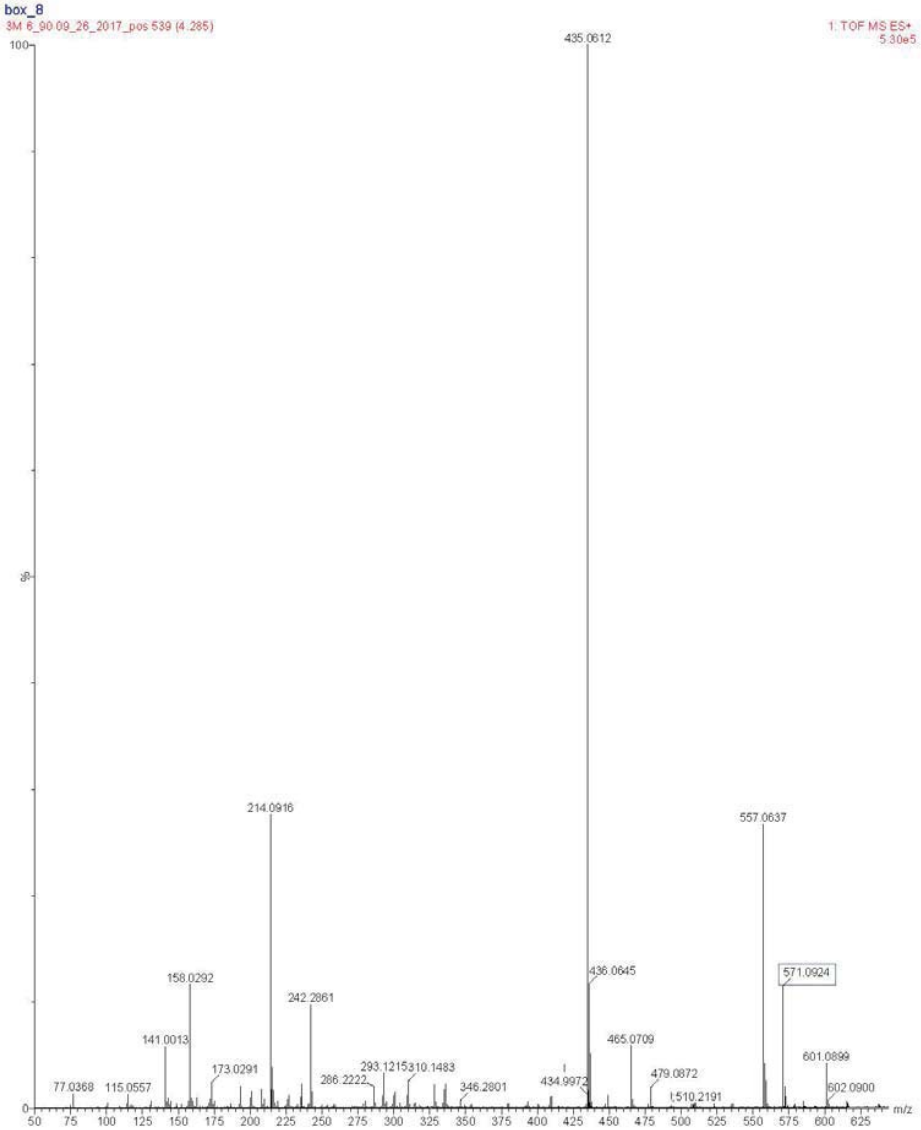

571.0924 m/z

Figure A4-12: Class 15 of 3M 6_90 - Positive

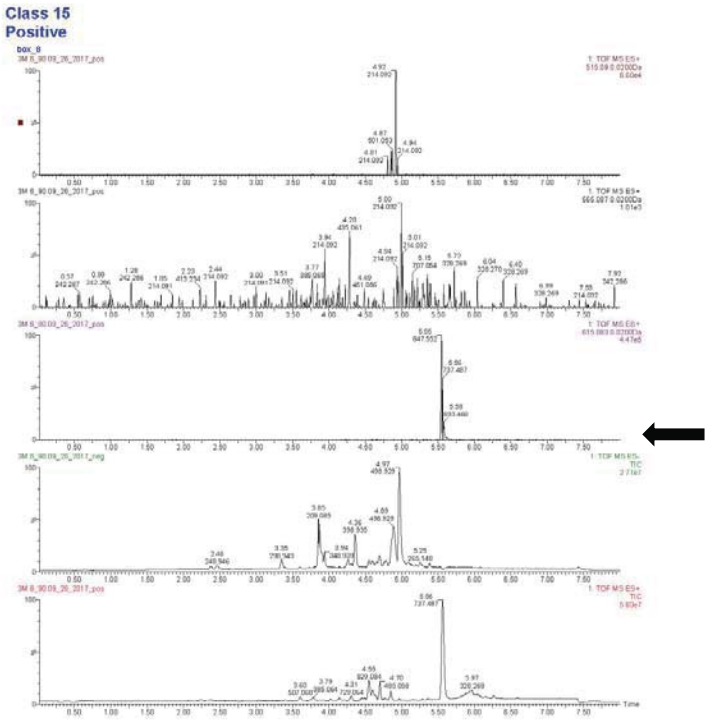

Class 15

Positive

box_8

3M 6_90 09_26_2017_pos 820 (4.921)

1: TOF MS ES+
1.44e5

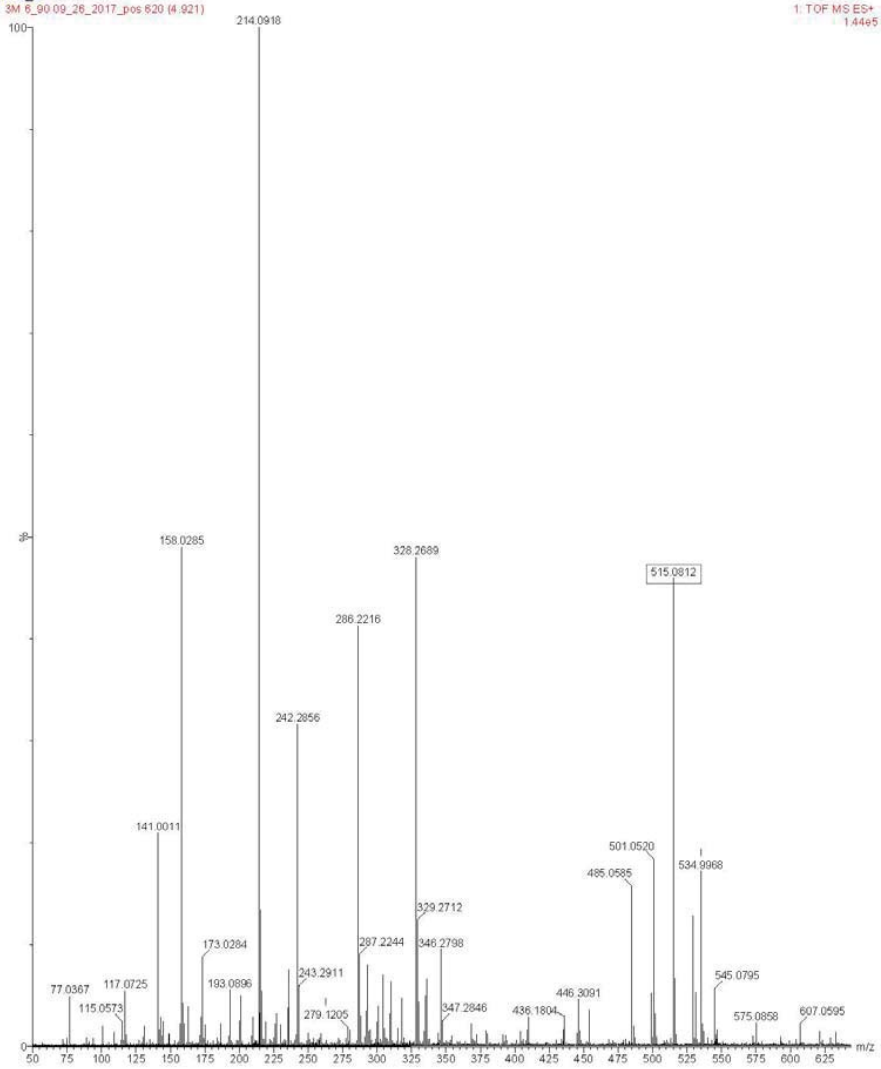

515.0812 m/z

Figure A4-13: Class 16 of 3M 6_90 - Positive

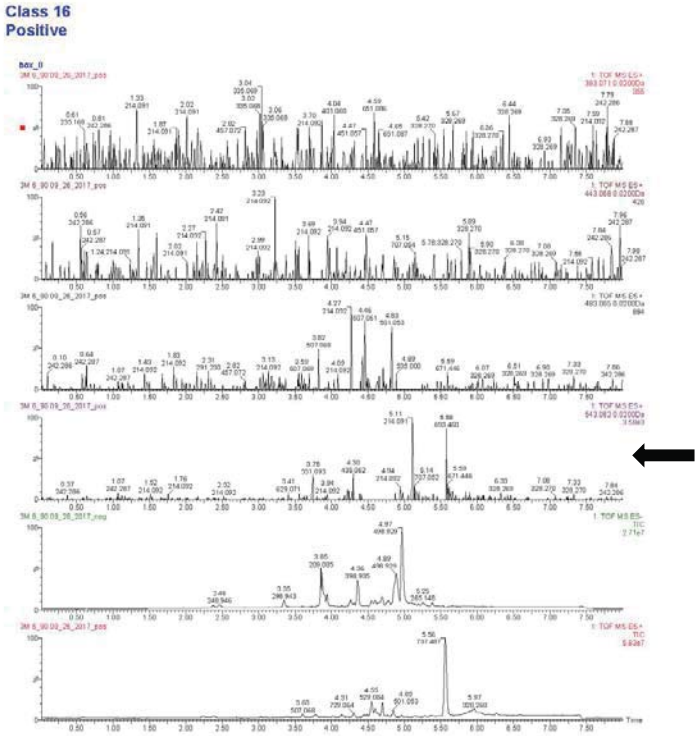

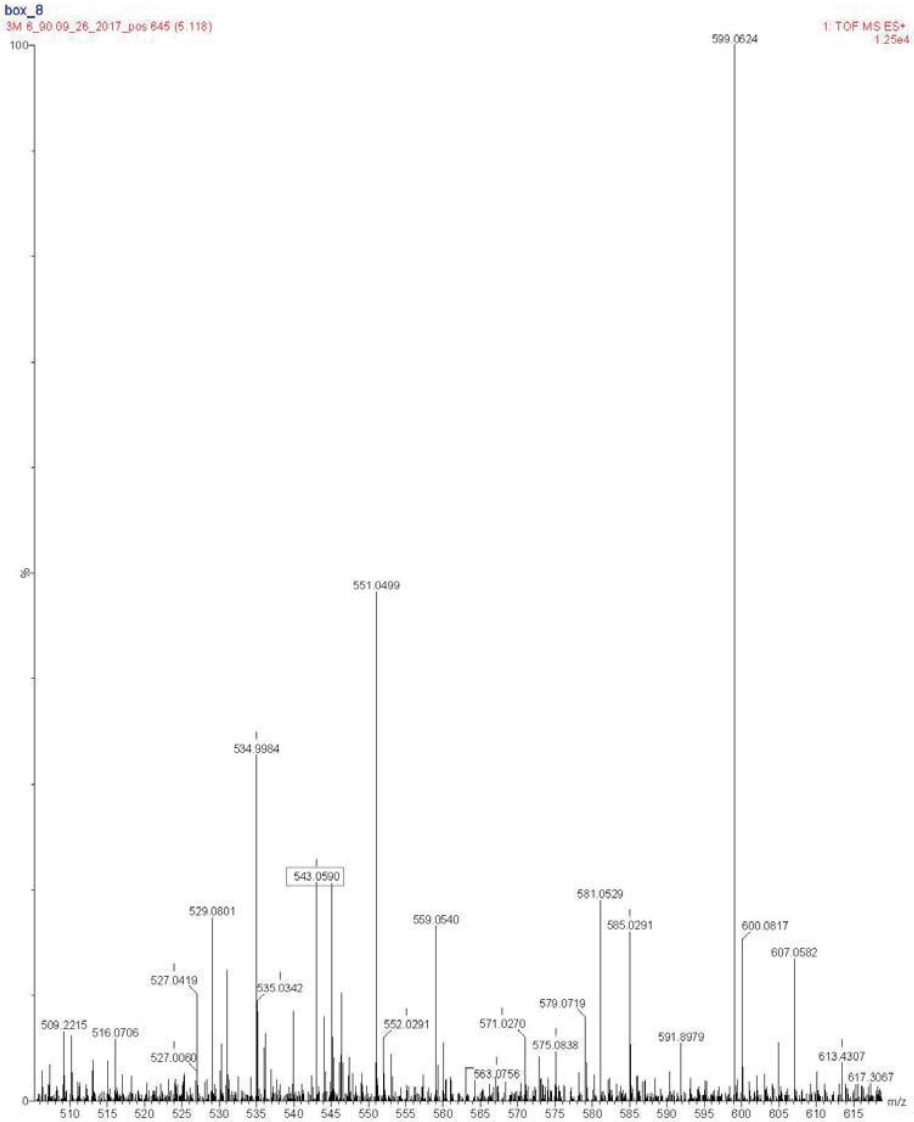

543.0590 m/z (only one of 4 clear)

Figure A4-14: Class 17 of 3M 6_90 - Positive

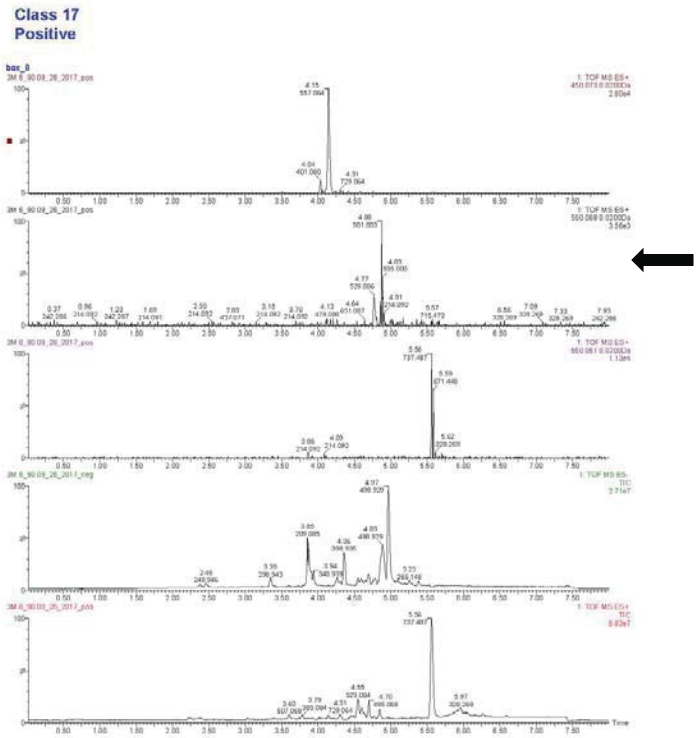

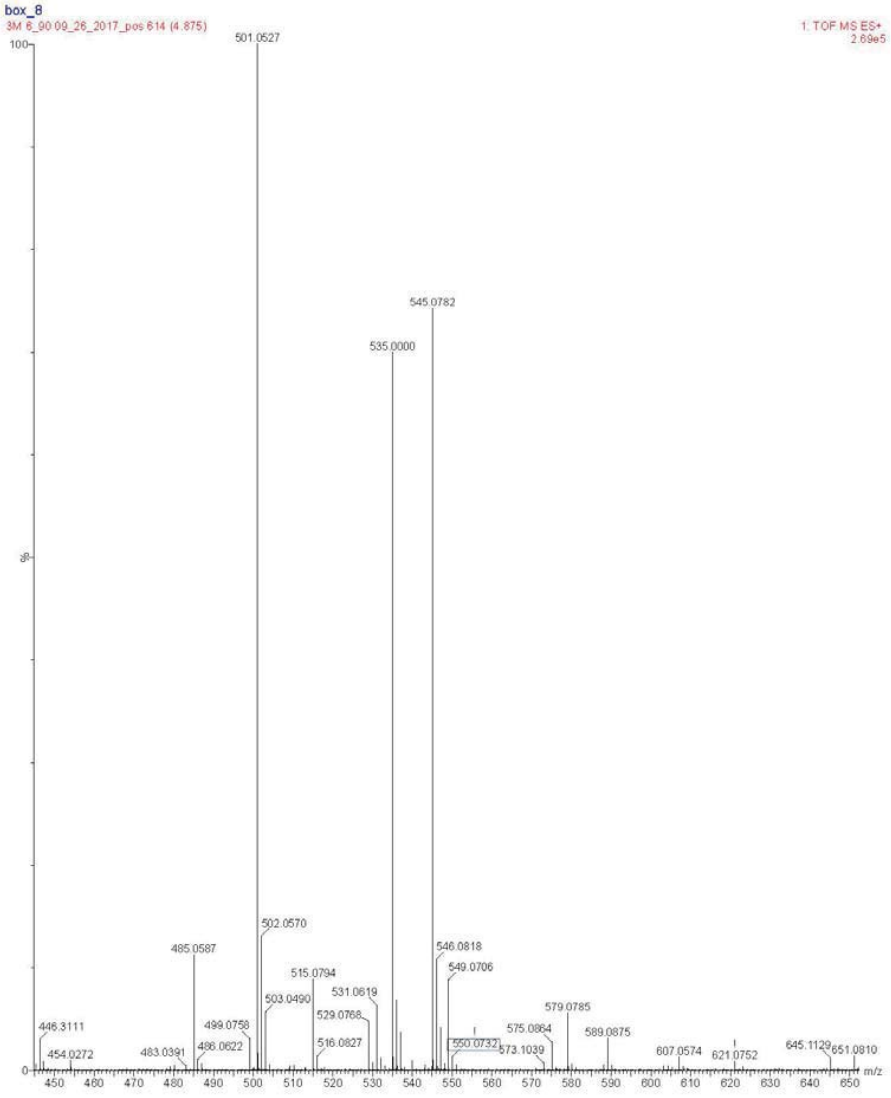

550.0732 m/z

Figure A4-15: Class 19 of 3M 6_90 - Positive

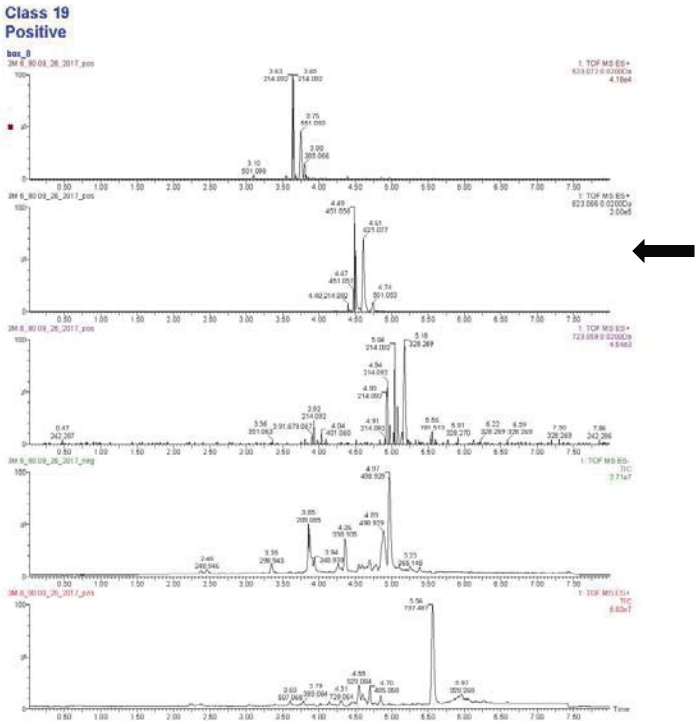

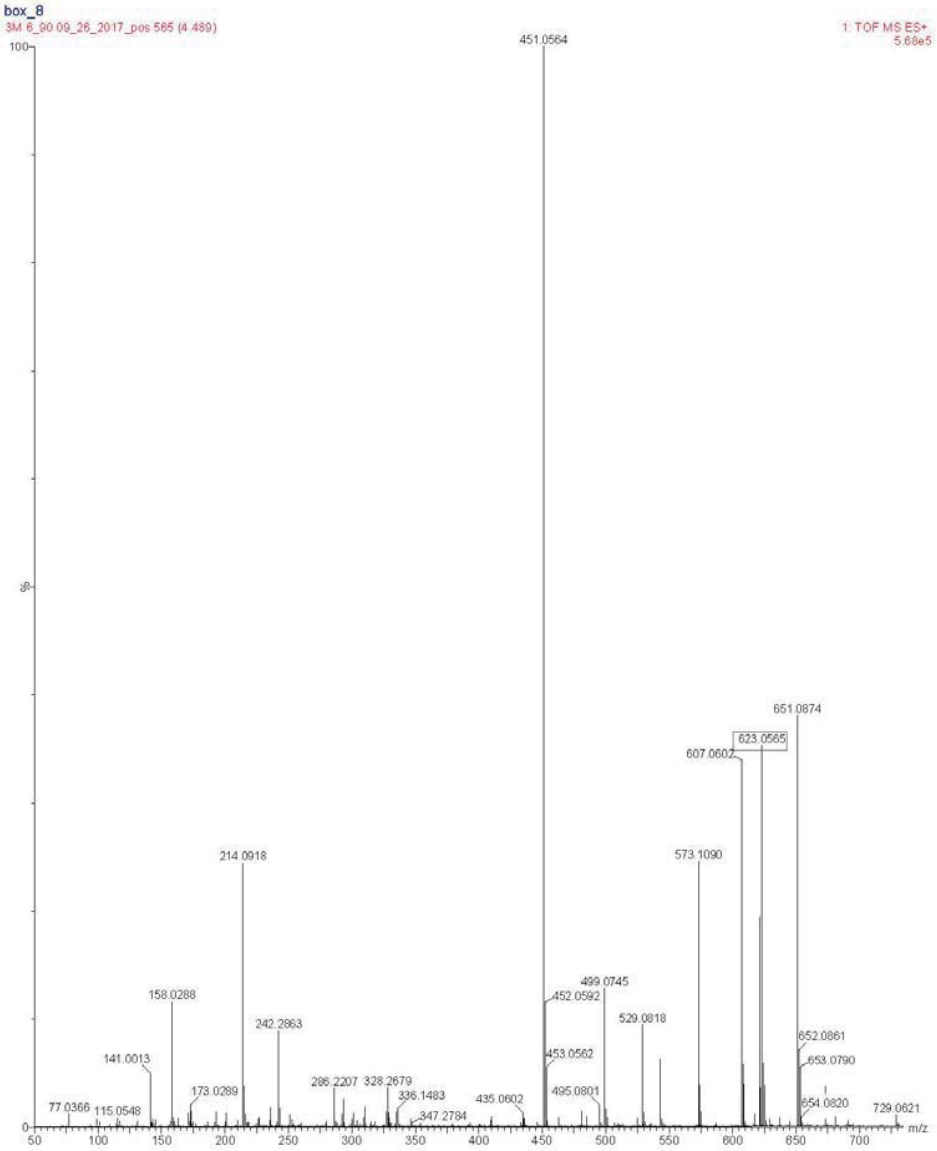

623.0565 m/z

Figure A4-16: Class 31 of 3M 6_90 - Positive

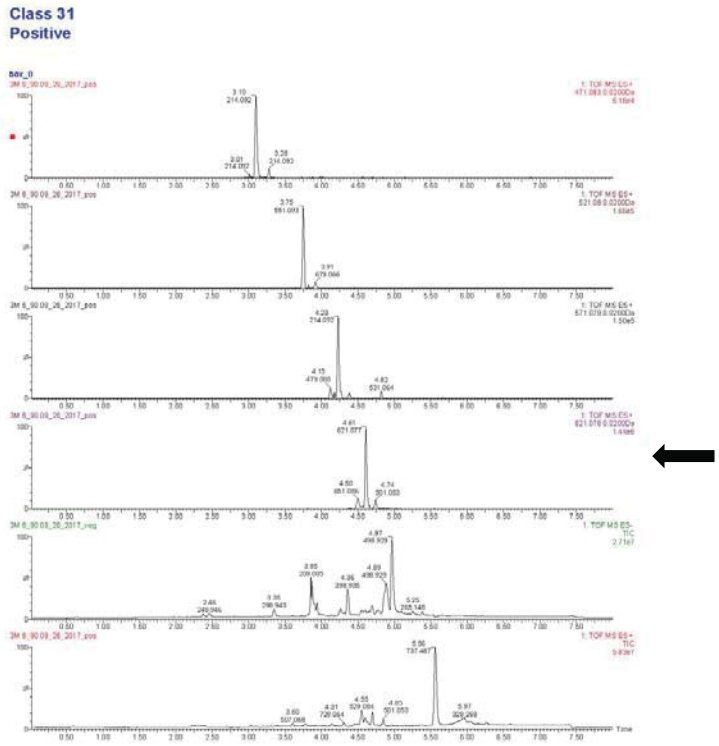

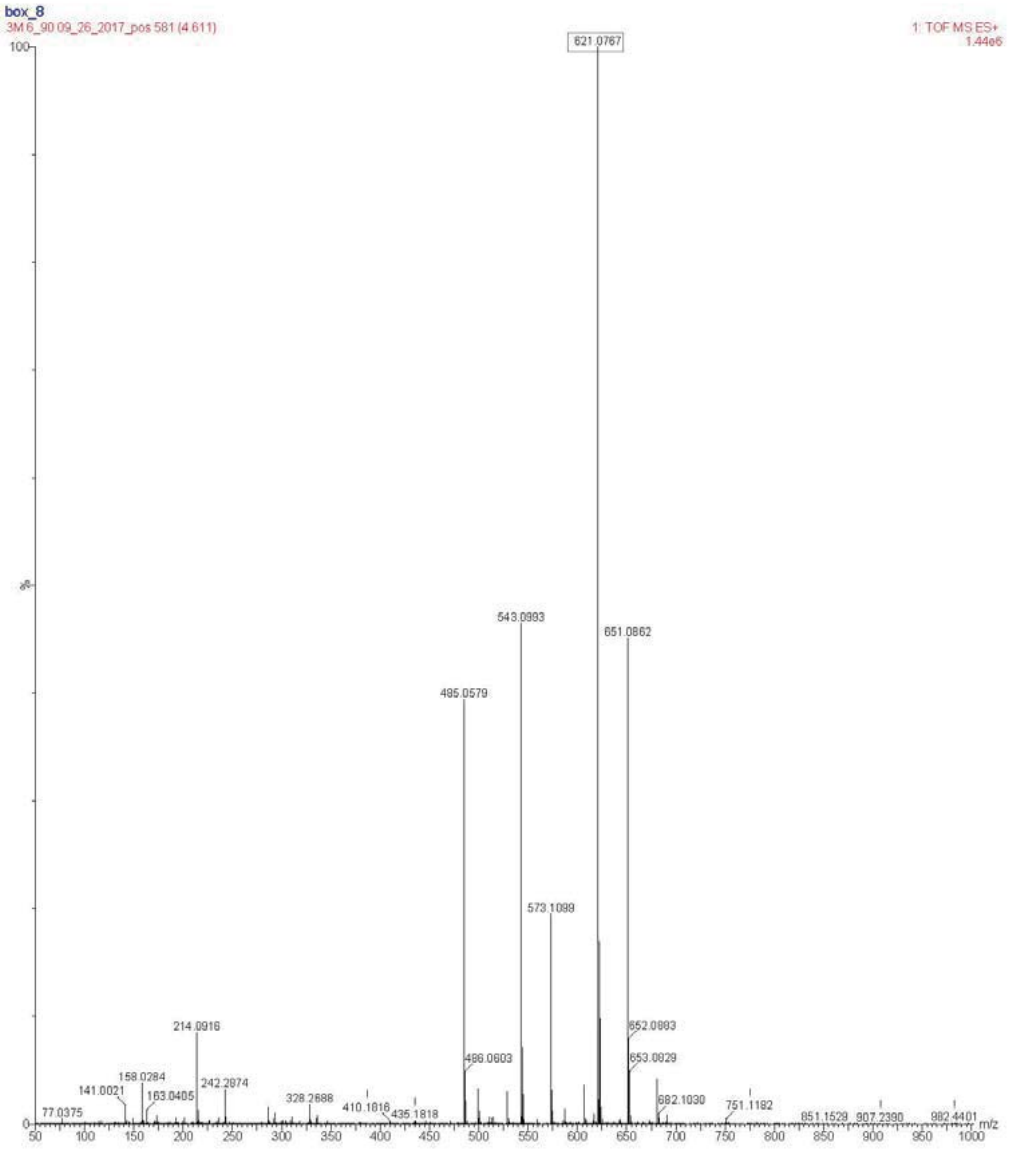

621.0767 m/z

Figure A4-17: Class 32 of 3M 6_90 - Positive

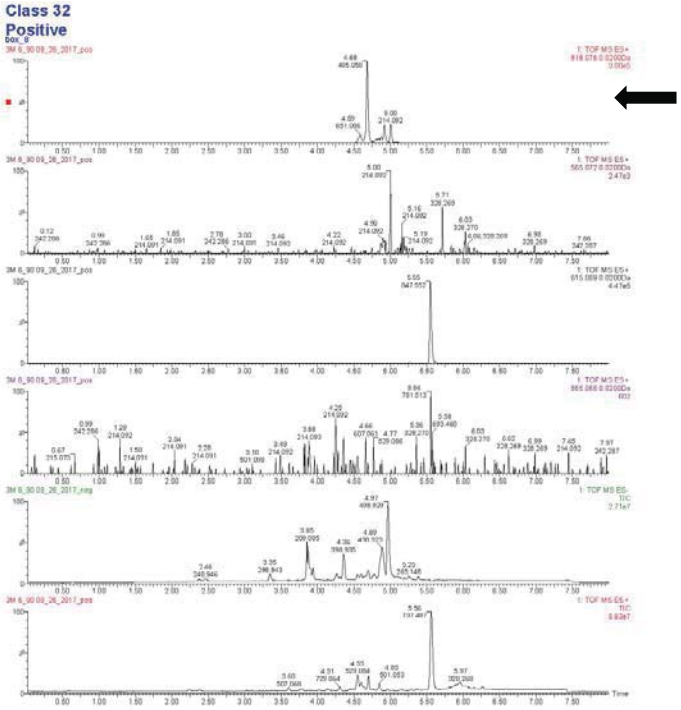

Class 32

Positive

box_8

3M 6_90 09_26_2017_pos 589 (4.679)

1: TOF MS ES+
1.45e6

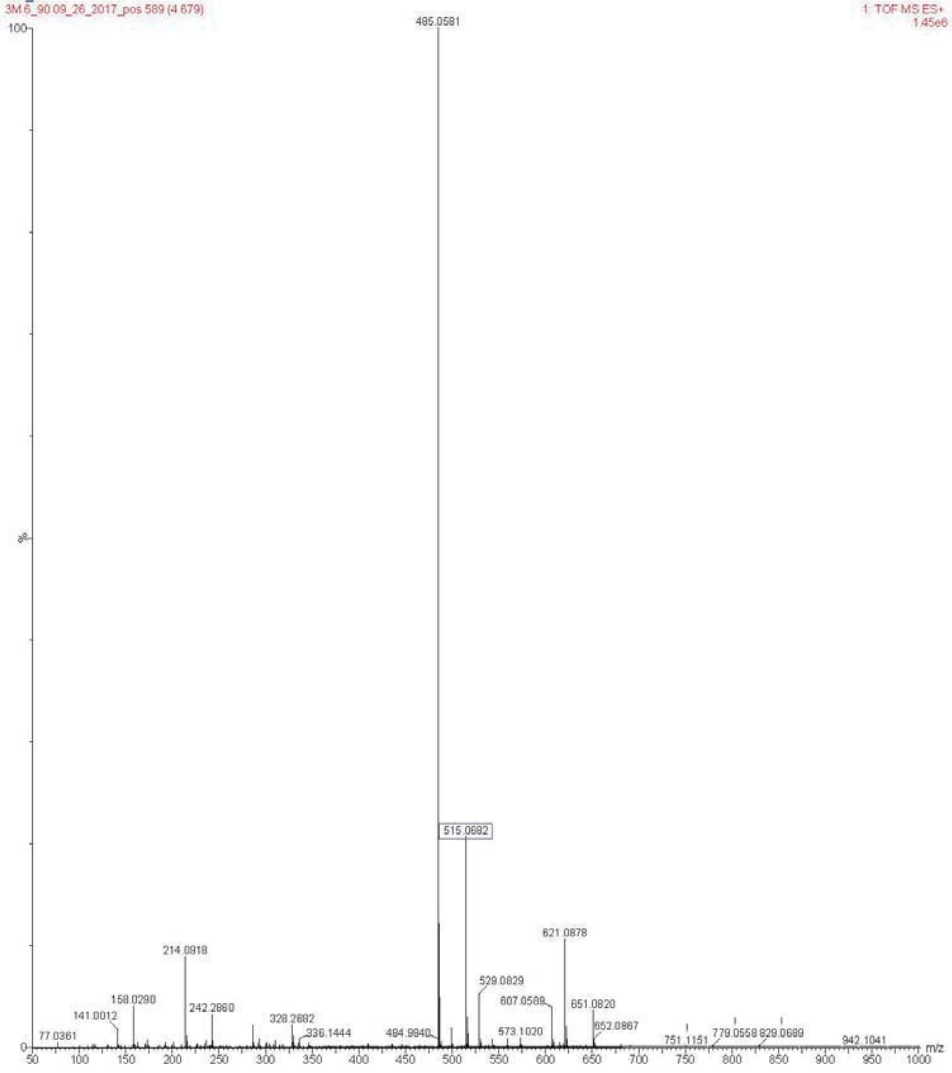

515.0682 m/z

Figure A4-18: Class 33 of 3M 6_90 - Positive

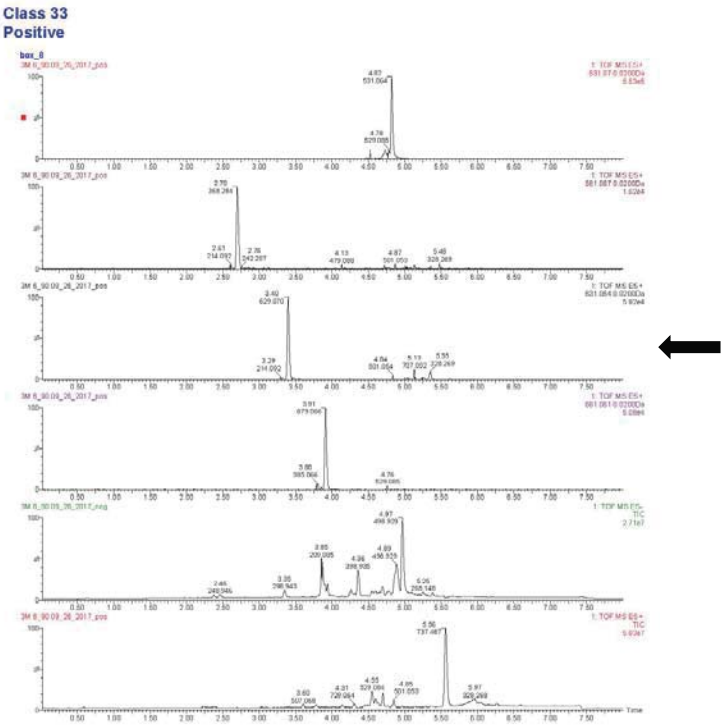

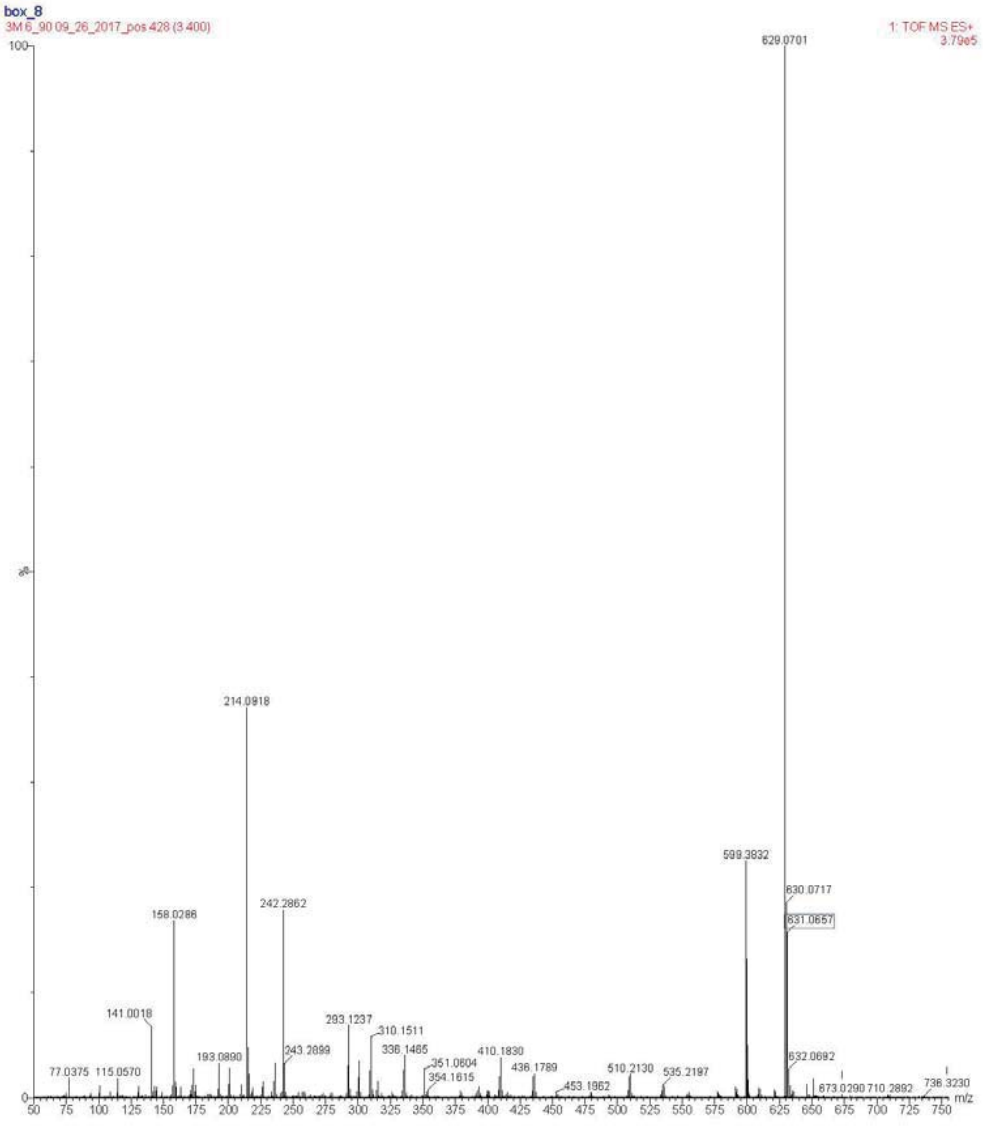

631.0657 m/z

Figure A4-19: Class 34 of 3M 6_90 - Positive

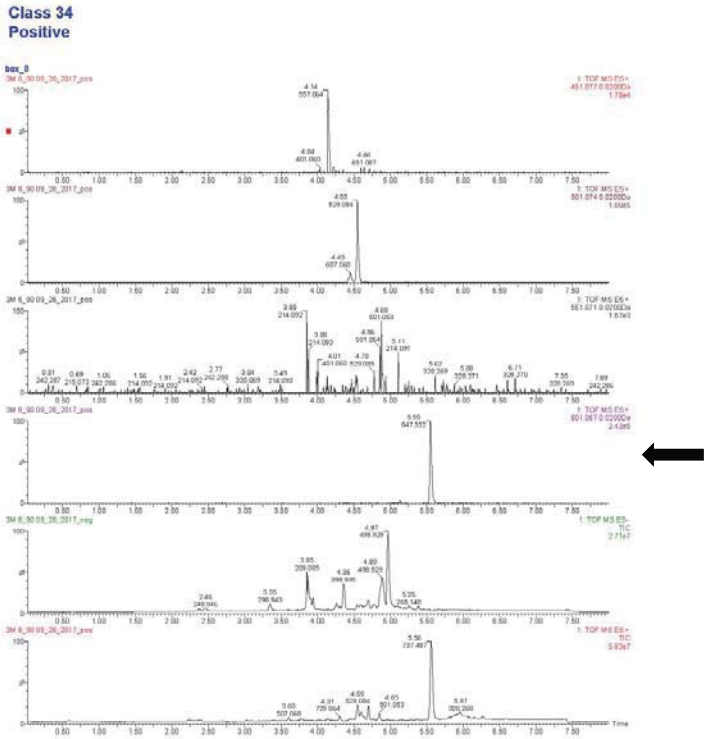

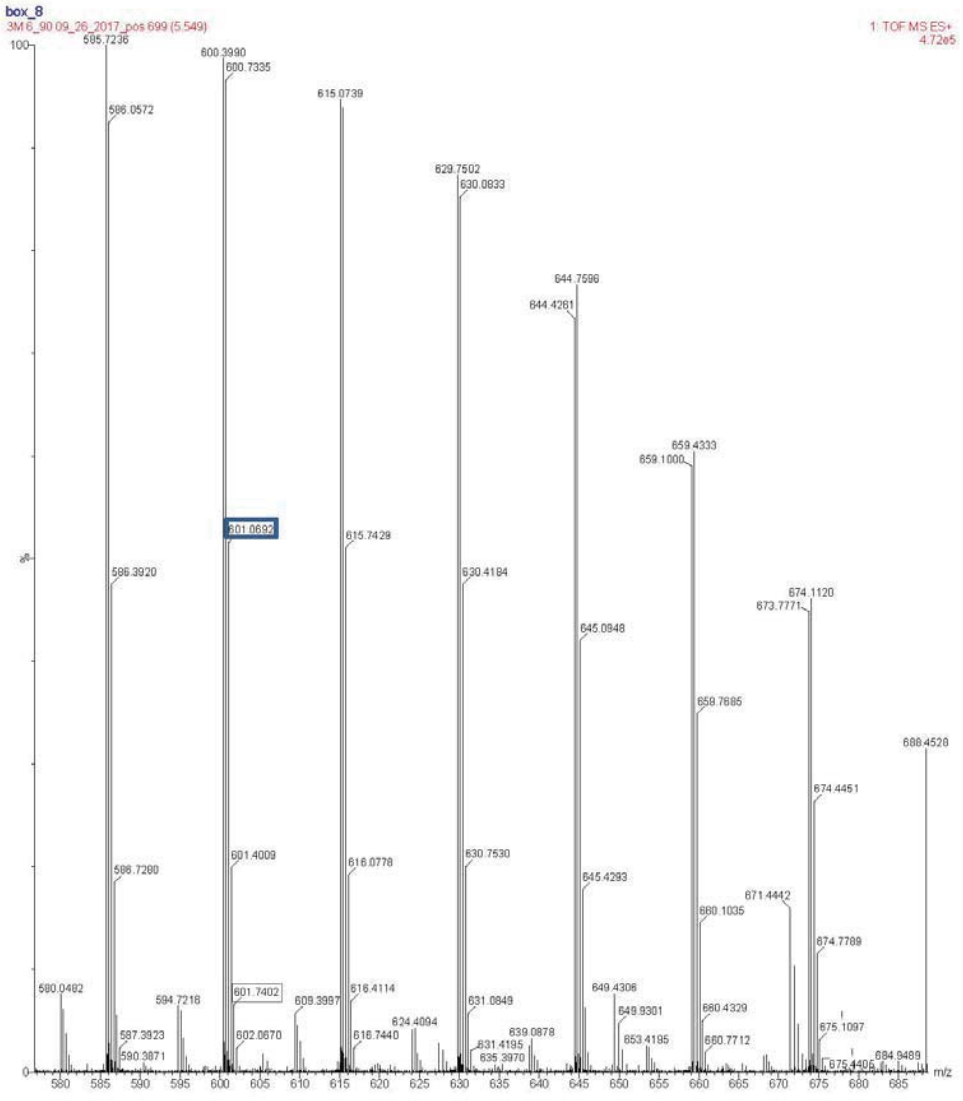

~~601.7402~~ 601.0692 m/z

Figure A4-20: Class 37 of 3M 6_90 - Positive

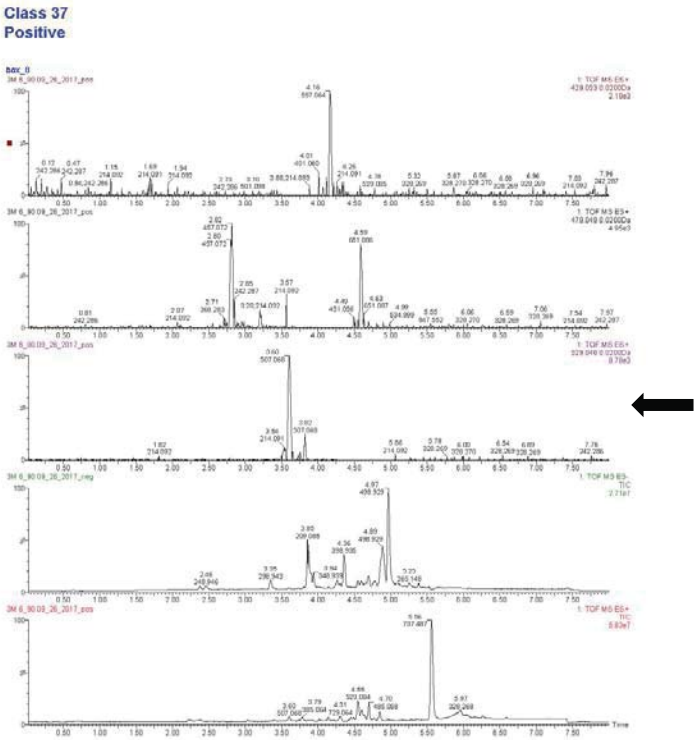

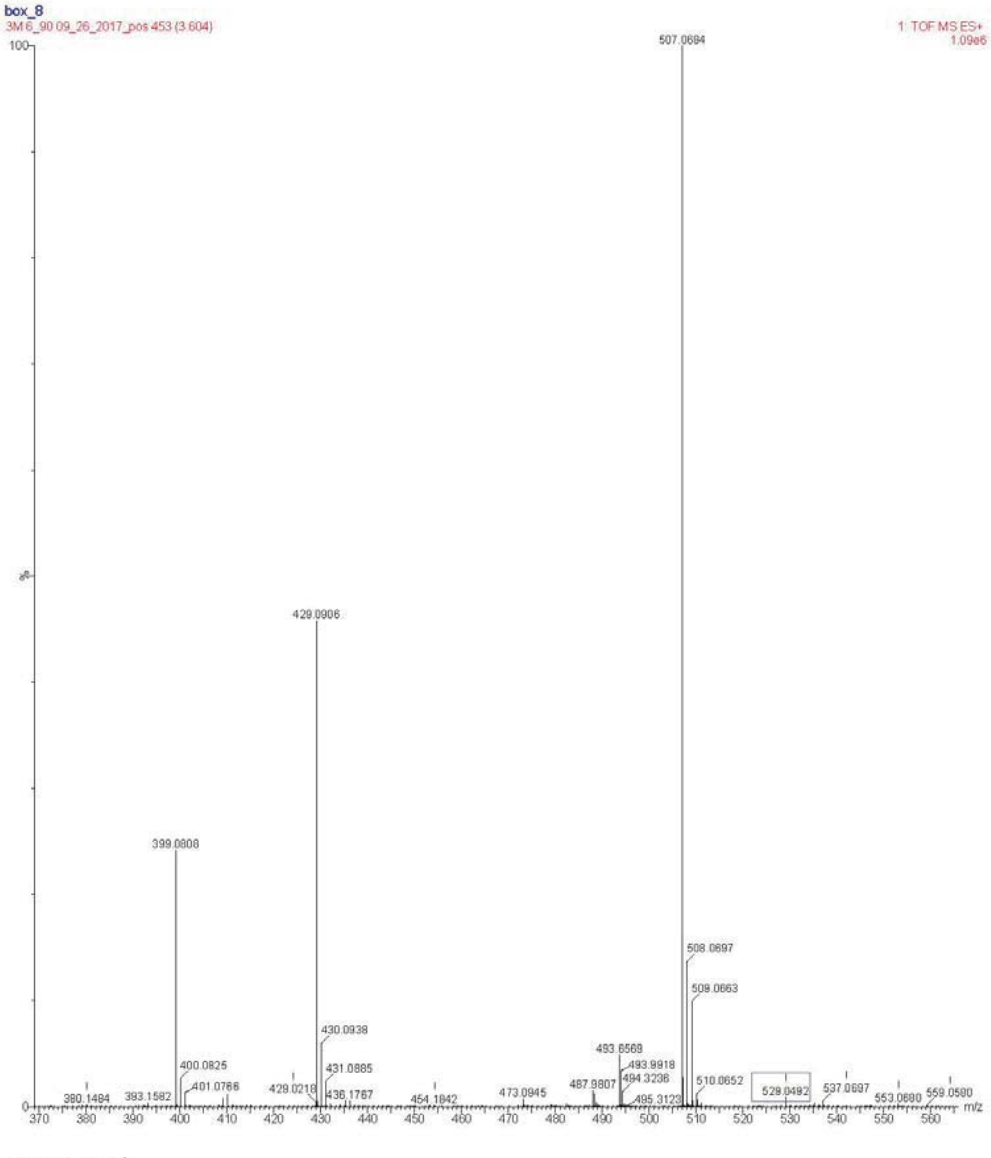

529.0492 m/z

Figure A4-21: Class 38 of 3M 6_90 - Positive

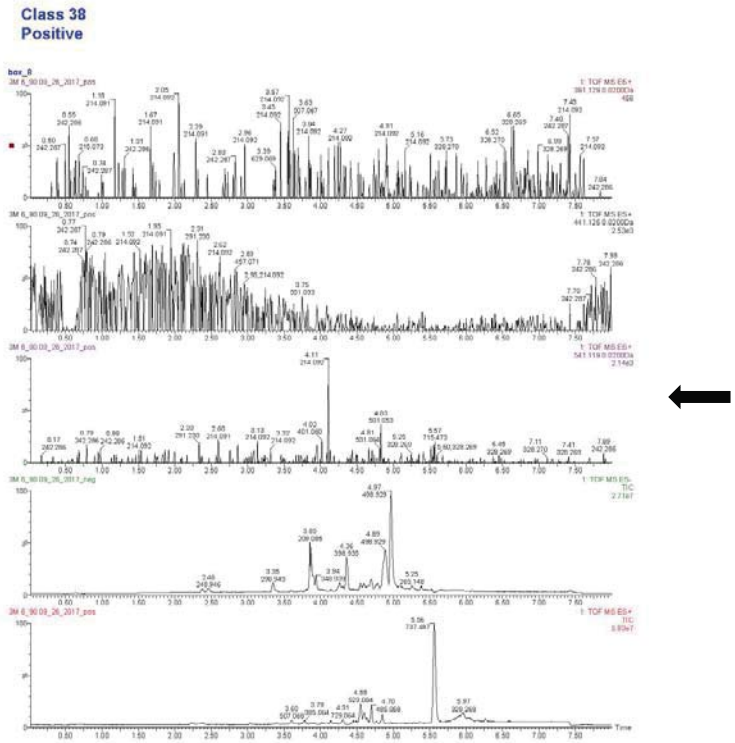

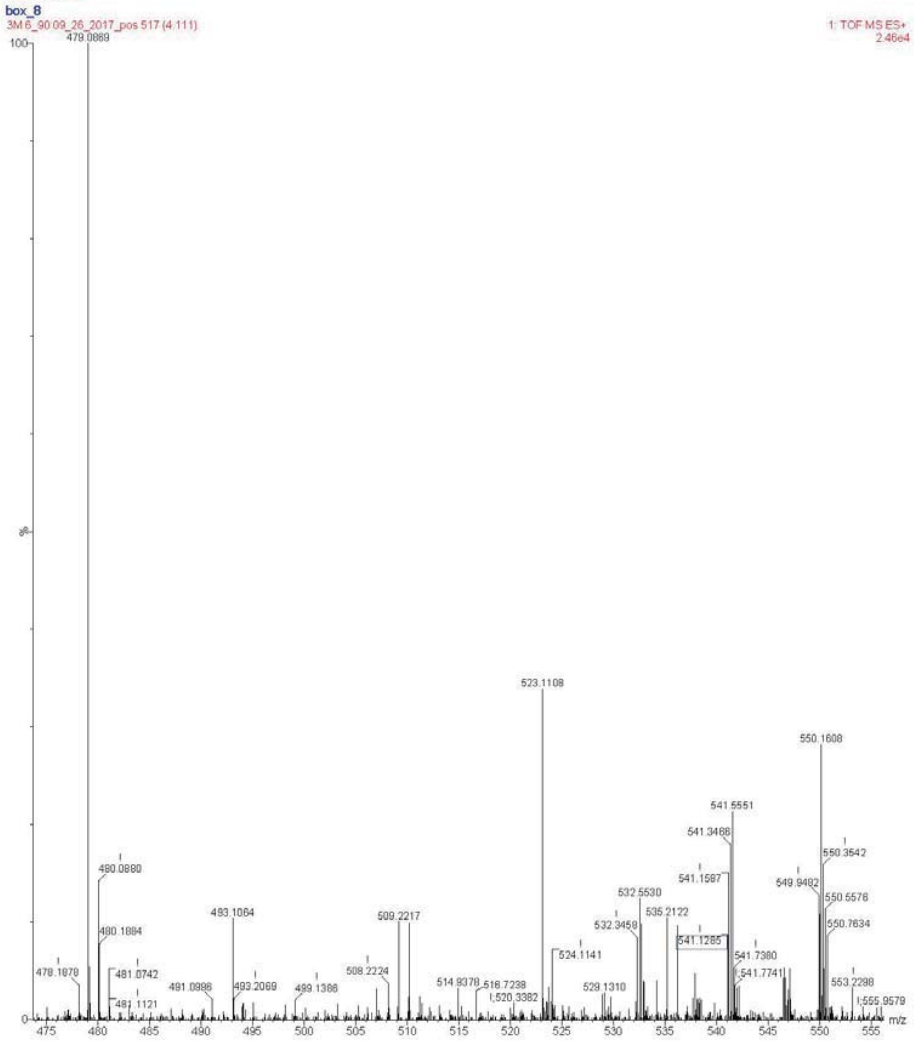

541.1285 m/z

Figure A4-22: Class 1 of 3M 6_90 - Negative

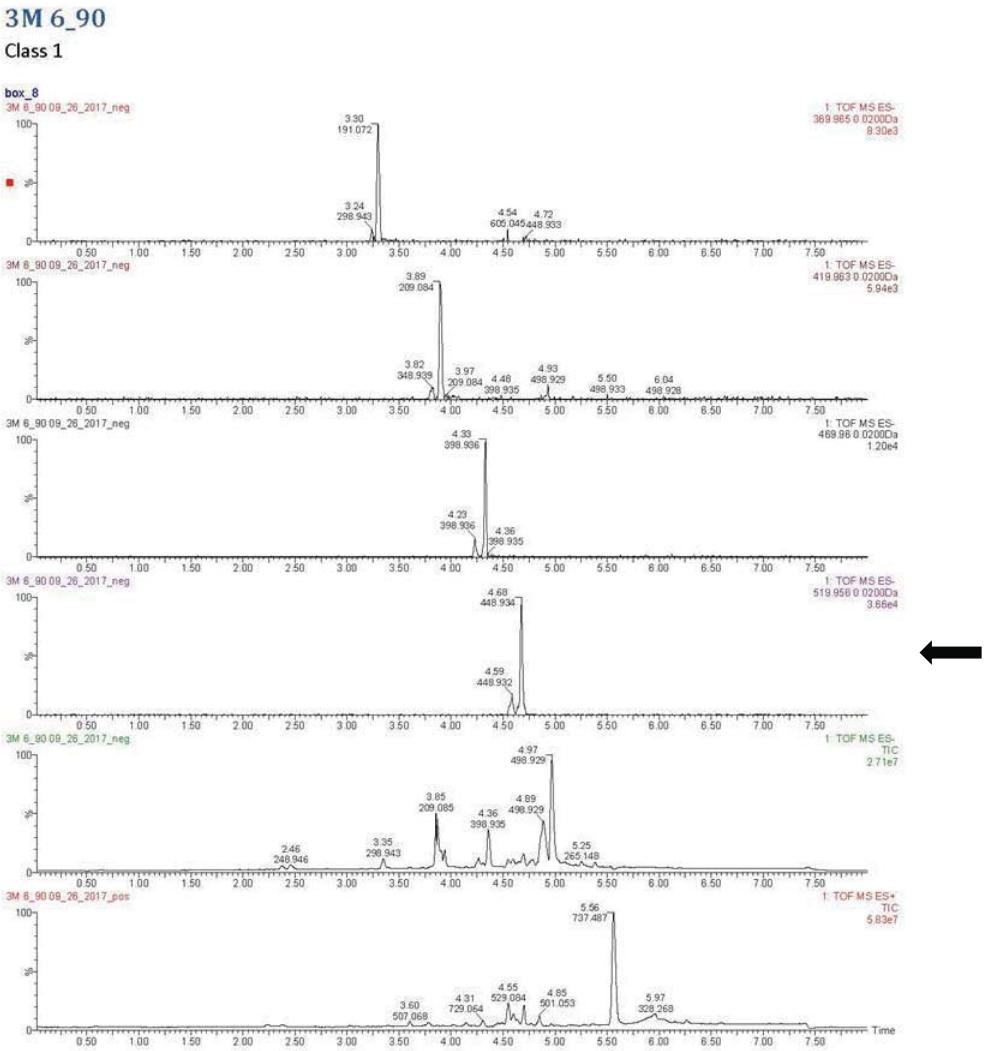

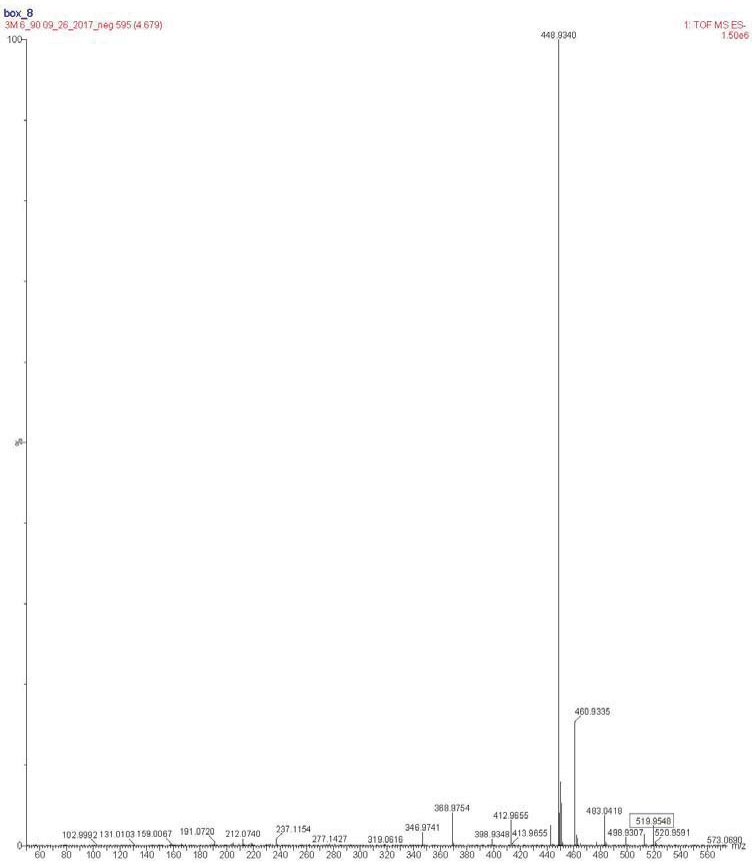

519.9548 m/z

Figure A4-23: Class 2 of 3M 6_90 - Negative

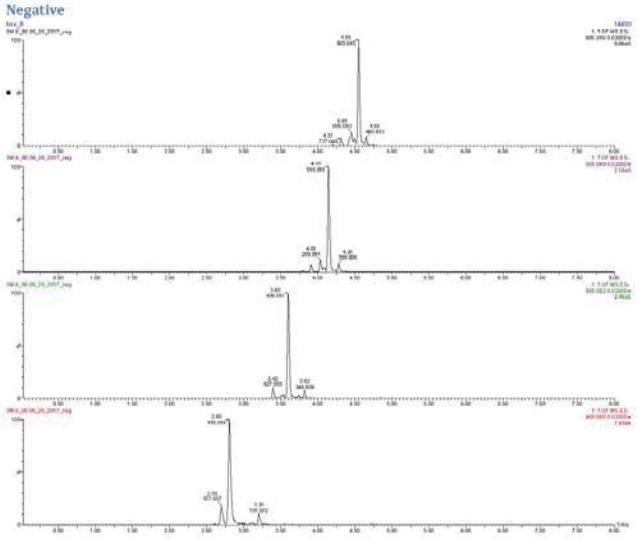

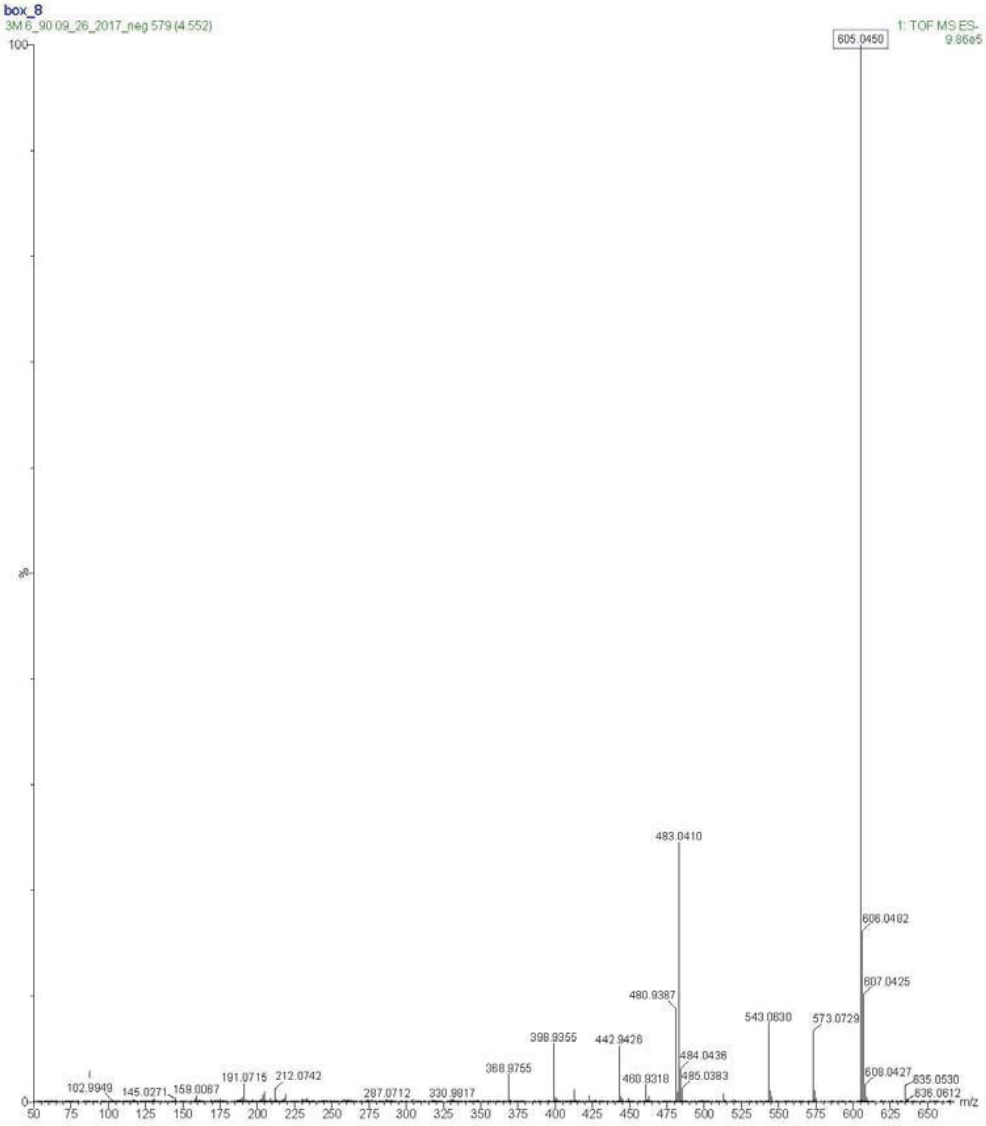

605.0450 m/z

Figure A4-24: Class 3 of 3M 6_90 - Negative

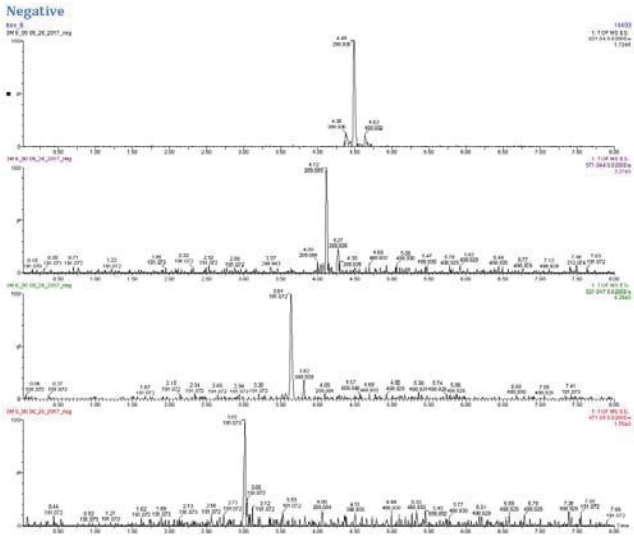

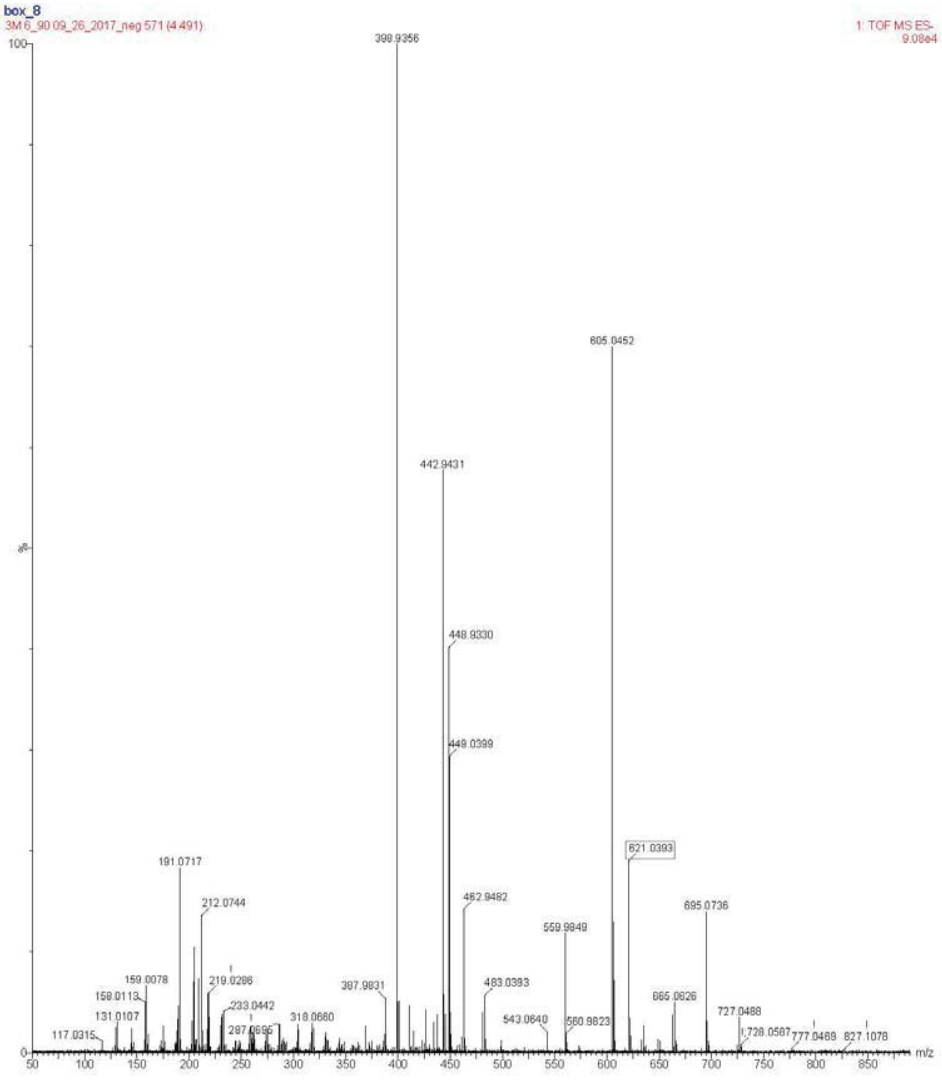

621.0393 m/z

Figure A4-25: Class 5 of 3M 6_90 - Negative

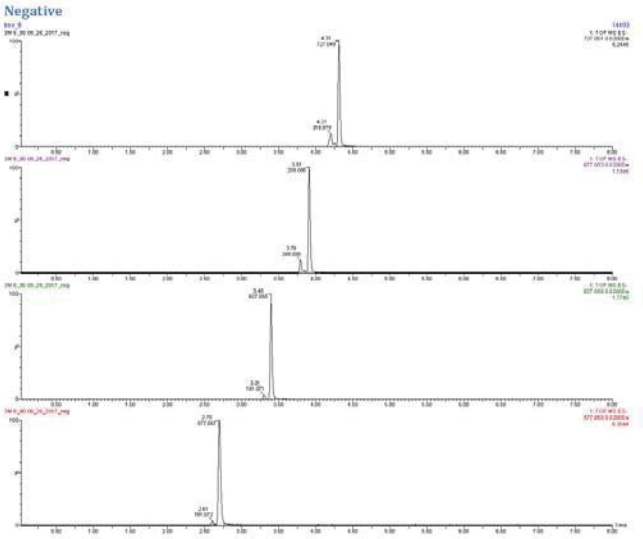

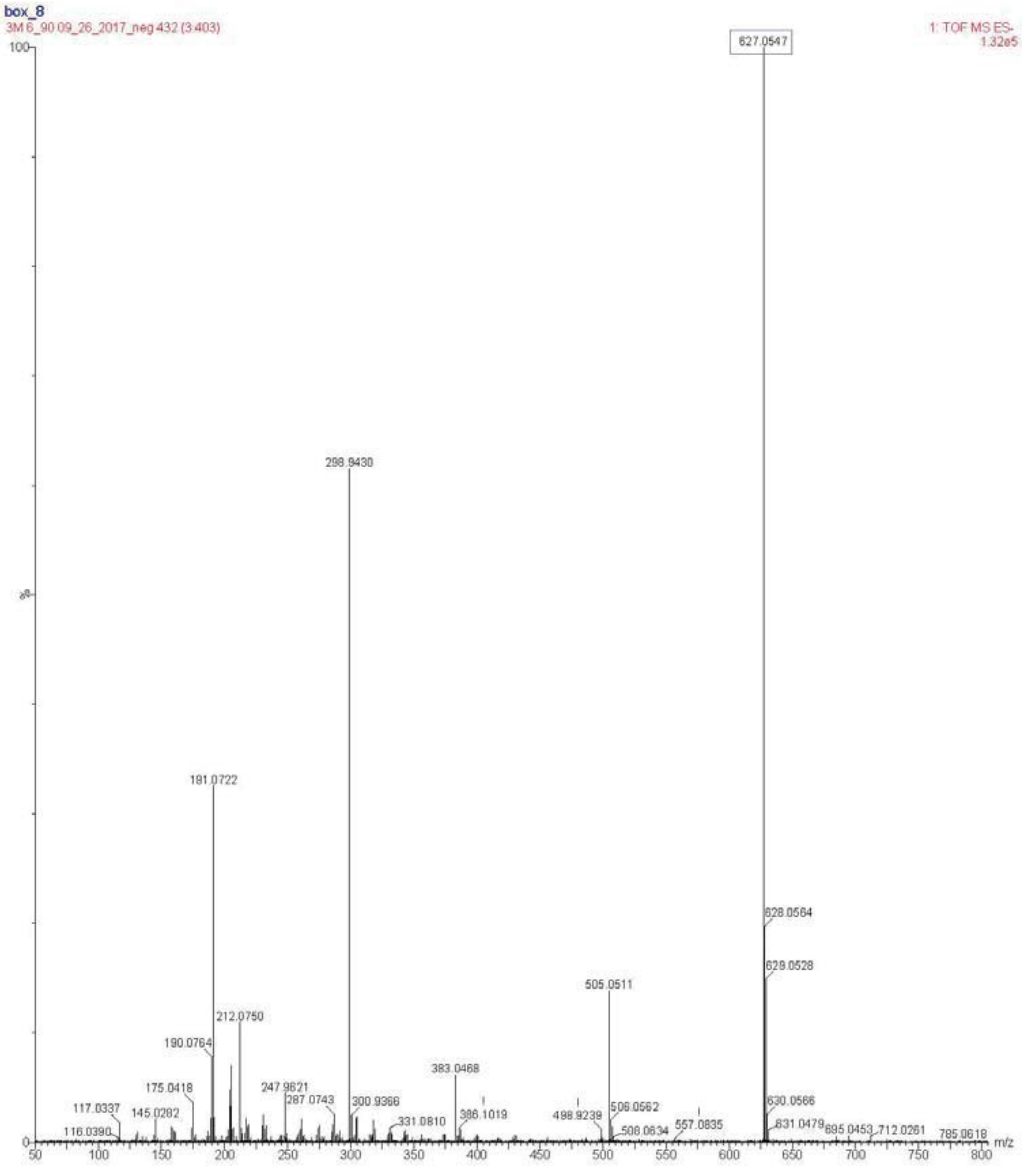

627.0547 m/z

Figure A4-26: Class 21 of 3M 6_90 - Negative

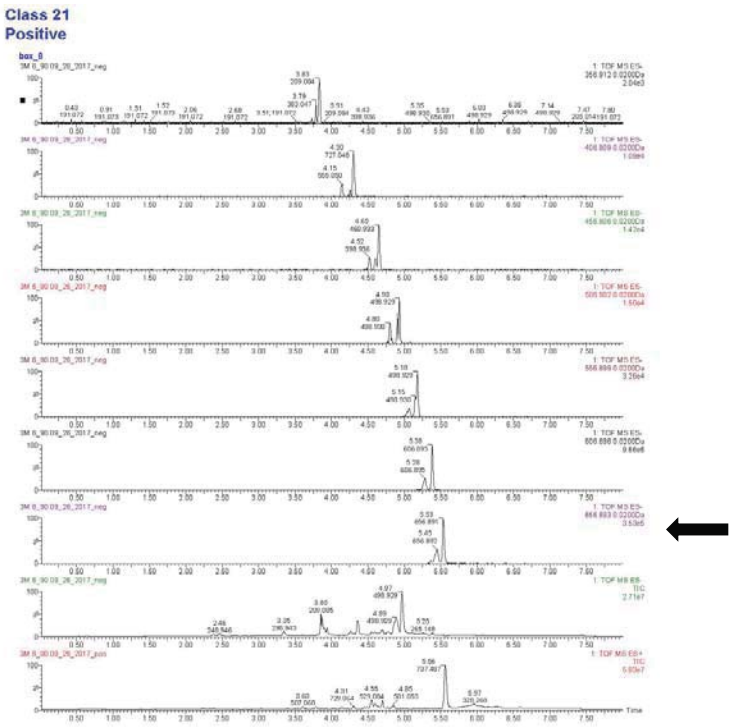

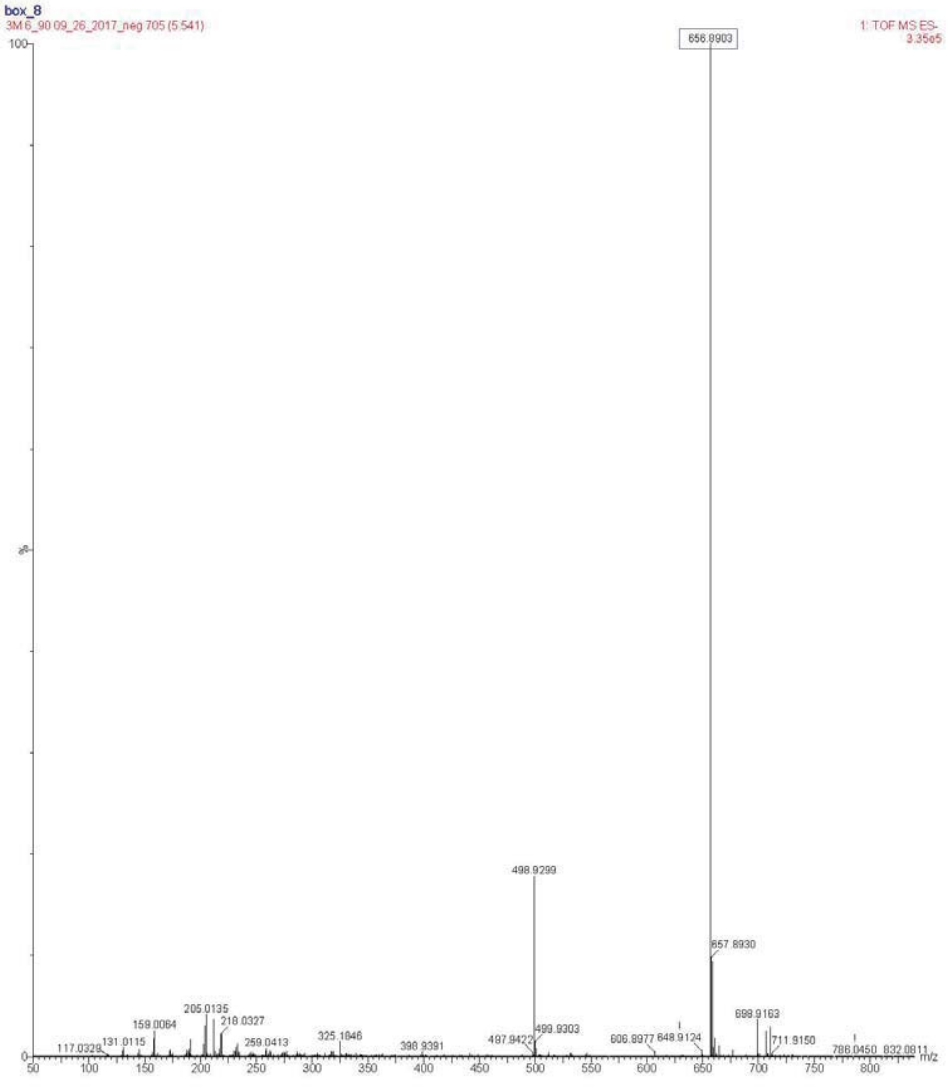

656.8903 m/z

Figure A4-27: Class 22 of 3M 6_90 - Negative

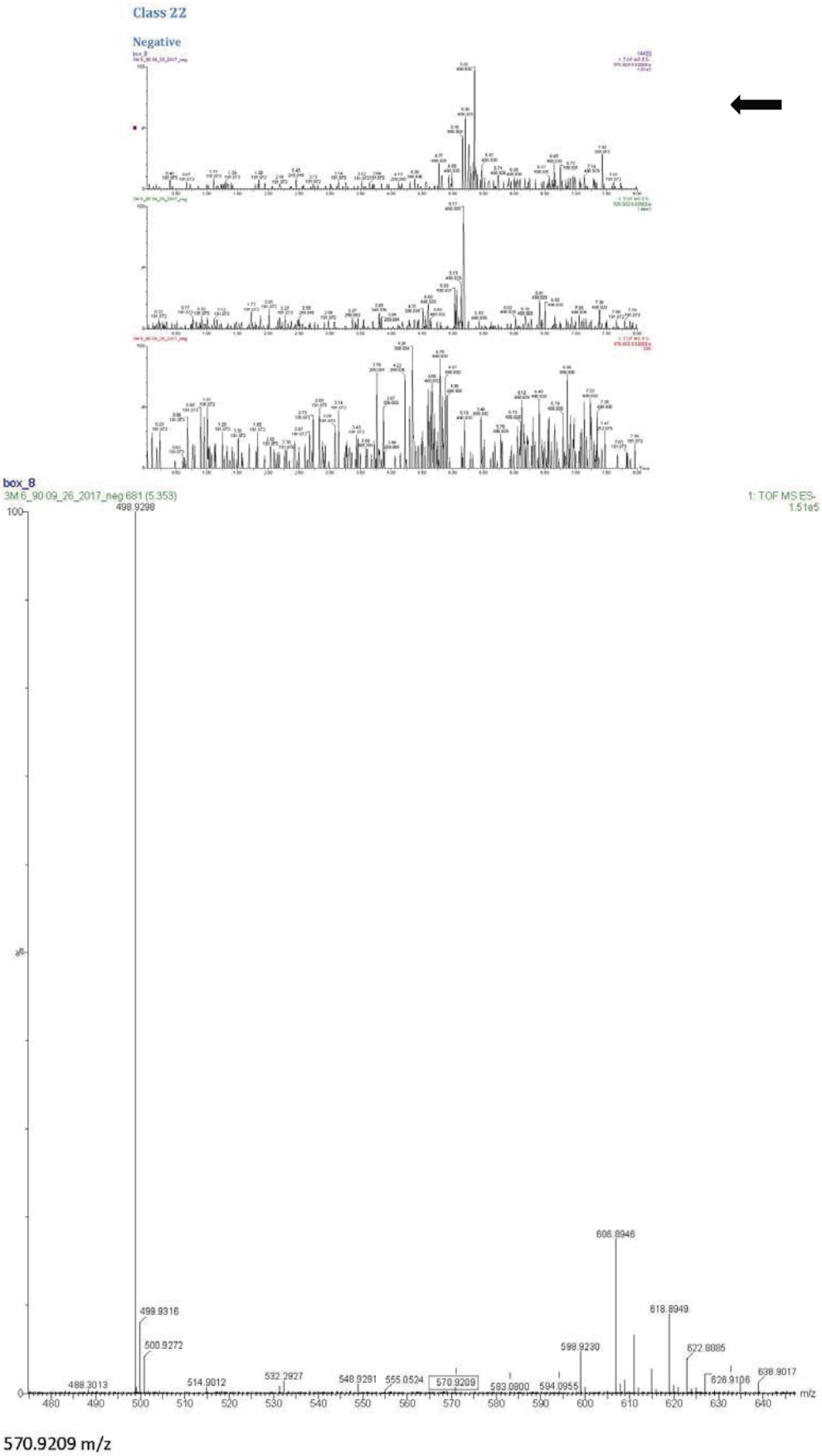

570.9209 m/z

Figure A4-28: Class 23 of 3M 6_90 - Negative

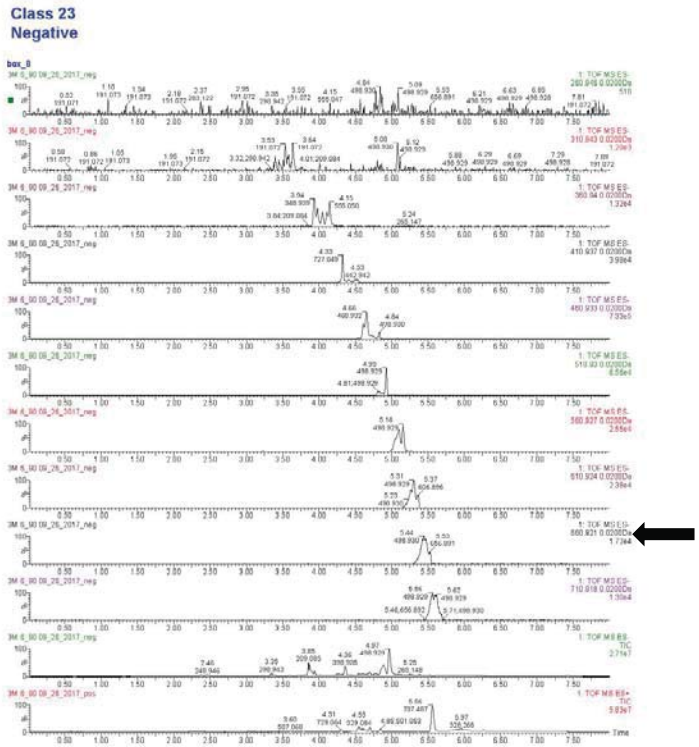

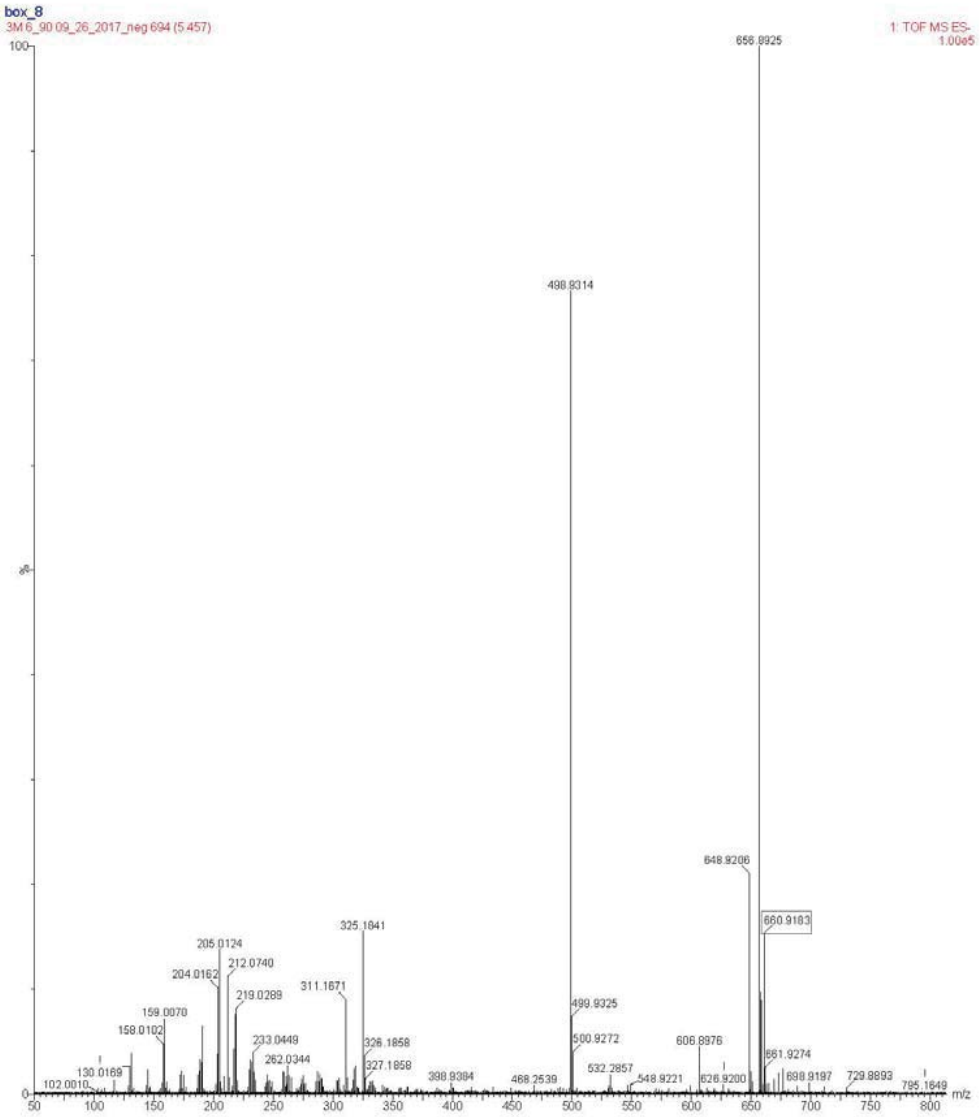

660.9183 m/z

Figure A4-29: Class 24 of 3M 6_90 - Negative

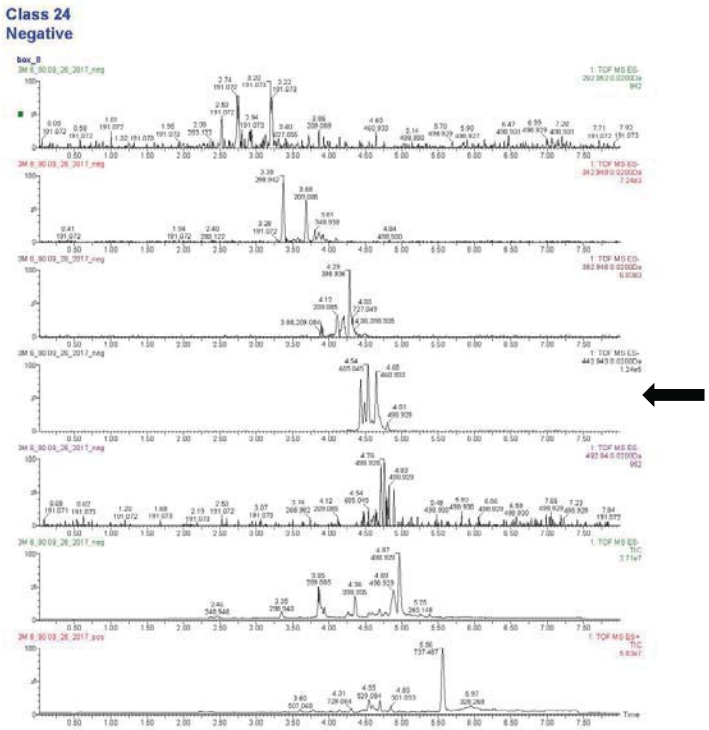

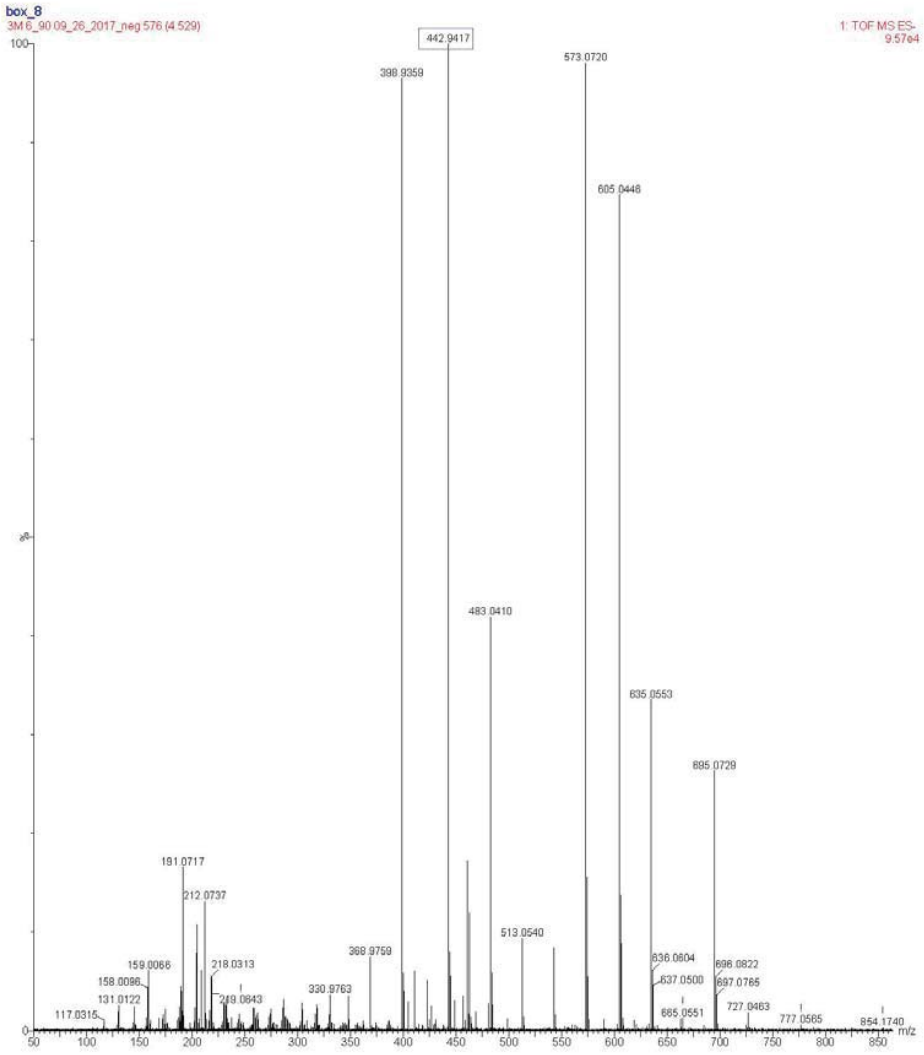

442.9417 m/z

Figure A4-30: Class 25 of 3M 6_90 - Negative

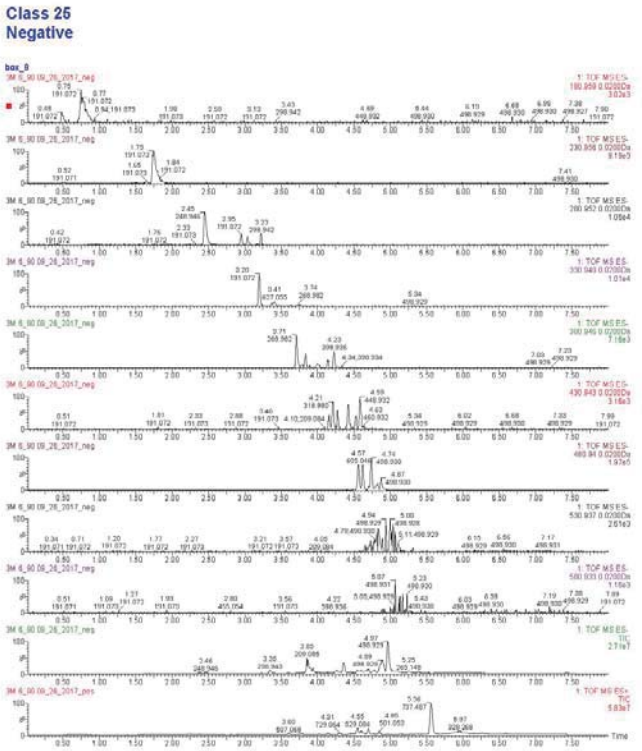

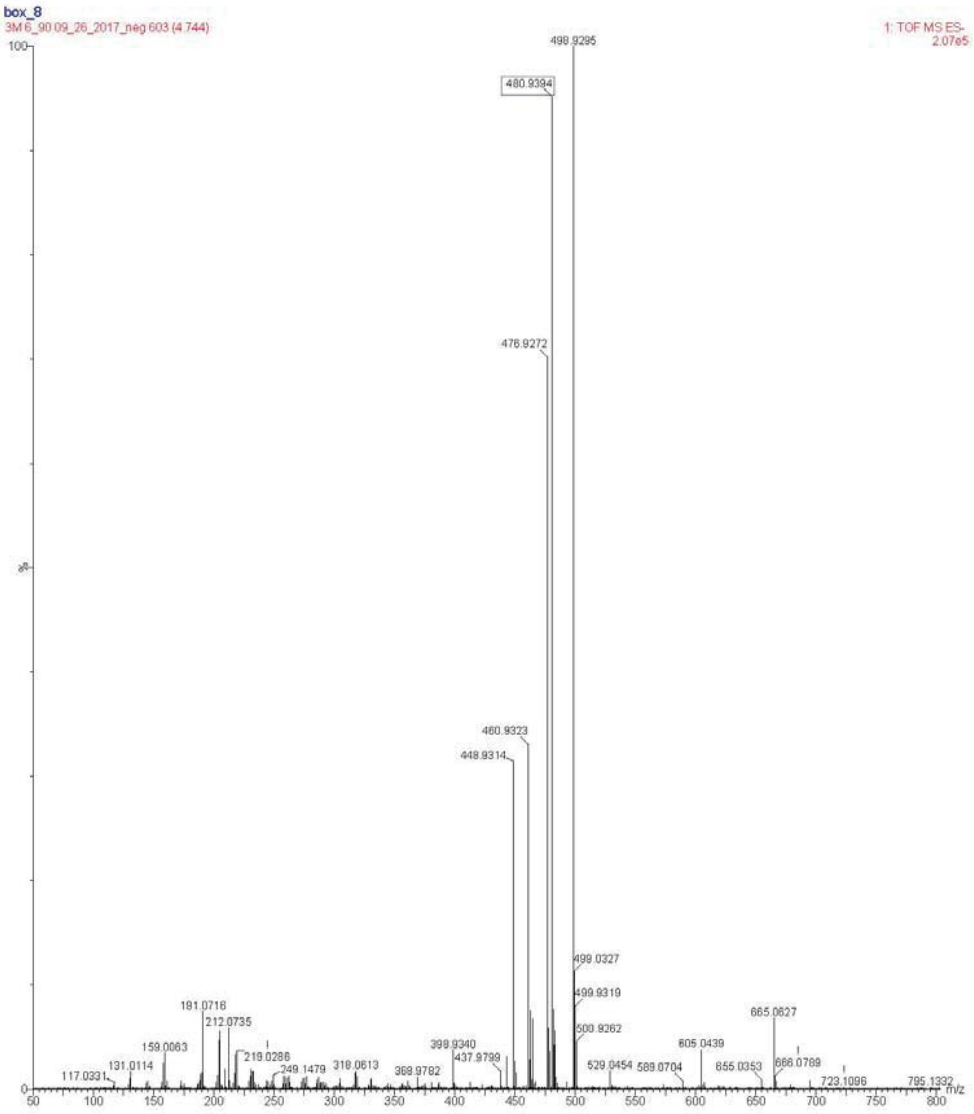

480.9394 m/z

Figure A4-31: Class 26 of 3M 6_90 - Negative

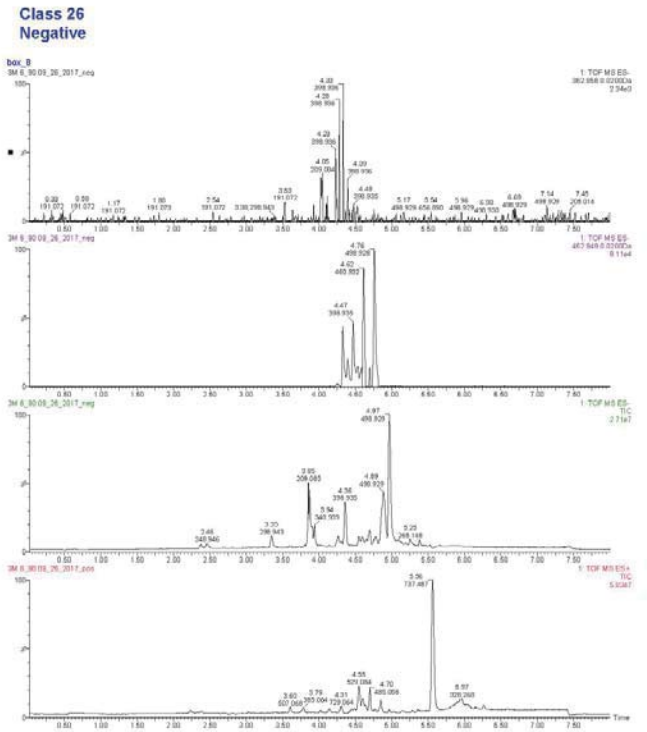

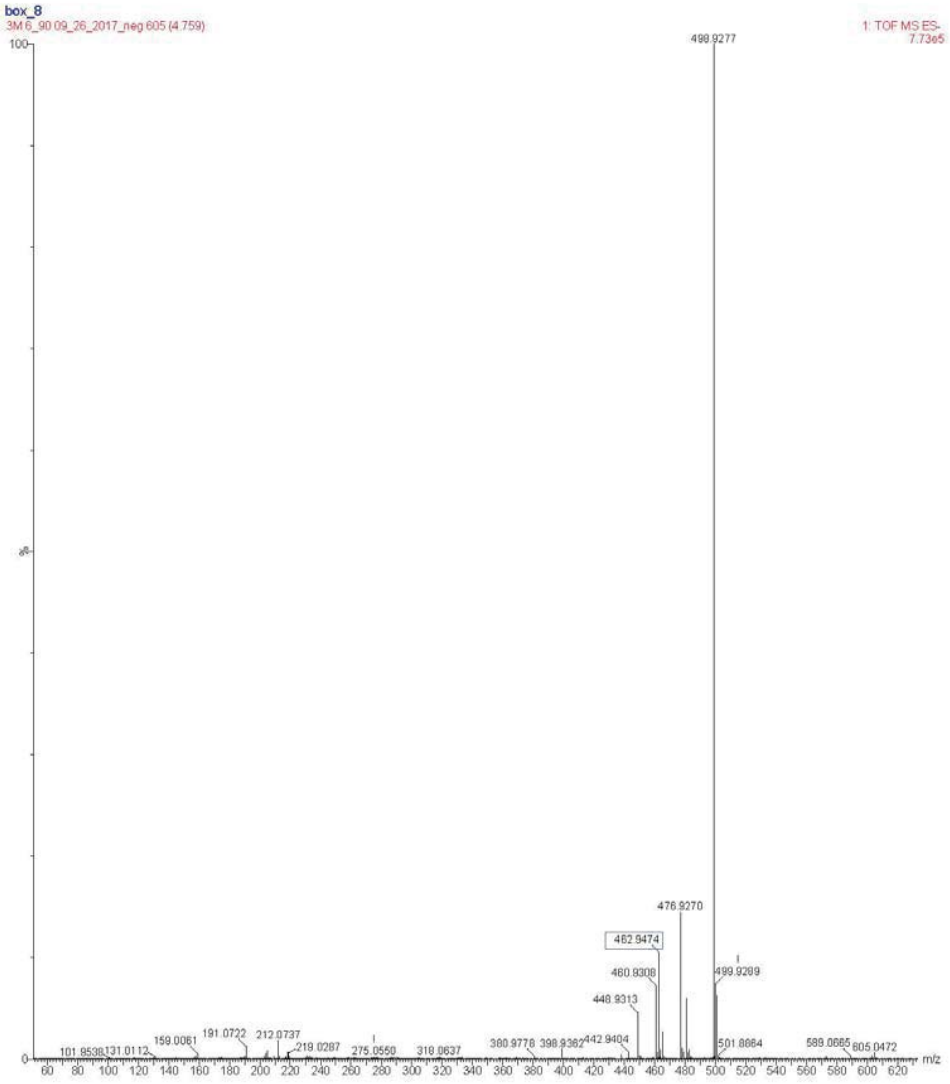

462.9474 m/z

Figure A4-32: Class 29 of 3M 6_90 - Negative

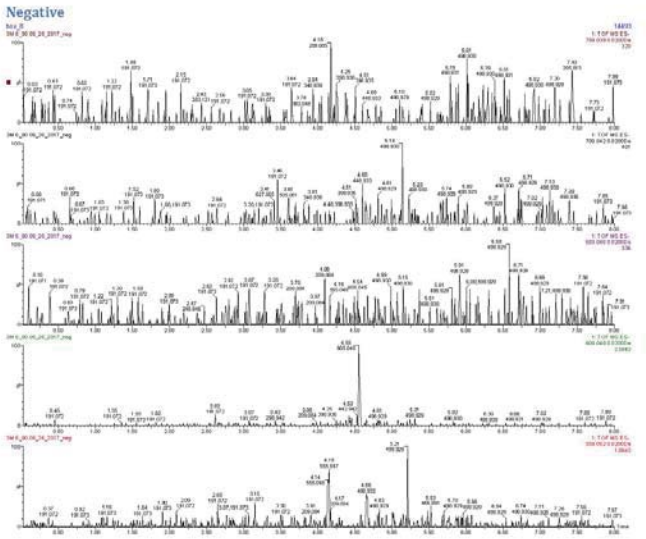

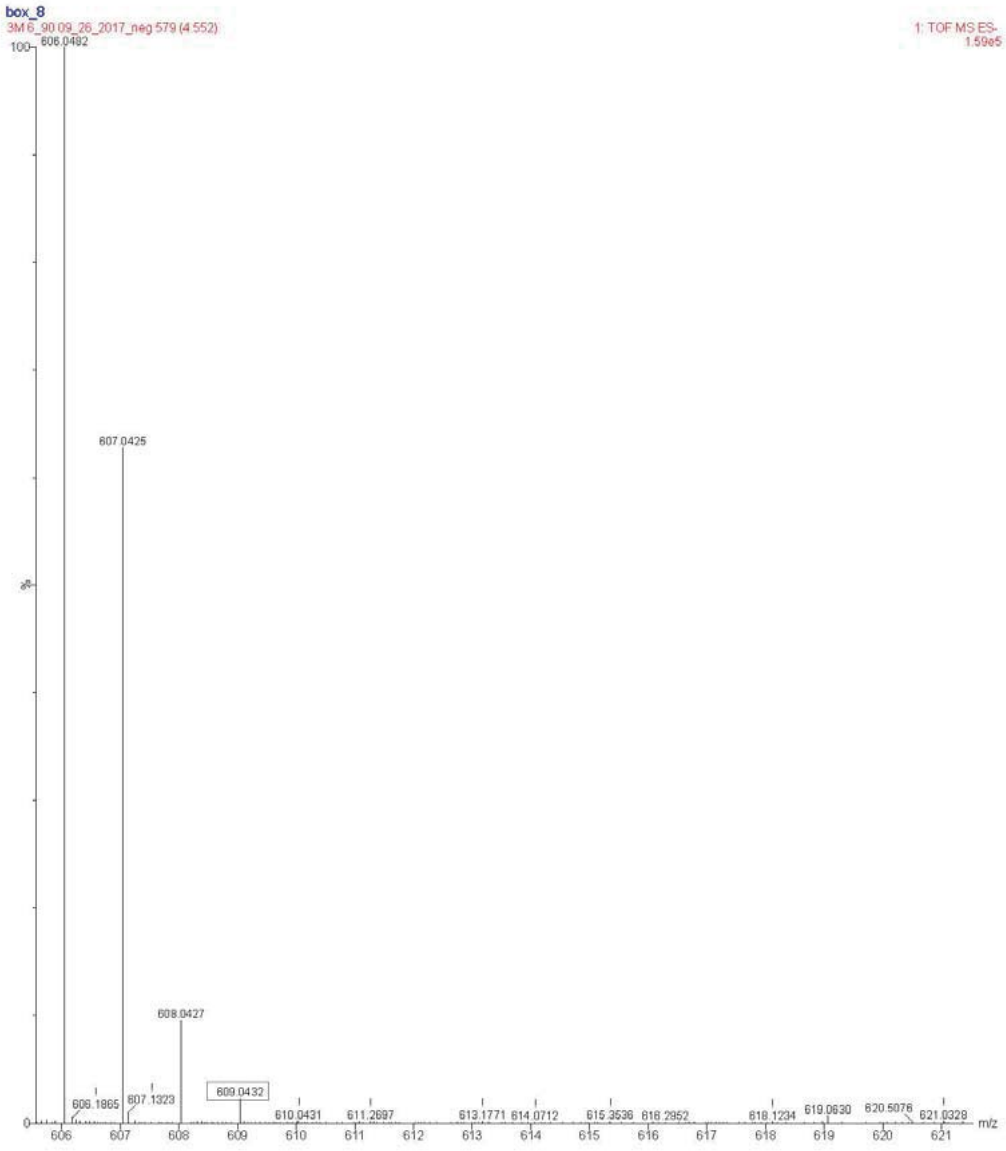

609.0432 m/z

Figure A4-33: Class 30 of 3M 6_90 - Negative

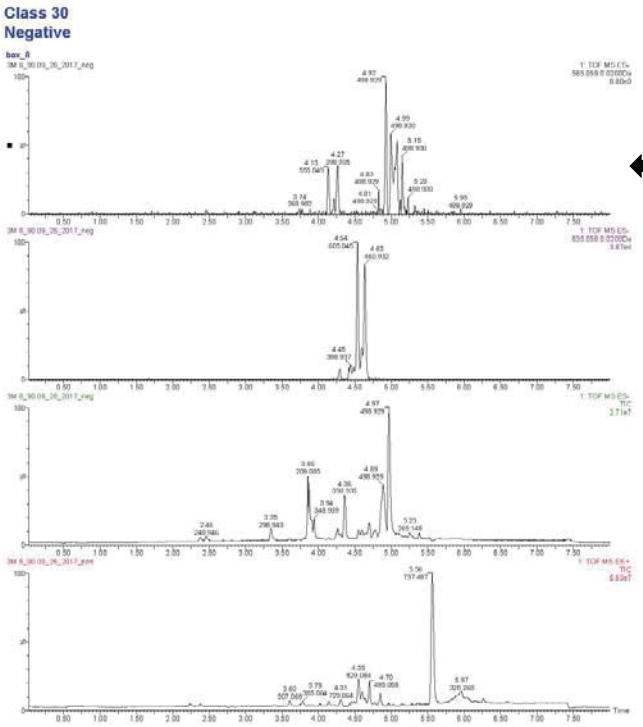

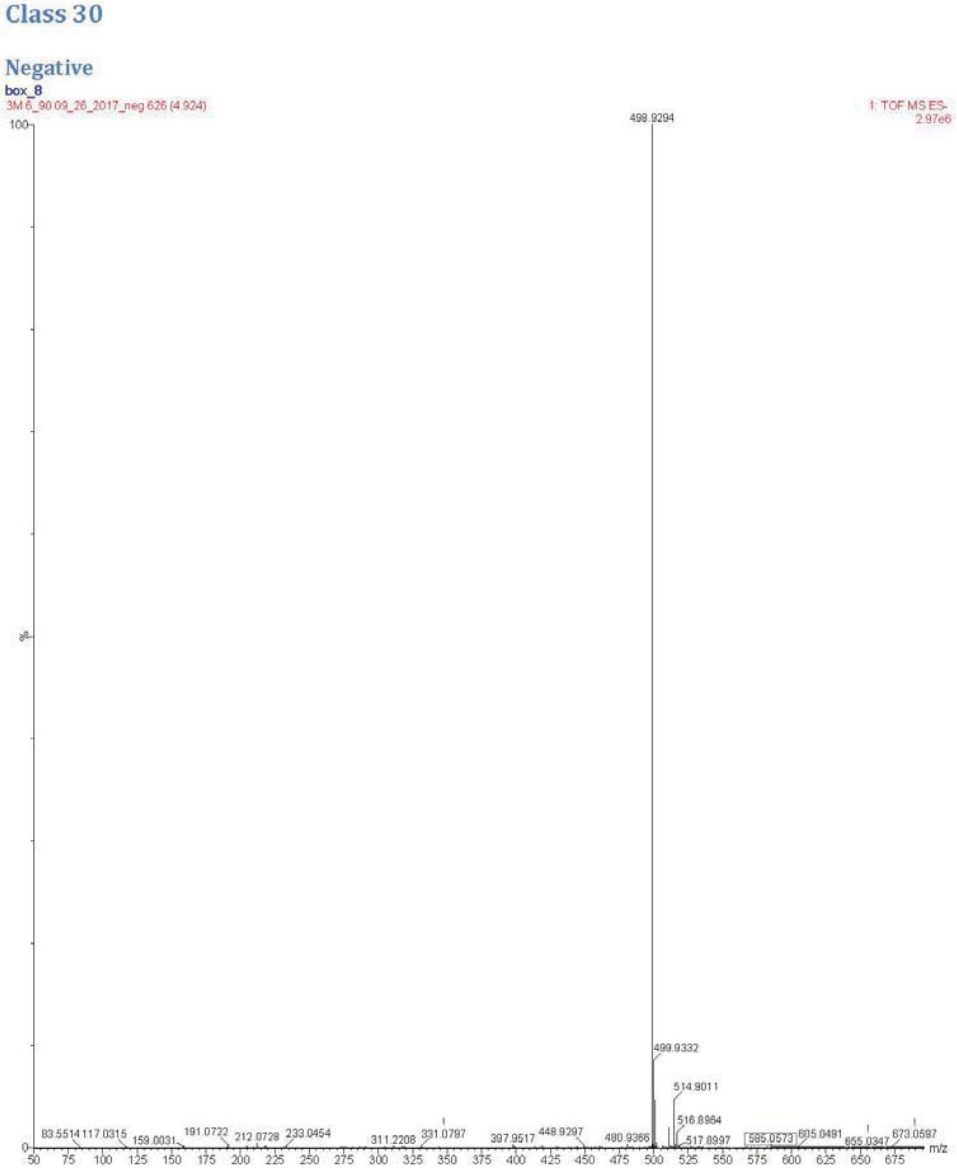

585.0573 m/z

Figure A4-34: Class 32 of 3M 6_90 - Negative

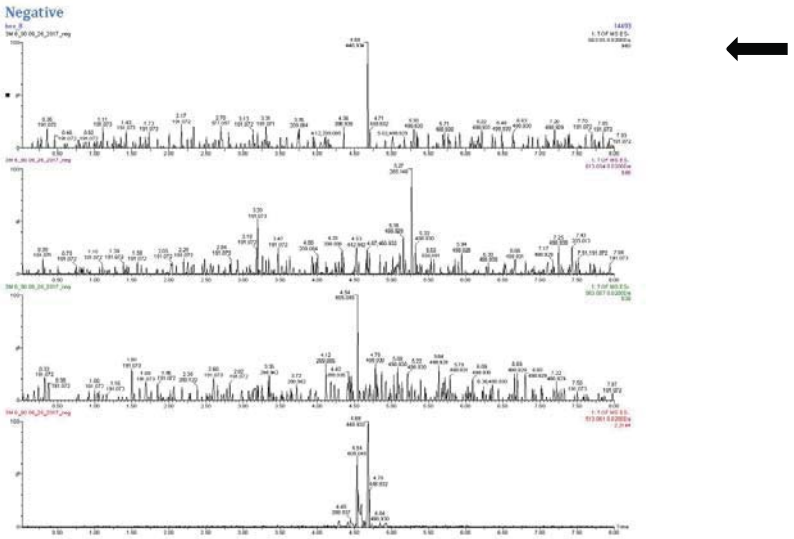

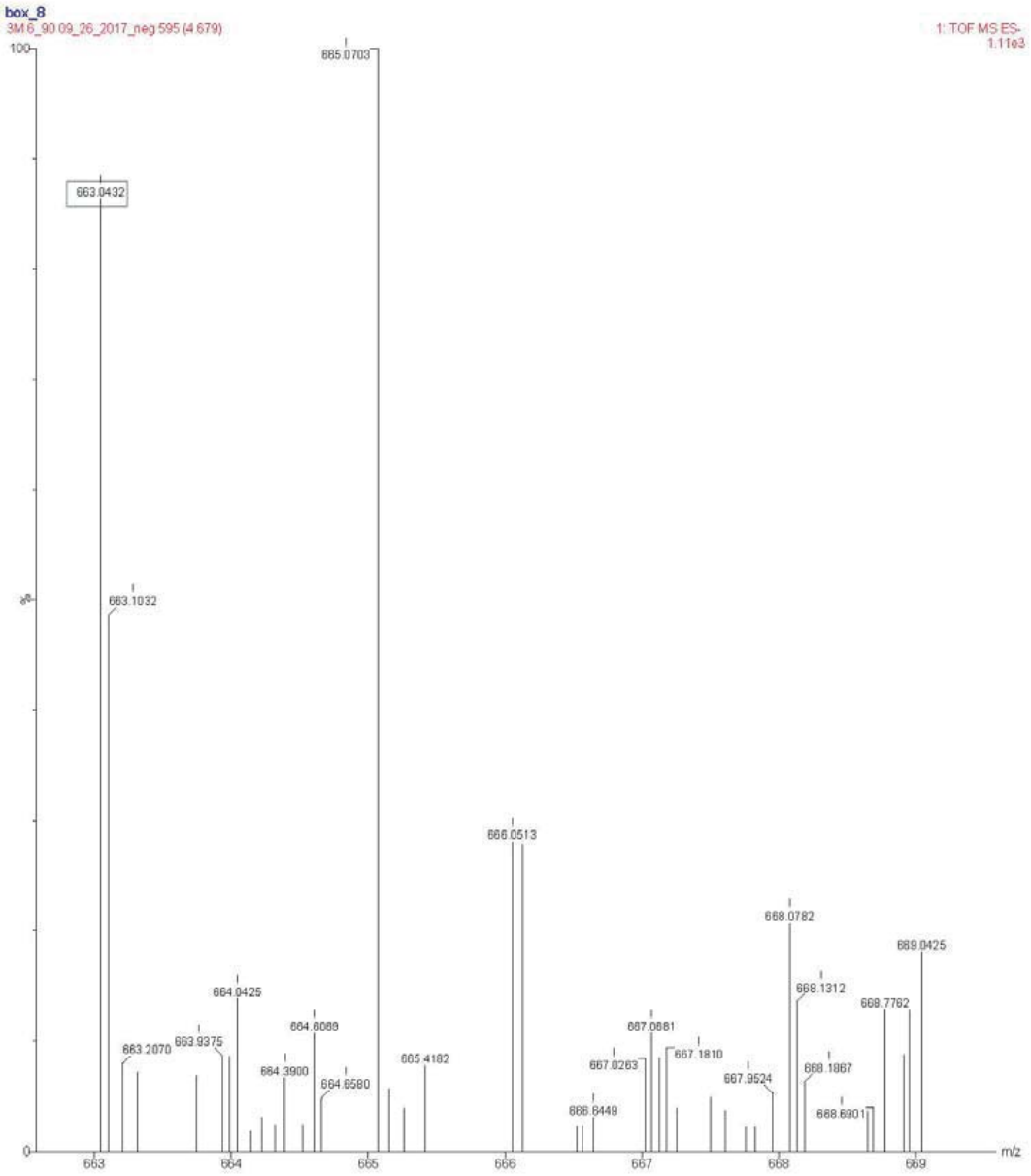

663.0432 m/z

Figure A4-35: Class 40 of 3M 6_90 - Negative

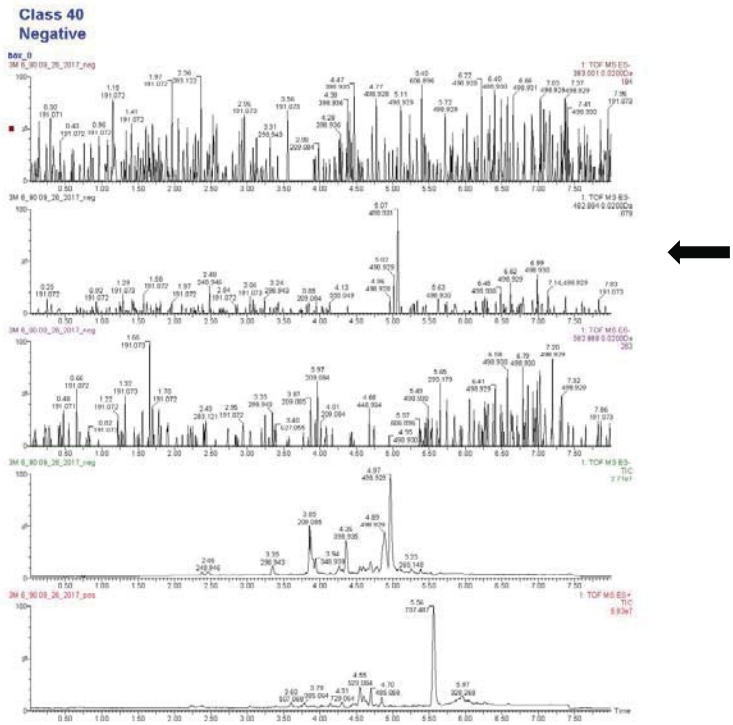

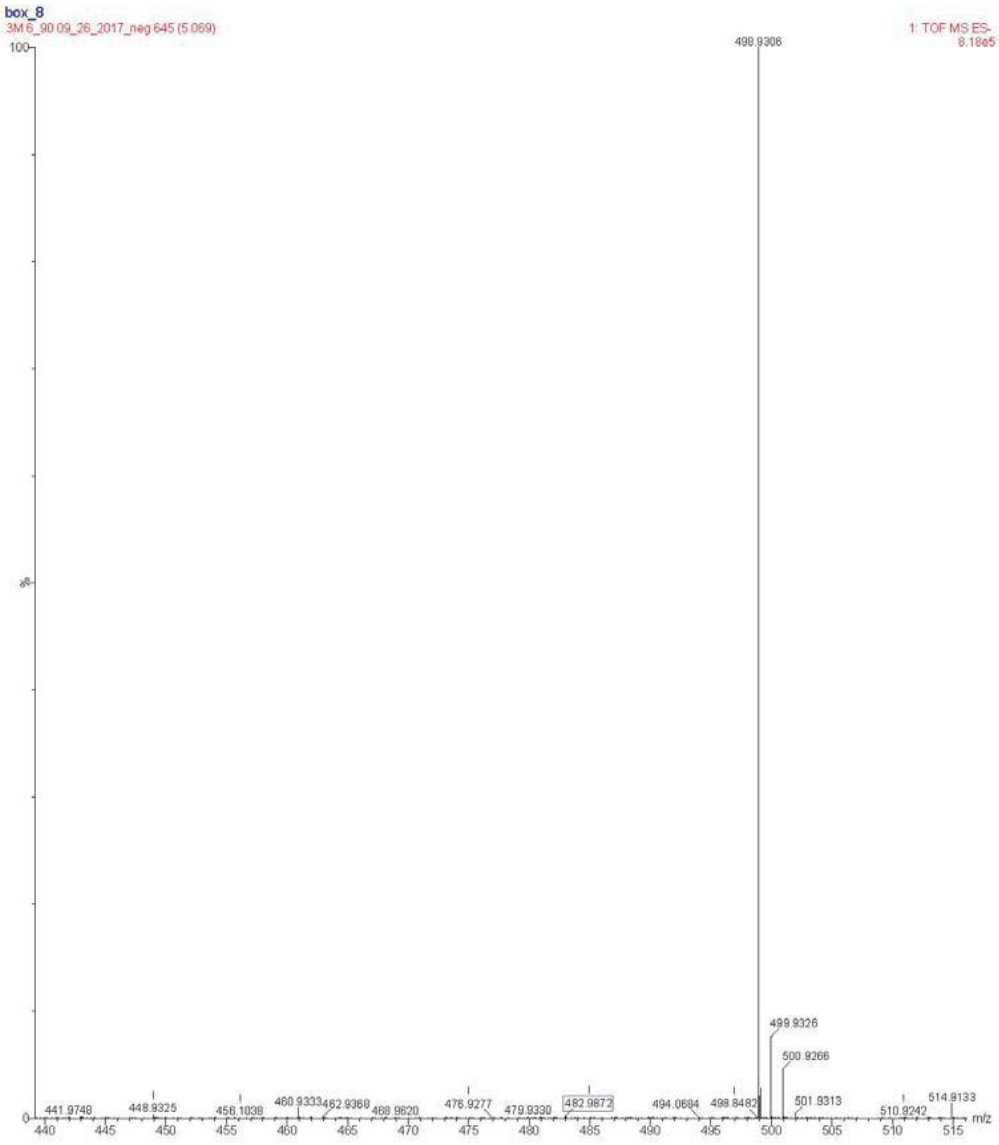

482.9872 m/z

3M 4_97 – Mass Spectrums and Chromatographs

Figure A5-1: Class 2 of 3M 4_97 - Positive

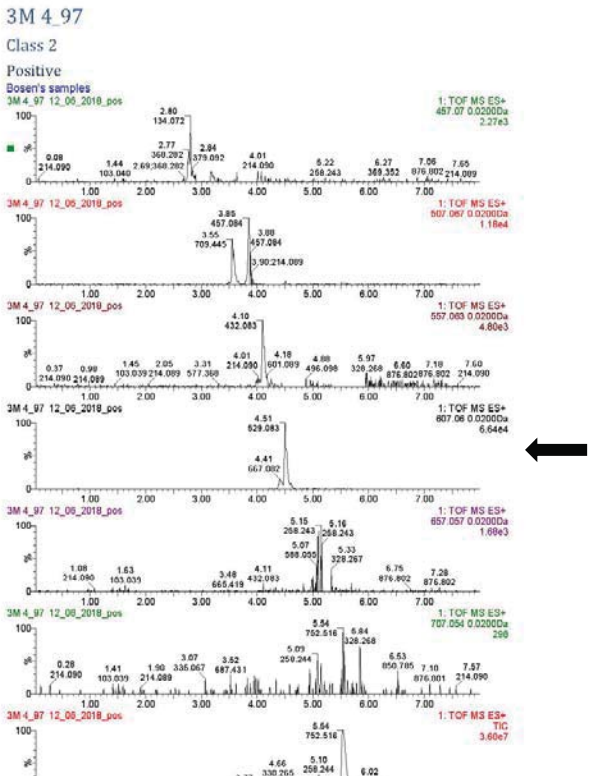

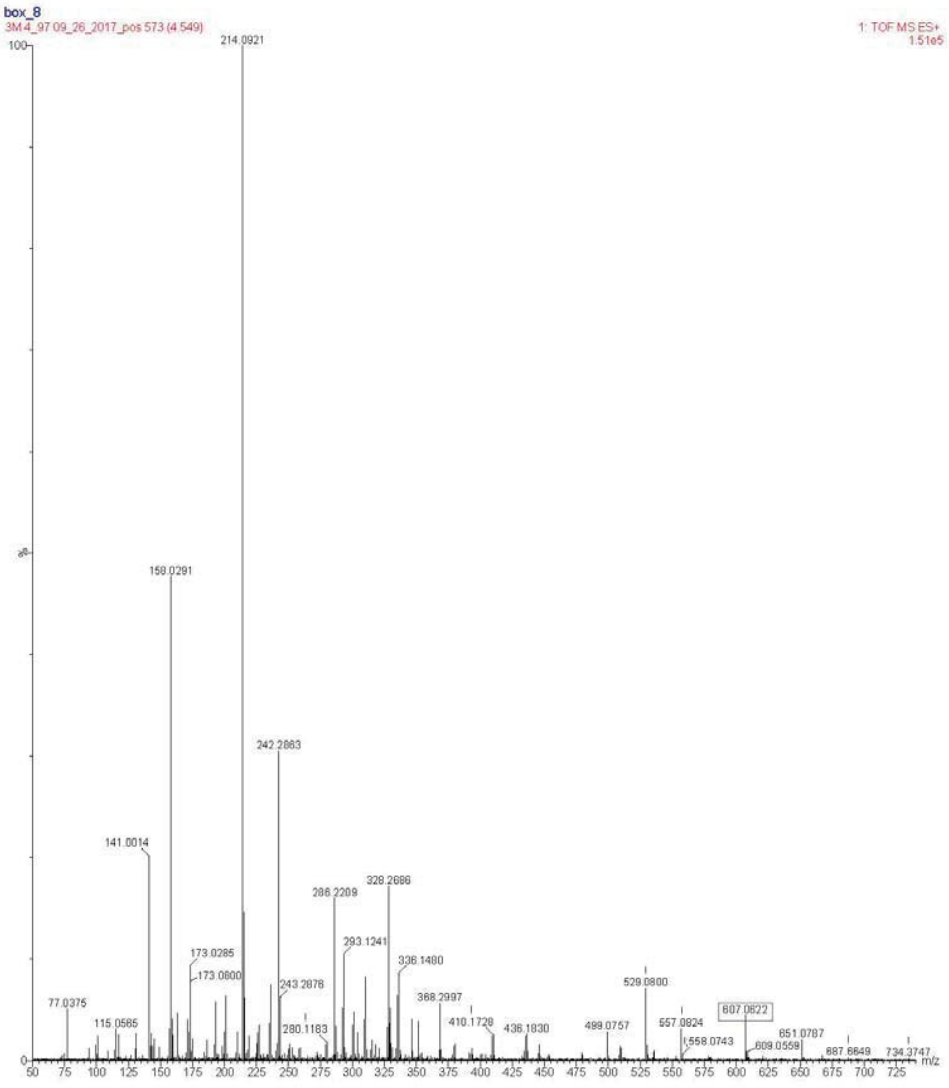

607.0622 m/z

Figure A5-2: Class 3 of 3M 4_97 - Positive

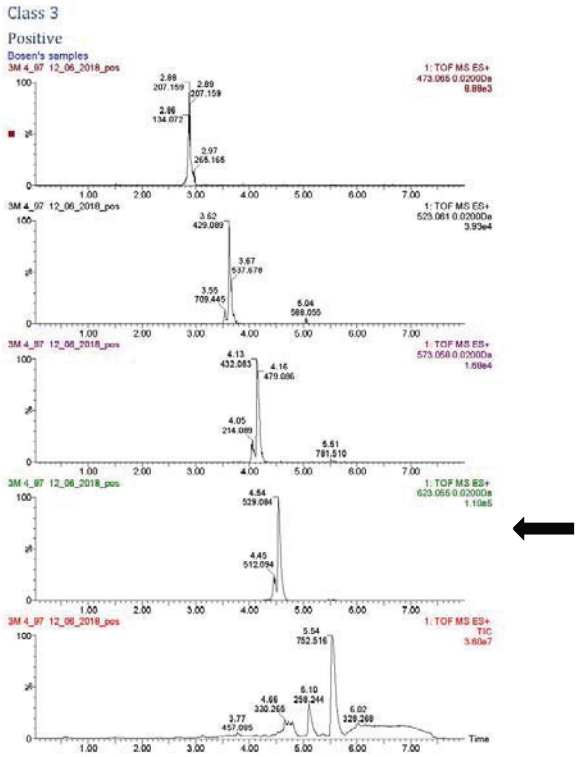

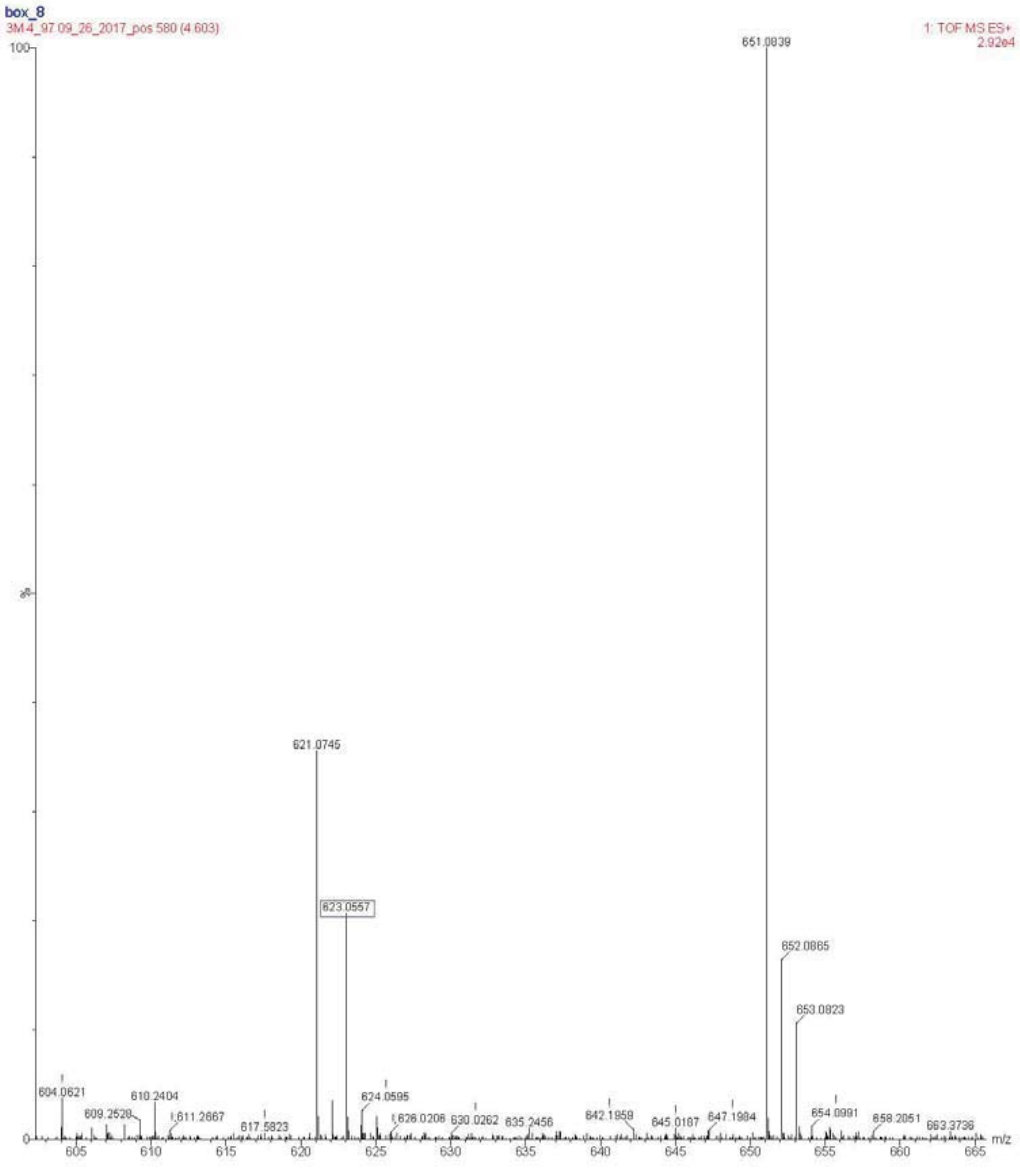

623.0557 m/z

Figure A5-3: Class 4 of 3M 4_97 - Positive

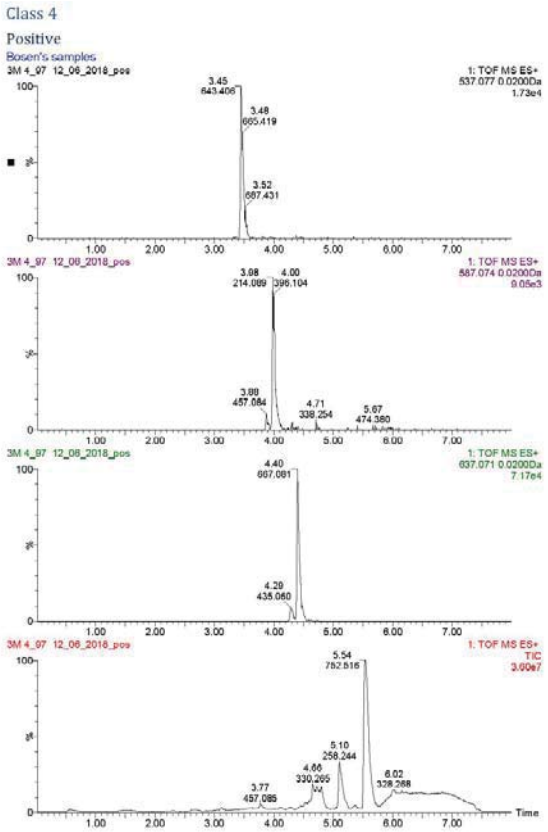

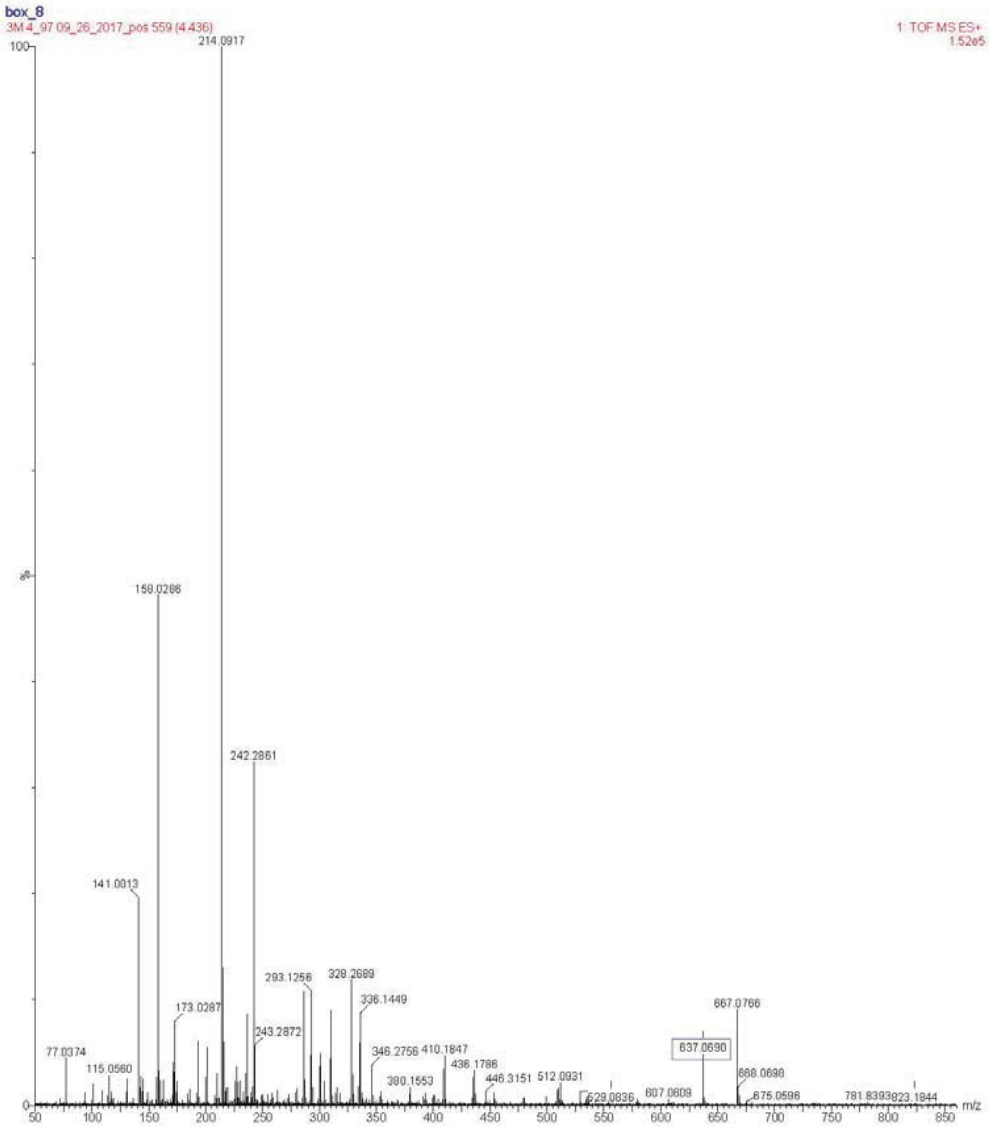

637.0690 m/z

Figure A5-4: Class 5 of 3M 4_97 - Positive

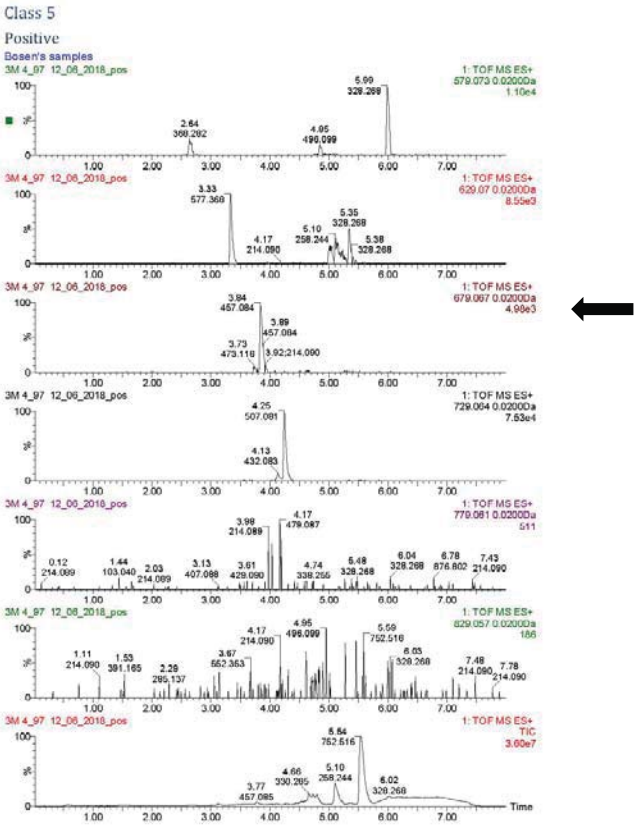

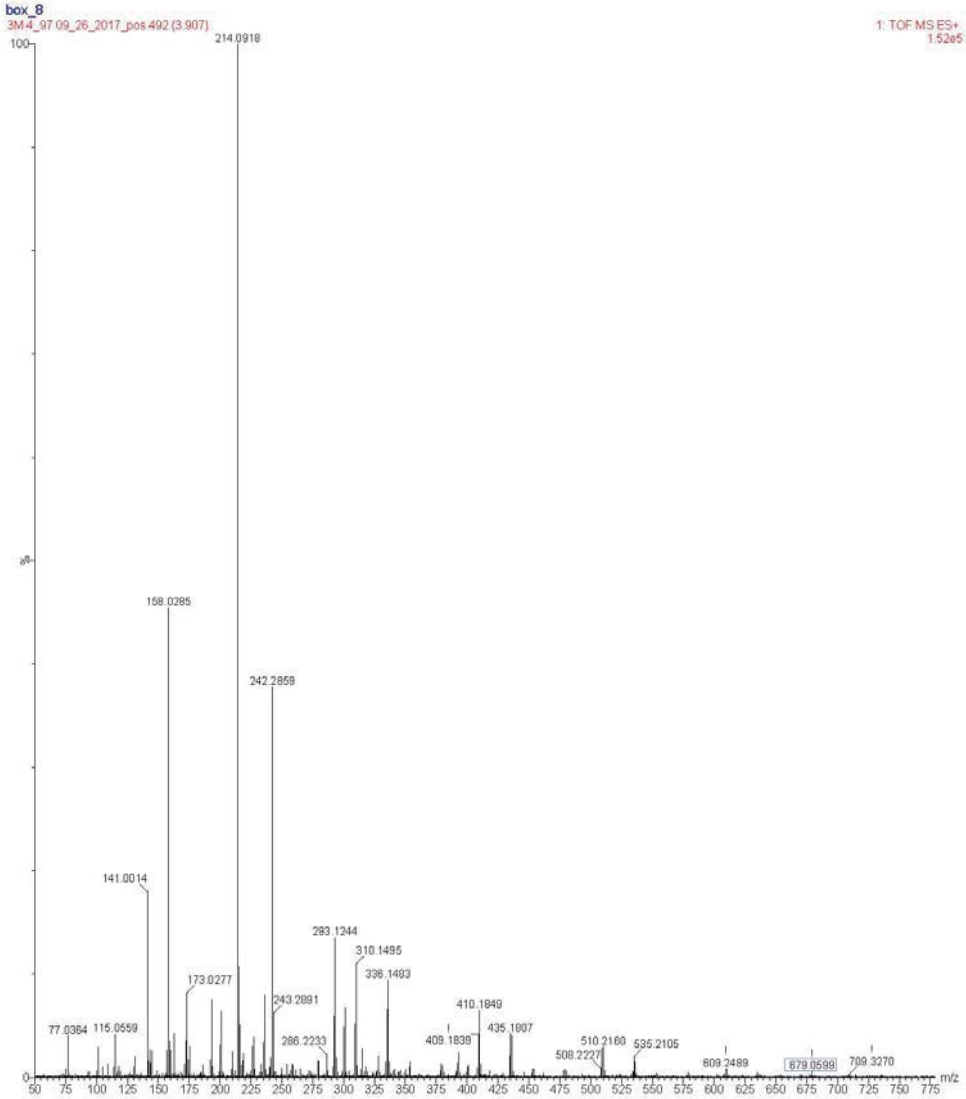

679.0599 m/z

Figure A5-5: Class 8 of 3M 4_97 - Positive

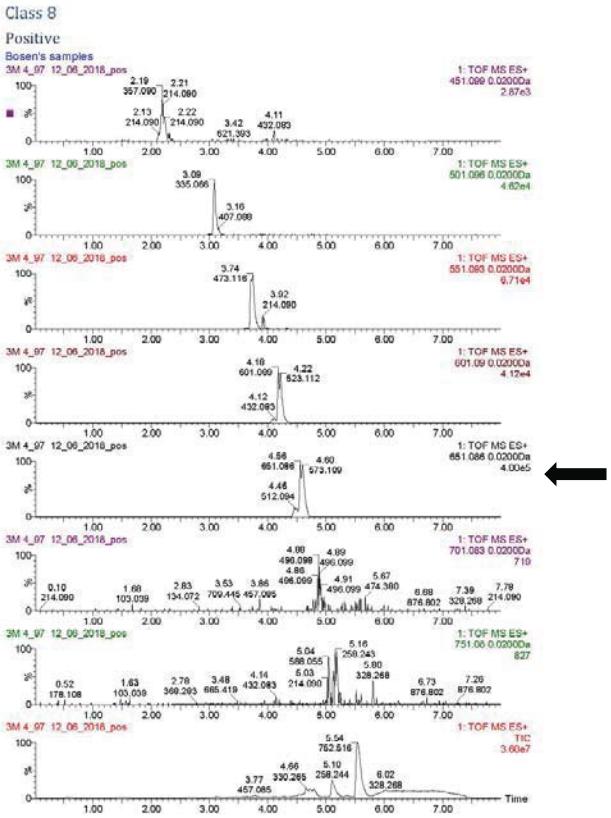

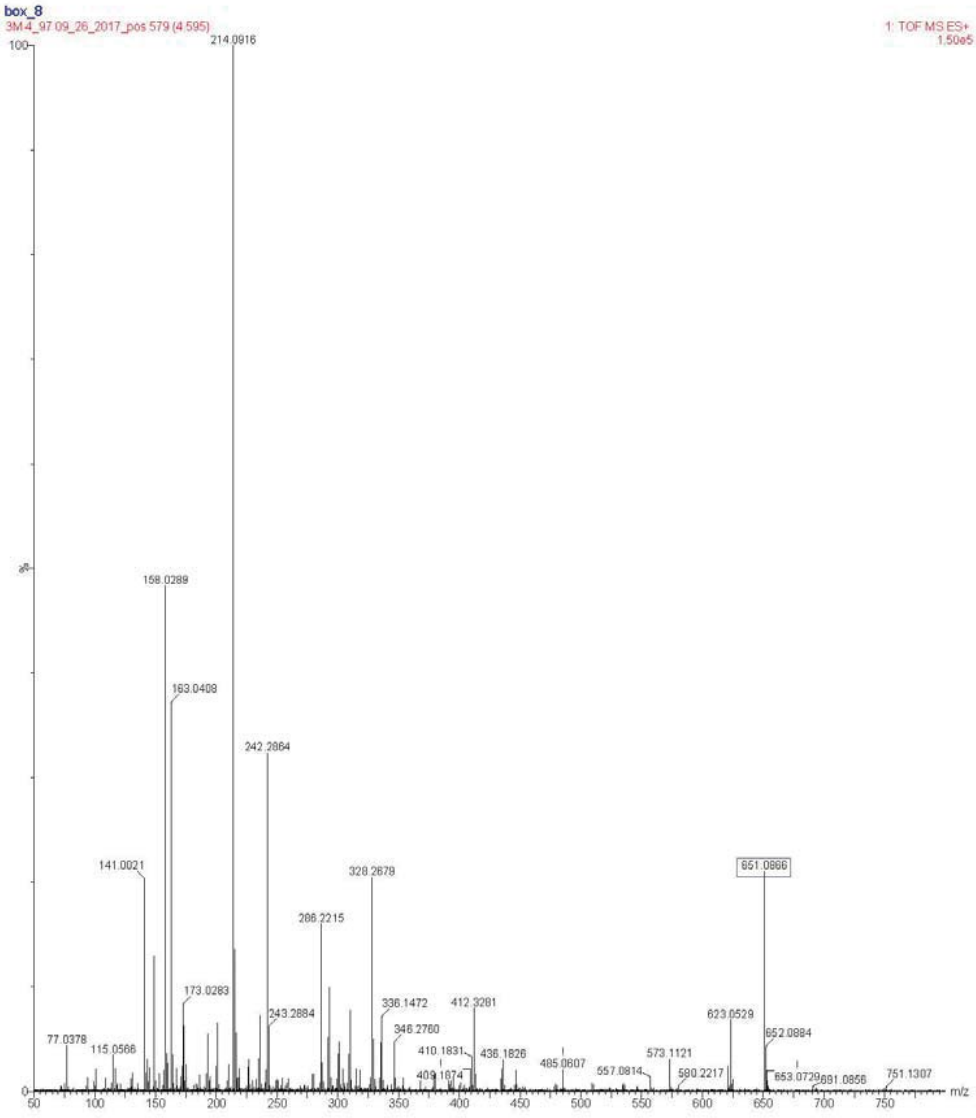

651.0866 m/z

Figure A5-6: Class 9 of 3M 4_97 - Positive

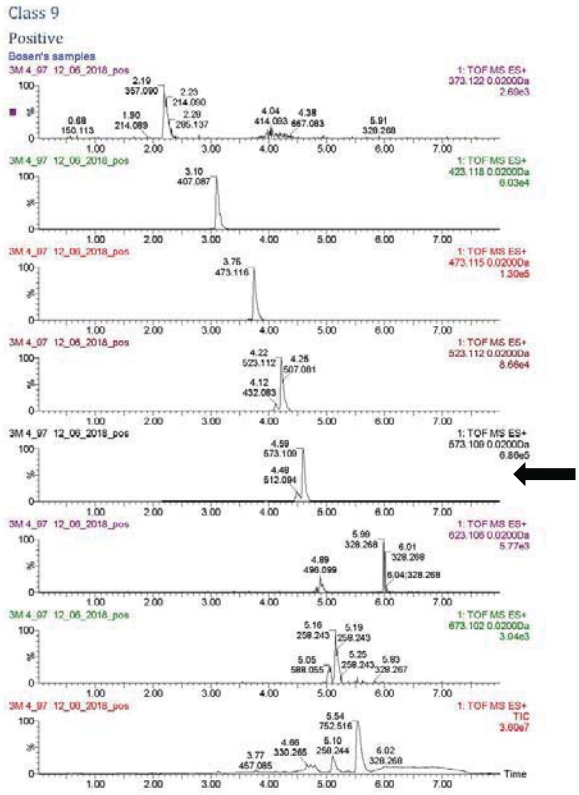

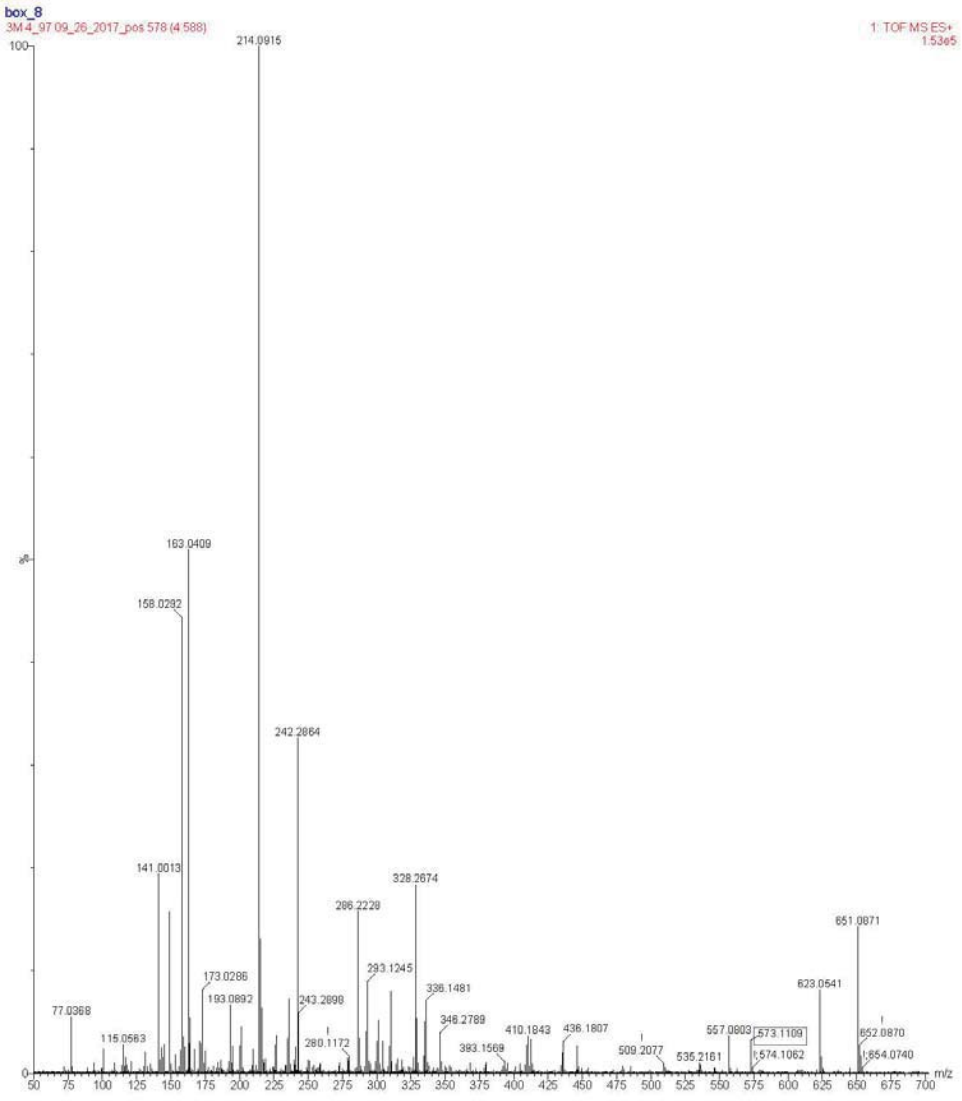

573.1109 m/z

Figure A5-7: Class 11 of 3M 4_97 - Positive

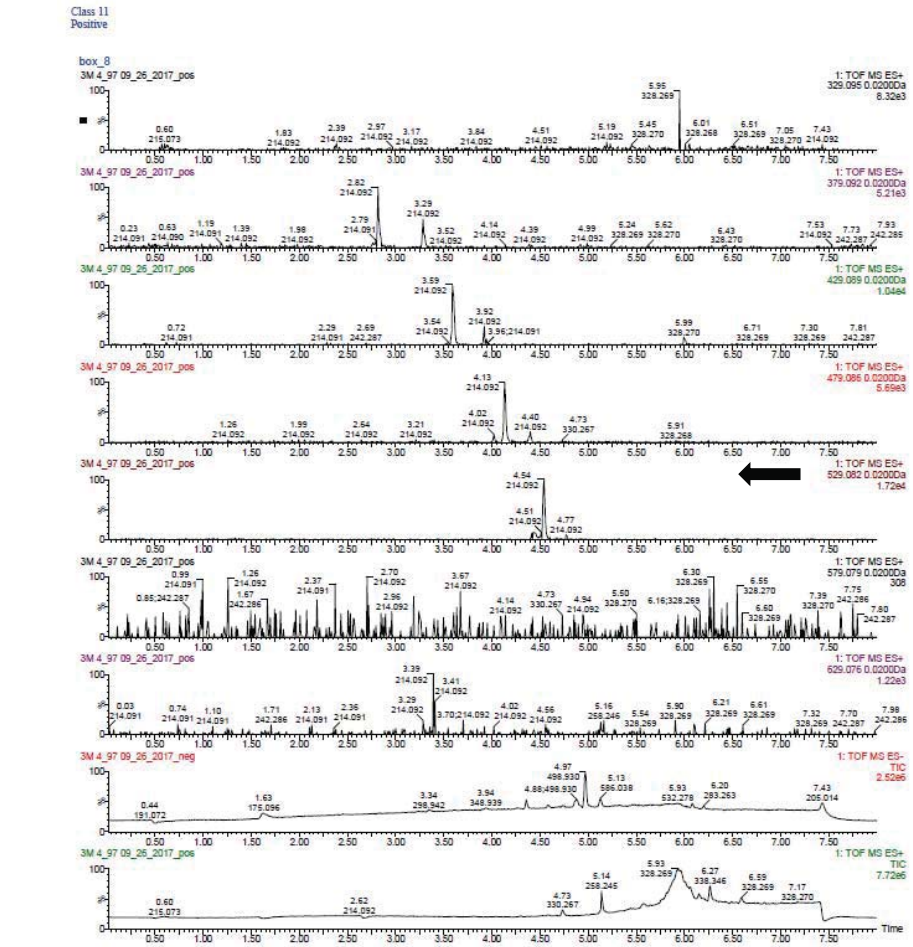

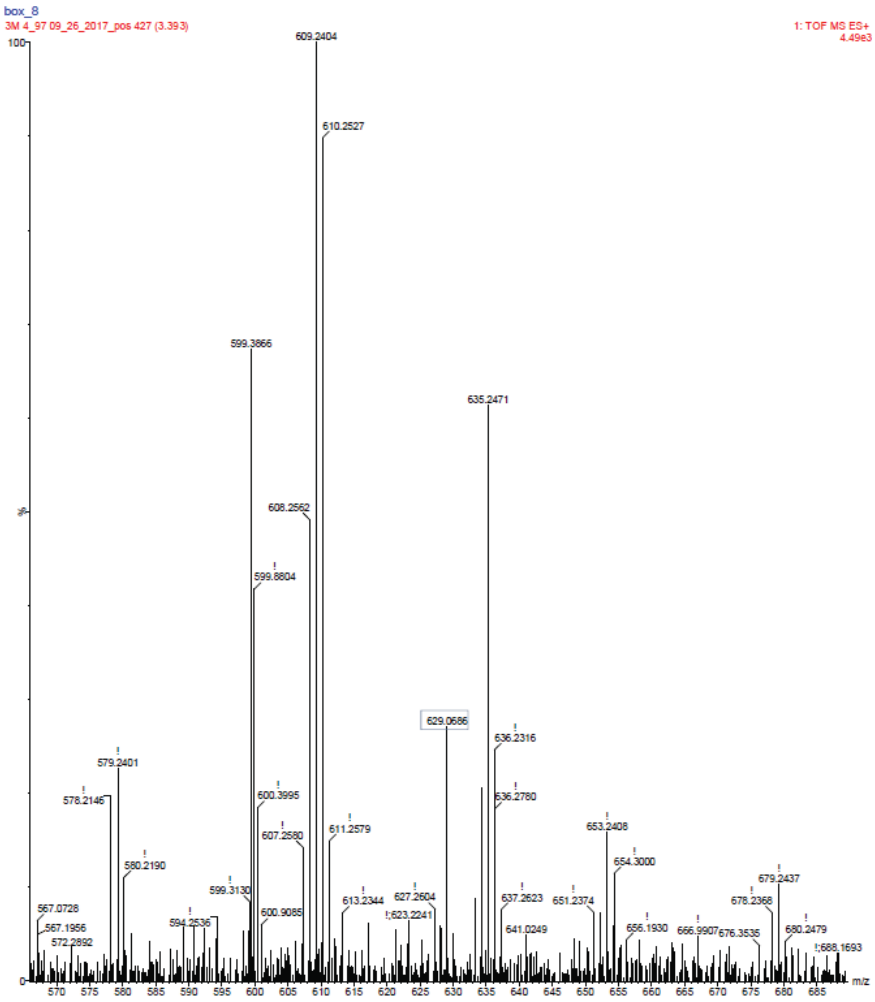

629.0686 m/z

Figure A5-8: Class 13 of 3M 4_97 - Positive

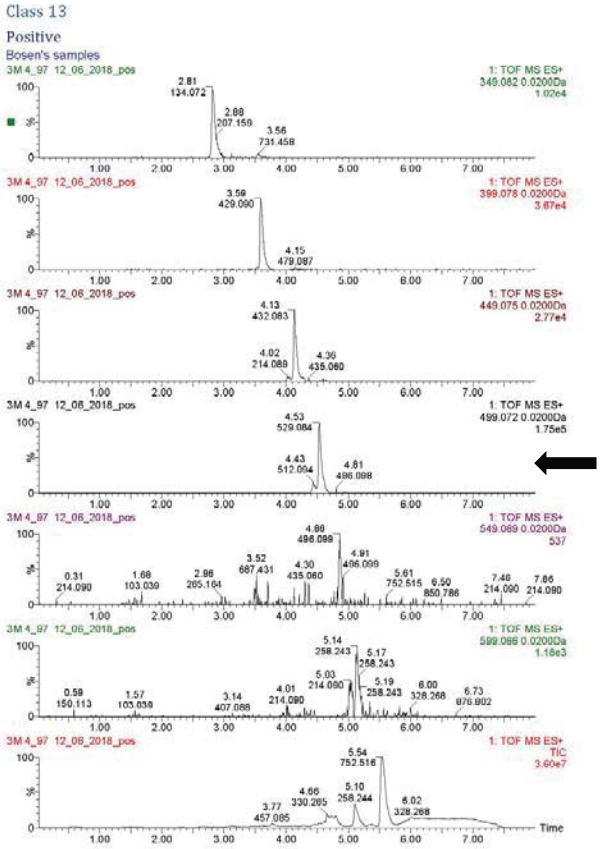

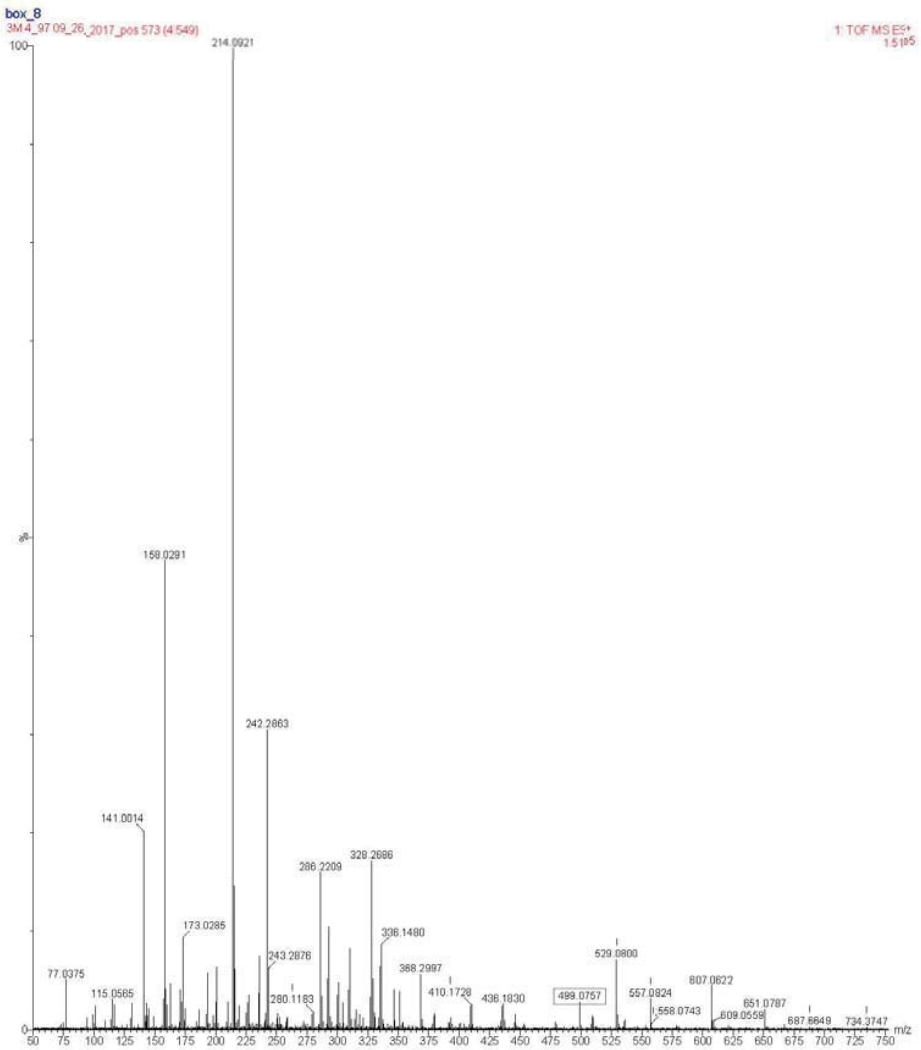

499.0757 m/z

Figure A5-9: Class 14 of 3M 4_97 - Positive

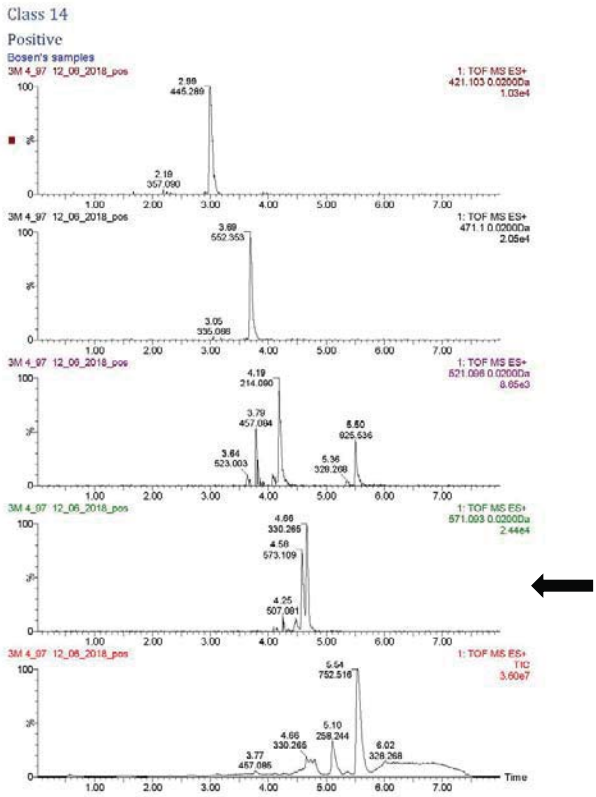

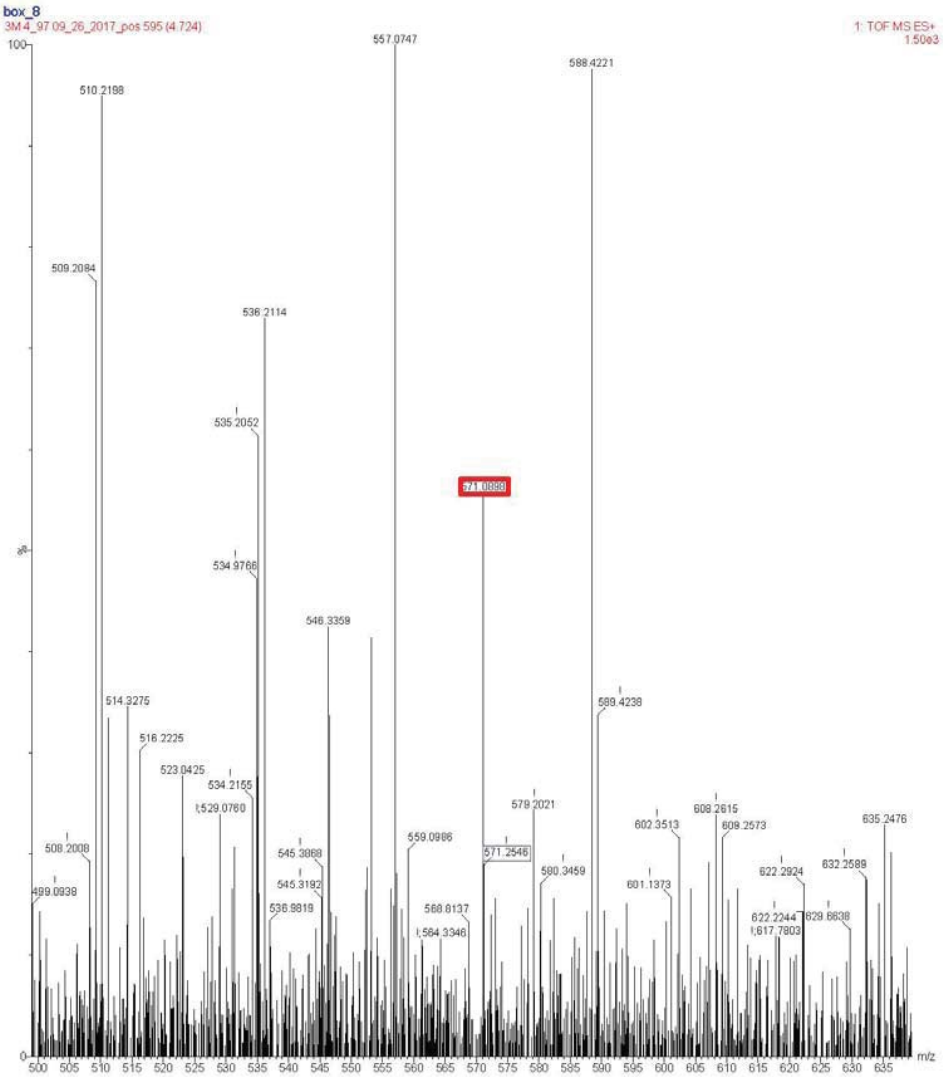

~~571.02546~~ 571.0898 m/z

Figure A5-10: Class 15 of 3M 4_97 - Positive

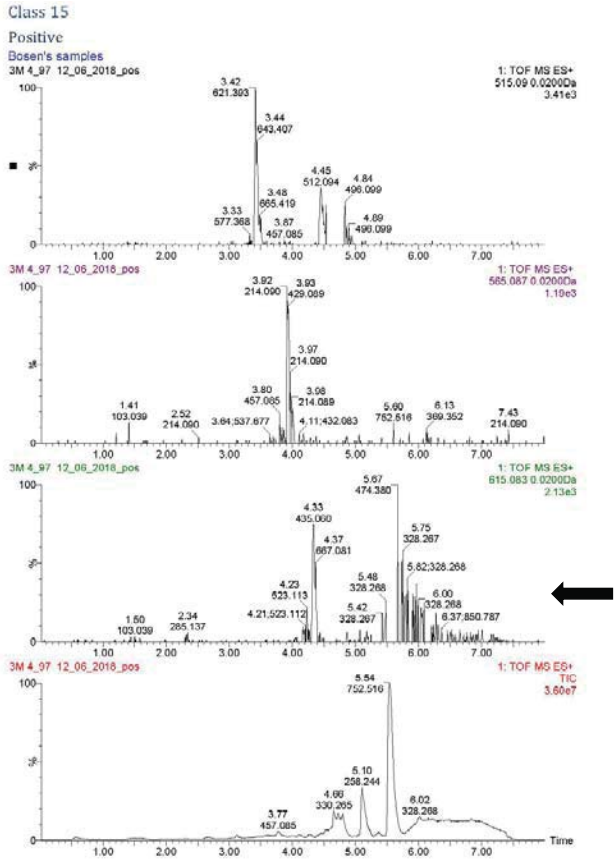

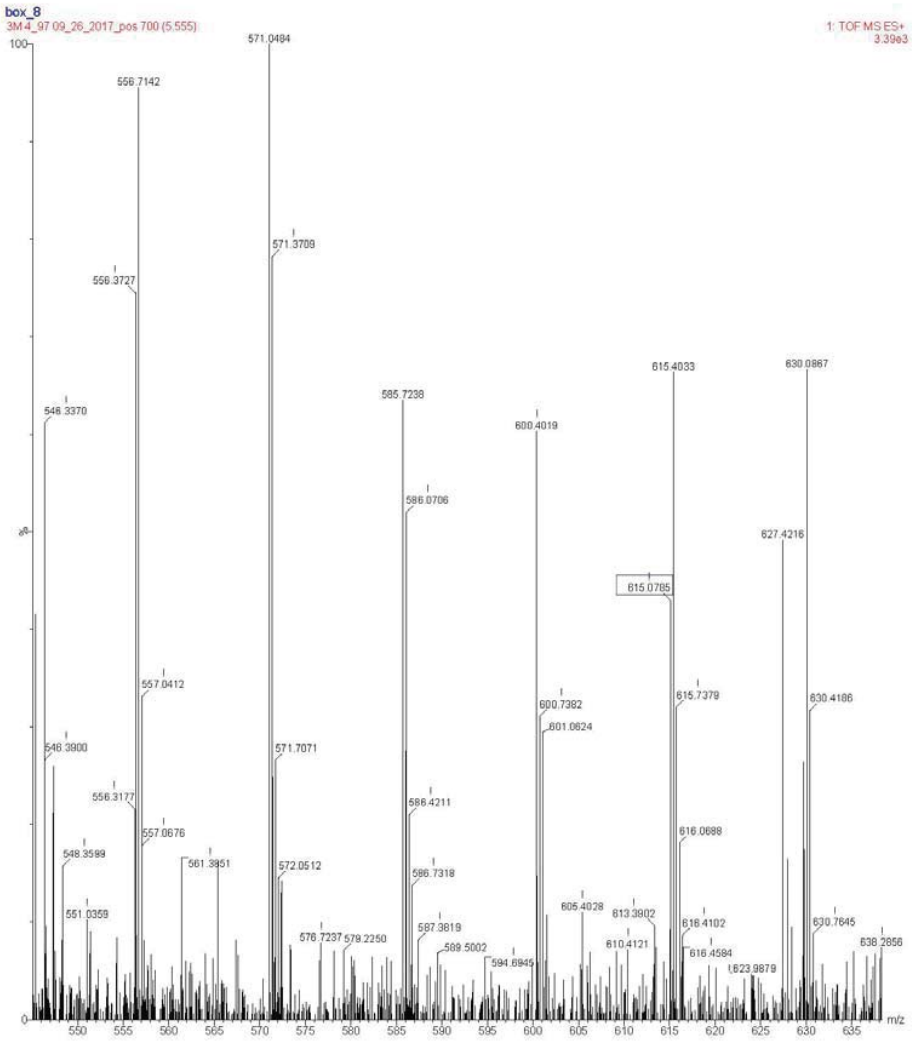

615.0785 m/z

Figure A5-11: Class 19 of 3M 4_97 - Positive

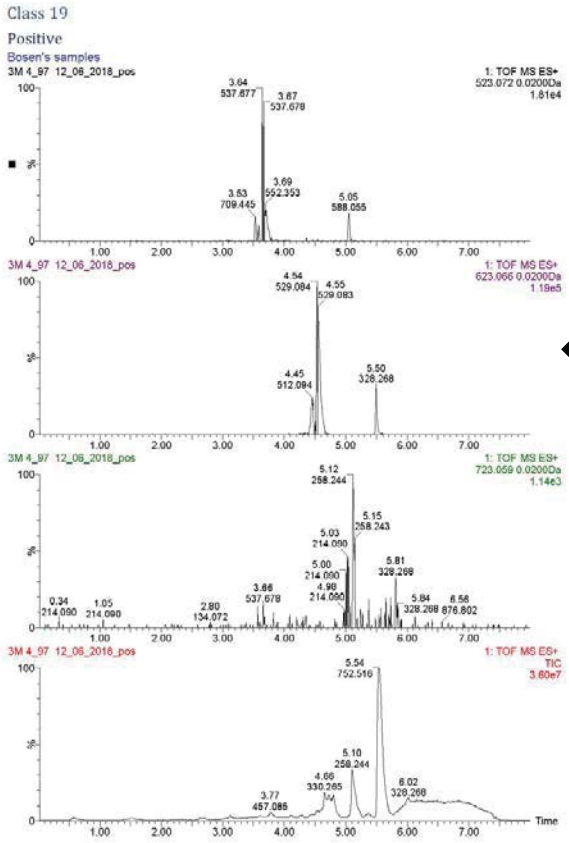

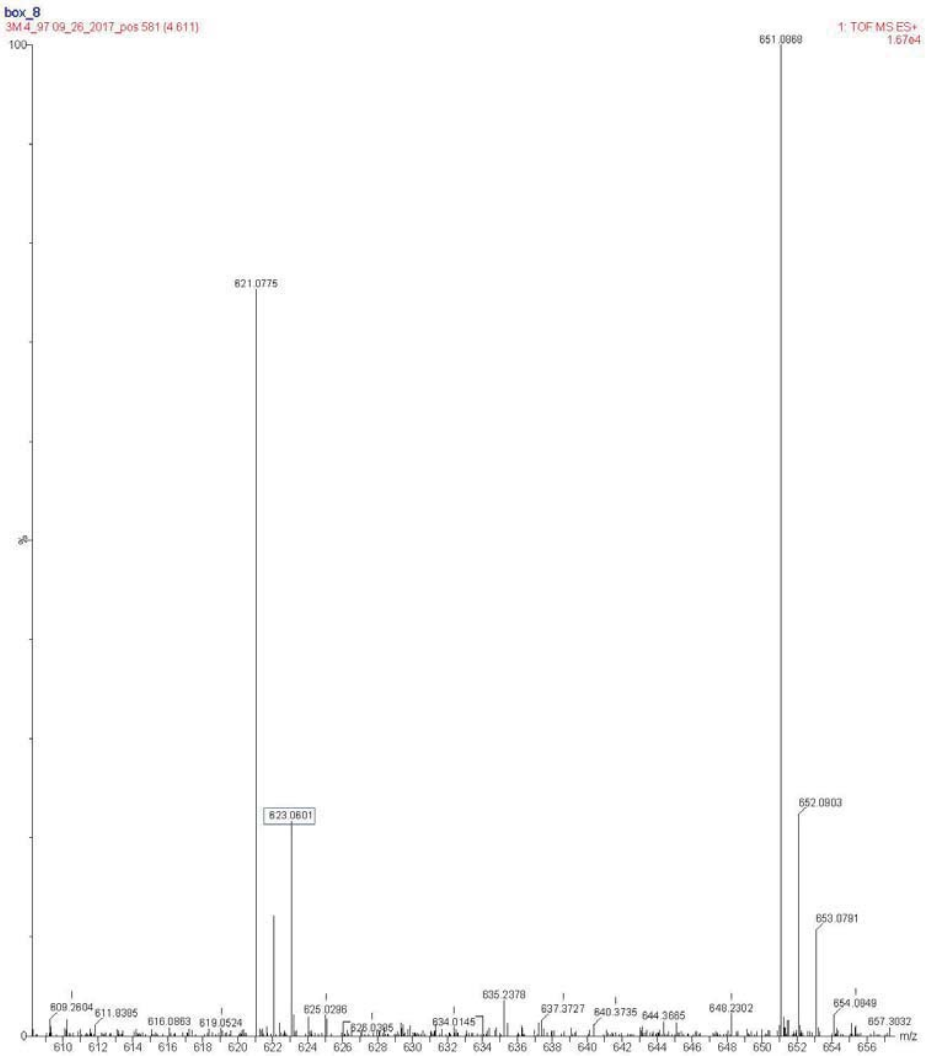

623.0601 m/z

Figure A5-12: Class 28 of 3M 4_97 - Positive

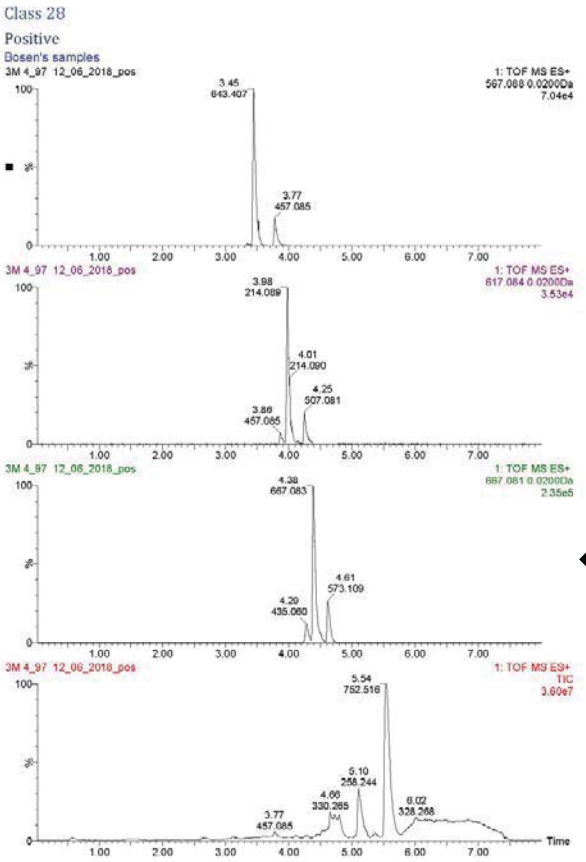

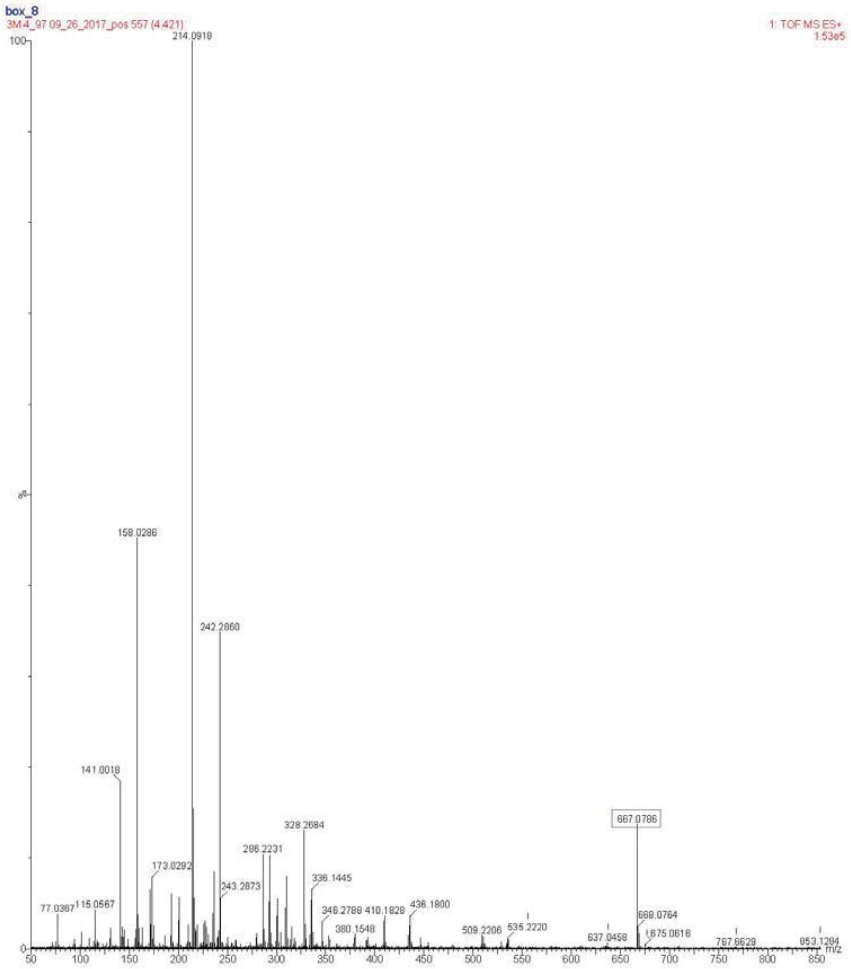

667.0786 m/z

Figure A5-13: Class 29 of 3M 4_97 - Positive

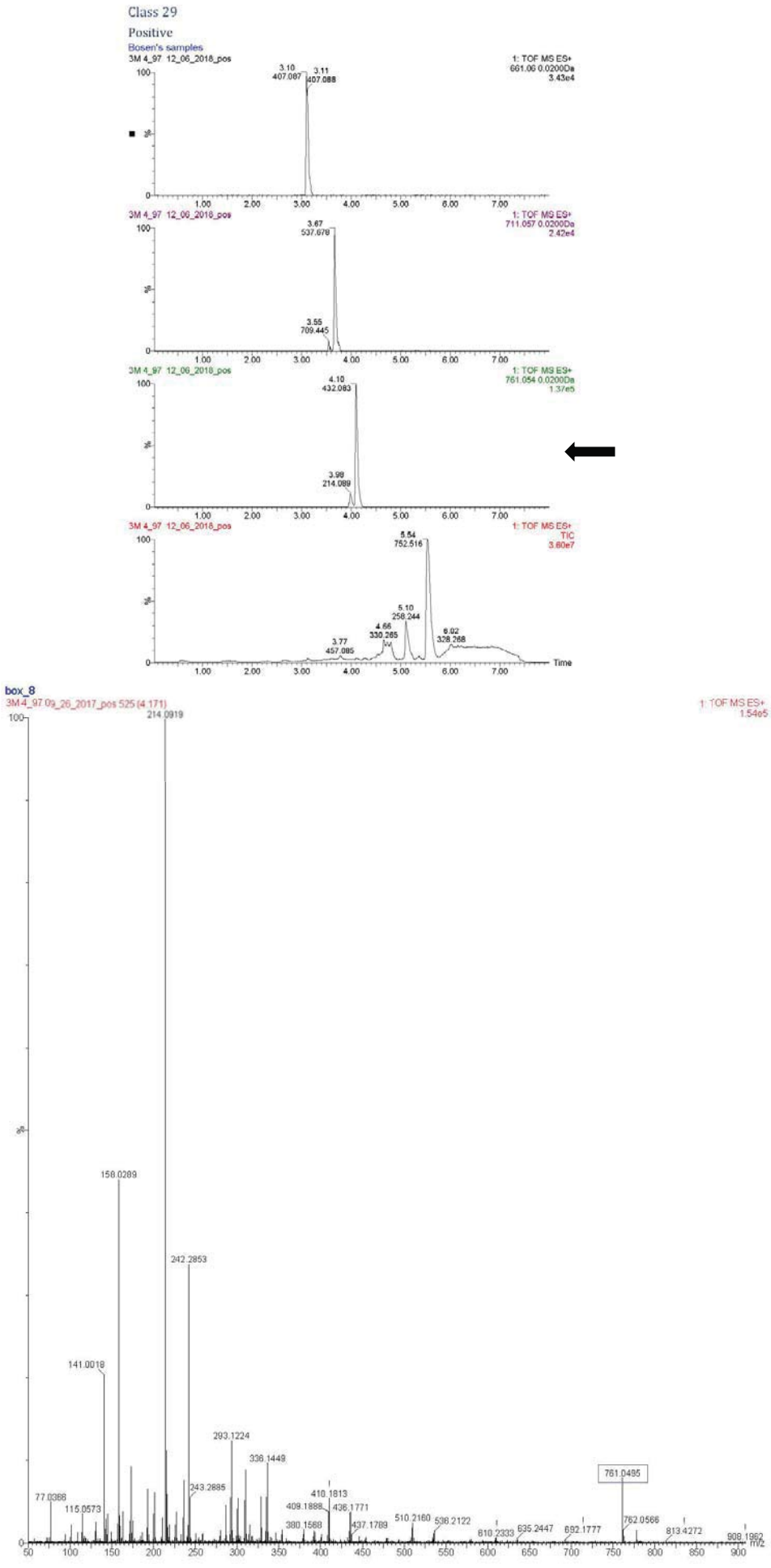

761.0495 m/z

Figure A5-14: Class 31 of 3M 4_97 - Positive

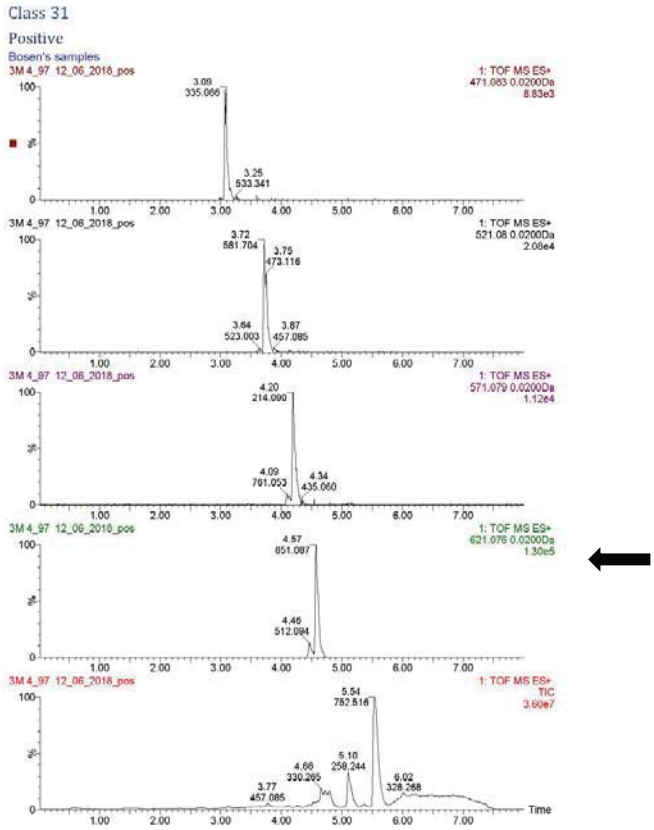

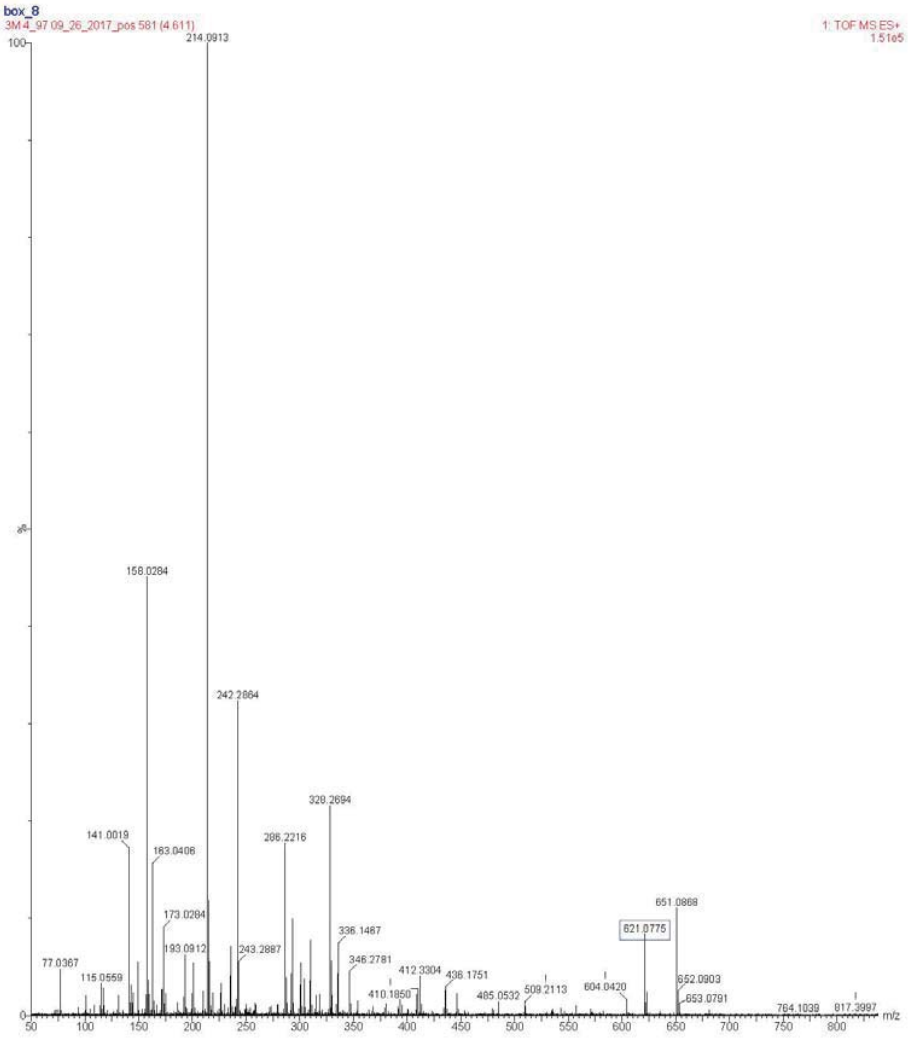

621.0775 m/z

Figure A5-15: Class 32 of 3M 4_97 - Positive

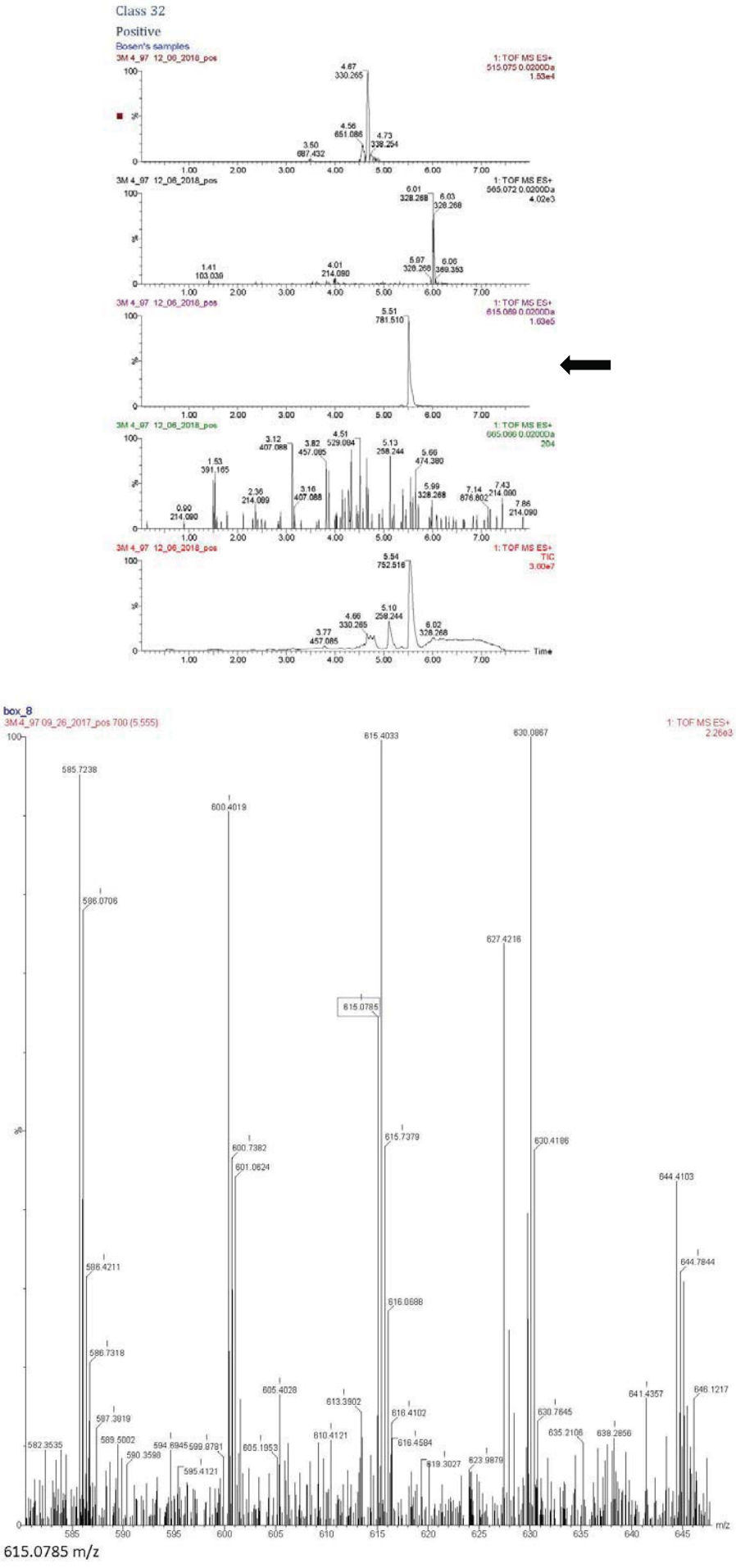

615.0785 m/z

Figure A5-16: Class 1 of 3M 3M 4_97 - Negative

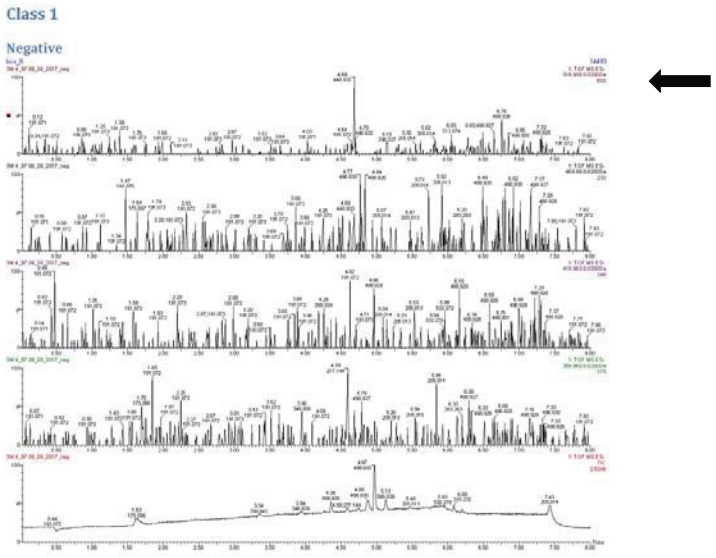

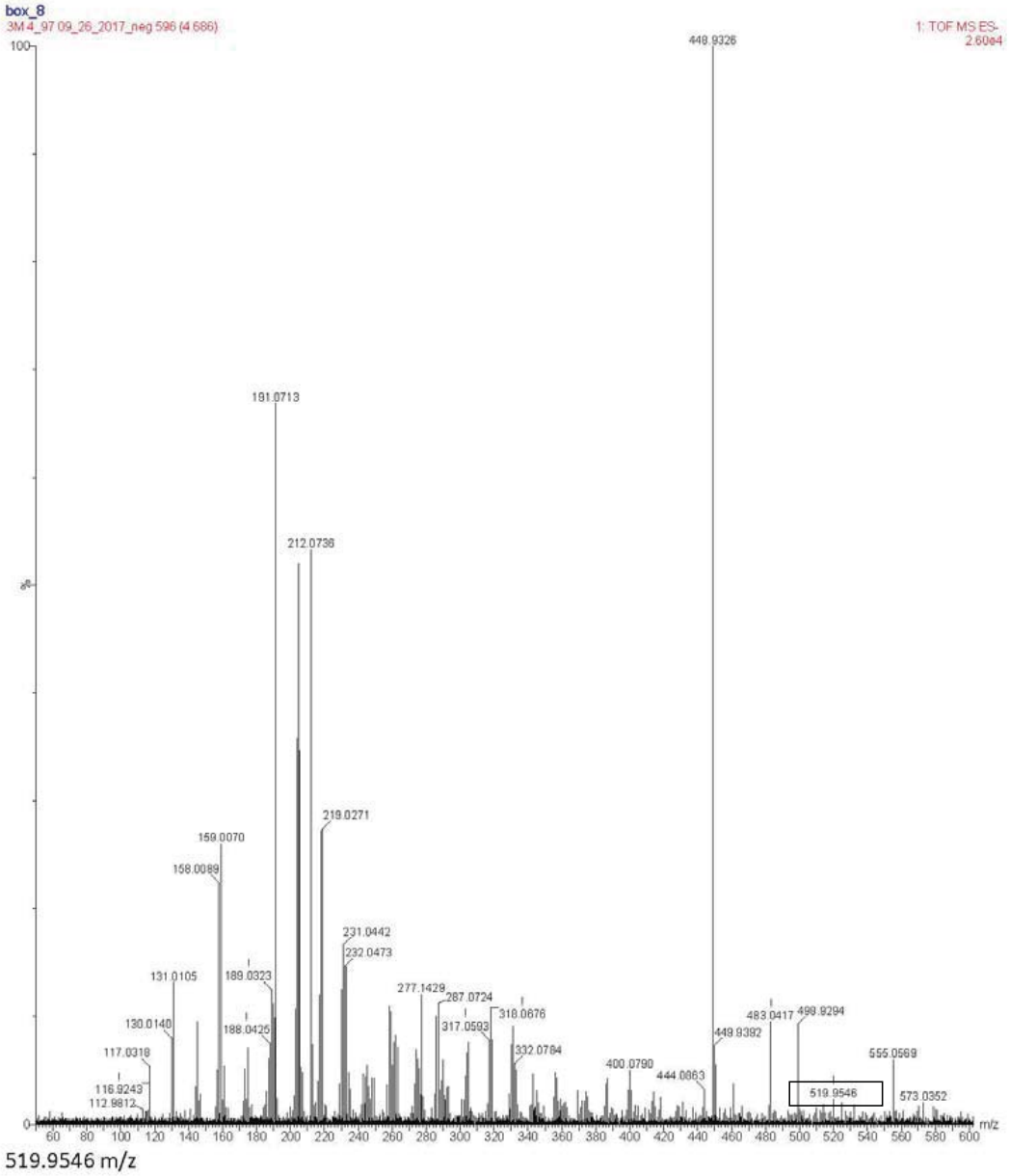

519.9546 m/z

Figure A5-17: Class 2 of 3M 4_97 - Negative

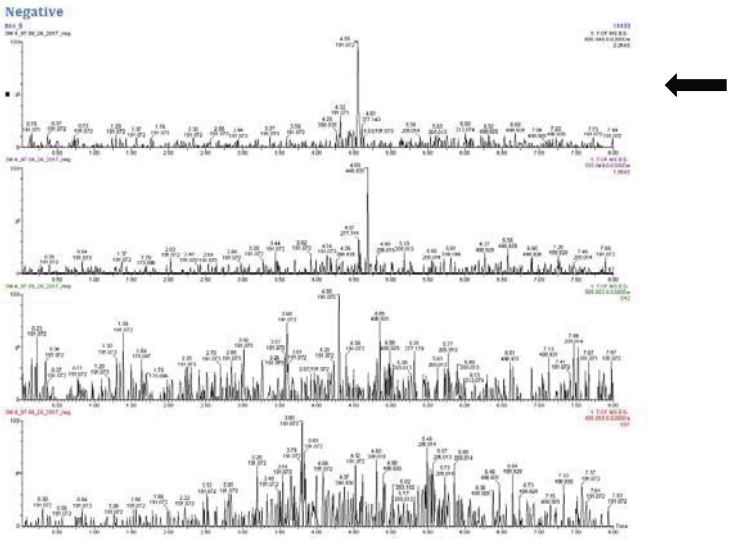

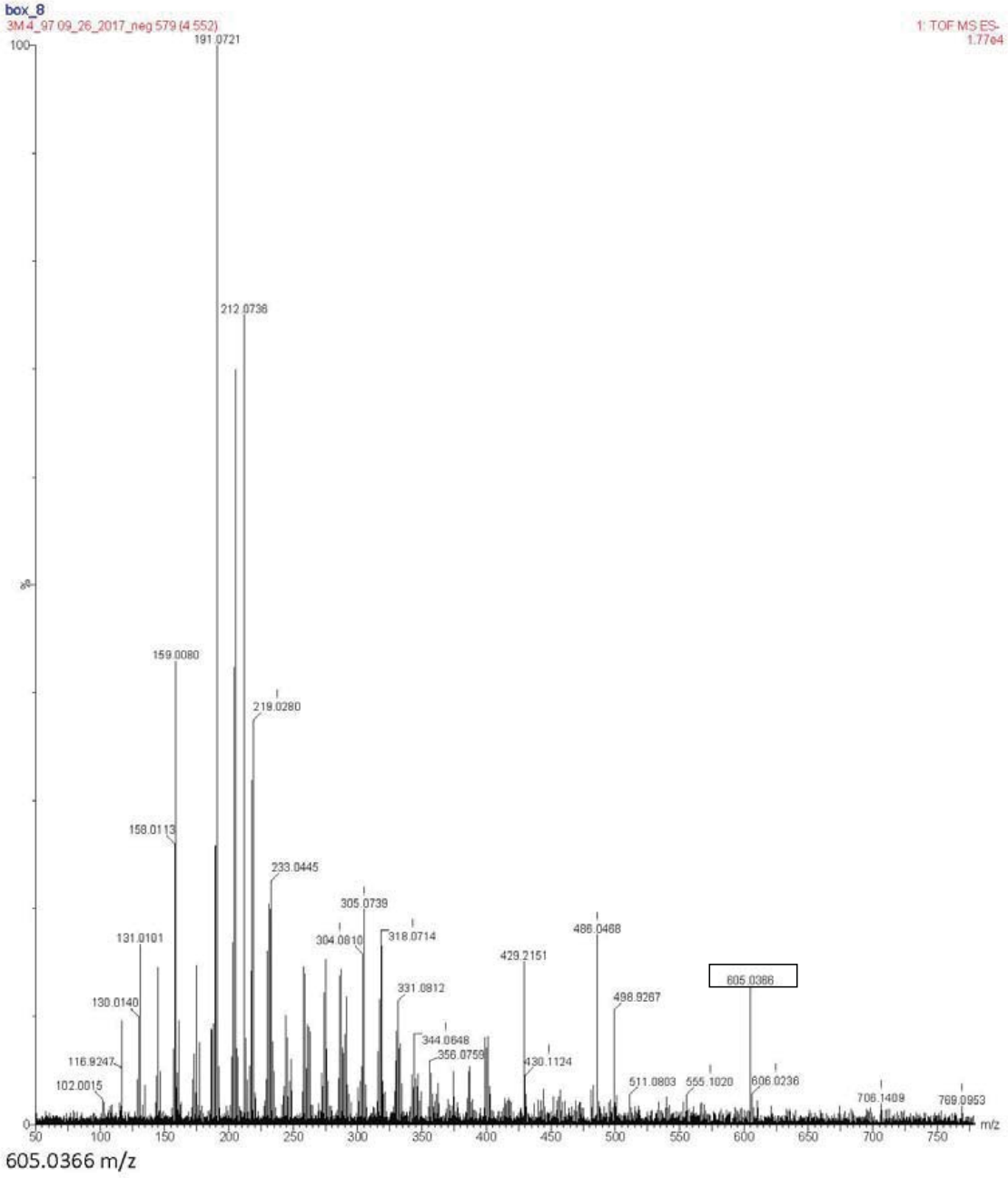

Figure A5-18: Class 3 of 3M 4_97 - Negative

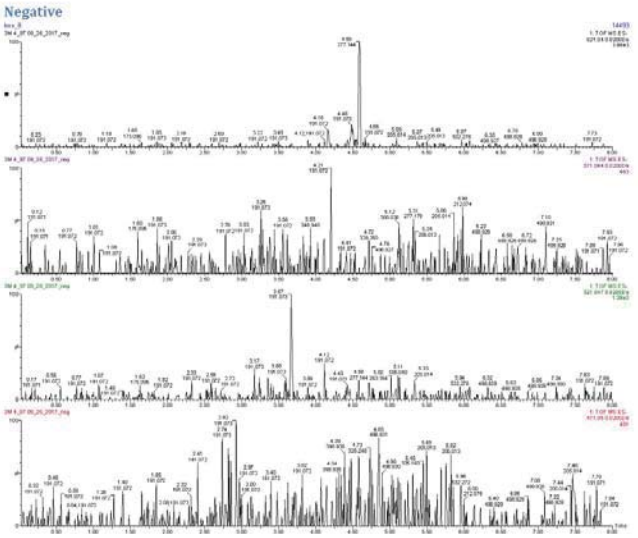

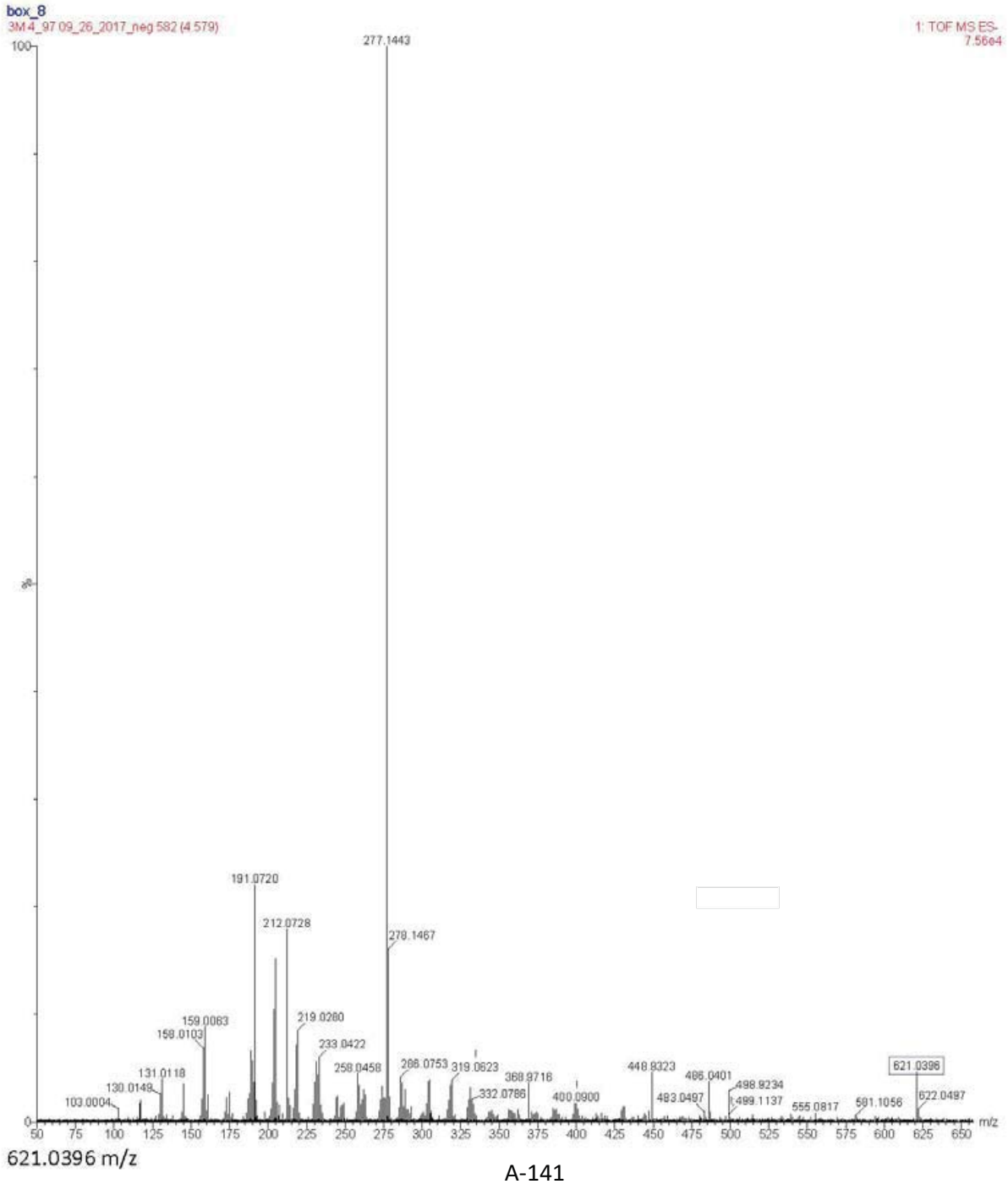

Figure A5-19: Class 5 of 3M 4_97 - Negative

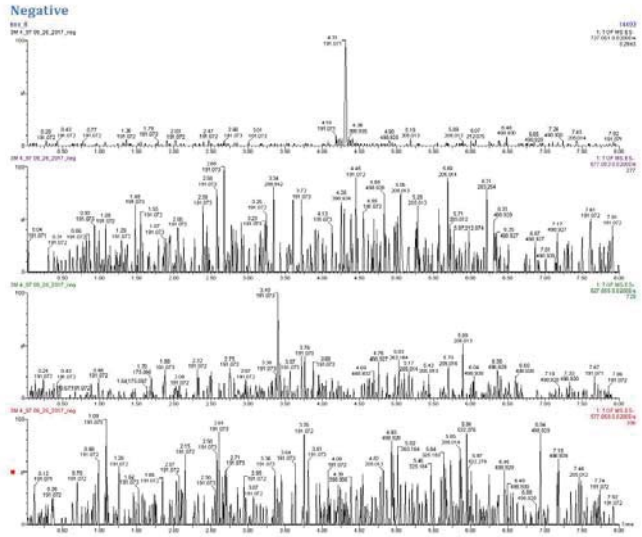

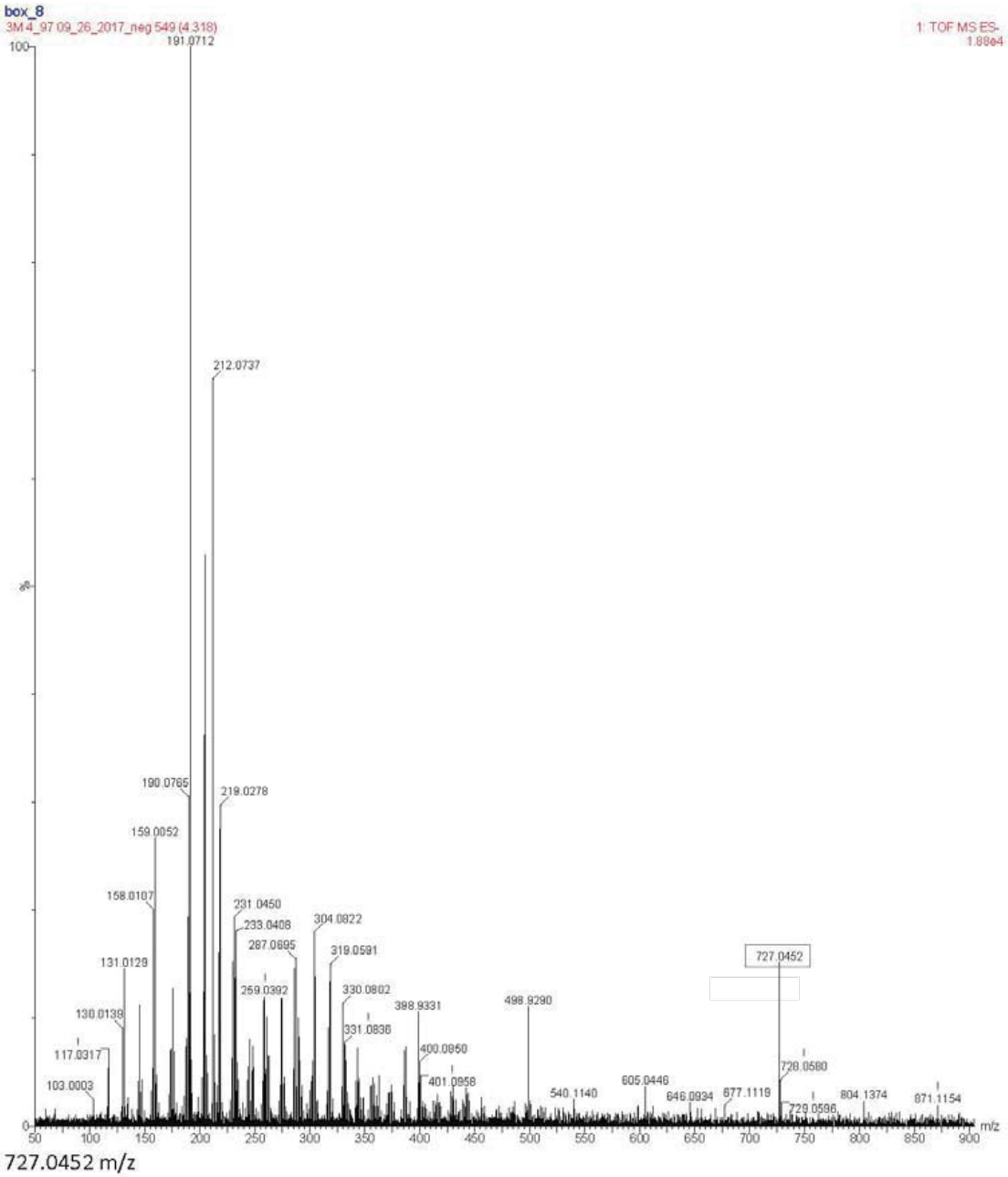

Figure A5-20: Class 29 of 3M 4_97 - Negative

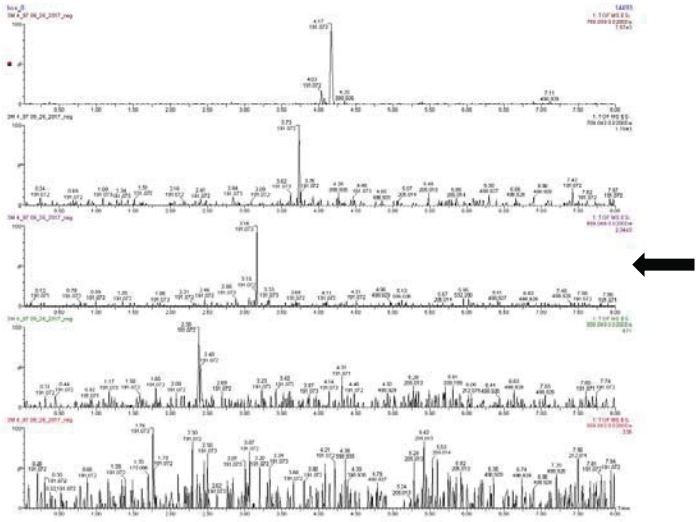

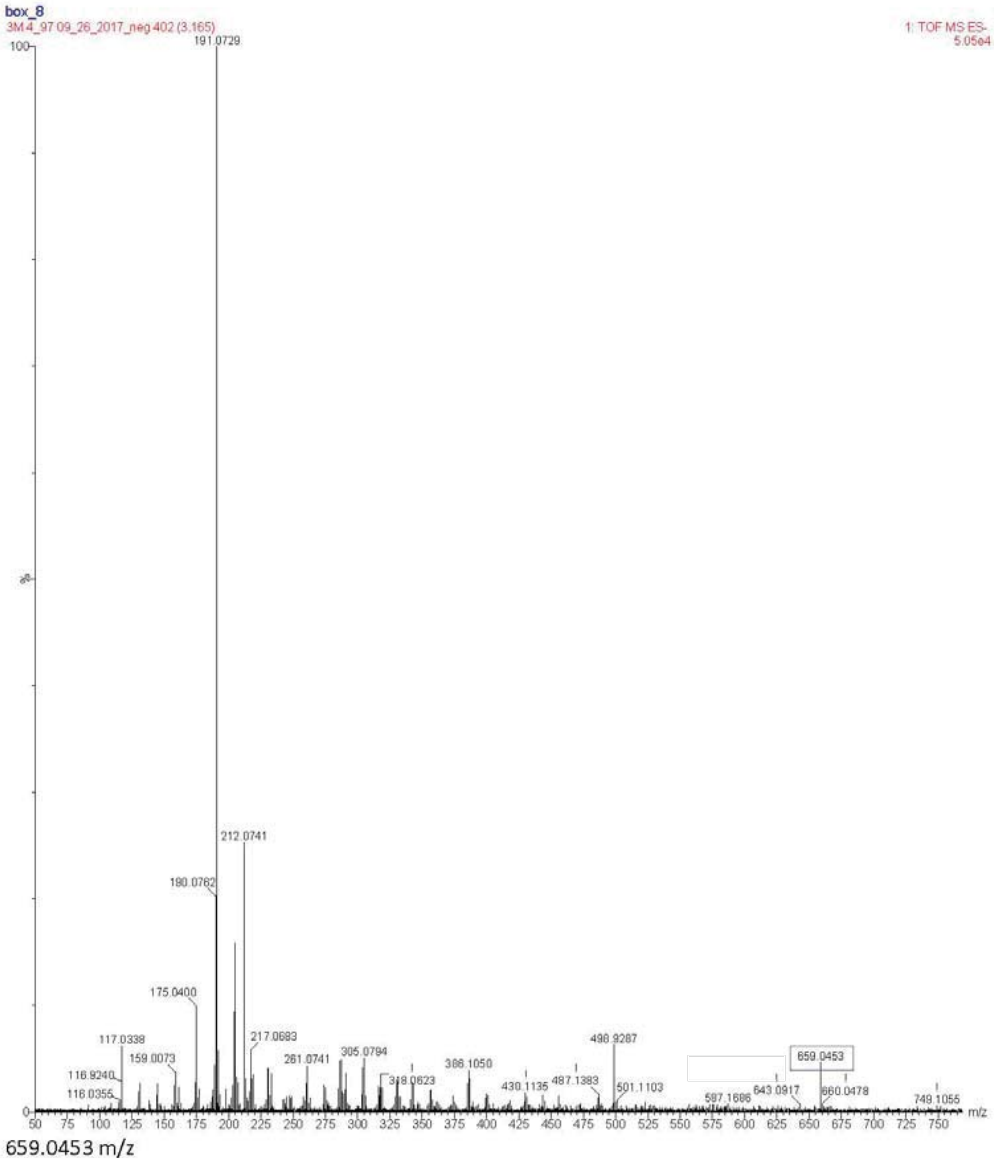

659.0453 m/z

Figure A6-1: Class 2 of 3M 3_98 - Positive

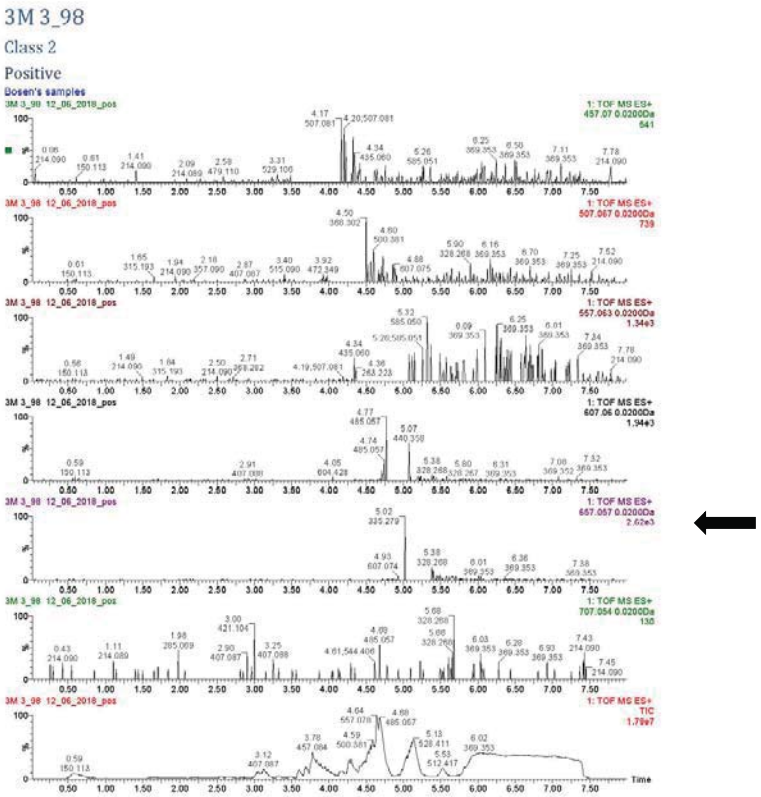

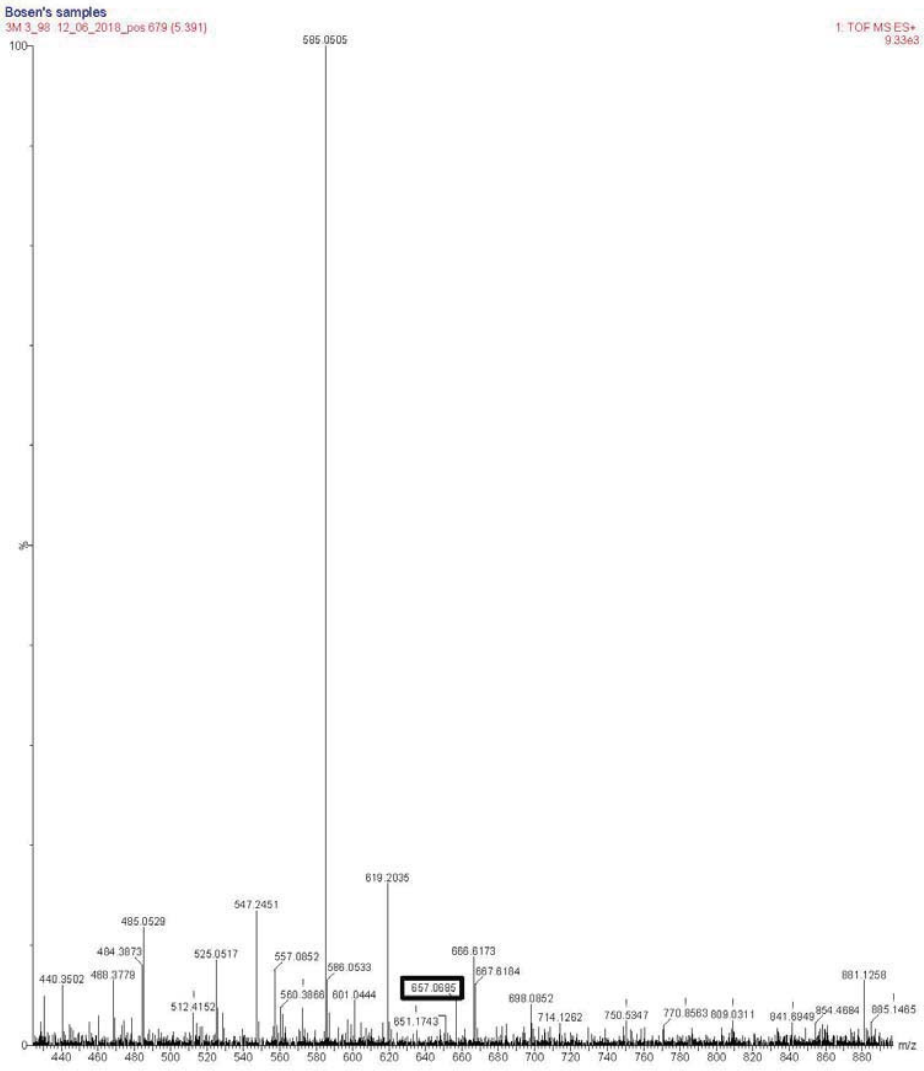

Mass value is found 657.0685 m/z

Figure A6-2: Class 3 of 3M 3_98 - Positive

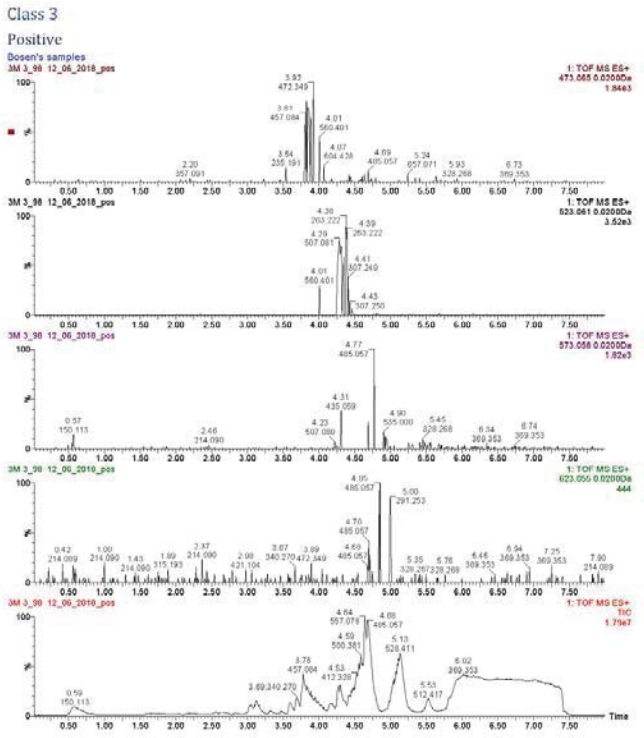

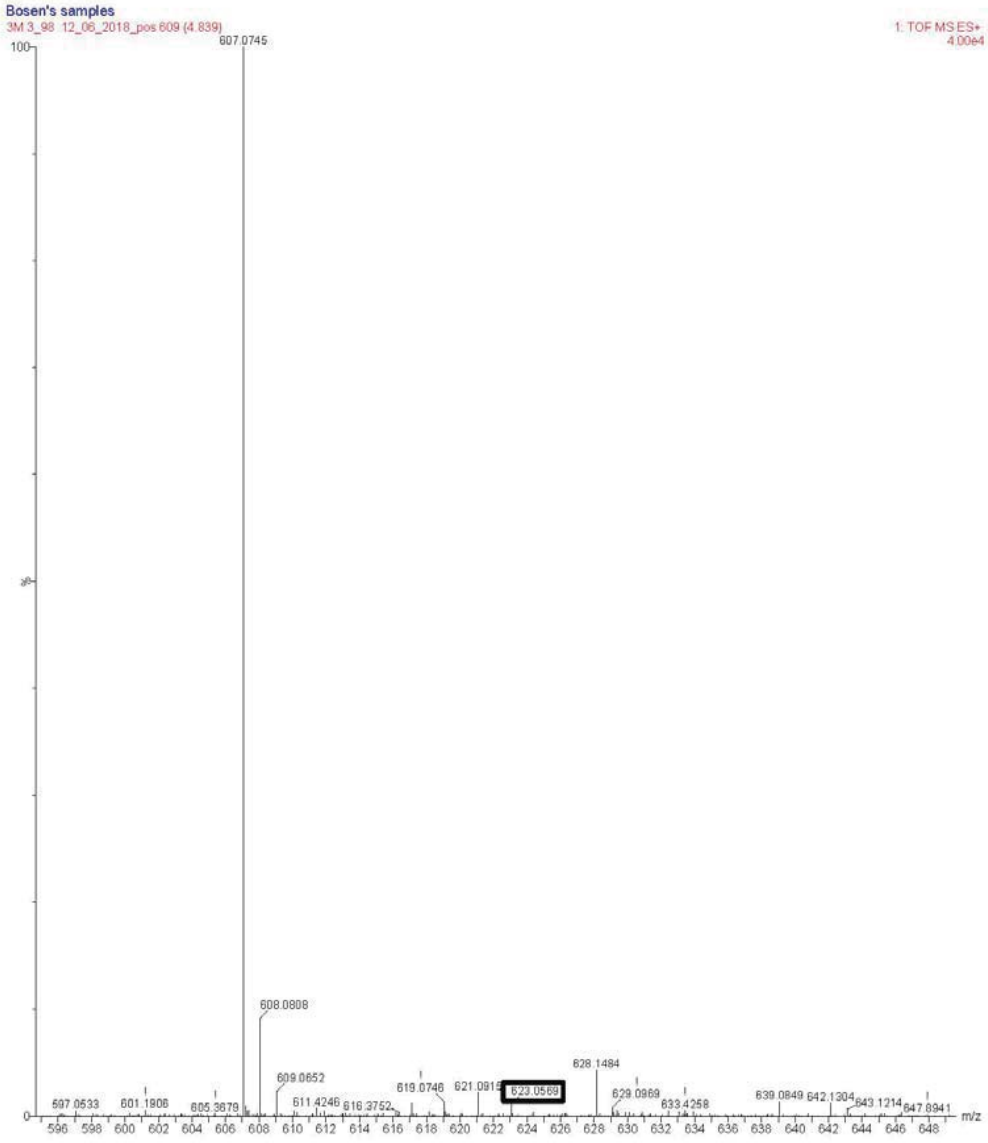

Mass value is found 623.0569 m/z

Figure A6-3: Class 12 of 3M 3_98 - Positive

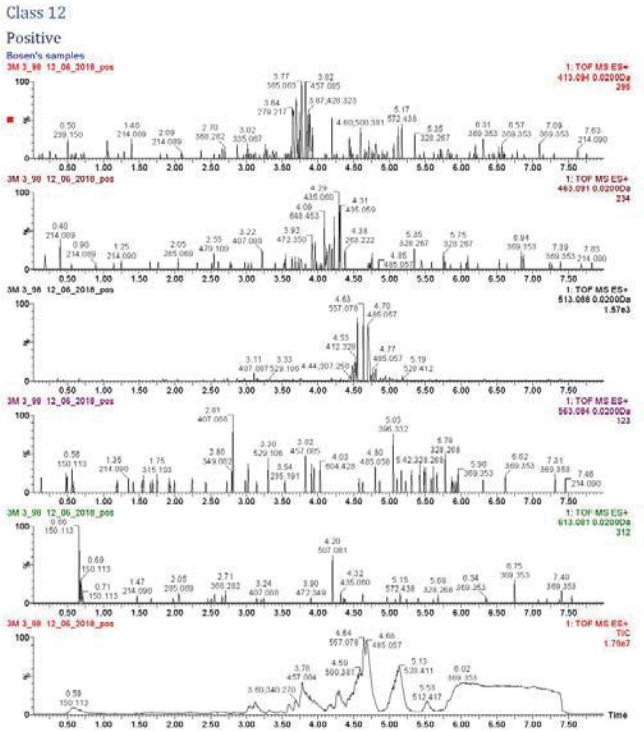

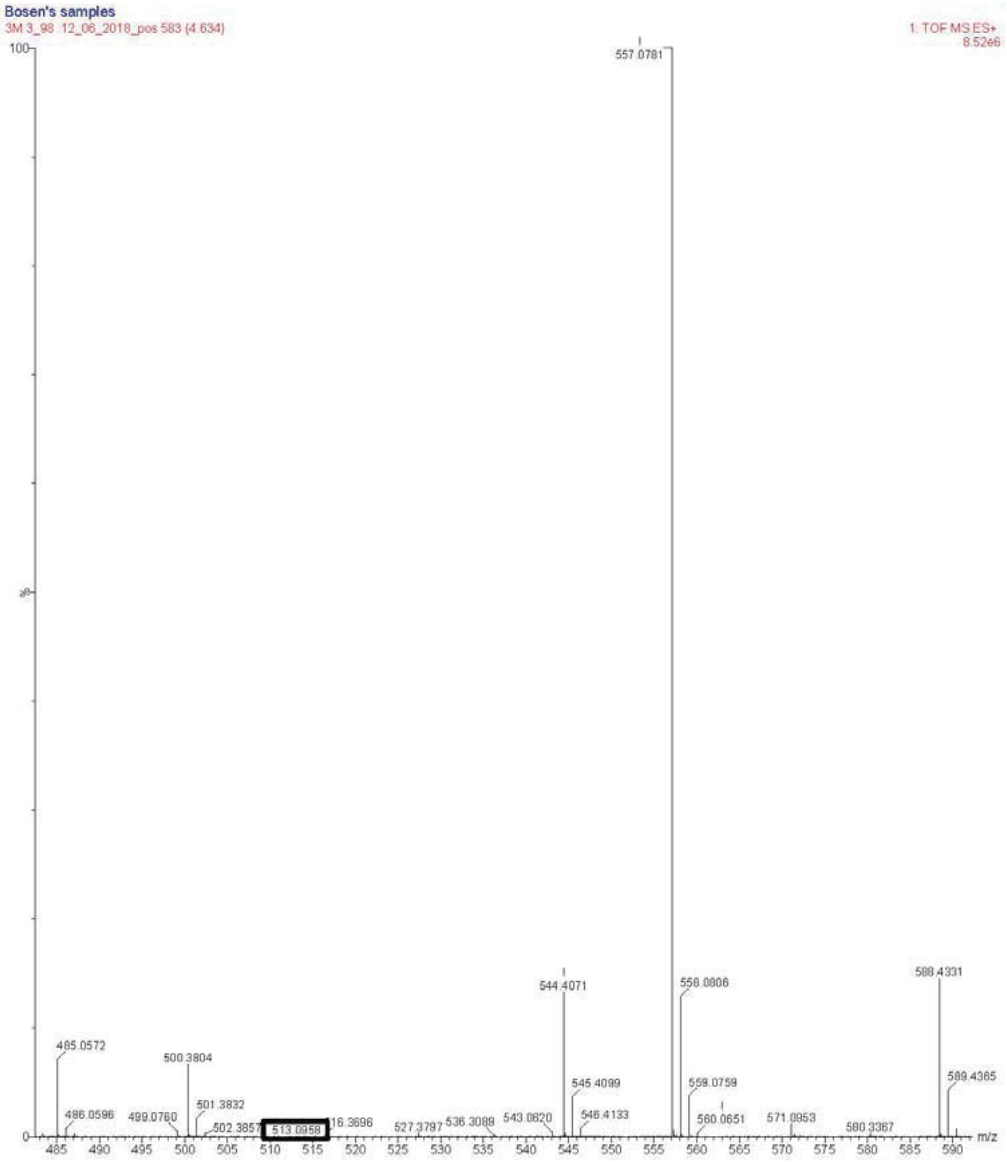

Mass value is found 513.0958 m/z

Figure A6-4: Class 13 of 3M 3_98 - Positive

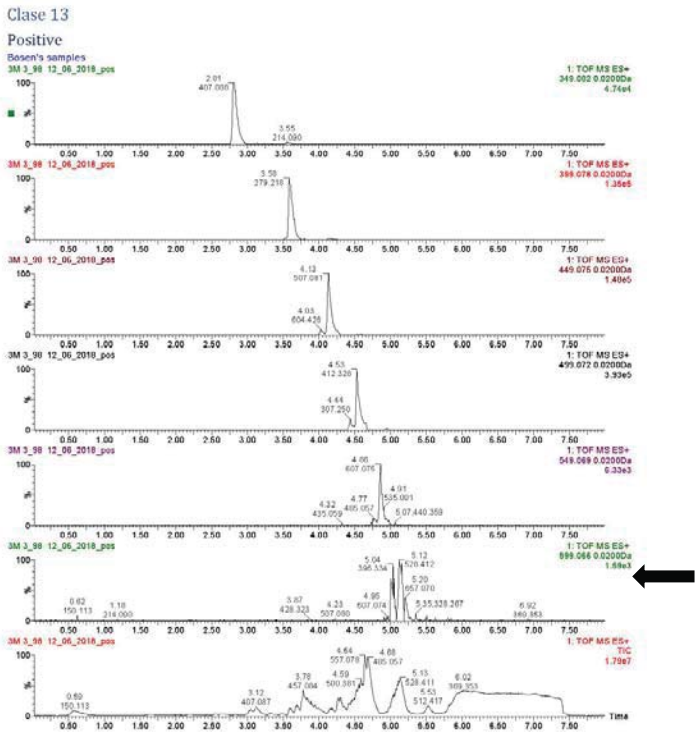

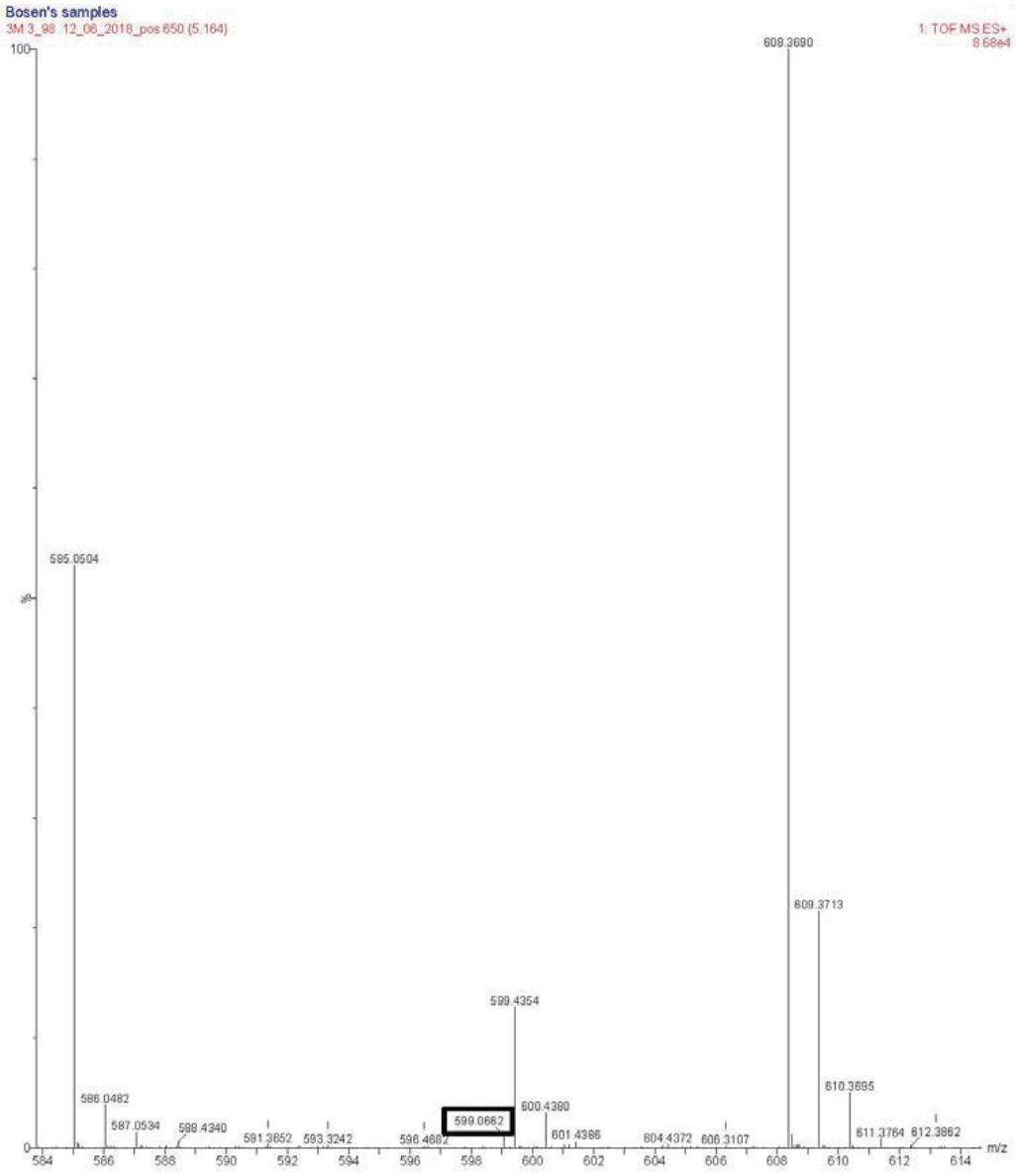

Mass value is found 599.0662 m/z

Figure A6-5: Class 14 of 3M 3_98 - Positive

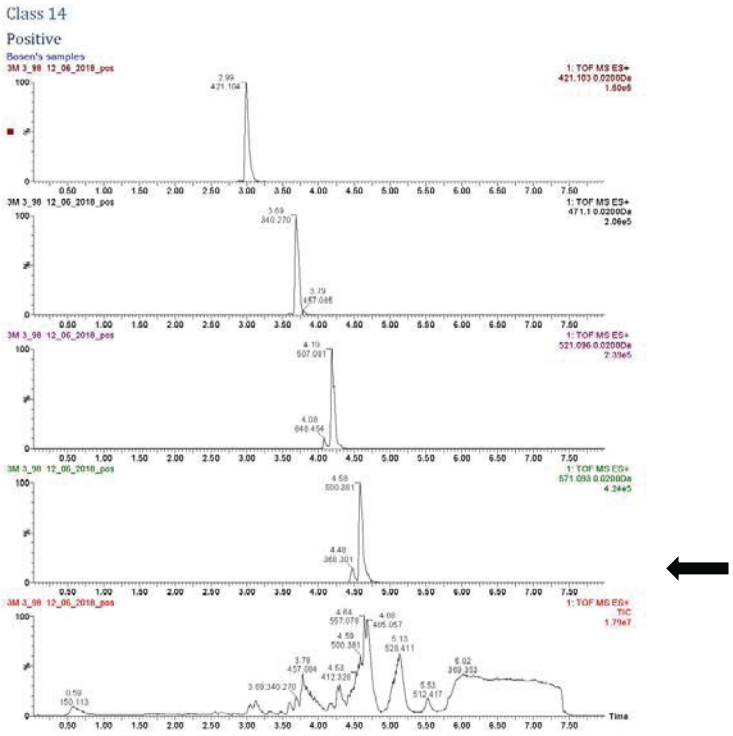

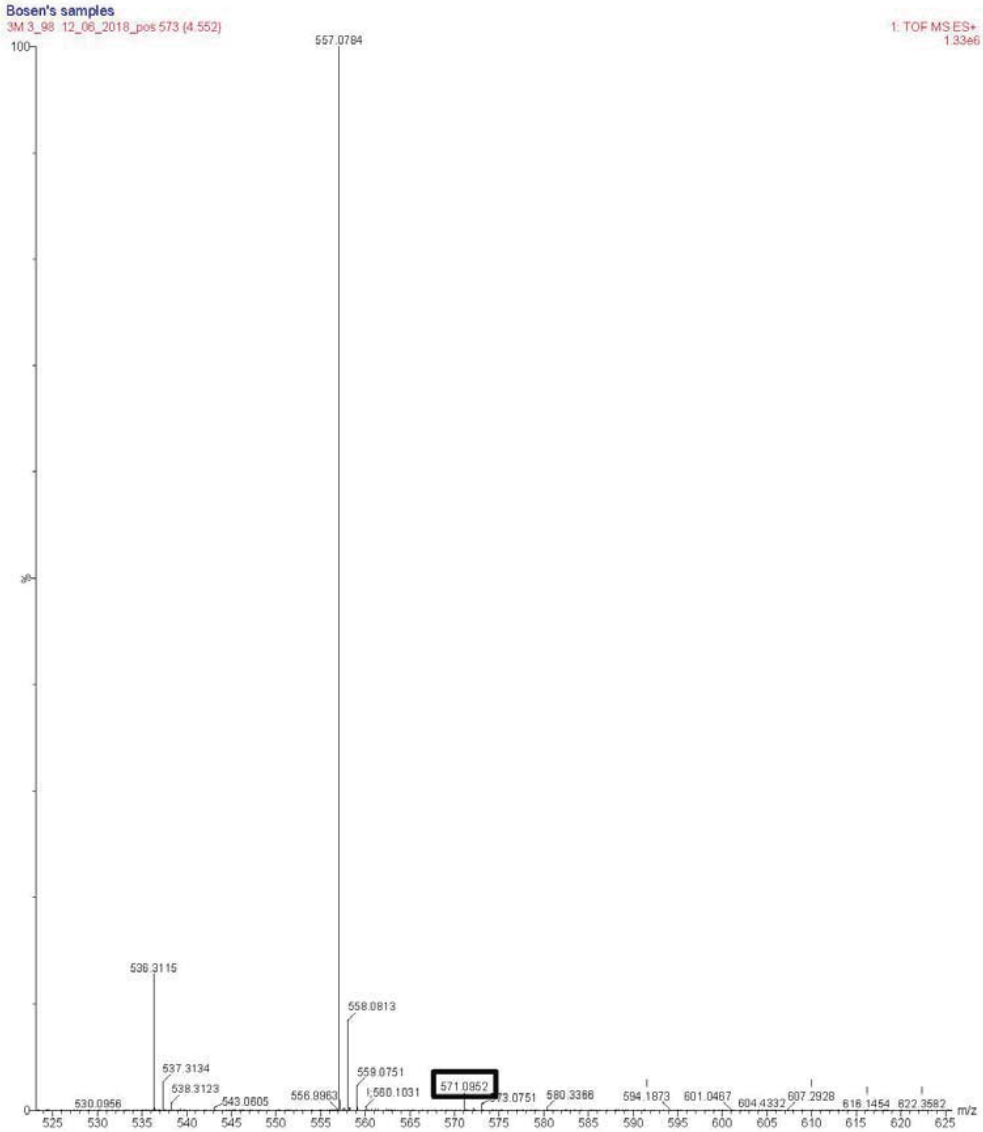

Mass value is found 571.0952 m/z

Figure A6-6: Class 15 of 3M 3_98 - Positive

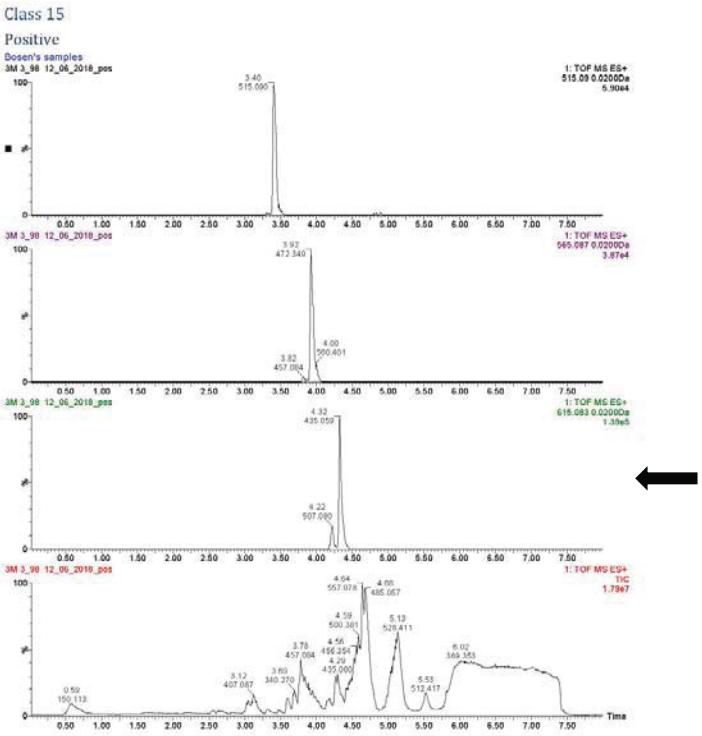

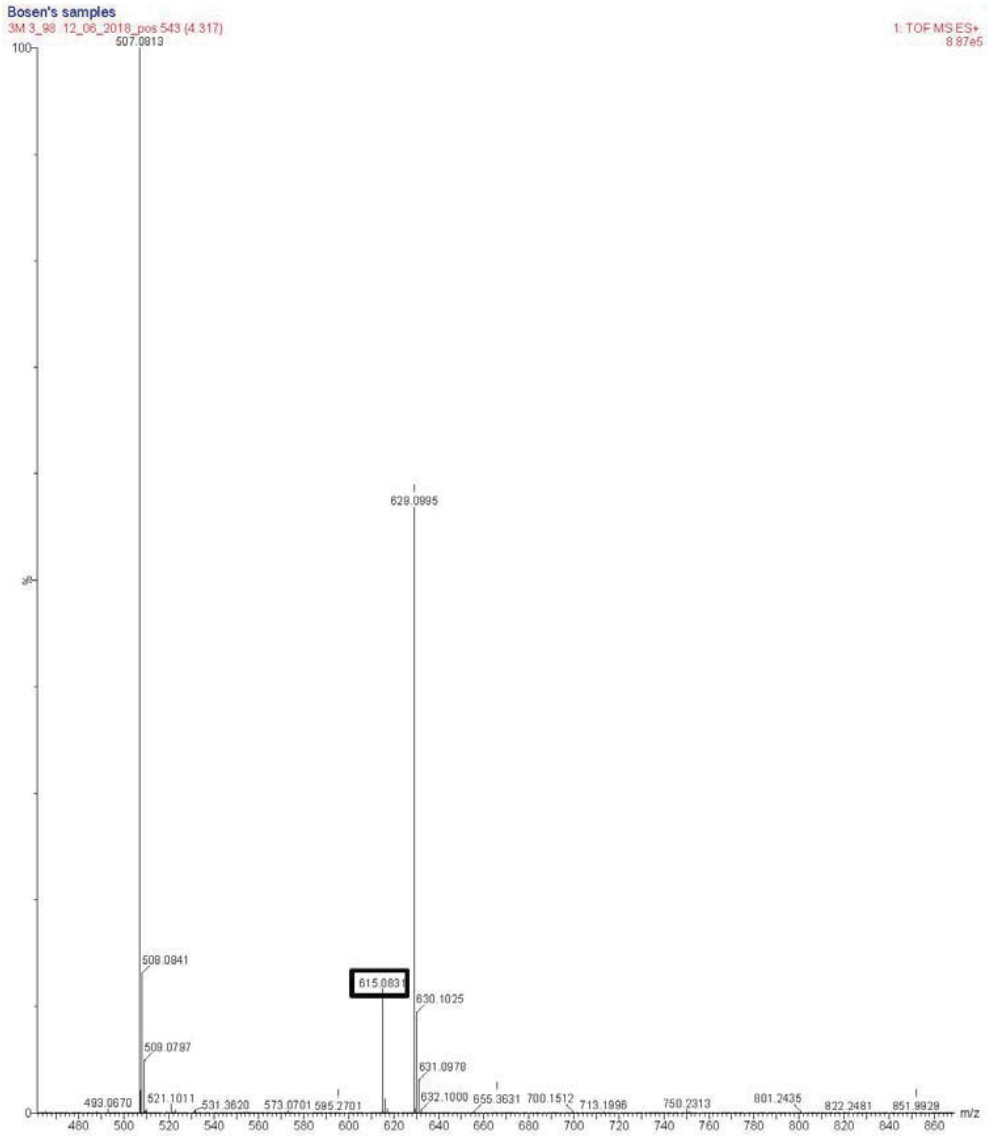

Mass value is found 615.0831 m/z

Figure A6-7: Class 16 of 3M 3_98 - Positive

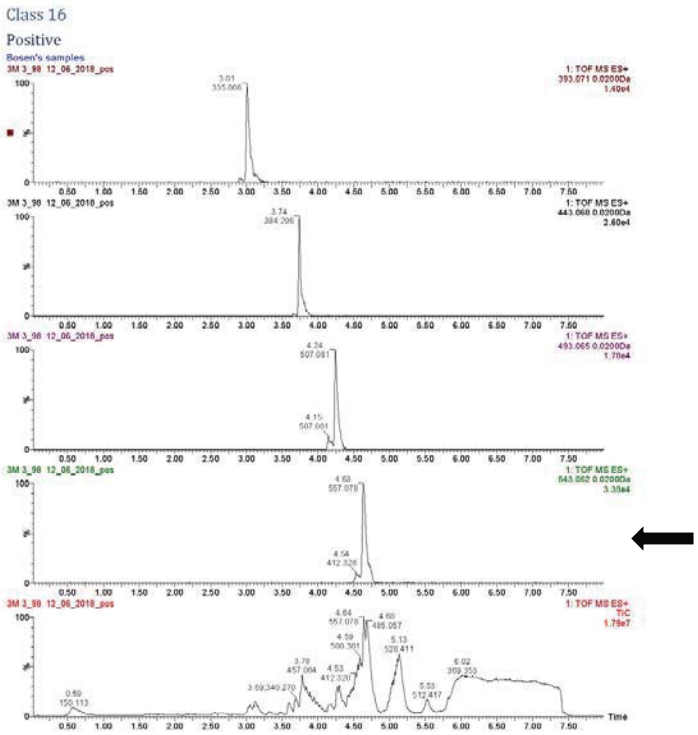

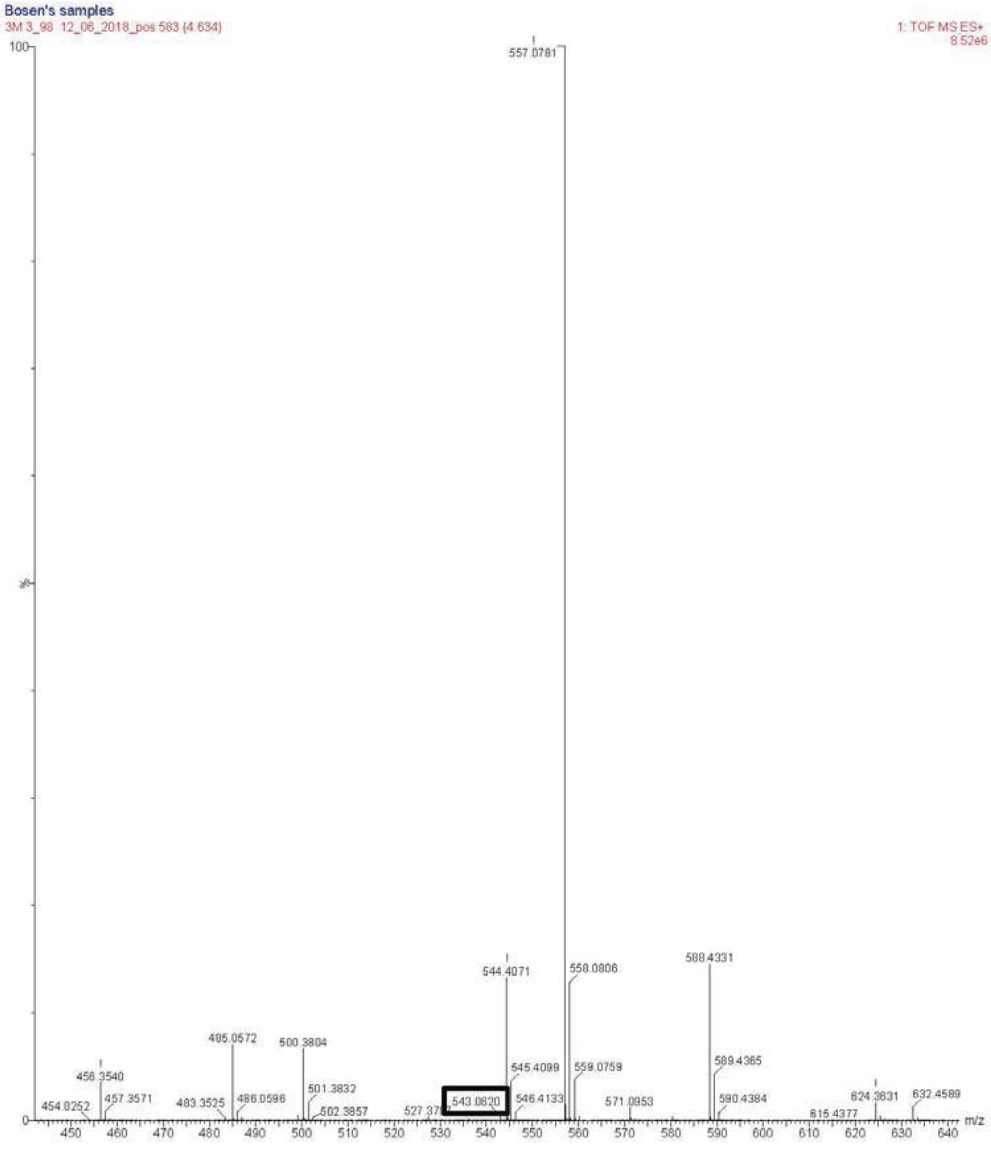

Mass value is found 543.0620 m/z

Figure A6-8: Class 17 of 3M 3_98 - Positive

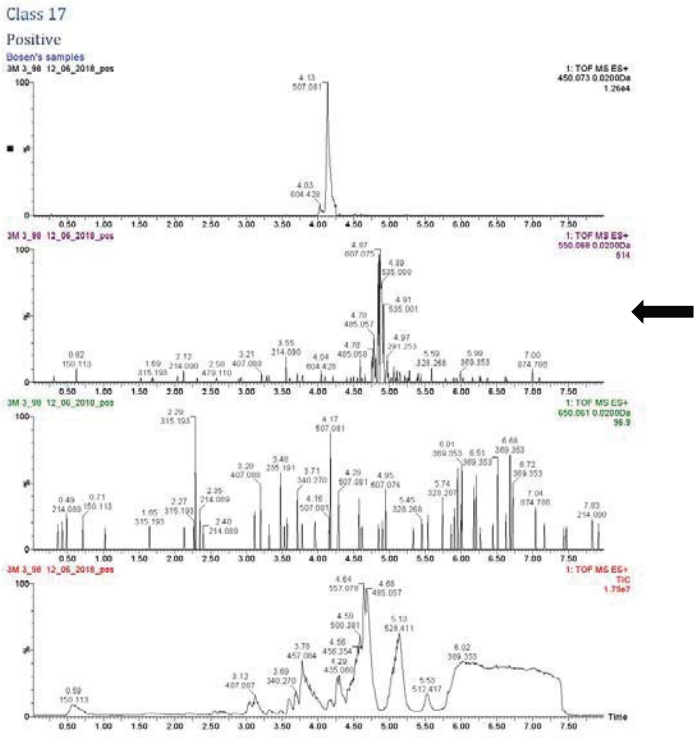

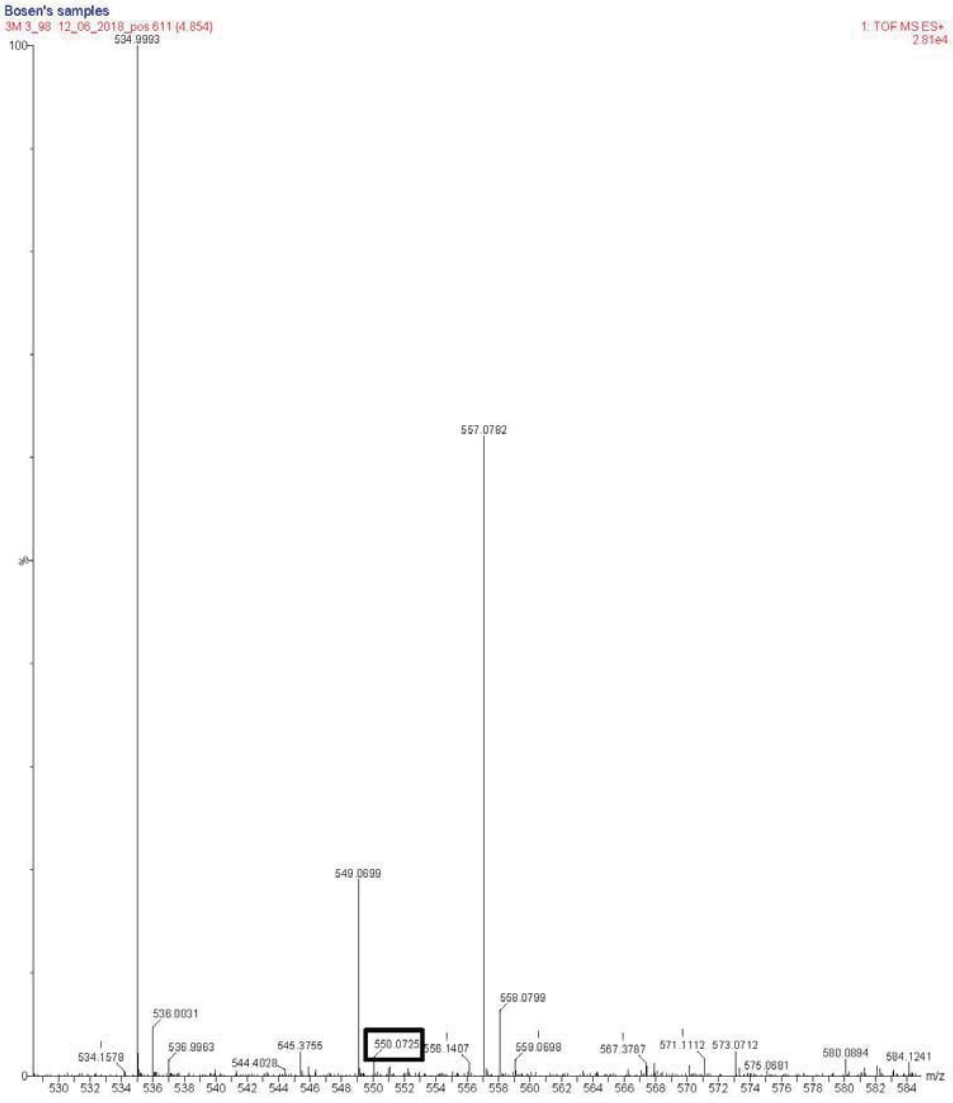

Mass value is found 550.0725 m/z

Figure A6-9: Class 19 of 3M 3_98 - Positive

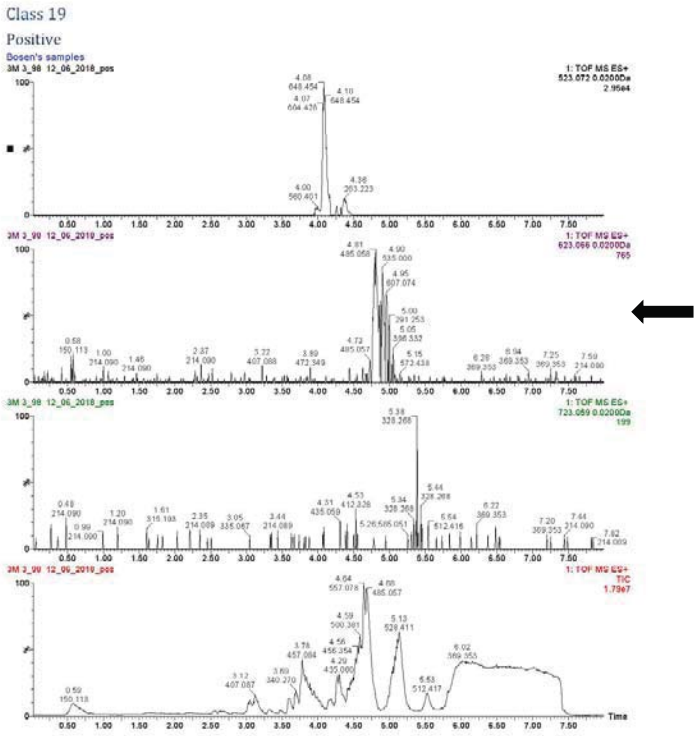

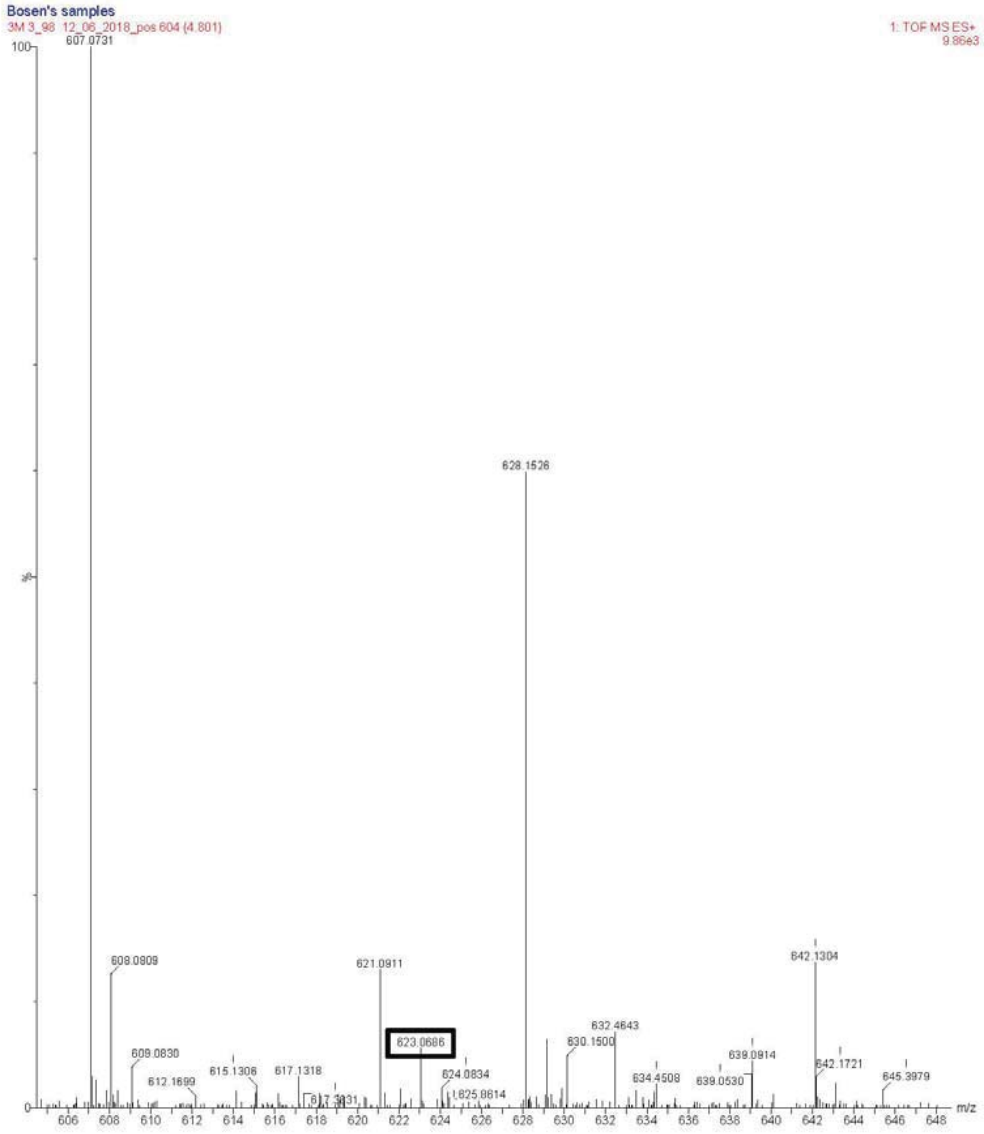

Mass value is found 623.0686 m/z

Figure A6-10: Class 28 of 3M 3_98 - Positive

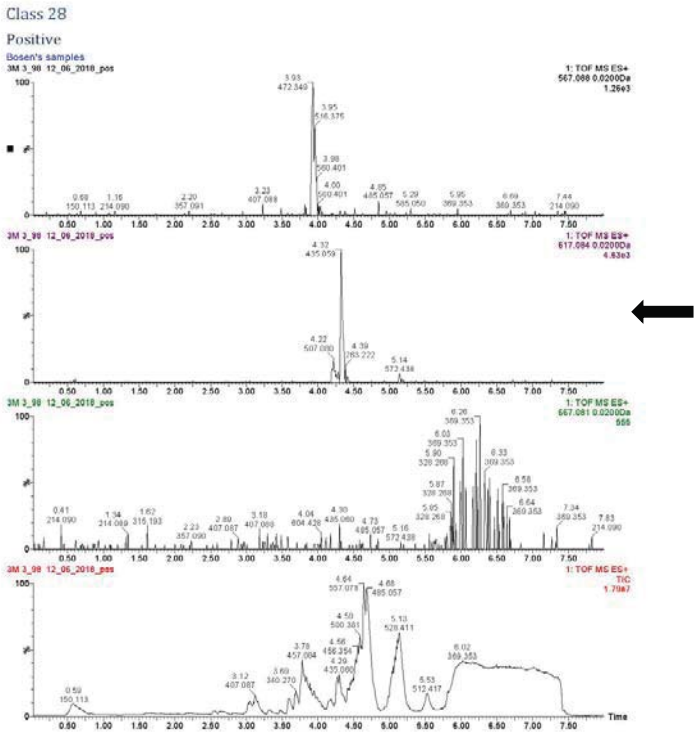

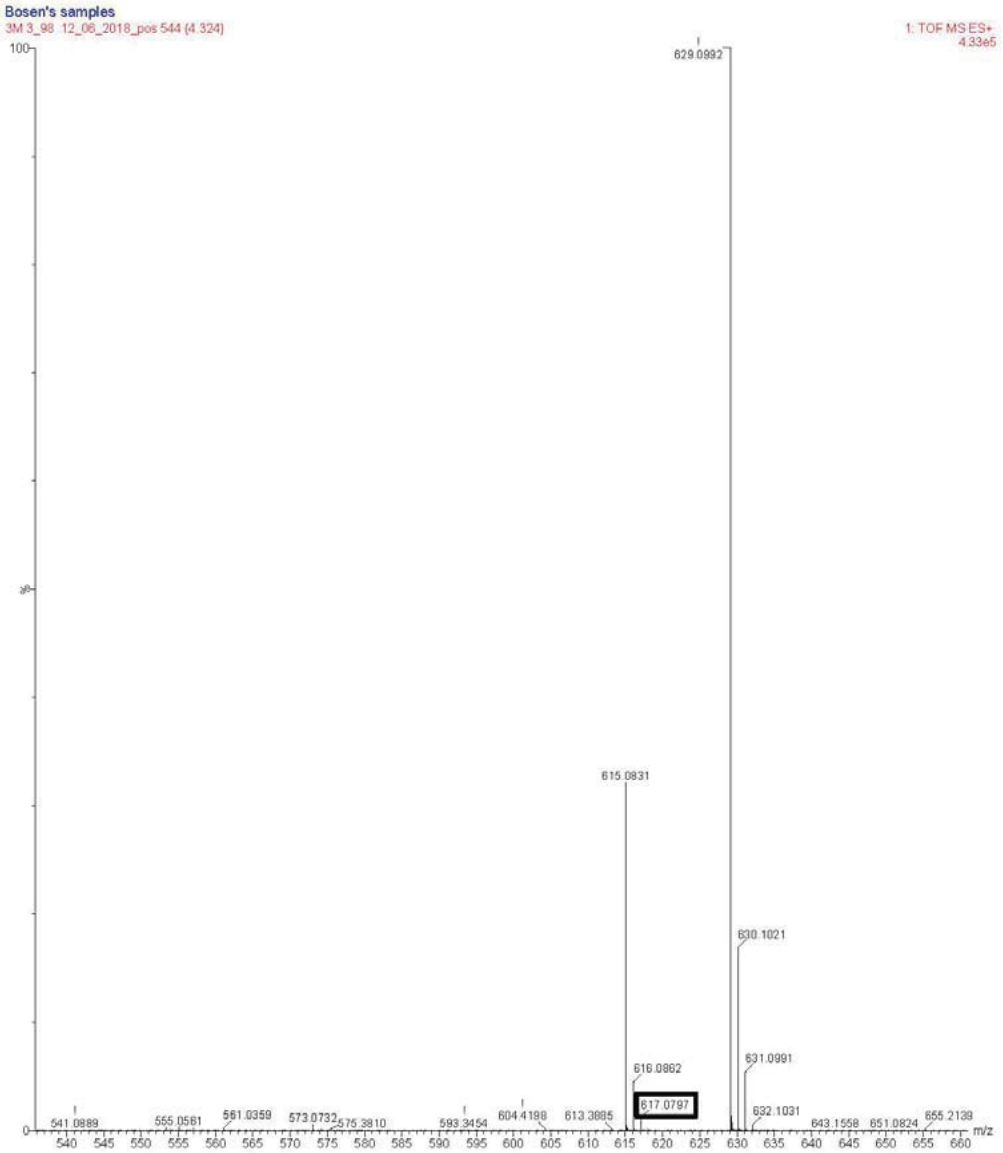

Mass value is found 617.0797 m/z

Figure A6-11: Class 31 of 3M 3_98 - Positive

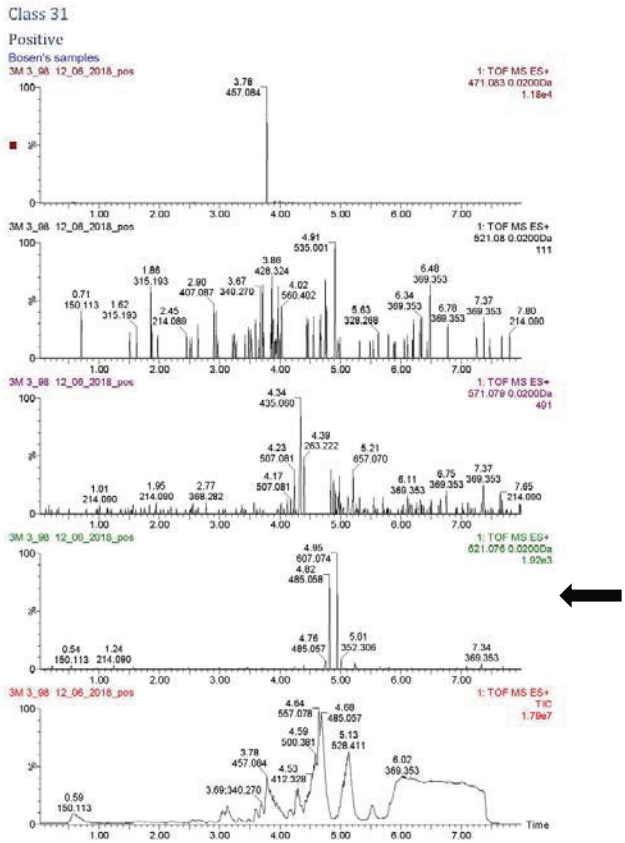

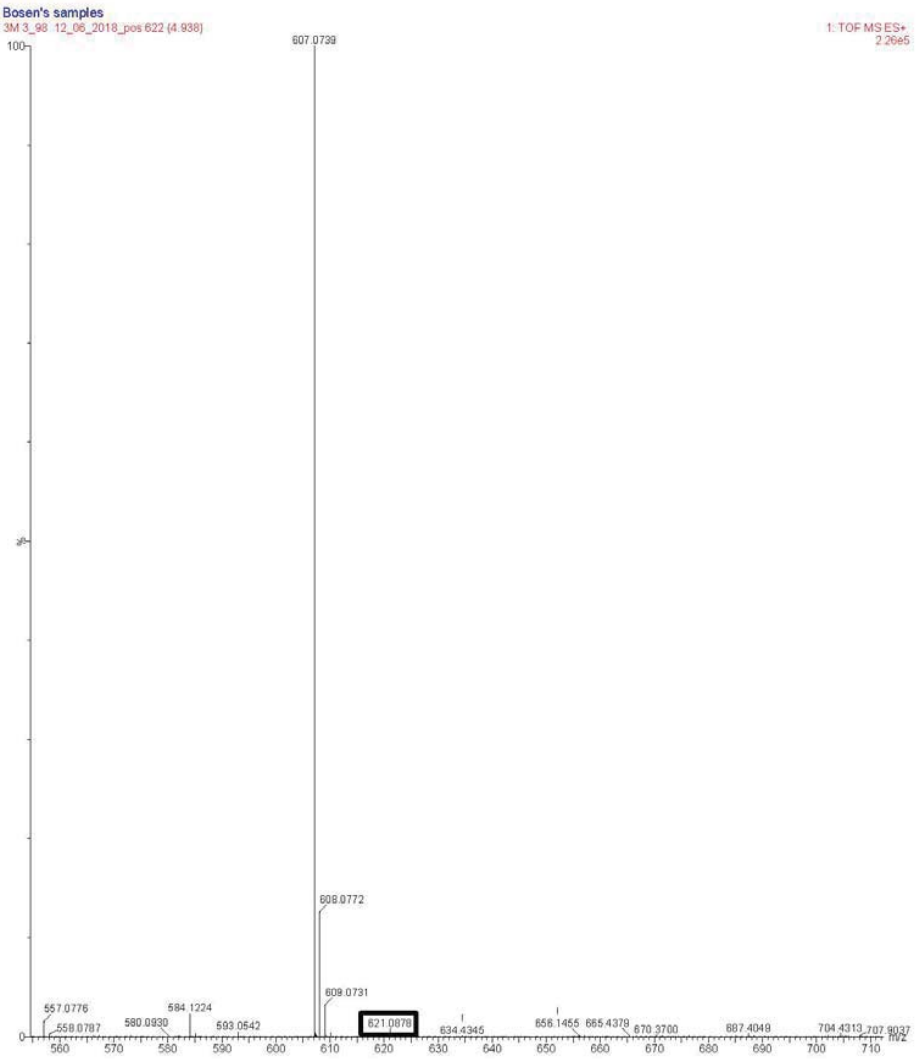

Mass value is found 621.0878 m/z

Figure A6-12: Class 32 of 3M 3_98 - Positive

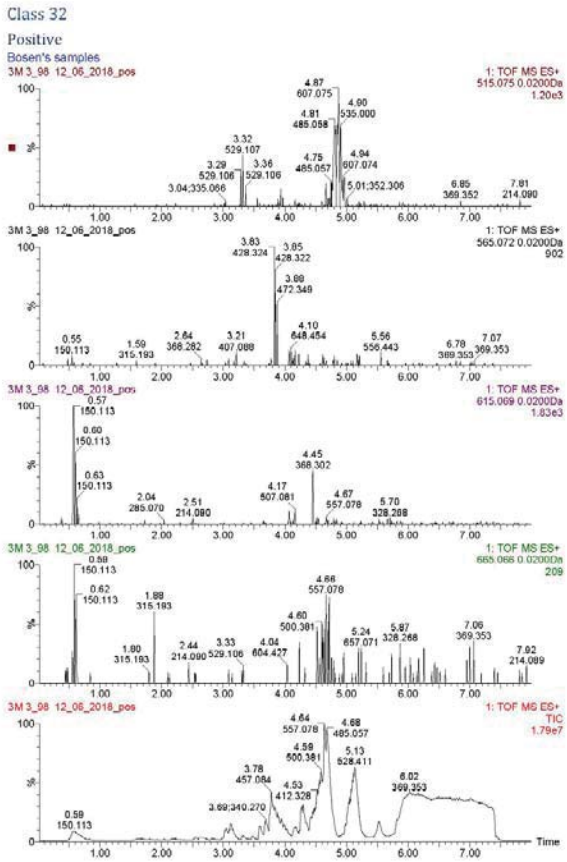

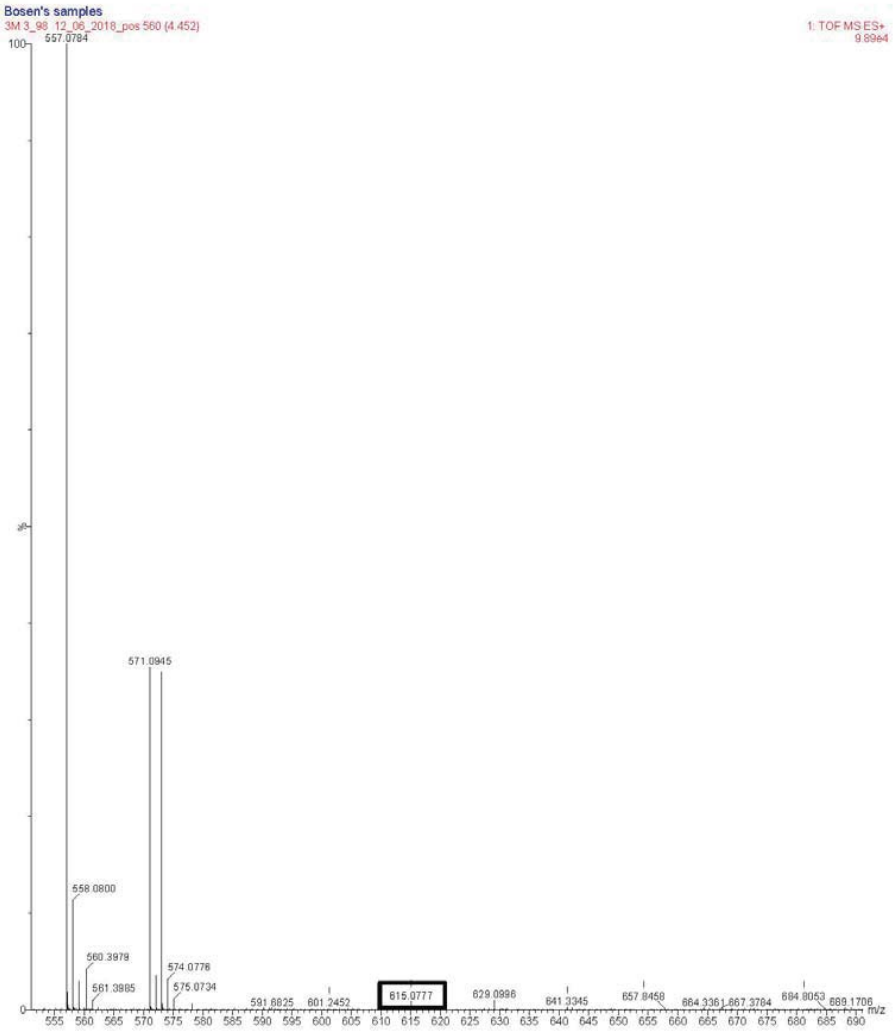

Mass value is found 615.0777 m/z

Figure A6-13: Class 34 of 3M 3_98 - Positive

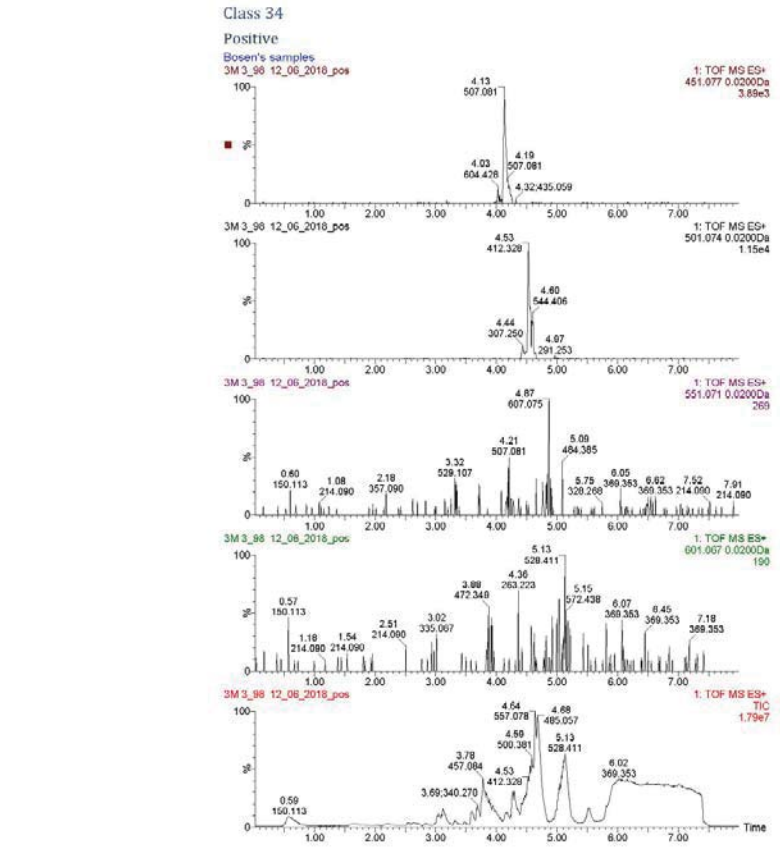

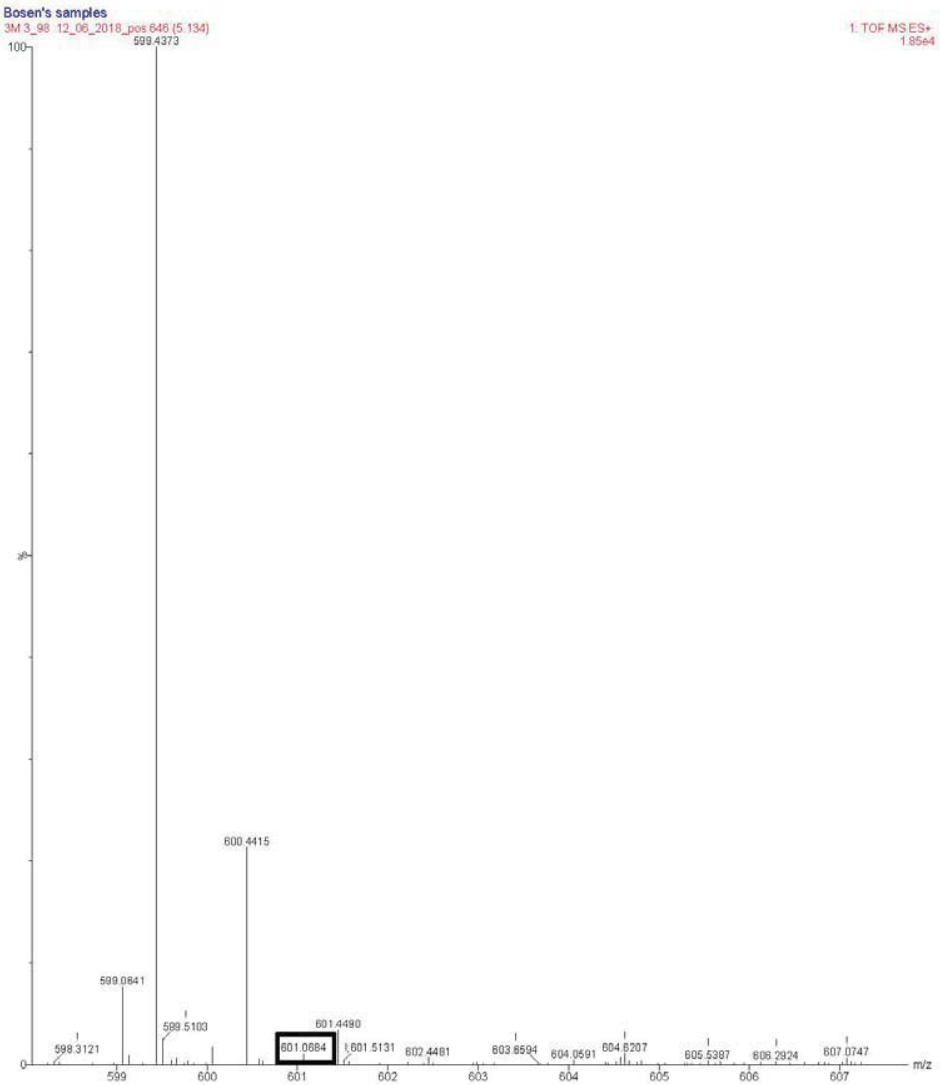

Mass value is found 601.0684 m/z

Figure A6-14: Class 37 of 3M 3_98 - Positive

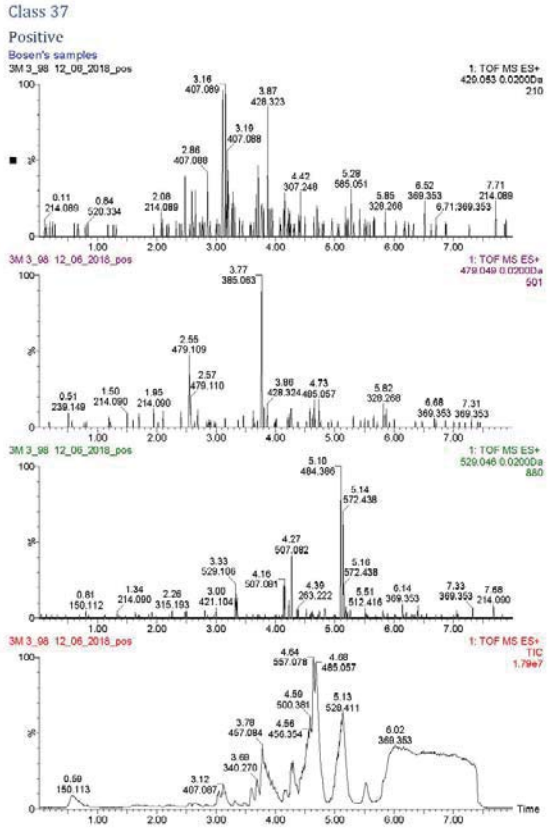

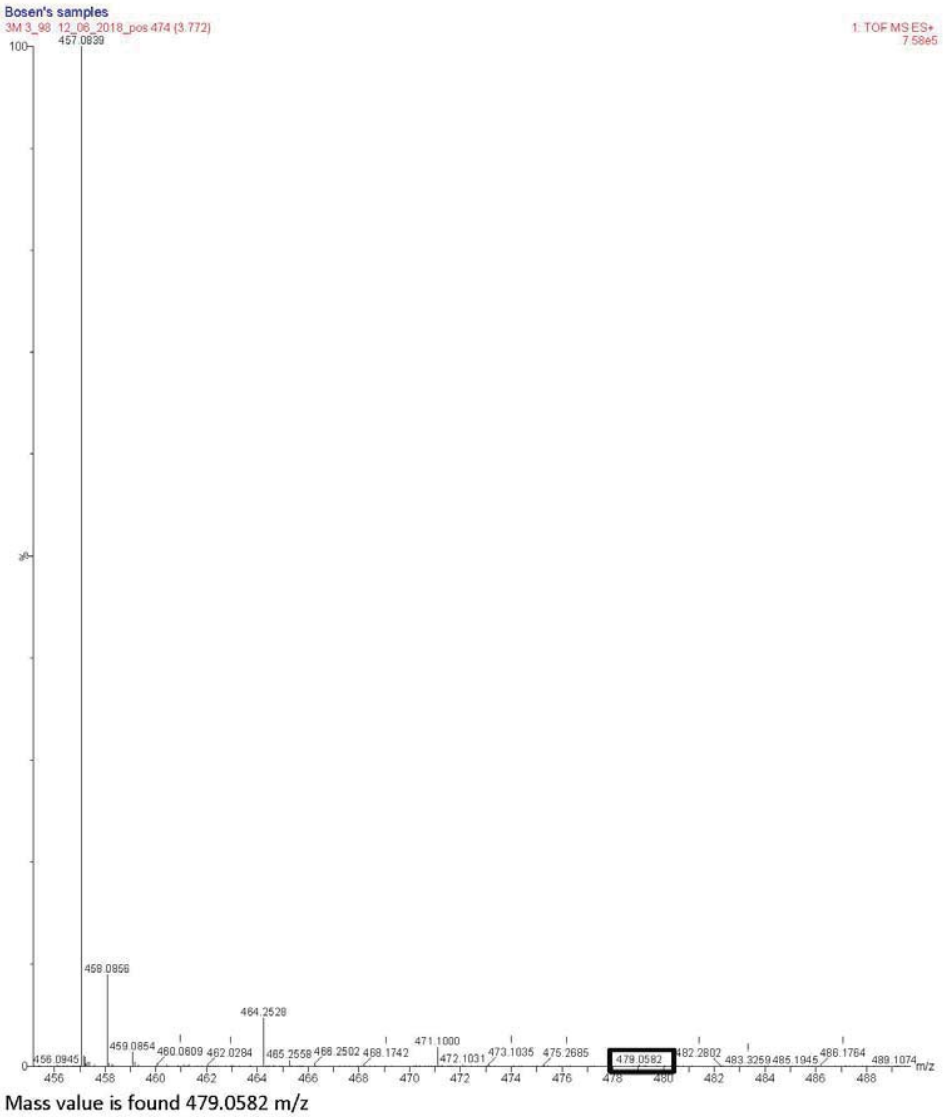

Mass value is found 479.0582 m/z

Figure A6-15: Class 21 of 3M 3_98 - Negative

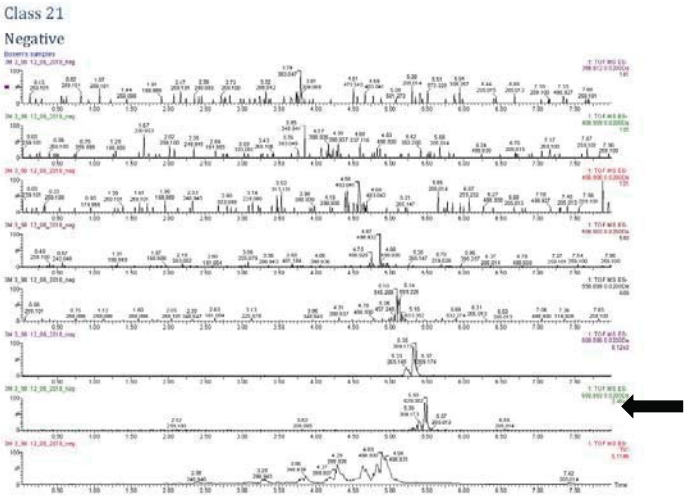

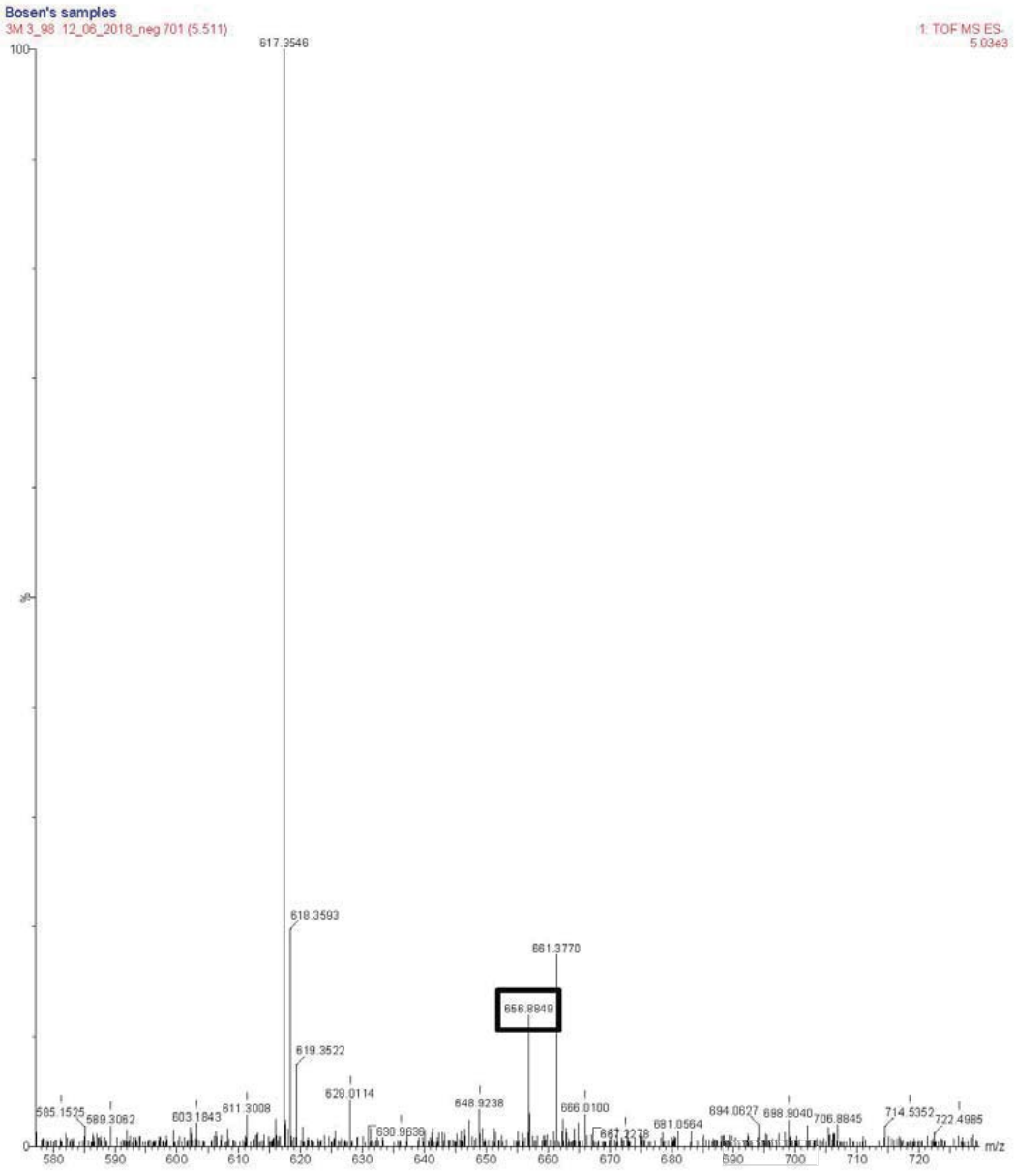

Mass value is found 656.8849 m/z

Figure A6-16: Class 23 of 3M 3_98 - Negative

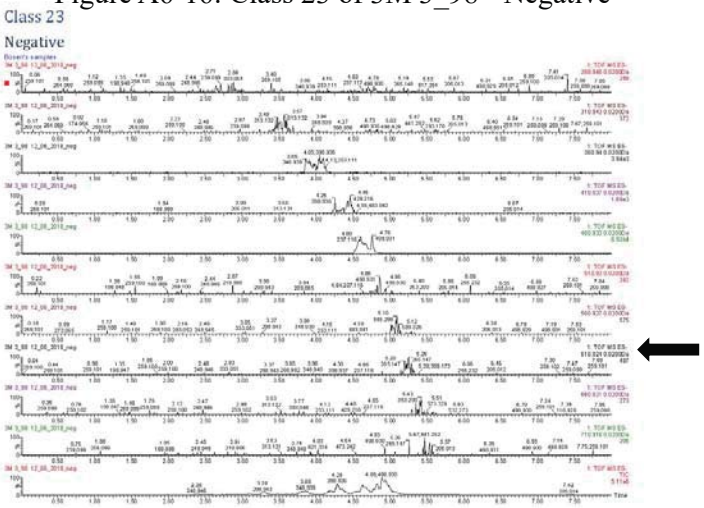

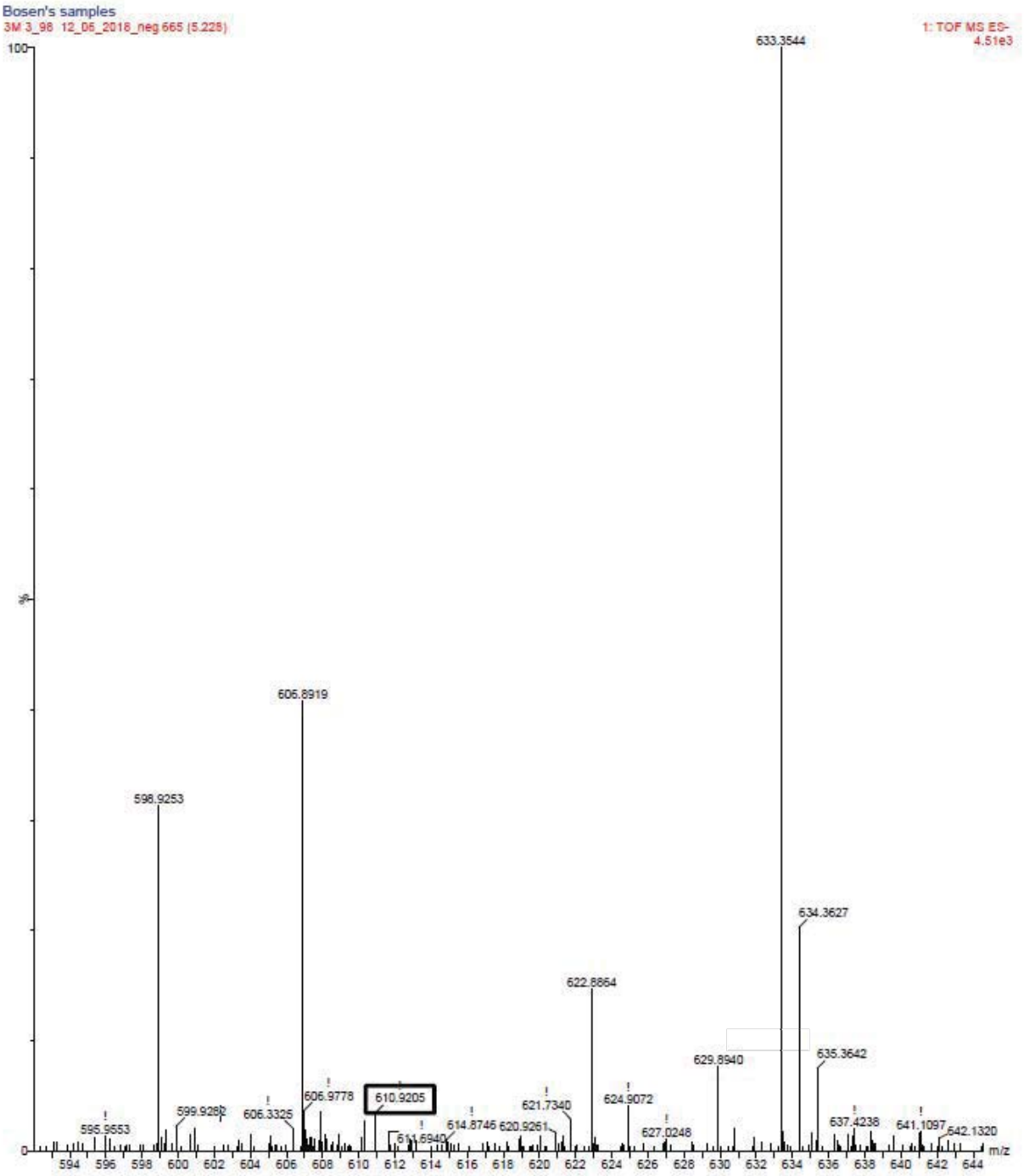

Mass value is found 610.9205 m/z

Figure A6-17: Class 24 of 3M 3_98 - Negative

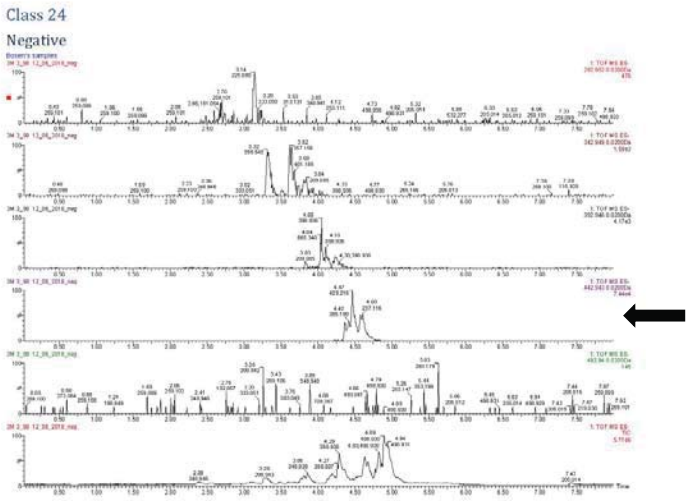

Mass value is 442.943 m/z

Figure A6-18: Class 25 of 3M 3_98 - Negative

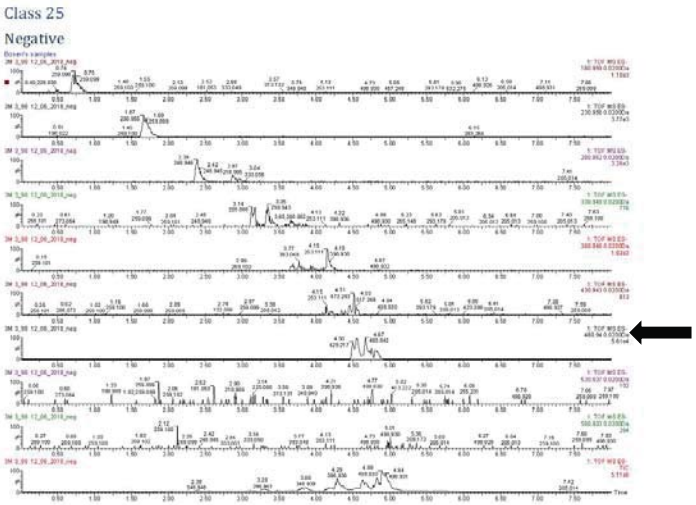

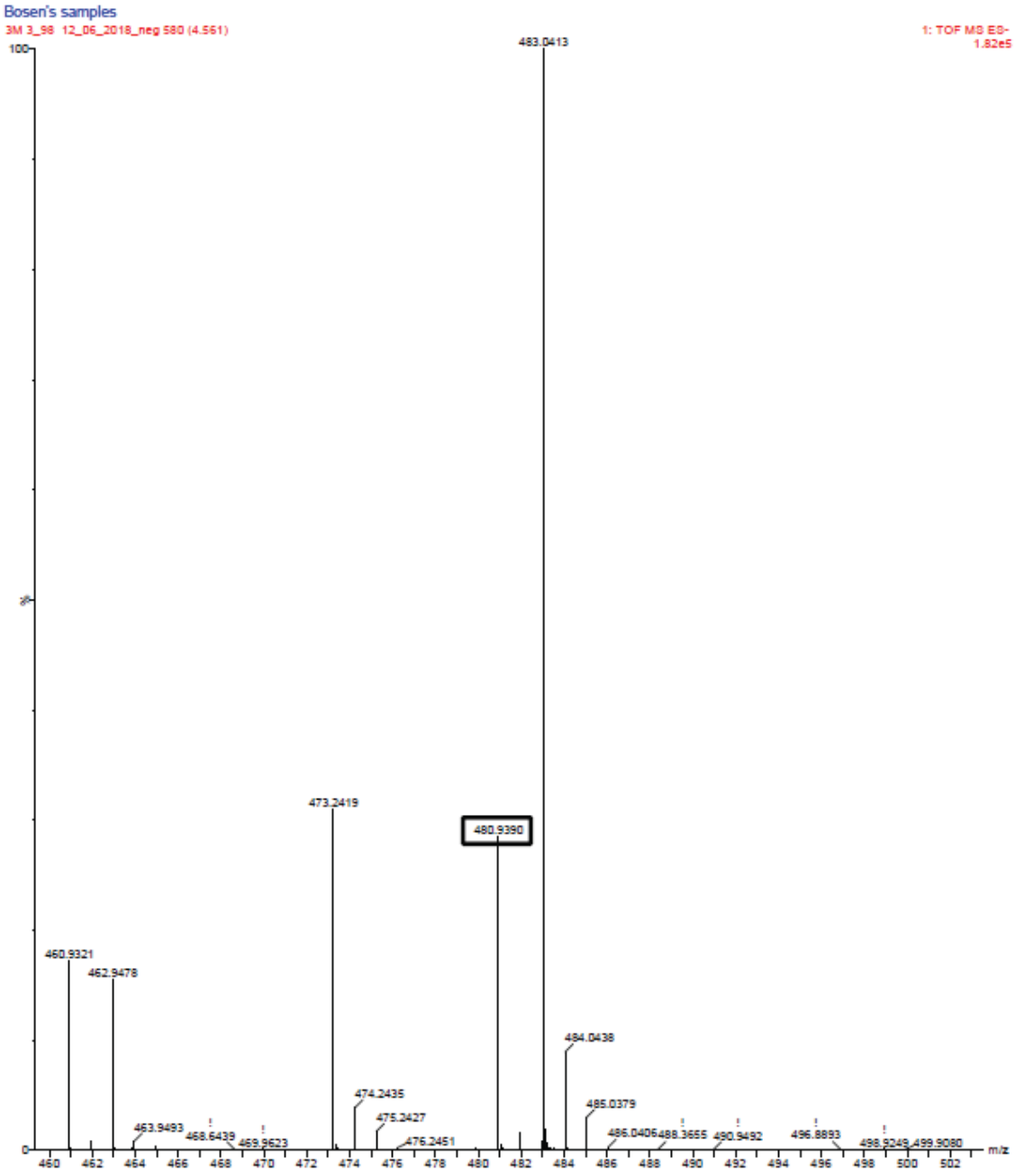

Mass value is found 480.9390 m/z

Figure A6-19: Class 26 of 3M 3_98 - Negative

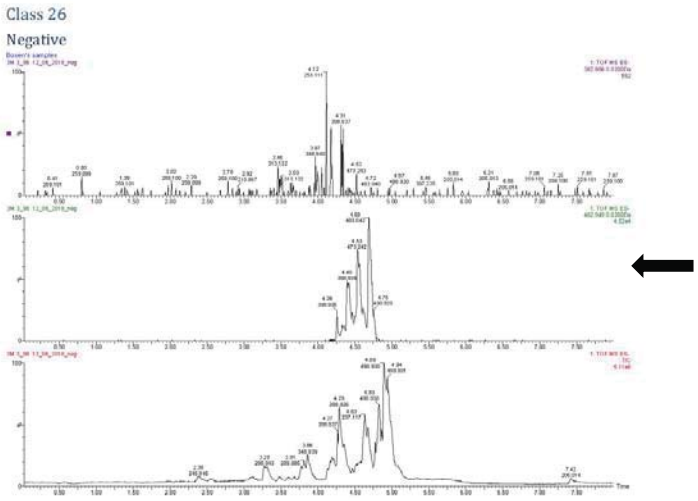

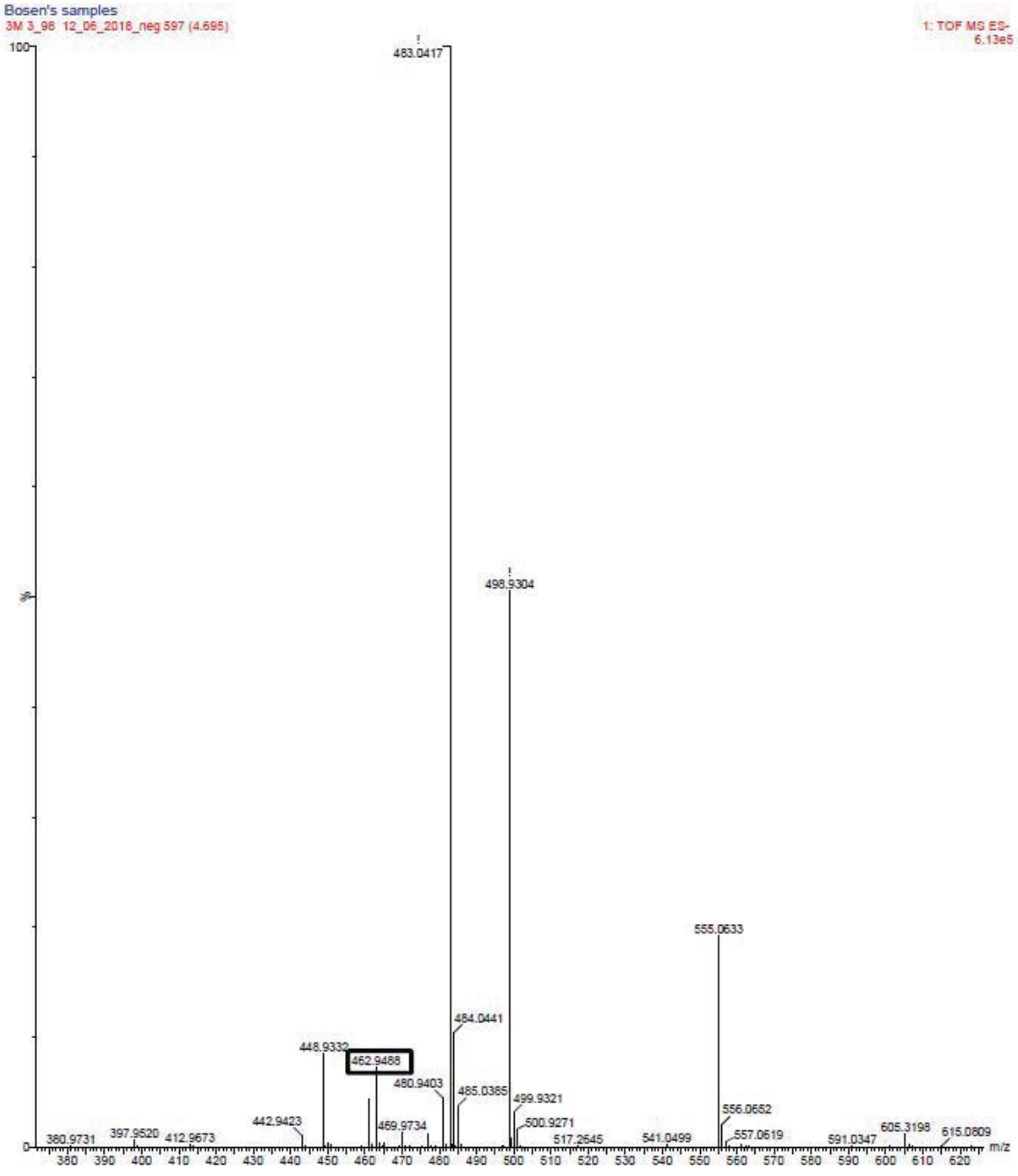

Mass value is found 462.9488 m/z

Figure A6-20: Class 30 of 3M 3_98 - Negative

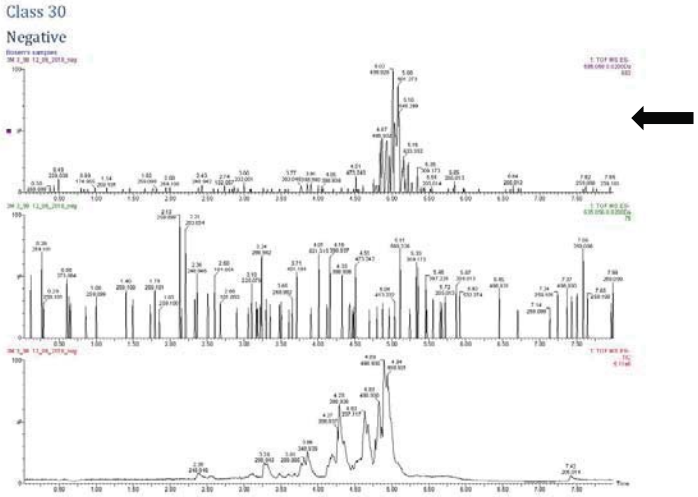

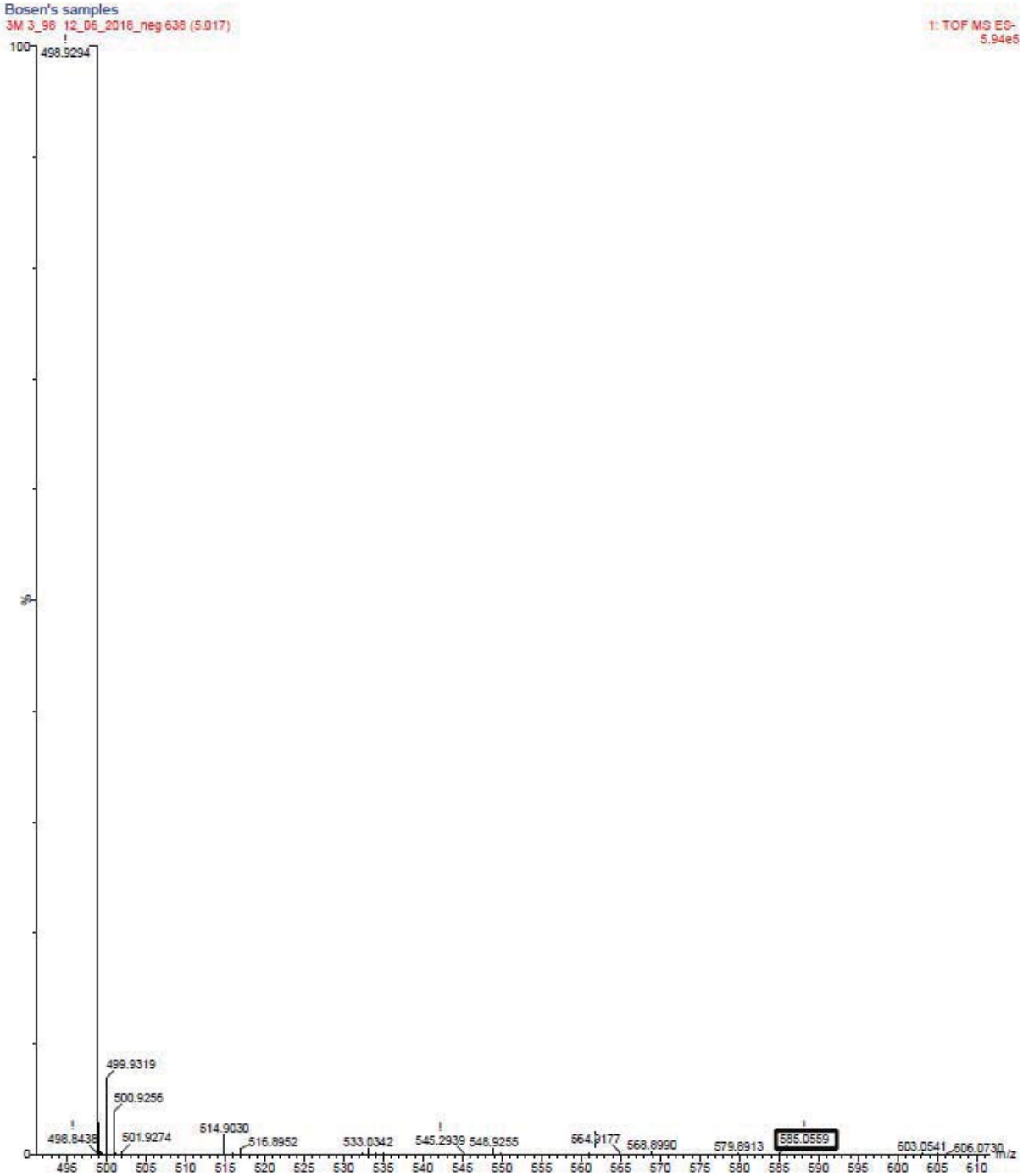

Mass value is found 585.0559 m/z

Figure A6-21: Class 40 of 3M 3_98 - Negative

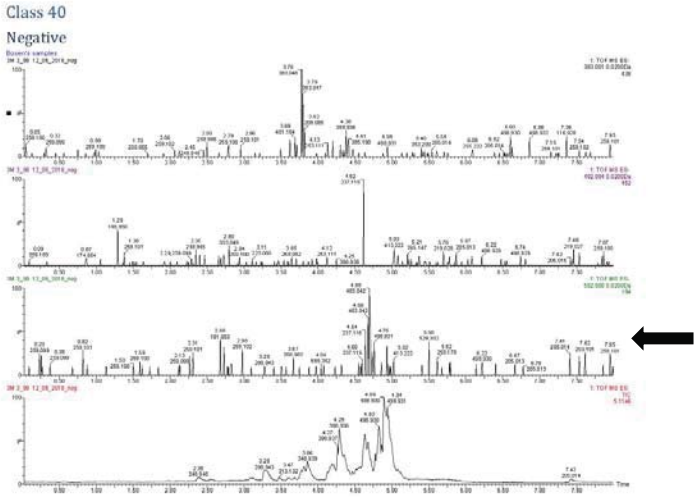

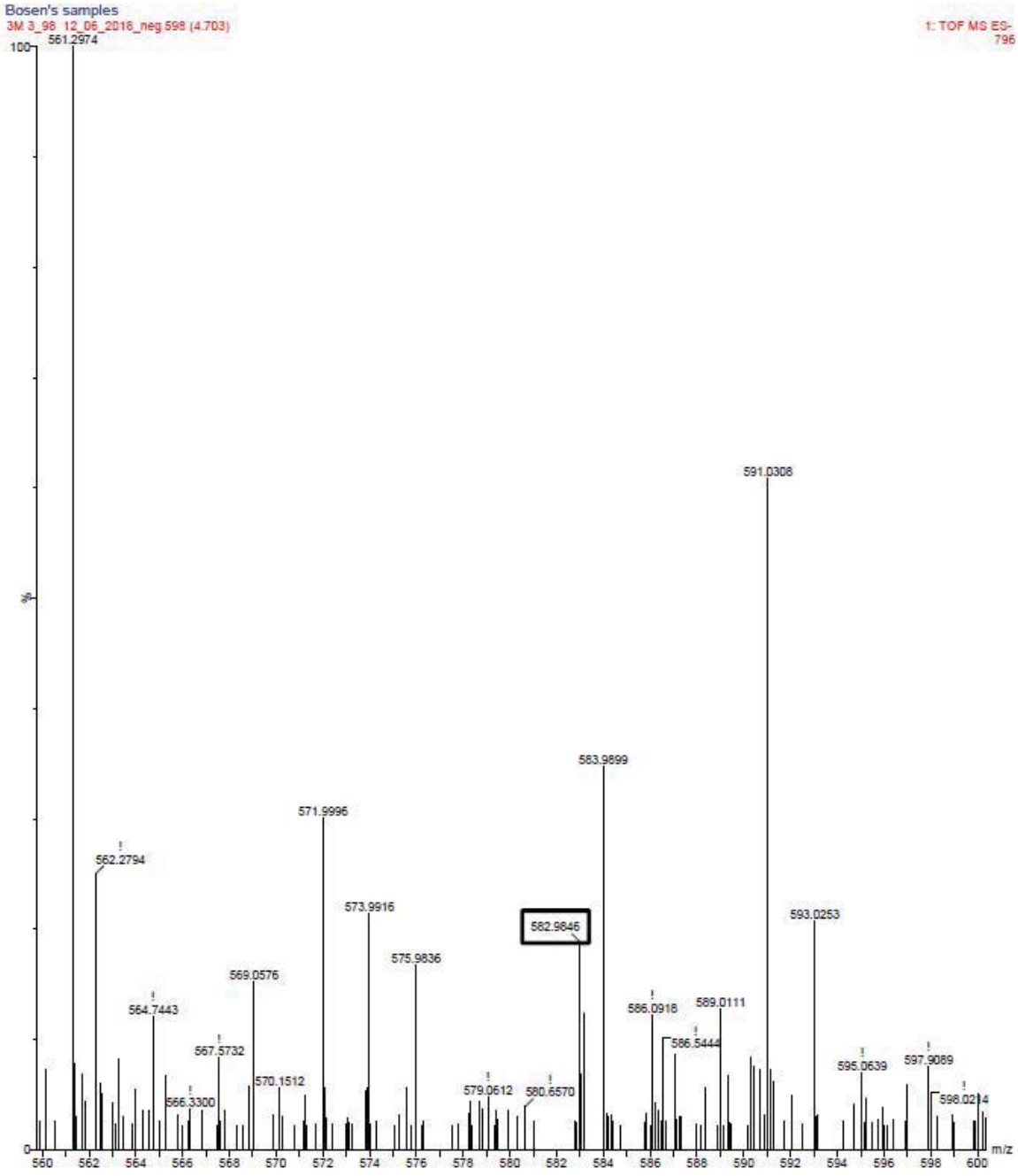

Mass value is found 582.9846 m/z

APPENDIX B - KMD RESULTS

Table B-1: KMD Results Listing

AFFF Formula Sample	Class	Mode (-/+)	Theoretical m/	Error	Inputed m/	Graph m/	Retention Time (min)	Notes
3M_3_98	23	-	310.943	-7.39685409	310.9407	310.941	5.34	Detected: Moderate noise but clear peak
3M_3_98	23	-	360.9398	-3.60170865	360.9385	360.939	4.05	Detected: Other close peaks
3M_3_98	24	-	392.9447	0	392.9447	392.945	4.05	Detected
3M_3_98	Class S/R/3B	-	405.0725	-2.46869388	405.0715	405.072	3.13	Detected
3M_3_98	23	-	410.9366	-1.46007924	410.936	410.936	4.46	Detected: Other close peaks
3M_3_98	24	-	442.9428	-2.03186506	442.9419	442.942	4.47	Detected
3M_3_98	Class S/R/3B	-	455.0693	-1.53822725	455.0686	455.069	3.78	Detected
3M_3_98	23	-	460.9334	-1.95255974	460.9325	460.933	4.76	Detected: Other close peaks
3M_3_98	Class S/R/3B	-	505.0661	-1.3859572	505.0654	505.065	4.26	Detected
3M_3_98	Class S/R/3B	-	555.0629	0.54047929	555.0632	555.063	4.63	Detected
3M_3_98	23	-	560.9270	-0.89138159	560.9265	560.927	4.58	Detected
3M_3_98	Class S/R/3B	-	655.0565		655.0547	655.055	5.20	Detected: Moderate noise but clear peak
3M_3_98	24	-	792.9193	0	792.9193	792.919	4.63	Detected
3M_4_90	Class 21	-	256.9183	2.72460156	256.9187	256.919	4.72	Detected: Other close peaks
3M_4_90	21	-	406.9087	-1.72028762	406.9077	406.908	4.30	Detected: Moderate noise but clear peak
3M_4_90	23	-	410.9366	-11.1939409	410.9346	410.932	4.33	Detected
3M_4_90	23	-	460.9334	-3.03731515	460.9319	460.932	4.66	Detected
3M_4_90	23	-	510.9302	-4.30587192	510.928	510.928	4.93	Detected
3M_4_90	21	-	556.8991	-1.97522316	556.8975	556.898	5.18	Detected
3M_4_90	23	-	560.9270	-5.34828953	560.9241	560.924	5.16	Detected: Other close peaks
3M_4_90	21	-	606.8659	46.303475	606.8939	606.894	5.38	Detected
3M_4_90	23	-	610.9238	-304.129582	610.738	610.738	5.31	Detected
3M_4_90	23	-	610.9238	-2.94635763	610.9217	610.922	5.31	Detected
3M_4_90	21	-	656.8977	-10.1994572	656.8907	656.891	5.54	Detected
3M_4_90	PR-3	-	676.9156	-5.31824056	676.9118	676.912	3.91	Detected
3M_4_90	23	-	710.9175	-3.51658244	710.9146	710.915	5.59	Detected: Other close peaks
3M_4_90	23	-	760.9112	-0.26284276	760.9112	760.911	5.70	Detected: Other close peaks
3M_5_79	Class PR-3	-	376.933	0	376.933	376.933	4.02	Detected: Other close peaks
3M_5_79	23	-	410.9366	-1.46007924	410.9358	410.936	4.27	Detected: Moderate noise but clear peak
3M_5_79	23	-	460.9334	-0.86780433	460.9328	460.933	4.58	Detected
3M_5_79	23	-	510.9302	-2.34865741	510.9292	510.929	4.87	Detected: Moderate noise but clear peak
3M_5_79	23	-	610.9238	-1.30949228	610.9227	610.923	3.45	Detected
3M_6_90	23	-	310.943	-5.46723998	310.9413	310.941	5.46	Detected
3M_6_90	23	-	410.9366	-5.11027735	410.9345	410.935	4.33	Detected
3M_6_90	23	-	460.9334	-2.16951082	460.9324	460.932	4.66	Detected: Other close peaks
3M_6_90	23	-	510.9302	-2.15293596	510.9291	510.929	4.93	Detected
3M_6_90	23	-	610.9238	-730.369319	610.4776	610.478	5.31	Detected
3M_6_90	23	-	610.9238	-3.2737307	610.9218	610.922	5.31	Detected
3M_6_90	PR-3	-	676.9156	-5.46596947	676.9119	676.912	3.91	Detected
3M_6_90	PR-3	-	726.9124	-6.46570343	726.9077	726.908	4.31	Detected

KMD Plots

3M 3_98: KMD Plots

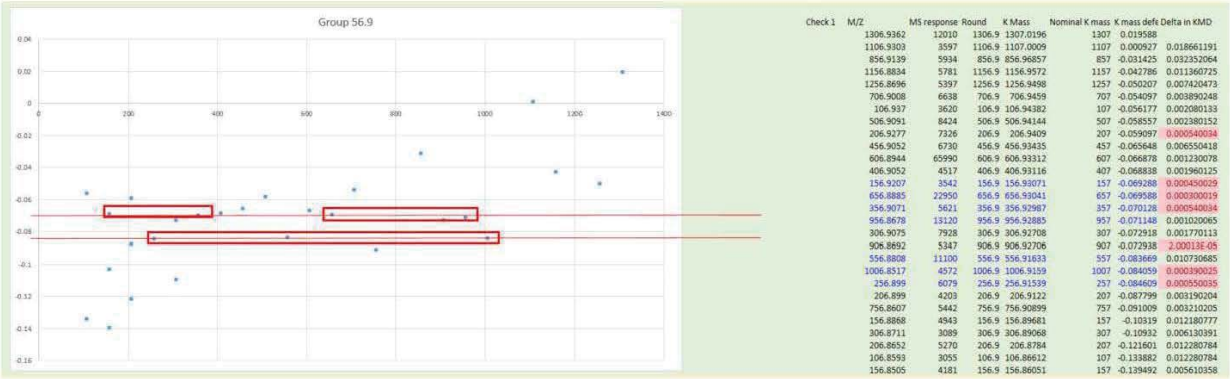

Check 1	M/Z	MS response	Round	K Mass	Nominal K mass	K mass defe	Delta in KMD
	1306.9362	12010	1306.9	1307.0196	1307	0.019588	
	1106.9303	3597	1106.9	1107.0009	1107	0.000927	0.018661191
	856.9139	5934	856.9	856.96857	857	-0.031425	0.032352064
	1156.8834	5781	1156.9	1156.9572	1157	-0.042786	0.011360725
	1256.8696	5397	1256.9	1256.9498	1257	-0.050207	0.007420473
	706.9008	6638	706.9	706.9459	707	-0.054097	0.003890248
	106.937	3620	106.9	106.94382	107	-0.056177	0.002080133
	506.9091	8424	506.9	506.94144	507	-0.058557	0.002380152
	206.9277	7326	206.9	206.9409	207	-0.059097	0.000540034
	456.9052	6730	456.9	456.93435	457	-0.065648	0.006550418
	606.8944	65990	606.9	606.93312	607	-0.066878	0.001230078
	406.9052	4517	406.9	406.93116	407	-0.068838	0.001960125
	156.9207	3542	156.9	156.93071	157	-0.069288	0.000450029
	656.8885	22950	656.9	656.93041	657	-0.069588	0.000300019
	356.9071	5621	356.9	356.92987	357	-0.070128	0.000540034
	956.8678	13120	956.9	956.92885	957	-0.071148	0.001020065
	306.9075	7928	306.9	306.92708	307	-0.072918	0.001770113
	906.8692	5347	906.9	906.92706	907	-0.072938	2.00013E-05
	556.8808	11100	556.9	556.91633	557	-0.083669	0.010730685
	1006.8517	4572	1006.9	1006.9159	1007	-0.084059	0.000390025
	256.899	6079	256.9	256.91539	257	-0.084609	0.000550035
	206.899	4203	206.9	206.9122	207	-0.087799	0.003190204
	756.8607	5442	756.9	756.90899	757	-0.091009	0.003210205
	156.8868	4943	156.9	156.89681	157	-0.10319	0.012180777
	306.8711	3089	306.9	306.89068	307	-0.10932	0.006130391
	206.8652	5270	206.9	206.8784	207	-0.121601	0.012280784
	106.8593	3055	106.9	106.86612	107	-0.133882	0.012280784
	156.8505	4181	156.9	156.86051	157	-0.139492	0.005610358

Figure B-1: KMD Plot for Class 21

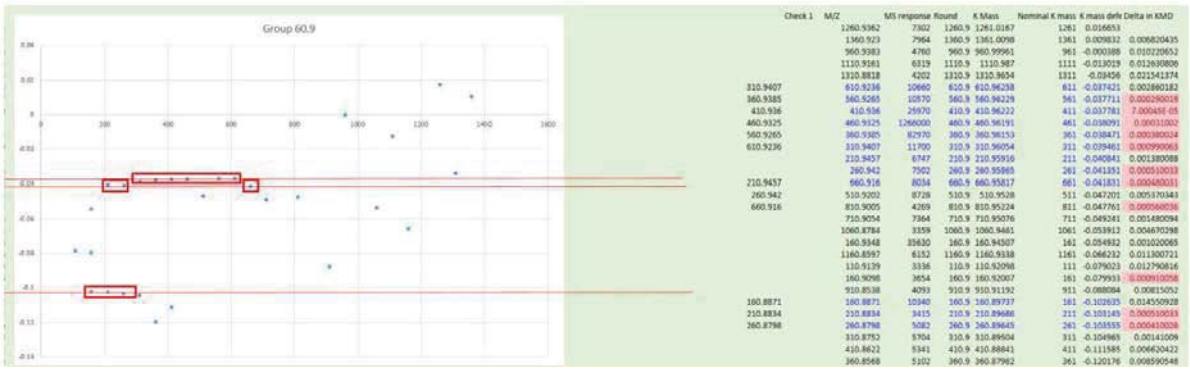

Check 1	M/Z	MS response	Round	K Mass	Nominal K mass	K mass defe	Delta in KMD
	1260.9362	7302	1260.9	1261.0167	1261	0.016653	
	1360.923	7964	1360.9	1361.0098	1361	0.009832	0.006820435
	960.9383	4760	960.9	960.99961	961	-0.000388	0.010220652
	1110.9161	6319	1110.9	1110.987	1111	-0.013019	0.012630806
	1310.8818	4202	1310.9	1310.9654	1311	-0.03456	0.021541374
310.9407	610.9236	10660	610.9	610.96258	611	-0.037421	0.002860182
160.9385	560.9265	10570	560.9	560.96229	561	-0.037711	0.000290028
410.936	410.936	25970	410.9	410.96222	411	-0.037781	7.00045E-05
460.9325	460.9325	1266000	460.9	460.96191	461	-0.038091	0.000310002
560.9265	360.9385	82970	360.9	360.98153	361	-0.038471	0.000380024
610.9236	310.9407	11700	310.9	310.96054	311	-0.039461	0.000990063
	210.9457	6747	210.9	210.95916	211	-0.040841	0.001380088
	260.942	7502	260.9	260.95865	261	-0.041151	0.000510033
210.9457	660.916	8034	660.9	660.95817	661	-0.041831	0.000680031
260.942	510.9202	8726	510.9	510.9528	511	-0.047201	0.005370340
660.916	810.9005	4269	810.9	810.95224	811	-0.047761	0.000560036
	710.9054	7364	710.9	710.95076	711	-0.049241	0.001480094
	1060.8784	3359	1060.9	1060.9461	1061	-0.053912	0.004670298
	160.9348	35630	160.9	160.94507	161	-0.054932	0.001020065
	1160.8597	6152	1160.9	1160.9338	1161	-0.066232	0.011300721
	110.9139	3336	110.9	110.92098	111	-0.079023	0.012790816
	160.9098	3854	160.9	160.92067	161	-0.079933	0.000910056
	910.8538	4093	910.9	910.91192	911	-0.088084	0.00815052
160.8871	160.8871	10340	160.9	160.89737	161	-0.102635	0.014550928
210.8834	210.8834	3415	210.9	210.89686	211	-0.103145	0.000510033
260.8798	260.8798	5082	260.9	260.89645	261	-0.103555	0.000410026
	310.8752	5704	310.9	310.89504	311	-0.104965	0.00141009
	410.8622	9341	410.9	410.88841	411	-0.111585	0.006620422
	360.8569	5102	360.9	360.87962	361	-0.120176	0.008590548

Figure B-2: KMD Plot for Class 23

3M 5_79: KMD Plots

	Check 1	M/Z	MS respo	Round	K Mass	Nominal K	K mass de	Delta in KMD
		960.947	9450	960.9	961.008	961	0.00841	
		910.938	5308	910.9	910.996	911	-0.0043	0.01269081
		810.943	6786	810.9	810.995	811	-0.0049	0.00058004
		760.923	7435	760.9	760.971	761	-0.0288	0.02389152
		710.923	11010	710.9	710.969	711	-0.0313	0.00259017
410.936		460.933	737000	460.9	460.962	461	-0.0378	0.00645041
460.933		560.926	24400	560.9	560.962	561	-0.0379	0.00013001
510.929		410.936	23980	410.9	410.962	411	-0.038	7.0004E-05
560.926		510.929	15530	510.9	510.962	511	-0.0382	0.00022001
610.923		610.923	20620	610.9	610.962	611	-0.0383	0.00013001
		360.938	32140	360.9	360.961	361	-0.0395	0.00115007
		310.938	9810	310.9	310.958	311	-0.0423	0.00279018
		660.915	11780	660.9	660.957	661	-0.0429	0.00067004
		210.942	4321	210.9	210.955	211	-0.0446	0.00171011
		260.928	4761	260.9	260.945	261	-0.0553	0.01061068
		210.908	6500	210.9	210.922	211	-0.0784	0.02319148
		310.899	5614	310.9	310.919	311	-0.0814	0.00292019
		260.889	4543	260.9	260.906	261	-0.0944	0.01299083
		210.87	4629	210.9	210.883	211	-0.117	0.02269145

B-3: KMD Plot for Class 23

REFERENCES

3M. (1999). *The science of organic fluorochemistry*. February 5, 1999. https://www.fluoridealert.org/wp-content/pesticides/pfos.fr.final.docket.0006.pdf

Alaska Department of Environmental Conservation (ADEC). (2019). Division of Spill Prevention and Response—Contaminated sites. https://dec.alaska.gov/spar/csp.aspx. Accessed multiple times in March-May 2019

Ahrens, L., Felizeter, S., Sturm, R., Xie, Z. Y., & Ebinghaus, R. (2009). Polyfluorinated compounds in waste water treatment plant effluents and surface waters along the River Elbe, Germany. *Marine Pollution Bulletin*, *58*(9), 1326–1333. https://doi.org/10.1016/j.marpolbul.2009.04.028

Ahrens, L., Shoeib, M., Harner, T., Lee, S. C., Guo, R., & Reiner, E. J. (2011). Wastewater treatment plant and landfills as sources of polyfluoroalkyl compounds to the atmosphere. *Environmental Science & Technology*, *45*(19), 8098–8105. https://doi.org/10.1021/es1036173

American Chemistry Society (ACS), Division of Chemical Toxicology Panel, & Panel Members Kurt Davis Pennel, J. D., Jon Sobus, Pamela J. Lein, & Dr. David Balshaw. (2020). *Chemical exposures and impacts on health*. American Chemistry Society (ACS) 2020 Fall Meeting. Virtual/Online. Aug 19, 2020.

American Society for Testing and Materials (ASTM). International. (2019). D7968 - 17a. Standard Test Method for Determination of Polyfluorinated Compounds in Soil by Liquid Chromatography Tandem Mass Spectrometry (LC/MS/MS). In *Book of Standards* (Vol. 11.04). 100 Barr Harbor Drive, PO Box C700, West Conshohocken, PA 19428-2959. United States: Copyright © ASTM International.

Anderson, R. H., Adamson, D. T., & Stroo, H. F. (2019). Partitioning of poly- and perfluoroalkyl substances from soil to groundwater within aqueous film-forming foam source zones. *Journal of Contaminant Hydrology*, *220*, 59–65. https://doi.org/10.1016/j.jconhyd.2018.11.011

Arvaniti, O. S., & Stasinakis, A. S. (2015). Review on the occurrence, fate and removal of perfluorinated compounds during wastewater treatment. *Science of the Total Environment*, *525*, 81–92. https://doi.org/10.1016/j.scitotenv.2015.04.023

Ateia, M., Maroli, A., Tharayil, N., & Karanfil, T. (2019). The overlooked short- and ultrashort-chain poly- and perfluorinated substances: A review. *Chemosphere*, *220*, 866–882. https://doi.org/10.1016/j.chemosphere.2018.12.186

Backe, W. J., Day, T. C., & Field, J. A. (2013). Zwitterionic, cationic, and anionic fluorinated chemicals in aqueous film forming foam formulations and groundwater from US military bases by nonaqueous large-volume injection HPLC-MS/MS. *Environmental Science and Technology*, *47*(10), 5226–5234. https://doi.org/10.1021/es3034999

Baduel, C., Mueller, J. F., Rotander, A., Corfield, J., & Gomez-Ramos, M. J. (2017). Discovery of novel per- and polyfluoroalkyl substances (PFAS) at a fire fighting training ground and preliminary investigation of their fate and mobility. *Chemosphere*, *185*, 1030-1038. https://doi.org/10.1016/j.chemosphere.2017.06.096

Barzen-Hanson, K. A., Davis, S. E., Kleber, M., & Field, J. A. (2017a). Sorption of fluorotelomer sulfonates, fluorotelomer sulfonamido betaines, and a fluorotelomer sulfonamido amine in national foam aqueous film-forming foam to soil. *Environmental Science and Technology*, *51*(21), 12394–12404. https://doi.org/10.1021/acs.est.7b03452

Barzen-Hanson, K. A., & Field, J. A. (2015). Discovery and Implications of C 2 and C 3 Perfluoroalkyl Sulfonates in Aqueous Film-Forming Foams and Groundwater. *Environmental Science and Technology Letters*, *2*(4), 95–99. https://doi.org/10.1021/acs.estlett.5b00049

Barzen-Hanson, K. A., Roberts, S. C., Choyke, S., Oetjen, K., McAlees, A., Riddell, N. . . Field, J. A. (2017b). Discovery of 40 classes of per- and polyfluoroalkyl substances in historical aqueous film-forming foams (AFFFs) and AFFF-impacted groundwater. *Environmental Science and Technology*, *51*(4), 2047–2057. https://doi.org/10.1021/acs.est.6b05843

Becker, A. M., Suchan, M., Gerstmann, S., & Frank, H. (2010). Perfluorooctanoic acid and perfluorooctane sulfonate released from a waste water treatment plant in Bavaria, Germany. *Environmental Science and Pollution Research International*, *17*(9), 1502–1507. https://doi.org/10.1007/s11356-010-0335-x

Benotti, M. J. (2020). PFAS fingerprinting presentation. *Newfields*. mbenotti@newfields.com.

Benotti, M. J., Fernandez, L. A., Peaslee, G. F., Douglas, G. S., Uhler, A. D., & Emsbo-Mattingly, S. (2020). A forensic approach for distinguishing PFAS materials. *Environmental Forensics*, *21*(3–4), 319–333. https://doi.org/10.1080/15275922.2020.1771631

Bird, D. R., & Furstenau, R. R. (1999). Applications and concepts in chemistry. Houghton Mifflin Harcourt Publishing Company of Boston, MA

Bolan, N., Sarkar, B., Yan, Y. B., Li, Q., Wijesekara, H., Kannan, K., . . . Rinklebe, J. (2021). Remediation of poly- and perfluoroalkyl substances (PFAS) contaminated soils—To mobilize or to immobilize or to degrade? *Journal of Hazardous Materials*, *401*, Article 123892. https://doi.org/10.1016/j.jhazmat.2020.123892

Boulanger, B., Vargo, J. D., Schnoor, J. L., & Hornbuckle, K. C. (2005). Evaluation of perfluorooctane surfactants in a wastewater treatment system and in a commercial surface protection product. *Environmental Science and Technology*, *39*(15), 5524–5530. https://doi.org/10.1021/es050213u

Brusseau, M. L. (2018). Assessing the potential contributions of additional retention processes to PFAS retardation in the subsurface. *Science of the Total Environment*, *614*, 176–185. https://doi.org/10.1016/j.scitotenv.2017.09.065

Brusseau, M. L., Yan, N., Van Glubt, S., Wang, Y. K., Chen, W., Lyu, Y., . . . Holguin, F. O. (2019). Comprehensive retention model for PFAS transport in subsurface systems. *Water Research*, *148*, 41–50. https://doi.org/10.1016/j.watres.2018.10.035

Bugsel, B., & Zwiener, C. (2020). LC-MS screening of poly- and perfluoroalkyl substances in contaminated soil by Kendrick mass analysis. *Analytical and Bioanalytical Chemistry*, *412*(20), 4797–4805. https://doi.org/10.1007/s00216-019-02358-0

Cerveny, D., Grabic, R., Fedorova, G., Grabicova, K., Turek, J., Kodes, V., . . . Randak, T. (2016). Perfluoroalkyl substances in aquatic environment-comparison of fish and passive sampling approaches. *Environmental Research*, *144*, 92–98. https://doi.org/10.1016/j.envres.2015.11.010

CFM-ID. (2019–20). 3.0. Online mass spectrum database. Retrieved from http://cfmid.wishartlab.com/predict. *Accessed* 2019–2020

D'Agostino, L. A., & Mabury, S. A. (2014). Identification of novel fluorinated surfactants in aqueous film forming foams and commercial surfactant concentrates. *Environmental Science and Technology*, *48*(1), 121–129. https://doi.org/10.1021/es403729e

D'Agostino, L. A., & Mabury, S. A. (2017). Certain perfluoroalkyl and polyfluoroalkyl substances associated with aqueous film forming foam are widespread in Canadian surface waters. *Environmental Science and Technology*, *51*(23), 13603–13613. https://doi.org/10.1021/acs.est.7b03994

Das, B. M. (1998). *Principles of geotechnical engineering*. PWS Publishing.

Dauchy, X., Boiteux, V., Bach, C., Colin, A., Hemard, J., Rosin, C., & Munoz, J. F. (2017). Mass flows and fate of per- and polyfluoroalkyl substances (PFAS) in the wastewater treatment plant of a fluorochemical manufacturing facility. *Science of the Total Environment*, *576*, 549–558. https://doi.org/10.1016/j.scitotenv.2016.10.130

Dauchy, X., Boiteux, V., Colin, A., Bach, C., Rosin, C., & Munoz, J. F. (2019). Poly- and perfluoroalkyl substances in runoff water and wastewater sampled at a firefighter training area. *Archives of Environmental Contamination and Toxicology*, *76*(2), 206–215. https://doi.org/10.1007/s00244-018-0585-z

De Silva, A. O., Spencer, C., Scott, B. F., Backus, S., & Muir, D. C. G. (2011). Detection of a cyclic perfluorinated acid, perfluoroethylcyclohexane sulfonate, in the Great Lakes of North America. *Environmental Science and Technology*, *45*(19), 8060–8066. https://doi.org/10.1021/es200135c

Earnshaw, M. R., Paul, A. G., Loos, R., Tavazzi, S., Paracchini, B., Scheringer, M., . . . Sweetman, A. J. (2014). Comparing measured and modelled PFOS concentrations in a UK freshwater catchment and estimating emission rates. *Environment International*, *70*, 25–31. https://doi.org/10.1016/j.envint.2014.05.004

Erickson, M. (2008). Emerging contaminants and impaired waters/TMDLs. Retrieved September from https://wiki.umn.edu/pub/Wilson/TMDL-SpecialProblem/PFCs_and_Impaired_Waters-TMDLs.pdf

EUROFINS, E. A. Eaton Analytical briefing for PFAS identification. UND Educational briefing.

Federal Aviation Administration (FAA), D. o. T. (2004). Title 14, code of federal regulation (CFR) §. *Aircraft rescue and firefighting: Equipment and agents*. Retrieved from https://ecfr.io/Title-14/Section-139.317, *139.317*

Ferrey, M. L., Wilson, J. T., Adair, C., Su, C. M., Fine, D. D., Liu, X. Y., & Washington, J. W. (2012). Behavior and fate of PFOA and PFOS in sandy aquifer sediment. *Groundwater Monitoring and Remediation*, *32*(4), 63–71. https://doi.org/10.1111/j.1745-6592.2012.01395.x

Fetter, C. W., Thomas Boving and David Kreamer. (2018). Containment Hydrogeology. (Third ed.). Waveland Press, Inc

Fitts, C. R. (2002). *Groundwater science*. Academic Press—An Imprint of Elsevier Science Ltd.

Gallen, C., G. Eaglesham, D. Drage, T. Hue Nguyen, and J.F. Mueller. (2018). A mass estimate of perfluoroalkyl substance (PFAS) release from Australian wastewater treatment plants. Chemosphere, 208, 975-983. https://doi.org/10.1016/j.chemosphere.2018.06.024

Gebbink, W. A., Glynn, A., Darnerud, P. O., & Berger, U. (2015). Perfluoroalkyl acids and their precursors in Swedish food: The relative importance of direct and indirect dietary exposure. *Environmental Pollution*, *198*, 108–115. https://doi.org/10.1016/j.envpol.2014.12.022

Guelfo, J. L., & Higgins, C. P. (2013). Subsurface transport potential of perfluoroalkyl acids at aqueous film-forming foam (AFFF)-impacted sites. *Environmental Science and Technology*, *47*(9), 4164–4171. https://doi.org/10.1021/es3048043

Guo, B., Zeng, J. C., & Brusseau, M. L. (2020). A mathematical model for the release, transport, and retention of per- and polyfluoroalkyl substances (PFAS) in the vadose zone. *Water Resources Research*, *56*(2), article e2019WR026667. https://doi.org/10.1029/2019wr026667

Harris, D. C., & Charles, L. A. (2016). *Quantitative chemical analysis* (9th ed). W. H Freeman and Company.

Hatzinger, P. B., & Alexander, M. (1995). Effect of aging of chemicals in soil on their biodegradability and extractability. *Environmental Science and Technology*, *29*(2), 537–545. https://doi.org/10.1021/es00002a033

Higgins, C. P., & Luthy, R. G. (2006). Sorption of perfluorinated surfactants on sediments. *Environmental Science and Technology*, *40*(23), 7251–7256. https://doi.org/10.1021/es061000n

Høisæter, Å., Pfaff, A., & Breedveld, G. D. (2019). Leaching and transport of PFAS from aqueous film-forming foam (AFFF) in the unsaturated soil at a firefighting training facility under cold climatic conditions. *Journal of Contaminant Hydrology*, *222*, 112–122. https://doi.org/10.1016/j.jconhyd.2019.02.010

Hollender, J., van Bavel, B., Dulio, V., Farmen, E., Furtmann, K., Koschorreck, J., . . . Tornero, V. (2019). High resolution mass spectrometry-based non-target screening can support regulatory environmental monitoring and chemicals management. *Environmental Sciences Europe*, *31*, article 42. https://doi.org/10.1186/s12302-019-0225-x

Houtz, E., Wang, M. M., & Park, J. S. (2018). Identification and fate of aqueous film forming foam derived per- and polyfluoroalkyl substances in a wastewater treatment plant. *Environmental Science and Technology*, *52*(22), 13212–13221. https://doi.org/10.1021/acs.est.8b04028 Not used yet

Houtz, E. F., Higgins, C. P., Field, J. A., & Sedlak, D. L. (2013). Persistence of perfluoroalkyl acid precursors in AFFF-impacted groundwater and soil. *Environmental Science and Technology*, *47*(15), 8187–8195. https://doi.org/10.1021/es4018877

Hughey, C. A., Hendrickson, C. L., Rodgers, R. P., Marshall, A. G., & Qian, K. N. (2001). Kendrick mass defect spectrum: A compact visual analysis for ultrahigh-resolution broadband mass spectra. *Analytical Chemistry*, *73*(19), 4676–4681. https://doi.org/10.1021/ac010560w

Jamari, N. L. A., Dohmann, J. F., Raab, A., Krupp, E. M., & Feldmann, J. (2019). Novel non-targeted analysis of perfluorinated compounds using fluorine-specific detection regardless of their ionisability (HPLC-ICPMS/MS-ESI-MS). *Analytica Chimica Acta*, *1053*, 22–31. https://doi.org/10.1016/j.aca.2018.11.037

Jeon, J., Kannan, K., Lim, B. J., An, K. G., & Kim, S. D. (2011). Effects of salinity and organic matter on the partitioning of perfluoroalkyl acid (PFAs) to clay particles. *Journal of Environmental Monitoring*, *13*(6), 1803–1810. https://doi.org/10.1039/c0em00791a

Jin, Z. W., Simkins, S., & Xing, B. S. (1999). Bioavailability of freshly added and aged naphthalene in soils under gastric pH conditions. *Environmental Toxicology and Chemistry*, *18*(12), 2751–2758. https://doi.org/10.1002/etc.5620181215

Johnson, R. L., Anschutz, A. J., Smolen, J. M., Simcik, M. F., & Penn, R. L. (2007). The adsorption of perfluorooctane sulfonate onto sand, clay, and iron oxide surfaces. *Journal of Chemical and Engineering Data*, *52*(4), 1165–1170. https://doi.org/10.1021/je060285g

Kendrick, E. (1963). A mass scale based on CH_2=14.0000 for high resolution mass spectrometry of organic compounds. *Analytical Chemistry*, *35*(13), 2146–2154. https://doi.org/10.1021/ac60206a048

Kwadijk, C. J., Velzeboer, I., & Koelmans, A. A. (2013). Sorption of perfluorooctane sulfonate to carbon nanotubes in aquatic sediments. *Chemosphere*, *90*(5), 1631–1636. https://doi.org/10.1016/j.chemosphere.2012.08.041

Leppänen, M. T., & Kukkonen, J. V. K. (2000). Effect of sediment–chemical contact time on availability of sediment-associated pyrene and benzo[a]pyrene to oligochaete worms and semi-permeable membrane devices. *Aquatic Toxicology*, *49*(4), 227–241. https://doi.org/10.1016/s0166-445x(99)00085-5

Liang, X. W., Zhu, S. Z., Chen, P., & Zhu, L. Y. (2010). Bioaccumulation and bioavailability of polybrominated diphenyl ethers (PBDEs) in soil. *Environmental Pollution*, *158*(7), 2387–2392. https://doi.org/10.1016/j.envpol.2010.04.008

Lin, Y. F., Liu, R. Z., Hu, F. B., Liu, R. R., Ruan, T., & Jiang, G. B. (2016). Simultaneous qualitative and quantitative analysis of fluoroalkyl sulfonates in riverine water by liquid chromatography coupled with Orbitrap high resolution mass spectrometry. *Journal of Chromatography A*, *1435*, 66–74. https://doi.org/10.1016/j.chroma.2016.01.039

Liu, Y. N., D'Agostino, L. A., Qu, G. B., Jiang, G. B., & Martin, J. W. (2019). High-resolution mass spectrometry (HRMS) methods for nontarget discovery and characterization of poly- and per-fluoroalkyl substances (PFAS) in environmental and human samples. *TrAC Trends in Analytical Chemistry*, *121*, article 115420. https://doi.org/10.1016/j.trac.2019.02.021

Liu, Y. N., Pereira, Ados S., & Martin, J. W. (2015). Discovery of C5-C17 poly- and perfluoroalkyl substances in water by in-line SPE-HPLC-Orbitrap with in-source fragmentation flagging. *Analytical Chemistry*, *87*(8), 4260–4268. https://doi.org/10.1021/acs.analchem.5b00039

Lorenzo, M., Campo, J., & Picó, Y. (2018). Analytical challenges to determine emerging persistent organic pollutants in aquatic ecosystems. *TrAC Trends in Analytical Chemistry*, *103*, 137–155. https://doi.org/10.1016/j.trac.2018.04.003

Lougee, R. (2020, August 20). New CSRML-based features to categorize and fingerprint PFAS structure lists for cheminformatics analysis and read-across. American Chemistry Society (ACS) 2020 Fall Meeting. Virtual/Online.

Lv, X. Y., Sun, Y. Y., Ji, R., Gao, B., Wu, J. C., Lu, Q. S., & Jiang, H. (2018). Physicochemical factors controlling the retention and transport of perfluorooctanoic acid (PFOA) in saturated sand and limestone porous media. *Water Research*, *141*, 251–258. https://doi.org/10.1016/j.watres.2018.05.020

Lyu, X. Y., Liu, X., Sun, Y. Y., Gao, B., Ji, R., Wu, J. C., & Xue, Y. Q. (2020). Importance of surface roughness on perfluorooctanoic acid (PFOA) transport in unsaturated porous media. *Environmental Pollution*, *266*, article 115343. https://doi.org/10.1016/j.envpol.2020.115343

Lyu, Y., & Brusseau, M. L. (2020). The influence of solution chemistry on air-water interfacial adsorption and transport of PFOA in unsaturated porous media. *Science of the Total Environment*, *713*, article 136744. https://doi.org/10.1016/j.scitotenv.2020.136744

Lyu, Y., Brusseau, M. L., Chen, W., Yan, N., Fu, X. R., & Lin, X. Y. (2018). Adsorption of PFOA at the air-water interface during transport in unsaturated porous media. *Environmental Science and Technology*, *52*(14), 7745–7753. https://doi.org/10.1021/acs.est.8b02348

Ma, L. L., Zhang, J., Han, L. S., Li, W. M., Xu, L., Hu, F., & Li, H. X. (2012). The effects of aging time on the fraction distribution and bioavailability of PAH. *Chemosphere*, *86*(10), 1072–1078. https://doi.org/10.1016/j.chemosphere.2011.11.065

Margenau, H. (1939). Van der Waals forces. *Reviews of Modern Physics*, *11*(1), 0001–0035. https://doi.org/10.1103/RevModPhys.11.1

Mejia-Avendaño, S., Munoz, G., Vo Duy, S. V., Desrosiers, M., Benoît, P., Sauvé, S., & Liu, J. X. (2017). Novel fluoroalkylated surfactants in soils following firefighting foam deployment during the lac-megantic railway accident. *Environmental Science and Technology*, *51*(15), 8313–8323. https://doi.org/10.1021/acs.est.7b02028

Milinovic, J., Lacorte, S., Vidal, M., & Rigol, A. (2015). Sorption behaviour of perfluoroalkyl substances in soils. *Science of the Total Environment*, *511*, 63–71. https://doi.org/10.1016/j.scitotenv.2014.12.017

Miller, C. T., & Weber, W. J. (1984). Modeling organic contaminant partitioning in ground-water Systems. *Ground Water*, *22*(5), 584–592. https://doi.org/10.1111/j.1745-6584.1984.tb01429.x

Minnesota Pollution Control Agency (MPCA). (2007). *Washington County Landfill Remedy Feasibility Assessment. SEH* No. A-MNPCA0802.00. Effective Date: November 15, 2007. https://www.pca.state.mn.us/sites/default/files/pfc-wa-co-remedy-feasibility.pdf.

MPCA. (2008a). Closed Landfill Program, Remediation Division—Investigating PFCs in groundwater near the Washington Co. Landfill. c-clf2-03. https://www.pca.state.mn.us/sites/default/files/c-clf2-03.pdf

MPCA (2008b). Remediation Division, Superfund Program −3M Oakdale Disposal Site Proposed cleanup plan for PFCs - *c-s3-06* - May 2008. Retrieved from https://www.pca.state.mn.us/sites/default/files/c-s3-06.pdf

MPCA. (2008c). *Remedy decision document: Washington County Landfill, Lake Elmo, Minnesota. 6/18*/08. https://www.pca.state.mn.us/sites/default/files/pfc-washingtoncounty-rdd.pdf

MPCA. (2009). PFCs and Class B firefighting foam. Remediation ·. Retrieved from https://www.pca.state.mn.us/sites/default/files/pfc-classbfoam-factsheet.pdf

MPCA. (2013). Groundwater Monitoring Data. http://www.pca.state.mn.us/index.php/data/groundwater.html. Accessed October 2020)

Miyake, Y., Yamashita, N., Rostkowski, P., So, M. K., Taniyasu, S., Lam, P. K. S., & Kannan, K. (2007). Determination of trace levels of total fluorine in water using combustion ion chromatography for fluorine: A mass balance approach to determine individual

perfluorinated chemicals in water. *Journal of Chromatography. A*, *1143*(1–2), 98–104. https://doi.org/10.1016/j.chroma.2006.12.071

Munoz, G., Duy, S. V., Labadie, P., Botta, F., Budzinski, H., Lestremau, F., . . . Sauvé, S. (2016). Analysis of zwitterionic, cationic, and anionic poly- and perfluoroalkyl surfactants in sediments by liquid chromatography polarity-switching electrospray ionization coupled to high resolution mass spectrometry. *Talanta*, *152*, 447–456. https://doi.org/10.1016/j.talanta.2016.02.021

Murakami, M., Shinohara, H., & Takada, H. (2009). Evaluation of wastewater and street runoff as sources of perfluorinated surfactants (PFSs). *Chemosphere*, *74*(4), 487–493. https://doi.org/10.1016/j.chemosphere.2008.10.018

Nason, S. L., Koelmel, J., Zuverza-Mena, N., Stanley, C., Tamez, C., Bowden, J. A., & Godri Pollitt, K. J. (2021). Software comparison for nontargeted analysis of PFAS in AFFF-contaminated soil. *Journal of the American Society for Mass Spectrometry*, *32*(4), 840–846. https://doi.org/10.1021/jasms.0c00261

Ololade, I. A., Oladoja, N. A., Ololade, O. O., Oloye, F. F., Adeola, A. O., Alabi, A. B., . . . Owolabi, M. B. (2018). Geographical distribution of perfluorooctanesulfonate and perfluorooctanoate in selected rivers from Nigeria. *Journal of Environmental Chemical Engineering*, *6*(4), 4061–4069. https://doi.org/10.1016/j.jece.2018.06.020

Picó, Y., Farré, M., & Barceló, D. (2015). Quantitative profiling of perfluoroalkyl substances by ultrahigh-performance liquid chromatography and hybrid quadrupole time-of-flight mass spectrometry. *Analytical and Bioanalytical Chemistry*, *407*(15), 4247–4259. https://doi.org/10.1007/s00216-015-8459-y

Place, B., Backe, W., Houtz, E., Sedlak, D., & Field, J. (2012). Identification of the novel fluorochemical components in US military-use aqueous film-forming foams (AFFFs) using fast atom bombardment and high resolution mass spectrometry. Abstracts of the Papers of the American Chemical Society, 243.

Place, B. J., & Field, J. A. (2012). Identification of novel fluorochemicals in aqueous film-forming foams used by the US Military. *Environmental Science and Technology*, *46*(13), 7120–7127. https://doi.org/10.1021/es301465n

Plumb, R. H. (2004). *EPA Fingerprint Analysis of Contaminant Data A Forensic Tool for Evaluating Environmental Contamination.* Retrieved from https://nepis.epa.gov/Exe/ZyNET.exe/901P0R00.txt?ZyActionD=ZyDocument&Client=EPA&Index=2000%20Thru%202005&Docs=&Query=&Time=&EndTime=&SearchMethod=1&TocRestrict=n&Toc=&TocEntry=&QField=&QFieldYear=&QFieldMonth=&QFieldDay=&UseQField=&IntQFieldOp=0&ExtQFieldOp=0&XmlQuery=&File=D%3A%5CZYFILES%5CINDEX%20DATA%5C00THRU05%5CTXT%5C00000011%5C901P0R00.txt&User=ANONYMOUS&Password=anonymous&SortMethod=h%7C-&MaximumDocuments=1&FuzzyDegree=0&ImageQuality=r75g8/r75g8/x150y150g16/i425&Display=hpfr&DefSeekPage=x&SearchBack=ZyActionL&Back=ZyActionS&BackDesc=Results%20page&MaximumPages=1&ZyEntry=5

Roy, W. R., & Griffin, R. A. (1985). Mobility of organic solvents in water-saturated soil materials. *Environmental Geology and Water Sciences*, *7*(4), 241–247. https://doi.org/10.1007/bf02509925

Ruan, T., & Jiang, G. B. (2017). Analytical methodology for identification of novel per- and polyfluoroalkyl substances in the environment. *TrAC Trends in Analytical Chemistry*, *95*, 122–131. https://doi.org/10.1016/j.trac.2017.07.024

Ruan, T., Lin, Y. F., Wang, T., Jiang, G. B., & Wang, N. (2015). Methodology for studying biotransformation of polyfluoroalkyl precursors in the environment. *TrAC Trends in Analytical Chemistry*, *67*, 167–178. https://doi.org/10.1016/j.trac.2014.11.017

Salgado-Freiría, R., López-Doval, S., & Lafuente, A. (2018). Perfluorooctane sulfonate (PFOS) can alter the hypothalamic-pituitary-adrenal (HPA) axis activity by modifying CRF1 and glucocorticoid receptors. *Toxicology Letters*, *295*, 1–9. https://doi.org/10.1016/j.toxlet.2018.05.025

Schultz, M. M., Higgins, C. P., Huset, C. A., Luthy, R. G., Barofsky, D. F., & Field, J. A. (2006). Fluorochemical mass flows in a municipal wastewater treatment facility. *Environmental Science and Technology*, *40*(23), 7350–7357. https://doi.org/10.1021/es061025m :10.1021/es061025m

Schwarzenbach, R. R., Gschwend, P. M., & Imboden, D. M. (2003). *Environmental organic chemistry* (2nd ed). John Wiley & Sons, Inc.

Schymanski, E. L., Jeon, J., Gulde, R., Fenner, K., Ruff, M., Singer, H. P., & Hollender, J. (2014). Identifying small molecules via high resolution mass spectrometry: Communicating confidence. *Environmental Science and Technology*, *48*(4), 2097–2098. https://doi.org/10.1021/es5002105

ScienceStruck. (2020). *Isotopes of Carbon*. https://sciencestruck.com/isotopes-of-carbon#:~:text=Carbon%20has%20as%20many%20as%2015%20isotopes.%20They,in%20the%20nucleus.%20Most%20of%20them%20are%20radioactive

Silva, J. A. K., Martin, W. A., Johnson, J. L., & McCray, J. E. (2019). Evaluating air-water and NAPL-water interfacial adsorption and retention of perfluorocarboxylic acids within the vadose zone. *Journal of Contaminant Hydrology*, *223*, article 103472. https://doi.org/10.1016/j.jconhyd.2019.03.004

Sinclair, E., & Kannan, K. (2006). Mass loading and fate of perfluoroalkyl surfactants in wastewater treatment plants. *Environmental Science and Technology*, *40*(5), 1408–1414. https://doi.org/10.1021/es051798v

Sobus, J. (2020, August 19). TOXI Broadcast: EPA's research initiatives on non-targeted analyses of environmental chemicals. American Chemistry Society (ACS) 2020 Fall Meeting., Virtual/Online.

Sobus, J. R., Wambaugh, J. F., Isaacs, K. K., Williams, A. J., McEachran, A. D., Richard, A. M., . . . Newton, S. R. (2018). Integrating tools for non-targeted analysis research and chemical safety evaluations at the US EPA. *Journal of Exposure Science and Environmental Epidemiology*, *28*(5), 411–426. https://doi.org/10.1038/s41370-017-0012-y

Steinberg, S. M., Pignatello, J. J., & Sawhney, B. L. (1987). Persistence of 1,2-dibromoethane in soils: Entrapment in intraparticle micropores. *Environmental Science and Technology*, *21*(12), 1201–1208. https://doi.org/10.1021/es00165a007

United States Department of Health and Human Services (USDHHS), National Institute of Environmental Health Sciences (NIEHS). (2017). Testing status of perfluorobutane sulfonate (PFBS). Retrieved from https://ntp.niehs.nih.gov/testing/status/agents/ts-m040006.html#Known-Uses

United States Environmental Protection Agency (USEPA). (2009). Method 537 v1.1. Determination of selected perfluorinated alkyl acids in drinking water by solid-phase extraction and liquid chromatography/tandem mass spectrometry (LC/MS/MS). EPA Document #: EPA/*600/R-08/092*. September 2009. Retrieved from https://cfpub.epa.gov/si/si_public_record_report.cfm?dirEntryId=348508&Lab=CESER&simpleSearch=0&showCriteria=2&searchAll=537.1&TIMSType=&dateBeginPublishedPresented=03%2F24%2F2018

USEPA. (2016). Health effects support document for perfluorooctane sulfonate (PFOS). EPA 822-R-16-002. Retrieved from https://www.epa.gov/sites/production/files/2016-05/documents/pfos_hesd_final_508.pdf#:~:text=Health%20Effects%20Support%20Document%20for%20Perfluorooctane%20Sulfonate%20Acid,as%20public%20comments%20received%20on%20the%20draft%20document.

USEPA. (2017a) "Technical Fact Sheet – Perfluorooctanoic Sulfonate (PFOS) and Perfluorooctanoic Acid (PFOA)." EPA 505-F-17-001. November 2017. Retrieved from https://www.epa.gov/sites/production/files/2017-12/documents/ffrrofactsheet_contaminants_pfos_pfoa_11-20-17_508_0.pdf

USEPA. (2017b). The third unregulated contaminant monitoring rule (UCMR 3): Data summary, January 2017. Retrieved from https://www.epa.gov/sites/production/files/2017-02/documents/ucmr3-data-summary-january-2017.pdf. Retrieved from https://www.epa.gov/dwucmr/third-unregulated-contaminant-monitoring-rule

USEPA. (2018). Science in Action - Innovative Research for a Sustainable Future: EPA's Non-Targeted Analysis Collaborative Trial (ENTACT). Factsheet. Retrieved from https://www.epa.gov/sciencematters/epas-entact-study-breaks-new-ground-non-targeted-research#:~:text=Non%2Dtargeted%20analysis%20involves%20analyzing,may%20be%20in%20the%20samples.

USEPA. (2019a). EPA analytical methods for PFAS in Drinking Water. Fact Sheet. December 2019. Retrieved from https://www.epa.gov/pfas/epa-pfas-drinking-water-laboratory-methods

USEPA. (2019b). *Method 533. Determination of per- and polyfluoroylky substances in drinking water by isotope dilution anion exchange solid phase extraction and liquid chromatography/tandem mass spectrometry. Office of Water (MS-140).*EPA Document No. 815-B-19-020.EPA contract EP-C-17-014.

USEPA. (2020a). CompTox chemicals dashboard. Retrieved from https://comptox.epa.gov/dashboard

USEPA. (2020b). PFAS analytical methods development and sampling research. Retrieved from https://www.epa.gov/water-research/pfas-analytical-methods-development-and-sampling-research

Wang, Z. Y., Cousins, I. T., Scheringer, M., & Hungerbühler, K. (2013). Fluorinated alternatives to long-chain perfluoroalkyl carboxylic acids (PFCAs), perfluoroalkane sulfonic acids (PFSAs) and their potential precursors. *Environment International*, *60*, 242–248. https://doi.org/10.1016/j.envint.2013.08.021

Watson, J. T., & Sparkman, O. D. (2007). *Introduction to mass spectrometry: Instrumentation, applications, and strategies for data interpretation* (4th ed). John Wiley & Sons, Ltd. 2011.

Weber, A. K., Barber, L. B., LeBlanc, D. R., Sunderland, E. M., & Vecitis, C. D. (2017). Geochemical and hydrologic factors controlling subsurface transport of poly- and perfluoroalkyl substances, Cape Cod, Massachusetts. *Environmental Science and Technology*, *51*(8), 4269–4279. https://doi.org/10.1021/acs.est.6b05573

Wei, C. L., Song, X., Wang, Q., & Hu, Z. H. (2017). Sorption kinetics, isotherms and mechanisms of PFOS on soils with different physicochemical properties. *Ecotoxicology and Environmental Safety*, *142*, 40–50. https://doi.org/10.1016/j.ecoenv.2017.03.040

Weiner, B., Yeung, L. W. Y., Marchington, E. B., D'Agostino, L. A., & Mabury, S. A. (2013). Organic fluorine content in aqueous film forming foams (AFFFs) and biodegradation of the foam component 6: 2 fluorotelomermercaptoalkylamido sulfonate (6: 2 FTSAS). *Environmental Chemistry*, *10*(6), 486–493. https://doi.org/10.1071/en13128

White, J. C., Kelsey, J. W., Hatzinger, P. B., & Alexander, M. (1997). Factors affecting sequestration and bioavailability of phenanthrene in soils. *Environmental Toxicology and Chemistry*, *16*(10), 2040–2045. https://doi.org/10.1002/etc.5620161008

Williams, L. D. (2019). Molecular Interactions (Noncovalent Interactions) and the Behaviors of Biological Macromolecules. Chemistry & Biochemistry, Georgia Tech. Website. https://ww2.chemistry.gatech.edu/~lw26/structure/molecular_interactions/mol_int.html Accessed 4/18/2019.

Xiao, F. (2017). Emerging poly- and perfluoroalkyl substances in the aquatic environment: A review of current literature. *Water Research*, *124*, 482–495. https://doi.org/10.1016/j.watres.2017.07.024

Xiao, F., Golovko, S. A., & Golovko, M. Y. (2017). Identification of novel non-ionic, cationic, zwitterionic, and anionic polyfluoroalkyl substances using UPLC-TOF-MSE high-resolution parent ion search. *Analytica Chimica Acta*, *988*, 41–49. https://doi.org/10.1016/j.aca.2017.08.016

Xiao, F., Gulliver, J. S., & Simcik, M. F. (2013). Perfluorooctane sulfonate (PFOS) contamination of fish in urban lakes: A prioritization methodology for lake management. *Water Research*, *47*(20), 7264–7272. https://doi.org/10.1016/j.watres.2013.09.063

Xiao, F., Halbach, T. R., Simcik, M. F., & Gulliver, J. S. (2012). Input characterization of perfluoroalkyl substances in wastewater treatment plants: Source discrimination by exploratory data analysis. *Water Research*, *46*(9), 3101–3109. https://doi.org/10.1016/j.watres.2012.03.027

Xiao, F., Hanson, R., Golovko, S.A., Golovko, M.Y. and Arnold, W.A. (2018). PFOA and PFOS Are Generated from Zwitterionic and Cationic Precursor Compounds During Water Disinfection with Chlorine or Ozone. Environmental Science & Technology Letters, 5, 382–388. https://doi.org/10.1021/acs.estlett.8b00266

Xiao, F., Jin, B. S., Golovko, S. A., Golovko, M. Y., & Xing, B. S. (2019). Sorption and desorption mechanisms of cationic and zwitterionic per- and polyfluoroalkyl substances in natural soils: Thermodynamics and hysteresis. *Environmental Science and Technology*, *53*(20), 11818–11827. https://doi.org/10.1021/acs.est.9b05379

Xiao, F., & Pignatello, J. J. (2015). π(+)-π interactions between (hetero)aromatic amine cations and the graphitic surfaces of pyrogenic carbonaceous materials. *Environmental Science and Technology*, *49*(2), 906–914. https://doi.org/10.1021/es5043029

Xiao, F., & Pignatello, J. J. (2016). Effects of post-pyrolysis air oxidation of biomass chars on adsorption of neutral and ionizable compounds. *Environmental Science and Technology*, *50*(12), 6276–6283. https://doi.org/10.1021/acs.est.6b00362

Xiao, F., Simcik, M. F., Halbach, T. R., & Gulliver, J. S. (2015). Perfluorooctane sulfonate (PFOS) and perfluorooctanoate (PFOA) in soils and groundwater of a US metropolitan area: Migration and implications for human exposure. *Water Research*, *72*, 64–74. https://doi.org/10.1016/j.watres.2014.09.052

Xiao, F., Zhang, X. R., Penn, L., Gulliver, J. S., & Simcik, M. F. (2011). Effects of monovalent cations on the competitive adsorption of perfluoroalkyl acids by kaolinite: Experimental studies and modeling. *Environmental Science and Technology*, *45*(23), 10028–10035. https://doi.org/10.1021/es202524y

Yan, H., Zhang, C. J., Zhou, Q., Chen, L., & Meng, X. Z. (2012). Short- and long-chain perfluorinated acids in sewage sludge from Shanghai, China. *Chemosphere*, *88*(11), 1300–1305. https://doi.org/10.1016/j.chemosphere.2012.03.105

Yang, C. H., Tarkhov, A., Marusczyk, J., Bienfait, B., Gasteiger, J., Kleinoeder, T., . . . Rathman, J. (2015). New publicly available chemical query language, CSRML, to support chemotype

representations for application to data mining and modeling. *Journal of Chemical Information and Modeling*, *55*(3), 510–528. https://doi.org/10.1021/ci500667v

Yeung, L. W. Y., Stadey, C., & Mabury, S. A. (2017). Simultaneous analysis of perfluoroalkyl and polyfluoroalkyl substances including ultrashort-chain C2 and C3 compounds in rain and river water samples by ultra performance convergence chromatography. *Journal of Chromatography. A*, *1522*, 78–85. https://doi.org/10.1016/j.chroma.2017.09.049

Yin, N. Y., Yang, R. J., Liang, S. J., Liang, S. X., Hu, B. W., Ruan, T., & Faiola, F. (2018). Evaluation of the early developmental neural toxicity of F-53B, as compared to PFOS, with an in vitro mouse stem cell differentiation model. *Chemosphere*, *204*, 109–118. https://doi.org/10.1016/j.chemosphere.2018.04.011

You, C., Jia, C. X., & Pan, G. (2010). Effect of salinity and sediment characteristics on the sorption and desorption of perfluorooctane sulfonate at sediment-water interface. *Environmental Pollution*, *158*(5), 1343–1347. https://doi.org/10.1016/j.envpol.2010.01.009

Zacs, D., & Bartkevics, V. (2015). Analytical capabilities of high performance liquid chromatography - Atmospheric pressure photoionization - Orbitrap mass spectrometry (HPLC-APPI-Orbitrap-MS) for the trace determination of novel and emerging flame retardants in fish. *Analytica Chimica Acta*, *898*, 60–72. https://doi.org/10.1016/j.aca.2015.10.008

Zhao, S. Y., & Zhu, L. Y. (2017). Uptake and metabolism of 10:2 fluorotelomer alcohol in soil-earthworm (*Eisenia fetida*) and soil-wheat (*Triticum aestivum* L.) systems. *Environmental Pollution*, *220*, 124–131. https://doi.org/10.1016/j.envpol.2016.09.030

Zhao, Y. G., Wong, C. K. C., & Wong, M. H. (2012). Environmental contamination, human exposure and body loadings of perfluorooctane sulfonate (PFOS), focusing on Asian countries. *Chemosphere*, *89*(4), 355–368. https://doi.org/10.1016/j.chemosphere.2012.05.043